

University of Strathclyde
Department of Naval Architecture, Ocean and Marine Engineering

**Peridynamics Theory and its Applications in
Isotropic and Functionally Graded Beam and
Plate Structures**

By
Zhenghao Yang

A thesis submitted in fulfilment of the requirements for the degree of Doctor of
Philosophy

Glasgow, U.K.
2020

AUTHOR STATEMENT

This thesis is the result of the author's original research. It has been composed by the author and has not been previously submitted for examination which has led to the award of a degree.

The copyright of this thesis belongs to the author under the terms of the United Kingdom Copyright Acts as qualified by University of Strathclyde Regulation 3.50. Due acknowledgement must always be made of the use of any material contained in, or derived from, this thesis.

Signed:

Date:

Acknowledgement

First of all, I would like to express my special gratitude to my supervisors Dr. Erkan Oterkus, Prof. Nigel Barltrop and Dr. Selda Oterkus, for their excellent guidance and support as without them my PhD will never be a success.

I would like also to thank my parents, anti, uncle and grandparents. Their strong support and encourage throughout my study is highly appreciated.

Moreover, I am very grateful to my German families, Horst, Claudia, Sascha and Michelle for their kindness and having hosted me as a member of their family.

“Withholding information is the essence of tyranny. Control of the flow of information is the tool of the dictatorship.”

Bruce Coville

*To everyone who longs
for liberal democracy*

Abstract

In recent two decades, as an alternative formulation to Classical Continuum Mechanics (CCM), peridynamics (PD) has been rapidly progressed for solid mechanics applications. Instead of expressing equations of motion in partial differential equation form as in CCM, PD equations of motion are expressed in integro-differential equation form. Moreover, PD equations do not contain any spatial derivatives, which offer certain advantages especially for the solution of problems including displacement discontinuities due to the existence of cracks. This thesis emphasizes the introduction of governing equations for currently popular beam and plate models in peridynamics framework. The formulations are derived by using Euler-Lagrange equation and Taylor series expansion and verified by considering benchmark problems with comparison against finite element analysis results. In addition, the implementation of peridynamic beam and plate formulations in finite element framework is explained. Moreover, the classical peridynamic formulations (bond based, ordinary state based and non-ordinary state based) are revisited.

Contents

1. Introduction	1
1.1 Background of Peridynamics	1
1.2 Classification of Beams and Plates	2
1.3 Objectives and Motivations	3
1.4 Novelty.....	4
1.5 Outlines	6
2. Literature Review	7
2.1 Introduction.....	7
2.2 Development of Beam theories.....	8
2.3 Development of Plate Theories.....	14
2.4 Development of Functionally Graded Material (FGM).....	18
2.5 Conclusion	22
3. Peridynamic Theory	24
3.1 Introduction.....	24
3.2 Bond Based & State Based Peridynamics	25
3.3 Numerical Solution Method.....	40
3.4 Conclusion	45
4. PD formulation for Beam Theories	47
4.1 PD Formulations for Timoshenko Beam	47
4.2 PD Formulations for Higher Order Deformable Beams	54
4.3 PD Formulations for Transversely FGM Euler Beams.....	64
4.4 PD formation for FGM Timoshenko Beam	72
4.5 PD Formulations of FGM Higher Order Deformable Beam	82
4.6 Comparison Among PD Beam Theories.....	95
4.7 Conclusion	98
5. PD Formulations for Plate Theories	99
5.1 PD Formulation for Kirchhoff Plate Theory.....	99
5.2 PD Formulation for Functionally Graded Material Kirchhoff Plate.....	107
5.3 PD Formulations for Mindlin Plate.....	119

5.4 PD Formulations for FGM Mindlin Plate	129
5.5 PD Formulations for Higher Order Deformable Plate	141
5.6 PD Formulations for FGM Higher Order Deformable Plate	153
5.7 Comparison Among PD Plate Theories	174
5.8 Conclusion	177
6. Implementation of Peridynamics Beam and Plate Formulations in Finite Element Framework	178
6.1. PD Timoshenko Beam and Mindlin Plate Formulation.....	178
6.2 Implementation of Peridynamic Formulations in Finite Element Framework	184
6.3 Numerical Results	187
6.4 Conclusion	197
7. Conclusion	198
7.1 Future Work	200
Appendix A. Peridynamics Strain Energy Density Functions	202
A1. PD SED for Beam Theories	202
A2 PD SED for Plate Theories	218
Appendix B Boundary Conditions for PD Beam and Plate Theories	239
B1 Boundary Conditions for PD Beams	240
B2 Boundary Conditions for PD Plates	248
Appendix C Nomenclature	255
Appendix D List of Figures & Tables	256
Reference	261

1. Introduction

1.1 Background of Peridynamics

Classical continuum mechanics (CCM) developed by Cauchy has been widely used for the analysis of deformation behavior of materials and structures. Although CCM has been very successful in dealing with numerous complex problems of engineering, it encounters difficulties if the displacement field is discontinuous. This situation mainly arises when cracks occur inside the solution domain. In this case, the partial derivatives in the governing equations of CCM become invalid along the crack surfaces. Moreover, as the technology advances and nanoscale structures become a significant interest, accurate material characteristic at such a small scale cannot always be captured by CCM since CCM does not have a length scale parameter.

To overcome the aforementioned issues related with CCM, a new continuum mechanics formulation, peridynamics, was proposed by Silling (2000). The governing equations of peridynamics (PD) are in the form of integro-differential equations and do not contain any spatial derivatives. Therefore, they are always valid even if the displacement field is discontinuous. Moreover, it has a length scale parameter, horizon, which can be utilised to model structures at nano-scale. Besides, in PDs, the state of a material point is influenced by material points that are located at a finite distance within a domain of influence called horizon. This feature positions PDs within non-local continuum mechanics formulations. As highlighted by dell'Isola et al. (2016), the origins of PDs go back to Piola. Since its introduction, there has been rapid progress on PDs. The PD formulation has been applied to many different material systems, including linear elastic materials, metals and composite materials. The PD theory is not limited to macroscopic analysis, which allows researchers to use it for analyzing problems at the mesoscale and nano-scale. Moreover, it is currently possible to perform multi-physics analysis in a single PD framework by coupling mechanical field to thermal field, moisture diffusion, electric current, porous flow, etc. PD theory has also

been effectively used for impact analysis. An in-depth review of PD research is given by Madenci and Oterkus (2014) and Javili et al. (2019).

1.2 Classification of Beams and Plates

Beams and plates are structural elements whose transverse dimension (thickness) is much smaller than the characteristic dimension such that

$$h / L \ll 1 \quad (1.1)$$

where h is the thickness of the beam or plate, and L represents the span of the beam or minimum characteristic dimension of the plate, respectively.

Elastic beams and plates can be categorized based on the thickness into three different classes:

- (1) Slender beams / thin plates $\frac{h}{L} < \frac{1}{20}$
- (2) Moderate thick beams / plates $\frac{h}{L} \approx \frac{1}{10}$
- (3) Deep beams / thick plates $\frac{h}{L} > \frac{1}{10}$

A beam or plate is called slender or thin if the maximum value of the ratio is $\frac{h}{L} < \frac{1}{20}$. In this regard, it is admissible to have a negligible error for engineering requirement by omitting the transverse shear effect.

For a large number of practical applications, if the thickness – length ratio is beyond that range, neglecting transverse shear effect may violate the solution precision. And they are regarded as moderate thick beams / plates (if $\frac{h}{L} \approx \frac{1}{10}$) and deep beams / thick plates (if $\frac{h}{L} > \frac{1}{10}$) accordingly.

Moreover, beams can be also classified according to the geometries of the cross-section, such as rectangular beam, T-section beam, etc, as shown in Fig. 1.1.

The shape of cross section determines the properties (e.g. bending resistance, torsional strength). Thus, choosing appropriate model is one the most fundamental role of a designer by considering economy and constraint of functional requirements.

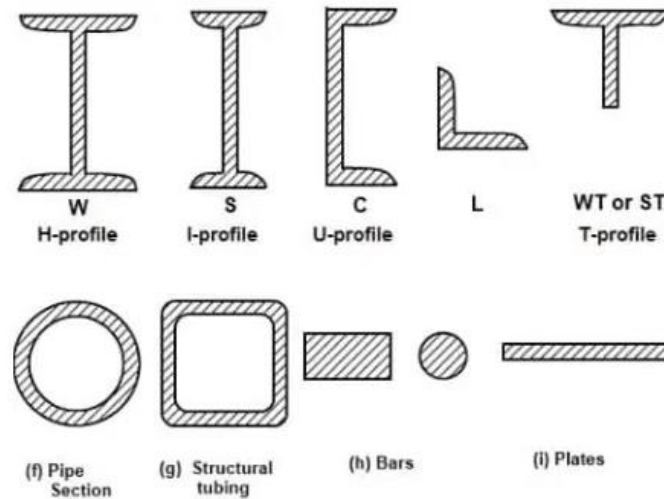


Figure 1.1 Beam cross sectional shapes (Hamakareem. M.I)

1.3 Objectives and Motivations

Beam and plate structures, as the major transverse loading carrying element, are widely used in mechanical, civil, aerospace and marine engineering applications. Indeed, beams and plates are obviously three-dimensional structure and can be analyzed in a straightforward manner by using three-dimensional governing equations of linear elasticity. However, the solution for three-dimensional problems is generally difficult and time-consuming for a computation. In order to simplify the solution of beams and plates, dimensional reduction that describes the deformation behavior by using the neutral axis and mid-plane for beams and plates, respectively, are utilised by researchers. Depending on the geometry and material properties, various theories of beam and plate theories arise. The classical beam and plate theories, i.e. Euler-Bernoulli Beam and Kirchhoff-Love Plate, neglect shear effects and are applicable to slender beams and thin plates. On the other hand, Timoshenko beam and Mindlin plate theories were developed by taking transverse shear deformation into consideration, which are applicable to

moderately thick structures. Regarding thicker beams and plates, several advanced theories arose in recent decades, which involve additional independent variables, and they are collectively known as higher order beam and plate theories.

Peridynamics, as a burgeoning theory in recent two decades, has significant capabilities in engineering applications. The main characteristic of peridynamics is that the governing equations are comprised of spatial integrations only rather than spatial partial derivatives. With the help of this advantage, discontinuous problems or singularities of the function due to cracks, fracture, corrosion etc. can be avoided. Although there has been ongoing research and development of peridynamics theory in solid mechanics, progress in development of peridynamic beam and plate structures is limited. The original formulation of peridynamics considers only translational degrees of freedom for material points and is capable of performing 3D analysis. However, this approach can be computationally expensive for certain geometries such as beam and plate structures. To model such structures, standard peridynamics mechanical model should be modified by taking into account bending moment for each peridynamics bond. Hence, 3-Dimensional geometries can be represented by 1-Dimensional models as beams or 2-Dimensional models as plates for simplicity. For this purpose, this thesis is aimed at developing peridynamics equations for the beam and plate models as mentioned above for researchers.

1.4 Novelty

Peridynamics is a new non-local continuum mechanics theory, which is very attractive for problems including discontinuities such as cracks and suitable for prediction and simulation of material crack propagation. Beam and plate structures, as the major transverse loading carrying element in industrial applications, bear the risk of material failure and crack propagation, which can cause catastrophic consequence. Thus, peridynamics would have ample scope for engineering safety precaution, due to its

advantage in material failure prediction. Although thin structures can be analyzed as a 3D model under traditional peridynamics formulations which were developed by Silling (2000), Silling et al. (2007) and Madenci and Oterkus (2014), the solutions for is generally difficult and computationally expensive. Hence, it is essential to develop particular simplified peridynamics formulations for such thin structures under beam and plate type idealizations. Current study of peridynamics has covered many physical areas but not much in beam and plate structures yet. Although, one of the most representative research outputs in this area, Diyaroglu et al. (2015), provided peridynamics formulations for Timoshenko beam and Mindlin plate, the limitation of Poisson's ratio of $1/3$ was assumed throughout their study. In this thesis, novel peridynamics formulations without limitation of Poisson's ratio are introduced and cover various types of beam and plate structures with isotropic and functionally graded material.

Bond based peridynamics (BBPD) and ordinary state based peridynamics (OSBPD), as two fundamental peridynamics theories, were developed by Silling (2000) and Silling et al. (2007), respectively. Although both theories were revisited and the derivation of peridynamics material parameters were re-explained by Madenci and Oterkus (2014), the concept of peridynamics state is still difficult to well understand for beginners. In this thesis, a novel derivation approach for peridynamics formulation based on utilization of Lagrange's equation and Taylor's series expansion rather than by equalizing the strain energy density between peridynamics and classical mechanics theory as in the previous study, are developed. The approach eliminates the limitation of the Poisson's ratio and unifies the BBPD and OSBPD together, which discards the need of introduction of peridynamics state concept. Moreover, this approach is well matched analytical mechanics point of view, which well clarifies the physical meaning of each peridynamics quantities and makes it facile for beginners.

In Addition to those above, this thesis provides a feasible approach to implement peridynamics beam and plate model in finite element framework. The principle of

coupling peridynamics with finite element analysis was originally introduced by Macek and Silling (2007). Diyaroglu (2016) extended the previous study and achieved the implementation of modelling peridynamics model within commercial finite element software, ANSYS, by using LINK or SPRING elements. Regarding peridynamics thin structures (1D and 2D models), modelling with LINK or SPRING elements are feasible to capture in-plane deformation, however, analyzing bending behaviors becomes incapable, due to the limitation of element degrees of freedom. In this thesis, a refined solution with utilizing BEAM element instead of LINK or SPRING is introduced in Chapter 6, which make it achievable to capture bending analysis for peridynamics beam and plate models in finite element software.

1.5 Outlines

Chapter 2 reviews the historical development of beam and plate theories. A list of several categories in the field of beam and plate theories is given and specifications are summarized.

Chapter 3 revisits the original PD formulations and re-derives them from analytical mechanics point of view.

Chapter 4 develops the PD formulations for beam structures comprising isotropic material and functionally graded material. The applicability and accuracy is validated from numerical results.

Chapter 5 is an extension of Chapter 4. Hierarchical classifications of plate models are presented and their corresponding PD equations of motion are derived. The governing equations are validated by numerical results.

Chapter 6 investigates the implementation of PD Timoshenko Beam and Mindlin Plate formulations in finite element framework. Deformation and buckling performances are

under consideration for demonstration. Moreover, crack propagation behaviors are also studied.

2. Literature Review

2.1 Introduction

As introduced in Chapter 1, PD theory, as a powerful tool for prediction of material failure, has been thrived by researcher during last years. The first milestone of PD development appeared in Silling (2000), which was the rudiment and often referred to as bond-based PD theory. Although this original version was neat, straightforward and simple to implement for beginners, the theory itself contained defect that the Poisson's ratio, ν , of material was restricted by value of 0.25, which limited the applicability in engineering. An improved version (ordinary stated based PD) thereafter published by Silling (2007), which eliminated the limitation of the Poisson ratio by introduction of concept of PD state. Another fundamental branch of PD theory that non-ordinary state based PD was released by Warren et al. (2009), and as a consequence, the theoretical framework of PD was basically established from then on. Madenci and Oterkus (2014) summarized former research achievements as a textbook which demonstrated PD engineering applications with varies of numerical examples. Moreover, simplified PD formulations for 1D rod and 2D plane stress problems were also represented within the textbook.

Based on the achievements mentioned above, there has been rapid development in PD research especially during the last years. According to dell'Isola et al. (2016), the origins of peridynamics go back to Piola. PD has been applied to analyse different material systems including metals (DeMeo et al., 2016), composites (Ozdemir et al., 2020), concrete (Oterkus et al., 2012), graphene (Liu al et., 2018), etc. Moreover, it is not limited to elasticity behaviour and PD based plasticity (Madenci and Oterkus, 2016), viscoelasticity (Madenci and Oterkus, 2017), and viscoplasticity (Amani al et., 2016)

formulations are available. In addition, PD equations has been extended to other fields to perform heat transfer (Gao and Oterkus, 2019), diffusion (Wang al et., 2018), porous flow (Oterkus al et., 2017), and fluid flow (Gao and Oterkus, 2019) analyses. An extensive review on peridynamics is given in Javili et al. (2019).

Simplified structures including beams, plates and shells can also be represented in PD framework. Taylor and Steigmann (2015) introduced a two-dimensional model for thin plates. In his study, the PD model was derived as a 2D approximation of the 3D bond-based theory of PD via an asymptotic analysis and fracture simulation of a brittle plate with a central crack under tensile loading was demonstrated. Diyaroglu et al. (2017) developed a PD isotropic Euler-beam. The effect of transverse shear deformation in thick plates was taken into account by Diyaroglu et al. (2015) by developing PD bond based Timoshenko and Mindlin plate formulations. O’Grady and Foster (2014) proposed Euler beam and Kirchhoff plate formulations by utilising non-ordinary state-based peridynamics. Chowdhury et al. (2016) developed a state-based PD formulation suitable for linear elastic shells.

The following sections of this Chapter review the development of beam and plate theories and functionally graded material according to the classical mechanics theory, and the corresponding theories based on PD framework are presented in Chapter 4 and 5, respectively.

2.2 Development of Beam theories

Beam, as one of the most popular elements in structural mechanics, is mostly designed to support transverse load and used in a wide range of structures such as bridges and buildings. Depending upon the geometries, uses and material properties, various beam theories have been developed since 1750s. The most important contributors were Euler and Bernoulli (1750s), who developed a suitable theory for slender beams, which is known as classical beam theory or Euler – Bernoulli beam theory. The next milestone

of beam theories was developed by Timoshenko in 1920s. On the basis of Euler-Bernoulli beam theory, Timoshenko provided a revised set of formulations with consideration of the effects of transverse shear deformations on the behavior of a beam, which enhanced the solution accuracy for analyzing moderately thick beams and is well known today as first order shear deformation theory or Timoshenko beam theory. Although the Timoshenko beam solutions are widely adopted in thick beam analysis, it contains limitations: the transverse normal must undergo no change in length during deformation, which means that both transverse normal strain, ε_z , and stress, σ_z , are omitted; the transverse normal must remain straight during deformation, which involves the need for the introduction of shear correction factor. In order to improve the applicability and accuracy, some advanced beam theories emerged thereafter. Soldatos and Elishakoff (1992) presented a theory with inclusion of both transverse shear deformation and transverse normal deformation. Another study reported by Heyliger and Reddy (1988) described a theory with higher order shear deformation, which eliminated the restriction that transverse normal must remain straight during deformation. Later, in addition to these, some refined displacement models of beams were developed by investigators such as Kant, Marurb and Rae (1998). In this section, we will briefly recapture the development of some representative beam theories.

2.2.1 Classical Beam theory

The first complete and adequate set of equation for linear theory of thin beams was developed by Euler and Bernoulli, which is also known as Euler – Bernoulli beam theory, thin beam theory or classical beam theory. According to Euler-Bernoulli beam theory, hypotheses made can be summarized as (Bauchau and Craig, 2009)

1. Small deformation is assumed.
2. Transverse normal remains straight during deformation.
3. Transverse normal stress, σ_z , is considered small compared to axial stress.
(This simplifies the 2D plane-stress Hooke's Law and make it a 1D material constitutive law.)

4. Transverse normal remains perpendicular to the neutral axis, or in other words, the transverse shear stress, τ_{xz} , is zero.
5. Transverse normal length remains unchanged, or in other words, the transverse normal stress, ε_z , is zero.

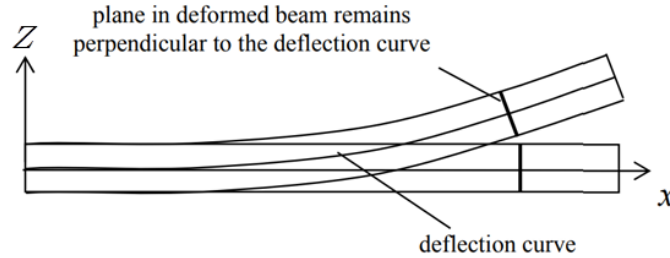


Figure 2.1 Deformation of Euler-Bernoulli Beam

(<http://www.parash.xyz/2019/02/26/structural-engineering>)

In view of the above, the displacement field in the Euler – Bernoulli beam can be written as

$$u(x, z, t) = z\theta(x, t) \quad (2.1a)$$

$$w(x, z, t) = \bar{w}(x, t) \quad (2.1b)$$

in which x and z represent the axial and transverse coordinate, respectively, and the "overbar" notation denotes the displacement of the neutral axis ($z = 0$) and θ represents the rotation of the material point located on neutral axis. Thus, strain – displacement relation can be expressed as

$$\gamma = \theta + \frac{\partial \bar{w}}{\partial x} = 0 \quad (2.2a)$$

$$\varepsilon = z \frac{\partial \theta}{\partial x} = -z \frac{\partial^2 \bar{w}}{\partial x^2} \quad (2.2b)$$

in which γ and ε represent the shear and normal strain, respectively. Note that, with the help of the hypothesizes mentioned above, the final governing equation of Euler – Bernoulli beam can be derived into a compact form and is widely used because of its simplicity. On the other hand, these hypothesizes restrict the deformation in terms of shearing and thickness change and lead that the beam is stiffer, therefore the deflection solution of Euler – Bernoulli beam is slightly smaller than reality. This issue can be neglected for slender beams but significant when the beams are thick. In order to

eliminate this effect, some improved beam theories emerged in the 20th century.

2.2.2 First Order Shear Deformation Beam Theory

First order shear deformation beam theory, sometimes referred as Timoshenko beam theory, was first introduced by Timoshenko early in the 20th century. Substantially better results for the thicker beams can be obtained by taking into account shear deformation and rotational bending effects. Timoshenko eliminated the assumption 4 which is given above, and this yields the strain components and linear strain energy density as (Timoshenko, 1983)

$$\varepsilon = z \frac{\partial \theta}{\partial x} \quad (2.3a)$$

$$\gamma = \theta + \frac{\partial \bar{w}}{\partial x} \quad (2.3b)$$

and

$$W = \frac{1}{2} \left[EI \left(\frac{\partial \theta}{\partial x} \right)^2 + \kappa GA \left(\theta + \frac{\partial \bar{w}}{\partial x} \right)^2 \right] \quad (2.4)$$

where κ is introduced as the shear correction factor, which depends upon the geometry of the cross-section, and EI , G and A represent the bending rigidity, shear modulus and cross section area, respectively. The equilibrium equations of Timoshenko beam can be derived by using minimum potential energy principle, which can be expressed in terms of displacements only as

$$\kappa GA \left(\frac{\partial^2 \bar{w}}{\partial x^2} - \frac{\partial \theta}{\partial x} \right) + p = 0 \quad (2.5a)$$

$$EI \frac{\partial^2 \theta}{\partial x^2} + \kappa GA \left(\frac{\partial \bar{w}}{\partial x} - \theta \right) = 0 \quad (2.5b)$$

2.2.3 Advanced Beam Theories

Beam theories are only approximate theories, with number of simplifications are made for the sake of reducing the dimension of the model.

In order to reduce the assumptions and enhance the applicability and solution accuracy for deeper beams as far as possible, varieties of new beam theories emerged thereafter.

In this section, three representative techniques are introduced.

2.2.3.1 Model 1 (Transverse shear and normal deformable beam)

In this theory, assumptions 3, 4 and 5 given in section 2.1.1 are eliminated. To achieve inclusion of transverse shear and normal strains, an additional independent displacement variable, w^* , is introduced and the displacement field of the beam can be written as (Soldatos and Elishakoff, 1992)

$$u(x, z, t) = z\theta(x, t) \quad (2.6a)$$

$$w(x, z, t) = \bar{w}(x, t) + z^2\dot{w}(x, t) \quad (2.6b)$$

This stipulation leads the strain-displacement relations as following:

$$\varepsilon_x = z \frac{\partial \theta}{\partial x} \quad (2.7a)$$

$$\varepsilon_z = 2z\dot{w} \quad (2.7b)$$

$$\gamma_{xz} = \theta + \frac{\partial \bar{w}}{\partial x} + z^2 \frac{\partial \dot{w}}{\partial x} \quad (2.7c)$$

Unlike the corresponding relations of the Timoshenko beam theory, where the transverse strain is zero, complete planar strain components are given in this theory. This implies that beams comply the 2D plane – stress material constitutive law rather than 1D Hooke's Law which is used in Timoshenko and Euler – Bernoulli beam theories.

2.2.3.2 Model 2 (Higher order shear deformable beam)

In this theory, assumptions 2 and 4 given in section 2.1.1 are eliminated by stipulation of the following displacement assumption (Kant and Gupta, 1988)

$$u(x, z, t) = z\theta(x, t) + z^3\theta'(x, t) \quad (2.8a)$$

$$w(x, z, t) = \bar{w}(x, t) \quad (2.8b)$$

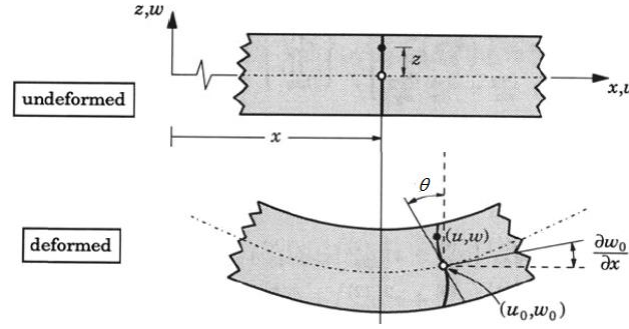


Figure 2.2 Deformation of higher order beam (Komeili et al., 2011)

where θ^* is introduced as a new independent generalized displacement. Strain components in this displacement field assumption can be expressed as

$$\varepsilon_x = z \frac{\partial \theta}{\partial x} + z^3 \frac{\partial \theta^*}{\partial x} \quad (2.9a)$$

$$\gamma_{xz} = \theta + \frac{\partial \bar{w}}{\partial x} + 3z^2 \theta^* \quad (2.9b)$$

Note that the planar strain components are incomplete (transverse normal strain, ε_z , is absent), and this implies the deformation behavior of the beam can be only abided by 1D Hooke's Law in this theoretical framework.

2.2.3.3 Model 3 (Refined Higher Order Deformable Beam)

In this theory, assumptions 2, 3, 4, 5 given in Section 2.1.1 can be eliminated by stipulating the displacement field as (Kant and Gupta, 1988)

$$u(x, z, t) = z\theta(x, t) + z^3\theta^*(x, t) \quad (2.10a)$$

$$w(x, z, t) = \bar{w}(x, t) + z^2\bar{w}^*(x, t) \quad (2.10b)$$

Hence, the strain components are given by

$$\varepsilon_x = z \frac{\partial \theta}{\partial x} + z^3 \frac{\partial \theta^*}{\partial x} \quad (2.11a)$$

$$\varepsilon_z = 2z\bar{w}^* \quad (2.11b)$$

$$\gamma_{xz} = \theta + \frac{\partial \bar{w}}{\partial x} + z^2 \left(3\theta^* + \frac{\partial \bar{w}^*}{\partial x} \right) \quad (2.11c)$$

In comparison with the corresponding relation given by Model 1, the shear strain component varies parabolically with the thickness, which is more realistic. Moreover, unlike the strain components given by Model 2, planar strain components are complete in this theory, which implies 2D plane – stress material constitutive law can be applied

for the stress analysis.

2.3 Development of Plate Theories

As an extension of beam theory, varieties of plate theories have been investigated since 18th century. One of the first plate theories developed for thin plate was presented by Love and Kirchhoff (1888), which is known as thin plate theory or Kirchhoff – Love plate theory. Similarly with the Euler – Bernoulli beam’s assumption, transverse shear effect is ignored. Due to this limitation, Kirchhoff – Love plate formulation is usually used only in thin plate analysis and not tenable for moderate thick plates. Later around 1940s, an improved plate theory developed for moderately thick plates was investigated by Reissner (1945) and Mindlin (1951), which is known as Mindlin – Reissner plate theory today. This theory takes shear deformation into account by involving rotations as the additional independent displacements, which extends the applicability of the plate formulation. Similar to Timoshenko beam theory, although Mindlin – Reissner plate theory obviates the most problems that beset thick plate analyses based on Kirchhoff – Love theory, it still has limitations: the transverse normal must undergo no change in length during deformation, which means that both transverse normal strain, ϵ_z , and stress, σ_z , are omitted; the transverse normal must remain straight during deformation, which involves the need for the introduction of shear correction factor. In order to overcome the limitations due to the assumptions made for formulation simplicity, some novel plate theories were developed with inclusion of additional generalized displacement variables in last 50 years, such as discussed by Lo and Wu (1977), Reddy (1984), Kant (1980) and in numerous subsequent publications. In this section, we will briefly recapture the development of some representative plate theories.

2.3.1 Kirchhoff – Love Plate Theory

Similar to Euler – Bernoulli beam, as the most elemental plate theory, Kirchhoff – Love plate theory proposed the following assumptions for simplifying the model:

1. Small deformation is assumed.

2. Transverse normal remains straight during deformation.
3. Transverse normal stress, σ_z , is considered small compared to other in-plane stress components, σ_x , σ_y and τ_{xy} . (This simplifies the 3D Hooke's Law and makes it a 2D plane – stress material constitutive law.)
4. Transverse normal remains perpendicular to the mid-plane, or in other words, the transverse shear stresses, τ_{xz} and τ_{yz} , are zero.
5. Transverse normal length remains unchanged, or in other words, the transverse normal stress, ε_z , is zero.

Therefore, the displacement field and strain – displacement relations can be written accordingly as following

$$u(x, y, z, t) = z\theta_x(x, y, t) \quad (2.12a)$$

$$v(x, y, z, t) = z\theta_y(x, y, t) \quad (2.12b)$$

$$w(x, y, z, t) = \bar{w}(x, y, t) \quad (2.12c)$$

and

$$\gamma_{xz} = \theta_x + \frac{\partial \bar{w}}{\partial x} = 0 \quad (2.13a)$$

$$\gamma_{yz} = \theta_y + \frac{\partial \bar{w}}{\partial y} = 0 \quad (2.13b)$$

$$\varepsilon_x = z \frac{\partial \theta_x}{\partial x} = -z \frac{\partial^2 \bar{w}}{\partial x^2} \quad (2.13c)$$

$$\varepsilon_y = z \frac{\partial \theta_y}{\partial y} = -z \frac{\partial^2 \bar{w}}{\partial y^2} \quad (2.13d)$$

$$\gamma_{xy} = z \left(\frac{\partial \theta_x}{\partial y} + \frac{\partial \theta_y}{\partial x} \right) = -2z \frac{\partial^2 \bar{w}}{\partial x \partial y} \quad (2.13e)$$

2.3.2 Mindlin – Reissner Plate Theory

As mentioned above, an improved plate theory was represented by Mindlin and Reissner with consideration of transverse shear effects during the deformation (assumption 4 given in section 2.2.1 is eliminated). The displacements field has no distinction with that of given in Kirchhoff – Love plate theory, and strain components can be written as following

$$\varepsilon_x = z \frac{\partial \theta_x}{\partial x} \quad (2.14a)$$

$$\varepsilon_y = z \frac{\partial \theta_y}{\partial y} \quad (2.14b)$$

$$\gamma_{xy} = z \left(\frac{\partial \theta_x}{\partial y} + \frac{\partial \theta_y}{\partial x} \right) \quad (2.14c)$$

$$\gamma_{xz} = \theta_x + \frac{\partial \bar{w}}{\partial x} \quad (2.14d)$$

$$\gamma_{yz} = \theta_y + \frac{\partial \bar{w}}{\partial y} \quad (2.14e)$$

It can be seen that θ_x and θ_y are introduced as two additional independent displacement variables due to the elimination of assumption 4 given in the section 2.2.1. This increases the degree of complexity and enhanced the solution accuracy especially for thick plates meanwhile.

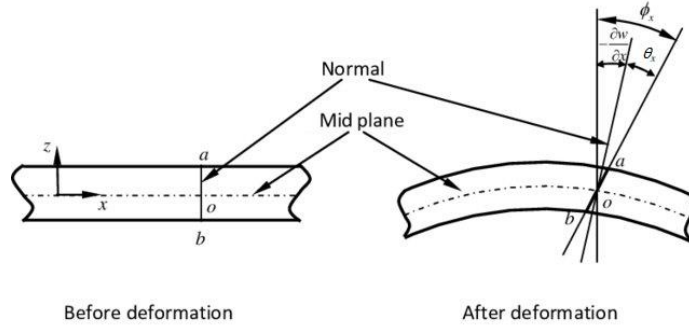


Figure 2.3 Deformation of Mindlin Plate (Chen and Kumar, 2013)

2.3.3 Advanced Plate Theories

2.3.3.1 Model 1 Transverse Shear and Normal Deformable Plate

This theory eliminates the assumptions 3, 4 and 5 given in section 2.3.1 by assuming such displacement field

$$u(x, y, z, t) = z\theta_x(x, y, t) \quad (2.15a)$$

$$v(x, y, z, t) = z\theta_y(x, y, t) \quad (2.15b)$$

$$w(x, y, z, t) = \bar{w}(x, y, t) + z^2\bar{w}'(x, y, t) \quad (2.15c)$$

Hence the strain-displacement relation can be written as

$$\varepsilon_x = z \frac{\partial \theta_x}{\partial y} \quad (2.16a)$$

$$\varepsilon_y = z \frac{\partial \theta_y}{\partial x} \quad (2.16b)$$

$$\varepsilon_z = 2z\bar{w}' \quad (2.16c)$$

$$\gamma_{xy} = z \left(\frac{\partial \theta_x}{\partial y} + \frac{\partial \theta_y}{\partial x} \right) \quad (2.16d)$$

$$\gamma_{xz} = \theta_x + \frac{\partial W_0}{\partial x} + z^2 \frac{\partial \dot{W}}{\partial x} \quad (2.16e)$$

$$\gamma_{yz} = \theta_y + \frac{\partial W_0}{\partial y} + z^2 \frac{\partial \dot{W}}{\partial y} \quad (2.16f)$$

It can be seen that strain components are completely defined in this theory, and hence, the deformation performance will comply 3D Hooke's Law.

2.3.3.2 Model 2 Higher Order Transverse Shear Deformable Plate

This theory eliminates the assumptions 2 and 4 given in section 2.3.1 by stipulating such displacement field

$$u(x, y, z, t) = z\theta_x(x, y, t) + z^3\theta'_x(x, y, t) \quad (2.17a)$$

$$v(x, y, z, t) = z\theta_y(x, y, t) + z^3\theta'_y(x, y, t) \quad (2.17b)$$

$$w(x, y, z, t) = \bar{w}(x, y, t) \quad (2.17c)$$

Therefore the strain-displacement relation can be expressed accordingly as

$$\begin{aligned} \varepsilon_x &= z \frac{\partial \theta_x}{\partial x} + z^3 \frac{\partial \theta'_x}{\partial x} \\ \varepsilon_y &= z \frac{\partial \theta_y}{\partial y} + z^3 \frac{\partial \theta'_y}{\partial y} \\ \varepsilon_z &= 0 \\ \gamma_{xy} &= z \left(\frac{\partial \theta_x}{\partial y} + \frac{\partial \theta_y}{\partial x} \right) + z^3 \left(\frac{\partial \theta'_x}{\partial y} + \frac{\partial \theta'_y}{\partial x} \right) \\ \gamma_{xz} &= \theta_x + \frac{\partial \bar{W}}{\partial x} + 3z^2\theta'_x \\ \gamma_{yz} &= \theta_y + \frac{\partial \bar{W}}{\partial y} + 3z^2\theta'_y \end{aligned} \quad (2.18a - f)$$

The absence of transverse normal strain and omittance of transverse normal stress yield the deformation behaviors which will follow a partial Hooke's Law (in accordance to Mindlin plate theory).

2.3.3.3 Model 3 Refined Higher Order Deformable Plate

This theory eliminates the assumptions 2, 3, 4 and 5 given in section 2.3.1 by assuming such displacements field (Lo al et., 1977)

$$u(x, y, z, t) = z\theta_x(x, y, t) + z^3\theta'_x(x, y, t) \quad (2.19a)$$

$$v(x, y, z, t) = z\theta_y(x, y, t) + z^3\theta_y^*(x, y, t) \quad (2.19b)$$

$$w(x, y, z, t) = \bar{w}(x, y, t) + z^2\bar{w}^*(x, y, t) \quad (2.19c)$$

Stipulation of the displacement field gives the strain components as

$$\varepsilon_x = z \frac{\partial \theta_x}{\partial x} + z^3 \frac{\partial \theta_x^*}{\partial x} \quad (2.20a)$$

$$\varepsilon_y = z \frac{\partial \theta_y}{\partial y} + z^3 \frac{\partial \theta_y^*}{\partial y} \quad (2.20b)$$

$$\varepsilon_z = 2z\bar{w}^*(x, y, t) \quad (2.20c)$$

$$\gamma_{xy} = z \left(\frac{\partial \theta_x}{\partial y} + \frac{\partial \theta_y}{\partial x} \right) + z^3 \left(\frac{\partial \theta_x^*}{\partial y} + \frac{\partial \theta_y^*}{\partial x} \right) \quad (2.20d)$$

$$\gamma_{xz} = \theta_x + \frac{\partial \bar{w}}{\partial x} + z^2 \left(3\theta_x^* + \frac{\partial \bar{w}^*}{\partial x} \right) \quad (2.20e)$$

$$\gamma_{yz} = \theta_y + \frac{\partial \bar{w}}{\partial y} + z^2 \left(3\theta_y^* + \frac{\partial \bar{w}^*}{\partial y} \right) \quad (2.20f)$$

It can be seen that strain components are fully defined in this theory, which yields that 3D Hooke's Law can be applied to describe the constitutive relation. Moreover, the need for introduction of shear correction factor is eliminated.

2.4 Development of Functionally Graded Material (FGM)

With the development of advanced manufacturing technologies, the importance of functionally graded materials (FGM) is increasing due to their advantages over widely used traditional composites. According to functionally graded material concept, the material properties are continuously varying based on a certain distribution. Therefore, functionally graded materials do not suffer from stress concentrations in the thickness direction due to the laminated structure used for fiber reinforced composites, and failure due to delamination can be avoided. Functionally graded materials are usually made of a mixture of ceramic and metal to resist ultra-high-temperature environments and eliminate interface problems. Moreover, they are used in various engineering fields including aerospace, defence, electronics and biomedical industries to remove stress concentrations, reduce residual stresses and increase bond strength (Simsek, 2010). Significant amount of research studies are available in the literature focusing on the

analysis of functionally graded materials including beam and plate formulations.

2.4.1 Development of Functionally Graded Beam

Due to the increase in usage of FGMs, numerous beam formulations for FGMs are available in the literature. Amongst these, Li (2008) developed a unified approach to analyze the static and dynamic behaviours of functionally graded beams by including rotary inertia and shear deformation. Kadoli et al. (2008) performed static analysis of functionally graded beams using higher order shear deformation theory. Kahrobaiyan et al. (2012) proposed a size-dependent functionally graded Euler-Bernoulli beam model based on strain gradient theory. Thai and Vo (2012) performed bending and free vibration analysis of functionally graded beams using various higher-order shear deformation beam theories. Lu et al. (2008) presented elasticity solutions for bending and thermal deformations of functionally graded beams with various end conditions using the state space-based differential quadrature method. Su et al. (2013) developed the dynamic stiffness method to investigate the free vibration behaviour of functionally graded beams. Simsek et al. (2012) performed linear dynamic analysis of an axially functionally graded beam with simply supported edges and subjected to a moving harmonic load based on Euler-Bernoulli beam theory. Li and Batra (2013) investigated relationships between buckling loads of functionally graded Timoshenko and homogenous Euler-Bernoulli beams. Sankar (2001) presented an elasticity solution for a functionally graded Euler-Bernoulli beam subjected to transverse loads. Birsan et al. (2012) performed deformation analysis of functionally graded beams by using direct approach which is based on the deformable curve model with a triad of rotating directors attached to each point. Nguyen et al. (2013) investigated static and free vibration behaviour of axially loaded functionally graded beams based on the first-order shear deformation theory. Filippi et al. (2015) used 1D Carrera Unified Formulation (CUF) to perform static analysis of functionally graded beams. Ebrahimi and Zia (2015) studied the functionally graded porous Timoshenko beams. Calim (2016) performed dynamic analysis of functionally graded Timoshenko beams with variable cross-section.

Ashgari et al. (2011) presented a size-dependent functionally graded Timoshenko beam formulation based on modified couple stress theory. Simsek (2010) investigated the dynamic behaviour of functionally graded Timoshenko beams subjected to a moving harmonic load. In another study, Tajalli et al. (2013) derived a size-dependent formulation for functionally graded Timoshenko beams using strain gradient theory. Ebrahimi and Barati (2016) investigated the free vibration behaviour of functionally graded nanobeams utilizing third-order shear deformation beam theory. Simsek and Reddy (2013) analysed functionally graded microbeams using modified couple stress theory and different higher order beam theories. Sun et. al. (2016) investigated buckling and post-buckling deformations of a functionally graded Timoshenko beam resting on an elastic foundation subjected to temperature rise using the shooting method. Pydah and Batra (2017) developed a shear deformation theory for thick circular beams which was used to analytically solve static deformations of bi-directional functionally graded circular beams. In another study, Fariborz and Batra (2019) performed free vibration analysis of functionally graded circular beams using a shear deformation theory by incorporating through-the-thickness logarithmic variation of the circumferential displacement and has a parabolic through-the-thickness distribution of shear strain. More recently, Menasria et al. (2020) presented dynamic analysis of functionally graded sandwich plates rested on elastic foundation using refined shear deformation theory. Zine et al. (2020) investigated the bending response of functionally graded plates utilizing cubic shear deformation theory. Rabhi et al. (2020) examined the buckling and vibration responses of exponentially graded sandwich plates resting on elastic medium using trigonometric shear deformation theory. Matouk et al. (2020) analyzed the free vibrational behaviour of functionally graded nano-beams resting on elastic foundation exposed to hygro-thermal environment utilizing Timoshenko beam theory. Chikr et al. (2020) and Refrafi et al. (2020) performed buckling analysis of functionally graded sandwich plates based on a refined trigonometric shear deformation theory. Rahmani et al. (2020) investigated the effect of boundary conditions on the bending and free vibration behaviour of functionally graded sandwich plates resting on elastic foundation using higher order shear deformation theory. Kaddari et al. (2020) studied static and

free vibration behavior of functionally graded porous plates resting on elastic foundation utilizing quasi-3D hyperbolic shear deformation theory. Tounsi et al. (2020) developed a four-variable trigonometric integral shear deformation model for the hygro-thermo-mechanical analysis of functionally graded ceramic-metal plates resting on an elastic foundation. Boussoula et al. (2020) performed thermomechanical analysis of functionally graded sandwich plates by employing n th-order shear deformation theory.

2.4.3 Development of Functionally Graded Plate

There are currently numerous studies in the literature focusing on plate formulations of functionally graded materials. Amongst these Vel and Batra (2004) provided three-dimensional exact solution for the vibration of functionally graded rectangular plates. Shen (2002) obtained nonlinear bending response of functionally graded plates subjected to transverse loading by using Reddy's higher order shear deformation plate theory. Zenkour (2006) presented generalised shear deformation theory for bending analysis of functionally graded plates. Bian et al. (2005) derived analytical solutions for functionally graded plates under cylindrical bending using first - and third-order shear deformation theories. Carrera et al. (2011) investigated the effect of thickness stretching in functionally graded plates by using Carrera's Unified Formulation. Ferreira et. al. (2005) used meshless method and third-order shear deformation theory to analyse functionally graded plates. Kashtalyan (2004) utilized Plevako general solution of the equilibrium equations for inhomogeneous isotropic media to obtain three-dimensional elasticity solution for functionally graded simply supported plates. Xiang and Kang (2013) performed bending analysis of functionally graded plates by using n th-order shear deformation theory and meshless global collocation method based on the thin plate spline radial basis function. Qian and Batra (2004) performed thermoelastic analysis of a thick functionally graded plate by using higher order shear and normal deformable plate theory and a meshless Petrov-Galerkin method. Ferreira et al. (2005) utilised the collocation multiquadric radial basis functions and meshless method to

determine the static deformations of a simply supported functionally graded plate based on a third-order shear deformation theory. Cheng and Batra (2000) examined a functionally graded plate by considering first-order and third-order shear deformation theories. Batra (2007) used principle of virtual work and higher-order shear and normal deformable theory to examine functionally graded incompressible linear elastic plates. Belabed et al. (2014) developed a new higher order shear and normal deformation theory for functionally graded plates by considering hyperbolic variation of all displacements along the thickness direction and without using shear correction factor. Zhang et al. (2020) introduced a semi-analytical approach to analyse in-plane functionally graded plates using scaled boundary finite element method.

2.5 Conclusion

In this section, the historical overview of classical beam and plate theories are recaptured and some improved novel techniques are outlined, as well as their advantages and limitations. Thereafter, the development of functionally graded material beam and plate theories is introduced. Basically, beam and plate theories are only approximate theories. The core conception is to reduce the dimension of the problem that describe the deformation of the body by using only the material points at neutral axis or mid-plane, with variety of assumptions made, for the sake of simplification and computational time reduction. The more advanced theories result in more accurate solution, but degree of complexity will therewith increase. In the practical applications, choosing a suitable theory of beam or plate should be based on the actual problem circumstances and engineering accuracy requirements. The characteristics of each beam and plate theory mentioned above can be summarized in the tables 2.1 and 2.2.

Table 2.1. Summary of beam theories

Beams	Transverse Shear	Transverse Normal	Degree of Freedom	Constitutive Law	Applications
Euler - Bernoulli	No	No	1 (w)	1D	Slender Beams
Timoshenko	1 st Order	No	2 (w, θ)	1D	Moderate Thick Beams
Model 1	1 st Order	1 st Order	3 (w, θ, w^*)	2D Plane-Stress	Thick Beams
Model 2	3 rd Order	No	3 (w, θ, θ^*)	1D	Thick Beams
Model 3	3 rd Order	1 st Order	4 (w, θ, w^*, θ^*)	2D Plane-Stress	Thick beams

Table 2.2. Summary of plate theories

Plates	Transverse Shear	Transverse Normal	Degree of Freedom	Constitutive Law	Applications
Kirchhoff-Love	No	No	1 (w)	2D Plane Stress	Thin Plates
Mindlin-Reissner	1 st Order	No	3 (w, θ_x, θ_y)	Partial Hooke's Law	Moderate Thick Plates
Model 1	1 st Order	1 st Order	4 ($w, \theta_x, \theta_y, w^*$)	3D Hooke's Law	Thick Plates
Model 2	3 rd Order	No	5 ($w, \theta_x, \theta_y, \theta_x^*, \theta_y^*$)	Partial Hooke's Law	Thick Plates
Model 3	3 rd Order	1 st Order	6 ($w, \theta_x, \theta_y, \theta_x^*, \theta_y^*, w^*$)	3D Hooke's Law	Thick Plates

3. Peridynamic Theory

3.1 Introduction

Unlike the local continuum theory, in PD theory, each state of a material point is not only influenced by the material points located in its immediate vicinity but also influenced by material points that are located within a region of finite radius named as the “horizon,” H . Therefore, the general PD equations of motion can be expressed as

$$\rho(\mathbf{x}, t) \ddot{\mathbf{u}}(\mathbf{x}, t) = \int_H \mathbf{f}(\mathbf{x}, \mathbf{x}', \mathbf{u}, \mathbf{u}', t) dV' + \mathbf{b}(\mathbf{x}, t) \quad (3.1a)$$

or in discrete form for the material point k as

$$\rho_{(k)} \ddot{\mathbf{u}}_{(k)} = \sum_j^{N_{(k)}} \mathbf{f}_{(k)(j)} V_{(j)} + \mathbf{b}_{(k)} \quad (3.1b)$$

where $N_{(k)}$ denotes the total number of family members of material point k , and the summation takes over the family member material points of k and ρ , u , V and b represent the density, displacement, material point volume and the body load density vector, respectively. The interaction force vector, $\mathbf{f}_{(k)(j)}$, between material points k and j has a unit of “force per unit volume squared,” defined as

$$\mathbf{f}_{(k)(j)} = \mathbf{t}_{(k)(j)} - \mathbf{t}_{(j)(k)} \quad (3.2)$$

As shown in Fig. 3.1, the PD force density vector $\mathbf{t}_{(k)(j)}$ represents the force acting on the main material point k by its family member material point j , and, in contrast, $\mathbf{t}_{(j)(k)}$ represents the force acting on material point j by its family member material point k .

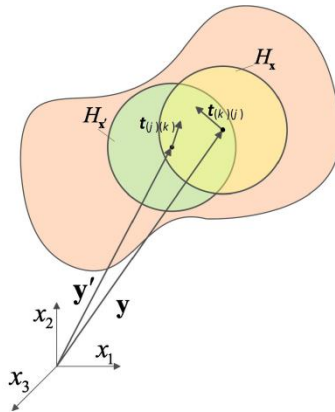


Figure 3.1 Interaction between material points

3.2 Bond Based & State Based Peridynamics

PD equations for small deformation analysis can be derived from Lagrange's equation. If we assume the system is initially at rest, then the generalized coordinates can be expressed in terms of the displacements, which give the Lagrange's equation as

$$\frac{d}{dt} \frac{\partial L}{\partial \dot{\mathbf{u}}_{(k)}} - \frac{\partial L}{\partial \mathbf{u}_{(k)}} = 0 \quad (3.3)$$

where $L = T - U$ is the Lagrangian and the $\mathbf{u}_{(k)}$ and $\dot{\mathbf{u}}_{(k)}$ represent the displacement vector and velocity vector of material point k , respectively. The total kinetic energy, T , of the system can be written in discretized form as

$$T = \frac{1}{2} \sum_{n=1}^N \rho_{(n)} \dot{\mathbf{u}}_{(n)} \cdot \dot{\mathbf{u}}_{(n)} V_{(n)} \quad (3.4)$$

where N represents the total material point number of the system, and ρ and V represent the material density and material point volume, respectively.

Since PD is a non-local theory, its strain energy density function has a non-local form such that the strain energy density of a certain material point k depends on both its displacement and all other material points in its family, which can be expressed as

$$W_{\text{D}}^{(k)} = W_{\text{D}}^{(k)}(\mathbf{u}_{(k)}, \mathbf{u}_{(1^k)}, \mathbf{u}_{(2^k)}, \mathbf{u}_{(3^k)}, \dots) \quad (3.5)$$

where $\mathbf{u}_{(i^k)}$ ($i = 1, 2, 3 \dots$) is the displacement vector of the i th material point within the horizon of the material point k .

Similar to Eq.(3.4), assume the system is conservative, the total potential energy stored in the body can be obtained by summing the potential energies of all material points including strain energy and energy due to external loads as

$$U = \sum_k W_{\text{D}}^{(k)}(\mathbf{u}_{(k)}, \mathbf{u}_{(1^k)}, \mathbf{u}_{(2^k)}, \mathbf{u}_{(3^k)}, \dots) V_{(k)} - \sum_k \mathbf{b}_{(k)} \mathbf{u}_{(k)} V_{(k)} \quad (3.6)$$

where \mathbf{b} is the body force density vector.

Since the potential energy is implicit of time variable, then the first term of the Lagrange's equation can be obtained by plugging Eq.(3.4) into (3.3) as

$$\frac{d}{dt} \frac{\partial L}{\partial \dot{\mathbf{u}}_{(k)}} = \frac{d}{dt} \frac{\partial T}{\partial \dot{\mathbf{u}}_{(k)}} = \rho_{(k)} \ddot{\mathbf{u}}_{(k)} V_{(k)} \quad (3.7)$$

Similarly, the second term of the Lagrange's equation becomes

$$\begin{aligned} -\frac{\partial L}{\partial \mathbf{u}_{(k)}} &= \frac{\partial}{\partial \mathbf{u}_{(k)}} \sum_n W_{(n)}^{PD}(\mathbf{u}_{(n)}, \mathbf{u}_{(1^n)}, \mathbf{u}_{(2^n)}, \mathbf{u}_{(3^n)}, \dots) V_{(n)} - \frac{\partial}{\partial \mathbf{u}_{(k)}} \sum_n \mathbf{b}_{(n)} \mathbf{u}_{(n)} V_{(n)} \\ &= \sum_n \frac{\partial W_{(n)}^{PD}}{\partial \mathbf{u}_{(k)}} (\delta_{nk} + \delta_{n^k}) V_{(n)} - \sum_n \mathbf{b}_{(n)} \delta_{nk} V_{(n)} \\ &= \left(\frac{\partial W_{(k)}^{PD}}{\partial \mathbf{u}_{(k)}} V_{(k)} + \sum_i \frac{\partial W_{(i^k)}^{PD}}{\partial \mathbf{u}_{(k)}} V_{(i^k)} \right) - \mathbf{b}_{(k)} V_{(k)} \end{aligned} \quad (3.8)$$

Inserting Eqs.(3.7) and (3.8) into Eq.(3.3) and renaming the summation index results in the general form PD equation of motion for small deformation analysis as

$$\rho_{(k)} \ddot{\mathbf{u}}_{(k)} = - \left(\frac{\partial W_{(k)}^{PD}}{\partial \mathbf{u}_{(k)}} + \sum_j \frac{\partial W_{(j)}^{PD}}{\partial \mathbf{u}_{(k)}} \frac{V_{(j)}}{V_{(k)}} \right) + \mathbf{b}_{(k)} \quad (3.9)$$

Eq. (3.9) can also be named as the fundamental Lagrange's equation in PD framework.

3.2.1 PD Formulation for 1D Bar Structure

Assume the neutral axis is aligned with the x -coordinate, the strain and stress of the bar structure can be expressed in terms of displacement, u , only as

$$\varepsilon = \frac{\partial u}{\partial x} \quad (3.10a)$$

$$\sigma = E \frac{\partial u}{\partial x} \quad (3.10b)$$

where E represents the Young's modulus of the body.

For an isotropic bar, the elastic strain energy density in the classical continuum mechanics can be casted as

$$W_{cm} = \frac{1}{2} \sigma \varepsilon = \frac{E}{2} \left(\frac{\partial u}{\partial x} \right)^2 \quad (3.11)$$

In order to write the non-local form of strain energy function of the material point k , Eq. (3.11), it is necessary to transform all the local terms into an equivalent PD form by also considering PD strain energy expression given in Eq. (3.5). This can be achieved by utilizing Taylor series expansion.

The axial displacement function, $u(x, t)$, can be Taylor series expanded up to 1st order

terms about point x :

$$u(x + \xi) - u(x) = \frac{\partial u(x)}{\partial x} \xi \quad (3.12)$$

Squaring both sides of Eq.(3.12) and dividing each terms by $|\xi|$ results in

$$\frac{[u(x + \xi) - u(x)]^2}{|\xi|} = \left(\frac{\partial u(x)}{\partial x} \right)^2 |\xi| \quad (3.13)$$

Considering x as a fixed point, integrating both sides of Equation (3.13) over a symmetric domain with centre of x yields

$$\int_{-\delta}^{\delta} \frac{[u(x + \xi) - u(x)]^2}{|\xi|} d\xi = \left(\frac{\partial u(x)}{\partial x} \right)^2 \int_{-\delta}^{\delta} |\xi| d\xi \quad (3.14)$$

which gives

$$\left(\frac{\partial u(x)}{\partial x} \right)^2 = \frac{1}{\delta^2} \int_{-\delta}^{\delta} \frac{[u(x + \xi) - u(x)]^2}{|\xi|} d\xi \quad (3.15a)$$

which can be written in the discretized form as

$$\left(\frac{\partial u_{(k)}}{\partial x} \right)^2 = g_{(k)} \frac{1}{\delta^2 A} \sum_i \frac{[u_{(i^k)} - u_{(k)}]^2}{|\xi_{(i^k)(k)}|} V_{(i^k)} \quad (3.15b)$$

where A represents the cross-sectional area of the bar and g is introduced as the surface correction factor for the sake of correcting the error occurred during the discretization, which is explained in the Section 3.2.4.

Substituting Eq.(3.15b) into (3.11) gives the strain energy density of material point k in PD form as

$$W_{(k)}^p = g_{(k)} \frac{E}{2\delta^2 A} \sum_i \frac{[u_{(i^k)} - u_{(k)}]^2}{|\xi_{(i^k)(k)}|} V_{(i^k)} \quad (3.16a)$$

Regarding the SED for the material point j , a similar form will hold if we replace the index k with j as

$$W_{(j)}^p = g_{(j)} \frac{E}{2\delta^2 A} \sum_i \frac{[u_{(i^j)} - u_{(j)}]^2}{|\xi_{(i^j)(j)}|} V_{(i^j)} \quad (3.16b)$$

Clearly, the following results can be obtained after performing algebraic manipulations as

$$\frac{\partial W_{(k)}^{PD}}{\partial \mathbf{u}_{(k)}} = -g_{(k)} \frac{E}{\delta^2 A} \sum_j \frac{u_{(j)} - u_{(k)}}{|\xi_{(j)(k)}|} \mathbf{V}_{(j)} \quad (3.17a)$$

$$\sum_j \frac{\partial W_{(j)}^{PD}}{\partial \mathbf{u}_{(k)}} \mathbf{V}_{(j)} = \frac{E}{\delta^2 A} \sum_j g_{(j)} \frac{u_{(k)} - u_{(j)}}{|\xi_{(k)(j)}|} \mathbf{V}_{(j)} \quad (3.17b)$$

Substituting Eq. (3.17) into (3.9) results in the final PD EoM for 1D bar as

$$\rho_{(k)} \ddot{\mathbf{u}}_{(k)} = \frac{2E}{\delta^2 A} \sum_j g_{(k)(j)} \frac{u_{(j)} - u_{(k)}}{|\xi_{(j)(k)}|} \mathbf{V}_{(j)} + \mathbf{b}_{(k)} \quad (3.18)$$

where $g_{(k)(j)}$ represents the resultant correction factor, which is defined as

$$g_{(k)(j)} = \frac{g_{(k)} + g_{(j)}}{2} \quad (3.19)$$

Moreover, the pairwise PD force density vectors, $\mathbf{t}_{(k)(j)}$ and $\mathbf{t}_{(j)(k)}$ can be obtained from Eq.(3.17) as

$$\mathbf{t}_{(k)(j)} = g_{(k)(j)} \frac{E}{\delta^2 A} \frac{u_{(j)} - u_{(k)}}{|\xi_{(j)(k)}|} \quad (3.20a)$$

and

$$\mathbf{t}_{(j)(k)} = g_{(k)(j)} \frac{E}{\delta^2 A} \frac{u_{(k)} - u_{(j)}}{|\xi_{(j)(k)}|} \quad (3.20b)$$

3.2.2 PD Formulation for 2D Plane Structures

If the length of the prismatic body along z axis is very small, then we shall have a thin plate of thickness loaded over the lateral surfaces (edges) by forces parallel to its faces. Since the thickness of plate is very small, the stress components associated with transverse effects can be considered to be vanishingly small, in other words, we assume

$$\tau_{zx} = \tau_{zy} = \sigma_z = 0 \quad (3.21)$$

The other stresses, σ_x , σ_y and τ_{xy} will vary very slightly along thickness direction. If the thickness is extremely small, we can assume them to be independent of z , and the following conditions are satisfied

$$\sigma_x = \sigma_x(x, y) \quad (3.22a)$$

$$\sigma_y = \sigma_y(x, y) \quad (3.22b)$$

$$\tau_{xy} = \tau_{xy}(x, y) \quad (3.22c)$$

In the view of these assumptions, the analysis of a thin plate can be simplified as the well-known 2D plane stress problem. The strain-displacement relations can be written as

$$\varepsilon_{xx} = \frac{\partial u}{\partial x} \quad (3.23a)$$

$$\varepsilon_{yy} = \frac{\partial v}{\partial y} \quad (3.23b)$$

$$\varepsilon_{xy} = \varepsilon_{yx} = \frac{1}{2} \left(\frac{\partial u}{\partial y} + \frac{\partial v}{\partial x} \right) \quad (3.23c)$$

For the isotropic material, the constitutive relations will look like

$$\sigma_{xx} = \frac{E}{1-\nu^2} (\varepsilon_{xx} + \nu \varepsilon_{yy}) \quad (3.24a)$$

$$\sigma_{yy} = \frac{E}{1-\nu^2} (\varepsilon_{yy} + \nu \varepsilon_{xx}) \quad (3.24b)$$

$$\sigma_{xy} = \frac{E}{1+\nu} \varepsilon_{xy} = \sigma_{yx} = \frac{E}{1+\nu} \varepsilon_{yx} \quad (3.24c)$$

where E and ν represent the Young's modulus and Poisson's ratio, respectively.

Eq.(3.23) and (3.24) can also be expressed in tensorial form as

$$\varepsilon_{IJ} = \frac{1}{2} \left(\frac{\partial u_I}{\partial x_J} + \frac{\partial u_J}{\partial x_I} \right) \quad (3.25a)$$

$$\sigma_{IJ} = \frac{E\nu}{1-\nu^2} \delta_{IJ} \varepsilon_{\mathcal{K}\mathcal{K}} + \frac{E}{2(1+\nu)} (\varepsilon_{IJ} + \varepsilon_{JI}) \quad (3.25b)$$

Note that, the subscript indices, I, J, \dots , take up the values of 1 ($= x$) and 2 ($= y$), and this convention will be applied throughout this section.

The strain energy density function in the classical continuum mechanics can be expressed as

$$W_{\text{CM}} = \frac{1}{2} \varepsilon_{IJ} \sigma_{IJ} \quad (3.26)$$

Plugging Eq.(3.25) into (3.26) and performing some algebraic manipulations results in

$$W_{\text{CM}} = \frac{1}{2} G \left[\left(\frac{\partial u_I}{\partial x_J} \frac{\partial u_I}{\partial x_J} + \frac{\partial u_I}{\partial x_J} \frac{\partial u_J}{\partial x_I} + \frac{\partial u_I}{\partial x_I} \frac{\partial u_J}{\partial x_J} \right) + \frac{3\nu-1}{1-\nu} \left(\frac{\partial u_I}{\partial x_I} \right)^2 \right] \quad (3.27)$$

where $G = \frac{E}{2(1+\nu)}$ represents the shear modulus of the material.

In order to write the non-local form of strain energy function of the material point k , Eq. (3.27), it is necessary to transform all the local terms into an equivalent PD form by also considering PD strain energy expression given in Eq. (3.5). This can be achieved by utilizing Taylor expansion.

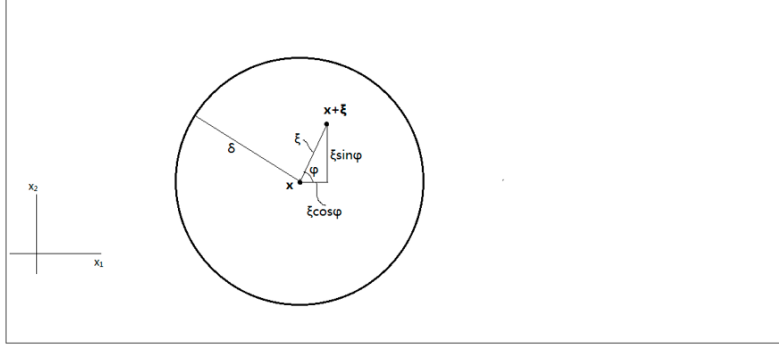


Figure 3.2 PD interaction between two material points inside the horizon

As shown in Fig. 3.2, the in-plane displacement function, $\mathbf{u}(x, y)$, can be Taylor series expanded up to 1st order terms about point x :

$$u_l(\mathbf{x} + \boldsymbol{\xi}) - u_l(\mathbf{x}) = \frac{\partial u_l(\mathbf{x})}{\partial x_j} \xi n_j \quad (3.28a)$$

and

$$u_k(\mathbf{x} + \boldsymbol{\xi}) - u_k(\mathbf{x}) = \frac{\partial u_k(\mathbf{x})}{\partial x_L} \xi n_L \quad (3.28b)$$

where $\xi = |\boldsymbol{\xi}|$ and the unit directional vector \mathbf{n} is defined as

$$\mathbf{n} = \begin{Bmatrix} n_1 \\ n_2 \end{Bmatrix} = \begin{Bmatrix} \cos \varphi \\ \sin \varphi \end{Bmatrix} \quad (3.29)$$

Multiplying Eq.(3.28a) with (3.28b) and dividing each term by ξ gives

$$\frac{[u_l(\mathbf{x} + \boldsymbol{\xi}) - u_l(\mathbf{x})][u_k(\mathbf{x} + \boldsymbol{\xi}) - u_k(\mathbf{x})]}{\xi} = \frac{\partial u_l(\mathbf{x})}{\partial x_j} \frac{\partial u_k(\mathbf{x})}{\partial x_L} \xi n_L n_j \quad (3.30)$$

Multiplying both sides of Eq.(3.30) twice by directional vector yields

$$\frac{[u_l(\mathbf{x} + \boldsymbol{\xi}) - u_l(\mathbf{x})][u_k(\mathbf{x} + \boldsymbol{\xi}) - u_k(\mathbf{x})]}{\xi} n_R n_S = \frac{\partial u_l(\mathbf{x})}{\partial x_j} \frac{\partial u_k(\mathbf{x})}{\partial x_L} \xi n_L n_j n_R n_S \quad (3.31)$$

Considering \mathbf{x} as a fixed point, integrating both sides of Eq. (3.31) over a circular domain with centre of \mathbf{x} and radius of δ yields:

$$\begin{aligned} & \int_0^{2\pi} \int_0^\delta \frac{[u_l(\mathbf{x} + \boldsymbol{\xi}) - u_l(\mathbf{x})][u_k(\mathbf{x} + \boldsymbol{\xi}) - u_k(\mathbf{x})]}{\xi} n_R n_S \xi d\xi d\varphi \\ &= \frac{\partial u_l(\mathbf{x})}{\partial x_j} \frac{\partial u_k(\mathbf{x})}{\partial x_L} \int_0^{2\pi} n_L n_j n_R n_S d\varphi \int_0^\delta \xi^2 d\xi \\ &= \frac{\pi \delta^3}{12} \frac{\partial u_l(\mathbf{x})}{\partial x_j} \frac{\partial u_k(\mathbf{x})}{\partial x_L} (\delta_{jL} \delta_{RS} + \delta_{jR} \delta_{LS} + \delta_{jS} \delta_{LR}) \\ &= \frac{\pi \delta^3}{12} \left(\frac{\partial u_l(\mathbf{x})}{\partial x_j} \frac{\partial u_k(\mathbf{x})}{\partial x_j} \delta_{RS} + \frac{\partial u_l(\mathbf{x})}{\partial x_R} \frac{\partial u_k(\mathbf{x})}{\partial x_S} + \frac{\partial u_l(\mathbf{x})}{\partial x_S} \frac{\partial u_k(\mathbf{x})}{\partial x_R} \right) \end{aligned} \quad (3.32)$$

Multiplying both sides of Eq. (3.32) by $\delta_{RI} \delta_{KS}$ and rearranging the dummy indices results in:

$$\begin{aligned} & \frac{\partial u_i(\mathbf{x})}{\partial x_j} \frac{\partial u_i(\mathbf{x})}{\partial x_j} + \frac{\partial u_i(\mathbf{x})}{\partial x_i} \frac{\partial u_j(\mathbf{x})}{\partial x_j} + \frac{\partial u_i(\mathbf{x})}{\partial x_j} \frac{\partial u_j(\mathbf{x})}{\partial x_i} \\ &= \frac{12}{\pi\delta^3} \int_0^{2\pi} \int_0^\delta \frac{[u_i(\mathbf{x} + \boldsymbol{\xi}) - u_i(\mathbf{x})][u_j(\mathbf{x} + \boldsymbol{\xi}) - u_j(\mathbf{x})]}{\xi} n_i n_j \xi d\xi d\varphi \end{aligned} \quad (3.33)$$

Recalling Eq.(3.28a)

$$u_i(\mathbf{x} + \boldsymbol{\xi}) - u_i(\mathbf{x}) = \frac{\partial u_i(\mathbf{x})}{\partial x_j} \xi n_j \quad (3.34)$$

and multiplying both sides by the unit direction vector gives

$$\frac{u_i(\mathbf{x} + \boldsymbol{\xi}) - u_i(\mathbf{x})}{\xi} n_\kappa = \frac{\partial u_i(\mathbf{x})}{\partial x_j} n_j n_\kappa \quad (3.35)$$

Considering \mathbf{x} as a fixed point, integrating both sides of Eq. (3.35) over a circular domain with centre of \mathbf{x} and radius of δ yields:

$$\begin{aligned} \int_0^{2\pi} \int_0^\delta \frac{u_i(\mathbf{x} + \boldsymbol{\xi}) - u_i(\mathbf{x})}{\xi} n_\kappa \xi d\xi d\varphi &= \frac{\partial u_i(\mathbf{x})}{\partial x_j} \int_0^{2\pi} n_j n_\kappa d\varphi \int_0^\delta \xi d\xi \\ &= \frac{\pi\delta^2}{2} \frac{\partial u_i(\mathbf{x})}{\partial x_j} \delta_{j\kappa} \\ &= \frac{\pi\delta^2}{2} \frac{\partial u_i(\mathbf{x})}{\partial x_\kappa} \end{aligned} \quad (3.36)$$

Multiplying both sides of Eq. (3.36) by δ_{IK} results in:

$$\frac{\partial u_i(\mathbf{x})}{\partial x_I} = \frac{2}{\pi\delta^2} \int_0^{2\pi} \int_0^\delta \frac{u_i(\mathbf{x} + \boldsymbol{\xi}) - u_i(\mathbf{x})}{\xi} n_I \xi d\xi d\varphi \quad (3.37)$$

Eq.(3.33) and (3.37) can also be written in a discretized form for material point k as

$$\begin{aligned} & \frac{\partial u_i^{(k)}}{\partial x_j} \frac{\partial u_i^{(k)}}{\partial x_j} + \frac{\partial u_i^{(k)}}{\partial x_i} \frac{\partial u_j^{(k)}}{\partial x_j} + \frac{\partial u_i^{(k)}}{\partial x_j} \frac{\partial u_j^{(k)}}{\partial x_i} \\ &= \frac{12}{\pi\delta^3 h} g_{(k)}' \sum_i \frac{(u_i^{(i^k)} - u_i^{(k)})(u_j^{(j^k)} - u_j^{(k)})}{\xi_{(i^k)(k)}} n_i^{(i^k)(k)} n_j^{(j^k)(k)} V_{(i^k)} \end{aligned} \quad (3.38a)$$

and

$$\frac{\partial u_i^{(k)}}{\partial x_I} = \frac{2}{\pi\delta^2 h} g_{(k)}' \sum_i \frac{u_i^{(i^k)} - u_i^{(k)}}{\xi_{(i^k)(k)}} n_i^{(i^k)(k)} V_{(i^k)} \quad (3.38b)$$

Similar to as mentioned in Section 3.2.1, g is introduced as the surface correction factor, in order to correct the error occurs from the discretization, and h represents the thickness of the plate.

Substituting Eq.(3.38a) and (3.38b) into the SED function, Eq.(3.27), results in the corresponding function in PD form for the material point k as

$$W_{(k)}^{\text{PD}} = \frac{1}{2} \mathbf{G} \left[\begin{aligned} & \frac{12}{\pi \delta^3 h} g'_{(k)} \sum_i \frac{\left[(u_i^{i^k}) - u_i^{(k)} \right] n_i^{i^k(k)} \left[n_i^{i^k(k)} \right]^2}{\xi_{(i^k)(k)}} V_{(i^k)} \\ & + \frac{3\nu - 1}{1 - \nu} \left(\frac{2}{\pi \delta^2 h} \right)^2 \left(g''_{(k)} \sum_i \frac{u_i^{i^k} - u_i^{(k)}}{\xi_{(i^k)(k)}} n_i^{i^k(k)} V_{(i^k)} \right)^2 \end{aligned} \right] \quad (3.39a)$$

Regarding the SED for the material point j , a similar form will hold if we replace the index k with j as

$$W_{(j)}^{\text{PD}} = \frac{1}{2} \mathbf{G} \left[\begin{aligned} & \frac{12}{\pi \delta^3 h} g'_{(j)} \sum_i \frac{\left[(u_i^{i^j}) - u_i^{(j)} \right] n_i^{i^j(j)} \left[n_i^{i^j(j)} \right]^2}{\xi_{(i^j)(j)}} V_{(i^j)} \\ & + \frac{3\nu - 1}{1 - \nu} \left(\frac{2}{\pi \delta^2 h} \right)^2 \left(g''_{(j)} \sum_i \frac{u_i^{i^j} - u_i^{(j)}}{\xi_{(i^j)(j)}} n_i^{i^j(j)} V_{(i^j)} \right)^2 \end{aligned} \right] \quad (3.39b)$$

Recall Eq.(3.9) given in Section 3.2,

$$\rho_{(k)} \ddot{\mathbf{u}}_{(k)} = - \left(\frac{\partial W_{(k)}^{\text{PD}}}{\partial \mathbf{u}_{(k)}} + \sum_j \frac{\partial W_{(j)}^{\text{PD}}}{\partial \mathbf{u}_{(k)}} \frac{V_{(j)}}{V_{(k)}} \right) + \mathbf{b}_{(k)} \quad (3.40)$$

the first two terms at the right hand side can be obtained by plugging Eq.(3.39a) and (3.39b) as

$$\frac{\partial W_{(k)}^{\text{PD}}}{\partial u_L^{(k)}} = -\mathbf{G} \left[\begin{aligned} & \frac{12}{\pi \delta^3 h} g'_{(k)} \sum_j \frac{u_i^{(j)} - u_i^{(k)}}{\xi_{(j)(k)}} n_i^{(j)(k)} n_L^{(j)(k)} V_{(j)} \\ & + \frac{3\nu - 1}{1 - \nu} \left(\frac{2}{\pi \delta^2 h} \right)^2 \sum_j g''_{(k)} \frac{n_L^{(j)(k)}}{\xi_{(j)(k)}} g''_{(k)} \sum_i \frac{u_i^{i^k} - u_i^{(k)}}{\xi_{(i^k)(k)}} n_i^{i^k(k)} V_{(i^k)} V_{(j)} \end{aligned} \right] \quad (3.41a)$$

and

$$\sum_j \frac{\partial W_{(j)}^{\text{PD}}}{\partial \mathbf{u}_{(k)}} \frac{V_{(j)}}{V_{(k)}} = \mathbf{G} \left[\begin{aligned} & \frac{12}{\pi \delta^3 h} \sum_j g'_{(j)} \frac{u_i^{(k)} - u_i^{(j)}}{\xi_{(k)(j)}} n_i^{(k)(j)} n_L^{(k)(j)} V_{(k)} + \\ & \frac{3\nu - 1}{1 - \nu} \left(\frac{2}{\pi \delta^2 h} \right)^2 \sum_j g''_{(j)} \frac{n_L^{(k)(j)}}{\xi_{(k)(j)}} g''_{(j)} \sum_i \frac{u_i^{i^j} - u_i^{(j)}}{\xi_{(i^j)(j)}} n_i^{i^j(j)} V_{(i^j)} V_{(j)} \end{aligned} \right] \quad (3.41b)$$

Inserting the above expressions into Eq.(3.40) yields the final PD EoM for 2D plane-stress problems as

$$\rho_{(k)} \ddot{u}_L^{(k)} = \mathbf{G} \left[\begin{aligned} & \frac{24}{\pi \delta^3 h} \sum_j g'_{(j)(k)} \frac{u_i^{(j)} - u_i^{(k)}}{\xi_{(j)(k)}} n_i^{(j)(k)} n_L^{(j)(k)} V_{(j)} + \\ & \frac{3\nu - 1}{1 - \nu} \left(\frac{2}{\pi \delta^2 h} \right)^2 \sum_j \frac{n_L^{(j)(k)}}{\xi_{(j)(k)}} \left(\begin{aligned} & (g''_{(k)})^2 \sum_i \frac{u_i^{i^k} - u_i^{(k)}}{\xi_{(i^k)(k)}} n_i^{i^k(k)} V_{(i^k)} \\ & + (g''_{(j)})^2 \sum_i \frac{u_i^{i^j} - u_i^{(j)}}{\xi_{(i^j)(j)}} n_i^{i^j(j)} V_{(i^j)} \end{aligned} \right) V_{(j)} \end{aligned} \right] + \mathbf{b}_L^{(k)} \quad (3.42)$$

where $g_{(j)(k)}$ represents the pairwise correction factor, which is defined as

$$g_{(j)(k)} = \frac{g_{(j)} + g_{(k)}}{2} \quad (3.43)$$

In particular case, when the Poisson's ratio is $\nu = \frac{1}{3}$, Eq.(3.42) can be reduced to a compact form (sometimes referred as bond-based formulation), as

$$\rho_{(k)} \ddot{u}_L^{(k)} = c \sum_j g_{(j)(k)} \frac{u_L^{(j)} - u_L^{(k)}}{\xi_{(j)(k)}} n_L^{(j)(k)} n_L^{(j)(k)} V_{(j)} + \mathbf{b}_L^{(k)} \quad (3.44)$$

where c represents the PD bond constant as

$$c = \frac{24G}{\pi\delta^3 h} = \frac{9E}{\pi\delta^3 h} \quad (3.45)$$

Moreover, the pairwise PD force density vectors, $\mathbf{t}_{(k)(j)}$ and $\mathbf{t}_{(j)(k)}$ can be expressed as

$$\mathbf{t}_L^{(k)(j)} = \left(\begin{array}{l} \frac{12G}{\pi\delta^3 h} g_{(j)(k)} \frac{u_L^{(j)} - u_L^{(k)}}{\xi_{(j)(k)}} n_L^{(j)(k)} n_L^{(j)(k)} \\ + G \frac{3\nu - 1}{1 - \nu} \left(\frac{2}{\pi\delta^2 h} \right)^2 (g_{(k)}^{(j)})^2 \frac{n_L^{(j)(k)}}{\xi_{(j)(k)}} \sum_i \frac{u_L^{(i^k)} - u_L^{(k)}}{\xi_{(i^k)(k)}} n_L^{(i^k)(k)} V_{(i^k)} \end{array} \right) \quad (3.46a)$$

and

$$\mathbf{t}_L^{(j)(k)} = \left(\begin{array}{l} \frac{12G}{\pi\delta^3 h} g_{(j)(k)} \frac{u_L^{(k)} - u_L^{(j)}}{\xi_{(j)(k)}} n_L^{(k)(j)} n_L^{(k)(j)} \\ + G \frac{3\nu - 1}{1 - \nu} \left(\frac{2}{\pi\delta^2 h} \right)^2 \frac{n_L^{(k)(j)}}{\xi_{(j)(k)}} (g_{(j)}^{(k)})^2 \sum_i \frac{u_L^{(i^j)} - u_L^{(j)}}{\xi_{(i^j)(j)}} n_L^{(i^j)(j)} V_{(i^j)} \end{array} \right) \quad (3.46b)$$

It can be concluded that

$$\begin{cases} \mathbf{t}_{(k)(j)} = -\mathbf{t}_{(j)(k)} & \text{if } \nu = \frac{1}{3} \\ \mathbf{t}_{(k)(j)} \neq -\mathbf{t}_{(j)(k)} & \text{if } \nu \neq \frac{1}{3} \end{cases} \quad (3.47)$$

Regarding the plane strain problems, similar EoM will hold if we manipulate the following material constants transformation:

$$E \rightarrow \frac{E}{1 - \nu^2} \quad \text{and} \quad \nu \rightarrow \frac{\nu}{1 - \nu} \quad (3.48a, b)$$

3.2.3 PD Formulation for 3D Solid Structures

The strain-displacement relation for a 3D solid structure can be written in the tensorial form as

$$\varepsilon_{ij} = \frac{1}{2} \left(\frac{\partial u_i}{\partial x_j} + \frac{\partial u_j}{\partial x_i} \right) \quad (3.49)$$

where the subscript indices, i, j, \dots , take up the value 1(= x), 2(= y) and 3(= z).

The stress components can be expressed as

$$\sigma_{ij} = C_{ijkl} \varepsilon_{kl} \quad (3.50)$$

where C is the 4th order stiffness tensor, which can be defined for the isotropic material as

$$C_{ijkl} = G(\delta_{il}\delta_{jk} + \delta_{ik}\delta_{jl}) + \frac{2G\nu}{1-2\nu} \delta_{ij} \delta_{kl} \quad (3.51)$$

The strain energy density function in classical continuum mechanics theory can be written as

$$W_{\text{con}} = \frac{1}{2} \sigma_{ij} \varepsilon_{ij} = \frac{1}{2} C_{ijkl} \varepsilon_{kl} \varepsilon_{ij} \quad (3.52)$$

The SED can be rewritten in terms displacement components by substituting Eqs.(3.49) and (3.51) into Eq.(3.52) as

$$W_{\text{con}} = \frac{G}{2} \left(\frac{\partial u_i}{\partial x_j} \frac{\partial u_j}{\partial x_i} + \frac{\partial u_i}{\partial x_j} \frac{\partial u_j}{\partial x_i} + \frac{\partial u_i}{\partial x_i} \frac{\partial u_j}{\partial x_j} \right) + \frac{G(4\nu-1)}{2(1-2\nu)} \left(\frac{\partial u_i}{\partial x_i} \right)^2 \quad (3.53)$$

In order to write the non-local form of strain energy function of the material point k , Eqn. (3.53), it is necessary to transform all the local terms into an equivalent PD form by also considering PD strain energy expression given in Eqn. (3.5). This can be achieved by utilizing Taylor series expansion.

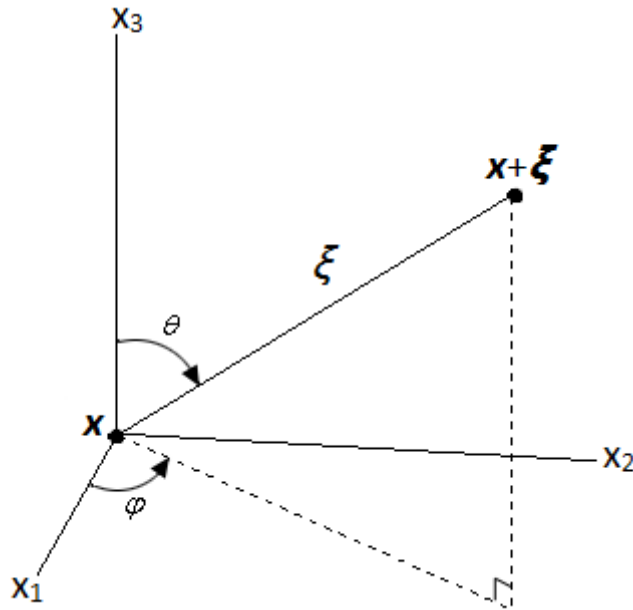


Figure 3.3 PD interaction between two material points

As shown in Fig. (3.3), the displacement function, $\mathbf{u}(x, y, z)$, can be Taylor expanded up to 1st order terms about point \mathbf{x} as

$$u_i(\mathbf{x} + \boldsymbol{\xi}) - u_i(\mathbf{x}) = \frac{\partial u_i(\mathbf{x})}{\partial x_j} \xi n_j \quad (3.54a)$$

and with other index notations as

$$u_k(\mathbf{x} + \boldsymbol{\xi}) - u_k(\mathbf{x}) = \frac{\partial u_k(\mathbf{x})}{\partial x_l} \xi n_l \quad (3.54b)$$

where $\xi = |\boldsymbol{\xi}|$ and the unit orientation vector \mathbf{n} is defined as

$$\mathbf{n} = \begin{Bmatrix} n_1 \\ n_2 \\ n_3 \end{Bmatrix} = \begin{Bmatrix} \sin \theta \cos \varphi \\ \sin \theta \sin \varphi \\ \cos \theta \end{Bmatrix} \quad (3.55)$$

Multiplying Eq.(3.54a) with (3.54b) gives

$$\frac{[u_i(\mathbf{x} + \boldsymbol{\xi}) - u_i(\mathbf{x})][u_k(\mathbf{x} + \boldsymbol{\xi}) - u_k(\mathbf{x})]}{\xi} = \frac{\partial u_i(\mathbf{x})}{\partial x_j} \frac{\partial u_k(\mathbf{x})}{\partial x_l} \xi n_j n_l \quad (3.56)$$

Multiplying both sides of Eq.(3.56) by unit orientation vector twice gives

$$\frac{[u_i(\mathbf{x} + \boldsymbol{\xi}) - u_i(\mathbf{x})][u_k(\mathbf{x} + \boldsymbol{\xi}) - u_k(\mathbf{x})]}{\xi} n_r n_s = \frac{\partial u_i(\mathbf{x})}{\partial x_j} \frac{\partial u_k(\mathbf{x})}{\partial x_l} \xi n_j n_l n_r n_s \quad (3.57)$$

Considering \mathbf{x} as a fixed point, integrating both sides of Eq. (3.57) over a spherical domain with centre of \mathbf{x} and radius of δ yields:

$$\begin{aligned} & \int_0^{2\pi} \int_0^\pi \int_0^\delta \frac{[u_i(\mathbf{x} + \boldsymbol{\xi}) - u_i(\mathbf{x})][u_k(\mathbf{x} + \boldsymbol{\xi}) - u_k(\mathbf{x})]}{\xi} n_r n_s \xi^2 \sin \theta d\xi d\theta d\varphi \\ &= \frac{\partial u_i(\mathbf{x})}{\partial x_j} \frac{\partial u_k(\mathbf{x})}{\partial x_l} \int_0^{2\pi} \int_0^\pi \int_0^\delta \xi n_j n_l n_r n_s \xi^2 \sin \theta d\xi d\theta d\varphi \\ &= \frac{\delta^4 \pi}{15} \frac{\partial u_i(\mathbf{x})}{\partial x_j} \frac{\partial u_k(\mathbf{x})}{\partial x_l} (\delta_{jl} \delta_{rs} + \delta_{jr} \delta_{ls} + \delta_{js} \delta_{rl}) \\ &= \frac{\delta^4 \pi}{15} \left(\frac{\partial u_i(\mathbf{x})}{\partial x_j} \frac{\partial u_k(\mathbf{x})}{\partial x_l} \delta_{rs} + \frac{\partial u_i(\mathbf{x})}{\partial x_r} \frac{\partial u_k(\mathbf{x})}{\partial x_s} + \frac{\partial u_i(\mathbf{x})}{\partial x_s} \frac{\partial u_k(\mathbf{x})}{\partial x_r} \right) \end{aligned} \quad (3.58)$$

Multiplying both sides of Eq.(3.58) by $\delta_{ir} \delta_{ks}$ and rearranging the dummy indices yields

$$\begin{aligned} & \frac{\partial u_i(\mathbf{x})}{\partial x_j} \frac{\partial u_i(\mathbf{x})}{\partial x_j} + \frac{\partial u_i(\mathbf{x})}{\partial x_i} \frac{\partial u_j(\mathbf{x})}{\partial x_j} + \frac{\partial u_i(\mathbf{x})}{\partial x_j} \frac{\partial u_j(\mathbf{x})}{\partial x_i} \\ &= \frac{15}{\delta^4 \pi} \int_0^{2\pi} \int_0^\pi \int_0^\delta \frac{[u_i(\mathbf{x} + \boldsymbol{\xi}) - u_i(\mathbf{x})][u_k(\mathbf{x} + \boldsymbol{\xi}) - u_k(\mathbf{x})]}{\xi} n_i n_k \xi^2 \sin \theta d\xi d\theta d\varphi \end{aligned} \quad (3.59)$$

Recalling Eq.(3.54):

$$u_i(\mathbf{x} + \boldsymbol{\xi}) - u_i(\mathbf{x}) = \frac{\partial u_i(\mathbf{x})}{\partial x_j} \xi n_j \quad (3.60)$$

and multiplying both sides by the unit orientation vector gives

$$\frac{u_i(\mathbf{x} + \boldsymbol{\xi}) - u_i(\mathbf{x})}{\xi} n_k = \frac{\partial u_i(\mathbf{x})}{\partial x_j} n_j n_k \quad (3.61)$$

Considering \mathbf{x} as a fixed point, integrating both sides of Eq. (3.61) over a spherical domain with centre of \mathbf{x} and radius of δ yields:

$$\begin{aligned} & \int_0^{2\pi} \int_0^\pi \int_0^\delta \frac{u_i(\mathbf{x} + \boldsymbol{\xi}) - u_i(\mathbf{x})}{\xi} n_k \xi^2 \sin \theta d\xi d\theta d\varphi \\ &= \frac{\partial u_i(\mathbf{x})}{\partial x_j} \int_0^{2\pi} \int_0^\pi \int_0^\delta n_j n_k \xi^2 \sin \theta d\xi d\theta d\varphi \\ &= \frac{4\delta^3 \pi}{9} \frac{\partial u_i(\mathbf{x})}{\partial x_j} \delta_{jk} \\ &= \frac{4\delta^3 \pi}{9} \frac{\partial u_i(\mathbf{x})}{\partial x_k} \end{aligned} \quad (3.62)$$

Multiplying both sides of Eq.(3.62) by δ_{ik} results in

$$\frac{\partial u_i(\mathbf{x})}{\partial x_i} = \frac{9}{4\delta^3 \pi} \int_0^{2\pi} \int_0^\pi \int_0^\delta \frac{u_i(\mathbf{x} + \boldsymbol{\xi}) - u_i(\mathbf{x})}{\xi} n_i \xi^2 \sin \theta d\xi d\theta d\varphi \quad (3.63)$$

Eq.(3.59) and (3.63) can be discretized for material point k as

$$\begin{aligned} & \frac{\partial u_r^{(k)}}{\partial x_s} \frac{\partial u_r^{(k)}}{\partial x_s} + \frac{\partial u_r^{(k)}}{\partial x_r} \frac{\partial u_s^{(k)}}{\partial x_s} + \frac{\partial u_r^{(k)}}{\partial x_s} \frac{\partial u_s^{(k)}}{\partial x_r} \\ &= \frac{15}{\delta^4 \pi} g_{(k)}' \sum_i \frac{(u_r^{(i^k)} - u_r^{(k)})(u_s^{(i^k)} - u_s^{(k)})}{\xi_{(i^k)(k)}} n_r^{(i^k)(k)} n_s^{(i^k)(k)} V_{(i^k)} \end{aligned} \quad (3.64a)$$

and

$$\frac{\partial u_r^{(k)}}{\partial x_r} = \frac{9}{4\delta^3 \pi} g_{(k)}'' \sum_i \frac{u_r^{(i^k)} - u_r^{(k)}}{\xi_{(i^k)(k)}} n_r^{(i^k)(k)} V_{(i^k)} \quad (3.64b)$$

where g is introduced as the surface correction factor in order to correct the error occurring from the discretization. Substituting Eq.(3.64) into (3.53) yields the PD SED function for material point k as

$$W_{\text{PD}}^{(k)} = \left\{ \begin{aligned} & \frac{G}{2\delta^4 \pi} g_{(k)}' \sum_i \frac{[(u_r^{(i^k)} - u_r^{(k)}) n_r^{(i^k)(k)}]^2}{\xi_{(i^k)(k)}} V_{(i^k)} \\ & + \frac{G}{2(1-2\nu)} \left(\frac{9}{4\delta^3 \pi} \right)^2 \left(g_{(k)}'' \sum_i \frac{u_r^{(i^k)} - u_r^{(k)}}{\xi_{(i^k)(k)}} n_r^{(i^k)(k)} V_{(i^k)} \right)^2 \end{aligned} \right\} \quad (3.65a)$$

Regarding the SED for the material point j , a similar form will hold if we replace the index k with j as

$$W_{\text{PD}}^{(j)} = \left\{ \begin{aligned} & \frac{G}{2\delta^4\pi} g'_{(j)} \sum_i \left[\frac{(u_r^{i^j}) - u_r^{(j)}}{\xi_{(i^j)(j)}} n_r^{i^j(j)} \right]^2 V_{(i^j)} \\ & + \frac{G}{2(1-2\nu)} \left(\frac{9}{4\delta^3\pi} \right)^2 \left(g''_{(j)} \sum_i \frac{u_r^{i^j} - u_r^{(j)}}{\xi_{(i^j)(j)}} n_r^{i^j(j)} V_{(i^j)} \right)^2 \end{aligned} \right\} \quad (3.65b)$$

The final PD EoM for 3D structures can be obtained by inserting Eq.(3.65) into (3.8)

as

$$\rho_{(k)} \ddot{u}_l^{(k)} = \left\{ \begin{aligned} & \frac{G}{\delta^4\pi} \sum_j g'_{(j)(k)} \frac{u_r^{(j)} - u_r^{(k)}}{\xi_{(j)(k)}} n_r^{(j)(k)} n_l^{(j)(k)} V_{(j)} \\ & + \frac{G}{(1-2\nu)} \left(\frac{9}{4\delta^3\pi} \right)^2 \sum_j \frac{n_l^{(j)(k)}}{\xi_{(j)(k)}} \left(\begin{aligned} & (g''_{(k)})^2 \sum_i \frac{u_r^{i^k} - u_r^{(k)}}{\xi_{(i^k)(k)}} n_r^{i^k(k)} V_{(i^k)} \\ & + (g''_{(j)})^2 \sum_i \frac{u_r^{i^j} - u_r^{(j)}}{\xi_{(i^j)(j)}} n_r^{i^j(j)} V_{(i^j)} \end{aligned} \right) V_{(j)} \end{aligned} \right\} + b_l^{(k)} \quad (3.66)$$

In particular case, when the Poisson's ratio is $\nu = \frac{1}{4}$, Eq.(3.66) can be reduced to a compact form (sometimes refer to bond-based formulation), as

$$\rho_{(k)} \ddot{u}_l^{(k)} = \frac{30G}{\delta^4\pi} \sum_j g'_{(j)(k)} \frac{u_r^{(j)} - u_r^{(k)}}{\xi_{(j)(k)}} n_r^{(j)(k)} n_l^{(j)(k)} V_{(j)} + b_l^{(k)} \quad (3.67)$$

Moreover, the pairwise PD force density vectors, $\mathbf{t}_{(k)(j)}$ and $\mathbf{t}_{(j)(k)}$ can be expressed

as

$$\mathbf{t}_l^{(k)(j)} = \left\{ \begin{aligned} & \frac{G}{\delta^4\pi} g'_{(j)(k)} \frac{u_r^{(j)} - u_r^{(k)}}{\xi_{(j)(k)}} n_r^{(j)(k)} n_l^{(j)(k)} \\ & + \frac{G}{(1-2\nu)} \left(\frac{9}{4\delta^3\pi} \right)^2 \frac{n_l^{(j)(k)}}{\xi_{(j)(k)}} (g''_{(k)})^2 \sum_i \frac{u_r^{i^k} - u_r^{(k)}}{\xi_{(i^k)(k)}} n_r^{i^k(k)} V_{(i^k)} \end{aligned} \right\} \quad (3.68a)$$

and

$$\mathbf{t}_l^{(j)(k)} = \left\{ \begin{aligned} & \frac{G}{\delta^4\pi} g'_{(k)(j)} \frac{u_r^{(k)} - u_r^{(j)}}{\xi_{(j)(k)}} n_r^{(k)(j)} n_l^{(k)(j)} \\ & + \frac{G}{(1-2\nu)} \left(\frac{9}{4\delta^3\pi} \right)^2 \frac{n_l^{(k)(j)}}{\xi_{(j)(k)}} (g''_{(j)})^2 \sum_i \frac{u_r^{i^j} - u_r^{(j)}}{\xi_{(i^j)(j)}} n_r^{i^j(j)} V_{(i^j)} \end{aligned} \right\} \quad (3.68b)$$

It can be concluded that

$$\begin{cases} \mathbf{t}_{(k)(j)} = -\mathbf{t}_{(j)(k)} & \text{if } \nu = \frac{1}{4} \\ \mathbf{t}_{(k)(j)} \neq -\mathbf{t}_{(j)(k)} & \text{if } \nu \neq \frac{1}{4} \end{cases} \quad (3.69)$$

3.2.4 Surface Correction Factor

As introduced above, PD is a non-local continuum mechanics theory with EoM expressed in integro-differential form. In numerical analysis, the PD model is usually discretized with finite number of material points and volumes and the integral formulation is replaced by a finite sum. This brings the need for introduction of so-called surface correction factor (SCF), for the sake of reducing the errors occurring from discretization for the numerical calculation. In this study, the approach for casting the SCF for 2D plane-stress model will be introduced, and this approach can be generalized analogically for 1D and 3D models.

Generally, the SCF at a certain material point can be obtained by equalizing the SED in classical theory with the corresponding SED in PD theory. Recalling Eq.(3.27), the SED function of material point k according to the classical continuum mechanics can be written in terms of strain components as

$$\mathcal{W}_{\text{CM}}(\mathbf{x}_{(k)}) = G \left[\left(\varepsilon_{IJ}^{(k)} \varepsilon_{IJ}^{(k)} + \frac{1}{2} \varepsilon_{II}^{(k)} \varepsilon_{JJ}^{(k)} \right) + \frac{3\nu - 1}{2(1 - \nu)} \varepsilon_{II}^{(k)} \varepsilon_{JJ}^{(k)} \right] \quad (3.70)$$

where the subscripts I, J, \dots take up the values $1(=x)$ and $2(=y)$, and $\varepsilon_{IJ}^{(k)} = \frac{1}{2} \left(\frac{\partial u_I^{(k)}}{\partial x_J} + \frac{\partial u_J^{(k)}}{\partial x_I} \right)$ represents the strain components. Let Eq.(3.70) be written separately

into two parts:

$$\mathcal{W}_{\text{CM}}(\mathbf{x}_{(k)}) = \mathcal{W}_{\text{CM}}^I(\mathbf{x}_{(k)}) + \mathcal{W}_{\text{CM}}^{II}(\mathbf{x}_{(k)}) \quad (3.71)$$

where

$$\mathcal{W}_{\text{CM}}^I(\mathbf{x}_{(k)}) = G \left(\varepsilon_{IJ}^{(k)} \varepsilon_{IJ}^{(k)} + \frac{1}{2} \varepsilon_{II}^{(k)} \varepsilon_{JJ}^{(k)} \right) \quad (3.72a)$$

and

$$\mathcal{W}_{\text{CM}}^{II}(\mathbf{x}_{(k)}) = G \frac{3\nu - 1}{2(1 - \nu)} \varepsilon_{II}^{(k)} \varepsilon_{JJ}^{(k)} \quad (3.72b)$$

Their counterparts in PD theory can be expressed as

$$\mathcal{W}_{\text{PD}}^I(\mathbf{x}_{(k)}) = \frac{6G}{\pi \delta^3 h} \sum_i \frac{\left[\left(u_i^{(i^k)} - u_i^{(k)} \right) \eta_i^{(i^k)(k)} \right]^2}{\xi_{(i^k)(k)}} V_{(i^k)} \quad (3.73a)$$

and

$$W'_{PD}(\mathbf{x}_{(k)}) = \frac{G}{2} \frac{3\nu - 1}{1 - \nu} \left(\frac{2}{\pi \delta^2 h} \right)^2 \left(\sum_i \frac{u_i^{(i^k)} - u_i^{(k)}}{\xi_{(i^k)(k)}} n_i^{(i^k)(k)} V_{(i^k)} \right)^2 \quad (3.73b)$$

Considering the body is undergoing a homogeneous deformation that

$$\varepsilon_{i,j}(\mathbf{x}) = c_{i,j} = c_{j,i} = \text{const}. \quad (3.74)$$

And this can be achieved by enforcing such displacement fields as

$$u_i(\mathbf{x}) = c_{i,j} x_j \quad (3.75)$$

Thus, the strain energy density functions according to classical continuum mechanics theory become

$$W'_{CM}(\mathbf{x}_{(k)}) = G \left(c_{i,j}^2 + \frac{1}{2} c_{ii}^2 \right) \quad (3.76a)$$

and

$$W'_{CM}(\mathbf{x}_{(k)}) = G \frac{3\nu - 1}{2(1 - \nu)} c_{ii}^2 \quad (3.76b)$$

and their counterpart PD functions are

$$W'_{PD}(\mathbf{x}_{(k)}) = \frac{6G}{\pi \delta^3 h} \sum_i \frac{\left[c_{i,j} (x_j^{(i^k)} - x_j^{(k)}) n_i^{(i^k)(k)} \right]^2}{\xi_{(i^k)(k)}} V_{(i^k)} \quad (3.77a)$$

and

$$W'_{PD}(\mathbf{x}_{(k)}) = \frac{G}{2} \frac{3\nu - 1}{1 - \nu} \left(\frac{2}{\pi \delta^2 h} \right)^2 \left(\sum_i c_{i,j} \frac{x_j^{(i^k)} - x_j^{(k)}}{\xi_{(i^k)(k)}} n_i^{(i^k)(k)} V_{(i^k)} \right)^2 \quad (3.77b)$$

Therefore, the surface correction factors for the material point k can be calculated by equalizing Eq.(3.76) with Eq.(3.77) correspondingly as

$$g'_{(k)} = \frac{W'_{PD}(\mathbf{x}_{(k)})}{W'_{CM}(\mathbf{x}_{(k)})} \quad (3.78a)$$

and

$$g''_{(k)} = \sqrt{\frac{W'_{PD}(\mathbf{x}_{(k)})}{W'_{CM}(\mathbf{x}_{(k)})}} \quad (3.78b)$$

Surface correction factors for 1D and 2D cases can be achieved in an analogical manner.

Moreover, for some family members whose volumes are partially embedded in the horizon, as shown in Fig. 3.4 donated in yellow, another correction factor so-called volume correction factor, α , is also necessarily being involved. The volume correction factor is related to the proportion of the material volume embedded in the horizon with

the entire material volume, which can be approximately casted as

$$\alpha_{(j)} = \begin{cases} 1 & \text{if } \xi_{(j)(k)} \leq \delta - \frac{dx}{2} \\ \frac{1}{2} + \frac{\delta - \xi_{(j)(k)}}{dx} & \text{otherwise} \end{cases} \quad (3.79)$$

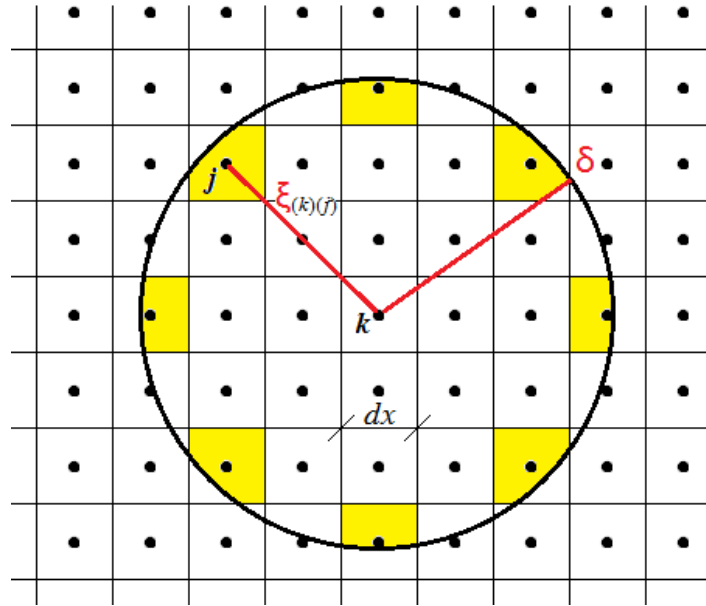


Figure 3.4 Material volumes in PD horizon

3.3 Numerical Solution Method

PD theory as introduced in previous sections is based on integro-differential equations and these equations are generally difficult to be solved by using analytical techniques. Therefore, numerical approximations, especially with meshless method, have been widely used. The PD model can be discretized uniformly into finite cubic subdomains with material points attached at the center, see Fig. 3.5. Therefore, PD equations of motion can be represented corresponding to each material points and systematized into a matrix equation system. In this section, the PD numerical solution procedure will be explained with 1D PD rod model as example, solution of more complex structures can be approached analogically.

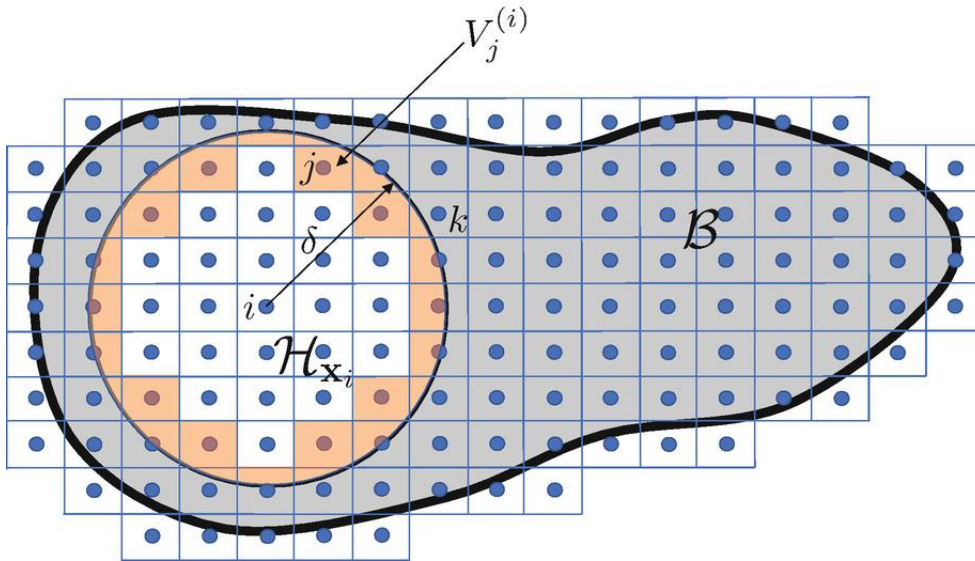


Figure 3.5 PD discretization method (Seleson P. and Littlewood D.J., 2018)

As shown in Fig 3.6, clamped – free rod subjected longitudinal body load density of $b = b(x)$ is taken into consideration. The geometry and material parameters are denoted by L (length), A (cross-section area), ρ (density) and E (Young’s modulus), respectively. The corresponding PD model is discretized uniformly into N material points and therefore the spacing between material point is $\Delta x = L/N$. Fictitious regions (denoted by green) with size of δ are introduced outside the two boundaries for the sake of ensuing each material point (denoted by orange) adjacent to boundary is fully embedded its PD horizon, as shown in Fig. 3.7.

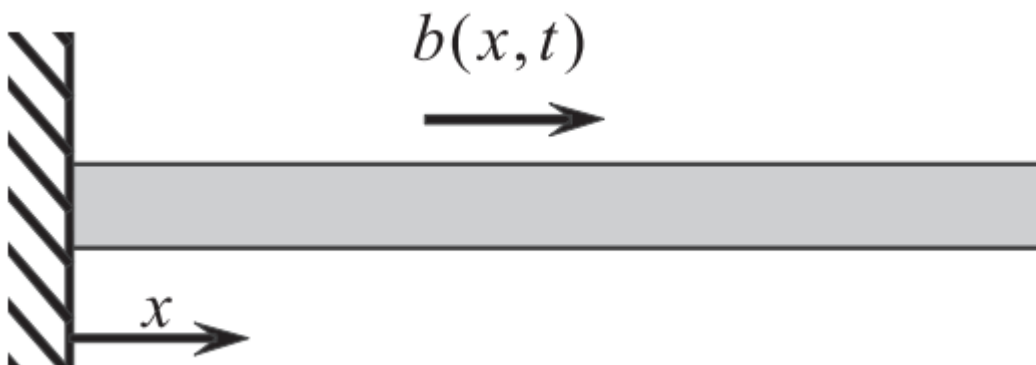


Figure 3.6 Clamped – Free rod (Schoeftner and Littlewood, 2016)

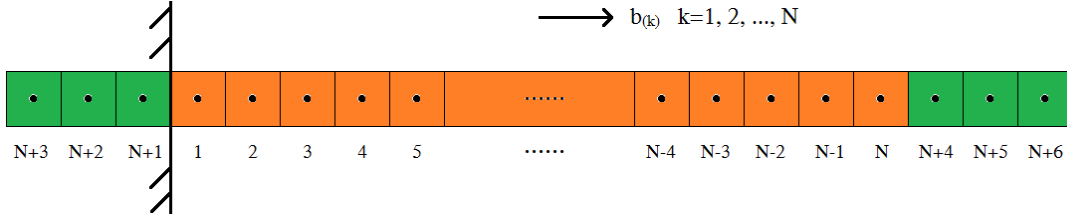


Figure 3.7 PD discretization model of clamped – free rod

3.3.1 Dynamics Solution

Dynamics analysis can be directly performed by using the PD equations of motion given in the previous sections in this chapter. In this case, the corresponding PD equation of motion, Eq. (3.18), can be rewritten with consideration of damping factor for n th time step as

$$\rho_{(k)} \ddot{u}_{(k)}^n = c \sum_{j=1}^{M_{(k)}} \frac{u_{(j)}^n - u_{(k)}^n}{|\xi_{(j)(k)}|} V_{(j)} + b_{(k)}^n - \eta \dot{u}_{(k)}^n \quad (3.80)$$

where

- | | |
|---|---------------------------------------|
| n : time step | c : PD material constant |
| $M_{(k)}$: number of family member of material point k | η : damping factor of the system |

Assume the initial conditions of the system are prescribed as

$$\begin{cases} u(\mathbf{x}_{(k)}, 0) = u_{(k)}^0 \\ \dot{u}(\mathbf{x}_{(k)}, 0) = \dot{u}_{(k)}^0 \end{cases} \quad (3.81a, b)$$

Boundary conditions can be prescribed by using mirror-displacement method (refer to Appendix B1.3) as

$$\begin{cases} u(\mathbf{x}, t) = -u(-\mathbf{x}, t) \\ u(L - \mathbf{x}, t) = u(L + \mathbf{x}, t) \end{cases} \quad 0 < \mathbf{x} < \delta \quad (3.82a, b)$$

for clamped end and free end, respectively, which can be written in the discretized form for this case as

$$u_{(N+1)}^n = -u_{(1)}^n \quad u_{(N+2)}^n = -u_{(2)}^n \quad u_{(N+3)}^n = -u_{(3)}^n \quad (3.83a, b, c)$$

and

$$u_{(N+4)}^n = u_{(N)}^n \quad u_{(N+5)}^n = u_{(N-1)}^n \quad u_{(N+6)}^n = u_{(N-2)}^n \quad (3.84a, b, c)$$

Eq. (3.80) can be performed central difference with respect to time variable at 0th time step as

$$\rho_{(k)} \frac{u_{(k)}^{-1} - 2u_{(k)}^0 + u_{(k)}^1}{(\Delta t)^2} = c \sum_{j=1}^{M_{(k)}} \frac{u_{(j)}^0 - u_{(k)}^0}{|\xi_{(j)(k)}|} V_{(j)} + b_{(k)}^0 - \eta \frac{u_{(k)}^1 - u_{(k)}^{-1}}{2\Delta t} \quad (3.85)$$

where Δt represents the time step size. Performing central difference with respect to time variable for the initial condition, Eq. (3.81b) results in

$$\dot{u}_{(k)}^0 = \frac{u_{(k)}^1 - u_{(k)}^{-1}}{2\Delta t} \quad (3.86a)$$

which gives

$$u_{(k)}^{-1} = u_{(k)}^1 - 2(\Delta t) \dot{u}_{(k)}^0 \quad (3.86b)$$

Plugging Eq. (3.86b) into (3.85) and performing some algebra results in the starting algorithm for PD dynamics solution as

$$u_{(k)}^1 = \frac{c}{\rho_{(k)}} \frac{(\Delta t)^2}{2} \sum_{j=1}^{M_{(k)}} \frac{u_{(j)}^0 - u_{(k)}^0}{|\xi_{(j)(k)}|} V_{(j)} + u_{(k)}^0 + \left[1 - \frac{\eta}{\rho_{(k)}} \frac{\Delta t}{2} \right] (\Delta t) \dot{u}_{(k)}^0 + \frac{b_{(k)}^0}{\rho_{(k)}} \frac{(\Delta t)^2}{2} \quad (3.87)$$

$(k = 1, 2, 3, \dots, N)$

Note that the choice of time step size Δt is preferred to be small in order to maintain the time-stepping scheme stable. The time step chosen criterion can be referred to Madenci and Oterkus (2014).

3.3.2 Static Solution

On the other hand, the PD numerical solution for statics analysis can be obtained by eliminating the inertial forces from the PD EoMs, which in this case, Eq. (3.18) reduces to

$$c \sum_{j=1}^{M_{(k)}} \frac{u_{(j)} - u_{(k)}}{|\xi_{(j)(k)}|} V_{(j)} = -b_{(k)} \quad (3.88)$$

With taking boundary conditions into consideration, PD statics solution can be obtained by solving the following system of linear equations

$$\begin{cases} c \sum_{j=1}^{M(k)} \frac{u_{(j)} - u_{(k)}}{|\xi_{(j)(k)}|} V_{(j)} = -b_{(k)} & \text{for } k = 1, 2, \dots, N \\ u_{(N+1)} = -u_{(1)} & u_{(N+2)} = -u_{(2)} & u_{(N+3)} = -u_{(3)} \\ u_{(N+4)} = u_{(N)} & u_{(N+5)} = u_{(N-1)} & u_{(N+6)} = u_{(N-2)} \end{cases} \quad (3.89)$$

Coupling the PD governing equations with the boundary conditions, Eq. (3.89) can be written in matrix form as

$$[K]_{N \times N} \{U\}_{N \times 1} = -\{B\}_{N \times 1} \quad (3.90)$$

where $[K]$ represents the stiffness matrix, which contains the PD parameter, the reference length of each bond and the material point's volume as well as the volume and the surface correction factors, the entries of $\{U\} = \{u_{(1)} \ u_{(2)} \ \dots \ u_{(N)}\}^T$ and $\{B\} = \{b_{(1)} \ b_{(2)} \ \dots \ b_{(N)}\}^T$ indicate the components of the displacement and external load vectors, respectively.

Thus, the displacement field can be directly solved by taking inverse of stiffness matrix from Eq. (3.90) as

$$\{U\} = -[K]^{-1} \{B\} \quad (3.91)$$

Overall, the PD solution procedure is more compact and straightforward than classical numerical method. A comparison between PD and finite element method (FEM) solution procedure can be generally described by using flow chart, as shown in Fig. 3.8.

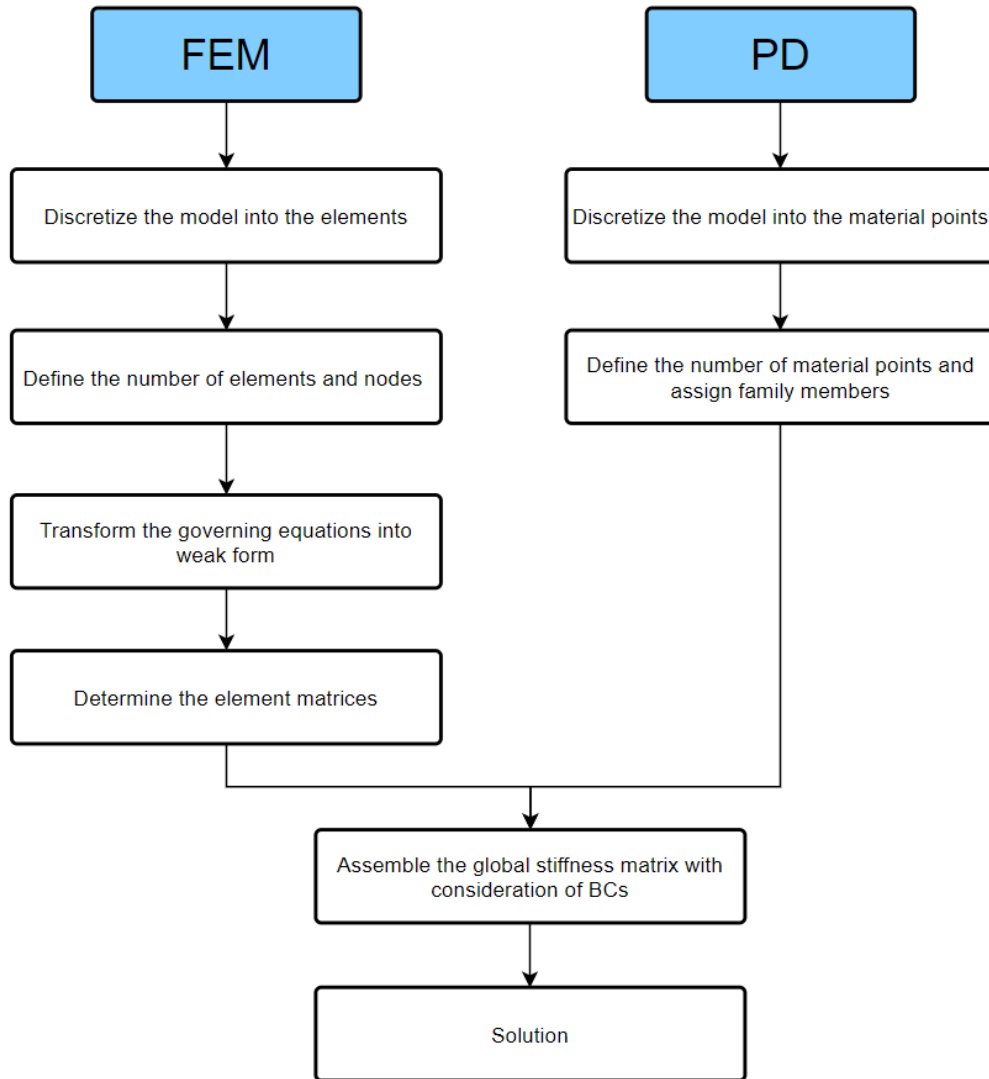


Figure 3.8 FEM and PD numerical solution procedure

As illustrated in Fig. 3.8, PD solution procedure eliminates the need of weak form governing equation transformation and local element matrices determination, which makes it more straightforward and suitable for computational programming.

3.4 Conclusion

In this section, PD EoM for small deformation analyses were re-derived emphatically in section 3.2. In general, PD formulations can be obtained based on analytical mechanics method, and the procedure can summarized as follows:

1. Write down the SED function in classical theory form

2. Transform each local (partial derivative) terms into the corresponding PD terms by using Taylor expansion to obtain the PD SED function
3. Substitute the PD strain energy function into the Lagrange's Equation to obtain the final PD EoM

Moreover, regarding the PD failure criterion, details can be referred to the textbook "Peridynamic theory and its applications" Chapter 6.

PD numerical solution methods with respect to dynamics and static analysis are explained in section 3.3. In this subsection, a 1D clamped – free rod is chosen as an example, and the general idea of the solution procedure can be expanded into more complex structures. Moreover, due to the advantage of directness, PD static solution method (section 3.3.2) has a good consociation ability with programing software, such as Matlab, and.as a consequence, it is widely used in section 4 and 5 for generating numerical results.

4. PD formulation for Beam Theories

In this chapter, PD formulations are developed for various beam theories, as well as functionally graded material beams. Beams with constant cross-section are considered. The equation of motion is developed based on analytical mechanics point of view and with small deformation assumption. Different boundary conditions are considered including pinned support, roller support, clamped and free ends. Validation and accuracy are verified by comparing PD results against finite element analysis results (ANSYS).

4.1 PD Formulations for Timoshenko Beam

4.1.1 Timoshenko Beam Theory

A complete and adequate set of equation for first order shear deformation linear theory of deep beam was developed by Timoshenko, which is also known as Timoshenko beam theory. It is reiterated that a transverse normal to the central axis of the beam in the undeformed state remains straight and no change in length during deformation.

According to the assumptions of the Timoshenko beam theory, the displacement field of any material points at the transverse normal can be represented in terms of the displacement field of the material point at locus of central axis in xz plane as

$$u(x, z, t) = z\theta(x, t) \quad (4.1a)$$

and

$$w(x, z, t) = \bar{w}(x, t) \quad (4.1b)$$

Where, $\theta(x, t)$ and $\bar{w}(x, t)$ denote the rotation and transverse displacement of the material point at central axis, respectively. Thus, the strain-displacement relation can be written as

$$\varepsilon_x = z \frac{\partial \theta}{\partial x} \quad (4.2a)$$

$$\gamma_{xz} = \theta + \frac{\partial \bar{w}}{\partial x} \quad (4.2b)$$

According to the 1D Hooke's Law, the stress function can be written in terms of displacement components as

$$\sigma_x = E\bar{\epsilon} \frac{\partial \theta}{\partial x} \quad (4.3a)$$

$$\tau_{xz} = G \left(\theta + \frac{\partial \bar{w}}{\partial x} \right) \quad (4.3b)$$

The average cross-sectional strain energy density of the beam can be expressed in classical theory as

$$W_{\text{com}} = \frac{1}{2A} \int_A (\sigma \bar{\epsilon} + \kappa \tau \gamma) dA \quad (4.4)$$

where A represents the cross-section and κ is introduced as the shear correction factor, which depends upon the geometry of the cross-section. Substituting Eq.(4.2) and (4.3) into (4.4) gives

$$W_{\text{com}} = \frac{1}{2A} \left[E \left(\frac{\partial \theta}{\partial x} \right)^2 + \kappa GA \left(\theta + \frac{\partial \bar{w}}{\partial x} \right)^2 \right] \quad (4.5)$$

Where I represents the second moment of the cross-section area, which is defined as

$$I = \int_A z^2 dA \quad (4.6)$$

4.1.2 PD EoM for Timoshenko Beam

Assume the system is initially at rest, the PD equations of motion can be derived by utilising Lagrange's equation:

$$\frac{d}{dt} \frac{\partial L}{\partial \dot{\mathbf{u}}_{(k)}} - \frac{\partial L}{\partial \mathbf{u}_{(k)}} = 0 \quad (4.7)$$

where $L = T - U$ is the Lagrangian and \mathbf{u} represents the displacement vector, which is defined in this study as

$$\mathbf{u} = [\theta \quad \bar{w}]^T \quad (4.8)$$

According to the stipulation of the displacement field given in Eqs. (4.1), the total kinetic energy of the beam, T , can be written as

$$T = \frac{1}{2} \int_0^l \int_A \rho (\dot{u}^2 + \dot{w}^2) dA dx = \frac{1}{2} \sum_k \rho_{(k)} \left(\frac{I}{A} \dot{\theta}_{(k)}^2 + \dot{\bar{w}}_{(k)}^2 \right) V_{(k)} \quad (4.9)$$

in which l represents the length of the beam. For a conservative system, since the

potential energy, U , is implicit of time variable, the first terms of the Lagrange's equation can be casted as

$$\frac{d}{dt} \frac{\partial L}{\partial \dot{\mathbf{u}}_{(k)}} = \frac{d}{dt} \frac{\partial T}{\partial \dot{\mathbf{u}}_{(k)}} = \left\{ \begin{array}{c} \rho_{(k)} \frac{l}{A} \ddot{\theta}_{(k)} \\ \rho_{(k)} \ddot{\mathbf{w}}_{(k)} \end{array} \right\} V_{(k)} \quad (4.10)$$

The PD strain energy density function has a non-local form such that the strain energy of a certain material point k depends on both its displacement and all other material points in its family, which can be expressed as

$$W_{(k)}^{PD} = \sum_k W_{(k)}^{PD}(\mathbf{u}_{(k)}, \mathbf{u}_{(1^k)}, \mathbf{u}_{(2^k)}, \mathbf{u}_{(3^k)}, \dots) \quad (4.11)$$

where $\mathbf{u}_{(k)}$ is the displacement vector of material point k and $\mathbf{u}_{(i^k)}$ ($i = 1, 2, 3, \dots$) is the displacement vector of the i th material point within the horizon of the material point k .

The total potential energy stored in the body can be obtained by summing potential energies of all material points including strain energy and energy due to external loads as

$$U = \sum_k W_{(k)}^{PD}(\mathbf{u}_{(k)}, \mathbf{u}_{(1^k)}, \mathbf{u}_{(2^k)}, \mathbf{u}_{(3^k)}, \dots) V_{(k)} - \sum_k \mathbf{b}_{(k)} \mathbf{u}_{(k)} V_{(k)} \quad (4.12)$$

where \mathbf{b} is the body force density vector, which in this study has the following components

$$\mathbf{b} = [b_\theta \quad b_z]^T \quad (4.13)$$

where b_θ and b_z correspond to moments and transverse body loads, respectively.

Recall the pre-proved result, Eq.(3.8), the second term of the Lagrange's equation becomes

$$-\frac{\partial L}{\partial \mathbf{u}_{(k)}} = \frac{\partial W_{(k)}^{PD}}{\partial \mathbf{u}_{(k)}} V_{(k)} + \sum_j \frac{\partial W_{(j)}^{PD}}{\partial \mathbf{u}_{(k)}} V_{(j)} - \mathbf{b}_{(k)} V_{(k)} \quad (4.14)$$

Plugging Eq.(4.10) and (4.14) into the Lagrange's equation arises

$$\begin{Bmatrix} \rho_{(k)} \frac{I}{A} \ddot{\theta}_{(k)} \\ \rho_{(k)} \ddot{\bar{w}}_{(k)} \end{Bmatrix} = - \begin{pmatrix} \frac{\partial W_{(k)}^{PD}}{\partial \theta_{(k)}} + \sum_j \frac{\partial W_{(j)}^{PD}}{\partial \theta_{(k)}} \frac{V_{(j)}}{V_{(k)}} \\ \frac{\partial W_{(k)}^{PD}}{\partial \bar{w}_{(k)}} + \sum_j \frac{\partial W_{(j)}^{PD}}{\partial \bar{w}_{(k)}} \frac{V_{(j)}}{V_{(k)}} \end{pmatrix} + \begin{Bmatrix} b_{\theta}^{(k)} \\ b_z^{(k)} \end{Bmatrix} \quad (4.15)$$

In order to nonlocalize the strain energy density function, Eq.(4.5), at a certain material point k , it is necessary to transform all the differential terms into an equivalent form of integration, and the nonlocalized strain energy density function should be in accordance with the form of PD's assumption, i.e. Eq.(4.11). As derived in Appendix A1.1, the strain energy density function at material point k , and its family member j can be expressed as

$$W_{(k)}^{PD} = \frac{1}{2} \frac{1}{\delta^2 A^2} \left\{ \Theta \sum_i \frac{(\theta_{(i^k)} - \theta_{(k)})^2}{|\xi_{(i^k)(k)}|} V_{(k)} + \kappa GA \sum_i \frac{\left(\bar{w}_{(i^k)} - \bar{w}_{(k)} + \frac{\theta_{(i^k)} + \theta_{(k)}}{2} \xi_{(i^k)(k)} \right)^2}{|\xi_{(i^k)(k)}|} V_{(i^k)} \right\} \quad (4.16a)$$

and

$$W_{(j)}^{PD} = \frac{1}{2} \frac{1}{\delta^2 A^2} \left\{ \Theta \sum_i \frac{(\theta_{(i^j)} - \theta_{(j)})^2}{|\xi_{(i^j)(j)}|} V_{(j)} + \kappa GA \sum_i \frac{\left(\bar{w}_{(i^j)} - \bar{w}_{(j)} + \frac{\theta_{(i^j)} + \theta_{(j)}}{2} \xi_{(i^j)(j)} \right)^2}{|\xi_{(i^j)(j)}|} V_{(i^j)} \right\} \quad (4.16b)$$

Substituting Eq.(4.16a) and (4.16b) into (4.15) and renaming the summation indices, final PD EoM for Timoshenko beam can be written as

$$\rho_{(k)} \frac{I}{A} \ddot{\theta}_{(k)} = c_b \sum_j \frac{\theta_{(j)} - \theta_{(k)}}{|\xi_{(j)(k)}|} V_{(j)} - \frac{1}{2} c_s \sum_j \left(\bar{w}_{(j)} - \bar{w}_{(k)} + \frac{\theta_{(j)} + \theta_{(k)}}{2} \xi_{(j)(k)} \right) \text{sgn}(\xi_{(j)(k)}) V_{(j)} + b_{\theta}^{(k)} \quad (4.17a)$$

and

$$\rho_{(k)} \ddot{\bar{w}}_{(k)} = c_s \sum_j \left[\frac{\bar{w}_{(j)} - \bar{w}_{(k)}}{|\xi_{(j)(k)}|} + \frac{\theta_{(k)} + \theta_{(j)}}{2} \text{sgn}(\xi_{(j)(k)}) \right] V_{(j)} + b_z^{(k)} \quad (4.17b)$$

where c_b and c_s are the PD material parameters associate with bending and transverse shear deformation, respectively, which are defined as

$$c_b = \frac{2\Theta}{\delta^2 A^2} \quad (4.18a)$$

and

$$c_s = \frac{2\kappa G}{\delta^2 A} \quad (4.18b)$$

4.1.3 Numerical Results

In order to validate the current Peridynamic Timoshenko beam formulation, several different benchmark problems were considered for a beam subjected to central loading under simply supported, clamped and mixed (clamped-simply supported) boundary conditions. The implementation of Peridynamics boundary conditions were explained in Appendix B1.1. Peridynamic solutions were compared against finite element analysis results.

4.1.3.1 Simply supported beam subjected to a central point force

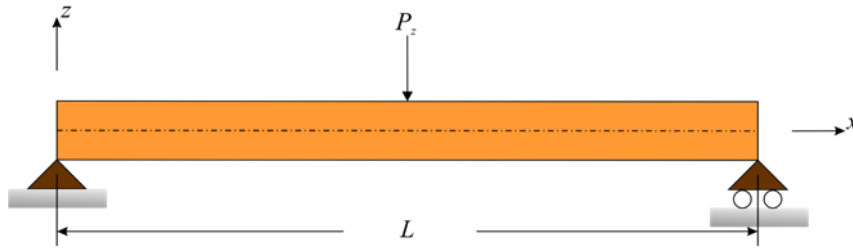


Figure 4.1. Simply supported beam subjected to a central point force.

In the first example case, a Timoshenko beam having 1 m length, 0.05 m width and 0.1 m thickness is considered as shown in Fig. 4.1. The elastic modulus and Poisson's ratio are specified as 200 GPa and 0.3, respectively. The shear correction factor is specified as $\kappa = 5/6$. For spatial discretization, a discretization size of $\Delta = 0.002$ m is utilized. The horizon size is chosen as $\delta = 3\Delta$. The steady-state solution is obtained by using adaptive dynamic relaxation scheme presented in Kilic and Madenci (2010). A point load of $F = 100$ N is applied at the center of the beam which can be convert as a body load density of $b = \frac{F}{\Delta \times A} = \frac{100}{0.002 \times 0.1 \times 0.05} = 10^7$ N/m³. The simply supported boundary conditions were applied by introducing fictitious regions both at the left and right edges. Finite element analysis (FEA) solution was obtained by using ANSYS, a commercial

finite element software. Finite element model was created by using BEAM188 elements with 100 element divisions along the beam central axis.

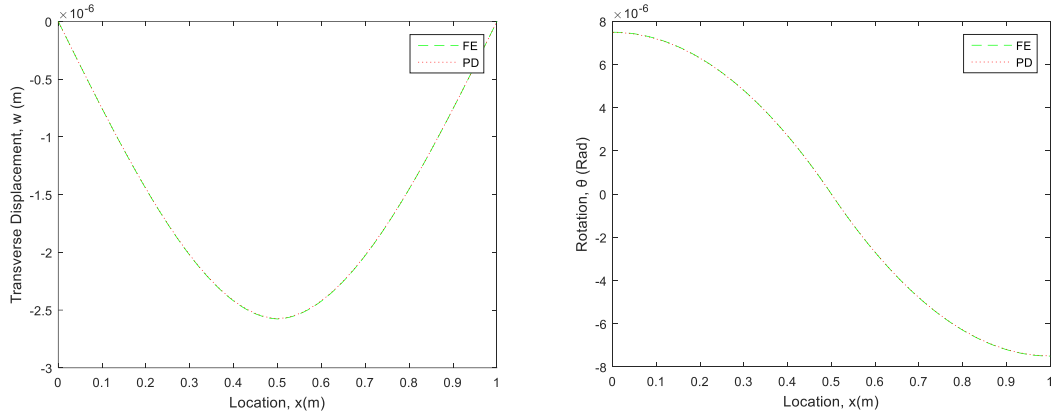


Figure 4.2. Variation of (a) transverse displacement, (b) rotation along the beam

Variation of transverse displacement and rotation along the beam is shown in Fig. 4.2. PD results are compared against FEA results and a very good agreement is observed between the two solutions.

4.1.3.2 Clamped beam subjected to a central point force

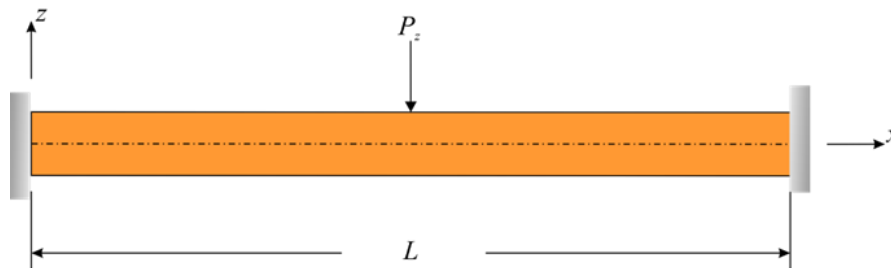


Figure 4.3 Clamped beam subjected to a central point force.

In the second example case, as shown in Fig. 4.3, the simply-supported boundary conditions were replaced with clamped boundary conditions at both right and left edges. Variation of transverse displacement and rotation along the beam is depicted in Fig. 4.4 and a very good agreement was obtained between PD and FEA results.

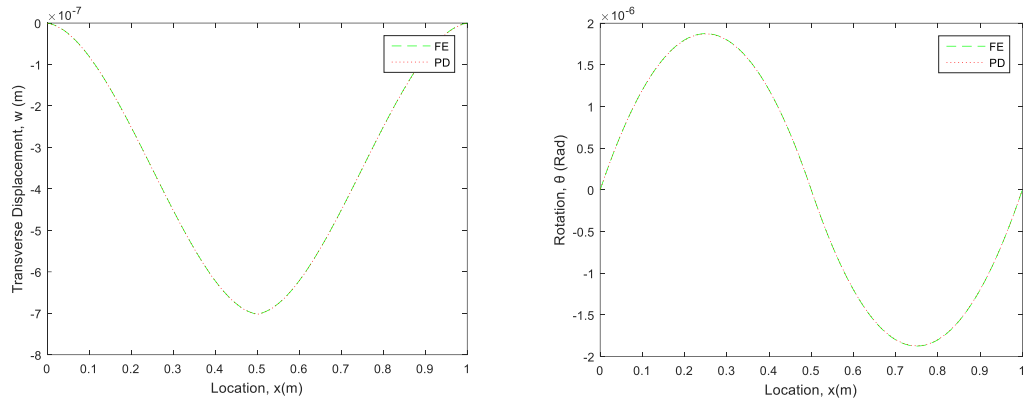


Figure 4.4. Variation of (a) transverse displacement, (b) rotation along the beam

4.1.3.3 Beam subjected to a central point force and mixed boundary conditions

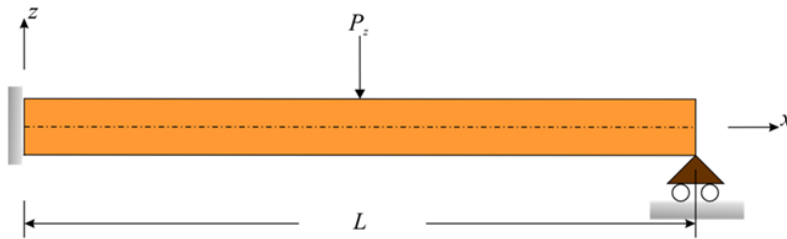


Figure 4.5 Beam subjected to a central point force and mixed boundary conditions.

In the last example case, a mixed boundary condition was considered by assigning clamped boundary condition at the left edge and simply supported boundary condition at the right edge as shown in Fig. 4.5. Variation of transverse displacement and rotation results along the beam was compared between PD and FEA results. As depicted in Fig. 4.6, a very good match was observed between the two approaches.

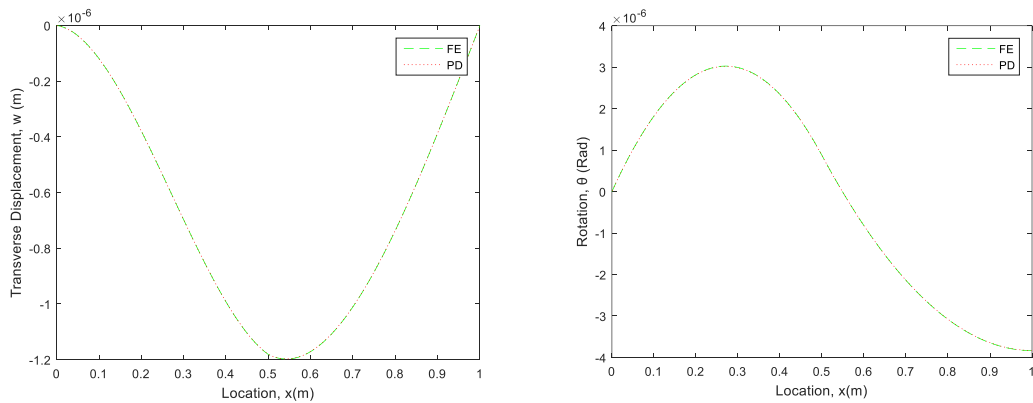


Figure 4.6. Variation of (a) transverse displacement, (b) rotation along the beam

4.2 PD Formulations for Higher Order Deformable Beams

4.2.1 Higher Order Beam Theory

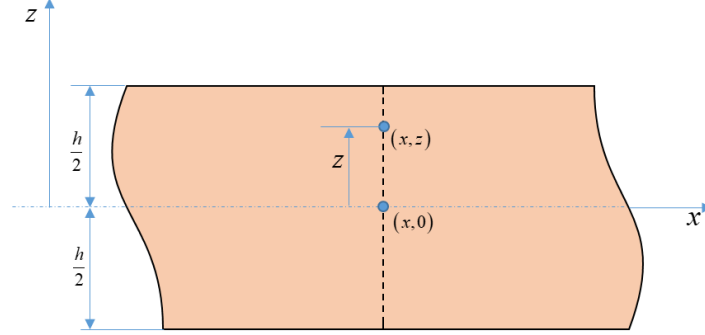


Figure 4.7 Deformation of higher order deformable beam

The displacement field of any material point in a beam can be represented in terms of the displacement field of a material point along the central axis in xz plane by using Taylor expansion as (see Fig. 4.7)

$$u(x, z, t) = u(x, 0, t) + z \left(\frac{\partial u}{\partial z} \right) \Big|_{z=0} + \frac{1}{2} z^2 \left(\frac{\partial^2 u}{\partial z^2} \right) \Big|_{z=0} + \frac{1}{3!} z^3 \left(\frac{\partial^3 u}{\partial z^3} \right) \Big|_{z=0} + \dots \quad (4.19a)$$

and

$$w(x, z, t) = w(x, 0, t) + z \left(\frac{\partial w}{\partial z} \right) \Big|_{z=0} + \frac{1}{2} z^2 \left(\frac{\partial^2 w}{\partial z^2} \right) \Big|_{z=0} + \frac{1}{3!} z^3 \left(\frac{\partial^3 w}{\partial z^3} \right) \Big|_{z=0} + \dots \quad (4.19b)$$

where $u(x, z, t)$ and $w(x, z, t)$ are the displacement components of the material point in x - and z -directions, respectively. In this study, only flexural deformations are taken into consideration. Thus, eliminating axial deformation effects and higher order terms in Eq.(4.19), the components of the displacement field can be expressed as

$$u(x, z, t) = z\alpha(x, t) + z^3\theta^*(x, t) \quad (4.20a)$$

and

$$w(x, z, t) = \bar{w}(x, t) + z^2\bar{w}^*(x, t) \quad (4.20b)$$

where \bar{w} represent the transverse displacement of the material point along neutral axis, and θ , θ^* and \bar{w}^* are arisen out of the Taylor series expansion and introduced as three new independent variables which are defined respectively as (see Fig.4.8)

$$\alpha(x, t) = \left. \frac{\partial u}{\partial x} \right|_{z=0} \quad (4.21a)$$

$$\theta'(x, t) = \frac{1}{3!} \frac{\partial^3 u}{\partial z^3} \Big|_{z=0} \quad (4.21b)$$

$$\dot{w}(x, t) = \frac{1}{2} \frac{\partial^2 w}{\partial z^2} \Big|_{z=0} \quad (4.21c)$$

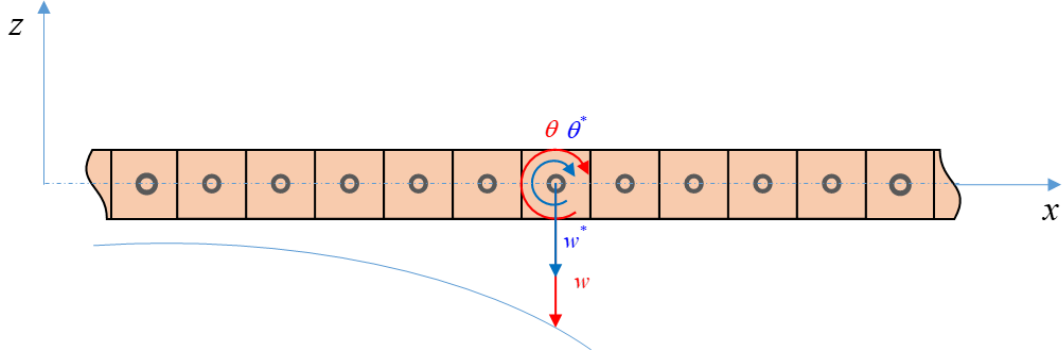


Figure 4.8 Degrees-of-freedom per node used in higher-order beam theory.

In order to simplify the expressions, hereafter $\bar{w}(x, t)$, $\theta(x, 0)$, $\dot{w}(x, 0)$ and $\theta'(x, 0)$ will be written simply as \bar{w} , θ , \dot{w} and θ' , respectively. Utilising the expressions given in Eqs. (4.20) for the displacement components, the three well-known strain-displacement relationships of the plane stress elasticity can be written as

$$\varepsilon_{xx} = z \frac{\partial \theta}{\partial x} + z^3 \frac{\partial \theta'}{\partial x} \quad (4.22a)$$

$$\varepsilon_{zz} = 2z\dot{w} \quad (4.22b)$$

$$\gamma_{xz} = \theta + \frac{\partial \bar{w}}{\partial x} + 3z^2\theta' + z^2 \frac{\partial \dot{w}}{\partial x} \quad (4.22c)$$

Note that the strain-displacement relationships given in Eqs. (4.22) are much more realistic with respect to Timoshenko beam theory where the axial normal strain, ε_{xx} and transverse shear strain, γ_{xz} vary linearly in the thickness direction and the transverse normal strain, ε_{zz} is equivalent to zero. This also eliminates the need for the introduction of shear correction factor which is widely used in Timoshenko beam analysis.

Assuming the material is isotropic and plane-stress condition is applicable, the stress-strain relationships can be expressed as

$$\begin{Bmatrix} \sigma_{xx} \\ \sigma_{zz} \\ \tau_{xz} \end{Bmatrix} = \frac{E}{1-\nu^2} \begin{bmatrix} 1 & \nu & 0 \\ \nu & 1 & 0 \\ 0 & 0 & \frac{1-\nu}{2} \end{bmatrix} \begin{Bmatrix} \varepsilon_{xx} \\ \varepsilon_{zz} \\ \gamma_{xz} \end{Bmatrix} \quad (4.23)$$

where E and ν represent elastic modulus and Poisson's ratio, respectively. Substituting Eqs. (4.22) into Eq. (4.23) yields

$$\sigma_{xx} = \frac{Ez}{1-\nu^2} \left(\frac{\partial \theta}{\partial x} + 2\nu \dot{w} \right) + \frac{E}{1-\nu^2} z^3 \frac{\partial \theta'}{\partial x} \quad (4.24a)$$

$$\sigma_{zz} = \frac{Ez}{1-\nu^2} \left(\nu \frac{\partial \theta}{\partial x} + 2\dot{w} \right) + \frac{E}{1-\nu^2} z^3 \left(\nu \frac{\partial \theta'}{\partial x} \right) \quad (4.24b)$$

$$\tau_{xz} = G \left(\theta + \frac{\partial \bar{w}}{\partial x} \right) + Gz^2 \left(3\theta' + \frac{\partial \dot{w}}{\partial x} \right) \quad (4.24c)$$

According to the classical continuum mechanics theory, the average cross-sectional strain energy density can then be casted as

$$W_{\text{com}} = \frac{1}{2A} \int_A (\sigma_{xx} \varepsilon_{xx} + \sigma_{zz} \varepsilon_{zz} + \tau_{xz} \gamma_{xz}) dA \quad (4.25)$$

where A represents the cross-section the beam.

Substituting Eqs. (4.22) and (4.24) into Eq. (4.25) results in

$$W_{\text{com}} = \frac{1}{2A} \left\{ \begin{aligned} & \frac{E}{1-\nu^2} \left[I \left(\left(\frac{\partial \theta}{\partial x} + 2\dot{w} \right)^2 - 4(1-\nu) \dot{w} \frac{\partial \theta}{\partial x} \right) + 2I^* \frac{\partial \theta'}{\partial x} \left(\frac{\partial \theta}{\partial x} + 2\nu \dot{w} \right) + I^{**} \left(\frac{\partial \theta'}{\partial x} \right)^2 \right] \\ & + G \left[A \left(\theta + \frac{\partial \bar{w}}{\partial x} \right)^2 + 2I \left(\theta + \frac{\partial \bar{w}}{\partial x} \right) \left(3\theta' + \frac{\partial \dot{w}}{\partial x} \right) + I^* \left(3\theta' + \frac{\partial \dot{w}}{\partial x} \right)^2 \right] \end{aligned} \right\} \quad (4.26)$$

where I represents the second moment of cross-section area, and I^* and I^{**} represent the higher order moments of cross-section area, which are defined respectively as

$$I = \int_A z^2 dA \quad (4.27a)$$

$$I^* = \int_A z^4 dA \quad (4.27b)$$

$$I^{**} = \int_A z^6 dA \quad (4.27c)$$

4.2.2 PD Formulations for Higher Order Beam

The PD equation of motion can be obtained by using Euler-Lagrange equation as

$$\frac{d}{dt} \frac{\partial L}{\partial \dot{\mathbf{u}}_{(k)}} - \frac{\partial L}{\partial \mathbf{u}_{(k)}} = 0 \quad (4.28)$$

where $\mathbf{u} = [\theta \ \theta' \ \bar{w} \ \bar{w}']^T$ represent the displacement vector and $L = T - U$ is the Lagrangian. The kinetic energy per unit length of the beam, \bar{T} , can be expressed as

$$\bar{T} = \frac{1}{2} \int_A \rho (\dot{u}^2 + \dot{w}^2) dA \quad (4.29)$$

Substituting Eqs.(4.20) into (4.29) results in

$$\begin{aligned} \bar{T} &= \frac{1}{2} \int_A \rho \left[\dot{\bar{w}}^2 + z^2 (\dot{\theta}^2 + 2\dot{\bar{w}}\dot{\theta}') + z^4 (2\dot{\theta}\dot{\theta}' + (\dot{w}')^2) + z^6 (\dot{\theta}')^2 \right] dA \\ &= \frac{1}{2} \rho \left[A\dot{\bar{w}}^2 + I (\dot{\theta}^2 + 2\dot{\bar{w}}\dot{\theta}') + I' (2\dot{\theta}\dot{\theta}' + (\dot{w}')^2) + I'' (\dot{\theta}')^2 \right] \end{aligned} \quad (4.30)$$

The total kinetic energy of the system can be expressed as

$$T = \int_0^L \bar{T} dx \quad (4.31)$$

which can be discretized as

$$T = \sum_k \frac{1}{2} \rho_{(k)} \left[\dot{\bar{w}}_{(k)}^2 + \frac{I}{A} (\dot{\theta}_{(k)}^2 + 2\dot{\bar{w}}_{(k)}\dot{\theta}'_{(k)}) + \frac{I'}{A} (2\dot{\theta}_{(k)}\dot{\theta}'_{(k)} + (\dot{w}'_{(k)})^2) + \frac{I''}{A} (\dot{\theta}'_{(k)})^2 \right] V_{(k)} \quad (4.32)$$

For a conservative system, since the potential energy, U , is implicit of time variable, the first terms of the Lagrange's equation can be casted as

$$\frac{d}{dt} \frac{\partial L}{\partial \dot{\mathbf{u}}_{(k)}} = \frac{d}{dt} \frac{\partial T}{\partial \dot{\mathbf{u}}_{(k)}} = \rho_{(k)} \left\{ \begin{array}{l} \frac{I}{A} \ddot{\theta}_{(k)} + \frac{I'}{A} \ddot{\theta}'_{(k)} \\ \frac{I''}{A} \ddot{\theta}'_{(k)} + \frac{I'}{A} \ddot{\theta}_{(k)} \\ \ddot{\bar{w}}_{(k)} + \frac{I}{A} \ddot{\theta}'_{(k)} \\ \frac{I'}{A} \ddot{\theta}'_{(k)} + \frac{I}{A} \ddot{\bar{w}}_{(k)} \end{array} \right\} V_{(k)} \quad (4.33)$$

Utilizing the pre-obtained result, Eq.(3.8), the second term of the Lagrange's equation becomes

$$-\frac{\partial L}{\partial \mathbf{u}_{(k)}} = \frac{\partial W_{(k)}^{FD}}{\partial \mathbf{u}_{(k)}} V_{(k)} + \sum_j \frac{\partial W_{(j)}^{FD}}{\partial \mathbf{u}_{(k)}} V_{(j)} - \mathbf{b}_{(k)} V_{(k)} \quad (4.34)$$

where body force density vector, \mathbf{b} , has the following entries in this study as

$$\mathbf{b} = [b_\theta \ 0 \ b_z \ 0]^T \quad (4.35)$$

where b_θ and b_z correspond to the loading density of bending moment and transverse force, respectively.

Inserting Eq.(4.32) and (4.34) into (4.28) results in the Lagrange's equation as

$$\rho_{(k)} \begin{Bmatrix} \frac{I}{A} \ddot{\theta}_{(k)} + \frac{I^*}{A} \ddot{\theta}_{(k)}^* \\ \frac{I^{**}}{A} \ddot{\theta}_{(k)}^* + \frac{I^*}{A} \ddot{\theta}_{(k)} \\ \ddot{w}_{(k)} + \frac{I}{A} \ddot{w}_{(k)}^* \\ \frac{I^*}{A} \ddot{w}_{(k)}^* + \frac{I}{A} \ddot{w}_{(k)} \end{Bmatrix} V_{(k)} = - \begin{pmatrix} \frac{\partial W_{(k)}^{PD}}{\partial \theta_{(k)}} V_{(k)} + \sum_j \frac{\partial W_{(j)}^{PD}}{\partial \theta_{(k)}} V_{(j)} \\ \frac{\partial W_{(k)}^{PD}}{\partial \theta_{(k)}^*} V_{(k)} + \sum_j \frac{\partial W_{(j)}^{PD}}{\partial \theta_{(k)}^*} V_{(j)} \\ \frac{\partial W_{(k)}^{PD}}{\partial w_{(k)}} V_{(k)} + \sum_j \frac{\partial W_{(j)}^{PD}}{\partial w_{(k)}} V_{(j)} \\ \frac{\partial W_{(k)}^{PD}}{\partial w_{(k)}^*} V_{(k)} + \sum_j \frac{\partial W_{(j)}^{PD}}{\partial w_{(k)}^*} V_{(j)} \end{pmatrix} + \begin{Bmatrix} b_{\theta}^{(k)} \\ 0 \\ 0 \\ b_z^{(k)} \end{Bmatrix} V_{(k)} \quad (4.36)$$

As explained in Appendix A1.2, the PD SED function material point k and its family member material point j can be written as

$$W_{PD}^{(k)} = \frac{1}{2\delta^2 A^2} \left\{ \begin{array}{l} \frac{E}{1-\nu^2} \left[I \sum_{i^k} \frac{(\theta_{(i^k)} - \theta_{(k)})^2 + 2\nu(\dot{w}_{(i^k)}^* + \dot{w}_{(k)}^*) (\theta_{(i^k)} - \theta_{(k)}) \xi_{(i^k)(k)} + (\dot{w}_{(i^k)}^* + \dot{w}_{(k)}^*)^2 \xi_{(i^k)(k)}^2}{|\xi_{(i^k)(k)}|} V_{(i^k)} + \right. \\ \left. 2I^* \sum_{i^k} \frac{[\theta_{(i^k)} - \theta_{(k)} + \nu(\dot{w}_{(i^k)}^* + \dot{w}_{(k)}^*) \xi_{(i^k)(k)}] (\theta_{(i^k)}^* - \theta_{(k)}^*)}{|\xi_{(i^k)(k)}|} V_{(i^k)} + I^{**} \sum_{i^k} \frac{(\theta_{(i^k)}^* - \theta_{(k)}^*)^2}{|\xi_{(i^k)(k)}|} V_{(i^k)} \right] + \\ G \left[A \sum_{i^k} \frac{1}{|\xi_{(i^k)(k)}|} \left(\bar{w}_{(i^k)} - \bar{w}_{(k)} + \frac{\theta_{(i^k)} + \theta_{(k)}}{2} \xi_{(i^k)(k)} \right)^2 V_{(i^k)} + I^* \sum_{i^k} \frac{1}{|\xi_{(i^k)(k)}|} \left(\dot{w}_{(i^k)}^* - \dot{w}_{(k)}^* + 3 \frac{\theta_{(i^k)}^* + \theta_{(k)}^*}{2} \xi_{(i^k)(k)} \right)^2 V_{(i^k)} \right. \\ \left. 2I \sum_{i^k} \frac{1}{|\xi_{(i^k)(k)}|} \left(\bar{w}_{(i^k)} - \bar{w}_{(k)} + \frac{\theta_{(i^k)} + \theta_{(k)}}{2} \xi_{(i^k)(k)} \right) \left(\dot{w}_{(i^k)}^* - \dot{w}_{(k)}^* + 3 \frac{\theta_{(i^k)}^* + \theta_{(k)}^*}{2} \xi_{(i^k)(k)} \right) V_{(i^k)} \right] \end{array} \right\} \quad (4.37a)$$

$$W_{PD}^{(j)} = \frac{1}{2\delta^2 A^2} \left\{ \begin{array}{l} \frac{E}{1-\nu^2} \left[I \sum_{i^j} \frac{(\theta_{(i^j)} - \theta_{(j)})^2 + 2\nu(\dot{w}_{(i^j)}^* + \dot{w}_{(j)}^*) (\theta_{(i^j)} - \theta_{(j)}) \xi_{(i^j)(j)} + (\dot{w}_{(i^j)}^* + \dot{w}_{(j)}^*)^2 \xi_{(i^j)(j)}^2}{|\xi_{(i^j)(j)}|} V_{(i^j)} + \right. \\ \left. 2I^* \sum_{i^j} \frac{[\theta_{(i^j)} - \theta_{(j)} + \nu(\dot{w}_{(i^j)}^* + \dot{w}_{(j)}^*) \xi_{(i^j)(j)}] (\theta_{(i^j)}^* - \theta_{(j)}^*)}{|\xi_{(i^j)(j)}|} V_{(i^j)} + I^{**} \sum_{i^j} \frac{(\theta_{(i^j)}^* - \theta_{(j)}^*)^2}{|\xi_{(i^j)(j)}|} V_{(i^j)} \right] + \\ G \left[A \sum_{i^j} \frac{1}{|\xi_{(i^j)(j)}|} \left(\bar{w}_{(i^j)} - \bar{w}_{(j)} + \frac{\theta_{(i^j)} + \theta_{(j)}}{2} \xi_{(i^j)(j)} \right)^2 V_{(i^j)} + I^* \sum_{i^j} \frac{1}{|\xi_{(i^j)(j)}|} \left(\dot{w}_{(i^j)}^* - \dot{w}_{(j)}^* + 3 \frac{\theta_{(i^j)}^* + \theta_{(j)}^*}{2} \xi_{(i^j)(j)} \right)^2 V_{(i^j)} \right. \\ \left. 2I \sum_{i^j} \frac{1}{|\xi_{(i^j)(j)}|} \left(\bar{w}_{(i^j)} - \bar{w}_{(j)} + \frac{\theta_{(i^j)} + \theta_{(j)}}{2} \xi_{(i^j)(j)} \right) \left(\dot{w}_{(i^j)}^* - \dot{w}_{(j)}^* + 3 \frac{\theta_{(i^j)}^* + \theta_{(j)}^*}{2} \xi_{(i^j)(j)} \right) V_{(i^j)} \right] \end{array} \right\} \quad (4.37b)$$

Substituting Eqs.(4.37) into (4.36) arises the final PD EoM for higher order deformable beams as

$$\begin{aligned}
& \rho_{(k)} \left(\frac{I}{A} \ddot{\theta}_{(k)} + \frac{I \cdot}{A} \ddot{\theta}_{(k)}^* \right) \\
&= \frac{E}{1-\nu^2} \frac{2}{\delta^2 A^2} \left[I \sum_j \left(\frac{(\theta_{(j)} - \theta_{(k)})}{|\xi_{(j)(k)}|} + \nu (\dot{w}_{(k)} + \dot{w}_{(j)}) \operatorname{sgn}(\xi_{(j)(k)}) \right) V_{(j)} + I \cdot \sum_j \frac{(\theta_{(j)}^* - \theta_{(k)}^*)}{|\xi_{(j)(k)}|} V_{(j)} \right] \\
&- \frac{G}{\delta^2 A} \left\{ \sum_j \left[(\bar{w}_{(j)} - \bar{w}_{(k)}) \operatorname{sgn}(\xi_{(j)(k)}) + \frac{\theta_{(j)} + \theta_{(k)}}{2} |\xi_{(j)(k)}| \right] V_{(j)} \right. \\
&\quad \left. + \frac{I}{A} \sum_j \left[(\dot{w}_{(j)} - \dot{w}_{(k)}) \operatorname{sgn}(\xi_{(j)(k)}) + 3 \frac{\theta_{(j)}^* + \theta_{(k)}^*}{2} |\xi_{(j)(k)}| \right] V_{(j)} \right\} + \mathbf{d}_{\theta}^{(k)}
\end{aligned} \tag{4.38a}$$

$$\begin{aligned}
& \rho_{(k)} \left(\frac{I \cdot \cdot}{A} \ddot{\theta}_{(k)} + \frac{I \cdot}{A} \ddot{\theta}_{(k)}^* \right) \\
&= \frac{E}{1-\nu^2} \frac{2}{\delta^2 A^2} \left[I \cdot \sum_j \left(\frac{(\theta_{(j)} - \theta_{(k)})}{|\xi_{(j)(k)}|} + \nu (\dot{w}_{(k)} + \dot{w}_{(j)}) \operatorname{sgn}(\xi_{(j)(k)}) \right) V_{(j)} + I \cdot \cdot \sum_j \frac{(\theta_{(j)}^* - \theta_{(k)}^*)}{|\xi_{(j)(k)}|} V_{(j)} \right] \\
&- \frac{3G}{\delta^2 A^2} \left\{ I \sum_j \left[(\bar{w}_{(j)} - \bar{w}_{(k)}) \operatorname{sgn}(\xi_{(j)(k)}) + \frac{\theta_{(j)} + \theta_{(k)}}{2} |\xi_{(j)(k)}| \right] V_{(j)} \right. \\
&\quad \left. + I \cdot \sum_j \left[(\dot{w}_{(j)} - \dot{w}_{(k)}) \operatorname{sgn}(\xi_{(j)(k)}) + 3 \frac{\theta_{(j)}^* + \theta_{(k)}^*}{2} |\xi_{(j)(k)}| \right] V_{(j)} \right\}
\end{aligned} \tag{4.38b}$$

$$\rho_{(k)} \left(\dot{w}_{(k)} + \frac{I}{A} \dot{w}_{(k)}^* \right) = \frac{2G}{\delta^2 A} \left\{ \sum_j \left[\frac{(\bar{w}_{(j)} - \bar{w}_{(k)})}{|\xi_{(j)(k)}|} + \frac{(\theta_{(k)} + \theta_{(j)})}{2} \operatorname{sgn}(\xi_{(j)(k)}) \right] V_{(j)} \right. \\
\left. + \frac{I}{A} \sum_j \left[\frac{(\dot{w}_{(j)} - \dot{w}_{(k)})}{|\xi_{(j)(k)}|} + 3 \frac{(\theta_{(k)}^* + \theta_{(j)}^*)}{2} \operatorname{sgn}(\xi_{(j)(k)}) \right] V_{(j)} \right\} + \mathbf{d}_z^{(k)} \tag{4.38c}$$

and

$$\begin{aligned}
\rho_{(k)} \left(\frac{I}{A} \ddot{w}_{(k)} + \frac{I \cdot}{A} \ddot{w}_{(k)}^* \right) &= -\frac{E}{1-\nu^2} \frac{2}{\delta^2 A^2} \left[I \sum_j \left(\nu (\theta_{(j)} - \theta_{(k)}) \operatorname{sgn}(\xi_{(j)(k)}) + (\dot{w}_{(j)} + \dot{w}_{(k)}) |\xi_{(j)(k)}| \right) V_{(j)} \right. \\
&\quad \left. + I \cdot \sum_j \nu (\theta_{(j)}^* - \theta_{(k)}^*) \operatorname{sgn}(\xi_{(j)(k)}) V_{(j)} \right] \\
&+ \frac{2G}{\delta^2 A^2} \left\{ I \sum_j \left[\frac{(\bar{w}_{(j)} - \bar{w}_{(k)})}{|\xi_{(j)(k)}|} + \frac{\theta_{(k)} + \theta_{(j)}}{2} \operatorname{sgn}(\xi_{(j)(k)}) \right] V_{(j)} \right. \\
&\quad \left. + I \cdot \sum_j \left[\frac{(\dot{w}_{(j)} - \dot{w}_{(k)})}{|\xi_{(j)(k)}|} + \frac{3}{2} (\theta_{(k)}^* + \theta_{(j)}^*) \operatorname{sgn}(\xi_{(j)(k)}) \right] V_{(j)} \right\}
\end{aligned} \tag{4.38d}$$

4.2.3 Numerical Results

In this section, several different numerical examples are considered to demonstrate the capability of the current PD formulation. A rectangular cross sectional beam with a

length of 1m, a thickness of 0.2m and a width of 0.005m is considered. The material properties of the beam are specified as elastic modulus of 200 GPa and Poisson's ratio of 1/3. PD model is obtained by using discretisation size of $\Delta x=1/1000\text{m}$. The horizon size is chosen as $\delta=3.015\Delta x$. The boundary conditions are applied through a fictitious region as explained in Appendix B1.2 with a size of $3\Delta x$. All example problems are static problems and the numerical solution is obtained by directly assigning inertia terms in equations of motion given in Eqs. (4.38) to 0 and solving a matrix system of equations. The solution procedure can be referred to Section 3.3 analogically. PD results are compared against FEM results generated using ANSYS, a commercial finite element software. PLANE182 element type is utilised by creating 100 elements along the beam with 8 elements along the thickness direction.

4.2.3.1 Simply supported beam with distributed load

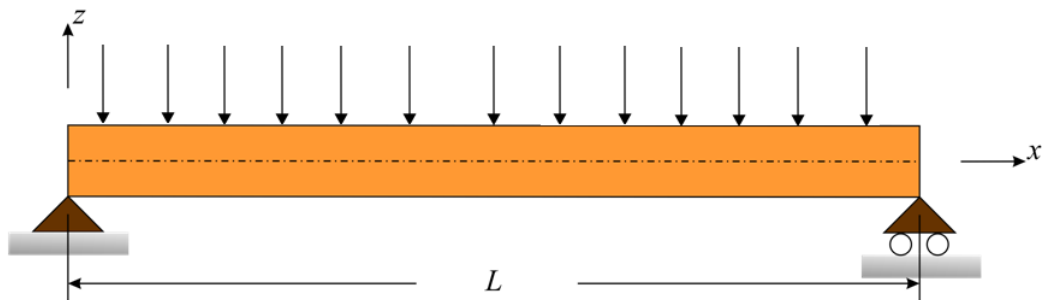


Figure 4.9 Simply supported beam subjected to distributed loading

In the first example, a simply supported beam subjected to a distributed loading of 100 N/m is considered as shown in Fig. 4.9. Regarding the PD model, the distributed loading can be converted into a body force density of $b_z = \frac{100 \times 1}{1000 \times 0.2 \times 0.05 \times 1/1000} = 10^5 \text{N/m}^3$ and acted on each material points of the beam. Comparison of transverse displacements obtained from PD and FEM analyses are depicted in Fig. 4.10 and a very good agreement is observed between the two approaches.

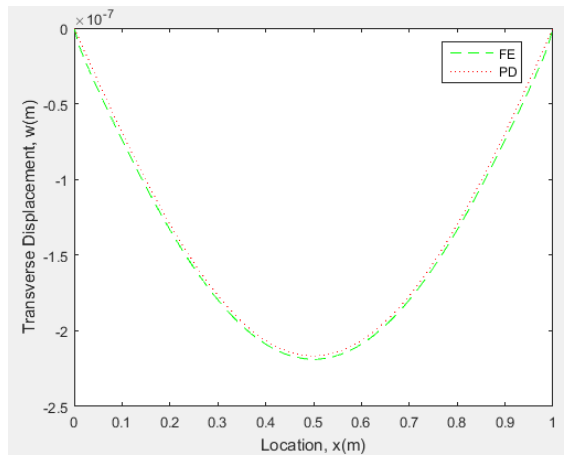


Figure 4.10 Variation of transverse displacements along the beam

4.2.3.2 Simply supported beam with concentrated load

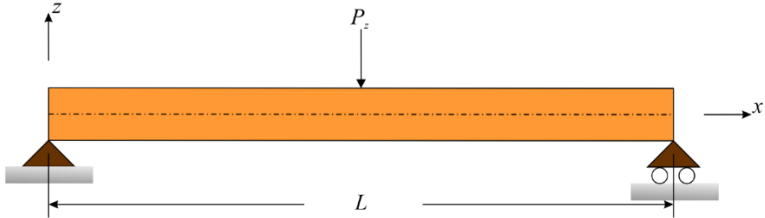


Figure 4.11 Simply supported beam subjected to concentrated load.

In the second example, the simply supported beam considered in the previous example is subjected to a concentrated load of $P_z = 100 \text{ N}$, which can be converted into body force density of $b_z = 10^7 \text{ N/m}^3$ acting at the center of the beam as shown in Fig. 4.11. Based on the comparison given in Fig. 4.12, PD results agree very well with FEM results.

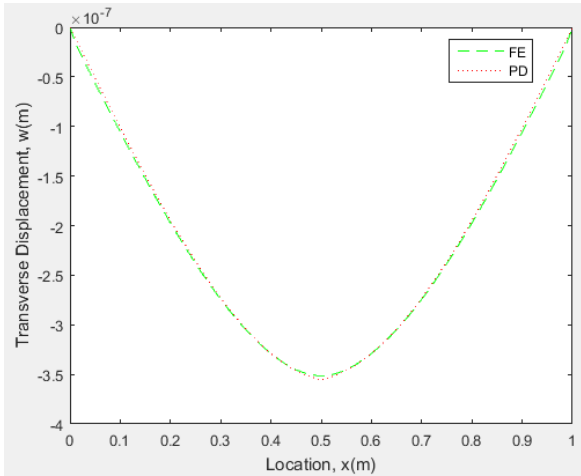


Figure 4.12 Variation of transverse displacements along the beam

4.2.3.3 Clamped-Clamped beam with distributed load

In the third example, the simply supported beam subjected to distributed loading considered in the first example case is subjected clamped-clamped boundary conditions as shown in Fig. 4.13. The distributed load is specified as 100N/m.

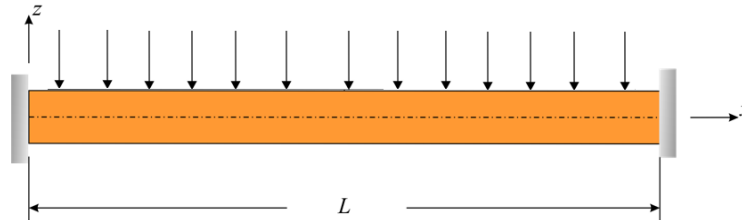


Figure 4.13 Clamped-clamped beam subjected to distributed loading

As demonstrated in Fig. 4.14, a very good agreement is observed between PD and FEM results in terms of transverse displacements.

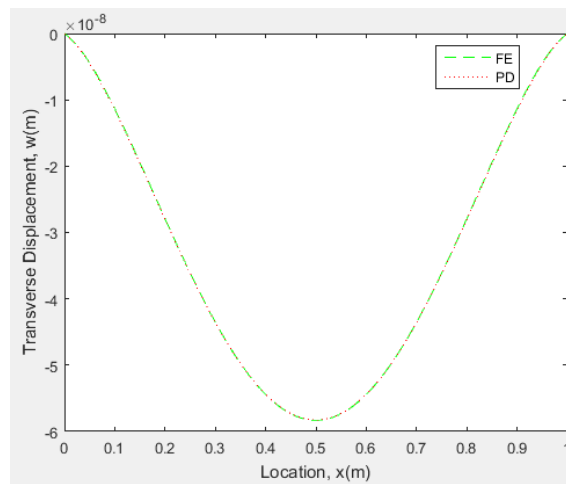


Figure 4.14 Variation of transverse displacements along the beam

4.2.3.4 Cantilever beam subjected to a point load at its free end

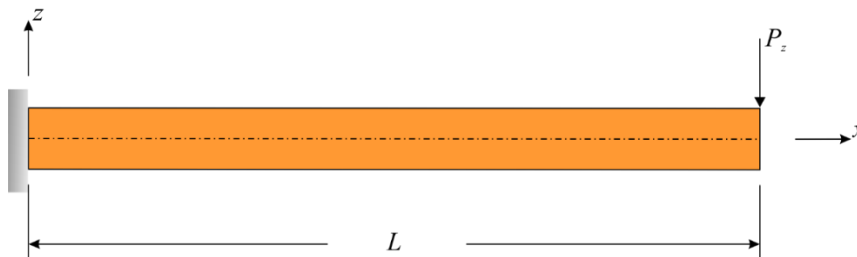


Figure 4.15 Cantilever beam subjected to a point load at its free end

In the fourth example case, a cantilever beam is considered as shown in Fig. 4.15. The beam is subjected to a point load of $P_z = 100$ N at its free end. As depicted in Fig. 4.16, PD results agree very well with FEM results.

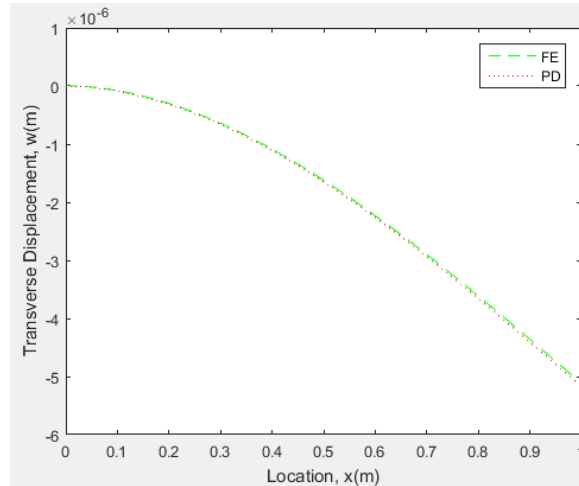


Figure 4.16 Variation of transverse displacements along the beam

4.2.3.5 Cantilever beam subjected to a moment at its free end

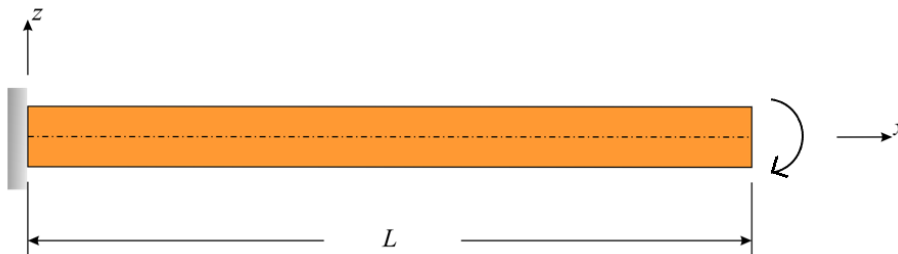


Figure 4.17 Cantilever beam subjected to a moment at its free end

In the final example case, the cantilever beam is subjected to a moment of 100 Nm at its free end as shown in Fig. 4.17. The moment loading is applied through a body load of $b_\theta = 10^7$ N m³ acting on a single material point at the right edge. As depicted in Fig. 4.18, there is a very good agreement between PD and FEM results for the transverse displacement along the beam.

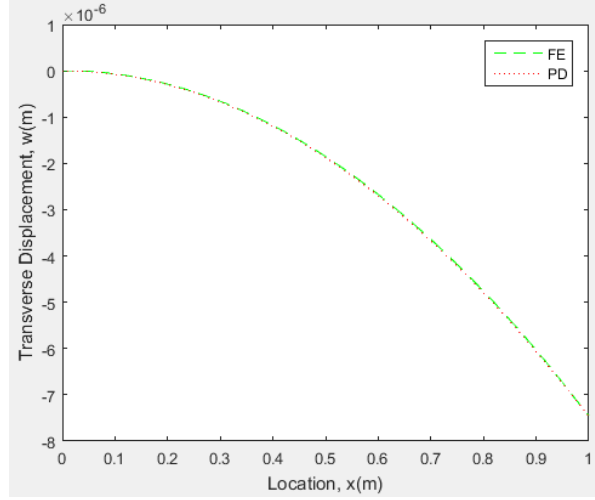


Figure 4.18 Variation of transverse displacements along the beam

4.3 PD Formulations for Transversely FGM Euler Beams

4.3.1 Euler-Bernoulli Beam Theory for FGM

A complete and adequate set of equation for linear theory of thin beams was developed by Euler and Bernoulli, which is also known as Euler-Bernoulli beam theory. According to Euler-Bernoulli beam theory, a transverse normal to the central axis of the beam in the undeformed state remains straight, normal to the central axis and its length doesn't change during deformation. Based on the assumptions of the Euler-Bernoulli beam theory, with considering axial deformation, the displacement field of any material point can be represented in terms of the displacement field of the material points along the central axis in xz plane as

$$u(x, z, t) = \bar{u}(x, t) + z\theta(x, t) \quad (4.39a)$$

$$w(x, z, t) = \bar{w}(x, t) \quad (4.39b)$$

where \bar{u} , \bar{w} and θ represent the axial displacement, transverse displacement and rotational displacement of the material points along neutral axis, respectively. Hereafter, $\bar{u}(x, t)$ and $\bar{w}(x, t)$ will be written as \bar{u} and \bar{w} , respectively, for compaction.

The strain-displacement relations can be written as

$$\varepsilon = \frac{\partial \bar{u}}{\partial x} + z \frac{\partial \theta}{\partial x} \quad (4.40a)$$

$$\gamma = \theta + \frac{\partial \bar{w}}{\partial x} = 0 \quad (4.40b)$$

Eliminating θ , the strain component can be expressed in terms of two independent displacement variables as

$$\varepsilon = \frac{\partial \bar{u}}{\partial x} - z \frac{\partial^2 \bar{w}}{\partial x^2} \quad (4.41)$$

According to the 1D Hooke's Law, the stress can be expressed as

$$\sigma = E(z)\varepsilon = E(z) \left(\frac{\partial \bar{u}}{\partial x} - z \frac{\partial^2 \bar{w}}{\partial x^2} \right) \quad (4.42)$$

where E represents Young's modulus which is a function of z-coordinate.

The average cross-sectional strain energy density of the beam can be expressed as

$$W_{\text{com}} = \frac{1}{2A} \int_A \sigma \varepsilon dA \quad (4.43)$$

Inserting Eq.(4.41) and (4.42) into (4.43) arises

$$W_{\text{com}} = \frac{1}{2A} \int_A E(z) \left[\left(\frac{\partial \bar{u}}{\partial x} \right)^2 - 2z \frac{\partial \bar{u}}{\partial x} \frac{\partial^2 \bar{w}}{\partial x^2} + z^2 \left(\frac{\partial^2 \bar{w}}{\partial x^2} \right)^2 \right] dA \quad (4.44)$$

4.3.2 PD Theory for FGM Euler-Bernoulli Beam

The PD EoM can be obtained by solving the Lagrange's Equation

$$\frac{d}{dt} \frac{\partial L}{\partial \dot{\mathbf{u}}_{(k)}} - \frac{\partial L}{\partial \mathbf{u}_{(k)}} = 0 \quad (4.45)$$

The displacement vector, \mathbf{u} , in this study contains the entries as following

$$\mathbf{u} = [\bar{u} \quad \bar{w}]^T \quad (4.46)$$

The total kinetic energy of the beam, T , can be written as

$$T = \frac{1}{2} \sum_k \rho_{(k)} \left(\dot{\bar{u}}_{(k)}^2 + \dot{\bar{w}}_{(k)}^2 \right) V_{(k)} \quad (4.47)$$

For a conservative system, since the potential energy, U , is implicit of time variable, the first terms of the Lagrange's equation can be casted as

$$\frac{d}{dt} \frac{\partial L}{\partial \dot{\mathbf{u}}_{(k)}} = \frac{d}{dt} \frac{\partial T}{\partial \dot{\mathbf{u}}_{(k)}} = \rho_{(k)} \left\{ \begin{array}{l} \ddot{\bar{u}}_{(k)} \\ \ddot{\bar{w}}_{(k)} \end{array} \right\} V_{(k)} \quad (4.48)$$

Recall Eq.(3.8), the second term of the Lagrange's equation under PD assumption can

be expressed as

$$-\frac{\partial L}{\partial \mathbf{u}_{(k)}} = \frac{\partial W_{(k)}^{PD}}{\partial \mathbf{u}_{(k)}} \mathbf{V}_{(k)} + \sum_j \frac{\partial W_{(j)}^{PD}}{\partial \mathbf{u}_{(k)}} \mathbf{V}_{(j)} - \mathbf{b}_{(k)} \mathbf{V}_{(k)} \quad (4.49)$$

where \mathbf{b} represents the body force density vector, which contains the following entries in this study

$$\mathbf{b} = [b_x \quad b_z]$$

Plugging Eq.(4.48) and (4.49) into the Lagrange's equation arises

$$\rho_{(k)} \begin{Bmatrix} \ddot{\bar{u}}_{(k)} \\ \ddot{\bar{w}}_{(k)} \end{Bmatrix} = - \begin{pmatrix} \frac{\partial W_{(k)}^{PD}}{\partial \bar{u}_{(k)}} + \sum_j \frac{\partial W_{(j)}^{PD}}{\partial \bar{u}_{(k)}} \frac{\mathbf{V}_{(j)}}{\mathbf{V}_{(k)}} \\ \frac{\partial W_{(k)}^{PD}}{\partial \bar{w}_{(k)}} + \sum_j \frac{\partial W_{(j)}^{PD}}{\partial \bar{w}_{(k)}} \frac{\mathbf{V}_{(j)}}{\mathbf{V}_{(k)}} \end{pmatrix} + \begin{Bmatrix} b_x^{(k)} \\ b_z^{(k)} \end{Bmatrix} \quad (4.50)$$

As explained in Appendix A1.3, the PD SED function for at material point k and its family member point j can be written as

$$W_{(k)}^{PD} = \frac{1}{2} \frac{1}{\delta^2 A^2} \left[\begin{aligned} & A \int_A E dA \sum_i \frac{(\bar{u}_{(i^k)} - \bar{u}_{(k)})^2}{|\xi_{(i^k)(k)}^\xi|} \mathbf{V}_{(i^k)} + \int_A E^2 z^2 dA \left(\sum_i \frac{\bar{w}_{(i^k)} - \bar{w}_{(k)}}{\xi_{(i^k)(k)}^2} \mathbf{V}_{(i^k)} \right)^2 \\ & - \int_A E z dA \sum_i \frac{\bar{u}_{(i^k)} - \bar{u}_{(k)}}{\xi_{(i^k)(k)}} \mathbf{V}_{(i^k)} \sum_i \frac{\bar{w}_{(i^k)} - \bar{w}_{(k)}}{\xi_{(i^k)(k)}^2} \mathbf{V}_{(i^k)} \end{aligned} \right] \quad (4.51a)$$

and

$$W_{(j)}^{PD} = \frac{1}{2} \frac{1}{\delta^2 A^2} \left[\begin{aligned} & A \int_A E dA \sum_i \frac{(\bar{u}_{(i^j)} - \bar{u}_{(j)})^2}{|\xi_{(i^j)(j)}^\xi|} \mathbf{V}_{(i^j)} + \int_A E^2 z^2 dA \left(\sum_i \frac{\bar{w}_{(i^j)} - \bar{w}_{(j)}}{\xi_{(i^j)(j)}^2} \mathbf{V}_{(i^j)} \right)^2 \\ & - \int_A E z dA \sum_i \frac{\bar{u}_{(i^j)} - \bar{u}_{(j)}}{\xi_{(i^j)(j)}} \mathbf{V}_{(i^j)} \sum_i \frac{\bar{w}_{(i^j)} - \bar{w}_{(j)}}{\xi_{(i^j)(j)}^2} \mathbf{V}_{(i^j)} \end{aligned} \right] \quad (4.51b)$$

Substituting Eqs.(4.51) into (4.50) arises the final PD EoM for FGB Euler-Bernoulli Beams

$$\rho_{(k)} \ddot{\bar{u}}_{(k)} = \frac{1}{\delta^2 A^3} \left[\begin{aligned} & 2A \int_A E dA \sum_j \frac{\bar{u}_{(j)} - \bar{u}_{(k)}}{|\xi_{(j)(k)}^\xi|} \mathbf{V}_{(j)} \\ & - \frac{1}{2} \int_A E z dA \sum_j \frac{1}{\xi_{(j)(k)}^\xi} \left(\sum_i \frac{\bar{w}_{(i^k)} - \bar{w}_{(k)}}{\xi_{(i^k)(k)}^2} \mathbf{V}_{(i^k)} + \sum_i \frac{\bar{w}_{(i^j)} - \bar{w}_{(j)}}{\xi_{(i^j)(k)}^2} \mathbf{V}_{(i^j)} \right) \mathbf{V}_{(j)} \end{aligned} \right] + b_x^{(k)} \quad (4.52a)$$

and

$$\rho_{(k)} \ddot{\bar{w}}_{(k)} = \frac{1}{\delta^2 A^3} \left[\begin{aligned} & \int_A E z^2 dA \sum_j \frac{1}{\xi_{(j)(k)}^2} \left(\sum_i \frac{\bar{w}_{(i^k)} - \bar{w}_{(k)}}{\xi_{(i^k)(k)}^2} \mathbf{V}_{(i^k)} + \sum_i \frac{\bar{w}_{(i^j)} - \bar{w}_{(j)}}{\xi_{(i^j)(k)}^2} \mathbf{V}_{(i^j)} \right) \mathbf{V}_{(j)} - \\ & \frac{1}{2} \int_A E z dA \sum_j \frac{1}{\xi_{(j)(k)}^\xi} \left(\sum_i \frac{\bar{u}_{(i^k)} - \bar{u}_{(k)}}{\xi_{(i^k)(k)}} \mathbf{V}_{(i^k)} + \sum_i \frac{\bar{u}_{(i^j)} - \bar{u}_{(j)}}{\xi_{(i^j)(k)}} \mathbf{V}_{(i^j)} \right) \mathbf{V}_{(j)} \end{aligned} \right] + b_z^{(k)} \quad (4.52b)$$

4.3.3 Numerical Results

To verify the validity of the PD formulation for functionally graded Euler-Bernoulli beams, the PD solutions are compared with the corresponding finite element (FE) analysis results. In this study, a FGM beam with rectangular cross-section is taken into consideration. The material property is chosen as Young's Modulus, $E(z)$, and it is assumed to vary linearly through the thickness as

$$E(z) = (E_t - E_b) \frac{z}{h} + \frac{1}{2}(E_t + E_b) \quad (GPa) \quad (4.53)$$

where E_t and E_b denote the Young's modulus of the top and bottom surfaces of the beam, and h donates the total thickness of the beam as shown in Fig. 4.19. All numerical examples considered in this section are for statics analysis. For all numerical examples, the horizon size is chosen as $\delta = 3\Delta x$ where Δx is the distance between material points.



Figure 4.19 Functionally graded Euler-Bernoulli beam

4.3.3.1 Functionally Graded Beam Subjected to Pinned Support-Roller Support Boundary Condition

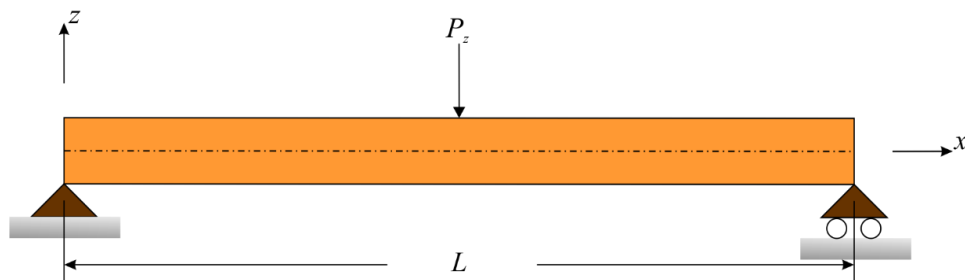
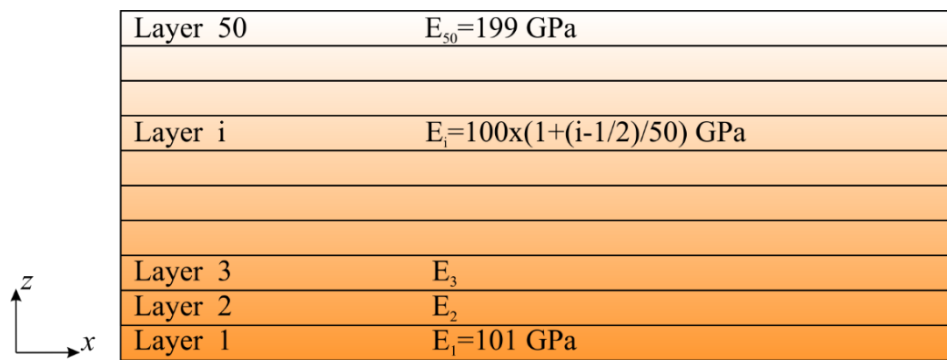


Figure 4.20 Functionally graded beam subjected to Pinned Support-Roller Support boundary condition

A simply supported functionally graded beam with length, width and thickness of $L = 1 \text{ m}$, $b = 0.01 \text{ m}$ and $h = 0.05 \text{ m}$, is considered as shown in Fig. 4.20. The beam is constrained by pinned support and roller support at left and right ends, respectively. The Young's modulus of the top and bottom surfaces are $E_t = 200 \text{ GPa}$ and $E_b = 100 \text{ GPa}$, respectively. The model is discretized into one single row of material points along the thickness and the distance between material points is $\Delta x = 1/101 \text{ m}$. A fictitious region is introduced outside the two ends as the external boundaries with a width of 2δ . The beam is subjected to a concentrated transverse load of $P_z = 1 \text{ N}$ at the center of the beam. The load is converted to a body load of $b = \frac{P_z}{\Delta V} = 202000 \text{ N/m}^3$ and it is subjected to central material points of the model.



Layer 50	$E_{50}=199 \text{ GPa}$
Layer i	$E_i=100x(1+(i-1/2)/50) \text{ GPa}$
Layer 3	E_3
Layer 2	E_2
Layer 1	$E_1=101 \text{ GPa}$

Figure 4.21 Variation of the Young's modulus in thickness direction for the FE model.

The FE model of the beam is created by using the SHELL181 element in ANSYS with dimensions of $1 \times 0.05 \times 0.01 \text{ m}^3$. To model the functionally graded beam, the model is divided into 50 layers by varying homogeneous material properties through the thickness. The Young's modulus varies linearly over the thickness from the first layer $E_1 = 101 \text{ GPa}$ to the last layer $E_{50} = 199 \text{ GPa}$, as shown in Fig. 4.21. The Poisson's ratio, $\nu = 0$, is applied in ANSYS for the sake of eliminating the Poisson's effect.

The PD and FE transverse and axial displacements are compared in Fig. 4.22. There is a very good agreement between PD and FE results. These results verify the accuracy of

the current PD formulation for a functionally graded beam subjected to pinned support – roller support boundary condition.

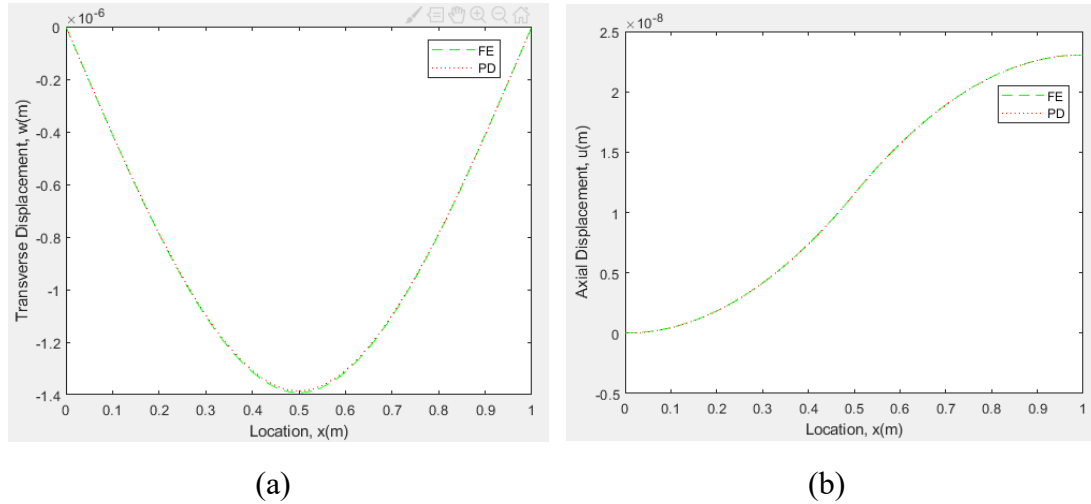


Figure 4.22 Comparison of PD and FE results; (a) transverse displacement, (b) axial displacement

4.3.3.2. Functionally Graded Beam Subjected to Pinned Support-Pinned Support Boundary Condition

In the second case, the functionally graded beam considered in the previous section is subjected to pinned support at both edges as shown in Fig. 4.23. Moreover, a horizontal load of $P_x = 1$ N is acting at the center of the beam in addition to the transverse load of $P_z = 1$ N.

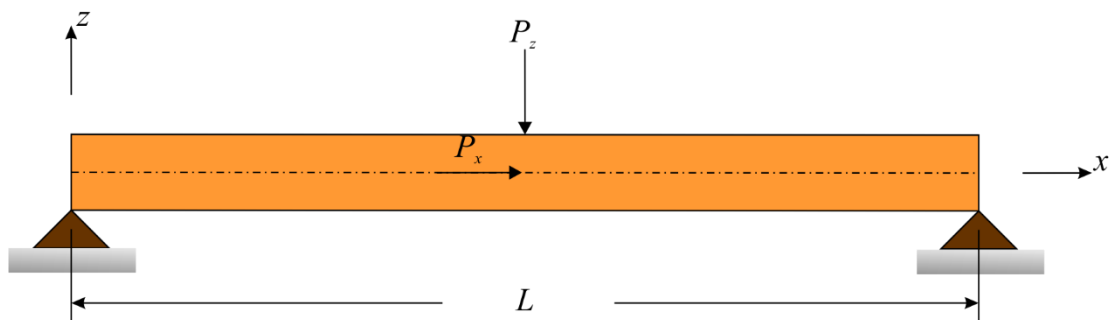


Figure 4.23 Functionally graded beam subjected to Pinned Support-Pinned Support boundary condition

PD results for transverse and axial deformations are compared against FE results as shown in Fig. 4.24 and there is a very good agreement between the two approaches.

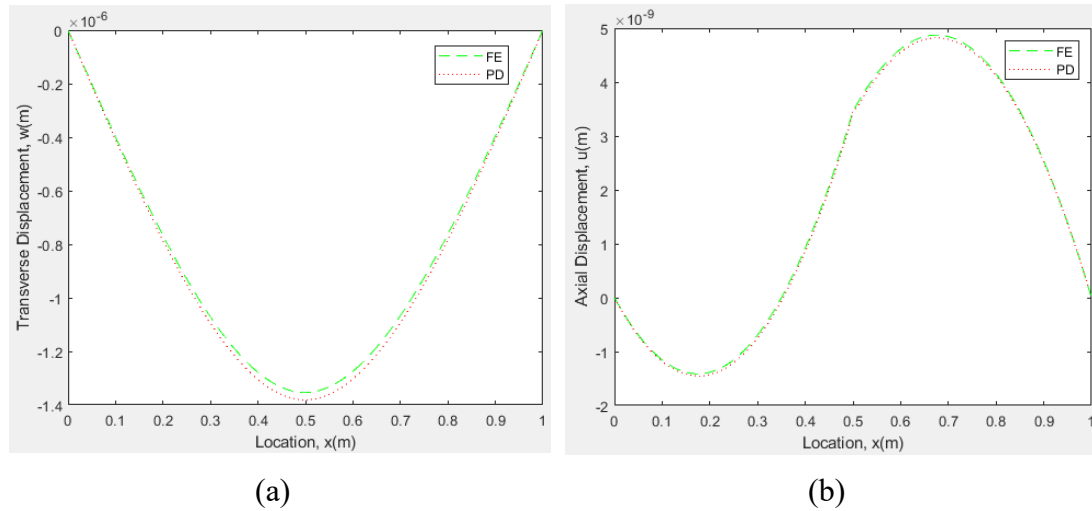


Figure 4.24 Comparison of PD and FE results; (a) transverse displacement, (b) axial displacement

4.3.3.3 Functionally Graded Beam Subjected to Clamped-Clamped Boundary Condition

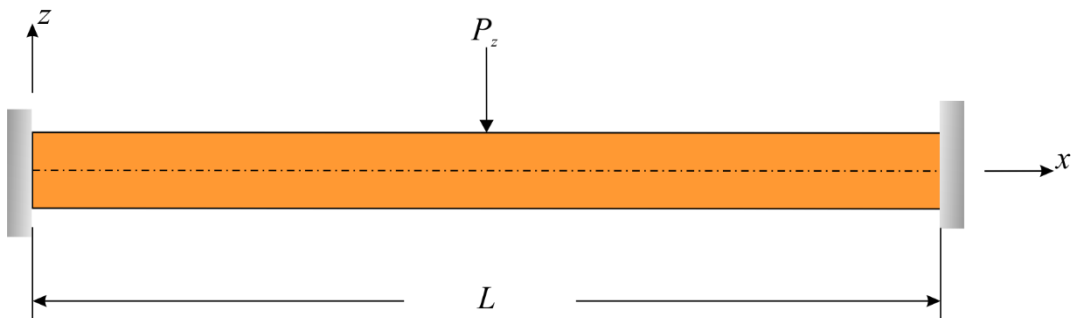


Figure 4.25 Functionally graded beam subjected to Clamped-Clamped boundary condition

In the third case, the functionally graded beam is subjected to clamped – clamped boundary condition as shown in Fig. 4.25. A transverse load of $P_z = 1$ N is applied at the centre of the beam. As demonstrated in Fig. 4.26, a very good match between PD and FE results is obtained for this particular condition.

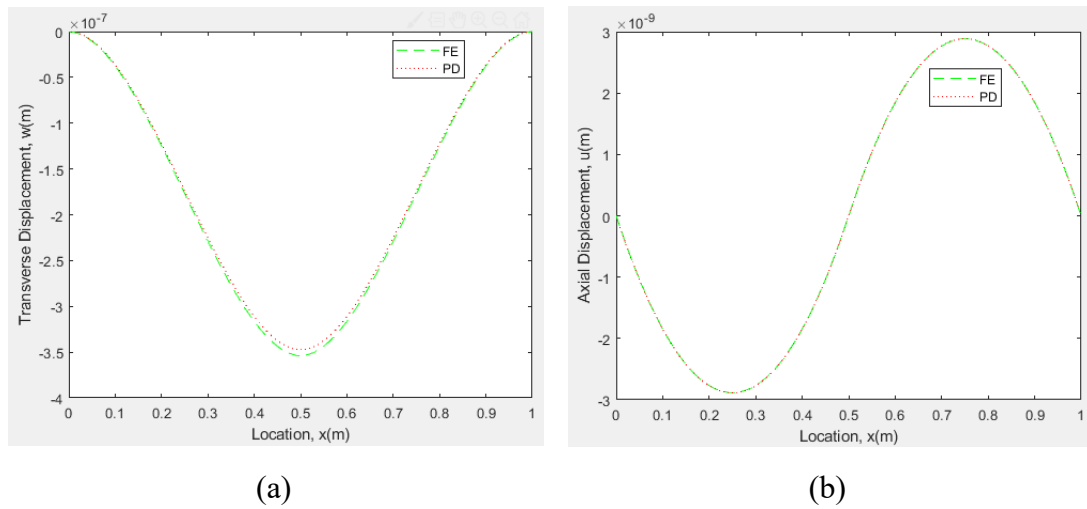


Figure 4.26 Comparison of PD and FE results; (a) transverse displacement, (b) axial displacement

Functionally Graded Beam Subjected to Clamped-Free Boundary Condition

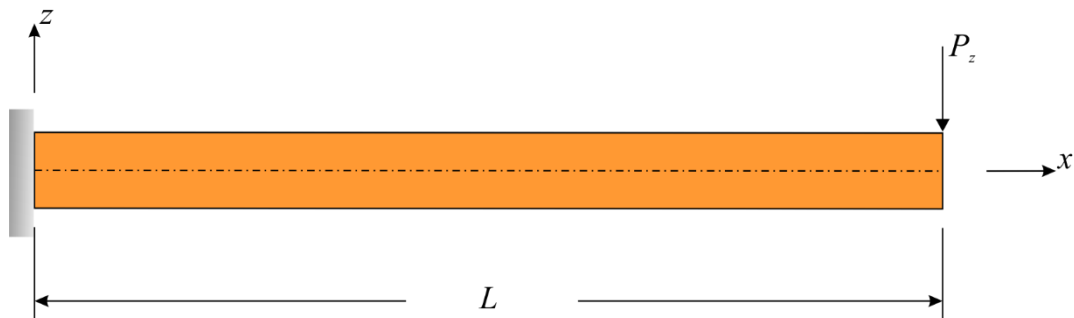


Figure 4.27 Functionally graded beam subjected to Clamped-Free boundary condition

In the final numerical case, the functionally graded beam is subjected to clamped – free boundary condition as shown in Fig. 4.27. A transverse load of $P_z = 1$ N is exerted at the free edge of the beam. As shown in Fig. 4.28, a very good agreement between PD and FE results is observed which shows that current PD formulation can capture accurate deformation behaviour for functionally graded beams subjected to different types of boundary conditions and loading.

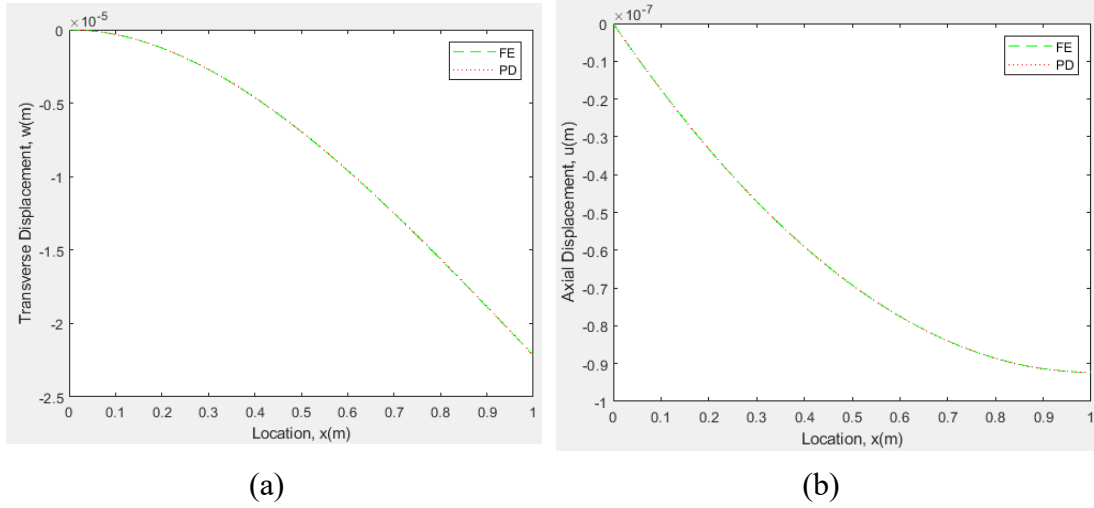


Figure 4.28 Comparison of PD and FE results; (a) transverse displacement, (b) axial displacement

4.4 PD formation for FGM Timoshenko Beam

4.4.1 Timoshenko Beam Theory for FGM

Timoshenko developed first order shear deformation theory for thick beams which is also known as Timoshenko beam theory. According to the assumptions of the Timoshenko beam theory, the displacement field of any material point can be expressed in terms of the displacement field of a material point along the central axis in xz plane as

$$u(x, z, t) = \bar{u}(x, t) + \alpha(x, t) \quad (4.54a)$$

$$w(x, z, t) = \bar{w}(x, t) \quad (4.54b)$$

where \bar{u} , \bar{w} and θ denote the axial displacement, transverse displacement and rotational displacement, respectively. Hereafter in this study, $\bar{u}(x, t)$, $\bar{w}(x, t)$ and $\theta(x, t)$ will be written shortly for u , w and θ for compaction, respectively. Hence, the strain-displacement relation can be expressed as

$$\varepsilon = \frac{\partial \bar{u}}{\partial x} + z \frac{\partial \theta}{\partial x} \quad (4.55a)$$

$$\gamma = \theta + \frac{\partial \bar{w}}{\partial x} \quad (4.55b)$$

The stress components can be written in terms of displacements only as

$$\sigma = E\varepsilon = E\left(\frac{\partial\bar{u}}{\partial x} + z\frac{\partial\theta}{\partial x}\right) \quad (4.56a)$$

$$\tau = \kappa G\gamma = \kappa G\left(\theta + \frac{\partial\bar{w}}{\partial x}\right) \quad (4.56b)$$

where $E = E(z)$ and $G = G(z)$ represent the Young's modulus and shear modulus, respectively, which are functions of the vertical coordinate, z , and κ is the shear correction factor, which depends upon the geometry of the cross-section.

The average cross-sectional strain energy density of the beam can be given as

$$W_{\text{cm}} = \frac{1}{2A} \int_A (\sigma\varepsilon + \tau\gamma) dA \quad (4.57)$$

where A represents the cross-section of the beam. Substituting Eq.(4.55) and (4.56) into (4.57) yields

$$W_{\text{cm}} = \frac{1}{2A} \left[\int_A E dA \left(\frac{\partial\bar{u}}{\partial x}\right)^2 + \int_A E z^2 dA \left(\frac{\partial\theta}{\partial x}\right)^2 + 2 \int_A E z dA \frac{\partial\bar{u}}{\partial x} \frac{\partial\theta}{\partial x} + \int_A \kappa G dA \left(\theta + \frac{\partial\bar{w}}{\partial x}\right)^2 \right] \quad (4.58)$$

4.4.2 PD Theory for FGM Timoshenko Beam

Assume the body is initially at rest, PD EoM can be derived from Lagrange's equation as following

$$\frac{d}{dt} \frac{\partial L}{\partial \dot{\mathbf{u}}_k} - \frac{\partial L}{\partial \mathbf{u}_k} = 0 \quad (4.59)$$

where $L = T - U$ represents the Lagrange and the displacement vector, \mathbf{u} , contains the following entries

$$\mathbf{u} = [\bar{u} \quad \theta \quad \bar{w}]^T \quad (4.60)$$

According to the displacement field assumption, Eqs. (4.54), the total kinetic energy of the systems can be written as

$$T = \frac{1}{2} \int_0^l \int_A \rho (\dot{u}^2 + \dot{w}^2) dA dx = \frac{1}{2} \sum_k \rho_{(k)} \left(\dot{\bar{u}}^2 + \frac{l}{A} \dot{\theta}^2 + \dot{\bar{w}}^2 \right) V_{(k)} \quad (4.61)$$

The total potential energy of the system can be expressed as

$$U = \sum_k W_{PD}^{(k)} (\mathbf{u}_{(k)}, \mathbf{u}_{(1^k)}, \mathbf{u}_{(2^k)}, \mathbf{u}_{(3^k)}, \dots) V_{(k)} - \sum_k \mathbf{b}_{(k)} \mathbf{u}_{(k)} V_{(k)} \quad (4.62)$$

Where $W_{PD}^{(k)}$ represents the PD strain energy density of the beam, and \mathbf{b} denotes the body force density vector, which is defined in this study as

$$\mathbf{b} = [b_x \quad b_\theta \quad b_z]^T \quad (4.63)$$

Here, the entries of the body force density vector, b_x , b_θ , and b_z correspond to axial force along x-axis, bending moment and transverse force densities, respectively.

For a conservative system, the first term of the Lagrange's Equation can be obtained by inserting Eq.(4.61) into (4.59) as

$$\frac{d}{dt} \frac{\partial L}{\partial \dot{\mathbf{u}}_{(k)}} = \frac{d}{dt} \frac{\partial T}{\partial \dot{\mathbf{u}}_{(k)}} = \rho_{(k)} \left\{ \begin{array}{c} \ddot{\mathbf{u}}_{(k)} \\ \frac{I}{A} \ddot{\theta}_{(k)} \\ \ddot{\mathbf{w}}_{(k)} \end{array} \right\} \mathbf{V}_{(k)} \quad (4.64)$$

Utilizing the pre-proved result, Eq.(3.8), the second term of the Lagrange's equation can be expressed as

$$-\frac{\partial L}{\partial \mathbf{u}_{(k)}} = \frac{\partial W_{(k)}^{PD}}{\partial \mathbf{u}_{(k)}} \mathbf{V}_{(k)} + \sum_j \frac{\partial W_{(j)}^{PD}}{\partial \mathbf{u}_{(k)}} \mathbf{V}_{(j)} - \mathbf{b}_{(k)} \mathbf{V}_{(k)} \quad (4.65)$$

which gives

$$\left\{ \begin{array}{c} \frac{\partial L}{\partial \bar{\mathbf{u}}_{(k)}} \\ \frac{\partial L}{\partial \theta_{(k)}} \\ \frac{\partial L}{\partial \bar{\mathbf{w}}_{(k)}} \end{array} \right\} = \left\{ \begin{array}{c} \frac{\partial W_{(k)}^{PD}}{\partial \bar{\mathbf{u}}_{(k)}} \mathbf{V}_{(k)} + \sum_j \frac{\partial W_{(j)}^{PD}}{\partial \bar{\mathbf{u}}_{(k)}} \mathbf{V}_{(j)} \\ \frac{\partial W_{(k)}^{PD}}{\partial \theta_{(k)}} \mathbf{V}_{(k)} + \sum_j \frac{\partial W_{(j)}^{PD}}{\partial \theta_{(k)}} \mathbf{V}_{(j)} \\ \frac{\partial W_{(k)}^{PD}}{\partial \bar{\mathbf{w}}_{(k)}} \mathbf{V}_{(k)} + \sum_j \frac{\partial W_{(j)}^{PD}}{\partial \bar{\mathbf{w}}_{(k)}} \mathbf{V}_{(j)} \end{array} \right\} - \left\{ \begin{array}{c} b_x^{(k)} \\ b_\theta^{(k)} \\ b_z^{(k)} \end{array} \right\} \mathbf{V}_{(k)} \quad (4.66)$$

Combining Eq.(4.64) with (4.66) arises

$$\rho_{(k)} \left\{ \begin{array}{c} \ddot{\mathbf{u}}_{(k)} \\ \frac{I}{A} \ddot{\theta}_{(k)} \\ \ddot{\mathbf{w}}_{(k)} \end{array} \right\} = \left\{ \begin{array}{c} \frac{\partial W_{(k)}^{PD}}{\partial \bar{\mathbf{u}}_{(k)}} + \sum_j \frac{\partial W_{(j)}^{PD}}{\partial \bar{\mathbf{u}}_{(k)}} \frac{\mathbf{V}_{(j)}}{\mathbf{V}_{(k)}} \\ \frac{\partial W_{(k)}^{PD}}{\partial \theta_{(k)}} + \sum_j \frac{\partial W_{(j)}^{PD}}{\partial \theta_{(k)}} \frac{\mathbf{V}_{(j)}}{\mathbf{V}_{(k)}} \\ \frac{\partial W_{(k)}^{PD}}{\partial \bar{\mathbf{w}}_{(k)}} + \sum_j \frac{\partial W_{(j)}^{PD}}{\partial \bar{\mathbf{w}}_{(k)}} \frac{\mathbf{V}_{(j)}}{\mathbf{V}_{(k)}} \end{array} \right\} - \left\{ \begin{array}{c} b_x^{(k)} \\ b_\theta^{(k)} \\ b_z^{(k)} \end{array} \right\} \quad (4.67)$$

As explained in Appendix A1.4, the PD SED function for material point k and its family member j can be given as

$$W_{PD}^{(k)} = \frac{1}{2} \frac{1}{\delta^2 \mathcal{A}^2} \left[\int_A E dz \sum_i \frac{(\bar{u}_{(i^k)} - \bar{u}_{(k)})^2}{|\xi_{(i^k)(k)}|} V_{(i^k)} + 2 \int_A E z dz \sum_i \frac{(\bar{u}_{(i^k)} - \bar{u}_{(k)}) (\theta_{(i^k)} - \theta_{(k)})}{|\xi_{(i^k)(k)}|} V_{(i^k)} \right. \\ \left. + \int_A E z^2 dz \sum_i \frac{(\theta_{(i^k)} - \theta_{(k)})^2}{|\xi_{(i^k)(k)}|} V_{(i^k)} \right. \\ \left. + \kappa \int_A G dz \sum_i \frac{1}{|\xi_{(i^k)(k)}|} \left(\frac{\theta_{(i^k)} + \theta_{(k)}}{2} \xi_{(i^k)(k)} + \bar{w}_{(i^k)} - \bar{w}_{(k)} \right)^2 V_{(i^k)} \right] \quad (4.68a)$$

and

$$W_{PD}^{(j)} = \frac{1}{2} \frac{1}{\delta^2 \mathcal{A}^2} \left[\int_A E dz \sum_i \frac{(\bar{u}_{(i^j)} - \bar{u}_{(j)})^2}{|\xi_{(i^j)(j)}|} V_{(i^j)} + 2 \int_A E z dz \sum_i \frac{(\bar{u}_{(i^j)} - \bar{u}_{(j)}) (\theta_{(i^j)} - \theta_{(j)})}{|\xi_{(i^j)(j)}|} V_{(i^j)} \right. \\ \left. + \int_A E z^2 dz \sum_i \frac{(\theta_{(i^j)} - \theta_{(j)})^2}{|\xi_{(i^j)(j)}|} V_{(i^j)} \right. \\ \left. + \kappa \int_A G dz \sum_i \frac{1}{|\xi_{(i^j)(j)}|} \left(\frac{\theta_{(i^j)} + \theta_{(j)}}{2} \xi_{(i^j)(j)} + \bar{w}_{(i^j)} - \bar{w}_{(j)} \right)^2 V_{(i^j)} \right] \quad (4.68b)$$

Substituting Eqs. (4.68) into (4.67) yields the final PD EoM for FGM Timoshenko beam

as

$$\rho_{(k)} \ddot{u}_{(k)} = \frac{2}{\delta^2 \mathcal{A}^2} \left(\int_A E dA \sum_j \frac{\bar{u}_{(j)} - \bar{u}_{(k)}}{|\xi_{(j)(k)}|} V_{(j)} + \int_A E z dA \sum_j \frac{\theta_{(j)} - \theta_{(k)}}{|\xi_{(j)(k)}|} V_{(j)} \right) + b_x^{(k)} \quad (4.69a)$$

$$\rho_{(k)} \frac{I}{A} \ddot{\theta}_{(k)} = \frac{2}{\delta^2 \mathcal{A}^2} \left(\int_A E z^2 dA \sum_j \frac{\theta_{(j)} - \theta_{(k)}}{|\xi_{(j)(k)}|} V_{(j)} + \int_A E z dA \sum_j \frac{\bar{u}_{(j)} - \bar{u}_{(k)}}{|\xi_{(j)(k)}|} V_{(j)} - \right. \\ \left. \frac{1}{2} \kappa \int_A G dA \sum_j \left(\bar{w}_{(j)} - \bar{w}_{(k)} + \frac{\theta_{(j)} + \theta_{(k)}}{2} \xi_{(j)(k)} \right) \text{sgn}(\xi_{(j)(k)}) V_{(j)} \right) + b_\theta^{(k)} \quad (4.69b)$$

and

$$\rho_{(k)} \ddot{w}_{(k)} = \frac{2}{\delta^2 \mathcal{A}^2} \kappa \int_A G dA \sum_j \left(\frac{\bar{w}_{(j)} - \bar{w}_{(k)}}{|\xi_{(j)(k)}|} + \frac{\theta_{(j)} + \theta_{(k)}}{2} \text{sgn}(\xi_{(j)(k)}) \right) V_{(j)} + b_z^{(k)} \quad (4.69c)$$

4.4.3 Numerical Cases

To verify the validity of the PD formulation for functionally graded Timoshenko beams, the PD solutions are compared with the corresponding finite element (FE) analysis results. In this study, the functionally graded material properties are chosen as Young's Modulus, $E(z)$ and shear modulus $G(z)$ and they are assumed to vary linearly through the thickness as

$$E(z) = (E_t - E_b) \frac{z}{h} + \frac{1}{2}(E_t + E_b) \quad (GPa) \quad (4.70a)$$

and

$$G(z) = \frac{E(z)}{2(1 + 0.3)} \quad (4.70b)$$

where E_t and E_b denote the Young's modulus of the top and bottom surfaces of the beam, and h denotes the total thickness of the beam as shown in Fig. 4.29. All numerical examples considered in this section are for static analysis and the numerical solution procedure is given in Appendix B. For all numerical examples, the horizon size is chosen as $\delta = 3\Delta x$ where Δx is the distance between material points.



Figure 4.29 Material variation along the thickness direction for the functionally graded material

4.4.3.1 Timoshenko beam with pinned support – roller support boundary conditions

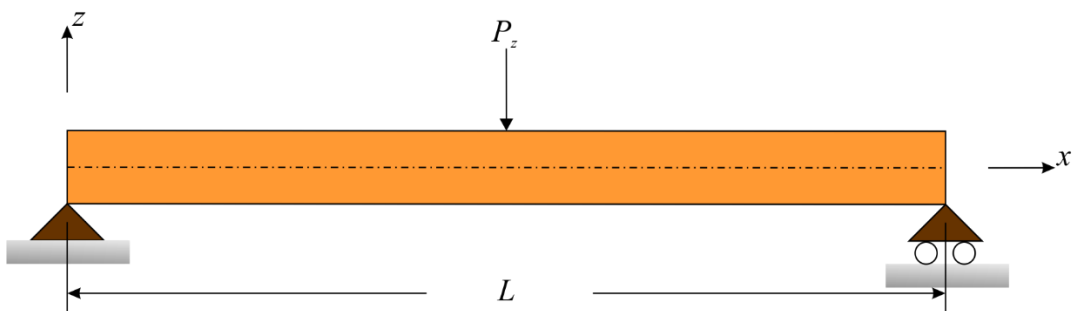


Figure 4.30 Timoshenko beam with pinned support – roller support boundary conditions

A simply supported functionally graded beam with length, width and thickness of $L = 1$ m, $W = 0.01$ m and $t = 0.1$ m is considered as shown in Fig. 4.30. The beam is constrained by pinned support and roller support at the left and right ends, respectively.

The Young's modulus of the top and bottom surfaces are specified as $E_t = 200$ GPa and $E_b = 100$ GPa, respectively. The model is discretized into one single row of material points along with the thickness and the distance between material points is $\Delta x = 0.002$ m. A fictitious region is introduced outside the actual solution domain as the external boundaries with a width of δ . The beam is subjected to a concentrated transverse load of $P_z = 100$ N at the central point. The load is converted to a body load of $b_z = \frac{P_z}{2\Delta V} = 2.5e7$ N/m³ and it is applied to two central material volumes of the model (see Fig. 4.31).

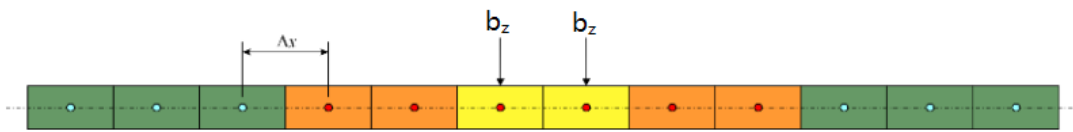


Figure 4.31 Discretization, applied loading and fictitious region.

The FE model of the beam is created by using SHELL181 element in ANSYS with dimensions of $1 \text{ m} \times 0.01 \text{ m} \times 0.1 \text{ m}$. The FE model is meshed with 100 elements along the length. To model the functionally graded beam, the model is divided to 50 layers with varying homogeneous materials properties through the thickness. The Young's modulus varies linearly over the thickness from the first layer $E_1 = 101$ GPa to the last layer $E_{50} = 199$ GPa, as shown in Fig. 4.32. The Poisson's ratio, $\nu = 0.3$, is applied in ANSYS.

Layer 50	$E_{50}=199$ GPa
Layer i	$E_i=100x(1+(i-1/2)/50)$ GPa
Layer 3	E_3
Layer 2	E_2
Layer 1	$E_1=101$ GPa

Figure 4.32 Material variation in the thickness direction for the finite element model

The PD and FE transverse displacements, $w(x)$, rotations, $\theta(x)$, and axial displacements, $u(x)$ are compared in Fig. 4.33. Both approaches yield similar

displacement and rotation variations. These results verify the accurateness of the current PD formulation for a functionally graded beam theory for pinned support – roller support boundary condition.

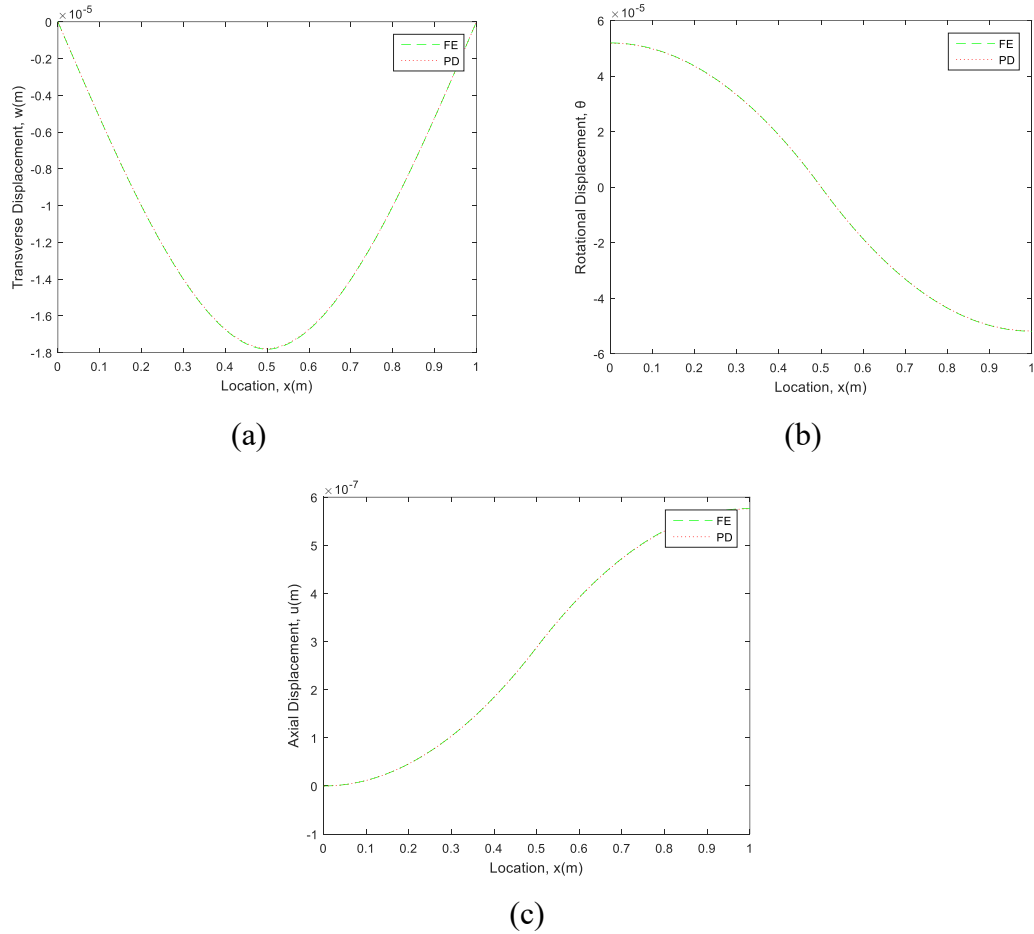


Figure 4.33 Comparison of PD and FE results for (a) transverse displacements, (b) rotations, and (c) axial displacements.

4.3.3.2 Timoshenko beam with clamped – roller support boundary conditions

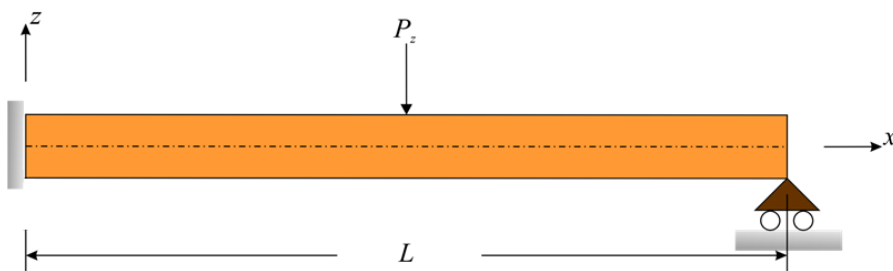


Figure 4.34 Timoshenko beam with clamped – roller support boundary conditions

The Timoshenko beam with clamped – roller supported boundary conditions is under consideration. The beam has the same geometrical and elastic properties as previous case. The model is discretized into one single row of material points along with the thickness and the distance between material points is $\Delta x = 0.002$ m. A fictitious region is introduced outside the ends as the external boundaries with a width of δ . The beam is subjected to a concentrated transverse load of $P_z = 100$ N at the central point. The load is converted to a body load of $b_z = \frac{P_z}{2\Delta V} = 2.5e7$ N/m³ and it is subjected to two central material volumes of the model.

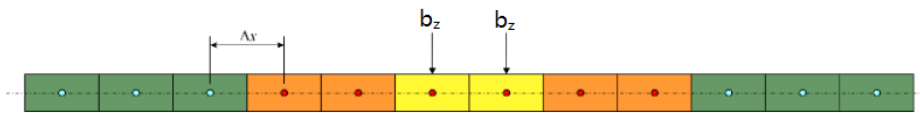
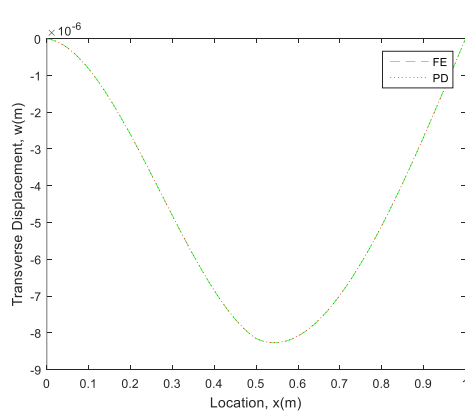
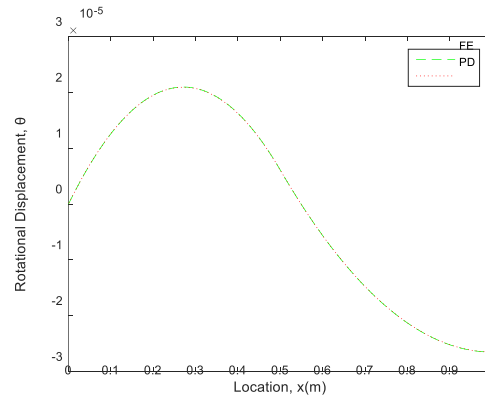


Figure 4.35 Discretization, applied loading and fictitious region

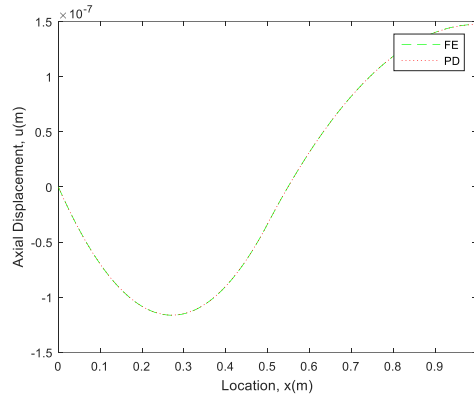
As depicted in Fig. 4.36, for transverse displacements, $w(x)$, rotations, $\theta(x)$, and axial displacements, $u(x)$, a very good agreement is obtained between PD and FE results.



(a)



(b)



(c)

Figure 4.36 Comparison of PD and FE results for (a) transverse displacements, (b) rotations, and (c) axial displacements

4.4.3.3 Timoshenko beam with clamped – free boundary conditions

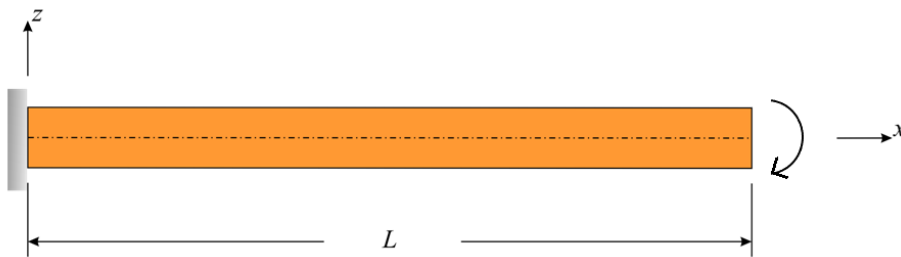


Figure 4.37 Timoshenko beam with clamped – free boundary conditions

The performance of a cantilever beam is under investigation. The beam has the same geometrical and elastic properties as previous case. The model is discretized into one single row of material points along with the thickness and the distance between material points is $\Delta x = 0.002$ m. A fictitious region is introduced outside the ends as the external boundaries with a width of δ . The beam is subjected to a bending moment of $M = 100$ Nm at the free end. The load is converted to a body load of $b_\theta = \frac{M}{\Delta V} = 5e7$ N/m² and it is applied to the last material point adjacent to the free end.

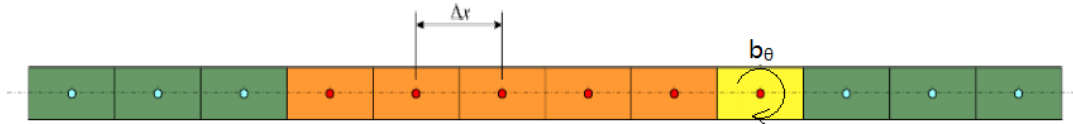


Figure 4.38 Discretization, applied loading and fictitious region

The transverse displacements, $w(x)$, rotations, $\theta(x)$, and axial displacements, $u(x)$ along the beam are obtained from both PD and FE analysis. As shown in Fig. 4.39, a very good agreement is observed between the two approaches.

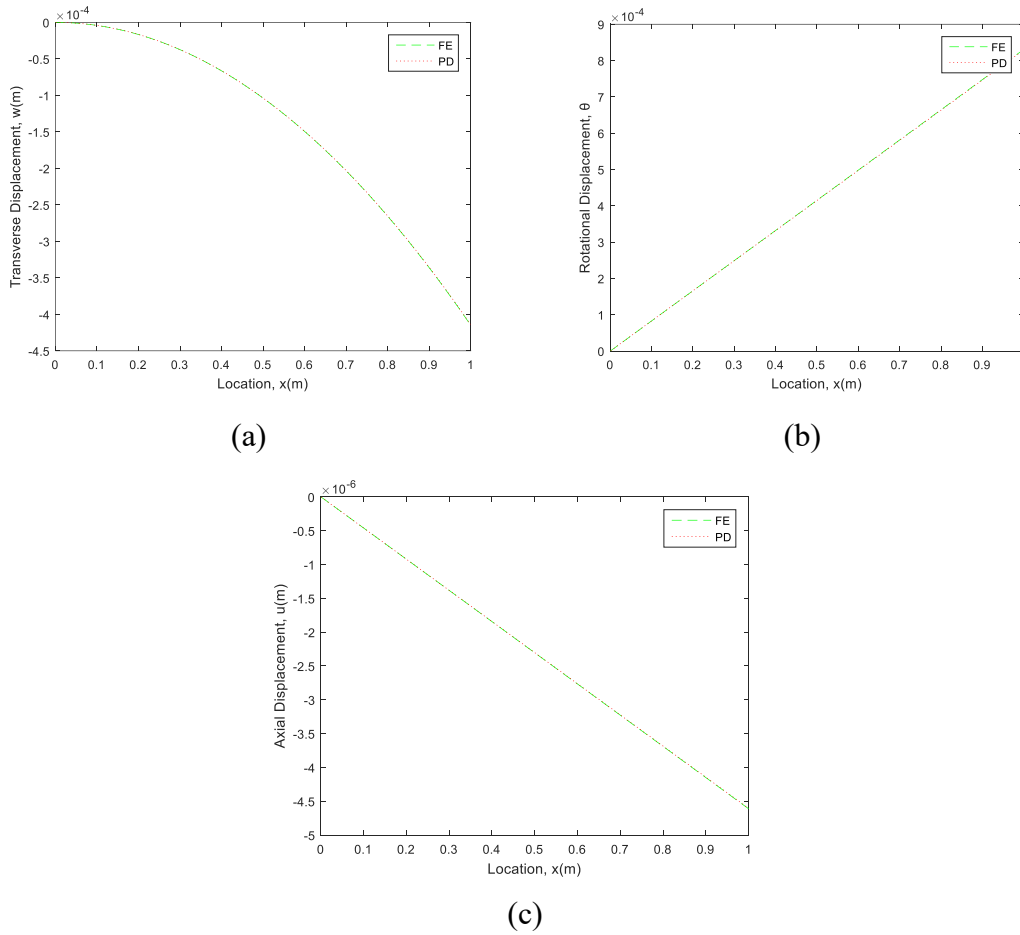


Figure 4.39 Comparison of PD and FE results for (a) transverse displacements, (b) rotations, and (c) axial displacements

4.5 PD Formulations of FGM Higher Order Deformable Beam

4.5.1 FGM Higher Order Deformable Beam Theory

The displacement field of any material points at the transverse normal can be represented in terms of the displacement field of the material point at locus of central axis in xz plane by using Taylor expansion as

$$u(x, z, t) = u(x, 0, t) + z \left. \frac{\partial u}{\partial z} \right|_{z=0} + \frac{1}{2} z^2 \left. \frac{\partial^2 u}{\partial z^2} \right|_{z=0} + \frac{1}{3!} z^3 \left. \frac{\partial^3 u}{\partial z^3} \right|_{z=0} + \dots \quad (4.71a)$$

$$w(x, z, t) = w(x, 0, t) + z \left. \frac{\partial w}{\partial z} \right|_{z=0} + \frac{1}{2} z^2 \left. \frac{\partial^2 w}{\partial z^2} \right|_{z=0} + \frac{1}{3!} z^3 \left. \frac{\partial^3 w}{\partial z^3} \right|_{z=0} + \dots \quad (4.71b)$$

Ignore the higher order terms of Eq.(4.71), the displacements field of the deep beam can be written as

$$u(x, z, t) = \bar{u}(x, t) + z\theta(x, t) + z^2 u^*(x, t) + z^3 \theta^*(x, t) \quad (4.72a)$$

$$w(x, z, t) = \bar{w}(x, t) + z\theta_z(x, t) + z^2 w^*(x, t) \quad (4.72b)$$

where \bar{u} and \bar{w} represent the axial displacement and transverse displacement of the material points along the neutral axis, and θ , u^* , θ^* , θ_z and w^* represent the higher order terms arise out of the Taylor expansion, which can be defined as

$$\theta(x, t) = \left. \frac{\partial u(x, z, t)}{\partial z} \right|_{z=0} \quad (4.73a)$$

$$u^*(x, t) = \left. \frac{1}{2} \frac{\partial^2 u(x, z, t)}{\partial z^2} \right|_{z=0} \quad (4.73b)$$

$$\theta^*(x, t) = \left. \frac{1}{3!} \frac{\partial^3 u(x, z, t)}{\partial z^3} \right|_{z=0} \quad (4.73c)$$

$$\theta_z(x, t) = \left. \frac{\partial w(x, z, t)}{\partial z} \right|_{z=0} \quad (4.73d)$$

$$w^*(x, t) = \left. \frac{1}{2} \frac{\partial^2 w(x, z, t)}{\partial z^2} \right|_{z=0} \quad (4.73e)$$

Hereafter, $\bar{u}(x, t)$, $\theta(x, t)$, $u^*(x, t)$, $\theta^*(x, t)$, $\bar{w}(x, t)$, $\theta_z(x, t)$ and $w^*(x, t)$ will be written simply as \bar{u} , θ , u^* , θ^* , \bar{w} , θ_z and w^* , respectively.

According to the stipulation of the displacement field assumption, Eq. (4.72), the strain components can be written as

$$\varepsilon_x = \frac{\partial \bar{u}}{\partial x} + z \frac{\partial \theta}{\partial x} + z^2 \frac{\partial u^*}{\partial x} + z^3 \frac{\partial \theta^*}{\partial x} \quad (4.74a)$$

$$\varepsilon_z = \theta_z + 2zw' \quad (4.74b)$$

$$\gamma_{xz} = \left(\theta + \frac{\partial \bar{w}}{\partial x} \right) + z \left(2u' + \frac{\partial \theta_z}{\partial x} \right) + z^2 \left(3\theta' + \frac{\partial w'}{\partial x} \right) \quad (4.74c)$$

Unlike the strain-displacement relations in the classical beam theories, wherein the transverse normal is zero and the shearing strain varies linearly along the thickness, these relations in our study are more realistic. This also eliminates the need for introducing the shear correction factor, which is widely used in the Timoshenko beam theory.

Assume the material is only axially isotropic, and obey the plane-stress constitutive relation, the stress components can be given by

$$\sigma_x = \frac{E}{1-\nu^2} (\varepsilon_x + \nu\varepsilon_z) \quad (4.75a)$$

$$\sigma_z = \frac{E}{1-\nu^2} (\varepsilon_z + \nu\varepsilon_x) \quad (4.75b)$$

$$\tau_{xz} = G\gamma_{xz} \quad (4.75c)$$

Where $E = E(z)$, $\nu = \nu(z)$ and $G = G(z)$ are the Young's modulus, Poisson's ratio and shear modulus, respectively, and they are variational with the thickness coordinate z .

According to the classical continuum mechanics theory, the average cross-sectional strain energy density function can be expressed as

$$W_{\text{OM}} = \frac{1}{2A} \int_A (\sigma_x \varepsilon_x + \sigma_z \varepsilon_z + \tau_{xz} \gamma_{xz}) dA \quad (4.76)$$

Inserting Eqs. (4.75) and (4.75) into (4.76) results in

$$\begin{aligned}
W_{\text{com}} = \frac{1}{2A} & \left\{ \int_A \frac{E}{1-\nu^2} dA \left[\left(\frac{\partial \bar{u}}{\partial x} \right)^2 + (\theta_z)^2 \right] + \int_A \frac{2Ez}{1-\nu^2} dA \left(\frac{\partial \bar{u}}{\partial x} \frac{\partial \theta}{\partial x} + 2\theta_z \dot{w} \right) \right. \\
& + \int_A \frac{Ez^2}{1-\nu^2} dA \left[\left(\frac{\partial \theta}{\partial x} \right)^2 + 2 \frac{\partial \bar{u}}{\partial x} \frac{\partial \dot{u}^*}{\partial x} + 4(\dot{w}^*)^2 \right] \\
& + \int_A \frac{2Ez^3}{1-\nu^2} dA \left(\frac{\partial \bar{u}}{\partial x} \frac{\partial \theta^*}{\partial x} + \frac{\partial \theta}{\partial x} \frac{\partial \dot{u}^*}{\partial x} \right) + \int_A \frac{Ez^4}{1-\nu^2} dA \left[\left(\frac{\partial \dot{u}^*}{\partial x} \right)^2 + 2 \frac{\partial \theta}{\partial x} \frac{\partial \theta^*}{\partial x} \right] \\
& \left. + \int_A \frac{2Ez^5}{1-\nu^2} dA \frac{\partial \dot{u}^*}{\partial x} \frac{\partial \theta^*}{\partial x} + \int_A \frac{Ez^6}{1-\nu^2} dA \left(\frac{\partial \theta^*}{\partial x} \right)^2 \right\} \\
& + \frac{1}{A} \left\{ \int_A \frac{Ev}{1-\nu^2} dA \frac{\partial \bar{u}}{\partial x} \theta_z + \int_A \frac{Evz}{1-\nu^2} dA \left(2 \frac{\partial \bar{u}}{\partial x} \dot{w} + \frac{\partial \theta}{\partial x} \theta_z \right) \right. \\
& + \int_A \frac{Evz^2}{1-\nu^2} dA \left(2 \frac{\partial \theta}{\partial x} \dot{w} + \frac{\partial \dot{u}^*}{\partial x} \theta_z \right) \\
& \left. + \int_A \frac{Evz^3}{1-\nu^2} dA \left(2 \frac{\partial \dot{u}^*}{\partial x} \dot{w} + \frac{\partial \theta^*}{\partial x} \theta_z \right) + \int_A \frac{2Evz^4}{1-\nu^2} dA \frac{\partial \theta^*}{\partial x} \dot{w} \right\} \\
& + \frac{1}{2A} \left\{ \int_A G dA \left(\theta + \frac{\partial \bar{w}}{\partial x} \right)^2 + 2 \int_A Gz dA \left(\theta + \frac{\partial \bar{w}}{\partial x} \right) \left(2\dot{u}^* + \frac{\partial \theta_z}{\partial x} \right) \right. \\
& + \int_A Gz^2 dA \left[\left(2\dot{u}^* + \frac{\partial \theta_z}{\partial x} \right)^2 + 2 \left(\theta + \frac{\partial \bar{w}}{\partial x} \right) \left(3\theta^* + \frac{\partial \dot{w}^*}{\partial x} \right) \right] \\
& \left. + 2 \int_A Gz^3 dA \left(2\dot{u}^* + \frac{\partial \theta_z}{\partial x} \right) \left(3\theta^* + \frac{\partial \dot{w}^*}{\partial x} \right) + \int_A Gz^4 dA \left(3\theta^* + \frac{\partial \dot{w}^*}{\partial x} \right)^2 \right\}
\end{aligned} \tag{4.77}$$

4.5.2 PD Formulations for FGM Higher Order Deformable Beam

If we assume the beam is initially at rest, the PD EoM can be derived from the Lagrange's equation as

$$\frac{d}{dt} \frac{\partial L}{\partial \dot{\mathbf{u}}_k} - \frac{\partial L}{\partial \mathbf{u}_k} = 0 \tag{4.78}$$

where $L = T - U$ represents the Lagrange and the displacement vector, \mathbf{u} , contains the following entries

$$\mathbf{u} = [\bar{u} \quad \theta \quad \dot{u}^* \quad \theta^* \quad \bar{w} \quad \theta_z \quad \dot{w}^*] \tag{4.79}$$

The cross-sectional kinetic energy, \bar{T} , can be written as

$$\bar{T} = \frac{1}{2} \int_A \rho (\dot{u}^2 + \dot{w}^2) dA \tag{4.80}$$

Substitute Eqs. (4.72) into (4.80) gives

$$\bar{T} = \frac{1}{2} \rho \left\{ A(\dot{\bar{u}}^2 + \dot{\bar{w}}^2) + I (\dot{\theta}^2 + 2\dot{u}^* \dot{\theta} + \dot{\theta}_z^2 + 2\dot{w}^*) + I^* [(\dot{u}^*)^2 + 2\dot{\theta} \dot{\theta}^* + (\dot{w}^*)^2] + I^{**} (\dot{\theta}^*)^2 \right\} \tag{4.81}$$

where I represents the second moment of the cross-section area and I^* and I^{**}

represent the higher order moment of the cross-section area, which are defined as

$$I = \int_A z^2 dA \quad (4.82a)$$

$$I^* = \int_A z^4 dA \quad (4.82b)$$

$$I^{**} = \int_A z^4 dA \quad (4.82c)$$

The total kinetic energy of the system can be casted by integrating Eq.() throughout the entire beam as

$$T = \int_0^l \bar{T} dx = \frac{1}{2} \int_0^l \rho \left\{ A(\dot{u}^2 + \dot{w}^2) + I(\dot{\theta}^2 + 2\dot{u}\dot{u}' + \dot{\theta}_z^2 + 2\dot{w}\dot{w}') \right. \\ \left. + I^*[(\dot{u}')^2 + 2\dot{\theta}\dot{\theta}' + (\dot{w}')^2] + I^{**}(\dot{\theta}')^2 \right\} dx \quad (4.83a)$$

which can be discretized as

$$T = \frac{1}{2} \sum_k \frac{\rho_{(k)}}{A} \left\{ A(\dot{u}_{(k)}^2 + \dot{w}_{(k)}^2) + I \left[\dot{\theta}_{(k)}^2 + 2\dot{u}_{(k)}\dot{u}'_{(k)} + (\dot{\theta}_z^{(k)})^2 + 2\dot{w}_{(k)}\dot{w}'_{(k)} \right] \right. \\ \left. + I^* [(\dot{u}'_{(k)})^2 + 2\dot{\theta}_{(k)}\dot{\theta}'_{(k)} + (\dot{w}'_{(k)})^2] + I^{**}(\dot{\theta}'_{(k)})^2 \right\} V_{(k)} \quad (4.83b)$$

Assume the system is conservative, the first term of the Lagrange's equation becomes

$$\frac{d}{dt} \frac{\partial L}{\partial \dot{\mathbf{u}}_{(k)}} = \frac{d}{dt} \left\{ \begin{array}{c} \frac{\partial T}{\partial \dot{u}_{(k)}} \\ \frac{\partial T}{\partial \dot{\theta}_{(k)}} \\ \frac{\partial T}{\partial \dot{u}'_{(k)}} \\ \frac{\partial T}{\partial \dot{\theta}'_{(k)}} \\ \frac{\partial T}{\partial \dot{w}_{(k)}} \\ \frac{\partial T}{\partial \dot{w}'_{(k)}} \\ \frac{\partial T}{\partial \dot{\theta}_z^{(k)}} \\ \frac{\partial T}{\partial \dot{w}'_{(k)}} \end{array} \right\} = \rho_{(k)} \left\{ \begin{array}{c} \ddot{u}_{(k)} + \frac{I}{A} \ddot{u}'_{(k)} \\ \frac{I}{A} \ddot{\theta}_{(k)} + \frac{I^*}{A} \ddot{\theta}'_{(k)} \\ \frac{I^*}{A} \ddot{u}'_{(k)} + \frac{I}{A} \ddot{u}_{(k)} \\ \frac{I^{**}}{A} \ddot{\theta}'_{(k)} + \frac{I^*}{A} \ddot{\theta}_{(k)} \\ \ddot{w}_{(k)} + \frac{I}{A} \ddot{w}'_{(k)} \\ \frac{I}{A} \ddot{\theta}_z^{(k)} \\ \frac{I^*}{A} \ddot{w}'_{(k)} + \frac{I}{A} \ddot{w}_{(k)} \end{array} \right\} V_{(k)} \quad (4.84)$$

The PD SED function has a non-local form such that the strain energy of a certain material point k depends on both its displacement and all other material points in its family, which can be expressed as

$$W_{FD}^{(k)} = W_{FD}^{(k)}(\mathbf{u}_{(k)}, \mathbf{u}_{(1^k)}, \mathbf{u}_{(2^k)}, \mathbf{u}_{(3^k)}, \dots) \quad (4.85)$$

Similar to Eq. (4.83b), the total potential energy stored in the body can be obtained by summing potential energies of all material points including strain energy and energy due to external loads as

$$\mathbf{U}_{PD}^{(k)} = \sum_k W_{PD}^{(k)} (\mathbf{u}_{(k)}, \mathbf{u}_{(1^k)}, \mathbf{u}_{(2^k)}, \mathbf{u}_{(3^k)}, \dots) \mathbf{V}_{(k)} - \sum_k \mathbf{b}_{(k)} \mathbf{u}_{(k)} \mathbf{V}_{(k)} \quad (4.86)$$

where \mathbf{b} represents the body force density vector, which includes the components as following

$$\mathbf{b} = [b_x \quad b_\theta \quad 0 \quad 0 \quad b_z \quad 0 \quad 0]^T \quad (4.87)$$

where b_x , b_θ and b_z correspond to the densities of axial force, moments and transverse force, respectively.

Recall the pre-proved result, Eq.(3.8):

$$-\frac{\partial L}{\partial \mathbf{u}_{(k)}} = \frac{\partial W_{PD}^{(k)}}{\partial \mathbf{u}_{(k)}} \mathbf{V}_{(k)} + \sum_j \frac{\partial W_{PD}^{(j)}}{\partial \mathbf{u}_{(k)}} \mathbf{V}_{(j)} - \mathbf{b}_{(k)} \mathbf{V}_{(k)} \quad (4.88)$$

Substituting Eq. (4.86) into and (4.88) and combining with (4.83b) into (4.78) arises

$$\rho_{(k)} \left\{ \begin{array}{l} \ddot{\mathbf{u}}_{(k)} + \frac{I}{A} \ddot{\mathbf{u}}_{(k)}^* \\ \frac{I}{A} \ddot{\theta}_{(k)} + \frac{I^*}{A} \ddot{\theta}_{(k)}^* \\ \frac{I^*}{A} \ddot{\mathbf{u}}_{(k)}^* + \frac{I}{A} \ddot{\mathbf{u}}_{(k)} \\ \frac{I^*}{A} \ddot{\theta}_{(k)}^* + \frac{I}{A} \ddot{\theta}_{(k)} \\ \ddot{\mathbf{w}}_{(k)} + \frac{I}{A} \ddot{\mathbf{w}}_{(k)}^* \\ \frac{I}{A} \ddot{\theta}_z^{(k)} \\ \frac{I^*}{A} \ddot{\mathbf{w}}_{(k)}^* + \frac{I}{A} \ddot{\mathbf{w}}_{(k)} \end{array} \right\} \mathbf{V}_{(k)} = - \left\{ \begin{array}{l} \frac{\partial W_{(k)}}{\partial \mathbf{u}_{(k)}} \mathbf{V}_{(k)} + \sum_j \frac{\partial W_{(j)}}{\partial \mathbf{u}_{(k)}} \mathbf{V}_{(j)} \\ \frac{\partial W_{(k)}}{\partial \theta_{(k)}} \mathbf{V}_{(k)} + \sum_j \frac{\partial W_{(j)}}{\partial \theta_{(k)}} \mathbf{V}_{(j)} \\ \frac{\partial W_{(k)}}{\partial \mathbf{u}_{(k)}^*} \mathbf{V}_{(k)} + \sum_j \frac{\partial W_{(j)}}{\partial \mathbf{u}_{(k)}^*} \mathbf{V}_{(j)} \\ \frac{\partial W_{(k)}}{\partial \theta_{(k)}^*} \mathbf{V}_{(k)} + \sum_j \frac{\partial W_{(j)}}{\partial \theta_{(k)}^*} \mathbf{V}_{(j)} \\ \frac{\partial W_{(k)}}{\partial \mathbf{w}_{(k)}} \mathbf{V}_{(k)} + \sum_j \frac{\partial W_{(j)}}{\partial \mathbf{w}_{(k)}} \mathbf{V}_{(j)} \\ \frac{\partial W_{(k)}}{\partial \theta_z^{(k)}} \mathbf{V}_{(k)} + \sum_j \frac{\partial W_{(j)}}{\partial \theta_z^{(k)}} \mathbf{V}_{(j)} \\ \frac{\partial W_{(k)}}{\partial \mathbf{w}_{(k)}^*} \mathbf{V}_{(k)} + \sum_j \frac{\partial W_{(j)}}{\partial \mathbf{w}_{(k)}^*} \mathbf{V}_{(j)} \end{array} \right\} + \left\{ \begin{array}{l} \mathbf{b}_x^{(k)} \\ \mathbf{b}_\theta^{(k)} \\ 0 \\ 0 \\ \mathbf{b}_z^{(k)} \\ 0 \\ 0 \end{array} \right\} \mathbf{V}_{(k)} \quad (4.89)$$

As derived in Appendix A1.5, the PD SED function for material point k and its family member j can be written as following

$$\begin{aligned}
W_{FD}^{(k)} = & \frac{1}{2} \frac{1}{\delta^2 A^2} \left\{ \int_A \frac{E}{1-\nu^2} dA \sum_i \left[\frac{(\bar{u}_{i^k} - \bar{u}_k)^2}{|\xi_{i^k}^{(k)}|} + \left(\frac{\theta_z^{i^k} + \theta_z^{(k)}}{2} \right)^2 \left| \xi_{i^k}^{(k)} \right| \right] V_{i^k} + \int_A \frac{2Ez}{1-\nu^2} dA \sum_i \left[\frac{(\bar{u}_{i^k} - \bar{u}_k)(\theta_{i^k} - \theta_k)}{|\xi_{i^k}^{(k)}|} + \frac{\theta_z^{i^k} + \theta_z^{(k)}}{2} (\dot{w}_{i^k}^* + \dot{w}_k^*) \left| \xi_{i^k}^{(k)} \right| \right] V_{i^k} \right. \\
& + \int_A \frac{Ez^2}{1-\nu^2} dA \sum_i \left[\frac{(\theta_{i^k} - \theta_k)^2}{|\xi_{i^k}^{(k)}|} + 2 \frac{(\bar{u}_{i^k} - \bar{u}_k)(\dot{u}_{i^k}^* - \dot{u}_k^*)}{|\xi_{i^k}^{(k)}|} + (\dot{w}_{i^k}^* + \dot{w}_k^*)^2 \left| \xi_{i^k}^{(k)} \right| \right] V_{i^k} \\
& + \int_A \frac{2Ez^3}{1-\nu^2} dA \sum_i \left[\frac{(\bar{u}_{i^k} - \bar{u}_k)(\theta_{i^k}^* - \theta_k^*)}{|\xi_{i^k}^{(k)}|} + \frac{(\theta_{i^k} - \theta_k)(\dot{u}_{i^k}^* - \dot{u}_k^*)}{|\xi_{i^k}^{(k)}|} \right] V_{i^k} \\
& \left. + \int_A \frac{Ez^4}{1-\nu^2} dA \sum_i \left[\frac{(\dot{u}_{i^k}^* - \dot{u}_k^*)^2}{|\xi_{i^k}^{(k)}|} + 2 \frac{(\theta_{i^k} - \theta_k)(\theta_{i^k}^* - \theta_k^*)}{|\xi_{i^k}^{(k)}|} \right] V_{i^k} + \int_A \frac{2Ez^5}{1-\nu^2} dA \sum_i \frac{(\dot{u}_{i^k}^* - \dot{u}_k^*)(\theta_{i^k}^* - \theta_k^*)}{|\xi_{i^k}^{(k)}|} V_{i^k} + \int_A \frac{Ez^6}{1-\nu^2} dA \sum_i \frac{(\theta_{i^k}^* - \theta_k^*)^2}{|\xi_{i^k}^{(k)}|} V_{i^k} \right\} \\
& + \frac{1}{\delta^2 A^2} \left\{ \int_A \frac{Ev}{1-\nu^2} dA \sum_i (\bar{u}_{i^k} - \bar{u}_k) \frac{\theta_z^{i^k} + \theta_z^{(k)}}{2} \operatorname{sgn}(\xi_{i^k}^{(k)}) V_{i^k} + \int_A \frac{Evz}{1-\nu^2} dA \sum_i \left[(\bar{u}_{i^k} - \bar{u}_k)(\dot{w}_{i^k}^* + \dot{w}_k^*) + (\theta_{i^k} - \theta_k) \frac{\theta_z^{i^k} + \theta_z^{(k)}}{2} \right] \operatorname{sgn}(\xi_{i^k}^{(k)}) V_{i^k} \right. \\
& + \int_A \frac{Evz^2}{1-\nu^2} dA \sum_i \left[(\theta_{i^k} - \theta_k)(\dot{w}_{i^k}^* + \dot{w}_k^*) + (\dot{u}_{i^k}^* - \dot{u}_k^*) \frac{\theta_z^{i^k} + \theta_z^{(k)}}{2} \right] \operatorname{sgn}(\xi_{i^k}^{(k)}) V_{i^k} \\
& \left. + \int_A \frac{Evz^3}{1-\nu^2} dA \sum_i \left[(\dot{u}_{i^k}^* - \dot{u}_k^*)(\dot{w}_{i^k}^* + \dot{w}_k^*) + (\theta_{i^k}^* - \theta_k^*) \frac{\theta_z^{i^k} + \theta_z^{(k)}}{2} \right] \operatorname{sgn}(\xi_{i^k}^{(k)}) V_{i^k} + \int_A \frac{Evz^4}{1-\nu^2} dA \sum_i (\theta_{i^k}^* - \theta_k^*)(\dot{w}_{i^k}^* + \dot{w}_k^*) \operatorname{sgn}(\xi_{i^k}^{(k)}) V_{i^k} \right\} \\
& + \frac{1}{2} \frac{1}{\delta^2 A^2} \left\{ \int_A \mathcal{G} dA \sum_i \frac{\left(\bar{w}_{i^k} - \bar{w}_k + \frac{\theta_{i^k} + \theta_k}{2} \xi_{i^k}^{(k)} \right)^2}{|\xi_{i^k}^{(k)}|} V_{i^k} + 2 \int_A \mathcal{G} z dA \sum_i \left(\bar{w}_{i^k} - \bar{w}_k + \frac{\theta_{i^k} + \theta_k}{2} \xi_{i^k}^{(k)} \right) \left(\frac{\theta_z^{i^k} - \theta_z^{(k)}}{|\xi_{i^k}^{(k)}|} + (\dot{u}_{i^k}^* - \dot{u}_k^*) \operatorname{sgn}(\xi_{i^k}^{(k)}) \right) V_{i^k} \right. \\
& + \int_A \mathcal{G} z^2 dA \sum_i \frac{\left[\frac{\theta_z^{i^k} - \theta_z^{(k)}}{|\xi_{i^k}^{(k)}|} + (\dot{u}_{i^k}^* + \dot{u}_k^*) \xi_{i^k}^{(k)} \right]^2 + 2 \left(\bar{w}_{i^k} - \bar{w}_k + \frac{\theta_{i^k} + \theta_k}{2} \xi_{i^k}^{(k)} \right) \left(\dot{w}_{i^k}^* - \dot{w}_k^* + 3 \frac{\theta_{i^k}^* + \theta_k^*}{2} \xi_{i^k}^{(k)} \right)}{|\xi_{i^k}^{(k)}|} V_{i^k} \\
& \left. + 2 \int_A \mathcal{G} z^3 dA \sum_i \frac{\theta_z^{i^k} - \theta_z^{(k)} + (\dot{u}_{i^k}^* + \dot{u}_k^*) \xi_{i^k}^{(k)}}{|\xi_{i^k}^{(k)}|} \left(\dot{w}_{i^k}^* - \dot{w}_k^* + 3 \frac{\theta_{i^k}^* + \theta_k^*}{2} \xi_{i^k}^{(k)} \right) V_{i^k} + \int_A \mathcal{G} z^4 dA \sum_i \frac{\left(\dot{w}_{i^k}^* - \dot{w}_k^* + 3 \frac{\theta_{i^k}^* + \theta_k^*}{2} \xi_{i^k}^{(k)} \right)^2}{|\xi_{i^k}^{(k)}|} V_{i^k} \right\}
\end{aligned}$$

$$\begin{aligned}
W_{FD}^{(i)} = & \frac{1}{2} \frac{1}{\delta^2 A^2} \left\{ \int_A \frac{E}{1-\nu^2} dA \sum_i \left[\frac{(\bar{u}_{(i)} - \bar{u}_{(j)})^2}{|\xi_{(i)(j)}|} + \left(\frac{\theta_z^{(i)} + \theta_z^{(j)}}{2} \right)^2 |\xi_{(i)(j)}| \right] V_{(i)} + \int_A \frac{2Ez}{1-\nu^2} dA \sum_i \left[\frac{(\bar{u}_{(i)} - \bar{u}_{(j)})(\theta_{(i)} - \theta_{(j)})}{|\xi_{(i)(j)}|} + \frac{\theta_z^{(i)} + \theta_z^{(j)}}{2} (\dot{w}_{(i)} + \dot{w}_{(j)}) |\xi_{(i)(j)}| \right] V_{(i)} \right. \\
& + \int_A \frac{Ez^2}{1-\nu^2} dA \sum_i \left[\frac{(\theta_{(i)} - \theta_{(j)})^2}{|\xi_{(i)(j)}|} + 2 \frac{(\bar{u}_{(i)} - \bar{u}_{(j)})(\dot{u}_{(i)} - \dot{u}_{(j)})}{|\xi_{(i)(j)}|} + (\dot{w}_{(i)} + \dot{w}_{(j)})^2 |\xi_{(i)(j)}| \right] V_{(i)} \\
& + \int_A \frac{2Ez^3}{1-\nu^2} dA \sum_i \left[\frac{(\bar{u}_{(i)} - \bar{u}_{(j)})(\theta_{(i)}^* - \theta_{(j)}^*)}{|\xi_{(i)(j)}|} + \frac{(\theta_{(i)} - \theta_{(j)})(\dot{u}_{(i)} - \dot{u}_{(j)})}{|\xi_{(i)(j)}|} \right] V_{(i)} \\
& \left. + \int_A \frac{Ez^4}{1-\nu^2} dA \sum_i \left[\frac{(\dot{u}_{(i)} - \dot{u}_{(j)})^2}{|\xi_{(i)(j)}|} + 2 \frac{(\theta_{(i)} - \theta_{(j)})(\theta_{(i)}^* - \theta_{(j)}^*)}{|\xi_{(i)(j)}|} \right] V_{(i)} + \int_A \frac{2Ez^5}{1-\nu^2} dA \sum_i \frac{(\dot{u}_{(i)} - \dot{u}_{(j)})(\theta_{(i)}^* - \theta_{(j)}^*)}{|\xi_{(i)(j)}|} V_{(i)} + \int_A \frac{Ez^6}{1-\nu^2} dA \sum_i \frac{(\theta_{(i)}^* - \theta_{(j)}^*)^2}{|\xi_{(i)(j)}|} V_{(i)} \right\} \\
& + \frac{1}{\delta^2 A^2} \left\{ \int_A \frac{Ev}{1-\nu^2} dA \sum_i (\bar{u}_{(i)} - \bar{u}_{(j)}) \frac{\theta_z^{(i)} + \theta_z^{(j)}}{2} \operatorname{sgn}(\xi_{(i)(j)}) V_{(i)} + \int_A \frac{Evz}{1-\nu^2} dA \sum_i \left[(\bar{u}_{(i)} - \bar{u}_{(j)})(\dot{w}_{(i)} + \dot{w}_{(j)}) + (\theta_{(i)} - \theta_{(j)}) \frac{\theta_z^{(i)} + \theta_z^{(j)}}{2} \right] \operatorname{sgn}(\xi_{(i)(j)}) V_{(i)} \right. \\
& + \int_A \frac{Evz^2}{1-\nu^2} dA \sum_i \left[(\theta_{(i)} - \theta_{(j)})(\dot{w}_{(i)} + \dot{w}_{(j)}) + (\dot{u}_{(i)} - \dot{u}_{(j)}) \frac{\theta_z^{(i)} + \theta_z^{(j)}}{2} \right] \operatorname{sgn}(\xi_{(i)(j)}) V_{(i)} \\
& \left. + \int_A \frac{Evz^3}{1-\nu^2} dA \sum_i \left[(\dot{u}_{(i)} - \dot{u}_{(j)})(\dot{w}_{(i)} + \dot{w}_{(j)}) + (\theta_{(i)}^* - \theta_{(j)}^*) \frac{\theta_z^{(i)} + \theta_z^{(j)}}{2} \right] \operatorname{sgn}(\xi_{(i)(j)}) V_{(i)} + \int_A \frac{Evz^4}{1-\nu^2} dA \sum_i (\theta_{(i)}^* - \theta_{(j)}^*)(\dot{w}_{(i)} + \dot{w}_{(j)}) \operatorname{sgn}(\xi_{(i)(j)}) V_{(i)} \right\} \\
& + \frac{1}{2} \frac{1}{\delta^2 A^2} \left\{ \int_A Gz dA \sum_i \frac{\left(\bar{w}_{(i)} - \bar{w}_{(j)} + \frac{\theta_{(i)} + \theta_{(j)}}{2} \xi_{(i)(j)} \right)^2}{|\xi_{(i)(j)}|} V_{(i)} + 2 \int_A Gz dA \sum_i \left(\bar{w}_{(i)} - \bar{w}_{(j)} + \frac{\theta_{(i)} + \theta_{(j)}}{2} \xi_{(i)(j)} \right) \left(\frac{\theta_z^{(i)} - \theta_z^{(j)}}{|\xi_{(i)(j)}|} + (\dot{u}_{(i)} - \dot{u}_{(j)}) \operatorname{sgn}(\xi_{(i)(j)}) \right) V_{(i)} \right. \\
& + \int_A Gz^2 dA \sum_i \frac{\left[\frac{\theta_z^{(i)} - \theta_z^{(j)}}{|\xi_{(i)(j)}|} + (\dot{u}_{(i)} + \dot{u}_{(j)}) \xi_{(i)(j)} \right]^2 + 2 \left(\bar{w}_{(i)} - \bar{w}_{(j)} + \frac{\theta_{(i)} + \theta_{(j)}}{2} \xi_{(i)(j)} \right) \left(\dot{w}_{(i)} - \dot{w}_{(j)} + 3 \frac{\theta_{(i)}^* + \theta_{(j)}^*}{2} \xi_{(i)(j)} \right)}{|\xi_{(i)(j)}|} V_{(i)} \\
& \left. + 2 \int_A Gz^3 dA \sum_i \frac{\theta_z^{(i)} - \theta_z^{(j)} + (\dot{u}_{(i)} + \dot{u}_{(j)}) \xi_{(i)(j)}}{|\xi_{(i)(j)}|} \left(\dot{w}_{(i)} - \dot{w}_{(j)} + 3 \frac{\theta_{(i)}^* + \theta_{(j)}^*}{2} \xi_{(i)(j)} \right) V_{(i)} + \int_A Gz^4 dA \sum_i \frac{\left(\dot{w}_{(i)} - \dot{w}_{(j)} + 3 \frac{\theta_{(i)}^* + \theta_{(j)}^*}{2} \xi_{(i)(j)} \right)^2}{|\xi_{(i)(j)}|} V_{(i)} \right\}
\end{aligned}$$

(4.90a, b)

Substituting Eqs. (4.90) into (4.89) results in the final PD EoM for FGM higher order deformable beam as

$$\begin{aligned} & \rho_{(k)} \left(\ddot{u}_{(k)} + \frac{I}{A} \ddot{u}_{(k)} \right) \\ &= \frac{2}{\delta^2 \mathcal{A}^2} \left[\int_A \frac{E}{1-\nu^2} dA \sum_j \frac{\bar{u}_{(j)} - \bar{u}_{(k)}}{|\xi_{(j)(k)}|} V_{(j)} + \int_A \frac{E\nu}{1-\nu^2} dA \sum_j \frac{\theta_z^{(j)} + \theta_z^{(k)}}{2} \operatorname{sgn}(\xi_{(j)(k)}) V_{(j)} \right. \\ & \quad + \int_A \frac{Ez}{1-\nu^2} dA \sum_j \frac{\theta_{(j)} - \theta_{(k)}}{|\xi_{(j)(k)}|} V_{(j)} + \int_A \frac{E\nu z}{1-\nu^2} dA \sum_j (\dot{w}_{(j)} + \dot{w}_{(k)}) \operatorname{sgn}(\xi_{(j)(k)}) V_{(j)} \\ & \quad \left. + \int_A \frac{Ez^2}{1-\nu^2} dA \sum_j \frac{\dot{u}_{(j)} - \dot{u}_{(k)}}{|\xi_{(j)(k)}|} V_{(j)} + \int_A \frac{Ez^3}{1-\nu^2} dA \sum_j \frac{\theta_{(j)}^* - \theta_{(k)}^*}{|\xi_{(j)(k)}|} V_{(j)} \right] + b_x^{(k)} \end{aligned} \quad (4.91a)$$

$$\begin{aligned} & \rho_{(k)} \left(\frac{I}{A} \ddot{\theta}_{(k)} + \frac{I}{A} \ddot{\theta}_{(k)} \right) \\ &= \frac{2}{\delta^2 \mathcal{A}^2} \left[\int_A \frac{Ez}{1-\nu^2} dA \sum_j \frac{\bar{u}_{(j)} - \bar{u}_{(k)}}{|\xi_{(j)(k)}|} V_{(j)} + \int_A \frac{E\nu z}{1-\nu^2} dA \sum_j \frac{\theta_z^{(j)} + \theta_z^{(k)}}{2} \operatorname{sgn}(\xi_{(j)(k)}) V_{(j)} \right. \\ & \quad + \int_A \frac{Ez^2}{1-\nu^2} dA \sum_j \frac{\theta_{(j)} - \theta_{(k)}}{|\xi_{(j)(k)}|} V_{(j)} + \int_A \frac{E\nu z^2}{1-\nu^2} dA \sum_j (\dot{w}_{(j)} + \dot{w}_{(k)}) \operatorname{sgn}(\xi_{(j)(k)}) V_{(j)} \\ & \quad + \int_A \frac{Ez^3}{1-\nu^2} dA \sum_j \frac{\dot{u}_{(j)} - \dot{u}_{(k)}}{|\xi_{(j)(k)}|} V_{(j)} + \int_A \frac{Ez^4}{1-\nu^2} dA \sum_j \frac{\theta_{(j)}^* - \theta_{(k)}^*}{|\xi_{(j)(k)}|} V_{(j)} \\ & \quad - \int_A \frac{G}{2} dA \sum_j \left(\bar{w}_{(j)} - \bar{w}_{(k)} + \frac{\theta_{(j)} + \theta_{(k)}}{2} \xi_{(j)(k)} \right) \operatorname{sgn}(\xi_{(j)(k)}) V_{(j)} \\ & \quad - \int_A \frac{Gz}{2} dA \sum_j \left[\theta_z^{(j)} - \theta_z^{(k)} + (\dot{u}_{(j)} + \dot{u}_{(k)}) \xi_{(j)(k)} \right] \operatorname{sgn}(\xi_{(j)(k)}) V_{(j)} \\ & \quad \left. - \int_A \frac{Gz^2}{2} dA \sum_j \left[\dot{w}_{(j)} - \dot{w}_{(k)} + \frac{3}{2} (\theta_{(j)}^* + \theta_{(k)}^*) \xi_{(j)(k)} \right] \operatorname{sgn}(\xi_{(j)(k)}) V_{(j)} \right] \end{aligned} \quad (4.91b)$$

$$\rho_{(k)} \left(\ddot{w}_{(k)} + \frac{I}{A} \ddot{w}_{(k)} \right) = \frac{2}{\delta^2 \mathcal{A}^2} \left\{ \int_A Gz dA \sum_j \left[\frac{\bar{w}_{(j)} - \bar{w}_{(k)}}{|\xi_{(j)(k)}|} + \frac{\theta_{(j)} + \theta_{(k)}}{2} \operatorname{sgn}(\xi_{(j)(k)}) \right] V_{(j)} \right. \\ \left. + \int_A Gz dA \sum_j \left[\frac{\theta_z^{(j)} - \theta_z^{(k)}}{|\xi_{(j)(k)}|} + (\dot{u}_{(j)} + \dot{u}_{(k)}) \operatorname{sgn}(\xi_{(j)(k)}) \right] V_{(j)} \right. \\ \left. + \int_A Gz^2 dA \sum_j \left[\frac{\dot{w}_{(j)} - \dot{w}_{(k)}}{|\xi_{(j)(k)}|} + \frac{3}{2} (\theta_{(j)}^* + \theta_{(k)}^*) \operatorname{sgn}(\xi_{(j)(k)}) \right] V_{(j)} \right\} + b_z^{(k)} \quad (4.91c)$$

$$\rho_{(k)} \frac{I}{A} \ddot{\theta}_z^{(k)} = \frac{2}{\delta^2 A^2} \left\{ \begin{aligned} & - \int_A \frac{E}{1-\nu^2} dA \sum_j \frac{\theta_z^{(j)} + \theta_z^{(k)}}{4} |\xi_{(j)(k)}| V_{(j)} - \int_A \frac{E\nu}{1-\nu^2} dA \sum_j \frac{\bar{u}_{(j)} - \bar{u}_{(k)}}{2} \operatorname{sgn}(\xi_{(j)(k)}) V_{(j)} \\ & - \int_A \frac{Ez}{1-\nu^2} dA \sum_j \frac{\dot{w}_{(j)} + \dot{w}_{(k)}}{2} |\xi_{(j)(k)}| V_{(j)} - \int_A \frac{E\nu z}{1-\nu^2} dA \sum_j \frac{\theta_{(j)} - \theta_{(k)}}{2} \operatorname{sgn}(\xi_{(j)(k)}) V_{(j)} \\ & - \int_A \frac{E\nu z^2}{1-\nu^2} dA \sum_j \frac{\dot{u}_{(j)} - \dot{u}_{(k)}}{2} \operatorname{sgn}(\xi_{(j)(k)}) V_{(j)} - \int_A \frac{E\nu z^3}{1-\nu^2} dA \sum_j \frac{\theta_{(j)}^* - \theta_{(k)}^*}{2} \operatorname{sgn}(\xi_{(j)(k)}) V_{(j)} \\ & + \int_A G dA \sum_j \left[\frac{\bar{w}_{(j)} - \bar{w}_{(k)}}{|\xi_{(j)(k)}|} + \frac{\theta_{(j)} + \theta_{(k)}}{2} \operatorname{sgn}(\xi_{(j)(k)}) \right] V_{(j)} \\ & + \int_A G^2 dA \sum_j \left[\frac{\theta_z^{(j)} - \theta_z^{(k)}}{|\xi_{(j)(k)}|} + (\dot{u}_{(j)} + \dot{u}_{(k)}) \operatorname{sgn}(\xi_{(j)(k)}) \right] V_{(j)} \\ & + \int_A G^3 dA \sum_j \left[\frac{\dot{w}_{(j)} - \dot{w}_{(k)}}{|\xi_{(j)(k)}|} + \frac{3}{2} (\theta_{(j)}^* + \theta_{(k)}^*) \operatorname{sgn}(\xi_{(j)(k)}) \right] V_{(j)} \end{aligned} \right\} \quad (4.91d)$$

$$\rho_{(k)} \left(\frac{I^*}{A} \ddot{w}_{(k)} + \frac{I}{A} \ddot{\bar{w}}_{(k)} \right) = \frac{2}{\delta^2 A^2} \left\{ \begin{aligned} & - \int_A \frac{Ez}{1-\nu^2} dA \sum_j \frac{\theta_z^{(j)} + \theta_z^{(k)}}{2} |\xi_{(j)(k)}| V_{(j)} \\ & - \int_A \frac{E\nu z}{1-\nu^2} dA \sum_j (\bar{u}_{(j)} - \bar{u}_{(k)}) \operatorname{sgn}(\xi_{(j)(k)}) V_{(j)} \\ & - \int_A \frac{Ez^2}{1-\nu^2} dA \sum_j (\dot{w}_{(j)} + \dot{w}_{(k)}) |\xi_{(j)(k)}| V_{(j)} \\ & - \int_A \frac{E\nu z^2}{1-\nu^2} dA \sum_j (\theta_{(j)} - \theta_{(k)}) \operatorname{sgn}(\xi_{(j)(k)}) V_{(j)} \\ & - \int_A \frac{E\nu z^3}{1-\nu^2} dA \sum_j (\dot{u}_{(j)} - \dot{u}_{(k)}) \operatorname{sgn}(\xi_{(j)(k)}) V_{(j)} \\ & - \int_A \frac{E\nu z^4}{1-\nu^2} dA \sum_j (\theta_{(j)}^* - \theta_{(k)}^*) \operatorname{sgn}(\xi_{(j)(k)}) V_{(j)} \\ & + \int_A G^2 dA \sum_j \left[\frac{\bar{w}_{(j)} - \bar{w}_{(k)}}{|\xi_{(j)(k)}|} + \frac{\theta_{(j)} + \theta_{(k)}}{2} \operatorname{sgn}(\xi_{(j)(k)}) \right] V_{(j)} \\ & + \int_A G^3 dA \sum_j \left[\frac{\theta_z^{(j)} + \theta_z^{(k)}}{|\xi_{(j)(k)}|} + (\dot{u}_{(j)} + \dot{u}_{(k)}) \operatorname{sgn}(\xi_{(j)(k)}) \right] V_{(j)} \\ & + \int_A G^4 dA \sum_j \left[\frac{\dot{w}_{(j)} - \dot{w}_{(k)}}{|\xi_{(j)(k)}|} + \frac{3}{2} (\theta_{(j)}^* + \theta_{(k)}^*) \operatorname{sgn}(\xi_{(j)(k)}) \right] V_{(j)} \end{aligned} \right\} \quad (4.91e)$$

4.5.3 Numerical Cases

To verify the validity of the PD formulation for functionally graded higher order beams, the PD solutions are compared with the corresponding finite element (FE) analysis results. In this study, the functionally graded material properties are chosen as Young's Modulus, E and shear modulus G and they are assumed to vary linearly through the thickness as

$$E(z) = (E_t - E_b) \frac{z}{h} + \frac{1}{2}(E_t + E_b) \quad (4.92a)$$

$$Q(z) = \frac{E(z)}{2[1 + \nu(z)]} \quad (4.92b)$$

$$\nu(z) = 0.3 \quad (4.92c)$$

where E_t and E_b denote the Young's modulus of the top and bottom surfaces of the beam, and h denotes the total thickness of the beam.

In the following numerical cases, a functionally graded higher order beam with rectangular cross section, which subjected to different boundary conditions is taken under consideration. The length, thickness and width of the beam are chosen as $L = 1\text{m}$, $h = 0.15\text{m}$ and $b = 0.1\text{m}$, respectively. Thus, the cross-section area of the beam is $A = h \times b = 0.015 \text{ m}^2$. The Young's modulus of the top and bottom surface are chosen as $E_t = 200 \text{ GPa}$ and $E_b = 100 \text{ GPa}$.

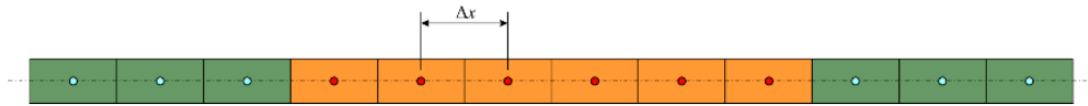


Fig. 4.40 PD model of functionally graded material beam

The PD models are discretized into one single row of material points through the thickness and 500 material points throughout the x axis. Thus, the distance between two adjacent material points is $\Delta x = 0.002\text{m}$. Two fictitious regions (denote in green) are introduced respectively outside the two ends as the external boundaries with a width of $3\Delta x$ (see Fig. 4.40).

The corresponding FE models are creating in ANSYS by using PLANE182 elements, with 100 elements along the x -direction and 50 elements along z -direction. In order to obtain the functionally graded character, varying materials properties are assigned to the elements through the thickness direction. The Young's modulus varies gradually over the thickness from the first layer $E_1 = 101 \text{ GPa}$ to the last layer $E_{50} = 199 \text{ GPa}$, as shown in Fig. 4.41. The Poisson's ratio, $\nu = 0.3$, is applied in ANSYS.

Layer 50	$E_{50}=199 \text{ GPa}$
Layer i	$E_i=100x(1+(i-1/2)/50) \text{ GPa}$
Layer 3	E_3
Layer 2	E_2
Layer 1	$E_1=101 \text{ GPa}$

Figure 4.41 Material variation in the thickness direction for the finite element model

Note that the PD results are preferably compared to PLANE element rather than BEAM element. This is because an entire 2D plane-stress Hooke's Law is considered in this studies, and BEAM element formulations are usually based on Euler-Bernoulli or Timoshenko beam theory, which are referred to as 1D Hooke's Law and may not be suitable for references.

4.5.3.1 Simply Supported Beam Subjected to Transverse Loading

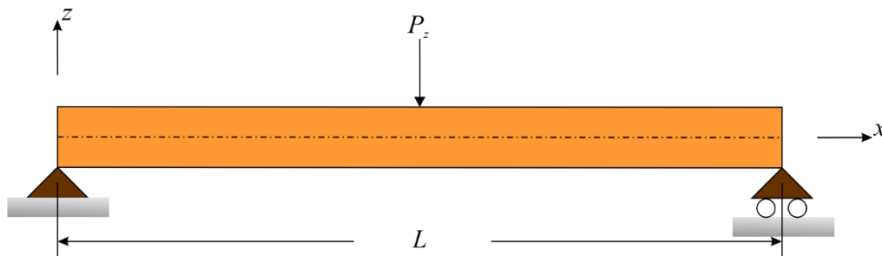


Figure 4.42 Beam with pinned support – roller support boundary conditions.

A simply supported functionally graded beam subjected to a concentrated force of $P_z = 1000 \text{ N}$ at the central is taken into consideration. With respect to PD model, the load is transformed into a body load of $b_z = \frac{P_z}{2A\Delta x} = 1.6667e7 \text{ N/m}^3$ and it is imposed on the two material points locate on the central position of the beam (see Fig. 4.43).

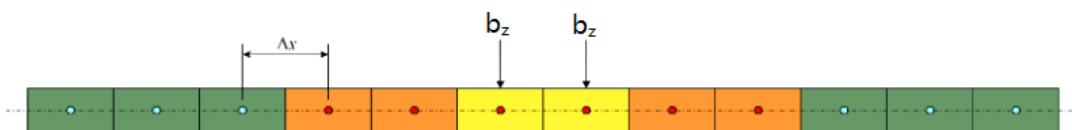


Figure 4.43 Discretization, applied loading and fictitious region

The PD and FE transverse displacements, $w(x)$ and axial displacements, $u(x)$ are compared in Fig. 4.44. Both approaches yield similar displacement variations. These results verify the accurateness of the current PD formulation for a higher order functionally graded beam theory for pinned support – roller support boundary condition.

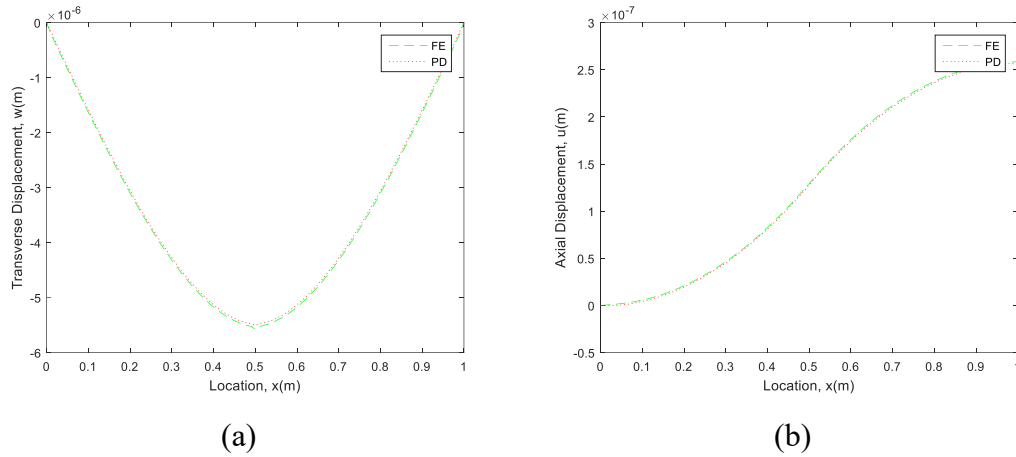


Figure 4.44 Comparison of PD and FE results; (a) transverse displacement, (b) axial displacement

4.5.3.2 Cantilever Beam Subjected to a Point End Load

In the second example, a cantilever functionally graded beam is considered as shown in Fig. 4.45. The beam is subjected to a concentrated force of $F = 1000\text{N}$ at the free end.

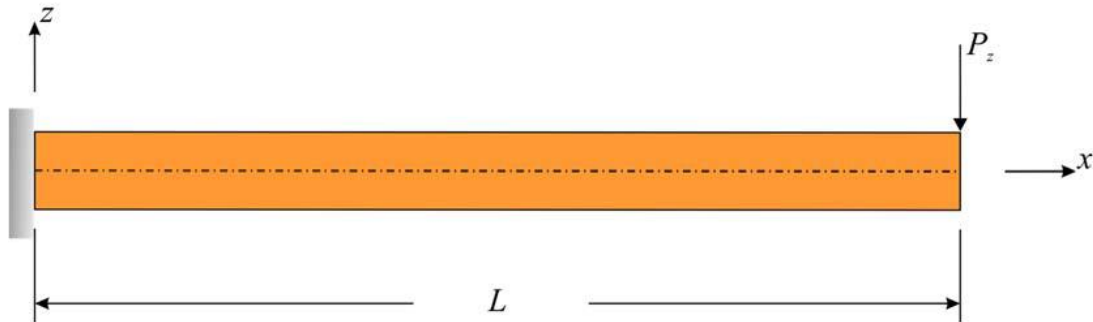


Figure 4.45. Cantilever beam subjected to a point end load.

As shown in Fig. 4.46, a very good agreement is observed between PD and FE results for both transverse and axial displacement results.

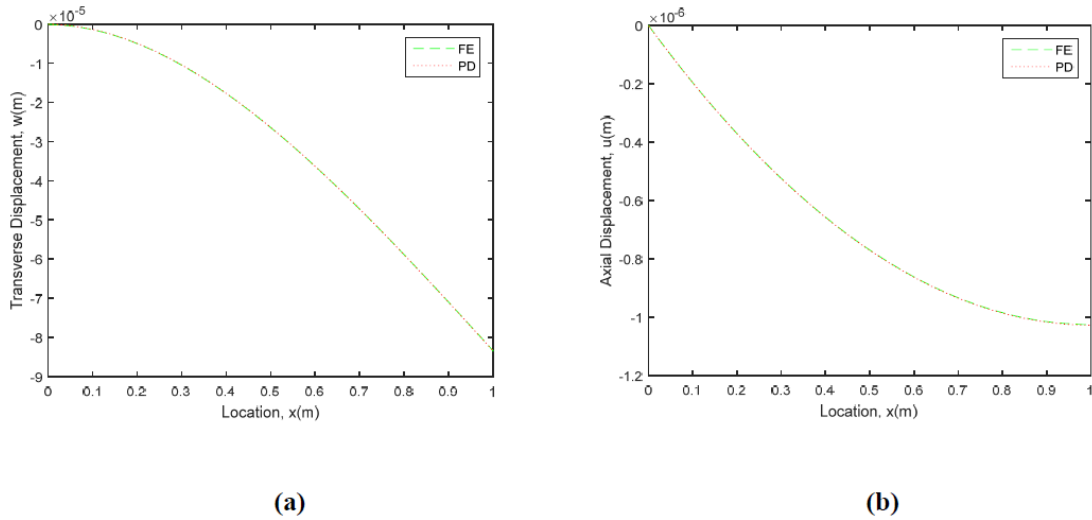


Figure 4.46. Variation of (a) transverse displacement, (b) axial displacement along the beam.

4.5.3.3 Clamped-Roller Supported Beam Subjected to Transverse Loading

In the final example, a clamped-roller supported functionally graded beam is considered as shown in Fig. 4.47. The beam is subjected to a concentrated force of $F = 1000\text{N}$ at its center.

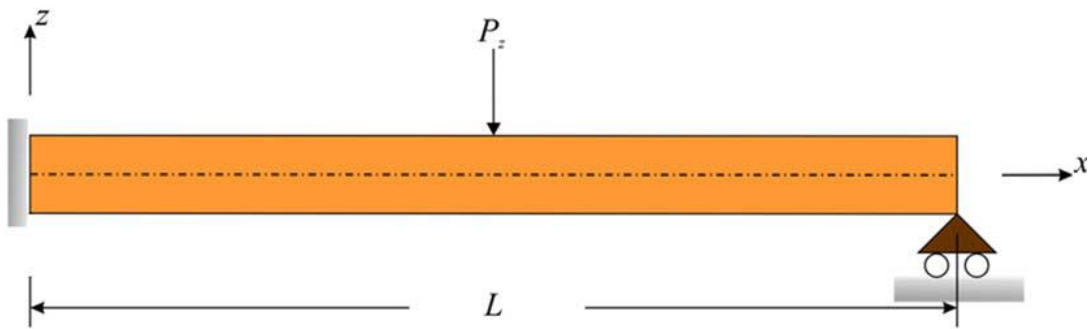


Figure 4.47. Clamped-simply supported beam subjected to transverse loading.

As in the previous cases, PD and FE results also agree with each other for this mixed (clamped-roller supported) boundary condition case for both axial and transverse displacement as shown in Fig. 4.48.

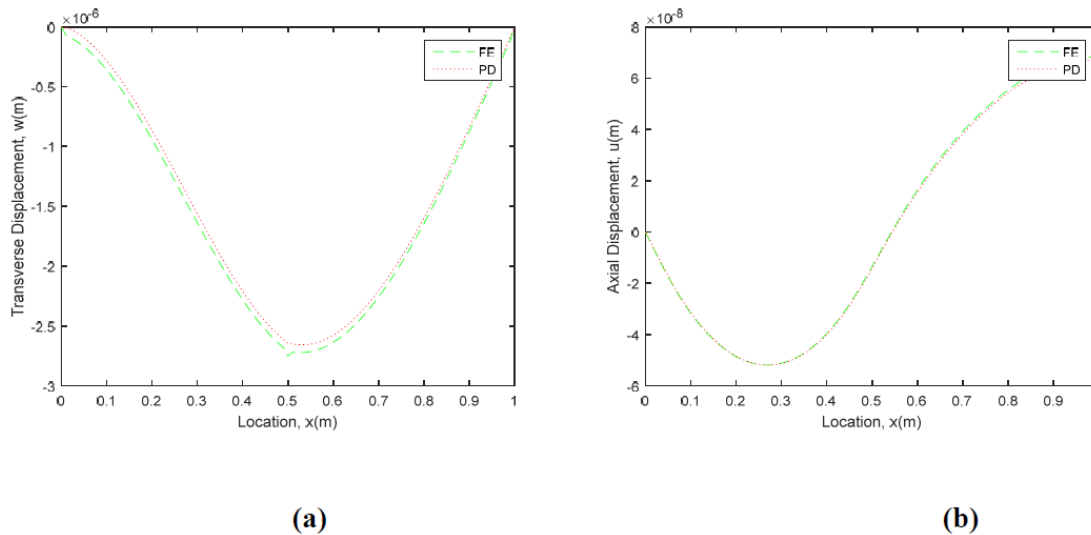


Figure 4.48. Variation of (a) transverse displacement, (b) axial displacement along the beam.

4.6 Comparison Among PD Beam Theories

In the previous sections, various of beam theories based on PD framework are introduced and their validation are verified by benchmark problems with comparison against the corresponding FE results. As mentioned in Chapter 2, Euler, Timoshenko and higher order beam theories based on classical mechanics theory are generally appropriate for thin, moderate thick and thick beam, respectively. In order to demonstrate that a similar conclusion can be obtained based on PD framework, three different types of PD beam theories are tested in the following numerical cases.

Three functionally graded beams with thickness of $h = 0.05m, 0.10m$ and $0.15m$ are considered for this study. The length and width are chosen as $L = 1m$ and $W = 0.01m$ equally for the three cases. Three beams are subjected to simply supported boundary conditions and a concentrated force of $p = 1000N$ at the center, as shown in Fig. 4.49.

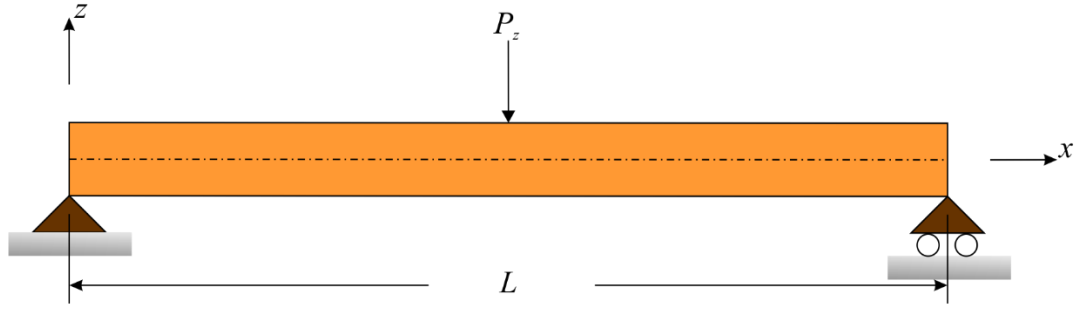


Figure 4.49 Simply supported FGM beam subjected to transverse load.

The functionally graded material properties are chosen as Young's Modulus, E and shear modulus G and they are assumed to vary linearly through the thickness as

$$E(z) = (E_t - E_b) \frac{z}{h} + \frac{1}{2}(E_t + E_b) \quad (4.93a)$$

$$G(z) = \frac{E(z)}{2[1 + \nu(z)]} \quad (4.93b)$$

$$\nu(z) = 0.3 \quad (4.93c)$$

where $E_t = 200GPa$ and $E_b = 100G$ denote the Young's modulus of the top and bottom surfaces of the beam, and h denotes the total thickness of the beam.

Three PD beam models are discretized into 101 material points and therefore the distance between material points is $\Delta x = 1/101m$. The PD horizon size is chosen as $\delta = 3\Delta x$.

As shown in Fig. 4.50, when the beam is thin, all the three solutions agree well with each other. As the thickness increases, PD Euler beam solution may not accurately capture the deformation behavior compared to PD Timoshenko and higher order results (see Fig. 4.51 and 4.52), which is in accordance with the conclusion from the classical mechanics theory.

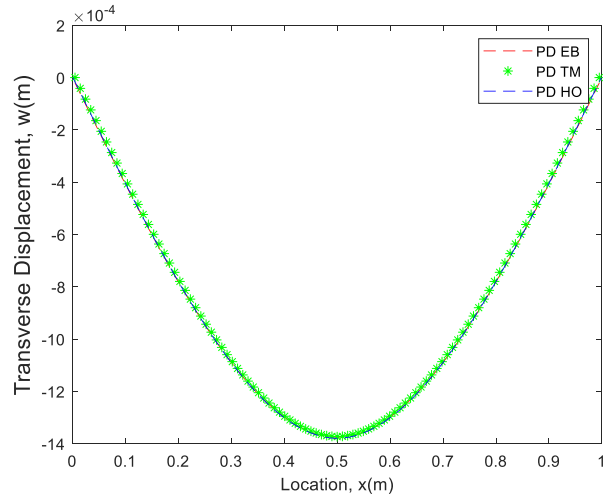


Figure 4.50 Deflections with thickness of $h = 0.05\text{m}$

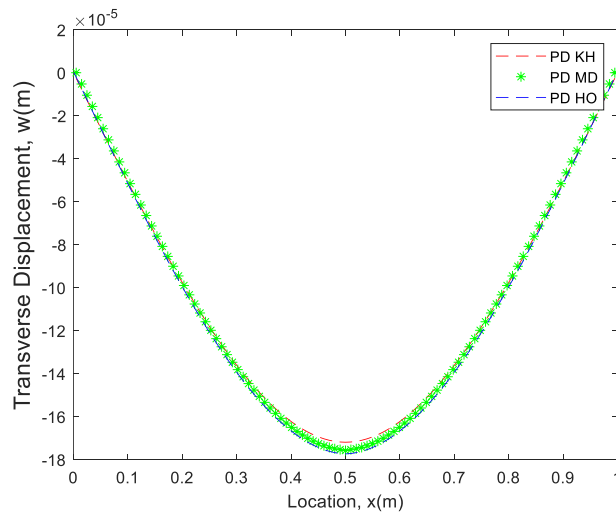


Figure 4.51 Deflections with thickness of $h = 0.10\text{m}$

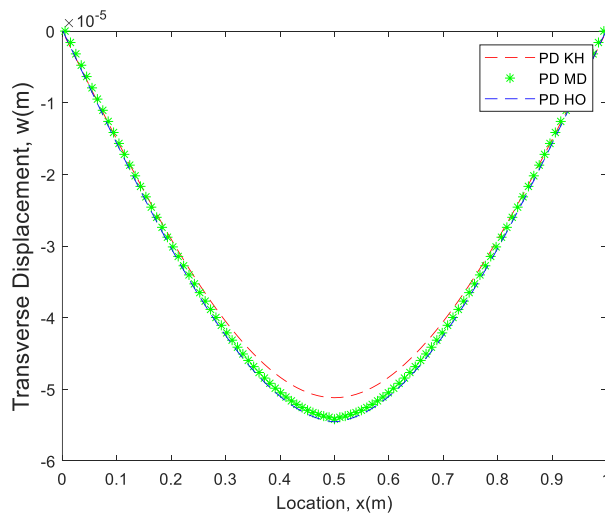


Figure 4.52 Deflections with thickness of $h = 0.15\text{m}$

4.7 Conclusion

In this section, PD formulations of Timoshenko beam, higher order deformable beam and FGM of Euler Beam, Timoshenko Beam and higher order beam are presented, respectively. These formulations are obtained by using Euler-Lagrange equations and Taylor's expansion. The derivation of PD SED functions and implementation of boundary conditions are explained in Appendix A1 and B1, respectively. To demonstrate the capability of the presented approach, several different beam configurations are considered including simply supported beam subjected to distributed loading, simply supported beam with concentrated load, clamped-clamped beam subjected to distributed loading, cantilever beam subjected to a point load at its free end and cantilever beam subjected to a moment at its free end. All the numerical results are based on PD static solution method, which is explained in section 3.3.2, and generated by using the commercial programming software, Matlab. Displacement results along the beam obtained from PD and finite element method are compared with each other and very good agreement is obtained between the two approaches. Therefore, it can be concluded that the proposed methodology is capable of representing beam theories in PD framework.

5. PD Formulations for Plate Theories

5.1 PD Formulation for Kirchhoff Plate Theory

5.1.1 Kirchhoff Plate Theory

Kirchhoff plate theory is based on the assumption that “normals to the mid-surface of the undeformed plate remain straight and normal to the mid-surface, and unstretched in length, during deformation” (Love, 1888). The displacement field of any material point can be represented in terms of the displacement field of the material points on mid-plane as

$$u(x, y, z, t) = z\theta_x(x, y, t) \quad (5.1a)$$

$$v(x, y, z, t) = z\theta_y(x, y, t) \quad (5.1b)$$

$$w(x, y, z, t) = \bar{w}(x, y, t) \quad (5.1c)$$

where $\theta_x(x, y, t)$ and $\theta_y(x, y, t)$ denote the rotation of the material points on the mid-plane about positive y -direction and negative x -direction, respectively, and $\bar{w}(x, y, t)$ denotes the transverse displacement of material points on mid-plane. Hereafter, $\theta_x(x, y, t)$, $\theta_y(x, y, t)$ and $\bar{w}(x, y, t)$ are written simply as θ_x , θ_y and \bar{w} , respectively.

Based on Eqs (5.1) and Kirchhoff Plate assumptions, the strain components can be given as

$$\varepsilon_x = z \frac{\partial \theta_x}{\partial x} \quad (5.2a)$$

$$\varepsilon_y = z \frac{\partial \theta_y}{\partial y} \quad (5.2b)$$

$$\gamma_{xy} = z \left(\frac{\partial \theta_x}{\partial y} + \frac{\partial \theta_y}{\partial x} \right) \quad (5.2c)$$

$$\gamma_{xz} = \theta_x + \frac{\partial \bar{w}}{\partial x} = 0 \quad (5.2d)$$

$$\gamma_{yz} = \theta_y + \frac{\partial \bar{w}}{\partial y} = 0 \quad (5.2e)$$

Eliminating θ_x and θ_y from Eqs. (5.2a, b, c) by taking use of Eq. (5.2d, e) gives

$$\varepsilon_x = -z \frac{\partial^2 \bar{w}}{\partial x^2} \quad (5.3a)$$

$$\varepsilon_y = -z \frac{\partial^2 \bar{w}}{\partial y^2} \quad (5.3b)$$

$$\gamma_{xy} = -2z \frac{\partial^2 \bar{w}}{\partial x \partial y} \quad (5.3c)$$

which can be written in the tensorial form as

$$\varepsilon_{IJ} = -z \frac{\partial^2 \bar{w}}{\partial x_I \partial x_J} \quad (5.4)$$

where the subscripts I, J, \dots take up the value 1(= x) and 2(= y), and this convention will be applied throughout this study.

According to the plane-stress constitutive law, the stress components can be written as

$$\sigma_{IJ} = C_{IJKL} \varepsilon_{KL} \quad (5.5)$$

where \mathbf{C} represents the stiffness tensor, which can be defined for isotropic material as

$$C_{IJKL} = \frac{E}{1-\nu^2} \left[\frac{1-\nu}{2} (\delta_{IL} \delta_{JK} + \delta_{IK} \delta_{JL}) + \nu \delta_{IJ} \delta_{KL} \right] \quad (5.6)$$

According to the elastic theory, the average strain energy density can be expressed as

$$W_{\text{com}} = \frac{1}{2h} \int_{-\frac{h}{2}}^{\frac{h}{2}} \sigma_{IJ} \varepsilon_{IJ} dz \quad (5.7)$$

which can be written in terms of transverse displacement only by utilizing the relations given in Eq. (5.4), (5.5) and (5.6) as

$$W_{\text{com}} = \frac{D}{2h} \left[\left(\frac{\partial^2 \bar{w}}{\partial x_I \partial x_I} \right)^2 + (1-\nu) \left(\frac{\partial^2 \bar{w}}{\partial x_I \partial x_J} \frac{\partial^2 \bar{w}}{\partial x_I \partial x_J} - \left(\frac{\partial^2 \bar{w}}{\partial x_I \partial x_I} \right)^2 \right) \right] \quad (5.8a)$$

where $D = \frac{Eh^3}{12(1-\nu^2)}$ represents the flexural rigidity.

Particularly, as explained in Appendix A2.1, for the Kirchhoff Plate subjected to only displacement constraints (i.e., no free boundaries), the SED function can be simplified as

$$W_{\text{com}} = \frac{D}{2h} \left(\frac{\partial^2 \bar{w}}{\partial x_I \partial x_I} \right)^2 \quad (5.8b)$$

5.1.2 PD Formulations for Kirchhoff Plate

The PD EoM can be derived by taking use of the Lagrange's equation

$$\frac{d}{dt} \frac{\partial L}{\partial \dot{\bar{W}}_{(k)}} - \frac{\partial L}{\partial \bar{W}_{(k)}} = 0 \quad (5.9)$$

where $L = T - U$ represents the Lagrangian.

The total kinetic energy of the system can be expressed as

$$T = \frac{1}{2} \sum_n \rho_{(n)} \dot{\bar{W}}_{(n)}^2 V_{(n)} \quad (5.10a)$$

The total potential energy of the system can be similarly written as

$$U = \sum_n W_{PD}^{(n)}(\bar{w}_{(n)}, \bar{w}_{(1^n)}, \bar{w}_{(2^n)}, \bar{w}_{(3^n)}, \dots) V_{(n)} - \sum_n b_{(n)} \bar{w}_{(n)} V_{(n)} \quad (5.10b)$$

where the PD SED function at material point n , $W_{PD}^{(n)}$, has a non-local form such that it depends on the transverse displacements of material point n , and all the other material points in its horizon, and $b_{(n)}$ represents the transverse force density subjected to material point n .

Assume a conservative system, the first term of Eq. (5.9) becomes

$$\frac{d}{dt} \frac{\partial L}{\partial \dot{\bar{W}}_{(k)}} = \frac{d}{dt} \frac{\partial T}{\partial \dot{\bar{W}}_{(k)}} = \rho_{(k)} \ddot{\bar{W}}_{(k)} V_{(k)} \quad (5.11a)$$

Recall the pre-obtained expression, Eq. (3.8), the second term of Eq. (5.9) becomes

$$-\frac{\partial L}{\partial \bar{W}_{(k)}} = \left(\frac{\partial W_{PD}^{(k)}}{\partial \bar{W}_{(k)}} V_{(k)} + \sum_j \frac{\partial W_{PD}^{(j)}}{\partial \bar{W}_{(k)}} V_{(j)} \right) - b_{(k)} V_{(k)} \quad (5.11b)$$

Substituting Eqs. (5.11) into (5.9) and renaming the summation notation gives

$$\rho_{(k)} \ddot{\bar{W}}_{(k)} = - \left(\frac{\partial W_{PD}^{(k)}}{\partial \bar{W}_{(k)}} + \sum_j \frac{\partial W_{PD}^{(j)}}{\partial \bar{W}_{(k)}} \frac{V_{(j)}}{V_{(k)}} \right) + b_{(k)} \quad (5.12)$$

As derived in Appendix A2.1, the SED function Eq. (5.8a) can be transformed into the corresponding PD form for material point k and its family member material point j as

$$W_{PD}^{(k)} = \left(\frac{2}{\pi \delta^2 h} \right)^2 \frac{D}{h} \left\{ \begin{aligned} & \left[2 - 5(1 - \nu) \right] \left(\sum_i \frac{\bar{w}_{(i^k)} - \bar{w}_{(k)}}{\xi_{(i^k)(k)}^2} V_{(i^k)} \right)^2 + \\ & 8(1 - \nu) \sum_i \frac{\bar{w}_{(i^k)} - \bar{w}_{(k)}}{\xi_{(i^k)(k)}^2} n_i^{i^k(k)} n_j^{i^k(k)} V_{(i^k)} \sum_j \frac{\bar{w}_{(j^k)} - \bar{w}_{(k)}}{\xi_{(j^k)(k)}^2} n_j^{j^k(k)} n_i^{j^k(k)} V_{(j^k)} \end{aligned} \right\} \quad (5.13a)$$

and

$$W_{PD}^{(j)} = \left(\frac{2}{\pi\delta^2 h} \right)^2 \frac{D}{h} \left\{ \begin{aligned} & \left[2 - 5(1-\nu) \right] \left(\sum_i \frac{\bar{w}_{(i^j)} - \bar{w}_{(j)}}{\xi_{(i^j)(j)}^2} V_{(i^j)} \right)^2 + \\ & 8(1-\nu) \sum_i \frac{\bar{w}_{(i^j)} - \bar{w}_{(j)}}{\xi_{(i^j)(j)}^2} n_i^{(i^j)(j)} n_j^{(i^j)(j)} V_{(i^j)} \sum_i \frac{\bar{w}_{(i^j)} - \bar{w}_{(j)}}{\xi_{(i^j)(j)}^2} n_i^{(i^j)(j)} n_j^{(i^j)(j)} V_{(i^j)} \end{aligned} \right\} \quad (5.13b)$$

where ξ represents the distance between two material points and \mathbf{n} represents the unit orientation vector which can be defined as (see Fig. 5.1)

$$\mathbf{n} = \begin{Bmatrix} n_1 \\ n_2 \end{Bmatrix} = \begin{Bmatrix} \cos \varphi \\ \sin \varphi \end{Bmatrix} \quad (5.14)$$

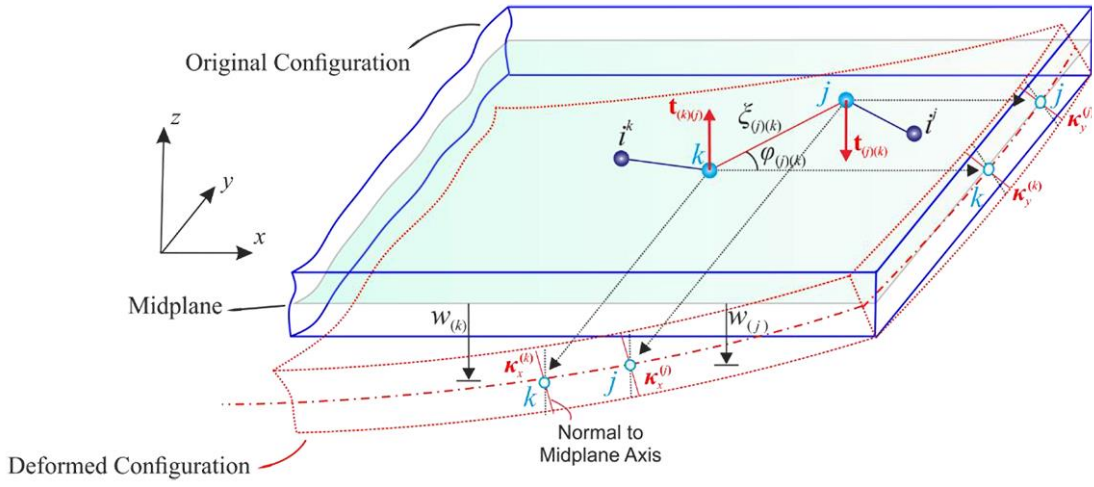


Figure. 5.1 Peridynamic interactions in Kirchhoff plate theory.

Regarding the special case that the plate subjected to displacement boundary conditions only, the PD SED function for material point k and its family member material point j becomes

$$W_{PD}^{(k)} = 2 \left(\frac{2}{\pi\delta^2 h} \right)^2 \frac{D}{h} \left(\sum_i \frac{\bar{w}_{(i^k)} - \bar{w}_{(k)}}{\xi_{(i^k)(k)}^2} V_{(i^k)} \right)^2 \quad (5.15a)$$

and

$$W_{PD}^{(j)} = 2 \left(\frac{2}{\pi\delta^2 h} \right)^2 \frac{D}{h} \left(\sum_i \frac{\bar{w}_{(i^j)} - \bar{w}_{(j)}}{\xi_{(i^j)(j)}^2} V_{(i^j)} \right)^2 \quad (5.15b)$$

Plugging Eqs. (5.13) into (5.12) and rearranging the summation notations results in the PD EoM for Kirchhoff Plate as

$$\rho_{(k)} \ddot{W}_{(k)} = c \left\{ \begin{array}{l} \left[1 - \frac{5}{2}(1-\nu) \right] \sum_j \frac{1}{\xi_{(j)(k)}^2} \left(\sum_i \frac{\bar{W}_{(i^k)} - \bar{W}_{(k)}}{\xi_{(i^k)(k)}^2} V_{(i^k)} - \sum_i \frac{\bar{W}_{(i^j)} - \bar{W}_{(j)}}{\xi_{(i^j)(j)}^2} V_{(i^j)} \right) V_{(j)} \\ + 4(1-\nu) \sum_j \frac{n_i^{(j)(k)} n_j^{(j)(k)}}{\xi_{(j)(k)}^2} \left(\begin{array}{l} \sum_i \frac{\bar{W}_{(i^k)} - \bar{W}_{(k)}}{\xi_{(i^k)(k)}^2} n_i^{(i^k)(k)} n_j^{(i^k)(k)} V_{(i^k)} \\ - \sum_i \frac{\bar{W}_{(i^j)} - \bar{W}_{(j)}}{\xi_{(i^j)(j)}^2} n_i^{(i^j)(j)} n_j^{(i^j)(j)} V_{(i^j)} \end{array} \right) V_{(j)} \end{array} \right\} + b_{(k)} \quad (5.16)$$

where the PD material constant c is defined as

$$c = \left(\frac{4}{\pi \delta^2 h} \right)^2 \frac{D}{h} \quad (5.17)$$

Particularly, when the plate subjected to fixed boundary conditions (simply supported and clamped) only, Eq. (5.16) can be simplified as

$$\rho_{(k)} \ddot{W}_{(k)} = c \sum_j \frac{1}{\xi_{(j)(k)}^2} \left(\sum_i \frac{\bar{W}_{(i^k)} - \bar{W}_{(k)}}{\xi_{(i^k)(k)}^2} V_{(i^k)} - \sum_i \frac{\bar{W}_{(i^j)} - \bar{W}_{(j)}}{\xi_{(i^j)(j)}^2} V_{(i^j)} \right) V_{(j)} + b_{(k)} \quad (5.18)$$

5.1.3 Numerical Cases

To verify the validity of the new PD formulation for a Kirchhoff plate, the PD solutions are compared with the corresponding finite element (FE) analysis results.

5.1.3.1 Clamped Plate

A clamped plate with a length and width of $L = W = 1\text{m}$ and a thickness of $h = 0.01$ is considered, as shown in Fig. 5.2. The Young's modulus and Poisson's ratio of the plate are $E = 200\text{ GPa}$ and $\nu = 0.3$, respectively. The model is discretized into one single row of material points along with the thickness and the distance between material points is $\Delta x = 0.01\text{m}$. A fictitious region is introduced outside the edges as the external boundaries with a width of 2δ . The plate is subjected to a distributed transverse load of $p = 100\text{ N/m}^3$ through the y -center line. The line load is converted to a body load of $b = \frac{pW}{2(W/\Delta x)\Delta V} = 5 \times 10^5\text{ N/m}^3$ and it is distributed to two columns of material volumes through the center line, as shown in Fig. 5.3.

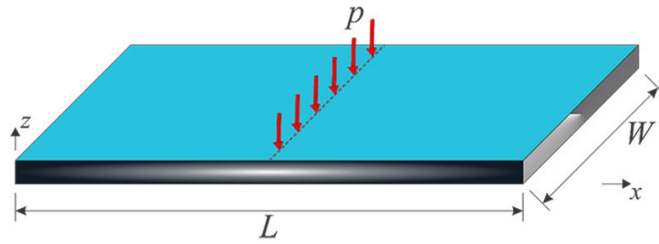


Figure 5.2 The geometry of a clamped Kirchhoff plate

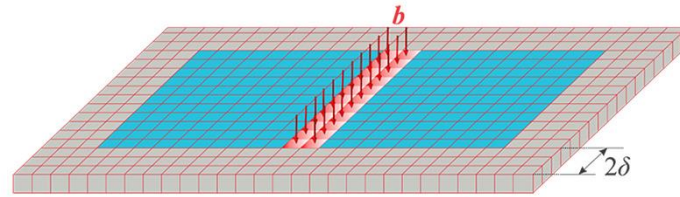


Figure 5.3 The peridynamic discretization of Kirchhoff plate

The FE model of the plate is created by using the SHELL181 element in ANSYS. The PD and FE transverse displacement contours are compared in Fig. 5.4. They yield similar displacement variations. The maximum difference between the PD and FE results is less than 0.5%. Moreover, the vertical displacement components along the central x - and y -axes are compared in Fig. 5.5. These results verify the accurateness of the current PD formulation for a Kirchhoff plate theory under clamped boundary conditions.

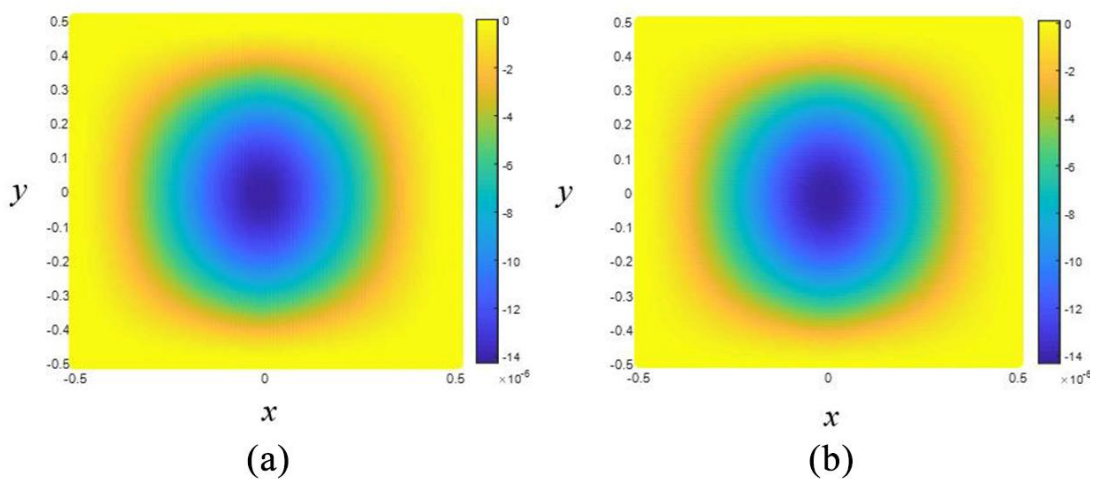


Figure 5.4 Comparison of the vertical displacement components of the (a) finite element and (b) peridynamic results (unit: m)

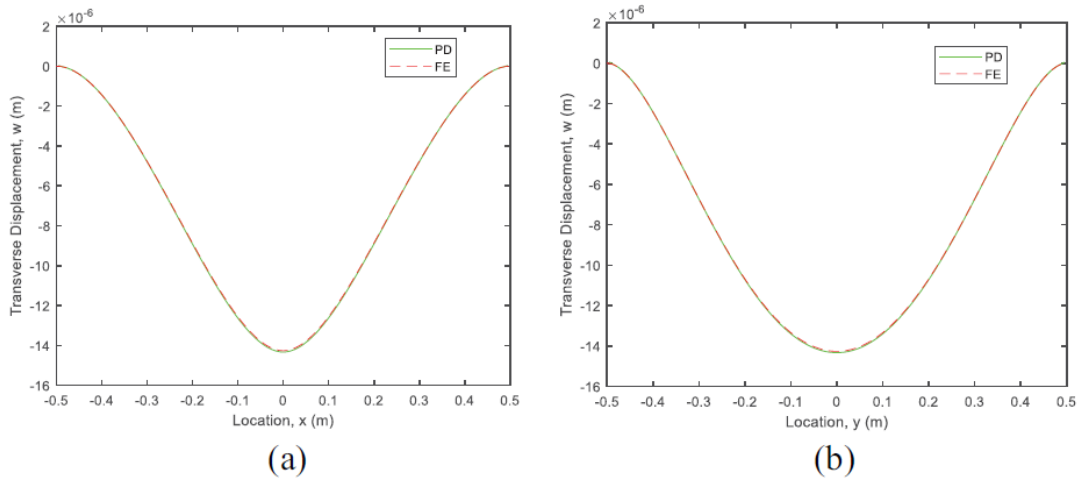


Figure 5.5 Comparison of the vertical displacements along the (a) x- and (b) y-central axes. PD: peridynamic; FE: finite element

5.1.3.2 Simply Supported Plate

A simply supported plate (Fig. 5.6) has the same geometrical and material properties as in the clamped plate case. Again, it is discretized with a single row of material points along the thickness direction and the discretization size is $\Delta x = 0.01m$. A fictitious region is created outside the region of boundaries and its width is equal to two times the size of the horizon, δ . The plate is subjected to a distributed transverse line load of $p = 100 N/m$ through the y-central line. It is imposed to two columns of material points with a body load of $b = 5 \times 10^5 N/m^3$, as in Figure 5.3.

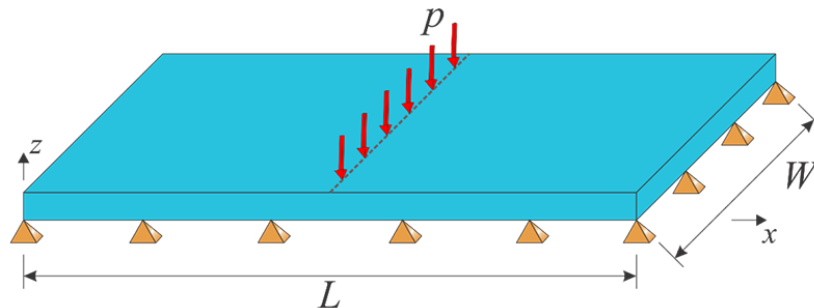


Figure 5.6 The geometry of a simply supported Kirchhoff plate.

The transverse displacement components of FE and PD theory show very close variations, as shown in Figure 5.7. The maximum difference between the PD and FE

results is less than 0.5%. Furthermore, the displacement variations along the central x - and y -axes are on top of each other for the FE and PD results, as shown in Figure 5.8. This confirms the current PD formulation of Kirchhoff plate theory under simply supported boundary conditions.

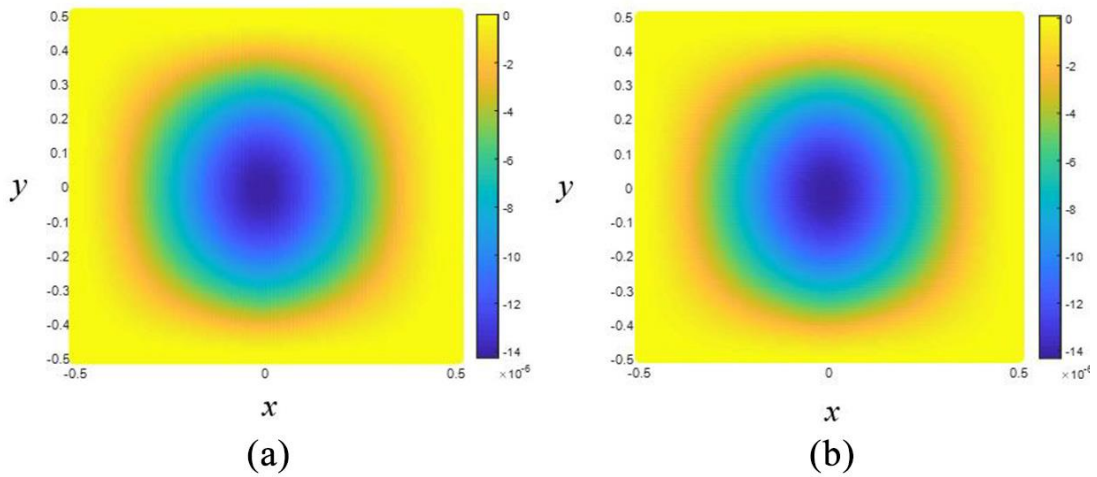


Figure 5.7 Comparison of the vertical displacement components of the (a) finite element and (b) peridynamic results (unit: m)

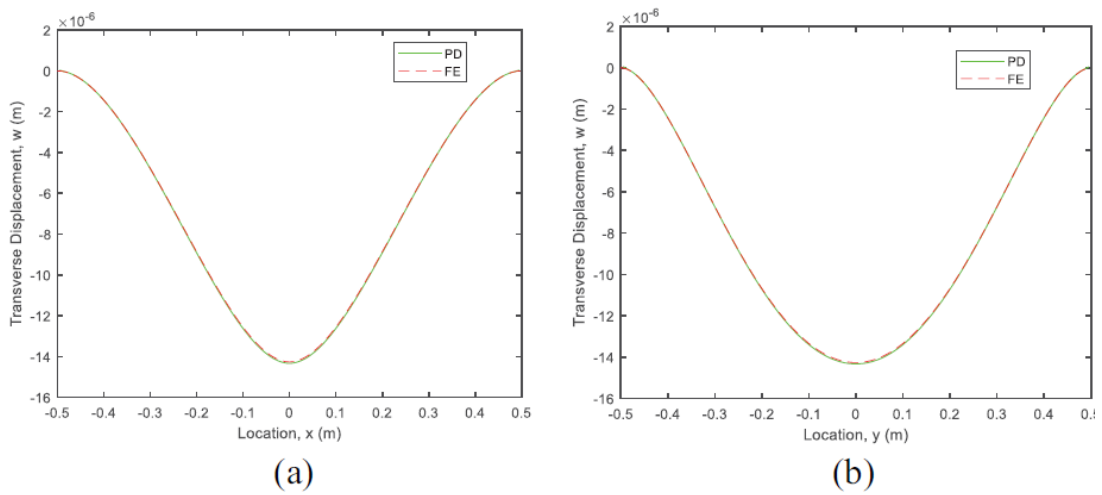


Figure 5.8 Comparison of the vertical displacements along the (a) x - and (b) y -central axes. PD: peridynamic; FE: finite element

5.2 PD Formulation for Functionally Graded Material Kirchhoff

Plate

5.2.1 Functionally Graded Material Kirchhoff Plate Theory

Unlike isotropic material Kirchhoff Plate theory, the displacement field of FGM Kirchhoff Plate takes consideration of in-plane deformation effect as

$$u(x, y, z, t) = \bar{u}(x, y, t) + z\theta_x(x, y, t) \quad (5.19a)$$

$$v(x, y, z, t) = \bar{v}(x, y, t) + z\theta_y(x, y, t) \quad (5.19b)$$

$$w(x, y, z, t) = \bar{w}(x, y, t) \quad (5.19c)$$

Where $\bar{u}(x, y, t)$ and $\bar{v}(x, y, t)$ denote the in-plane displacements of material points on mid-plane along x - and y - axis, and $\bar{w}(x, y, t)$ denotes the transverse displacement of material points on mid-plane, respectively.

Based on Eqs. (5.19) and Kirchhoff Plate assumptions, the strain components can be given as

$$\varepsilon_x = \frac{\partial \bar{u}}{\partial x} + z \frac{\partial \theta_x}{\partial x} \quad (5.20a)$$

$$\varepsilon_y = \frac{\partial \bar{v}}{\partial y} + z \frac{\partial \theta_y}{\partial y} \quad (5.20b)$$

$$\gamma_{xy} = \left(\frac{\partial \bar{u}}{\partial y} + \frac{\partial \bar{v}}{\partial x} \right) + z \left(\frac{\partial \theta_x}{\partial y} + \frac{\partial \theta_y}{\partial x} \right) \quad (5.20c)$$

$$\gamma_{xz} = \theta_x + \frac{\partial \bar{w}}{\partial x} = 0 \quad (5.20d)$$

$$\gamma_{yz} = \theta_y + \frac{\partial \bar{w}}{\partial y} = 0 \quad (5.20e)$$

Eliminating θ_x and θ_y from Eqs. (5.20a, b, c) by taking use of Eq. (5.20d, e) gives

$$\varepsilon_x = \frac{\partial \bar{u}}{\partial x} - z \frac{\partial^2 \bar{w}}{\partial x^2} \quad (5.21a)$$

$$\varepsilon_y = \frac{\partial \bar{v}}{\partial y} - z \frac{\partial^2 \bar{w}}{\partial y^2} \quad (5.21b)$$

$$\gamma_{xy} = \left(\frac{\partial \bar{u}}{\partial y} + \frac{\partial \bar{v}}{\partial x} \right) - 2z \frac{\partial^2 \bar{w}}{\partial x \partial y} \quad (5.21c)$$

which can be written in the tensorial form as

$$\varepsilon_{ij} = \frac{1}{2} \left(\frac{\partial \bar{u}_i}{\partial x_j} + \frac{\partial \bar{u}_j}{\partial x_i} \right) - z \frac{\partial^2 \bar{w}}{\partial x_i \partial x_j} \quad (5.22)$$

where the subscripts I, J, \dots take up the value 1(= x) and 2(= y), and this convention will be applied throughout this study.

According to the plane-stress constitutive law, the stress components can be written as

$$\sigma_{IJ} = C_{IJKL} \varepsilon_{KL} \quad (5.23)$$

where \mathbf{C} represents the stiffness tensor, which can be defined for isotropic material as

$$C_{IJKL} = \frac{E}{1-\nu^2} \left[\frac{1-\nu}{2} (\delta_{IL}\delta_{JK} + \delta_{IK}\delta_{JL}) + \nu\delta_{IJ}\delta_{KL} \right] \quad (5.24)$$

where $E = E(z)$ and $\nu = \nu(z)$ represent the Young's modulus and Poisson's ratio, respectively, and both of them vary in the thickness direction z .

According to the elastic theory, the average strain energy density can be expressed as

$$W_{\text{GM}} = \frac{1}{2h} \int_{-\frac{h}{2}}^{\frac{h}{2}} \sigma_{IJ} \varepsilon_{IJ} dz \quad (5.25)$$

which can be written in terms of transverse displacement only by utilizing the relations given in Eq. (5.22), (5.23) and (5.24) as

$$W_{\text{GM}} = \frac{1}{2h} \int_{-\frac{h}{2}}^{\frac{h}{2}} \frac{E}{1-\nu^2} \left\{ \begin{array}{l} \frac{1-\nu}{2} (\bar{u}_{I,J} \bar{u}_{I,J} + \bar{u}_{I,J} \bar{u}_{J,I} + \bar{u}_{I,I} \bar{u}_{J,J}) + \frac{3\nu-1}{2} (\bar{u}_{I,I})^2 \\ + z^2 \left[(\bar{w}_{,II})^2 + (1-\nu) (\bar{w}_{,IJ} \bar{w}_{,IJ} - (\bar{w}_{,II})^2) \right] \\ - 2z \left[\bar{u}_{I,I} \bar{w}_{,JJ} + (1-\nu) \left(\frac{1}{2} (\bar{u}_{I,J} + \bar{u}_{J,I}) \bar{w}_{,IJ} - \bar{u}_{I,I} \bar{w}_{,JJ} \right) \right] \end{array} \right\} dz \quad (5.26)$$

Note that Eq. (5.26) is composed of three independent parts. The first and second rows represent the strain energy densities that occur due to in-plane and flexural (bending) deformation, respectively, and the last row arises due to coupling of in-plane and flexural deformations. If the material properties are constant over the thickness, the last row of Eq. (5.26) will be cancelled out after integration and Eq. (5.26) will become uncoupled. Thus, the strain energy density of the plate can be written concisely as

$$W_{\text{GM}} = W_{\text{GM}}^I + W_{\text{GM}}^{II} + W_{\text{GM}}^{III} \quad (5.27)$$

where W_I , W_{II} and W_{III} denote the strain energy densities due to in-plane deformation, flexural deformation and coupled deformation, respectively, which can be written as

$$W_{\text{COM}}^I = \frac{1}{2h} \left[\int_{-\frac{h}{2}}^{\frac{h}{2}} \mathbf{G} \mathbf{z} (\bar{u}_{i,j} \bar{u}_{i,j} + \bar{u}_{i,j} \bar{u}_{j,i} + \bar{u}_{i,i} \bar{u}_{j,j}) + \int_{-\frac{h}{2}}^{\frac{h}{2}} \frac{E}{1-\nu^2} \frac{3\nu-1}{2} \mathbf{z} (\bar{u}_{i,i})^2 \right] \quad (5.28a)$$

$$W_{\text{COM}}^{II} = \frac{1}{2h} \left[\int_{-\frac{h}{2}}^{\frac{h}{2}} \frac{E \mathbf{z}^2}{1-\nu^2} \mathbf{z} (\bar{w}_{i,i})^2 + 2 \int_{-\frac{h}{2}}^{\frac{h}{2}} \mathbf{G}^2 \mathbf{z} (\bar{w}_{i,j} \bar{w}_{i,j} - (\bar{w}_{i,i})^2) \right] \quad (5.28b)$$

$$W_{\text{COM}}^{III} = -\frac{1}{h} \left[\int_{-\frac{h}{2}}^{\frac{h}{2}} \frac{E \mathbf{z}}{1-\nu^2} \mathbf{z} (\bar{u}_{i,i} \bar{w}_{j,j}) + \int_{-\frac{h}{2}}^{\frac{h}{2}} \mathbf{G} \mathbf{z} ((\bar{u}_{i,j} + \bar{u}_{j,i}) \bar{w}_{i,j} - 2\bar{u}_{i,i} \bar{w}_{j,j}) \right] \quad (5.28c)$$

Particularly, as explained in Appendix A2.2, when the Plate subjected to only displacement constraints (i.e., no free boundaries), the SED function, Eq. (5.26) can be simplified as

$$W_{\text{COM}} = \frac{1}{2h} \int_{-\frac{h}{2}}^{\frac{h}{2}} \frac{E}{1-\nu^2} \left\{ \begin{aligned} & \frac{1-\nu}{2} (\bar{u}_{i,j} \bar{u}_{i,j} + \bar{u}_{i,j} \bar{u}_{j,i} + \bar{u}_{i,i} \bar{u}_{j,j}) \\ & + \frac{3\nu-1}{2} (\bar{u}_{i,i})^2 + \mathbf{z}^2 (\bar{w}_{i,i})^2 - 2\mathbf{z} \bar{u}_{i,i} \bar{w}_{j,j} \end{aligned} \right\} \mathbf{z} \quad (5.29)$$

5.2.2 PD Formulations for Functionally Graded Material Kirchhoff Plate

The PD EoM can be derived by taking use of the Lagrange's equation

$$\frac{d}{dt} \frac{\partial L}{\partial \dot{\mathbf{u}}_k} - \frac{\partial L}{\partial \mathbf{u}_k} = 0 \quad (5.30)$$

where $L = T - U$ represents the Lagrangian and \mathbf{u} is the displacement vector, which contains the following entries in this study as

$$\mathbf{u} = [\bar{u} \quad \bar{v} \quad \bar{w}]^T \quad (5.31)$$

The total kinetic energy of the system can be expressed as

$$T = \frac{1}{2} \sum_n \rho_{(n)} (\dot{\bar{u}}_{(n)}^2 + \dot{\bar{v}}_{(n)}^2 + \dot{\bar{w}}_{(n)}^2) V_{(n)} \quad (5.32a)$$

The total potential energy of the system can be similarly written as

$$U = \sum_n W_{PD}^{(n)} (\mathbf{u}_{(n)}, \mathbf{u}_{(1^n)}, \mathbf{u}_{(2^n)}, \mathbf{u}_{(3^n)}, \dots) V_{(n)} - \sum_n \mathbf{b}_{(n)} \mathbf{u}_{(n)} V_{(n)} \quad (5.32b)$$

where the PD SED function at material point n , $W_{PD}^{(n)}$, has a non-local form such that it depends on the displacement of material point n , and all the other material points in its horizon, and $\mathbf{b}_{(n)}$ represents the force density vector subjected to material point n , which has the following components as

$$\mathbf{b} = [b_x \quad b_y \quad b_z]^T \quad (5.33)$$

Assume a conservative system, the first term of Eq. (5.9) becomes

$$\frac{d}{dt} \frac{\partial L}{\partial \dot{\mathbf{u}}_{(k)}} = \frac{d}{dt} \frac{\partial T}{\partial \dot{\mathbf{u}}_{(k)}} = \rho_{(k)} \begin{Bmatrix} \ddot{\mathbf{u}}_{(k)} \\ \ddot{\mathbf{v}}_{(k)} \\ \ddot{\mathbf{w}}_{(k)} \end{Bmatrix} \mathbf{V}_{(k)} \quad (5.34a)$$

Recall the pre-obtained expression, Eq. (3.8), the second term of Eq. (5.30) becomes

$$-\frac{\partial L}{\partial \mathbf{u}_{(k)}} = \begin{pmatrix} \frac{\partial W_{FD}^{(k)}}{\partial \bar{\mathbf{u}}_{(k)}} \mathbf{V}_{(k)} + \sum_j \frac{\partial W_{FD}^{(j)}}{\partial \bar{\mathbf{u}}_{(k)}} \mathbf{V}_{(j)} \\ \frac{\partial W_{FD}^{(k)}}{\partial \bar{\mathbf{v}}_{(k)}} \mathbf{V}_{(k)} + \sum_j \frac{\partial W_{FD}^{(j)}}{\partial \bar{\mathbf{v}}_{(k)}} \mathbf{V}_{(j)} \\ \frac{\partial W_{FD}^{(k)}}{\partial \bar{\mathbf{w}}_{(k)}} \mathbf{V}_{(k)} + \sum_j \frac{\partial W_{FD}^{(j)}}{\partial \bar{\mathbf{w}}_{(k)}} \mathbf{V}_{(j)} \end{pmatrix} - \begin{Bmatrix} b_x \\ b_y \\ b_z \end{Bmatrix} \mathbf{V}_{(k)} \quad (5.34b)$$

Substituting Eqs. (5.11) into (5.9) and renaming the summation notation gives

$$\rho_{(k)} \begin{Bmatrix} \ddot{\mathbf{u}}_{(k)} \\ \ddot{\mathbf{v}}_{(k)} \\ \ddot{\mathbf{w}}_{(k)} \end{Bmatrix} = - \begin{pmatrix} \frac{\partial W_{FD}^{(k)}}{\partial \bar{\mathbf{u}}_{(k)}} + \sum_j \frac{\partial W_{FD}^{(j)}}{\partial \bar{\mathbf{u}}_{(k)}} \frac{\mathbf{V}_{(j)}}{\mathbf{V}_{(k)}} \\ \frac{\partial W_{FD}^{(k)}}{\partial \bar{\mathbf{v}}_{(k)}} + \sum_j \frac{\partial W_{FD}^{(j)}}{\partial \bar{\mathbf{v}}_{(k)}} \frac{\mathbf{V}_{(j)}}{\mathbf{V}_{(k)}} \\ \frac{\partial W_{FD}^{(k)}}{\partial \bar{\mathbf{w}}_{(k)}} + \sum_j \frac{\partial W_{FD}^{(j)}}{\partial \bar{\mathbf{w}}_{(k)}} \frac{\mathbf{V}_{(j)}}{\mathbf{V}_{(k)}} \end{pmatrix} + \begin{Bmatrix} b_x^{(k)} \\ b_y^{(k)} \\ b_z^{(k)} \end{Bmatrix} \quad (5.35)$$

As derived in Appendix A2.2, the SED function Eq. (5.26) can be transformed into the corresponding PD form for material point k and its family member material point j as

$$\begin{aligned} W_{FD}^{(k)} = & \frac{6}{\pi \delta^3 h^2} \int_{-\frac{h}{2}}^{\frac{h}{2}} \mathcal{G} dz \sum_i \left[\frac{(\bar{\mathbf{u}}_i^{(i^k)} - \bar{\mathbf{u}}_i^{(k)}) n_i^{i^k(k)}}{\xi_{(i^k)(k)}} \right]^2 \mathbf{V}_{(i^k)} \\ & + \frac{1}{h} \left(\frac{1}{\pi \delta^2 h} \right)^2 \int_{-\frac{h}{2}}^{\frac{h}{2}} \frac{E(3\nu - 1)}{1 - \nu^2} dz \left(\sum_i \frac{\bar{\mathbf{u}}_i^{(i^k)} - \bar{\mathbf{u}}_i^{(k)}}{\xi_{(i^k)(k)}} n_i^{i^k(k)} \mathbf{V}_{(i^k)} \right)^2 \\ & + \frac{2}{h} \left(\frac{2}{\pi \delta^2 h} \right)^2 \left[\int_{-\frac{h}{2}}^{\frac{h}{2}} \left(\frac{E}{1 - \nu^2} - 5G \right) z^2 dz \left(\sum_i \frac{\bar{\mathbf{w}}_{(i^k)} - \bar{\mathbf{w}}_{(k)}}{\xi_{(i^k)(k)}} \mathbf{V}_{(i^k)} \right)^2 \right. \\ & \quad \left. + \int_{-\frac{h}{2}}^{\frac{h}{2}} \mathcal{G}^2 dz 8 \sum_i \frac{\bar{\mathbf{w}}_{(i^k)} - \bar{\mathbf{w}}_{(k)}}{\xi_{(i^k)(k)}^2} n_i^{i^k(k)} n_j^{j^k(k)} \mathbf{V}_{(i^k)} \sum_i \frac{\bar{\mathbf{w}}_{(i^k)} - \bar{\mathbf{w}}_{(k)}}{\xi_{(i^k)(k)}^2} n_i^{i^k(k)} n_j^{j^k(k)} \mathbf{V}_{(i^k)} \right] \\ & - \frac{2}{h} \left(\frac{2}{\pi \delta^2 h} \right)^2 \left[\int_{-\frac{h}{2}}^{\frac{h}{2}} \left(\frac{E}{1 - \nu^2} - 3G \right) z dz \sum_i \frac{\bar{\mathbf{u}}_i^{(i^k)} - \bar{\mathbf{u}}_i^{(k)}}{\xi_{(i^k)(k)}} n_i^{i^k(k)} \mathbf{V}_{(i^k)} \sum_i \frac{\bar{\mathbf{w}}_{(i^k)} - \bar{\mathbf{w}}_{(k)}}{\xi_{(i^k)(k)}^2} \mathbf{V}_{(i^k)} \right. \\ & \quad \left. + 4 \int_{-\frac{h}{2}}^{\frac{h}{2}} \mathcal{G} dz \sum_i \frac{\bar{\mathbf{w}}_{(i^k)} - \bar{\mathbf{w}}_{(k)}}{\xi_{(i^k)(k)}^2} n_i^{i^k(k)} n_j^{j^k(k)} \mathbf{V}_{(i^k)} \sum_i \frac{\bar{\mathbf{u}}_i^{(i^k)} - \bar{\mathbf{u}}_i^{(k)}}{\xi_{(i^k)(k)}} n_j^{j^k(k)} \mathbf{V}_{(i^k)} \right] \end{aligned} \quad (5.36a)$$

$$\begin{aligned}
W_{PD}^{(j)} = & \frac{6}{\pi\delta^3 h^2} \int_{-\frac{h}{2}}^{\frac{h}{2}} \mathcal{G}z \sum_i \frac{\left[(\bar{u}_i^{(ij)} - \bar{u}_i^{(j)}) n_i^{(ij)(j)} \right]^2}{\xi_{(i)(j)}} V_{(j)} \\
& + \frac{1}{h} \left(\frac{1}{\pi\delta^2 h} \right)^2 \int_{-\frac{h}{2}}^{\frac{h}{2}} \frac{E(3\nu-1)}{1-\nu^2} dz \left(\sum_i \frac{\bar{u}_i^{(ij)} - \bar{u}_i^{(j)}}{\xi_{(i)(j)}} n_i^{(ij)(j)} V_{(j)} \right)^2 \\
& + \frac{2}{h} \left(\frac{2}{\pi\delta^2 h} \right)^2 \left[\int_{-\frac{h}{2}}^{\frac{h}{2}} \left(\frac{E}{1-\nu^2} - 5G \right) z^2 dz \left(\sum_i \frac{\bar{w}_{(j)} - \bar{w}_{(j)}}{\xi_{(i)(j)}^2} V_{(j)} \right)^2 \right. \\
& \left. + \int_{-\frac{h}{2}}^{\frac{h}{2}} \mathcal{G}^2 dz 8 \sum_i \frac{\bar{w}_{(j)} - \bar{w}_{(j)}}{\xi_{(i)(j)}^2} n_i^{(ij)(j)} n_j^{(ij)(j)} V_{(j)} \sum_i \frac{\bar{w}_{(j)} - \bar{w}_{(j)}}{\xi_{(i)(j)}^2} n_i^{(ij)(j)} n_j^{(ij)(j)} V_{(j)} \right] \\
& - \frac{2}{h} \left(\frac{2}{\pi\delta^2 h} \right)^2 \left[\int_{-\frac{h}{2}}^{\frac{h}{2}} \left(\frac{E}{1-\nu^2} - 3G \right) z dz \sum_i \frac{\bar{u}_i^{(ij)} - \bar{u}_i^{(j)}}{\xi_{(i)(j)}} n_i^{(ij)(j)} V_{(j)} \sum_i \frac{\bar{w}_{(j)} - \bar{w}_{(j)}}{\xi_{(i)(j)}^2} V_{(j)} \right. \\
& \left. + 4 \int_{-\frac{h}{2}}^{\frac{h}{2}} \mathcal{G}z dz \sum_i \frac{\bar{w}_{(j)} - \bar{w}_{(j)}}{\xi_{(i)(j)}^2} n_i^{(ij)(j)} n_j^{(ij)(j)} V_{(j)} \sum_i \frac{\bar{u}_i^{(ij)} - \bar{u}_i^{(j)}}{\xi_{(i)(j)}} n_j^{(ij)(j)} V_{(j)} \right]
\end{aligned} \tag{5.36b}$$

Particularly, when the plate subjected to only displacement constraints (i.e., no free boundaries), the PD SED function, Eqs. (5.36) can be simplified as

$$\begin{aligned}
W_{PD}^{(k)} = & \left\{ \begin{aligned} & \frac{6}{\pi\delta^3 h^2} \int_{-\frac{h}{2}}^{\frac{h}{2}} \mathcal{G}z \sum_i \frac{\left[(\bar{u}_i^{(ik)} - \bar{u}_i^{(k)}) n_i^{(ik)(k)} \right]^2}{\xi_{(i)(k)}} V_{(k)} \\ & + \frac{1}{h} \left(\frac{1}{\pi\delta^2 h} \right)^2 \int_{-\frac{h}{2}}^{\frac{h}{2}} \frac{E(3\nu-1)}{1-\nu^2} dz \left(\sum_i \frac{\bar{u}_i^{(ik)} - \bar{u}_i^{(k)}}{\xi_{(i)(k)}} n_i^{(ik)(k)} V_{(k)} \right)^2 \\ & + \frac{2}{h} \left(\frac{2}{\pi\delta^2 h} \right)^2 \int_{-\frac{h}{2}}^{\frac{h}{2}} \frac{E}{1-\nu^2} z^2 dz \left(\sum_i \frac{\bar{w}_{(k)} - \bar{w}_{(k)}}{\xi_{(i)(k)}^2} V_{(k)} \right)^2 \\ & - \frac{2}{h} \left(\frac{2}{\pi\delta^2 h} \right)^2 \int_{-\frac{h}{2}}^{\frac{h}{2}} \frac{E}{1-\nu^2} z dz \sum_i \frac{\bar{u}_i^{(ik)} - \bar{u}_i^{(k)}}{\xi_{(i)(k)}} n_i^{(ik)(k)} V_{(k)} \sum_i \frac{\bar{w}_{(k)} - \bar{w}_{(k)}}{\xi_{(i)(k)}^2} V_{(k)} \end{aligned} \right\}
\end{aligned} \tag{5.37a}$$

and

$$\begin{aligned}
W_{PD}^{(j)} = & \left\{ \begin{aligned} & \frac{6}{\pi\delta^3 h^2} \int_{-\frac{h}{2}}^{\frac{h}{2}} \mathcal{G}z \sum_i \frac{\left[(\bar{u}_i^{(ij)} - \bar{u}_i^{(j)}) n_i^{(ij)(j)} \right]^2}{\xi_{(i)(j)}} V_{(j)} + \\ & \frac{1}{h} \left(\frac{1}{\pi\delta^2 h} \right)^2 \int_{-\frac{h}{2}}^{\frac{h}{2}} \frac{E(3\nu-1)}{1-\nu^2} dz \left(\sum_i \frac{\bar{u}_i^{(ij)} - \bar{u}_i^{(j)}}{\xi_{(i)(j)}} n_i^{(ij)(j)} V_{(j)} \right)^2 + \\ & \frac{2}{h} \left(\frac{2}{\pi\delta^2 h} \right)^2 \int_{-\frac{h}{2}}^{\frac{h}{2}} \frac{E}{1-\nu^2} z^2 dz \left(\sum_i \frac{\bar{w}_{(j)} - \bar{w}_{(j)}}{\xi_{(i)(j)}^2} V_{(j)} \right)^2 - \\ & \frac{2}{h} \left(\frac{2}{\pi\delta^2 h} \right)^2 \int_{-\frac{h}{2}}^{\frac{h}{2}} \frac{E}{1-\nu^2} z dz \sum_i \frac{\bar{u}_i^{(ij)} - \bar{u}_i^{(j)}}{\xi_{(i)(j)}} n_i^{(ij)(j)} V_{(j)} \sum_i \frac{\bar{w}_{(j)} - \bar{w}_{(j)}}{\xi_{(i)(j)}^2} V_{(j)} \end{aligned} \right\}
\end{aligned} \tag{5.37b}$$

Substituting Eqs. (5.36) into (5.35) yields the final PD EoM for FGM Kirchhoff Plate as

$$\rho_{(k)} \ddot{u}_L^{(k)} = \left[\begin{aligned} & \frac{24}{\pi \delta^3 h^2} \int_{-\frac{h}{2}}^{\frac{h}{2}} \mathbf{G} dz \sum_j \frac{\bar{u}_l^{(j)} - \bar{u}_l^{(k)}}{\xi_{(j)(k)}} n_l^{(j)(k)} n_L^{(j)(k)} V_{(j)} \\ & + \frac{2}{\pi \delta^2 h^2} \int_{-\frac{h}{2}}^{\frac{h}{2}} \frac{E(3\nu - 1)}{1 + \nu} dz \sum_j \frac{\Theta_{(j)} + \Theta_{(k)}}{\xi_{(j)(k)}} n_L^{(j)(k)} V_{(j)} \\ & - \left(\frac{2}{\pi \delta^2 h} \right)^2 \frac{2}{h} \int_{-\frac{h}{2}}^{\frac{h}{2}} \left(\frac{Ez}{1 - \nu^2} - 3\mathbf{G} \right) dz \sum_j \frac{n_L^{(j)(k)}}{\xi_{(j)(k)}} \left(\begin{aligned} & \sum_i \frac{\bar{w}_{(i^k)} - \bar{w}_{(k)}}{\xi_{(i^k)(k)}^2} V_{(i^k)} \\ & + \sum_i \frac{\bar{w}_{(i^j)} - \bar{w}_{(j)}}{\xi_{(i^j)(j)}^2} V_{(i^j)} \end{aligned} \right) V_{(j)} \\ & - \left(\frac{4}{\pi \delta^2 h} \right)^2 \frac{2}{h} \int_{-\frac{h}{2}}^{\frac{h}{2}} \mathbf{G} dz \sum_j \frac{n_l^{(j)(k)}}{\xi_{(j)(k)}} \left(\begin{aligned} & \sum_i \frac{\bar{w}_{(i^k)} - \bar{w}_{(k)}}{\xi_{(i^k)(k)}^2} n_l^{(i^k)(k)} n_L^{(i^k)(k)} V_{(i^k)} \\ & + \sum_i \frac{\bar{w}_{(i^j)} - \bar{w}_{(j)}}{\xi_{(i^j)(j)}^2} n_l^{(i^j)(j)} n_L^{(i^j)(j)} V_{(i^j)} \end{aligned} \right) V_{(j)} \end{aligned} \right] + \mathbf{b}_L^{(k)} \quad (5.38a)$$

and

$$\rho_{(k)} \ddot{w}_k = \frac{1}{h} \left(\frac{4}{\pi \delta^2 h} \right)^2 \left[\begin{aligned} & \int_{-\frac{h}{2}}^{\frac{h}{2}} \left(\frac{E}{1 - \nu^2} - 5\mathbf{G} \right) z^2 dz \sum_j \frac{1}{\xi_{(i^k)(k)}^2} \left(\begin{aligned} & \sum_i \frac{\bar{w}_{(i^k)} - \bar{w}_{(k)}}{\xi_{(i^k)(k)}^2} V_{(i^k)} \\ & - \sum_i \frac{\bar{w}_{(i^j)} - \bar{w}_{(j)}}{\xi_{(i^j)(j)}^2} V_{(i^j)} \end{aligned} \right) V_{(j)} \\ & + 8 \int_{-\frac{h}{2}}^{\frac{h}{2}} \mathbf{G}^2 dz \sum_i \frac{n_l^{(i^k)(k)} n_j^{(i^k)(k)}}{\xi_{(i^k)(k)}^2} \left(\begin{aligned} & \sum_i \frac{\bar{w}_{(i^k)} - \bar{w}_{(k)}}{\xi_{(i^k)(k)}^2} n_l^{(i^k)(k)} n_j^{(i^k)(k)} V_{(i^k)} \\ & - \sum_i \frac{\bar{w}_{(i^j)} - \bar{w}_{(j)}}{\xi_{(i^j)(j)}^2} n_l^{(i^j)(j)} n_j^{(i^j)(j)} V_{(i^j)} \end{aligned} \right) V_{(j)} \\ & - \frac{1}{2} \int_{-\frac{h}{2}}^{\frac{h}{2}} \left(\frac{E}{1 - \nu^2} - 3\mathbf{G} \right) z dz \sum_i \frac{1}{\xi_{(i^k)(k)}^2} \left(\begin{aligned} & \sum_i \frac{\bar{u}_l^{(i^k)} - \bar{u}_l^{(k)}}{\xi_{(i^k)(k)}} n_l^{(i^k)(k)} V_{(i^k)} \\ & - \sum_i \frac{\bar{u}_l^{(i^j)} - \bar{u}_l^{(j)}}{\xi_{(i^j)(j)}} n_l^{(i^j)(j)} V_{(i^j)} \end{aligned} \right) V_{(j)} \\ & + 2 \int_{-\frac{h}{2}}^{\frac{h}{2}} \mathbf{G} dz \sum_i \frac{n_l^{(i^k)(k)} n_j^{(i^k)(k)}}{\xi_{(i^k)(k)}^2} \left(\begin{aligned} & \sum_i \frac{\bar{u}_l^{(i^k)} - \bar{u}_l^{(k)}}{\xi_{(i^k)(k)}} n_j^{(i^k)(k)} V_{(i^k)} \\ & - \sum_i \frac{\bar{u}_l^{(i^j)} - \bar{u}_l^{(j)}}{\xi_{(i^j)(j)}} n_j^{(i^j)(j)} V_{(i^j)} \end{aligned} \right) V_{(j)} \end{aligned} \right] + \mathbf{b}_z^{(k)} \quad (5.38b)$$

Where Φ can be expressed as

$$\Theta_{(k)} = \frac{2}{\pi \delta^2 h} \sum_i \frac{\bar{u}_l^{(i^k)} - \bar{u}_l^{(k)}}{\xi_{(i^k)(k)}} n_l^{(i^k)(k)} V_{(i^k)} \quad (5.39a)$$

and

$$\Theta_{(j)} = \frac{2}{\pi \delta^2 h} \sum_i \frac{\bar{u}_l^{(i^j)} - \bar{u}_l^{(j)}}{\xi_{(i^j)(j)}} n_l^{(i^j)(j)} V_{(i^j)} \quad (5.39b)$$

For the plates subjected to fixed boundary conditions only, the PD EoM, Eqs. (5.38) can be simplified as

$$\rho_{(k)} \ddot{u}_L^{(k)} = \left\{ \begin{array}{l} \frac{24}{\pi \delta^3 h^2} \int_{-\frac{h}{2}}^{\frac{h}{2}} \alpha z \sum_j \frac{\bar{u}_l^{(j)} - \bar{u}_l^{(k)}}{\xi_{(j)(k)}} n_l^{(j)(k)} n_L^{(j)(k)} V_{(j)} \\ + \frac{2}{\pi \delta^2 h^2} \int_{-\frac{h}{2}}^{\frac{h}{2}} \frac{E(3\nu - 1)}{1 + \nu} dz \sum_j \frac{\Theta_{(j)} + \Theta_{(k)}}{\xi_{(j)(k)}} n_L^{(j)(k)} V_{(j)} \\ - \left(\frac{2}{\pi \delta^2 h} \right)^2 \frac{2}{h} \int_{-\frac{h}{2}}^{\frac{h}{2}} \frac{Ez}{1 - \nu^2} dz \sum_j \frac{n_L^{(j)(k)}}{\xi_{(j)(k)}} \left(\begin{array}{l} \sum_i \frac{\bar{w}_{(i^k)} - \bar{w}_{(k)}}{\xi_{(i^k)(k)}^2} V_{(i^k)} \\ + \sum_i \frac{\bar{w}_{(i^j)} - \bar{w}_{(j)}}{\xi_{(i^j)(j)}^2} V_{(i^j)} \end{array} \right) V_{(j)} \end{array} \right\} + b_L^{(k)} \quad (5.40a)$$

and

$$\rho_{(k)} \ddot{w}_{(k)} = \frac{1}{h} \left(\frac{4}{\pi \delta^2 h} \right)^2 \left[\begin{array}{l} \int_{-\frac{h}{2}}^{\frac{h}{2}} \frac{E}{1 - \nu^2} z^2 dz \sum_j \frac{1}{\xi_{(i^k)(k)}^2} \left(\begin{array}{l} \sum_i \frac{\bar{w}_{(i^k)} - \bar{w}_{(k)}}{\xi_{(i^k)(k)}^2} V_{(i^k)} \\ - \sum_i \frac{\bar{w}_{(i^j)} - \bar{w}_{(j)}}{\xi_{(i^j)(j)}^2} V_{(i^j)} \end{array} \right) V_{(j)} \\ - \frac{1}{2} \int_{-\frac{h}{2}}^{\frac{h}{2}} \frac{E}{1 - \nu^2} z dz \sum_i \frac{1}{\xi_{(i^k)(k)}^2} \left(\begin{array}{l} \sum_i \frac{\bar{u}_l^{(i^k)} - \bar{u}_l^{(k)}}{\xi_{(i^k)(k)}} n_l^{(i^k)(k)} V_{(i^k)} \\ - \sum_i \frac{\bar{u}_l^{(i^j)} - \bar{u}_l^{(j)}}{\xi_{(i^j)(j)}} n_l^{(i^j)(j)} V_{(i^j)} \end{array} \right) V_{(j)} \end{array} \right] + b_z^{(k)} \quad (5.40b)$$

5.2.3 Numerical Cases

To demonstrate the validity of the presented PD formulation for functionally graded Kirchhoff plates, the PD solutions are compared with the corresponding finite element (FE) analysis results. Here, the material properties are chosen such that Young's Modulus, $E(z)$, is assumed to be varied linearly through the thickness direction and Poisson's ratio, $\nu(z)$, remains a constant as

$$E(z) = (E_t - E_b) \frac{z}{h} + \frac{1}{2} (E_t + E_b) \quad (5.41a)$$

and

$$\nu(z) = \nu \quad (5.41b)$$

where E_t and E_b denote the Young's modulus of the top and bottom surfaces of the plate, and h represents the total thickness of the plate.

5.2.3.1 Clamped Plate Subjected to Transverse Loading

A clamped functionally graded plate with a length and width of $L = W = 1$ m and a thickness of $h = 0.02$ m is considered as shown in Fig. 5.9. The Poisson's ratio of

the plate is $\nu = 1/3$ and the Young's modulus of the top and bottom surfaces are $E_t = 200 \text{ GPa}$ and $E_b = 100 \text{ GPa}$, respectively. The model is discretized into one single row of material points along the thickness direction and the distance between material points is $\Delta x = 1/101 \text{ m}$. A fictitious region is introduced outside the edges as the external boundaries with a width of 2δ . The plate is subjected to a distributed transverse load of $p_z = 101 \text{ N/m}$ through the y -centre line, respectively. The line load is converted to a body load of $b = \frac{p_z W}{(W/\Delta x)\Delta V} = 510050 \text{ N/m}^3$ and it is distributed to one column of material volumes through the central line.

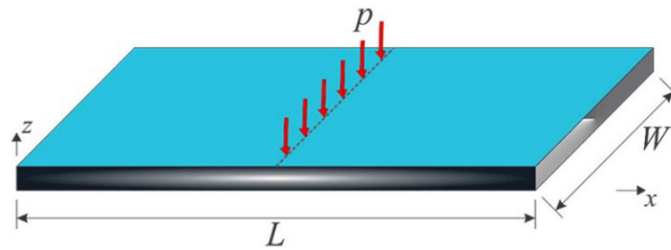


Figure 5.9 Clamped plate subjected to transverse loading

Layer 50	$E_{50}=199 \text{ GPa}$
Layer i	$E_i=100x(1+(i-1/2)/50) \text{ GPa}$
Layer 3	E_3
Layer 2	E_2
Layer 1	$E_1=101 \text{ GPa}$

Figure 5.10 Variation of the Young's modulus in thickness direction for the FE model

The FE model of the plate is created by using the SHELL181 element in ANSYS with dimensions of $1 \text{ m} \times 1 \text{ m} \times 0.02 \text{ m}$. To model the functionally graded plate, the model is divided to 50 layers with varying homogeneous materials properties through the thickness. The Young's modulus varies linearly over the thickness from the first layer $E_1 = 101 \text{ GPa}$ to the last layer $E_{50} = 199 \text{ GPa}$ as shown in Fig. 5.10. The model is meshed with 0.01 m element size.

The PD and FE transverse displacement contours are compared in Fig. 5.11. They yield similar displacement variations. The maximum difference between the PD and FE results is less than 0.5%. Moreover, the transverse and in-plane displacement components along the central y-axis are compared in Fig. 5.12 and very good agreement is obtained between the two approaches. These results verify the accuracy of the current PD formulation for a functionally graded Kirchhoff plate theory under clamped boundary conditions.

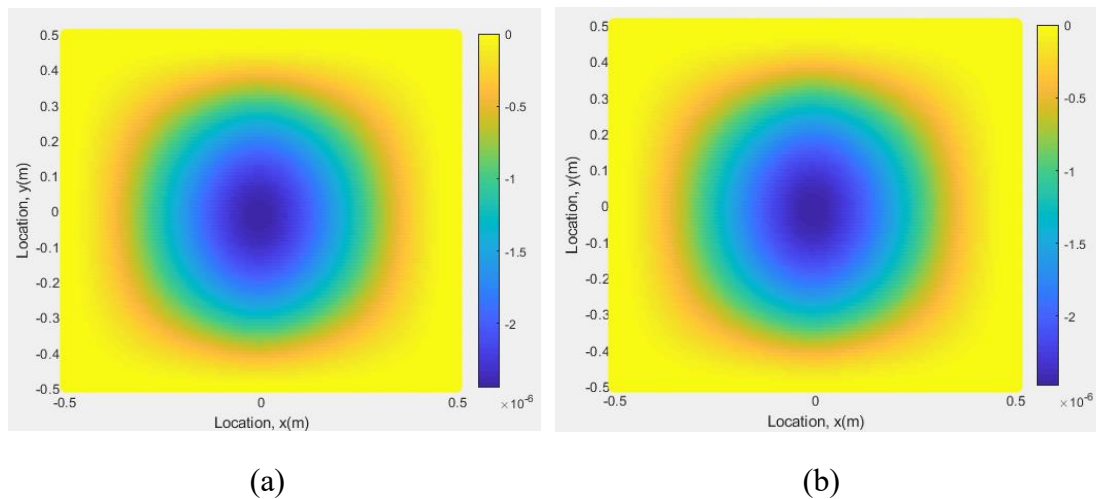


Figure 5.11 Variation of transverse displacements (a) PD, (b) FEM

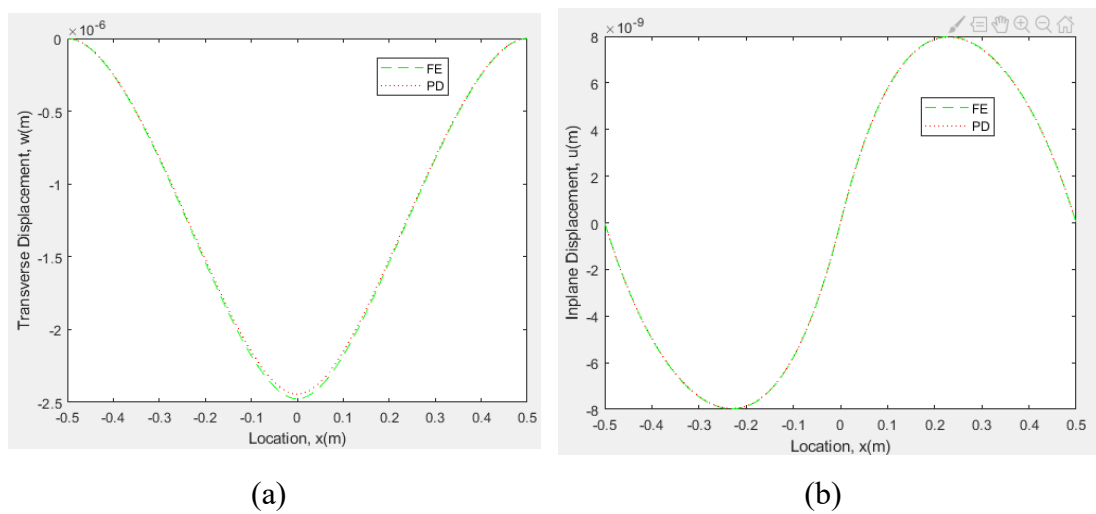


Figure 5.12 Variation of (a) transverse, w and (b) in-plane, u_1 , displacements along the central y-axis

5.2.3.2 Simply Supported Plate Subjected to Transverse Loading

A simply supported plate (see Fig. 5.13) has the same geometrical and material properties as in the clamped plate case. Again, it is discretized with a single row of material points along the thickness direction and the discretization size is $\Delta x = \frac{1}{101} m$. A fictitious region is created outside the region of boundaries and its width is equal to two times the size of the horizon, δ . The plate is subjected to a distributed transverse line load of $p_z = 101 \text{ N/m}$ through the y-central line. It is imposed to central column of material points with a body load of $b = \frac{p_z W}{(\frac{W}{\Delta x}) \Delta V} = 510050 \text{ N/m}^3$.

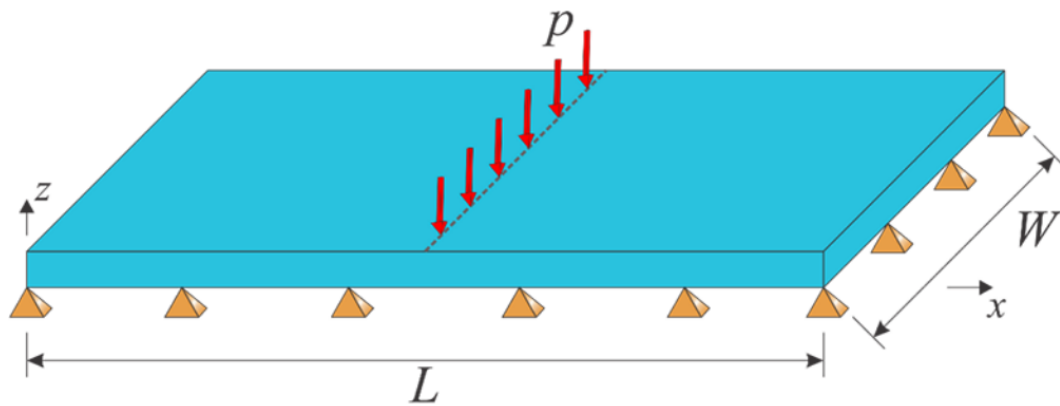


Figure 5.13 Simply supported plate subjected to transverse loading

The transverse displacement components of FE and PD theory show very close variations, as shown in Fig. 5.14. The maximum difference between the PD and FE results is less than 0.5%. Furthermore, the transverse and in-plane displacement variations along the central y-axis are on top of each other for the FE and PD results, as shown in Fig. 5.15. This confirms the current PD formulation of functionally graded plate theory under simply supported boundary conditions.

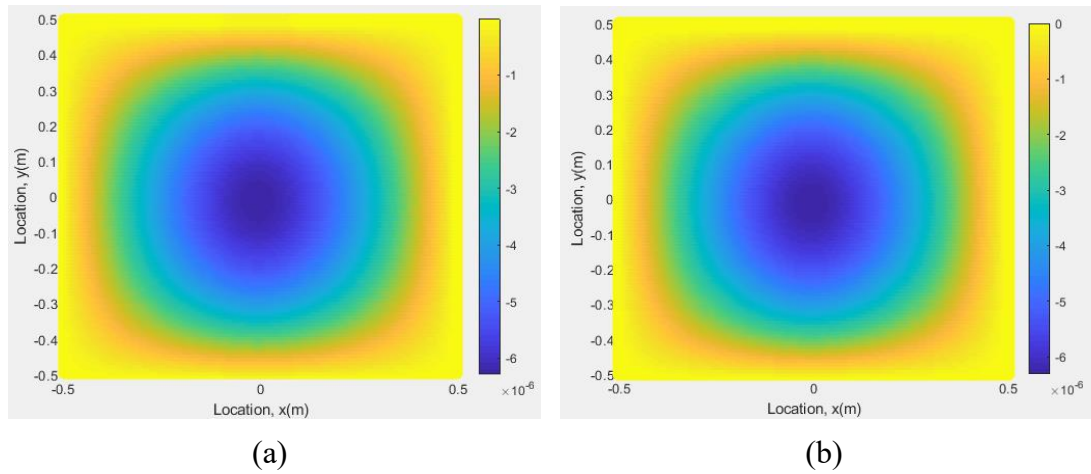


Figure 5.14 Variation of transverse displacements (a) PD, (b) FEM

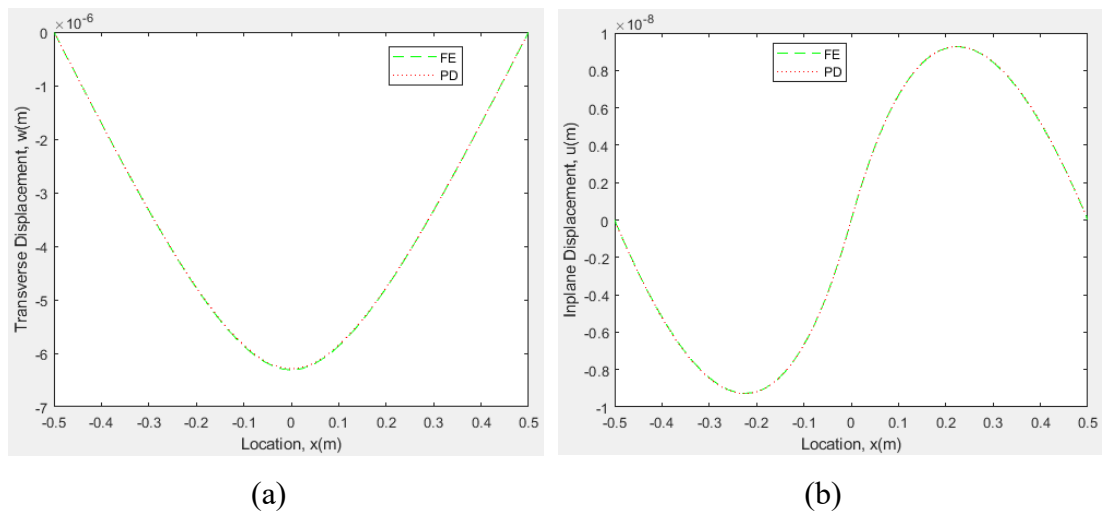


Figure 5.15 Variation of (a) transverse, w and (b) in-plane, u_1 , displacements along the central y -axis

5.2.3.3 Simply Supported Plate Subjected to Inclined Loading

This problem case is similar to the previous case except Poisson's ratio of 0.2 and an inclined load of $p_x = p_z = 101 \text{ N/m}$ through the y -central line are considered as shown in Fig. 5.16.

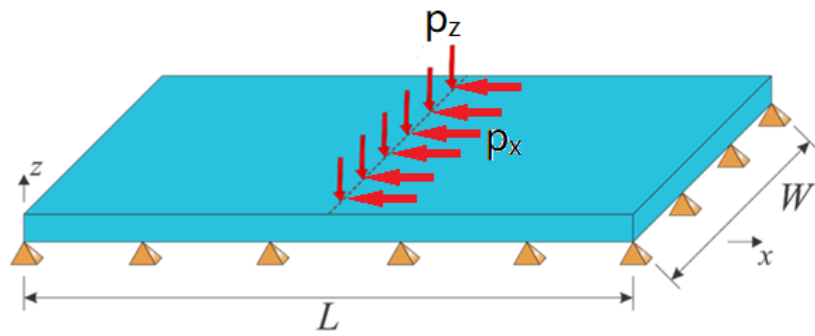
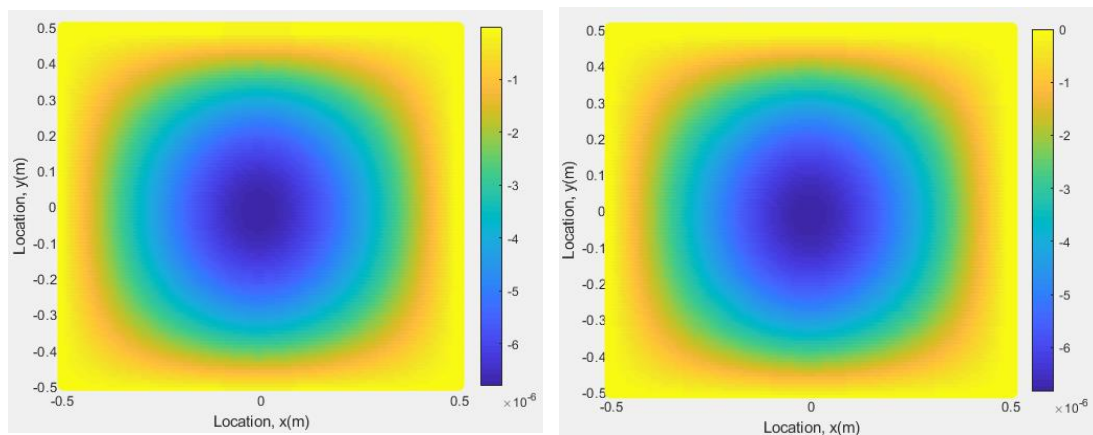


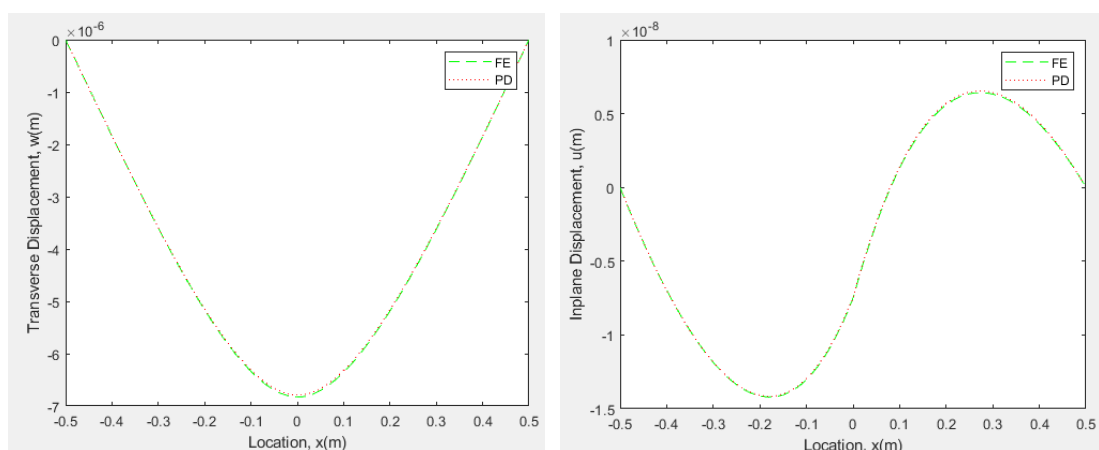
Figure 5.16 Simply supported plate subjected to inclined loading



(a)

(b)

Figure 5.17 Variation of transverse displacements (a) PD, (b) FEM



(a)

(b)

Figure 5.18 Variation of (a) transverse, w and (b) in-plane, u_1 , displacements along the central y -axis

As depicted in Fig. 5.17, the transverse displacement components of FE and PD theory agree very well with each other. Moreover, the transverse and in-plane displacements variations along the central y -axis are also in very good agreement as depicted in Fig. 5.18.

5.3 PD Formulations for Mindlin Plate

5.3.1 Mindlin Plate Theory

A complete and adequate set of equations for first order shear deformation linear theory of thick plates was developed by Mindlin, which is also known as Mindlin Plate theory. According to Mindlin plate theory, a transverse normal to the mid-plane of the plate in the undeformed state remains straight and there is no change in its length during deformation.

According to the assumptions of the Mindlin Plate theory, the displacement field of any material point can be represented in terms of the displacement field of the material points on the mid-plane (xy plane) as

$$u(x, y, z, t) = z\theta_x(x, y, t) \quad (5.42a)$$

$$v(x, y, z, t) = z\theta_y(x, y, t) \quad (5.42b)$$

$$w(x, y, z, t) = \bar{w}(x, y, t) \quad (5.42c)$$

where $\theta_x(x, y, t)$ and $\theta_y(x, y, t)$ denote the rotation of the material points on the mid-plane about positive y -direction and negative x -direction, respectively. Moreover, $\bar{w}(x, y, t)$ denotes the transverse displacement of the material points on the mid-plane. The positive set of the degrees-of-freedom is shown in Fig. 5.19.

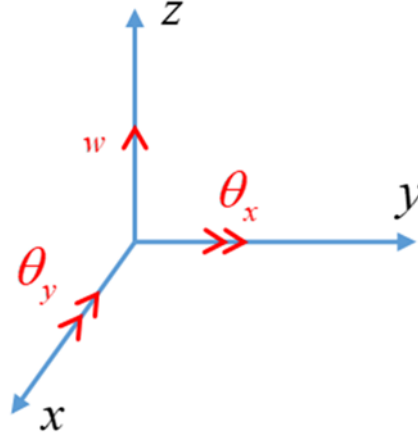


Figure 5.19 Degrees-of-freedom in peridynamic Mindlin formulation

Thus, the strain-displacement relationship can be written as

$$\varepsilon_{xx} = z \frac{\partial \theta_x}{\partial x} \quad (5.43a)$$

$$\varepsilon_{yy} = z \frac{\partial \theta_y}{\partial y} \quad (5.43b)$$

$$\varepsilon_{xy} = \varepsilon_{yx} = \frac{1}{2} z \left(\frac{\partial \theta_x}{\partial y} + \frac{\partial \theta_y}{\partial x} \right) \quad (5.43c)$$

$$\gamma_{xz} = \kappa_s \left(\theta_x + \frac{\partial w}{\partial x} \right) \quad (5.43d)$$

$$\gamma_{yz} = \kappa_s \left(\theta_y + \frac{\partial w}{\partial y} \right) \quad (5.43e)$$

which can be also expressed in terms of indicial notation as

$$\varepsilon_{IJ} = \frac{1}{2} z \left(\frac{\partial \theta_I}{\partial x_J} + \frac{\partial \theta_J}{\partial x_I} \right) \quad (5.44a)$$

$$\gamma_{I3} = \kappa_s \left(\theta_I + \frac{\partial w}{\partial x_I} \right) \quad (5.44b)$$

where κ_s is introduced as shear coefficient. Note that the subscript indices, $I, J, \dots = 1, 2$, and this convention will be applied throughout this study.

For isotropic materials, the stress-strain relationships can be written as:

$$\sigma_{xx} = \frac{E}{1-\nu^2} (\varepsilon_{xx} + \nu \varepsilon_{yy}) \quad (5.45a)$$

$$\sigma_{yy} = \frac{E}{1-\nu^2} (\varepsilon_{yy} + \nu \varepsilon_{xx}) \quad (5.45b)$$

$$\sigma_{xy} = G (\varepsilon_{xy} + \varepsilon_{yx}) \quad (5.45c)$$

$$\tau_{xz} = G \gamma_{xz} \quad (5.45d)$$

$$\tau_{yz} = G\gamma_{yz} \quad (5.45e)$$

Note that the transverse normal stress, σ_{zz} , is considered to be small compared to in-plane stresses. Thus, it is discarded from the stress components set for simplification.

The stress components can also be expressed in indicial notation as:

$$\sigma_{IJ} = C_{IJKL}\varepsilon_{KL} \quad (5.46a)$$

$$\tau_{I3} = G\gamma_{I3} \quad (5.46b)$$

where

$$C_{IJKL} = G(\delta_{IL}\delta_{JK} + \delta_{IK}\delta_{JL}) + \frac{Ev}{1-\nu^2}\delta_{IJ}\delta_{KL} \quad (5.47)$$

The average strain energy density of a particular material point on the mid-plane can be reasonably obtained by integrating the strain energy density function, through the transverse direction and dividing by the thickness as

$$W_{\text{com}} = \frac{1}{2h} \int_{-\frac{h}{2}}^{\frac{h}{2}} (\sigma_{IJ}\varepsilon_{IJ} + \tau_{I3}\gamma_{I3}) dz \quad (5.48a)$$

Inserting Eqs. (5.46) and (6) into (5.47) and rearranging indices yields

$$W_{\text{com}} = \frac{G}{2} \frac{h^2}{12} \left[\left(\frac{\partial\theta_I}{\partial x_J} \frac{\partial\theta_I}{\partial x_J} + \frac{\partial\theta_I}{\partial x_J} \frac{\partial\theta_J}{\partial x_I} + \frac{\partial\theta_I}{\partial x_I} \frac{\partial\theta_J}{\partial x_J} \right) + \frac{3\nu-1}{1-\nu} \frac{\partial\theta_I}{\partial x_I} \frac{\partial\theta_J}{\partial x_J} \right] + \kappa_s^2 \frac{G}{2} \left(\theta_I + \frac{\partial w}{\partial x_I} \right) \left(\theta_I + \frac{\partial w}{\partial x_I} \right) \quad (5.48b)$$

5.3.2 Peridynamic Mindlin Plate Formulation

The PD equations of motion can be derived by utilizing Lagrange's equation:

$$\frac{d}{dt} \frac{\partial L}{\partial \dot{\mathbf{u}}_{(k)}} - \frac{\partial L}{\partial \mathbf{u}_{(k)}} = 0 \quad (5.49)$$

where $L = T - U$ is the Lagrangian and \mathbf{u} represents the displacement vector, which can be defined in this study as\

$$\mathbf{u} = [\theta_1 \quad \theta_2 \quad \bar{w}]^T \quad (5.50)$$

The kinetic energy per unit area, \bar{T} , can be expressed as

$$\bar{T} = \frac{1}{2} \int_{-\frac{h}{2}}^{\frac{h}{2}} \rho (\dot{u}^2 + \dot{v}^2 + \dot{w}^2) dz \quad (5.51a)$$

Plugging Eqs. (5.42) into (5.51a) yields

$$\bar{T} = \frac{1}{2} \rho \left[\frac{h^3}{12} (\dot{\theta}_x^2 + \dot{\theta}_y^2) + h\dot{w}^2 \right] \quad (5.51b)$$

The total kinetic energy of the system, T , can be casted by integrating the areal kinetic energy density, Eq.(5.51b) over the mid-plane as

$$T = \int_A \bar{T} dA = \frac{1}{2} \int_A \rho \left[\frac{h^3}{12} (\dot{\theta}_x^2 + \dot{\theta}_y^2) + h\dot{w}^2 \right] dA \quad (5.52a)$$

which can be written in a discretized form as

$$T = \frac{1}{2} \sum_j \rho_{(j)} \left\{ \frac{h^2}{12} \left[(\dot{\theta}_1^{(j)})^2 + (\dot{\theta}_2^{(j)})^2 \right] + \dot{w}_{(j)}^2 \right\} V_{(j)} \quad (5.52b)$$

Therefore, the first term of the Lagrange's equation becomes

$$\frac{d}{dt} \frac{\partial L}{\partial \dot{\mathbf{u}}_{(k)}} = \frac{d}{dt} \frac{\partial T}{\partial \dot{\mathbf{u}}_{(k)}} = \rho_{(k)} \left\{ \begin{array}{c} \frac{h^2}{12} \ddot{\theta}_1^{(k)} \\ \frac{h^2}{12} \ddot{\theta}_2^{(k)} \\ \ddot{w}_{(k)} \end{array} \right\} V_{(k)} \quad (5.53)$$

The total potential energy stored in the body can be obtained by summing potential energies of all material points including strain energy and energy due to external loads as

$$U = \sum_n W_{FD}^{(n)} (\mathbf{u}_{(n)}, \mathbf{u}_{(1^n)}, \mathbf{u}_{(2^n)}, \mathbf{u}_{(3^n)}, \dots) V_{(n)} - \sum_n \mathbf{b}_{(n)} \mathbf{u}_{(n)} V_{(n)} \quad (5.54)$$

where the body force density vector, \mathbf{b} , can be expressed in this study as

$$\mathbf{b} = [\hat{b}_1 \quad \hat{b}_2 \quad b_z]^T \quad (5.55)$$

Here the entries of the body force density vector, \hat{b} , and b_z correspond to moment and transverse force, respectively. Utilizing the pre-obtained result, Eq. (3.8), the second term of the Lagrange's equation becomes

$$-\frac{\partial L}{\partial \mathbf{u}_{(k)}} = \left(\begin{array}{c} \frac{\partial W_{FD}^{(k)}}{\partial \theta_1^{(k)}} V_{(k)} + \sum_j \frac{\partial W_{FD}^{(j)}}{\partial \theta_1^{(k)}} V_{(j)} \\ \frac{\partial W_{FD}^{(k)}}{\partial \theta_2^{(k)}} V_{(k)} + \sum_j \frac{\partial W_{FD}^{(j)}}{\partial \theta_2^{(k)}} V_{(j)} \\ \frac{\partial W_{FD}^{(k)}}{\partial w_{(k)}} V_{(k)} + \sum_j \frac{\partial W_{FD}^{(j)}}{\partial w_{(k)}} V_{(j)} \end{array} \right) - \left\{ \begin{array}{c} \hat{b}_1 \\ \hat{b}_2 \\ b_z \end{array} \right\} V_{(k)} \quad (5.56)$$

Combining Eq. (5.53) and (5.56) into the Lagrange's equation gives

$$\rho_{(k)} \begin{Bmatrix} \frac{h^2}{12} \ddot{\theta}_1^{(k)} \\ \frac{h^2}{12} \ddot{\theta}_2^{(k)} \\ \ddot{w}_{(k)} \end{Bmatrix} V_{(k)} = - \begin{pmatrix} \frac{\partial W_{PD}^{(k)}}{\partial \theta_1^{(k)}} V_{(k)} + \sum_j \frac{\partial W_{PD}^{(j)}}{\partial \theta_1^{(k)}} V_{(j)} \\ \frac{\partial W_{PD}^{(k)}}{\partial \theta_2^{(k)}} V_{(k)} + \sum_j \frac{\partial W_{PD}^{(j)}}{\partial \theta_2^{(k)}} V_{(j)} \\ \frac{\partial W_{PD}^{(k)}}{\partial \bar{w}_{(k)}} V_{(k)} + \sum_j \frac{\partial W_{PD}^{(j)}}{\partial \bar{w}_{(k)}} V_{(j)} \end{pmatrix} + \begin{Bmatrix} \hat{b}_1 \\ \hat{b}_2 \\ b_z \end{Bmatrix} V_{(k)} \quad (5.57)$$

In order to write the non-local form of strain energy density function of the material point k , Eq. (5.48b), it is necessary to transform all the differential terms into an equivalent form of integration by considering PD strain energy density expression given in Eq. (5.55). As derived in Appendix A2.3, the strain energy density function of the material point k , and its family member j can be expressed as

$$W_{PD}^{(k)} = \frac{h^2 G}{12 \cdot 2} \left\{ \begin{aligned} & \frac{12}{\pi \delta^3 h} \sum_i \left[\frac{(\theta_i^{(k)} - \theta_i^{(k)}) n_i^{(i^k)(k)} \xi_{(i^k)(k)}}{\xi_{(i^k)(k)}} \right]^2 V_{(i^k)} \\ & + \frac{3\nu - 1}{1 - \nu} \left(\frac{2}{\pi \delta^2 h} \sum_i \frac{\theta_i^{(i^k)} - \theta_i^{(k)}}{\xi_{(i^k)(k)}} n_i^{(i^k)(k)} V_{(i^k)} \right)^2 \end{aligned} \right\} \quad (5.58a)$$

$$+ \kappa_s^2 \frac{G}{2} \frac{3}{\pi \delta^3 h} \sum_i \left(\frac{\bar{w}_{(i^k)} - \bar{w}_{(k)} + \frac{\theta_i^{(i^k)} + \theta_i^{(k)}}{2} n_i^{(i^k)(k)} \xi_{(i^k)(k)}}{\xi_{(i^k)(k)}} \right)^2 V_{(i^k)}$$

and

$$W_{PD}^{(j)} = \frac{h^2 G}{12 \cdot 2} \left\{ \begin{aligned} & \frac{12}{\pi \delta^3 h} \sum_i \left[\frac{(\theta_i^{(j)} - \theta_i^{(j)}) n_i^{(i^j)(j)} \xi_{(i^j)(j)}}{\xi_{(i^j)(j)}} \right]^2 V_{(i^j)} \\ & + \frac{3\nu - 1}{1 - \nu} \left(\frac{2}{\pi \delta^2 h} \sum_i \frac{\theta_i^{(i^j)} - \theta_i^{(j)}}{\xi_{(i^j)(j)}} n_i^{(i^j)(j)} V_{(i^j)} \right)^2 \end{aligned} \right\} \quad (5.58b)$$

$$+ \kappa_s^2 \frac{G}{2} \frac{3}{\pi \delta^3 h} \sum_i \left(\frac{\bar{w}_{(i^j)} - \bar{w}_{(j)} + \frac{\theta_i^{(i^j)} + \theta_i^{(j)}}{2} n_i^{(i^j)(j)} \xi_{(i^j)(j)}}{\xi_{(i^j)(j)}} \right)^2 V_{(i^j)}$$

Substituting Eqs. (5.58a) and (5.58b) into Eq. (5.57) and renaming the summation indices yield's the PD equations of motion for Mindlin plate as:

$$\rho_{(k)} \frac{h^2}{12} \ddot{\theta}_L^{(k)} = \frac{2Gh}{\pi \delta^3} \sum_j \frac{\theta_i^{(j)} - \theta_i^{(k)}}{\xi_{(j)(k)}} n_i^{(j)(k)} n_L^{(j)(k)} V_{(j)} + G \frac{3\nu - 1}{1 - \nu} \frac{h^2}{12} \frac{2}{\pi \delta^2 h} \sum_j \frac{\Phi_{(j)} + \Phi_{(k)}}{\xi_{(j)(k)}} n_L^{(j)(k)} V_{(j)} \quad (5.59a)$$

$$- \kappa_s^2 \frac{3G}{\pi \delta^3 h} \sum_j \left(\bar{w}_{(j)} - \bar{w}_{(k)} + \frac{\theta_i^{(k)} + \theta_i^{(j)}}{2} \xi_{(j)(k)} n_i^{(j)(k)} \right) n_L^{(j)(k)} V_{(j)} + \hat{b}_L \quad)$$

$$\rho_{(k)} \ddot{w}_{(k)} = \frac{6\kappa_s^2 G}{\pi \delta^3 h} \sum_j \left(\frac{\bar{w}_{(j)} - \bar{w}_{(k)}}{\xi_{(j)(k)}} + \frac{\theta_i^{(k)} + \theta_i^{(j)}}{2} n_i^{(j)(k)} \right) V_{(j)} + b_z^{(k)} \quad (5.59b)$$

where $\Phi_{(j)}$ and $\Phi_{(k)}$ appeared in Eq. (5.59a) can be expressed as

$$\Phi_{(k)} = \frac{2}{\pi\delta^2 h} \sum_i \frac{\theta_i^{(i^k)} + \theta_i^{(k)}}{\xi_{(i^k)(k)}} n_i^{(i^k)(k)} V_{(i^k)} \quad (5.60a)$$

$$\Phi_{(j)} = \frac{2}{\pi\delta^2 h} \sum_i \frac{\theta_i^{(i^j)} + \theta_i^{(j)}}{\xi_{(i^j)(j)}} n_i^{(i^j)(j)} V_{(i^j)} \quad (5.60b)$$

In particular case, Eqs. (5.59) can be simplified for the Poisson's ratio, $\nu = 1/3$ as:

$$\begin{aligned} \rho_{(k)} \frac{h^2}{12} \ddot{\theta}_L^{(k)} &= c_b \sum_j \frac{\theta_j^{(j)} - \theta_j^{(k)}}{\xi_{(j)(k)}} n_j^{(j)(k)} n_L^{(j)(k)} V_{(j)} \\ &\quad - \frac{c_s}{2} \sum_j \left(\bar{w}_{(j)} - \bar{w}_{(k)} + \frac{\theta_j^{(k)} + \theta_j^{(j)}}{2} \xi_{(j)(k)} n_j^{(j)(k)} \right) n_L^{(j)(k)} V_{(j)} + \hat{b}_L \end{aligned} \quad (5.61a)$$

$$\rho_{(k)} \ddot{w}_{(k)} = c_s \sum_j \left(\frac{\bar{w}_{(j)} - \bar{w}_{(k)}}{\xi_{(j)(k)}} + \frac{\theta_j^{(k)} + \theta_j^{(j)}}{2} n_j^{(j)(k)} \right) V_{(j)} + \hat{b}_z^{(k)} \quad (5.61b)$$

where c_b and c_s are the PD material parameters associated with bending and transverse shear deformation, respectively, which are defined as

$$c_b = \frac{3Eh}{4\pi\delta^3} \quad (5.62a)$$

$$c_s = \frac{9\kappa_s^2 E}{4\pi\delta^3 h} \quad (5.62b)$$

5.3.3 Numerical Cases

In this section, three different numerical examples are demonstrated for a Mindlin plate subjected to transverse loading and different types of boundary conditions including simply supported, clamped and mixed (clamped-simply supported). To verify the validity of the PD formulation, the PD solutions are compared with the corresponding finite element (FE) analysis results

5.3.3.1 Mindlin plate subjected to simply supported boundary conditions

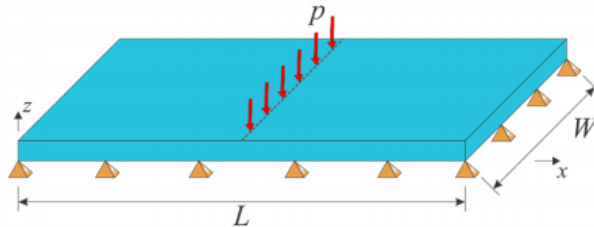


Figure 5.20 Simply supported plate subjected to transverse loading

A simply supported plate with a length and width of $L = W = 1\text{ m}$ and thickness of

$h = 0.1\text{m}$ is considered as shown in Fig. 5.20. The Young's modulus and Poisson's ratio of the plate are $E = 200\text{GPa}$ and $\nu = 1/3$, respectively. The shear coefficient is chosen as $\kappa_s^2 = \frac{\pi^2}{12}$. The model is discretized into one single row of material points along with the thickness direction and 101 material points throughout the length and width, respectively. The distance between two adjacent material points is $\Delta x = \frac{1}{101}\text{m}$. The horizon size is chosen as $\delta = 3.606\Delta x$. A fictitious region is introduced outside the edges as the external boundaries with a width of $3\Delta x$. The plate is subjected to a distributed transverse load of $p = 100\text{N/m}$ through the central line of plate as shown in Fig. 5.20. The load is converted to a body load of $b_z = \frac{pW}{101\Delta V} = 1.01e5 \text{ N/m}^3$ and it is imposed on a row of material points through the central line of the plate as shown in Fig. 5.21.

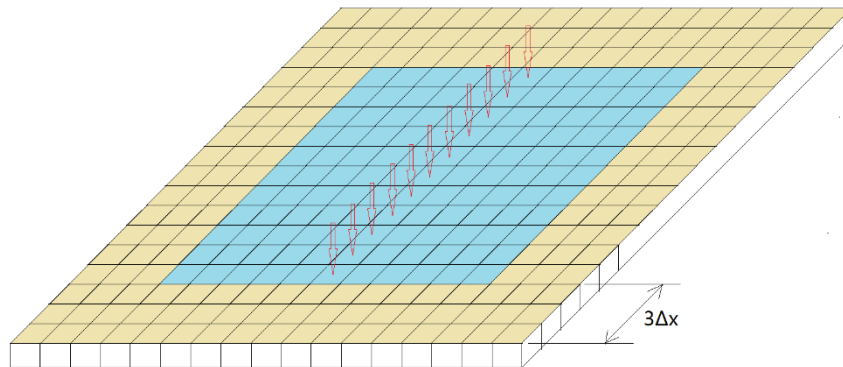


Figure 5.21 Discretisation and application of the body load

The FE model of the simply supported plate is created by using SHELL181 element in ANSYS and meshed with 50×50 elements throughout the body. The PD solution of the transverse displacement, w , and rotations, θ_L , along the central x - and y -axes are compared with the FE method results. As depicted in Figs. 5.22-5.23, the PD and the FE method results agree well with each other.

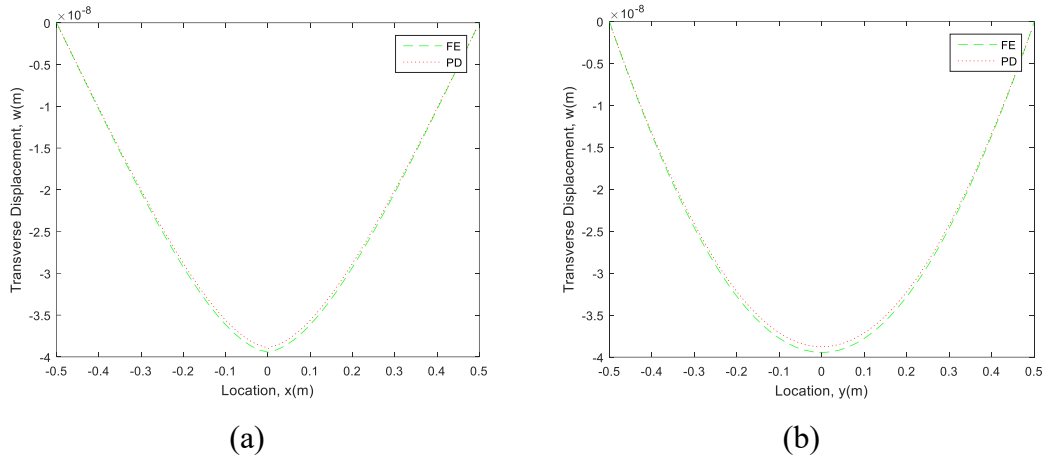


Figure 5.22 Variation of transverse displacements along the central (a) x -axis, (b) y -axis

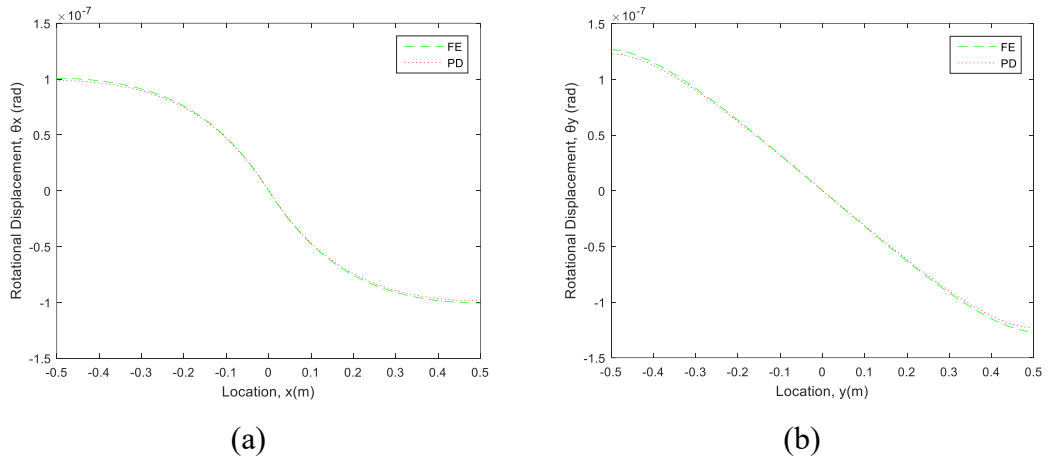


Figure 5.23 Variation of rotations along the central (a) x -axis, (b) y -axis.

5.3.3.2 Mindlin plate subjected to clamped boundary conditions

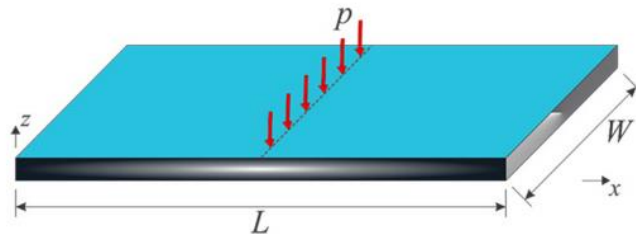


Figure 5.24 Clamped plated subjected to transverse loading

In the second case, same problem is considered as in the previous example case except

the Poisson's ratio being 0.3 and the boundary condition being clamped instead of simply-supported as shown in Fig. 5.24. The FE model of the simply supported plate is created by using SHELL181 element in ANSYS and meshed with 50x50 elements throughout the body. The PD solution of the transverse displacement, w , and rotations, θ_L , along the central x - and y -axes are compared with the FE method results. As depicted in Fig. 5.25-5.26, the PD and the FE method results agree well with each other.

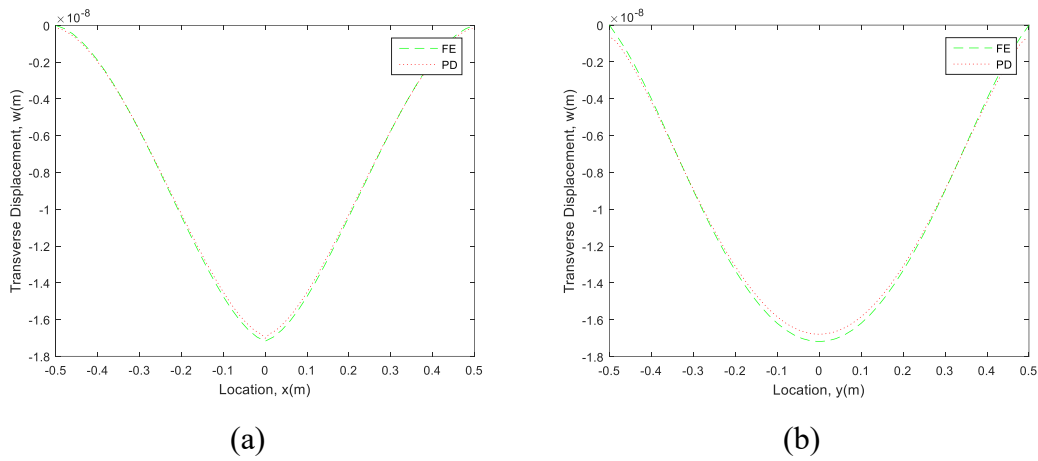


Figure 5.25 Variation of transverse displacements along the central (a) x -axis, (b) y -axis.

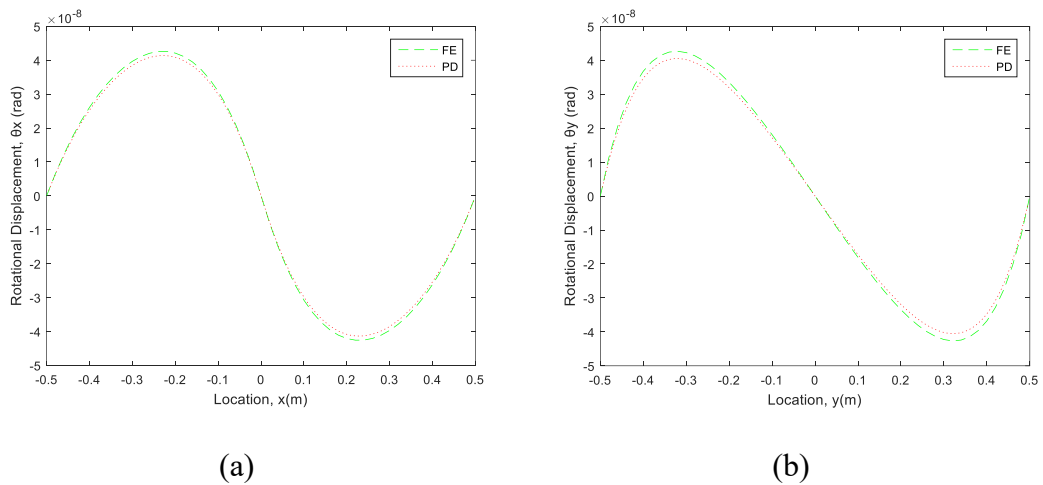


Figure 5.26 Variation of rotations along the central (a) x -axis, (b) y -axis.

5.3.3 Mindlin plate subjected to mixed (clamped – simply supported) boundary conditions

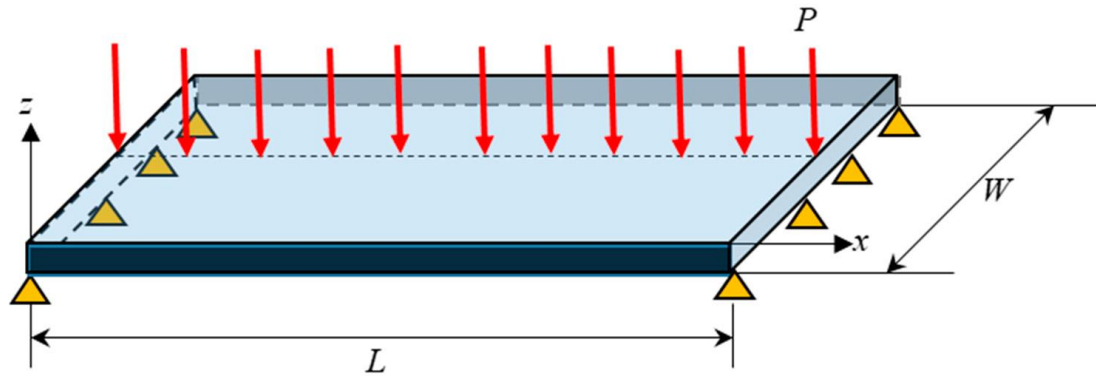


Figure 5.27 Mindlin plate subjected to mixed boundary conditions

In this final numerical case, as opposed to first and second numerical cases, Mindlin plate is subjected to mixed (clamped-simply supported) boundary conditions. The Poisson's Ratio is again chosen as 0.3. The FE model of the simply supported plate is created by using SHELL181 element in ANSYS and meshed with 50x50 elements through the body. The PD solution of the transverse displacement, w , and rotations, θ_L , are compared with the FE method results. As depicted in Fig. 5.28-5.29, the PD and the FE method results agree well with each other.

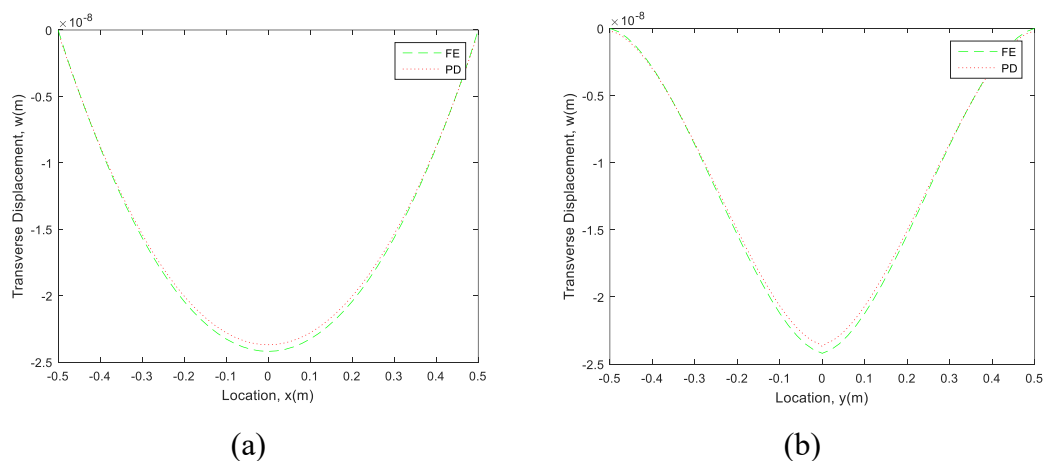


Figure 5.28 Variation of transverse displacements along the central (a) x -axis, (b) y -axis.

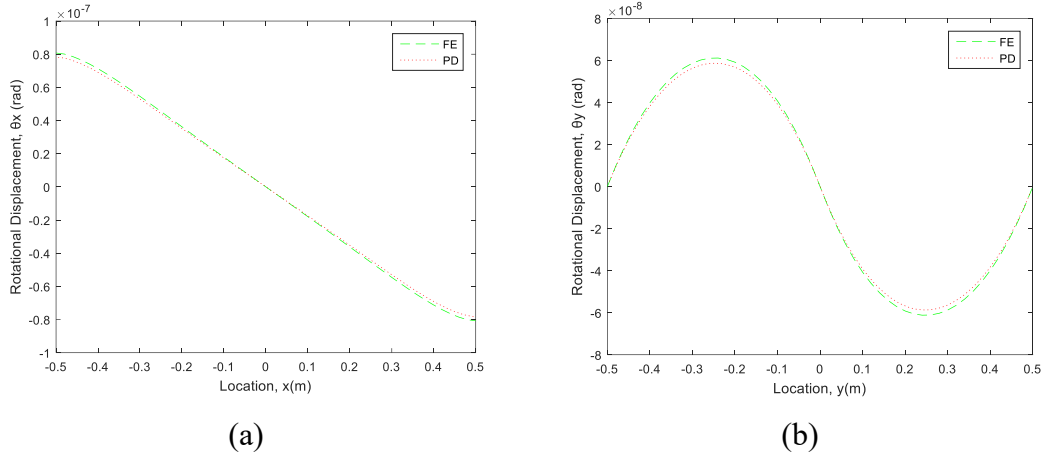


Figure 5.29 Variation of rotations along the central (a) x -axis, (b) y -axis

5.4 PD Formulations for FGM Mindlin Plate

5.4.1 FGM Mindlin Plate Theory

Mindlin plate formulation was developed to analyse relatively thick plates by taking into account transverse shear deformations which is neglected in Kirchhoff plate theory suitable for thin plates. According to Mindlin plate theory, the displacement of a material point can be expressed in terms of displacement and rotation fields of the material points along the mid-plane (xy -plane)

$$u(x, y, z, t) = \bar{u}(x, y, t) + z\theta_x(x, y, t) \quad (5.63a)$$

$$v(x, y, z, t) = \bar{v}(x, y, t) + z\theta_y(x, y, t) \quad (5.63b)$$

$$w(x, y, z, t) = \bar{w}(x, y, t) \quad (5.63c)$$

where $\bar{u}(x, y, t)$ and $\bar{v}(x, y, t)$ represent the in-plane displacement, $\bar{w}(x, y, t)$ represents the transverse displacement and $\theta_x(x, y, t)$ and $\theta_y(x, y, t)$ denote the rotational displacement about positive y -direction and negative x -direction, of the material points on the mid - plane, respectively. The positive set of the degrees - of - freedom is shown in Figure 5.30.

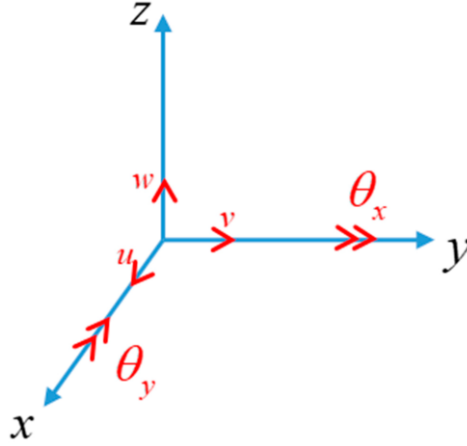


Figure 5.30. The positive set of the degrees - of - freedom for Mindlin plate formulation

Thus, the strain - displacement relationship can be written as

$$\varepsilon_{xx} = \frac{\partial \bar{u}}{\partial x} + z \frac{\partial \theta_x}{\partial x} \quad (5.64a)$$

$$\varepsilon_{yy} = \frac{\partial \bar{v}}{\partial y} + z \frac{\partial \theta_y}{\partial y} \quad (5.64b)$$

$$\varepsilon_{xy} = \varepsilon_{yx} = \frac{1}{2} \left[\left(\frac{\partial u}{\partial y} + \frac{\partial v}{\partial x} \right) z \left(\frac{\partial \theta_x}{\partial y} + \frac{\partial \theta_y}{\partial x} \right) \right] \quad (5.64c)$$

$$\gamma_{xz} = \kappa_s \left(\theta_x + \frac{\partial w}{\partial x} \right) \quad (5.64d)$$

$$\gamma_{yz} = \kappa_s \left(\theta_y + \frac{\partial w}{\partial y} \right) \quad (5.64e)$$

which can be also expressed in terms of indicial notation as

$$\varepsilon_{IJ} = \frac{1}{2} \left[\left(\frac{\partial u_I}{\partial x_J} + \frac{\partial u_J}{\partial x_I} \right) z \left(\frac{\partial \theta_I}{\partial x_J} + \frac{\partial \theta_J}{\partial x_I} \right) \right] \quad (5.65a)$$

$$\gamma_{I3} = \kappa_s \left(\theta_I + \frac{\partial w}{\partial x_I} \right) \quad (5.65b)$$

where κ_s is introduced as shear coefficient. Note that the subscript indices, I, J, \dots , take up the value 1(= x) and 2(= y), and this convention will be applied throughout this study.

According to plane-stress material constitutive law, the stress components can be given as

$$\sigma_{xx} = \frac{E}{1 - \nu^2} (\varepsilon_{xx} + \nu \varepsilon_{yy}) \quad (5.66a)$$

$$\sigma_{yy} = \frac{E}{1-\nu^2} (\varepsilon_{yy} + \nu\varepsilon_{xx}) \quad (5.66b)$$

$$\sigma_{xy} = 2G\varepsilon_{xy} \quad (5.66c)$$

$$\tau_{xz} = G\gamma_{xz} \quad (5.66d)$$

$$\tau_{yz} = G\gamma_{yz} \quad (5.66e)$$

which can be written in the tensorial form as

$$\sigma_{IJ} = 2G\varepsilon_{IJ} + \frac{E\nu}{1-\nu^2} \delta_{IJ}\varepsilon_{KK} \quad (5.67)$$

where $E = E(z)$, $G = G(z)$ and $\nu = \nu(z)$ represent the Young's modulus, shear modulus and Poisson's ratio, respectively.

The transverse average strain energy density can be reasonably calculated by integrating the strain energy density over the thickness and dividing by the thickness as

$$W_{\text{com}} = \frac{1}{2h} \int_{-\frac{h}{2}}^{\frac{h}{2}} (\sigma_{IJ}\varepsilon_{IJ} + \tau_{I3}\gamma_{I3}) dz \quad (5.68a)$$

Substituting Eqs. (5.65) and (5.66) into (5.68a) gives

$$W_{\text{com}} = \frac{1}{2h} \left[\int_{-\frac{h}{2}}^{\frac{h}{2}} G dz \left(\frac{\partial \bar{u}_I}{\partial x_J} \frac{\partial \bar{u}_I}{\partial x_J} + \frac{\partial \bar{u}_I}{\partial x_J} \frac{\partial \bar{u}_J}{\partial x_I} + \frac{\partial \bar{u}_I}{\partial x_I} \frac{\partial \bar{u}_J}{\partial x_J} \right) + \int_{-\frac{h}{2}}^{\frac{h}{2}} G^2 dz \left(\frac{\partial \theta_I}{\partial x_J} \frac{\partial \theta_I}{\partial x_J} + \frac{\partial \theta_I}{\partial x_J} \frac{\partial \theta_J}{\partial x_I} + \frac{\partial \theta_I}{\partial x_I} \frac{\partial \theta_J}{\partial x_J} \right) \right. \\ \left. + 2 \int_{-\frac{h}{2}}^{\frac{h}{2}} G dz \left(\frac{\partial \bar{u}_I}{\partial x_J} \frac{\partial \theta_I}{\partial x_J} + \frac{\partial \bar{u}_I}{\partial x_J} \frac{\partial \theta_J}{\partial x_I} + \frac{\partial \bar{u}_I}{\partial x_I} \frac{\partial \theta_J}{\partial x_J} \right) + \int_{-\frac{h}{2}}^{\frac{h}{2}} \kappa_s^2 G dz \left(\theta_I + \frac{\partial \bar{w}}{\partial x_I} \right) \left(\theta_I + \frac{\partial \bar{w}}{\partial x_I} \right) \right. \\ \left. + \int_{-\frac{h}{2}}^{\frac{h}{2}} G \frac{3\nu-1}{1-\nu} dz \left(\frac{\partial \bar{u}_I}{\partial x_I} \right)^2 + \int_{-\frac{h}{2}}^{\frac{h}{2}} G \frac{3\nu-1}{1-\nu} z^2 dz \left(\frac{\partial \theta_I}{\partial x_I} \right) + 2 \int_{-\frac{h}{2}}^{\frac{h}{2}} G \frac{3\nu-1}{1-\nu} z dz \frac{\partial \bar{u}_I}{\partial x_I} \frac{\partial \theta_J}{\partial x_J} \right] \quad (5.68b)$$

5.4.2 PD FGM Mindlin Plate Formulation

The PD equations of motion can be derived by utilizing Lagrange's equation:

$$\frac{d}{dt} \frac{\partial L}{\partial \dot{\mathbf{u}}_k} - \frac{\partial L}{\partial \mathbf{u}_k} = 0 \quad (5.69)$$

where $L = T - U$ is the Lagrangian and \mathbf{u} represents the displacement vector, which can be defined in this study as

$$\mathbf{u} = [\bar{u}_1 \quad \bar{u}_2 \quad \theta_1 \quad \theta_2 \quad \bar{w}]^T \quad (5.70)$$

The kinetic energy per unit area, \bar{T} , can be expressed as

$$\bar{T} = \frac{1}{2} \int_{-\frac{h}{2}}^{\frac{h}{2}} \rho (\dot{u}^2 + \dot{v}^2 + \dot{w}^2) dz \quad (5.71a)$$

Plugging Eqs. (5.63) into (5.71a) yields

$$\bar{T} = \frac{1}{2} \rho \left[\frac{h^3}{12} (\dot{\theta}_x^2 + \dot{\theta}_y^2) + h (\dot{u}^2 + \dot{v}^2 + \dot{w}^2) \right] \quad (5.71b)$$

The total kinetic energy of the system, T , can be casted by integrating the areal kinetic energy density, Eq.(5.71b) over the mid-plane as

$$T = \int_A \bar{T} dA = \frac{1}{2} \int_A \rho \left[\frac{h^3}{12} (\dot{\theta}_x^2 + \dot{\theta}_y^2) + h (\dot{u}^2 + \dot{v}^2 + \dot{w}^2) \right] dA \quad (5.72a)$$

which can be written in a discretized form as

$$T = \frac{1}{2} \sum_j \rho_{(j)} \left\{ \frac{h^2}{12} [(\dot{\theta}_1^{(j)})^2 + (\dot{\theta}_2^{(j)})^2] + (\dot{u}_1)^2 + (\dot{u}_2)^2 + \dot{w}_{(j)}^2 \right\} V_{(j)} \quad (5.72b)$$

Therefore, the first term of the Lagrange's equation becomes

$$\frac{d}{dt} \frac{\partial L}{\partial \dot{\mathbf{u}}_{(k)}} = \frac{d}{dt} \frac{\partial T}{\partial \dot{\mathbf{u}}_{(k)}} = \rho_{(k)} \left\{ \begin{array}{c} \ddot{u}_1 \\ \ddot{u}_2 \\ \frac{h^2}{12} \ddot{\theta}_1^{(k)} \\ \frac{h^2}{12} \ddot{\theta}_2^{(k)} \\ \ddot{w}_{(k)} \end{array} \right\} V_{(k)} \quad (5.73)$$

The total potential energy stored in the body can be obtained by summing potential energies of all material points including strain energy and energy due to external loads as

$$U = \sum_n V_{FD}^{(n)} (\mathbf{u}_{(n)}, \mathbf{u}_{(1^n)}, \mathbf{u}_{(2^n)}, \mathbf{u}_{(3^n)}, \dots) V_{(n)} - \sum_n \mathbf{b}_{(n)} \mathbf{u}_{(n)} V_{(n)} \quad (5.74)$$

where the body force density vector, \mathbf{b} , can be expressed in this study as

$$\mathbf{b} = [b_1 \quad b_2 \quad \hat{b}_1 \quad \hat{b}_2 \quad b_z]^T \quad (5.75)$$

Here the entries of the body force density vector, b_L , \hat{b}_L and b_z correspond to in-plane forces, moments, and transverse force respectively. Utilizing the pre-obtained result, Eq. (3.8), the second term of the Lagrange's equation becomes

$$-\frac{\partial L}{\partial \mathbf{u}_{(k)}} = \begin{pmatrix} \frac{\partial W_{FD}^{(k)}}{\partial \bar{u}_1^{(k)}} V_{(k)} + \sum_j \frac{\partial W_{FD}^{(j)}}{\partial \bar{u}_1^{(k)}} V_{(j)} \\ \frac{\partial W_{FD}^{(k)}}{\partial \bar{u}_2^{(k)}} V_{(k)} + \sum_j \frac{\partial W_{FD}^{(j)}}{\partial \bar{u}_2^{(k)}} V_{(j)} \\ \frac{\partial W_{FD}^{(k)}}{\partial \theta_1^{(k)}} V_{(k)} + \sum_j \frac{\partial W_{FD}^{(j)}}{\partial \theta_1^{(k)}} V_{(j)} \\ \frac{\partial W_{FD}^{(k)}}{\partial \theta_2^{(k)}} V_{(k)} + \sum_j \frac{\partial W_{FD}^{(j)}}{\partial \theta_2^{(k)}} V_{(j)} \\ \frac{\partial W_{FD}^{(k)}}{\partial \bar{w}_{(k)}} V_{(k)} + \sum_j \frac{\partial W_{FD}^{(j)}}{\partial \bar{w}_{(k)}} V_{(j)} \end{pmatrix} - \begin{Bmatrix} b_1 \\ b_2 \\ \hat{b}_1 \\ \hat{b}_2 \\ b_z \end{Bmatrix} V_{(k)} \quad (5.76)$$

Inserting Eq. (5.73) and (5.76) into the Lagrange's equation gives

$$\rho_{(k)} \begin{Bmatrix} \ddot{u}_L \\ \frac{h^2}{12} \ddot{\theta}_L^{(k)} \\ \ddot{w} \end{Bmatrix} V_{(k)} - \begin{pmatrix} \frac{\partial W_{FD}^{(k)}}{\partial \bar{u}_L^{(k)}} V_{(k)} + \sum_j \frac{\partial W_{FD}^{(j)}}{\partial \bar{u}_L^{(k)}} V_{(j)} \\ \frac{\partial W_{FD}^{(k)}}{\partial \theta_L^{(k)}} V_{(k)} + \sum_j \frac{\partial W_{FD}^{(j)}}{\partial \theta_L^{(k)}} V_{(j)} \\ \frac{\partial W_{FD}^{(k)}}{\partial \bar{w}_{(k)}} V_{(k)} + \sum_j \frac{\partial W_{FD}^{(j)}}{\partial \bar{w}_{(k)}} V_{(j)} \end{pmatrix} + \begin{Bmatrix} b_L \\ \hat{b}_L \\ b_z \end{Bmatrix} V_{(k)} \quad (5.77)$$

where the subscript L takes up the value 1 and 2.

In order to write the non-local form of strain energy density function of the material point k , Eq. (5.68b), it is necessary to transform all the differential terms into an equivalent form of integration by considering PD strain energy density expression given in Eq. (5.74). As derived in Appendix A2.4, the strain energy density function of the material point k , and its family member j can be expressed as

$$W_{FD}^{(k)} = \frac{6}{\pi \delta^3 h^2} \left\{ \int_{-\frac{h}{2}}^{\frac{h}{2}} \mathbf{G} dz \sum_i \frac{\left[(\bar{u}_i^{(i^k)} - \bar{u}_i^{(k)}) n_i^{(i^k)(k)} \right]^2}{\xi_{(i^k)(k)}} V_{(i^k)} + \int_{-\frac{h}{2}}^{\frac{h}{2}} \mathbf{G}^2 dz \sum_i \frac{\left[(\theta_i^{(i^k)} - \theta_i^{(k)}) n_i^{(i^k)(k)} \right]^2}{\xi_{(i^k)(k)}} V_{(i^k)} \right. \\ \left. + \kappa_s^2 \int_{-\frac{h}{2}}^{\frac{h}{2}} \frac{\mathbf{G}}{4} dz \sum_i \frac{1}{\xi_{(i^k)(k)}} \left(\bar{w}_{(i^k)} - \bar{w}_{(k)} + \frac{\theta_i^{(i^k)} + \theta_i^{(k)}}{2} n_i^{(i^k)(k)} \xi_{(i^k)(k)} \right)^2 V_{(i^k)} \right. \\ \left. 2 \int_{-\frac{h}{2}}^{\frac{h}{2}} \mathbf{G} dz \sum_i \frac{(\bar{u}_i^{(i^k)} - \bar{u}_i^{(k)}) (\theta_j^{(i^k)} - \theta_j^{(k)})}{\xi_{(i^k)(k)}} n_i^{(i^k)(k)} n_j^{(i^k)(k)} V_{(i^k)} \right\} \quad (5.78a)$$

$$+ \frac{1}{h} \left(\frac{2}{\pi \delta^2 h} \right)^2 \left[\int_{-\frac{h}{2}}^{\frac{h}{2}} \frac{\mathbf{G}}{2} \frac{3\nu - 1}{1 - \nu} dz \left(\sum_i \frac{\bar{u}_i^{(i^k)} - \bar{u}_i^{(k)}}{\xi_{(i^k)(k)}} n_i^{(i^k)(k)} V_{(i^k)} \right)^2 \right. \\ \left. + \int_{-\frac{h}{2}}^{\frac{h}{2}} \frac{\mathbf{G}}{2} \frac{3\nu - 1}{1 - \nu} z^2 dz \left(\sum_i \frac{\theta_i^{(i^k)} - \theta_i^{(k)}}{\xi_{(i^k)(k)}} n_i^{(i^k)(k)} V_{(i^k)} \right)^2 \right. \\ \left. + \int_{-\frac{h}{2}}^{\frac{h}{2}} \frac{\mathbf{G}}{2} \frac{3\nu - 1}{1 - \nu} z dz \sum_i \frac{\theta_i^{(i^k)} - \theta_i^{(k)}}{\xi_{(i^k)(k)}} n_i^{(i^k)(k)} V_{(i^k)} \sum_i \frac{\bar{u}_j^{(i^k)} - \bar{u}_j^{(k)}}{\xi_{(i^k)(k)}} n_j^{(i^k)(k)} V_{(i^k)} \right]$$

and

$$\begin{aligned}
W_{FD}^{(j)} = & \frac{6}{\pi\delta^3 h^2} \left\{ \int_{-\frac{h}{2}}^{\frac{h}{2}} G dz \sum_i \frac{\left[(\bar{u}_i^{(j)} - \bar{u}_i^{(j)}) n_i^{(j)(j)} \right]^2}{\xi_{(i)(j)}} V_{(i)} + \int_{-\frac{h}{2}}^{\frac{h}{2}} G^2 dz \sum_i \frac{\left[(\theta_i^{(j)} - \theta_i^{(j)}) n_i^{(j)(j)} \right]^2}{\xi_{(i)(j)}} V_{(i)} \right\} \\
& + \kappa_s^2 \int_{-\frac{h}{2}}^{\frac{h}{2}} \frac{G}{4} dz \sum_i \frac{1}{\xi_{(i)(j)}} \left(\bar{w}_{(i)} - \bar{w}_{(j)} + \frac{\theta_i^{(j)} + \theta_i^{(j)}}{2} n_i^{(j)(j)} \xi_{(i)(j)} \right)^2 V_{(i)} \\
& \left. 2 \int_{-\frac{h}{2}}^{\frac{h}{2}} G dz \sum_i \frac{(\bar{u}_i^{(j)} - \bar{u}_i^{(j)}) (\theta_i^{(j)} - \theta_i^{(j)})}{\xi_{(i)(j)}} n_i^{(j)(j)} n_j^{(j)(j)} V_{(i)} \right\} \quad (5.78b) \\
& + \frac{1}{h} \left(\frac{2}{\pi\delta^2 h} \right)^2 \left[\int_{-\frac{h}{2}}^{\frac{h}{2}} \frac{G}{2} \frac{3\nu - 1}{1 - \nu} dz \left(\sum_i \frac{\bar{u}_i^{(j)} - \bar{u}_i^{(j)}}{\xi_{(i)(j)}} n_i^{(j)(j)} V_{(i)} \right)^2 \right. \\
& \left. + \int_{-\frac{h}{2}}^{\frac{h}{2}} \frac{G}{2} \frac{3\nu - 1}{1 - \nu} z^2 dz \left(\sum_i \frac{\theta_i^{(j)} - \theta_i^{(j)}}{\xi_{(i)(j)}} n_i^{(j)(j)} V_{(i)} \right)^2 \right. \\
& \left. + \int_{-\frac{h}{2}}^{\frac{h}{2}} G \frac{3\nu - 1}{1 - \nu} z dz \sum_i \frac{\theta_i^{(j)} - \theta_i^{(j)}}{\xi_{(i)(j)}} n_i^{(j)(j)} V_{(i)} \sum_i \frac{\bar{u}_i^{(j)} - \bar{u}_i^{(j)}}{\xi_{(i)(j)}} n_j^{(j)(j)} V_{(i)} \right]
\end{aligned}$$

Substituting Eqs. (5.78a) and (5.78b) into Eq. (5.77) and renaming the summation indices yield's the PD equations of motion for FGM Mindlin plate as:

$$\begin{aligned}
\rho_{(k)} \ddot{u}_L^{(k)} = & \frac{24}{\pi\delta^3 h^2} \left(\int_{-\frac{h}{2}}^{\frac{h}{2}} G dz \sum_j \frac{\bar{u}_j^{(j)} - \bar{u}_j^{(k)}}{\xi_{(j)(k)}} n_j^{(j)(k)} n_L^{(j)(k)} V_{(j)} \right) \\
& + \int_{-\frac{h}{2}}^{\frac{h}{2}} G dz \sum_j \frac{\theta_j^{(j)} - \theta_j^{(k)}}{\xi_{(j)(k)}} n_j^{(j)(k)} n_L^{(j)(k)} V_{(j)} \quad (5.79a) \\
& + \frac{2}{\pi\delta^2 h^2} \left(\int_{-\frac{h}{2}}^{\frac{h}{2}} G \frac{3\nu - 1}{1 - \nu} dz \sum_j \frac{\Theta_{(j)} + \Theta_{(k)}}{\xi_{(j)(k)}} n_L^{(j)(k)} V_{(j)} \right) + b_L^{(k)} \\
& + \int_{-\frac{h}{2}}^{\frac{h}{2}} G \frac{3\nu - 1}{1 - \nu} z dz \sum_j \frac{\Phi_{(j)} + \Phi_{(k)}}{\xi_{(j)(k)}} n_L^{(j)(k)} V_{(j)}
\end{aligned}$$

$$\begin{aligned}
\rho_{(k)} \frac{h^2}{12} \ddot{\theta}_L^{(k)} = & \frac{24}{\pi\delta^3 h^2} \left(\int_{-\frac{h}{2}}^{\frac{h}{2}} G^2 dz \sum_j \frac{\theta_j^{(j)} - \theta_j^{(k)}}{\xi_{(j)(k)}} n_j^{(j)(k)} n_L^{(j)(k)} V_{(j)} \right) \\
& + \int_{-\frac{h}{2}}^{\frac{h}{2}} G dz \sum_j \frac{\bar{u}_j^{(j)} - \bar{u}_j^{(k)}}{\xi_{(j)(k)}} n_j^{(j)(k)} n_L^{(j)(k)} V_{(j)} \quad (5.79b) \\
& - \frac{3\kappa_s^2}{\pi\delta^3 h^2} \int_{-\frac{h}{2}}^{\frac{h}{2}} G dz \sum_j \left(\bar{w}_{(j)} - \bar{w}_{(k)} + \frac{\theta_j^{(j)} + \theta_j^{(k)}}{2} \xi_{(j)(k)} n_j^{(j)(k)} \right) n_L^{(j)(k)} V_{(j)} \\
& + \frac{2}{\pi\delta^2 h^2} \left(\int_{-\frac{h}{2}}^{\frac{h}{2}} G \frac{3\nu - 1}{1 - \nu} z^2 dz \sum_j \frac{\Phi_{(j)} + \Phi_{(k)}}{\xi_{(j)(k)}} n_L^{(j)(k)} V_{(j)} \right) + \hat{b}_L
\end{aligned}$$

and

$$\rho_{(k)} \ddot{w}_{(k)} = \frac{6}{\pi\delta^3 h^2} \kappa_s^2 \int_{-\frac{h}{2}}^{\frac{h}{2}} G dz \sum_j \left(\frac{\bar{w}_{(j)} - \bar{w}_{(k)}}{\xi_{(j)(k)}} + \frac{\theta_j^{(k)} + \theta_j^{(j)}}{2} n_j^{(j)(k)} \right) V_{(j)} + b_z^{(k)} \quad (5.79c)$$

where Φ and Θ can be expressed as

$$\Phi_{(k)} = \frac{2}{\pi\delta^2 h} \sum_i \frac{\theta_i^{(i^k)} + \theta_i^{(k)}}{\xi_{(i^k)(k)}} n_i^{(i^k)(k)} V_{(i^k)} \quad (5.80a)$$

$$\Phi_{(j)} = \frac{2}{\pi\delta^2 h} \sum_i \frac{\theta_i^{(i^j)} + \theta_i^{(j)}}{\xi_{(i^j)(j)}} n_i^{(i^j)(j)} V_{(i^j)} \quad (5.80b)$$

and

$$\Theta_{(k)} = \frac{2}{\pi\delta^2 h} \sum_i \frac{\bar{u}_i^{(i^k)} + \bar{u}_i^{(k)}}{\xi_{(i^k)(k)}} n_i^{(i^k)(k)} V_{(i^k)} \quad (5.81a)$$

$$\Theta_{(j)} = \frac{2}{\pi\delta^2 h} \sum_i \frac{\bar{u}_i^{(i^j)} + \bar{u}_i^{(j)}}{\xi_{(i^j)(j)}} n_i^{(i^j)(j)} V_{(i^j)} \quad (5.81b)$$

In particular case, Eqs. (5.79) can be simplified for the Poisson's ratio, $\nu = 1/3$ as:

where c_b and c_s are the PD material parameters associated with bending and transverse shear deformation, respectively, which are defined as

$$\rho_{(k)} \ddot{u}_L^{(k)} = \frac{9}{\pi\delta^3 h^2} \left(\int_{-\frac{h}{2}}^{\frac{h}{2}} E dz \sum_j \frac{\bar{u}_i^{(j)} - \bar{u}_i^{(k)}}{\xi_{(j)(k)}} n_i^{(j)(k)} n_L^{(j)(k)} V_{(j)} \right) + \mathbf{b}_L^{(k)} \quad (5.82a)$$

$$\rho_{(k)} \frac{h^2}{12} \ddot{\theta}_L^{(k)} = \frac{9}{\pi\delta^3 h^2} \left(\int_{-\frac{h}{2}}^{\frac{h}{2}} E z^2 dz \sum_j \frac{\theta_i^{(j)} - \theta_i^{(k)}}{\xi_{(j)(k)}} n_i^{(j)(k)} n_L^{(j)(k)} V_{(j)} \right) + \frac{9\kappa_s^2}{8\pi\delta^3 h^2} \int_{-\frac{h}{2}}^{\frac{h}{2}} E dz \sum_j \left(\bar{w}_{(j)} - \bar{w}_{(k)} + \frac{\theta_i^{(k)} + \theta_i^{(j)}}{2} \xi_{(j)(k)} n_i^{(j)(k)} \right) n_L^{(j)(k)} V_{(j)} + \hat{\mathbf{b}}_L \quad (5.82b)$$

$$\rho_{(k)} \ddot{\bar{w}}_{(k)} = \frac{9}{4\pi\delta^3 h^2} \kappa_s^2 \int_{-\frac{h}{2}}^{\frac{h}{2}} E dz \sum_j \left(\frac{\bar{w}_{(j)} - \bar{w}_{(k)}}{\xi_{(j)(k)}} + \frac{\theta_i^{(k)} + \theta_i^{(j)}}{2} n_i^{(j)(k)} \right) V_{(j)} + \mathbf{b}_z^{(k)} \quad (5.82c)$$

5.4.3 Numerical Results

To verify the validity of the PD formulation for functionally graded Mindlin plates, the PD solutions are compared with the corresponding finite element (FE) analysis results. In this study, the functionally graded material properties are chosen as Young's Modulus, $E(z)$, and shear modulus, $G(z)$, and they are assumed to vary linearly through the thickness as

$$E(z) = (E_t - E_b) \frac{z}{h} + \frac{1}{2} (E_t + E_b) \quad (5.83a)$$

$$G(z) = \frac{E(z)}{2(1 + 0.3)} \quad (5.83b)$$

$$\nu(z) = 0.3 \quad (5.83c)$$

where E_t and E_b denote the Young's modulus of the top and bottom surfaces of the plate, and h denotes the total thickness of the plate. The shear correction coefficient is chosen as $\kappa_s = \frac{\pi^2}{12}$.

In the following three numerical cases, a square plate with length and width of $L = W = 1m$ and thickness of $h = 0.15m$ is considered. The plate is subjected to different boundary conditions. The Young's modulus of the top and bottom surface are chosen as $E_t = 200 \text{ GPa}$ and $E_b = 100 \text{ GPa}$.

The PD models are discretized into one single row of material points through the thickness and 65×65 material points throughout the xy plane. Thus, the distance between two adjacent material points is $\Delta x = \frac{1}{65}m$ and the area attached on each material points is $\Delta A = \Delta x^2$. A fictitious region is introduced outside the edges as the external boundaries with a width of $6\Delta x$ to apply boundary conditions as explained in Appendix B2.4. The horizon size can be approximately chosen as $\delta = 3\Delta x$.

The corresponding FE models are created in ANSYS by using SHELL181 elements with 50×50 elements throughout the plate. In order to obtain the functionally graded character, the model is divided into 50 layers with varying homogeneous material properties throughout the thickness. The Young's modulus varies gradually over the thickness from the first layer $E_1 = 101 \text{ GPa}$ to the last layer $E_{50} = 199 \text{ GPa}$, as shown in Figure 5.31. The Poisson's ratio, $\nu = 0.3$, is applied in ANSYS.

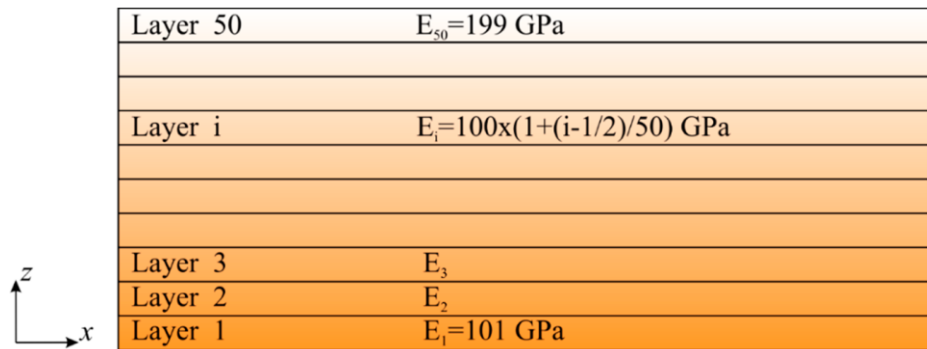


Figure 5.31 Variation of material properties through the thickness direction for the

5.4.3.1 Simply Supported Functionally Graded Mindlin Plate

In the first example case, a simply supported functionally graded Mindlin plate subjected to a distributed load of $p = 100,000 \text{ N/m}$ through the central line is taken into consideration (see Figure 5.32). For the PD model, the load is transformed into a body load of $b_z = \frac{pW}{65\Delta V} = 4.33 \times 10^7 \text{ N/m}^3$ and it is imposed on a row of material points through the central line of the plate as shown in Figure 5.32.

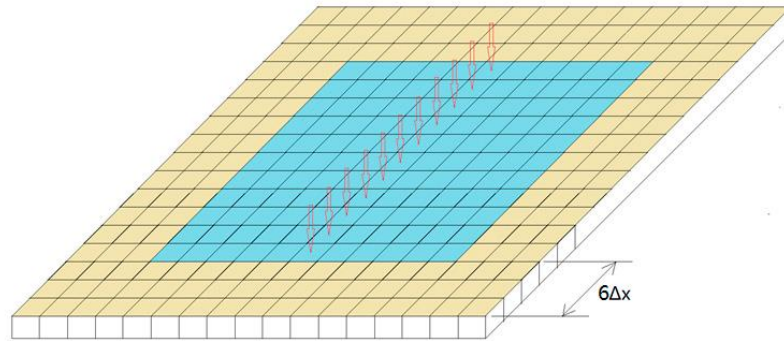
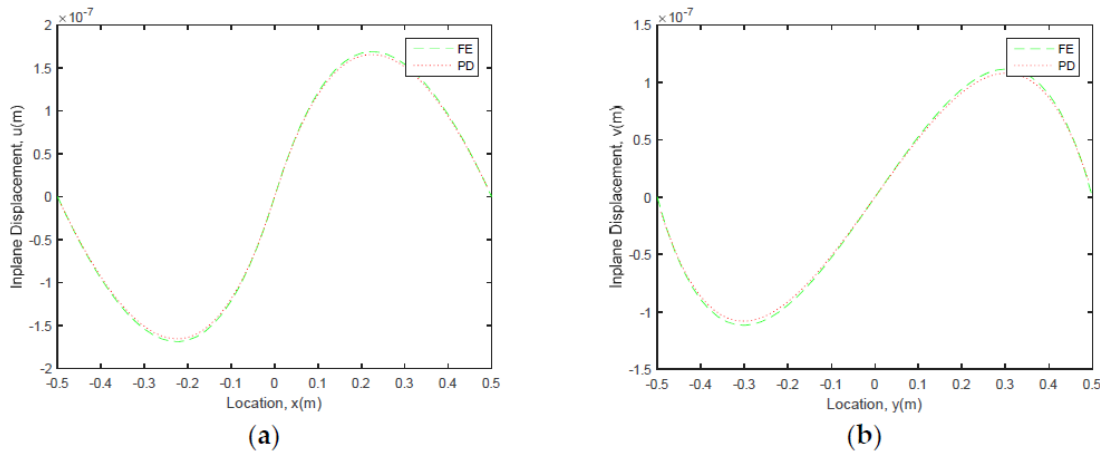


Figure 5.32 Numerical discretization, loading and fictitious region

The PD results for in - plane and transverse displacements, and rotations are obtained and compared with FEA results for the material points located along central x - and y - axes. As depicted in Figure 5.33, PD and FEA results agree very well with each other.



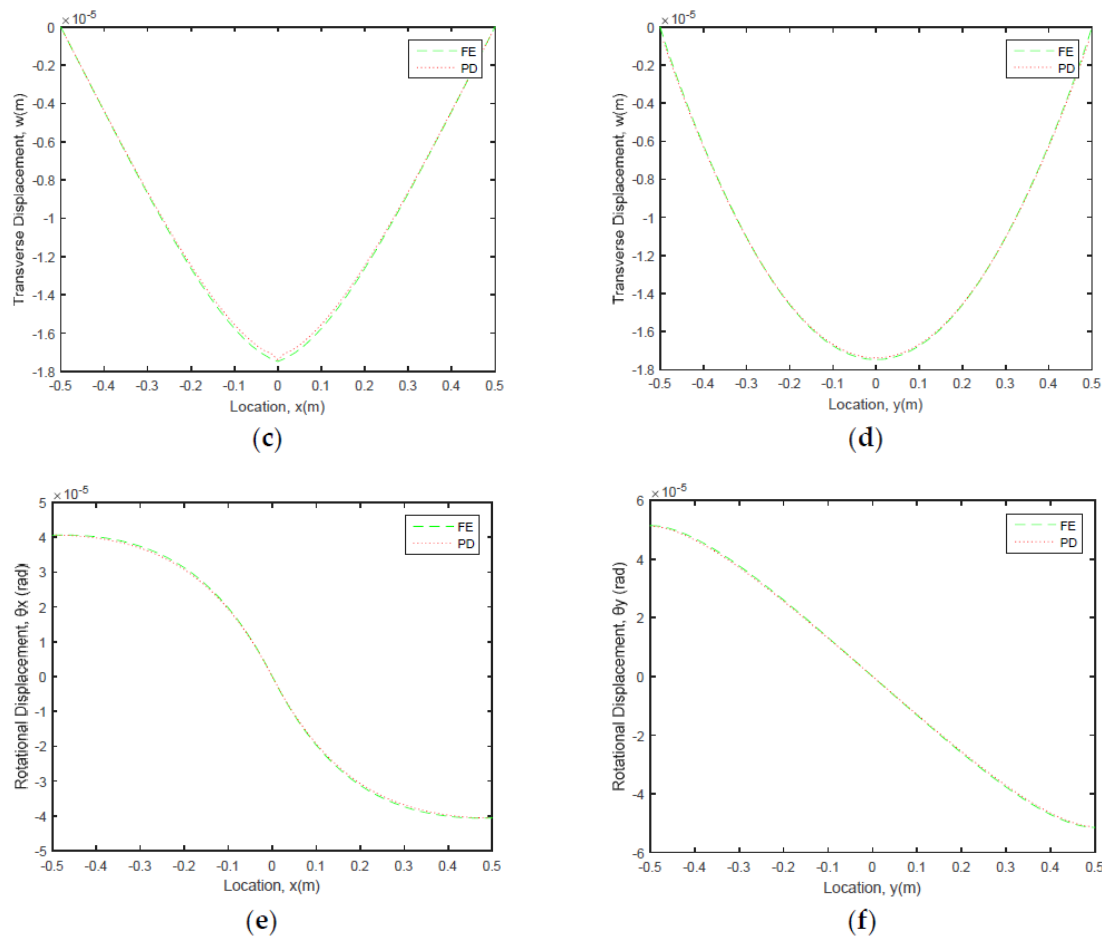


Figure 5.33 Comparison of PD and FEA results along the central x - and y - axes.

5.4.3.2 Fully Clamped Functionally Graded Mindlin Plate

In the second example case, the functionally graded Mindlin plate considered in the previous example is subjected to fully clamped boundary condition (see Figure 5.34). In ANSYS, the clamped boundary condition is achieved by constraining all degrees of freedom along the external boundaries.

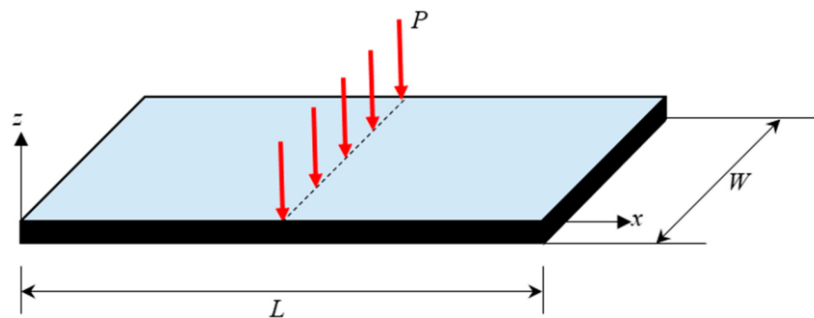


Figure 5.34 Fully clamped functionally graded Mindlin plate

Based on the comparison between the PD and FEA results as shown in Figure 5.35, it can be concluded that current PD formulation can also provide accurate results for fully clamped boundary condition.

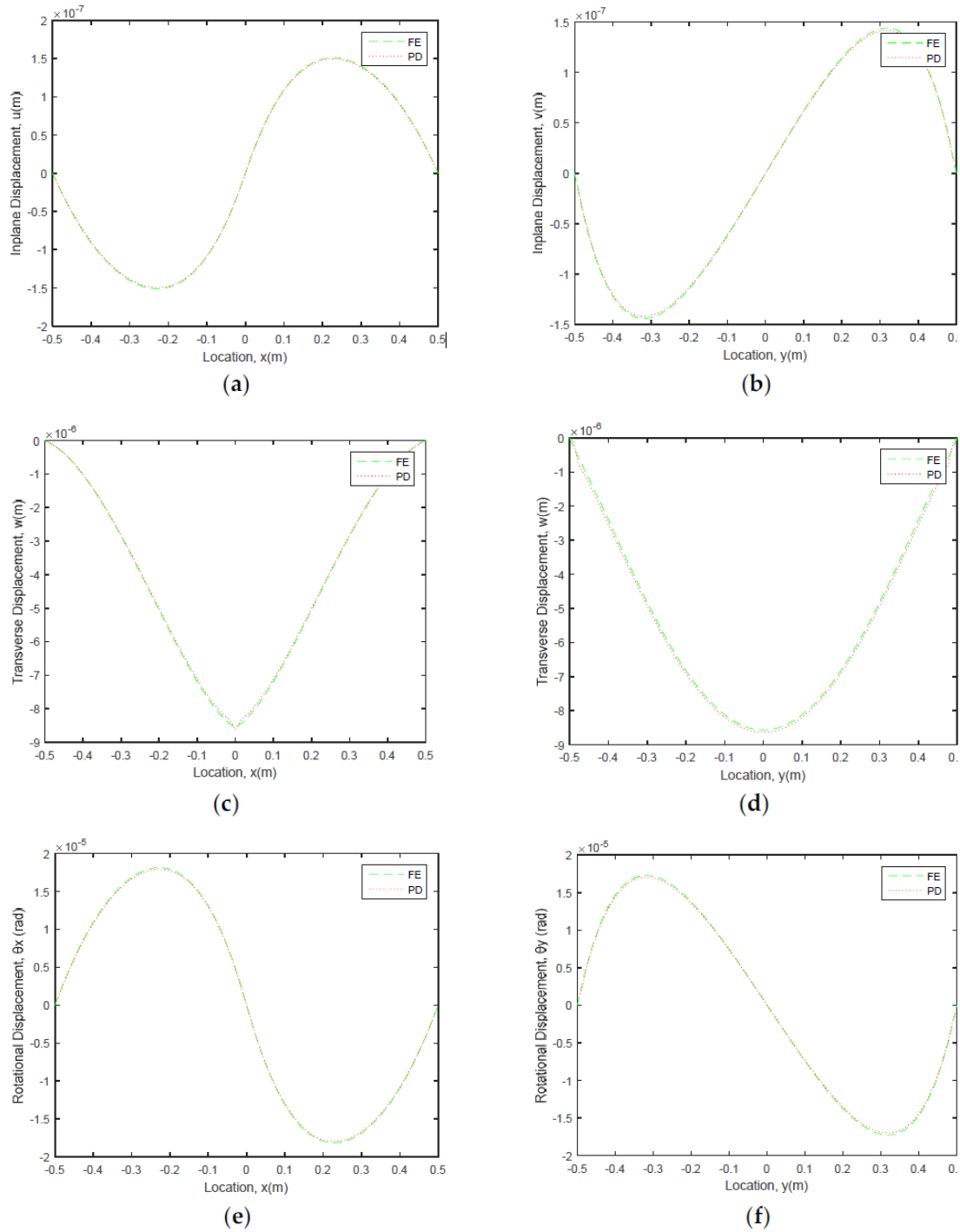


Figure 5.35 Comparison of PD and FEA results along the central x - and y - axes

5.4.3.3 Functionally Graded Mindlin Plate Subjected to Mixed Boundary Conditions

The last numerical case aims to verify the current PD formulation for mixed boundary conditions, i.e., clamped-simply supported. As shown in Figure 5.36, edges along the horizontal direction are subjected to clamped boundary conditions whereas the remaining two edges are subjected to simply supported boundary conditions.

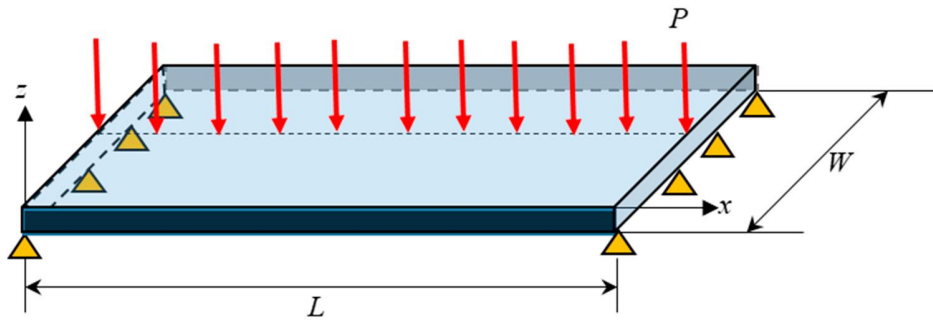
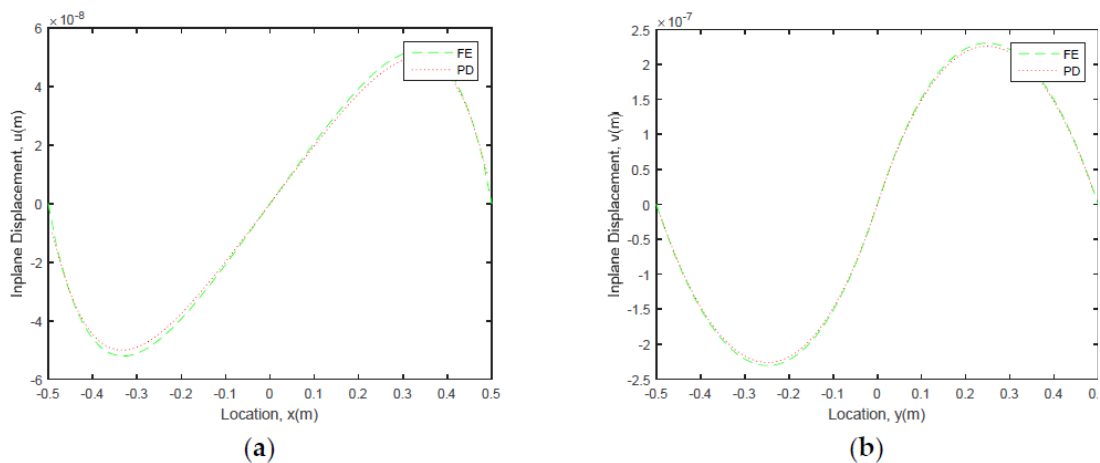


Figure 5.36 Functionally graded Mindlin plate subjected to mixed boundary conditions

As depicted in Figure 5.37, also for this mixed - boundary conditions case, PD and FEM results agree well with each other.



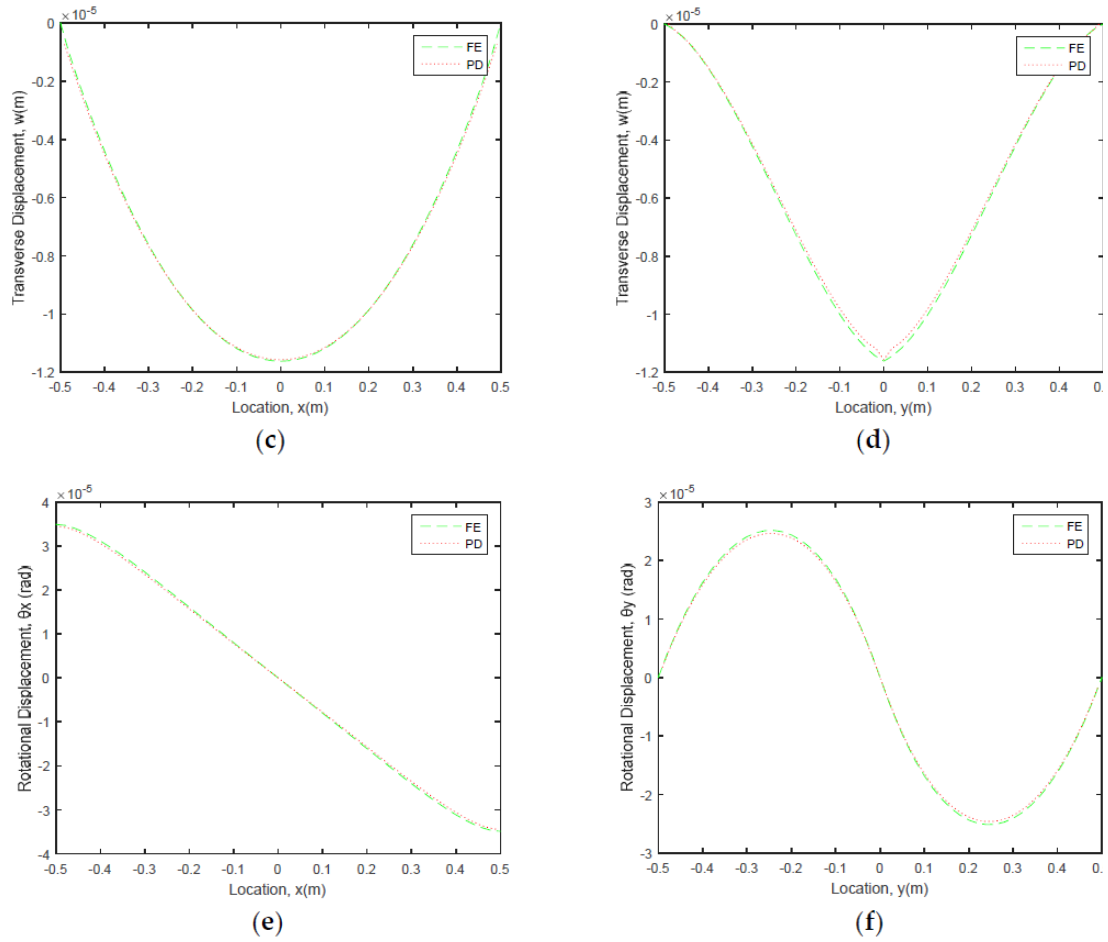


Figure 5.37 Comparison of PD and FEA results along the central x - and y - axes.

5.5 PD Formulations for Higher Order Deformable Plate

5.5.1 Higher Order Deformable Plate Theory

The displacement field of any material point, $u(x, y, z, t), v(x, y, z, t)$ and $w(x, y, z, t)$, can be represented in terms of the displacement field of a material point on the mid-plane, $u(x, y, 0, t), v(x, y, 0, t)$ and $w(x, y, 0, t)$, by using Taylor's expansion as

$$u(x, y, z, t) = u|_{z=0} + z \frac{\partial u}{\partial z} \Big|_{z=0} + \frac{1}{2} z^2 \frac{\partial^2 u}{\partial z^2} \Big|_{z=0} + \frac{1}{3!} z^3 \frac{\partial^3 u}{\partial z^3} \Big|_{z=0} + \dots \quad (5.84a)$$

$$v(x, y, z, t) = v|_{z=0} + z \frac{\partial v}{\partial z} \Big|_{z=0} + \frac{1}{2} z^2 \frac{\partial^2 v}{\partial z^2} \Big|_{z=0} + \frac{1}{3!} z^3 \frac{\partial^3 v}{\partial z^3} \Big|_{z=0} + \dots \quad (5.84b)$$

$$w(x, y, z, t) = w|_{z=0} + z \frac{\partial w}{\partial z} \Big|_{z=0} + \frac{1}{2} z^2 \frac{\partial^2 w}{\partial z^2} \Big|_{z=0} + \frac{1}{3!} z^3 \frac{\partial^3 w}{\partial z^3} \Big|_{z=0} + \dots \quad (5.84c)$$

In this study, only flexural deformations are taken into consideration. Thus, eliminating

in-plane deformation effects and higher order terms in Eqs. (5.84), the components of the displacement field can be expressed as

$$u(x, y, z, t) = z\theta_x(x, y, t) + z^3\theta_x^*(x, y, t) \quad (5.85a)$$

$$v(x, y, z, t) = z\theta_y(x, y, t) + z^3\theta_y^*(x, y, t) \quad (5.85b)$$

$$w(x, y, z, t) = \bar{w}(x, y, t) + z^2\dot{w}(x, y, t) \quad (5.85c)$$

where \bar{w} , θ_x and θ_y represent the mid-plane behaviors of transverse displacement, rotation about x -axis, rotation about negative y -axis, respectively, and θ_x^* , θ_x^* , θ_y and θ_y^* are higher order terms arose out of the Taylor expansion.

After utilising the displacement relationships given in Eqs. (5.85), strain-displacement relationships of 3-Dimensional elasticity can be expressed as

$$\varepsilon_{11} = z \frac{\partial \theta_1}{\partial x_1} + z^3 \frac{\partial \theta_1^*}{\partial x_1} \quad (5.86a)$$

$$\varepsilon_{22} = z \frac{\partial \theta_2}{\partial x_2} + z^3 \frac{\partial \theta_2^*}{\partial x_2} \quad (5.86b)$$

$$\varepsilon_{12} = \varepsilon_{21} = \frac{1}{2} \left[z \left(\frac{\partial \theta_1}{\partial x_2} + \frac{\partial \theta_2}{\partial x_1} \right) + z^3 \left(\frac{\partial \theta_1^*}{\partial x_2} + \frac{\partial \theta_2^*}{\partial x_1} \right) \right] \quad (5.86c)$$

$$\varepsilon_{13} = \varepsilon_{31} = \frac{1}{2} \left[\left(\theta_1 + \frac{\partial \bar{w}}{\partial x_1} \right) + z^2 \left(3\theta_x + \frac{\partial \dot{w}}{\partial x_1} \right) \right] \quad (5.86d)$$

$$\varepsilon_{23} = \varepsilon_{32} = \frac{1}{2} \left[\left(\theta_2 + \frac{\partial \bar{w}}{\partial x_2} \right) + z^2 \left(3\theta_y + \frac{\partial \dot{w}}{\partial x_2} \right) \right] \quad (5.86e)$$

$$\varepsilon_{33} = 2z\dot{w} \quad (5.86f)$$

with $x_1 = x$ and $x_2 = y$.

These strain-displacement relationships can be also expressed in following form by using indicial notation:

$$\begin{aligned} \varepsilon_{ij} = & \frac{1}{2} \left[z \left(\frac{\partial \theta_I}{\partial x_J} + \frac{\partial \theta_J}{\partial x_I} \right) + z^3 \left(\frac{\partial \theta_I^*}{\partial x_J} + \frac{\partial \theta_J^*}{\partial x_I} \right) \right] \delta_{Ii} \delta_{Jj} \\ & + \frac{1}{2} \left[\left(\theta_I + \frac{\partial \bar{w}}{\partial x_I} \right) + z^2 \left(3\theta_I^* + \frac{\partial \dot{w}}{\partial x_I} \right) \right] (\delta_{Ii} \delta_{3j} + \delta_{3i} \delta_{Ij}) + 2z\dot{w} \delta_{3i} \delta_{3j} \end{aligned} \quad (5.87)$$

where $i, j = 1, 2, 3$ and $I, J = 1, 2$. Note that this convention where capital letter

indices, e.g., I, J, K, \dots vary from 1 and 2, and lowercase letter indices, e.g., i, j, k, \dots vary from 1, 2 and 3, will be applied throughout this study.

Assuming the material is isotropic and obeys 3-Dimensional constitutive relationship, the stress components can be expressed as

$$\sigma_{ij} = C_{ijkl} \varepsilon_{kl} \quad (5.88)$$

where C_{ijkl} is the elastic modulus tensor which is defined for isotropic material as

$$C_{ijkl} = G(\delta_{il}\delta_{jk} + \delta_{ik}\delta_{jl}) + \frac{2G\nu}{1-2\nu} \delta_{ij} \delta_{kl} \quad (5.89)$$

with E and ν being the Young's modulus and Poisson's ratio, respectively.

Substituting Eq. (5.89) into (5.88) yields:

$$\sigma_{ij} = 2G\varepsilon_{ij} + \frac{2G\nu}{1-2\nu} \varepsilon_{ll} \delta_{ij} \quad (5.90)$$

The transverse average strain energy density can be reasonably calculated by integrating the strain energy density over the thickness and dividing by the thickness as

$$W_{\text{com}} = \frac{1}{2h} \int_{-\frac{h}{2}}^{\frac{h}{2}} \sigma_{ij} \varepsilon_{ij} dz \quad (5.91a)$$

Inserting Eqs. (5.87) and (5.90) into Eq. (5.91a) and rearranging the indices gives the expression of strain energy density as

$$W_{\text{com}} = \frac{G}{2} \left\{ \begin{aligned} & \left(\theta_l + \frac{\partial \bar{w}}{\partial x_l} \right) \left(\theta_l + \frac{\partial \bar{w}}{\partial x_l} \right) \\ & + \frac{h^2}{12} \left[\frac{\partial \theta_l}{\partial x_j} \frac{\partial \theta_l}{\partial x_j} + \frac{\partial \theta_l}{\partial x_j} \frac{\partial \theta_j}{\partial x_l} + \frac{\partial \theta_l}{\partial x_l} \frac{\partial \theta_j}{\partial x_j} \right. \\ & \left. + 2 \left(\theta_l + \frac{\partial \bar{w}}{\partial x_l} \right) \left(3\theta_l' + \frac{\partial \bar{w}'}{\partial x_l} \right) + \frac{8}{1-2\nu} \bar{w}' \left[(1-\nu) \bar{w}' + \nu \frac{\partial \theta_l}{\partial x_l} \right] \right] \\ & + 2 \frac{h^4}{80} \left[\frac{\partial \theta_l}{\partial x_j} \frac{\partial \theta_l'}{\partial x_j} + \frac{\partial \theta_l}{\partial x_j} \frac{\partial \theta_j'}{\partial x_l} + \frac{\partial \theta_l}{\partial x_l} \frac{\partial \theta_j'}{\partial x_j} \right. \\ & \left. + \frac{1}{2} \left(3\theta_l' + \frac{\partial \bar{w}'}{\partial x_l} \right) \left(3\theta_l' + \frac{\partial \bar{w}'}{\partial x_l} \right) + \frac{4\nu}{1-2\nu} \frac{\partial \theta_l'}{\partial x_l} \bar{w}' \right] \\ & + \frac{h^6}{448} \left(\frac{\partial \theta_l'}{\partial x_j} \frac{\partial \theta_l'}{\partial x_j} + \frac{\partial \theta_l'}{\partial x_j} \frac{\partial \theta_j'}{\partial x_l} + \frac{\partial \theta_l'}{\partial x_l} \frac{\partial \theta_j'}{\partial x_j} \right) \\ & + \frac{4\nu-1}{1-2\nu} \left[\frac{h^2}{12} \left(\frac{\partial \theta_l}{\partial x_l} \right)^2 + \frac{h^6}{448} \left(\frac{\partial \theta_l'}{\partial x_l} \right)^2 + 2 \frac{h^4}{80} \frac{\partial \theta_l}{\partial x_l} \frac{\partial \theta_j'}{\partial x_j} \right] \end{aligned} \right\} \quad (5.91b)$$

5.5.2 PD Formulations for Higher Order Deformable Plate

The PD equations of motion can be derived by utilizing Euler-Lagrange equation as

$$\frac{d}{dt} \frac{\partial L}{\partial \dot{\mathbf{u}}_{(k)}} - \frac{\partial L}{\partial \mathbf{u}_{(k)}} = 0 \quad (5.92)$$

where $L = T - U$ is the Lagrangian and \mathbf{u} represents the displacement vector, which can be defined in this study as

$$\mathbf{u} = [\theta_1 \ \theta_2 \ \dot{\theta}_1 \ \dot{\theta}_2 \ \bar{w} \ \dot{w}]^T \quad (5.93)$$

The kinetic energy per unit area, \bar{T} , can be expressed as

$$\bar{T} = \frac{1}{2} \int_{-\frac{h}{2}}^{\frac{h}{2}} \rho (\dot{u}^2 + \dot{v}^2 + \dot{w}^2) dz \quad (5.94a)$$

Plugging Eqs. (5.85) into (5.94a) yields

$$\bar{T} = \frac{1}{2} \rho \left[\frac{h^3}{12} \dot{\theta}_1 \dot{\theta}_1 + \frac{h^7}{447} \dot{\theta}_1^* \dot{\theta}_1^* + \frac{h^5}{40} \dot{\theta}_1 \dot{\theta}_1^* + h \dot{w}^2 + \frac{h^5}{80} (\dot{w}^*)^2 + \frac{h^3}{6} \dot{w} \dot{w}^* \right] \quad (5.94b)$$

The total kinetic energy of the system, T , can be casted by integrating the areal kinetic energy density, Eq.(5.94b) over the mid-plane as

$$T = \frac{1}{2} \int_A \rho \left[\frac{h^3}{12} \dot{\theta}_1 \dot{\theta}_1 + \frac{h^7}{447} \dot{\theta}_1^* \dot{\theta}_1^* + \frac{h^5}{40} \dot{\theta}_1 \dot{\theta}_1^* + h \dot{w}^2 + \frac{h^5}{80} (\dot{w}^*)^2 + \frac{h^3}{6} \dot{w} \dot{w}^* \right] dA \quad (5.95a)$$

which can be written in a discretized form as

$$T = \frac{1}{2} \sum_j \rho_{(j)} \left[\frac{h^2}{12} (\dot{\theta}_1^{(j)} \dot{\theta}_1^{(j)} + 2\dot{w}_{(j)}^* \dot{w}_{(j)}^*) + \frac{h^4}{80} (2\dot{\theta}_1^{(j)} \dot{\theta}_1^{*(j)} + (\dot{w}_{(j)}^*)^2) + \frac{h^6}{447} \dot{\theta}_1^{*(j)} \dot{\theta}_1^{*(j)} + \dot{w}_{(j)}^2 \right] V_{(j)} \quad (5.95b)$$

Therefore, the first term of the Lagrange's equation becomes

$$\frac{d}{dt} \frac{\partial L}{\partial \dot{\mathbf{u}}_{(k)}} = \frac{d}{dt} \frac{\partial T}{\partial \dot{\mathbf{u}}_{(k)}} = \rho_{(k)} \left\{ \begin{array}{l} \frac{h^2}{12} \ddot{\theta}_L^{(k)} + \frac{h^4}{80} \ddot{\theta}_L^{*(k)} \\ \frac{h^6}{448} \ddot{\theta}_L^{*(k)} + \frac{h^4}{80} \ddot{\theta}_L^{(k)} \\ \ddot{w}_{(k)} + \frac{h^2}{12} \ddot{w}_{(k)}^* \\ \frac{h^4}{80} \ddot{w}_{(k)}^* + \frac{h^2}{12} \ddot{w}_{(k)} \end{array} \right\} V_{(k)} \quad (5.96)$$

where the subscript L takes up the value 1 and 2.

The total potential energy stored in the body can be obtained by summing potential energies of all material points including strain energy and energy due to external loads as

$$U = \sum_n W_{PD}^{(n)} (\mathbf{u}_{(n)}, \mathbf{u}_{(1^n)}, \mathbf{u}_{(2^n)}, \mathbf{u}_{(3^n)}, \dots) V_{(n)} - \sum_n \mathbf{b}_{(n)} \cdot \mathbf{u}_{(n)} V_{(n)} \quad (5.97)$$

where the body force density vector, \mathbf{b} , can be expressed in this study as

$$\mathbf{b} = [\hat{b}_1 \quad \hat{b}_2 \quad 0 \quad 0 \quad b_z \quad 0]^T \quad (5.98)$$

Here the entries of the body force density vector, \hat{b}_L and b_z correspond to moments, and transverse force respectively. Utilizing the pre-obtained result, Eq. (3.8), the second term of the Lagrange's equation becomes

$$-\frac{\partial L}{\partial \mathbf{u}_{(k)}} = \begin{pmatrix} \frac{\partial W_{PD}^{(k)}}{\partial \theta_L^{(k)}} V_{(k)} + \sum_j \frac{\partial W_{PD}^{(j)}}{\partial \theta_L^{(k)}} V_{(j)} \\ \frac{\partial W_{PD}^{(k)}}{\partial \theta_L^{(k)}} V_{(k)} + \sum_j \frac{\partial W_{PD}^{(j)}}{\partial \theta_L^{(k)}} V_{(j)} \\ \frac{\partial W_{PD}^{(k)}}{\partial \bar{w}_{(k)}} V_{(k)} + \sum_j \frac{\partial W_{PD}^{(j)}}{\partial \bar{w}_{(k)}} V_{(j)} \\ \frac{\partial W_{PD}^{(k)}}{\partial \dot{w}_{(k)}} V_{(k)} + \sum_j \frac{\partial W_{PD}^{(j)}}{\partial \dot{w}_{(k)}} V_{(j)} \end{pmatrix} - \begin{Bmatrix} \hat{b}_L \\ 0 \\ b_z \\ 0 \end{Bmatrix} V_{(k)} \quad (5.99)$$

Inserting Eq. (5.96) and (5.99) into the Lagrange's equation gives

$$\rho_{(k)} \begin{Bmatrix} \frac{h^2}{12} \ddot{\theta}_L^{(k)} + \frac{h^4}{80} \ddot{\theta}_L^{(k)} \\ \frac{h^6}{448} \ddot{\theta}_L^{(k)} + \frac{h^4}{80} \ddot{\theta}_L^{(k)} \\ \ddot{w}_{(k)} + \frac{h^2}{12} \ddot{w}_{(k)} \\ \frac{h^4}{80} \ddot{w}_{(k)} + \frac{h^2}{12} \ddot{w}_{(k)} \end{Bmatrix} V_{(k)} - \begin{pmatrix} \frac{\partial W_{PD}^{(k)}}{\partial \theta_L^{(k)}} V_{(k)} + \sum_j \frac{\partial W_{PD}^{(j)}}{\partial \theta_L^{(k)}} V_{(j)} \\ \frac{\partial W_{PD}^{(k)}}{\partial \theta_L^{(k)}} V_{(k)} + \sum_j \frac{\partial W_{PD}^{(j)}}{\partial \theta_L^{(k)}} V_{(j)} \\ \frac{\partial W_{PD}^{(k)}}{\partial \bar{w}_{(k)}} V_{(k)} + \sum_j \frac{\partial W_{PD}^{(j)}}{\partial \bar{w}_{(k)}} V_{(j)} \\ \frac{\partial W_{PD}^{(k)}}{\partial \dot{w}_{(k)}} V_{(k)} + \sum_j \frac{\partial W_{PD}^{(j)}}{\partial \dot{w}_{(k)}} V_{(j)} \end{pmatrix} + \begin{Bmatrix} \hat{b}_L \\ 0 \\ b_z \\ 0 \end{Bmatrix} V_{(k)} \quad (5.100)$$

In order to express the strain energy density function given in Eq. (5.91b) in PD form for a particular material point k , it is necessary to transform all the differential terms into an equivalent form of integration and the nonlocalized strain energy density function should be in accordance with the form given in Eq.(5.97). As derived in Appendix A2.5, the strain energy density function for the material point k and its family member j can be expressed as

$$\begin{aligned}
W_D^{(k)} = & \frac{6G}{\pi\delta^3 h^2} \left\{ \frac{h^3}{12} \sum_i \frac{[(\theta_i^{(k)} - \theta_i^{(k)}) n_i^{(k)}]^2}{\xi_{(i^k)(k)}} V_{(i^k)} + \frac{h^7}{448} \sum_i \frac{[(\theta_i^{(i^k)} - \theta_i^{(k)}) n_i^{(k)}]^2}{\xi_{(i^k)(k)}} V_{(i^k)} \right\} \\
& + 2 \frac{h^5}{80} \sum_i \frac{(\theta_i^{(k)} - \theta_i^{(k)}) (\theta_j^{(i^k)} - \theta_j^{(k)})}{\xi_{(i^k)(k)}} n_i^{(k)} n_j^{(k)} V_{(i^k)} \\
& + \frac{G}{2} \frac{3}{\pi\delta^3 h^2} \left[h \sum_i \frac{\left(\bar{w}_{(i^k)} - \bar{w}_{(k)} + \frac{\theta_i^{(i^k)} + \theta_i^{(k)}}{2} \xi_{(i^k)(k)} n_i^{(k)} \right)^2}{\xi_{(i^k)(k)}} V_{(i^k)} \right. \\
& + \frac{h^5}{80} \sum_i \frac{\left(\dot{w}_{(i^k)} - \dot{w}_{(k)} + 3 \frac{\theta_i^{(i^k)} + \theta_i^{(k)}}{2} \xi_{(i^k)(k)} n_i^{(k)} \right)^2}{\xi_{(i^k)(k)}} V_{(i^k)} \\
& \left. + 2 \frac{h^3}{12} \sum_i \frac{\left(\bar{w}_{(i^k)} - \bar{w}_{(k)} + \frac{\theta_i^{(i^k)} + \theta_i^{(k)}}{2} \xi_{(i^k)(k)} n_i^{(k)} \right) \left(\dot{w}_{(i^k)} - \dot{w}_{(k)} + 3 \frac{\theta_j^{(i^k)} + \theta_j^{(k)}}{2} \xi_{(i^k)(k)} n_j^{(k)} \right)}{\xi_{(i^k)(k)}} V_{(i^k)} \right] \\
& + \frac{G}{1-2\nu} \frac{6}{\pi\delta^3 h^2} \left\{ \frac{h^3}{12} \sum_i (\dot{w}_{(i^k)} + \dot{w}_{(k)}) \left[\nu (\theta_i^{(i^k)} - \theta_i^{(k)}) n_i^{(k)} + \frac{1-\nu}{2} \frac{\dot{w}_{(i^k)} + \dot{w}_{(k)}}{2} \xi_{(i^k)(k)} \right] V_{(i^k)} \right\} \\
& + \frac{h^5}{80} \nu \sum_i (\dot{w}_{(i^k)} + \dot{w}_{(k)}) (\theta_i^{(i^k)} - \theta_i^{(k)}) n_i^{(k)} V_{(i^k)} \\
& + \frac{G}{2} \frac{4\nu - 1}{1-2\nu} \frac{1}{h} \left(\frac{2}{\pi\delta^2 h} \right)^2 \left[\frac{h^3}{12} \left(\sum_i \frac{\theta_i^{(i^k)} - \theta_i^{(k)}}{\xi_{(i^k)(k)}} n_i^{(k)} V_{(i^k)} \right)^2 + \frac{h^7}{448} \left(\sum_i \frac{\theta_i^{(i^k)} - \theta_i^{(k)}}{\xi_{(i^k)(k)}} n_i^{(k)} V_{(i^k)} \right)^2 \right] \\
& + 2 \frac{h^5}{80} \sum_i \frac{\theta_i^{(i^k)} - \theta_i^{(k)}}{\xi_{(i^k)(k)}} n_i^{(k)} V_{(i^k)} \sum_i \frac{\theta_j^{(i^k)} - \theta_j^{(k)}}{\xi_{(i^k)(k)}} n_j^{(k)} V_{(i^k)}
\end{aligned} \tag{5.101a}$$

and

$$\begin{aligned}
W_D^{(j)} = & \frac{6G}{\pi\delta^3 h^2} \left\{ \frac{h^3}{12} \sum_i \frac{[(\theta_i^{(j)} - \theta_i^{(j)}) n_i^{(j)}]^2}{\xi_{(i^j)(j)}} V_{(i^j)} + \frac{h^7}{448} \sum_i \frac{[(\theta_i^{(i^j)} - \theta_i^{(j)}) n_i^{(j)}]^2}{\xi_{(i^j)(j)}} V_{(i^j)} \right\} \\
& + 2 \frac{h^5}{80} \sum_i \frac{(\theta_i^{(j)} - \theta_i^{(j)}) (\theta_j^{(i^j)} - \theta_j^{(j)})}{\xi_{(i^j)(j)}} n_i^{(j)} n_j^{(j)} V_{(i^j)} \\
& + \frac{G}{2} \frac{3}{\pi\delta^3 h^2} \left[h \sum_i \frac{\left(\bar{w}_{(i^j)} - \bar{w}_{(j)} + \frac{\theta_i^{(i^j)} + \theta_i^{(j)}}{2} \xi_{(i^j)(j)} n_i^{(j)} \right)^2}{\xi_{(i^j)(j)}} V_{(i^j)} \right. \\
& + \frac{h^5}{80} \sum_i \frac{\left(\dot{w}_{(i^j)} - \dot{w}_{(j)} + 3 \frac{\theta_i^{(i^j)} + \theta_i^{(j)}}{2} \xi_{(i^j)(j)} n_i^{(j)} \right)^2}{\xi_{(i^j)(j)}} V_{(i^j)} \\
& \left. + 2 \frac{h^3}{12} \sum_i \frac{\left(\bar{w}_{(i^j)} - \bar{w}_{(j)} + \frac{\theta_i^{(i^j)} + \theta_i^{(j)}}{2} \xi_{(i^j)(j)} n_i^{(j)} \right) \left(\dot{w}_{(i^j)} - \dot{w}_{(j)} + 3 \frac{\theta_j^{(i^j)} + \theta_j^{(j)}}{2} \xi_{(i^j)(j)} n_j^{(j)} \right)}{\xi_{(i^j)(j)}} V_{(i^j)} \right] \\
& + \frac{G}{1-2\nu} \frac{6}{\pi\delta^3 h^2} \left\{ \frac{h^3}{12} \sum_i (\dot{w}_{(i^j)} + \dot{w}_{(j)}) \left[\nu (\theta_i^{(i^j)} - \theta_i^{(j)}) n_i^{(j)} + \frac{1-\nu}{2} \frac{\dot{w}_{(i^j)} + \dot{w}_{(j)}}{2} \xi_{(i^j)(j)} \right] V_{(i^j)} \right\} \\
& + \frac{h^5}{80} \nu \sum_i (\dot{w}_{(i^j)} + \dot{w}_{(j)}) (\theta_i^{(i^j)} - \theta_i^{(j)}) n_i^{(j)} V_{(i^j)} \\
& + \frac{G}{2} \frac{4\nu - 1}{1-2\nu} \frac{1}{h} \left(\frac{2}{\pi\delta^2 h} \right)^2 \left[\frac{h^3}{12} \left(\sum_i \frac{\theta_i^{(i^j)} - \theta_i^{(j)}}{\xi_{(i^j)(j)}} n_i^{(j)} V_{(i^j)} \right)^2 + \frac{h^7}{448} \left(\sum_i \frac{\theta_i^{(i^j)} - \theta_i^{(j)}}{\xi_{(i^j)(j)}} n_i^{(j)} V_{(i^j)} \right)^2 \right] \\
& + 2 \frac{h^5}{80} \sum_i \frac{\theta_i^{(i^j)} - \theta_i^{(j)}}{\xi_{(i^j)(j)}} n_i^{(j)} V_{(i^j)} \sum_i \frac{\theta_j^{(i^j)} - \theta_j^{(j)}}{\xi_{(i^j)(j)}} n_j^{(j)} V_{(i^j)}
\end{aligned} \tag{5.101b}$$

where $n_1 = \cos \varphi, n_2 = \sin \varphi$ with φ being the bond angle with respect to x -axis.

Substituting these PD strain energy expressions into Eq.(5.100) yields the final PD equations of motion for higher-order plate theory as:

$$\begin{aligned}
\rho_{(k)} \left(\frac{h^2}{12} \ddot{\theta}_L^{(k)} + \frac{h^4}{80} \dot{\theta}_L^{*(k)} \right) &= \frac{24G}{\pi\delta^3 h^2} \left(\frac{h^3}{12} \sum_j \frac{\theta_l^{(j)} - \theta_l^{(k)}}{\xi_{(j)(k)}} n_l^{(j)(k)} n_L^{(j)(k)} V_{(j)} + \frac{h^5}{80} \sum_j \frac{\theta_l^{*(j)} - \theta_l^{*(k)}}{\xi_{(j)(k)}} n_l^{(j)(k)} n_L^{(j)(k)} V_{(j)} \right) \\
&\quad - \frac{3G}{\pi\delta^3 h^2} \left[h \sum_j \left(\bar{w}_{(j)} - \bar{w}_{(k)} + \frac{\theta_l^{(j)} + \theta_l^{(k)}}{2} \xi_{(j)(k)} n_l^{(j)(k)} \right) n_L^{(j)(k)} V_{(j)} \right. \\
&\quad \left. + \frac{h^3}{12} \sum_j \left(\dot{w}_{(j)} - \dot{w}_{(k)} + 3 \frac{\theta_l^{*(j)} + \theta_l^{*(k)}}{2} \xi_{(j)(k)} n_l^{(j)(k)} \right) n_L^{(j)(k)} V_{(j)} \right] \\
&\quad + G \frac{4\nu - 1}{1 - 2\nu} \frac{2}{\pi\delta^2 h^2} \left(\frac{h^3}{12} \sum_j \frac{\Phi_{(j)} + \Phi_{(k)}}{\xi_{(j)(k)}} n_L^{(j)(k)} V_{(j)} + \frac{h^5}{80} \sum_j \frac{\Phi_{(j)}^* + \Phi_{(k)}^*}{\xi_{(j)(k)}} n_L^{(j)(k)} V_{(j)} \right) \\
&\quad - \frac{G\nu}{1 - 2\nu} \frac{h}{\pi\delta^3 h^2} \sum_j (\dot{w}_{(j)} + \dot{w}_{(k)}) n_L^{(j)(k)} V_{(j)} + \hat{b}_L^{(k)}
\end{aligned} \tag{5.102a}$$

$$\begin{aligned}
\rho_{(k)} \left(\frac{h^6}{448} \ddot{\theta}_L^{(k)} + \frac{h^4}{80} \dot{\theta}_L^{*(k)} \right) &= \frac{24G}{\pi\delta^3 h^2} \left(\frac{h^7}{448} \sum_j \frac{\theta_l^{(j)} - \theta_l^{(k)}}{\xi_{(j)(k)}} n_l^{(j)(k)} n_L^{(j)(k)} V_{(j)} + \frac{h^5}{80} \sum_j \frac{\theta_l^{*(j)} - \theta_l^{*(k)}}{\xi_{(j)(k)}} n_l^{(j)(k)} n_L^{(j)(k)} V_{(j)} \right) \\
&\quad - \frac{9G}{\pi\delta^3 h^2} \left[\frac{h^5}{80} \sum_j \left(\dot{w}_{(j)} - \dot{w}_{(k)} + 3 \frac{\theta_l^{*(j)} + \theta_l^{*(k)}}{2} \xi_{(j)(k)} n_l^{(j)(k)} \right) n_L^{(j)(k)} V_{(j)} \right. \\
&\quad \left. + \frac{h^3}{12} \sum_j \left(\bar{w}_{(j)} - \bar{w}_{(k)} + \frac{\theta_l^{(j)} + \theta_l^{(k)}}{2} \xi_{(j)(k)} n_l^{(j)(k)} \right) n_L^{(j)(k)} V_{(j)} \right] \\
&\quad + \frac{G\nu}{1 - 2\nu} \frac{12}{\pi\delta^3 h^2} \frac{h^5}{80} \sum_j (\dot{w}_{(j)} + \dot{w}_{(k)}) n_L^{(j)(k)} V_{(j)} \\
&\quad + G \frac{4\nu - 1}{1 - 2\nu} \frac{2}{\pi\delta^2 h^2} \left(\frac{h^5}{80} \sum_j \frac{\Phi_{(j)} + \Phi_{(k)}}{\xi_{(j)(k)}} n_L^{(j)(k)} V_{(j)} + \frac{h^7}{448} \sum_j \frac{\Phi_{(j)}^* + \Phi_{(k)}^*}{\xi_{(j)(k)}} n_L^{(j)(k)} V_{(j)} \right)
\end{aligned} \tag{5.102b}$$

$$\rho_{(k)} \left(\ddot{w}_{(k)} + \frac{h^2}{12} \dot{w}_{(k)}^* \right) = \frac{6G}{\pi\delta^3 h^2} \left[h \sum_j \left(\frac{\bar{w}_{(j)} - \bar{w}_{(k)}}{\xi_{(j)(k)}} + \frac{\theta_l^{(k)} + \theta_l^{(j)}}{2} n_l^{(j)(k)} \right) V_{(j)} \right. \\
\left. + \frac{h^3}{12} \sum_j \left(\frac{\dot{w}_{(j)} - \dot{w}_{(k)}}{\xi_{(j)(k)}} + 3 \frac{\theta_l^{*(k)} + \theta_l^{*(j)}}{2} n_l^{(j)(k)} \right) V_{(j)} \right] + \hat{b}_z^{(k)} \tag{5.102c}$$

$$\begin{aligned}
\rho_{(k)} \left(\frac{h^2}{12} \ddot{w}_{(k)} + \frac{h^4}{80} \dot{w}_{(k)}^* \right) &= \frac{6G}{\pi\delta^3 h^2} \left[\frac{h^3}{12} \sum_j \left(\frac{\bar{w}_{(j)} - \bar{w}_{(k)}}{\xi_{(j)(k)}} + \frac{\theta_l^{(k)} + \theta_l^{(j)}}{2} n_l^{(j)(k)} \right) V_{(j)} \right. \\
&\quad \left. + \frac{h^5}{80} \sum_j \left(\frac{\dot{w}_{(j)} - \dot{w}_{(k)}}{\xi_{(j)(k)}} + 3 \frac{\theta_l^{*(k)} + \theta_l^{*(j)}}{2} n_l^{(j)(k)} \right) V_{(j)} \right] \\
&\quad - \frac{G}{1 - 2\nu} \frac{12}{\pi\delta^3 h^2} \left\{ \frac{h^3}{12} \sum_j \left[\nu (\theta_l^{(j)} - \theta_l^{(k)}) n_l^{(j)(k)} + \frac{1 - \nu}{2} (\dot{w}_{(j)} + \dot{w}_{(k)}) \right] V_{(j)} \right\} \\
&\quad \left. + \frac{h^5}{80} \sum_j \nu (\theta_l^{*(j)} - \theta_l^{*(k)}) V_{(j)} \right\}
\end{aligned} \tag{5.102d}$$

where Φ and Φ^* can be defined as

$$\Phi_{(j)} = \frac{2}{\pi\delta^2 h} \sum_i \frac{\theta_i^{(j)} - \theta_i^{(k)}}{\xi_{(i)(j)}} n_i^{(j)(j)} V_{(j)} \quad (5.103a)$$

$$\Phi_{(k)} = \frac{2}{\pi\delta^2 h} \sum_i \frac{\theta_i^{(k)} - \theta_i^{(j)}}{\xi_{(i)(k)}} n_i^{(k)(k)} V_{(k)} \quad (5.103b)$$

and

$$\Phi_{(j)}^* = \frac{2}{\pi\delta^2 h} \sum_i \frac{\theta_i^{*(j)} - \theta_i^{*(k)}}{\xi_{(i)(j)}} n_i^{(j)(j)} V_{(j)} \quad (5.103c)$$

$$\Phi_{(k)}^* = \frac{2}{\pi\delta^2 h} \sum_i \frac{\theta_i^{*(k)} - \theta_i^{*(j)}}{\xi_{(i)(k)}} n_i^{(k)(k)} V_{(k)} \quad (5.103d)$$

In particular case, when the Poisson's ratio is $\nu = 0.25$, PD equations of motion will reduce to simpler forms:

$$\rho_{(k)} \left(\frac{h^2}{12} \ddot{\theta}_L^{(k)} + \frac{h^4}{80} \ddot{\theta}_L^{*(k)} \right) = \frac{24G}{\pi\delta^3 h^2} \left(\begin{aligned} & \left[\frac{h^3}{12} \sum_j \frac{\theta_j^{(j)} - \theta_j^{(k)}}{\xi_{(j)(k)}} n_j^{(j)(k)} n_L^{(j)(k)} V_{(j)} \right. \\ & \left. + \frac{h^5}{80} \sum_j \frac{\theta_j^{*(j)} - \theta_j^{*(k)}}{\xi_{(j)(k)}} n_j^{(j)(k)} n_L^{(j)(k)} V_{(j)} \right] \\ & - \frac{3G}{\pi\delta^3 h^2} \left[h \sum_j \left(\bar{w}_{(j)} - \bar{w}_{(k)} + \frac{\theta_j^{(j)} + \theta_j^{(k)}}{2} \xi_{(j)(k)} n_j^{(j)(k)} \right) n_L^{(j)(k)} V_{(j)} \right. \\ & \left. + \frac{h^3}{12} \sum_j \left(\dot{w}_{(j)} - \dot{w}_{(k)} + 3 \frac{\theta_j^{*(j)} + \theta_j^{*(k)}}{2} \xi_{(j)(k)} n_j^{(j)(k)} \right) n_L^{(j)(k)} V_{(j)} \right] \\ & + \frac{G}{2} \frac{h}{\pi\delta^3 h^2} \sum_j \left(\dot{w}_{(j)} + \dot{w}_{(k)} \right) n_L^{(j)(k)} V_{(j)} + \hat{b}_L^{(k)} \end{aligned} \right) \quad (5.104a)$$

$$\rho_{(k)} \left(\frac{h^6}{448} \ddot{\theta}_L^{*(k)} + \frac{h^4}{80} \ddot{\theta}_L^{(k)} \right) = \frac{24G}{\pi\delta^3 h^2} \left(\begin{aligned} & \left[\frac{h^7}{448} \sum_j \frac{\theta_j^{*(j)} - \theta_j^{*(k)}}{\xi_{(j)(k)}} n_j^{(j)(k)} n_L^{(j)(k)} V_{(j)} \right. \\ & \left. + \frac{h^5}{80} \sum_j \frac{\theta_j^{(j)} - \theta_j^{(k)}}{\xi_{(j)(k)}} n_j^{(j)(k)} n_L^{(j)(k)} V_{(j)} \right] \\ & - \frac{9G}{\pi\delta^3 h^2} \left[\frac{h^5}{80} \sum_j \left(\dot{w}_{(j)} - \dot{w}_{(k)} + 3 \frac{\theta_j^{*(j)} + \theta_j^{*(k)}}{2} \xi_{(j)(k)} n_j^{(j)(k)} \right) n_L^{(j)(k)} V_{(j)} \right. \\ & \left. + \frac{h^3}{12} \sum_j \left(\bar{w}_{(j)} - \bar{w}_{(k)} + \frac{\theta_j^{(j)} + \theta_j^{(k)}}{2} \xi_{(j)(k)} n_j^{(j)(k)} \right) n_L^{(j)(k)} V_{(j)} \right] \\ & + \frac{6G}{\pi\delta^3 h^2} \frac{h^5}{80} \sum_j \left(\dot{w}_{(j)} + \dot{w}_{(k)} \right) n_L^{(j)(k)} V_{(j)} \end{aligned} \right) \quad (5.104b)$$

$$\rho_{(k)} \left(\ddot{\bar{w}}_{(k)} + \frac{h^2}{12} \ddot{\dot{w}}_{(k)} \right) = \frac{6G}{\pi\delta^3 h^2} \left[\begin{aligned} & h \sum_j \left(\frac{\bar{w}_{(j)} - \bar{w}_{(k)}}{\xi_{(j)(k)}} + \frac{\theta_j^{(k)} + \theta_j^{(j)}}{2} n_j^{(j)(k)} \right) V_{(j)} \\ & + \frac{h^3}{12} \sum_j \left(\frac{\dot{w}_{(j)} - \dot{w}_{(k)}}{\xi_{(j)(k)}} + 3 \frac{\theta_j^{*(k)} + \theta_j^{*(j)}}{2} n_j^{(j)(k)} \right) V_{(j)} \end{aligned} \right] + \hat{b}_z^{(k)} \quad (5.104c)$$

$$\rho_{(k)} \left(\frac{h^2}{12} \ddot{W}_{(k)} + \frac{h^4}{80} \dot{W}_{(k)}^* \right) = \frac{6G}{\pi \delta^3 h^2} \left[\begin{aligned} & \frac{h^3}{12} \sum_j \left(\frac{\bar{w}_{(j)} - \bar{w}_{(k)}}{\xi_{(j)(k)}} + \frac{\theta_l^{(j)} + \theta_l^{(k)}}{2} r_l^{(j)(k)} \right) V_{(j)} \\ & + \frac{h^5}{80} \sum_j \left(\frac{w_{(j)}^* - w_{(k)}^*}{\xi_{(j)(k)}} + 3 \frac{\theta_l^{*(j)} + \theta_l^{*(k)}}{2} r_l^{(j)(k)} \right) V_{(j)} \end{aligned} \right] \quad (5.104d)$$

$$- \frac{6G}{\pi \delta^3 h^2} \left\{ \begin{aligned} & \frac{h^3}{12} \sum_j \left[(\theta_l^{(j)} - \theta_l^{(k)}) r_l^{(j)(k)} + (w_{(j)}^* + w_{(k)}^*) \right] V_{(j)} \\ & + \frac{h^5}{80} \sum_j (\theta_l^{*(j)} - \theta_l^{*(k)}) V_{(j)} \end{aligned} \right\}$$

5.5.3 Numerical Results

In order to verify the PD formulation for a higher-order plate theory, three numerical examples are considered for simply supported and clamped boundary conditions. The PD solutions are compared with the corresponding finite element (FE) analysis results.

5.5.3.1 Simply supported plate subjected to transverse loading

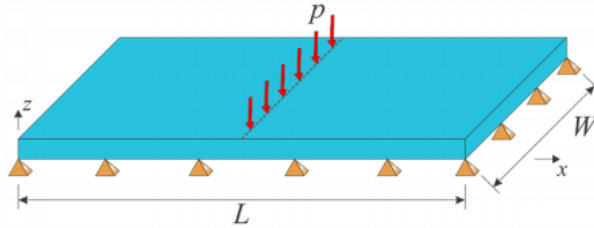


Figure 5.38 Simply supported plate subjected to transverse loading.

A simply supported plate with a length and width of $L = W = 1\text{m}$ and a thickness of $h = 0.2\text{m}$ is considered as shown in Fig. 5.38. The Young's modulus and Poisson's ratio of the plate are $E = 200\text{GPa}$ and $\nu = 1/4$, respectively. The model is discretized into one single row of material points along with the thickness direction and the distance between material points is $\Delta x = 1/70\text{ m}$. The horizon size is chosen as $\delta = 3.015\Delta x$. A fictitious region is introduced outside the edges as the external boundaries with a width of δ . The plate is subjected to a distributed transverse load of $p = 100\text{N/m}$ through the y -center line. The line load is converted to a body load of $b = \frac{pW}{2(\frac{W}{\Delta x})\Delta V} = 1.25 \times 10^4\text{N/m}^3$ and it is distributed to two columns of material points

through the center line as shown in Fig. 5.39.

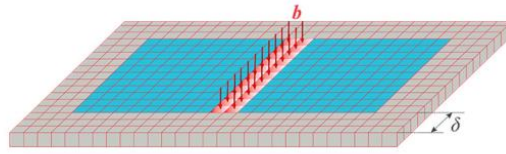


Figure 5.39 Application of transverse loading in PD model and fictitious region.

The FE model of the plate is created by using SOLID185 element in ANSYS with 50 elements along the length and width, and 8 elements along the thickness. Boundary conditions below were applied in ANSYS as:

$$u(0, y, 0) = u(L, y, 0) = u(x, 0, 0) = u(x, W, 0) = 0$$

$$v(0, y, 0) = v(L, y, 0) = v(x, 0, 0) = v(x, W, 0) = 0$$

$$w(0, y, 0) = w(L, y, 0) = w(x, 0, 0) = w(x, W, 0) = 0$$

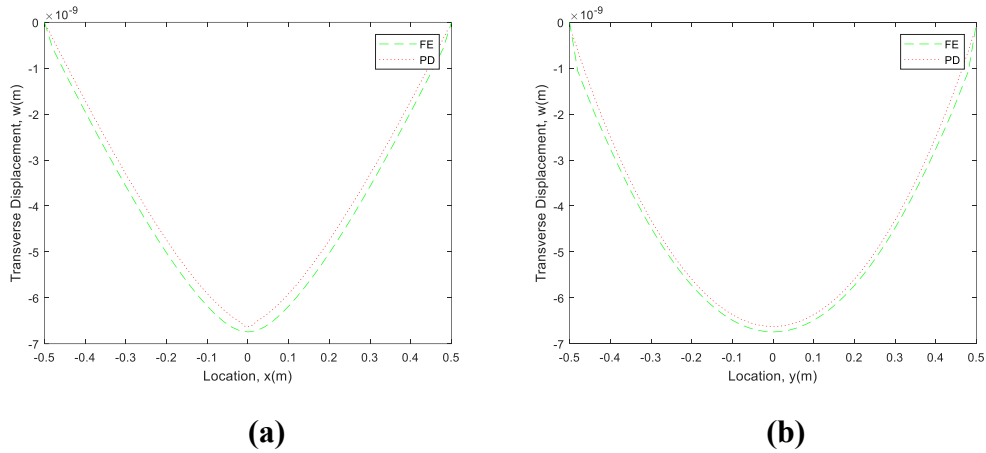


Figure 5.40 Variation of transverse displacements along (a) central x-axis and (b) central y-axis.

As depicted in Fig. 5.40, the transverse displacement variation results along the central x-axis and y-axis obtained from PD and FE analyses are compared with each other and a very good agreement is obtained between the two approaches.

5.5.3.2 Clamped plate subjected to transverse loading

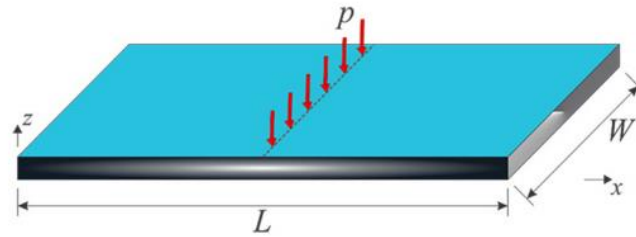


Figure 5.41 Clamped plate subjected to transverse loading.

A clamped plate with a length and width of $L = W = 1\text{m}$ and a thickness of $h = 0.15\text{m}$ is considered as shown in Fig. 5.41. Young's modulus and Poisson's ratio of the plate are $E = 200\text{GPa}$ and $\nu = 0.3$, respectively. The model is discretized into one single row of material points along with the thickness and the distance between material points is $\Delta x = 1/70\text{ m}$. The horizon size is chosen as $\delta = 3.015\Delta x$. A fictitious region is introduced outside the edges as the external boundaries with a width of 2δ . The plate is subjected to a distributed transverse load of $p = 100\text{N/m}$ through the y-center line. The line load is converted to a body load of $b = \frac{pW}{2(\frac{W}{\Delta x} - 2)\Delta V} = 1.3021 \times 10^4\text{ N/m}^3$ and it is distributed to two columns of material points through the center line as shown in Fig. 5.42.

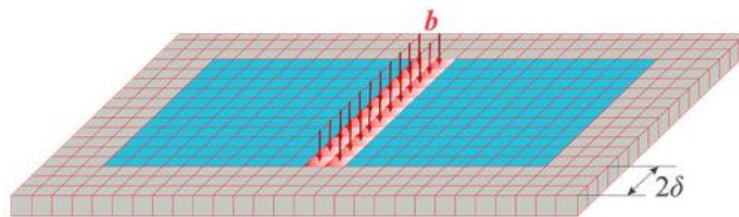


Figure 5.42 Application of transverse loading in PD model and fictitious region.

The FE model of the plate is created by using the SOLID185 element in ANSYS with 50 elements along the length and width, and 8 elements along the thickness. Boundary conditions below were applied in ANSYS as:

$$u(0, y, z) = u(L, y, z) = u(x, 0, z) = u(x, W, z) = 0$$

$$v(0, y, z) = v(L, y, z) = v(x, 0, z) = v(x, W, z) = 0$$

$$w(0, y, 0) = w(L, y, 0) = w(x, 0, 0) = w(x, W, 0) = 0$$

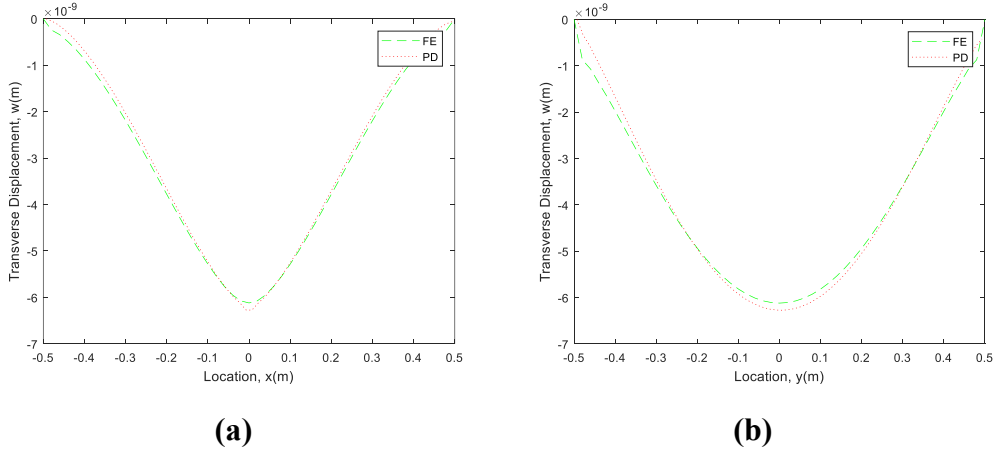


Figure 5.43 Variation of transverse displacements along (a) central x-axis and (b) central y-axis.

PD results for transverse deflection obtained along the central x-axis and y-axis are compared against FE results as shown in Fig. 5.43. PD results agree very well with FE results.

5.5.3.3 Plate subjected to transverse loading and mixed (simply supported – clamped) boundary conditions

In the final numerical case, a mixed (simply supported – clamped) boundary condition is considered. The plate has a length and width of $L = W = 1\text{m}$ and a thickness of $h = 0.2\text{m}$. The material properties are same as in the previous case. The plate is subjected to a distributed transverse load of $p = 100\text{N/m}$ through the y-center line. The line load is converted to a body load of $b = \frac{pW}{2(\frac{W}{\Delta x})\Delta V} = 1.25 \times 10^4\text{N/m}^3$ and it is distributed to two columns of material points through the center line.

The FE model of the plate is created by using the SOLID185 element in ANSYS with 50 elements along the length and width, and 8 elements along the thickness. Boundary

conditions below were applied in ANSYS as:

$$u(0, y, 0) = u(L, y, 0) = u(x, 0, z) = u(x, W, z) = 0$$

$$v(0, y, 0) = v(L, y, 0) = v(x, 0, z) = v(x, W, z) = 0$$

$$w(0, y, 0) = w(L, y, 0) = w(x, 0, 0) = w(x, W, 0) = 0$$

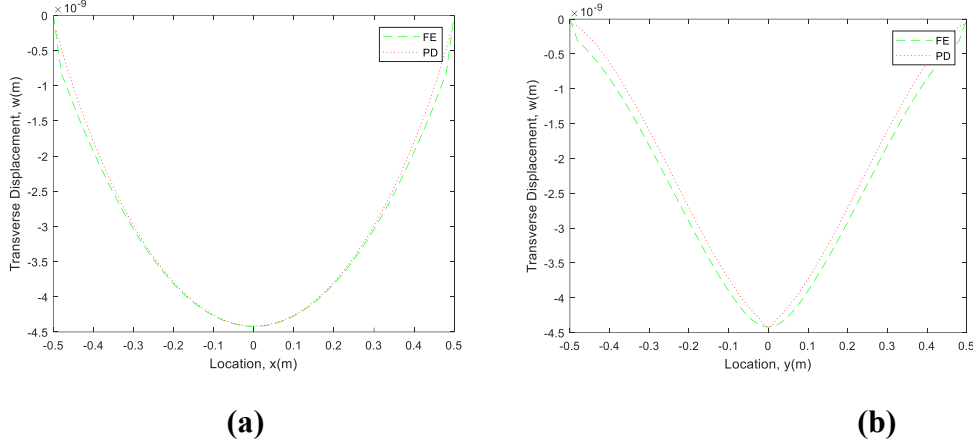


Figure 5.44 Variation of transverse displacements along (a) central x-axis and (b) central y-axis.

Transverse deflection results obtained along the central x-axis and y-axis are shown in Fig. 5.44 and PD and FE results agree very well with each other demonstrating that the current formulation is capable of considering mixed boundary conditions.

5.6 PD Formulations for FGM Higher Order Deformable Plate

5.6.1 FGM Higher Order Deformable Plate Theory

The displacement field of any material points at the transverse normal can be represented in terms of the displacement field of the material point at locus of mid-plane by using Taylor expansion as

$$u(x, y, z) = u(x, y, 0) + z \left. \frac{\partial u}{\partial z} \right|_{z=0} + \frac{1}{2} z^2 \left. \frac{\partial^2 u}{\partial z^2} \right|_{z=0} + \frac{1}{3!} z^3 \left. \frac{\partial^3 u}{\partial z^3} \right|_{z=0} + \dots \quad (5.105a)$$

$$v(x, y, z) = v(x, y, 0) + z \left. \frac{\partial v}{\partial z} \right|_{z=0} + \frac{1}{2} z^2 \left. \frac{\partial^2 v}{\partial z^2} \right|_{z=0} + \frac{1}{3!} z^3 \left. \frac{\partial^3 v}{\partial z^3} \right|_{z=0} + \dots \quad (5.105b)$$

$$w(x, y, z) = w(x, y, 0) + z \left. \frac{\partial w}{\partial z} \right|_{z=0} + \frac{1}{2} z^2 \left. \frac{\partial^2 w}{\partial z^2} \right|_{z=0} + \frac{1}{3!} z^3 \left. \frac{\partial^3 w}{\partial z^3} \right|_{z=0} + \dots \quad (5.105c)$$

Ignoring higher order terms in Eqs. (5.105), the components of the displacement field can be rewritten as follows

$$u(x, y, z) = \bar{u}(x, y) + z\theta_x(x, y) + z^2\dot{u}(x, y) + z^3\dot{\theta}_x^*(x, y) \quad (5.106a)$$

$$v(x, y, z) = \bar{v}(x, y) + z\theta_y(x, y) + z^2\dot{v}(x, y) + z^3\dot{\theta}_y^*(x, y) \quad (5.106b)$$

$$w(x, y, z) = \bar{w}(x, y) + z\theta_z(x, y) + z^2\dot{w}(x, y) \quad (5.106c)$$

Where \bar{u} , \bar{v} and \bar{w} represent the linear displacement of the material points on mid-plane along x , y and z direction, respectively, and θ_x , θ_x^* , θ_y , θ_y^* , θ_z , u^* , v^* and w^* are arisen out of the Taylor expansion and introduced as eight new independent variables. Particularly, θ_x and θ_y represent the rotation of the material points on mid-plane about y axis and negative x axis, respectively.

In order to compact the expressions, hereafter $\bar{u}(x, y)$, $\bar{v}(x, y)$, $\bar{w}(x, y)$, $\theta_x(x, y)$, $\theta_y(x, y)$, $\theta_z(x, y)$, $u^*(x, y)$, $v^*(x, y)$, $w^*(x, y)$, $\theta_x^*(x, y)$ and $\theta_y^*(x, y)$ are written simply as \bar{u} , \bar{v} , \bar{w} , θ_x , θ_y , θ_z , u^* , v^* , w^* , θ_x^* and θ_y^* , respectively.

Stipulation of the displacement assumptions, Eq.(5.106), in the three well-known strain-displacement relations of the 3D elasticity gives the following relations with indices notations

$$\varepsilon_{11} = \frac{\partial \bar{u}}{\partial x_1} + z \frac{\partial \theta_1}{\partial x_1} + z^2 \frac{\partial \dot{u}_1^*}{\partial x_1} + z^3 \frac{\partial \dot{\theta}_1^*}{\partial x_1} \quad (5.107a)$$

$$\varepsilon_{22} = \frac{\partial \bar{u}_2}{\partial x_2} + z \frac{\partial \theta_2}{\partial x_2} + z^2 \frac{\partial \dot{u}_2^*}{\partial x_2} + z^3 \frac{\partial \dot{\theta}_2^*}{\partial x_2} \quad (5.107b)$$

$$\varepsilon_{33} = \theta_z + 2z\dot{w} \quad (5.107c)$$

$$\varepsilon_{12} = \varepsilon_{21} = \frac{1}{2} \left[\left(\frac{\partial \bar{u}_1}{\partial x_2} + \frac{\partial \bar{u}_2}{\partial x_1} \right) + z \left(\frac{\partial \theta_1}{\partial x_2} + \frac{\partial \theta_2}{\partial x_1} \right) + z^2 \left(\frac{\partial \dot{u}_1^*}{\partial x_2} + \frac{\partial \dot{u}_2^*}{\partial x_1} \right) + z^3 \left(\frac{\partial \dot{\theta}_1^*}{\partial x_2} + \frac{\partial \dot{\theta}_2^*}{\partial x_1} \right) \right] \quad (5.107d)$$

$$\varepsilon_{13} = \varepsilon_{31} = \frac{1}{2} \left[\left(\theta_1 + \frac{\partial \bar{w}}{\partial x_1} \right) + z \left(2\dot{u}_1^* + \frac{\partial \theta_z}{\partial x_1} \right) + z^2 \left(3\dot{\theta}_1^* + \frac{\partial \dot{w}}{\partial x_1} \right) \right] \quad (5.107e)$$

$$\varepsilon_{23} = \varepsilon_{32} = \frac{1}{2} \left[\left(\theta_2 + \frac{\partial \bar{w}}{\partial x_2} \right) + z \left(2\dot{u}_2^* + \frac{\partial \theta_z}{\partial x_2} \right) + z^2 \left(3\dot{\theta}_2^* + \frac{\partial \dot{w}}{\partial x_2} \right) \right] \quad (5.107f)$$

These strain-displacement relations can be also expressed in terms of tensorial indices as:

$$\begin{aligned} \varepsilon_{ij} = & \frac{1}{2} \left[\left(\frac{\partial \bar{u}_i}{\partial x_j} + \frac{\partial \bar{u}_j}{\partial x_i} \right) + z \left(\frac{\partial \theta_i}{\partial x_j} + \frac{\partial \theta_j}{\partial x_i} \right) + z^2 \left(\frac{\partial u_i^*}{\partial x_j} + \frac{\partial u_j^*}{\partial x_i} \right) + z^3 \left(\frac{\partial \theta_i^*}{\partial x_j} + \frac{\partial \theta_j^*}{\partial x_i} \right) \right] \delta_{ii} \delta_{jj} \\ & + \frac{1}{2} \left[\left(\theta_i + \frac{\partial \bar{w}}{\partial x_i} \right) + z \left(2u_i^* + \frac{\partial \theta_z^*}{\partial x_i} \right) + z^2 \left(3\theta_i^* + \frac{\partial w^*}{\partial x_i} \right) \right] (\delta_{ii} \delta_{3j} + \delta_{3i} \delta_{jj}) \\ & + (\theta_z + 2zw^*) \delta_{3i} \delta_{3j} \end{aligned} \quad (5.108)$$

Where $i, j = 1, 2, 3$ and $I, J = 1, 2$. Note that this convention that capital letter indices, e.g., I, J, K, \dots take up the values 1 and 2, and small letter indices, e.g., i, j, k, \dots take up the values 1, 2 and 3, will be applied throughout the later study.

Assuming the material is planar isotropic and obeys 3D constitutive relation, the stress components can be given by

$$\sigma_{ij} = C_{ijkl} \varepsilon_{kl} \quad (5.109)$$

Where is C_{ijkl} the elastic modulus tensor, which is defined as

$$C_{ijkl} = G(\delta_{ii} \delta_{jj} + \delta_{ik} \delta_{jl}) + \frac{2G\nu}{1-2\nu} \delta_{ij} \delta_{kl} \quad (5.110)$$

where the shear modulus $G = G(z)$ and Poisson's ratio $\nu = \nu(z)$ vary through the thickness.

Plugging Eq.(5.110) into (5.109) gives

$$\sigma_{ij} = 2G\varepsilon_{ij} + \frac{2G\nu}{1-2\nu} \varepsilon_{kk} \delta_{ij} \quad (5.111)$$

According to the classical continuum mechanics theory, the average strain energy density of the plate can be written as:

$$W_{\text{cm}} = \frac{1}{2h} \int_{-\frac{h}{2}}^{\frac{h}{2}} \sigma_{ij} \varepsilon_{ij} dz \quad (5.112a)$$

where h represent the thickness of the plate.

Inserting Eq.(5.111) and (5.108) into (5.112a) and rearranging the tensorial indices gives the expression of strain energy density function as

$$\begin{aligned}
W_{\text{cm}} = \frac{1}{h} & \left\{ \int_{-\frac{h}{2}}^{\frac{h}{2}} \frac{G}{2} dz \left[\frac{\partial \bar{u}_i}{\partial x_j} \frac{\partial \bar{u}_i}{\partial x_j} + \frac{\partial \bar{u}_i}{\partial x_j} \frac{\partial \bar{u}_j}{\partial x_i} + \frac{\partial \bar{u}_i}{\partial x_j} \frac{\partial \bar{u}_j}{\partial x_i} + \left(\theta_i + \frac{\partial \bar{w}}{\partial x_i} \right) \left(\theta_i + \frac{\partial \bar{w}}{\partial x_i} \right) + 2\theta_z^2 \right] \right. \\
& + \int_{-\frac{h}{2}}^{\frac{h}{2}} \frac{G}{2} dz \left[\frac{\partial \bar{u}_i}{\partial x_j} \frac{\partial \theta_i}{\partial x_j} + \frac{\partial \bar{u}_i}{\partial x_j} \frac{\partial \theta_j}{\partial x_i} + \frac{\partial \bar{u}_i}{\partial x_j} \frac{\partial \theta_j}{\partial x_i} + \left(\theta_i + \frac{\partial \bar{w}}{\partial x_i} \right) \left(2\dot{u}_i + \frac{\partial \theta_z}{\partial x_i} \right) + 4\theta_z \dot{w} \right] \\
& + \int_{-\frac{h}{2}}^{\frac{h}{2}} \frac{G}{2} z^2 dz \left[\frac{\partial \theta_i}{\partial x_j} \frac{\partial \theta_i}{\partial x_j} + \frac{\partial \theta_i}{\partial x_j} \frac{\partial \theta_j}{\partial x_i} + \frac{\partial \theta_i}{\partial x_j} \frac{\partial \theta_j}{\partial x_i} + 2 \left(\frac{\partial \bar{u}_i}{\partial x_j} \frac{\partial \dot{u}_i}{\partial x_j} + \frac{\partial \bar{u}_i}{\partial x_j} \frac{\partial \dot{u}_j}{\partial x_i} + \frac{\partial \bar{u}_i}{\partial x_j} \frac{\partial \dot{u}_j}{\partial x_i} \right) \right. \\
& \left. + \left(2\dot{u}_i + \frac{\partial \theta_z}{\partial x_i} \right) \left(2\dot{u}_i + \frac{\partial \theta_z}{\partial x_i} \right) + 2 \left(\theta_i + \frac{\partial \bar{w}}{\partial x_i} \right) \left(3\dot{\theta}_i + \frac{\partial \dot{w}}{\partial x_i} \right) + 8(\dot{w})^2 \right] \\
& + \int_{-\frac{h}{2}}^{\frac{h}{2}} \frac{G}{2} z^3 dz \left[\frac{\partial \bar{u}_i}{\partial x_j} \frac{\partial \dot{\theta}_i}{\partial x_j} + \frac{\partial \bar{u}_i}{\partial x_j} \frac{\partial \dot{\theta}_j}{\partial x_i} + \frac{\partial \bar{u}_i}{\partial x_j} \frac{\partial \dot{\theta}_j}{\partial x_i} + \left(\frac{\partial \theta_i}{\partial x_j} \frac{\partial \dot{u}_i}{\partial x_j} + \frac{\partial \theta_i}{\partial x_j} \frac{\partial \dot{u}_j}{\partial x_i} + \frac{\partial \theta_i}{\partial x_j} \frac{\partial \dot{u}_j}{\partial x_i} \right) + \left(2\dot{u}_i + \frac{\partial \theta_z}{\partial x_i} \right) \left(3\dot{\theta}_i + \frac{\partial \dot{w}}{\partial x_i} \right) \right] \\
& + \int_{-\frac{h}{2}}^{\frac{h}{2}} \frac{G}{2} z^4 dz \left[\left(\frac{\partial \dot{u}_i}{\partial x_j} \frac{\partial \dot{u}_i}{\partial x_j} + \frac{\partial \dot{u}_i}{\partial x_j} \frac{\partial \dot{u}_j}{\partial x_i} + \frac{\partial \dot{u}_i}{\partial x_j} \frac{\partial \dot{u}_j}{\partial x_i} \right) + 2 \left(\frac{\partial \theta_i}{\partial x_j} \frac{\partial \dot{\theta}_i}{\partial x_j} + \frac{\partial \theta_i}{\partial x_j} \frac{\partial \dot{\theta}_j}{\partial x_i} + \frac{\partial \theta_i}{\partial x_j} \frac{\partial \dot{\theta}_j}{\partial x_i} \right) + \left(3\dot{\theta}_i + \frac{\partial \dot{w}}{\partial x_i} \right) \left(3\dot{\theta}_i + \frac{\partial \dot{w}}{\partial x_i} \right) \right] \\
& + \int_{-\frac{h}{2}}^{\frac{h}{2}} \frac{G}{2} z^5 dz \left(\frac{\partial \dot{u}_i}{\partial x_j} \frac{\partial \dot{\theta}_i}{\partial x_j} + \frac{\partial \dot{u}_i}{\partial x_j} \frac{\partial \dot{\theta}_j}{\partial x_i} + \frac{\partial \dot{u}_i}{\partial x_j} \frac{\partial \dot{\theta}_j}{\partial x_i} \right) + \int_{-\frac{h}{2}}^{\frac{h}{2}} \frac{G}{2} z^6 dz \left(\frac{\partial \dot{\theta}_i}{\partial x_j} \frac{\partial \dot{\theta}_i}{\partial x_j} + \frac{\partial \dot{\theta}_i}{\partial x_j} \frac{\partial \dot{\theta}_j}{\partial x_i} + \frac{\partial \dot{\theta}_i}{\partial x_j} \frac{\partial \dot{\theta}_j}{\partial x_i} \right) \\
& + \frac{1}{h} \left\{ \int_{-\frac{h}{2}}^{\frac{h}{2}} \frac{G\nu}{1-2\nu} dz \left(2 \frac{\partial \bar{u}_i}{\partial x_i} \theta_z + \theta_z^2 \right) + \int_{-\frac{h}{2}}^{\frac{h}{2}} \frac{2G\nu z}{1-2\nu} dz \left(2 \frac{\partial \bar{u}_i}{\partial x_i} \dot{w} + \frac{\partial \theta_i}{\partial x_i} \theta_z + 2\theta_z \dot{w} \right) \right. \\
& + \int_{-\frac{h}{2}}^{\frac{h}{2}} \frac{2G\nu z^2}{1-2\nu} dz \left[2 \frac{\partial \theta_i}{\partial x_i} \dot{w} + \frac{\partial \dot{u}_i}{\partial x_i} \theta_z + 2(\dot{w})^2 \right] + \int_{-\frac{h}{2}}^{\frac{h}{2}} \frac{2G\nu z^3}{1-2\nu} dz \left(2 \frac{\partial \dot{u}_i}{\partial x_i} \dot{w} + \frac{\partial \dot{u}_i}{\partial x_i} \theta_z \right) + \int_{-\frac{h}{2}}^{\frac{h}{2}} \frac{4G\nu z^4}{1-2\nu} dz \frac{\partial \dot{\theta}_i}{\partial x_i} \dot{w} \\
& + \frac{1}{h} \left\{ \int_{-\frac{h}{2}}^{\frac{h}{2}} \frac{G(4\nu-1)}{2(1-2\nu)} dz \left(\frac{\partial \bar{u}_i}{\partial x_i} \right)^2 + \int_{-\frac{h}{2}}^{\frac{h}{2}} \frac{G(4\nu-1)}{1-2\nu} z dz \frac{\partial \bar{u}_i}{\partial x_i} \frac{\partial \theta_j}{\partial x_j} \right. \\
& + \int_{-\frac{h}{2}}^{\frac{h}{2}} \frac{G(4\nu-1)}{2(1-2\nu)} z^2 dz \left[\left(\frac{\partial \theta_i}{\partial x_i} \right)^2 + 2 \frac{\partial \bar{u}_i}{\partial x_i} \frac{\partial \dot{u}_j}{\partial x_j} \right] + \int_{-\frac{h}{2}}^{\frac{h}{2}} \frac{G(4\nu-1)}{1-2\nu} z^3 dz \left(\frac{\partial \bar{u}_i}{\partial x_i} \frac{\partial \dot{\theta}_j}{\partial x_j} + \frac{\partial \theta_i}{\partial x_i} \frac{\partial \dot{u}_j}{\partial x_j} \right) \\
& + \int_{-\frac{h}{2}}^{\frac{h}{2}} \frac{G(4\nu-1)}{2(1-2\nu)} z^4 dz \left[\left(\frac{\partial \dot{u}_i}{\partial x_i} \right)^2 + 2 \frac{\partial \theta_i}{\partial x_i} \frac{\partial \dot{\theta}_j}{\partial x_j} \right] + \int_{-\frac{h}{2}}^{\frac{h}{2}} \frac{G(4\nu-1)}{1-2\nu} z^5 dz \frac{\partial \dot{u}_i}{\partial x_i} \frac{\partial \dot{\theta}_j}{\partial x_j} + \int_{-\frac{h}{2}}^{\frac{h}{2}} \frac{G(4\nu-1)}{2(1-2\nu)} z^6 dz \left(\frac{\partial \dot{\theta}_i}{\partial x_i} \right)^2 \right. \\
& \left. \left. \right\} \right. \\
& \left. \right\} \tag{5.112b}
\end{aligned}$$

5.6.2 PD Formulations for FBM Higher Order Deformable Plate

Assume the system is initially at rest, the PD equations of motion can be derived by utilising Euler-Lagrange's equation:

$$\frac{d}{dt} \frac{\partial L}{\partial \mathbf{u}_{(k)}} - \frac{\partial L}{\partial \mathbf{u}_{(k)}} = 0 \tag{5.113}$$

where $L = T - U$ is the Lagrangian and $\mathbf{u}_{(k)}$ is the displacement vector of material point k which contains the following entries in this study as

$$\mathbf{u} = (\bar{u}_1 \ \bar{u}_2 \ \theta_1 \ \theta_2 \ u_1^* \ u_2^* \ \theta_1^* \ \theta_2^* \ \bar{w} \ \theta_z \ w)^T \tag{5.114}$$

The kinetic energy per unit area of the plate, \bar{T} , can be expressed as

$$\bar{T} = \frac{1}{2} \int_{-\frac{h}{2}}^{\frac{h}{2}} \rho (\dot{u}^2 + \dot{v}^2 + \dot{w}^2) dz \tag{5.115a}$$

Substituting Equations (5.106) into Equation (5.115a) results in

$$\begin{aligned}
\bar{T} &= \frac{1}{2} \int_{-\frac{h}{2}}^{\frac{h}{2}} \rho \left\{ \left(\dot{u}_i \dot{u}_i + \dot{w}^2 \right) + 2z \left(\dot{u}_i \dot{\theta}_i + \dot{w} \dot{\theta}_z \right) + z^2 \left(\dot{\theta}_i \dot{\theta}_i + 2\dot{u}_i \dot{u}_i^* + 2\dot{w} \dot{w}^* + \dot{\theta}_z^2 \right) \right. \\
&\quad \left. + 2z^3 \left(\dot{u}_i \dot{\theta}_i^* + \dot{\theta}_i \dot{u}_i^* + \dot{\theta}_z \dot{w}^* \right) + z^4 \left[\dot{u}_i \dot{u}_i^* + 2\dot{\theta}_i \dot{\theta}_i^* + \left(\dot{w}^* \right)^2 \right] + 2z^5 \dot{u}_i^* \dot{\theta}_i^* + z^6 \dot{\theta}_i^* \dot{\theta}_i^* \right\} dz \\
&= \frac{1}{2} \rho \left\{ h \left(\dot{u}_i \dot{u}_i + \dot{w}^2 \right) + \frac{h^3}{12} \left(\dot{\theta}_i \dot{\theta}_i + 2\dot{u}_i \dot{u}_i^* + 2\dot{w} \dot{w}^* + \dot{\theta}_z^2 \right) \right. \\
&\quad \left. + \frac{h^5}{80} \left[\dot{u}_i \dot{u}_i^* + 2\dot{\theta}_i \dot{\theta}_i^* + \left(\dot{w}^* \right)^2 \right] + \frac{h^7}{448} \dot{\theta}_i^* \dot{\theta}_i^* \right\}
\end{aligned} \tag{5.115b}$$

The total kinetic energy of the body can be casted by integrating Equation (5.115b) over the whole mid-plane as

$$T = \frac{1}{2} \int_A \rho \left\{ h \left(\dot{u}_i \dot{u}_i + \dot{w}^2 \right) + \frac{h^3}{12} \left(\dot{\theta}_i \dot{\theta}_i + 2\dot{u}_i \dot{u}_i^* + 2\dot{w} \dot{w}^* + \dot{\theta}_z^2 \right) \right. \\
\left. + \frac{h^5}{80} \left[\dot{u}_i \dot{u}_i^* + 2\dot{\theta}_i \dot{\theta}_i^* + \left(\dot{w}^* \right)^2 \right] + \frac{h^7}{448} \dot{\theta}_i^* \dot{\theta}_i^* \right\} dA \tag{5.116a}$$

which can be written in discretised form as

$$T = \frac{1}{2} \sum_k \rho_{(k)} \left\{ \left(\dot{u}_i^{(k)} \dot{u}_i^{(k)} + \dot{w}_{(k)}^2 \right) + \frac{h^2}{12} \left[\dot{\theta}_i^{(k)} \dot{\theta}_i^{(k)} + 2\dot{u}_i^{(k)} \dot{u}_i^{*(k)} + 2\dot{w}_{(k)} \dot{w}_{(k)}^* + \left(\dot{\theta}_z^{(k)} \right)^2 \right] \right. \\
\left. + \frac{h^4}{80} \left[\dot{u}_i^{*(k)} \dot{u}_i^{(k)} + 2\dot{\theta}_i^{(k)} \dot{\theta}_i^{*(k)} + \left(\dot{w}_{(k)}^* \right)^2 \right] + \frac{h^6}{448} \dot{\theta}_i^{*(k)} \dot{\theta}_i^{(k)} \right\} V_{(k)} \tag{5.116b}$$

where $V_{(k)}$ is the volume that contains the material point k .

The total potential energy stored in the body can be obtained by summing potential energies of all material points including strain energy and energy due to external loads as

$$U = \sum_k W_{FD}^{(k)} \left(\mathbf{u}_{(k)}, \mathbf{u}_{(1^k)}, \mathbf{u}_{(2^k)}, \mathbf{u}_{(2^k)}, \dots \right) V_{(k)} - \sum_k \mathbf{b}_{(k)} \mathbf{u}_{(k)} V_{(k)} \tag{5.117}$$

where \mathbf{b} is the body force density vector, which in this study has the following components

$$\mathbf{b} = \left(b_1 \quad b_2 \quad \hat{b}_1 \quad \hat{b}_2 \quad 0 \quad 0 \quad 0 \quad 0 \quad b_z \quad 0 \quad 0 \right)^T \tag{5.118}$$

and b_L , \hat{b}_L and b_z correspond to in-plane loads, moments and transverse body loads, respectively.

Assume the system is conservative, the first term of the Euler-Lagrange's equation can be obtained by inserting Equations (5.114) and (5.116) into Equation (5.113) as

$$\frac{d}{dt} \frac{\partial L}{\partial \dot{\mathbf{u}}_{(k)}} = \frac{d}{dt} \frac{\partial T}{\partial \dot{\mathbf{u}}_{(k)}} = \rho_{(k)} \left\{ \begin{array}{l} \ddot{u}_L^{(k)} + \frac{h^2}{12} \dot{u}_L^{*(k)} \\ \frac{h^2}{12} \ddot{\theta}_L^{(k)} + \frac{h^4}{80} \dot{\theta}_L^{*(k)} \\ \frac{h^2}{12} \ddot{u}_L^{(k)} + \frac{h^4}{80} \dot{u}_L^{*(k)} \\ \frac{h^4}{80} \ddot{\theta}_L^{(k)} + \frac{h^6}{448} \dot{\theta}_L^{*(k)} \\ \ddot{w}_{(k)} + \frac{h^2}{12} \dot{w}_{(k)} \\ \frac{h^2}{12} \ddot{\theta}_z^{(k)} \\ \frac{h^2}{12} \ddot{w}_{(k)} + \frac{h^4}{80} \dot{w}_{(k)} \end{array} \right\} V_{(k)} \quad (5.119)$$

Utilizing the pre-obtained expression, Eq. (3.8), the second term of the Euler-Lagrange's equation can be written by taking use of Eqs. (114) and (118) as

$$-\frac{\partial L}{\partial \mathbf{u}_{(k)}} = \left\{ \begin{array}{l} \frac{\partial W_{FD}^{(k)}}{\partial \bar{u}_L^{(k)}} V_{(k)} + \sum_j \frac{\partial W_{FD}^{(j)}}{\partial \bar{u}_L^{(k)}} V_{(j)} \\ \frac{\partial W_{FD}^{(k)}}{\partial \theta_L^{(k)}} V_{(k)} + \sum_j \frac{\partial W_{FD}^{(j)}}{\partial \theta_L^{(k)}} V_{(j)} \\ \frac{\partial W_{FD}^{(k)}}{\partial u_L^{*(k)}} V_{(k)} + \sum_j \frac{\partial W_{FD}^{(j)}}{\partial u_L^{*(k)}} V_{(j)} \\ \frac{\partial W_{FD}^{(k)}}{\partial \theta_L^{*(k)}} V_{(k)} + \sum_j \frac{\partial W_{FD}^{(j)}}{\partial \theta_L^{*(k)}} V_{(j)} \\ \frac{\partial W_{FD}^{(k)}}{\partial \bar{w}_{(k)}} V_{(k)} + \sum_j \frac{\partial W_{FD}^{(j)}}{\partial \bar{w}_{(k)}} V_{(j)} \\ \frac{\partial W_{FD}^{(k)}}{\partial \theta_z^{(k)}} V_{(k)} + \sum_j \frac{\partial W_{FD}^{(j)}}{\partial \theta_z^{(k)}} V_{(j)} \\ \frac{\partial W_{FD}^{(k)}}{\partial w_{(k)}} V_{(k)} + \sum_j \frac{\partial W_{FD}^{(j)}}{\partial w_{(k)}} V_{(j)} \end{array} \right\} - \left\{ \begin{array}{l} b_{u_L}^{(k)} \\ b_{\theta_L}^{(k)} \\ 0 \\ 0 \\ b_z^{(k)} \\ 0 \\ 0 \end{array} \right\} V_{(k)} \quad (5.120)$$

Plugging Eqs. (5.119) and (5.120) into the Lagrange's equation yields

$$\rho_{(k)} \left\{ \begin{array}{l} \ddot{u}_L^{(k)} + \frac{h^2}{12} \dot{u}_L^{*(k)} \\ \frac{h^2}{12} \ddot{\theta}_L^{(k)} + \frac{h^4}{80} \dot{\theta}_L^{*(k)} \\ \frac{h^2}{12} \ddot{u}_L^{(k)} + \frac{h^4}{80} \dot{u}_L^{*(k)} \\ \frac{h^4}{80} \ddot{\theta}_L^{(k)} + \frac{h^6}{448} \dot{\theta}_L^{*(k)} \\ \ddot{w}_{(k)} + \frac{h^2}{12} \dot{w}_{(k)} \\ \frac{h^2}{12} \ddot{\theta}_z^{(k)} \\ \frac{h^2}{12} \ddot{w}_{(k)} + \frac{h^4}{80} \dot{w}_{(k)} \end{array} \right\} = - \left\{ \begin{array}{l} \frac{\partial W_{FD}^{(k)}}{\partial \bar{u}_L^{(k)}} + \sum_j \frac{\partial W_{FD}^{(j)}}{\partial \bar{u}_L^{(k)}} \frac{V_{(j)}}{V_{(k)}} \\ \frac{\partial W_{FD}^{(k)}}{\partial \theta_L^{(k)}} + \sum_j \frac{\partial W_{FD}^{(j)}}{\partial \theta_L^{(k)}} \frac{V_{(j)}}{V_{(k)}} \\ \frac{\partial W_{FD}^{(k)}}{\partial u_L^{*(k)}} + \sum_j \frac{\partial W_{FD}^{(j)}}{\partial u_L^{*(k)}} \frac{V_{(j)}}{V_{(k)}} \\ \frac{\partial W_{FD}^{(k)}}{\partial \theta_L^{*(k)}} + \sum_j \frac{\partial W_{FD}^{(j)}}{\partial \theta_L^{*(k)}} \frac{V_{(j)}}{V_{(k)}} \\ \frac{\partial W_{FD}^{(k)}}{\partial \bar{w}_{(k)}} + \sum_j \frac{\partial W_{FD}^{(j)}}{\partial \bar{w}_{(k)}} \frac{V_{(j)}}{V_{(k)}} \\ \frac{\partial W_{FD}^{(k)}}{\partial \theta_z^{(k)}} + \sum_j \frac{\partial W_{FD}^{(j)}}{\partial \theta_z^{(k)}} \frac{V_{(j)}}{V_{(k)}} \\ \frac{\partial W_{FD}^{(k)}}{\partial w_{(k)}} + \sum_j \frac{\partial W_{FD}^{(j)}}{\partial w_{(k)}} \frac{V_{(j)}}{V_{(k)}} \end{array} \right\} + \left\{ \begin{array}{l} b_{u_L}^{(k)} \\ b_{\theta_L}^{(k)} \\ 0 \\ 0 \\ b_z^{(k)} \\ 0 \\ 0 \end{array} \right\} \quad (5.121)$$

In order to write the non-local form of strain energy function of the material point k , Equation (5.112b), it is necessary to transform all the local terms into an equivalent PD form by also considering PD strain energy expression given in Equation (5.117). As derived in Appendix A2.6, the strain energy density function of the material point k and its family member j can be expressed as

$$W_{\text{D}}^{(k)} = \frac{3}{\pi \delta^3 h^2} \left\{ \int_{-\frac{h}{2}}^{\frac{h}{2}} \frac{G}{2} dz \left[4 \sum_i \frac{[(\bar{u}_i^{(i^k)} - \bar{u}_i^{(k)}) n_i^{(i^k)(k)}]^2}{\xi_{(i^k)(k)}} V_{(i^k)} + \sum_i \left[\frac{1}{\xi_{(i^k)(k)}} \left(\bar{w}_{(i^k)} - \bar{w}_{(k)} + \frac{\theta_i^{(i^k)} + \theta_i^{(k)}}{2} \xi_{(i^k)(k)} n_i^{(i^k)(k)} \right)^2 + \left(\frac{\theta_z^{(i^k)} + \theta_z^{(k)}}{2} \right)^2 \xi_{(i^k)(k)} \right] V_{(i^k)} \right] \right. \\
+ \int_{-\frac{h}{2}}^{\frac{h}{2}} G dz \left\{ 4 \sum_i \frac{(\bar{u}_i^{(i^k)} - \bar{u}_i^{(k)}) (\theta_j^{(i^k)} - \theta_j^{(k)}) n_i^{(i^k)(k)} n_j^{(i^k)(k)}}{\xi_{(i^k)(k)}} V_{(i^k)} \right. \\
+ \left. \sum_i \left[\left(\bar{w}_{(i^k)} - \bar{w}_{(k)} + \frac{\theta_i^{(i^k)} + \theta_i^{(k)}}{2} \xi_{(i^k)(k)} n_i^{(i^k)(k)} \right) \left(\frac{\theta_z^{(i^k)} - \theta_z^{(k)}}{\xi_{(i^k)(k)}} + (u_i^{*(i^k)} + u_i^{*(k)}) n_i^{(i^k)(k)} \right) + \frac{(\theta_z^{(i^k)} + \theta_z^{(k)}) (w_{(i^k)}^* + w_{(k)}^*)}{2} \xi_{(i^k)(k)} \right] V_{(i^k)} \right\} \\
+ \int_{-\frac{h}{2}}^{\frac{h}{2}} \frac{G}{2} z^2 dz \left[4 \sum_i \frac{[(\theta_i^{(i^k)} - \theta_i^{(k)}) n_i^{(i^k)(k)}]^2 + 2(\bar{u}_i^{(i^k)} - \bar{u}_i^{(k)}) (u_j^{*(i^k)} - u_j^{*(k)}) n_i^{(i^k)(k)} n_j^{(i^k)(k)}}{\xi_{(i^k)(k)}} V_{(i^k)} \right. \\
+ \left. \sum_i \left[\frac{1}{\xi_{(i^k)(k)}} (\theta_z^{(i^k)} - \theta_z^{(k)} + (u_i^{*(i^k)} + u_i^{*(k)}) \xi_{(i^k)(k)} n_i^{(i^k)(k)})^2 + (w_{(i^k)}^* + w_{(k)}^*)^2 \xi_{(i^k)(k)} \right. \right. \\
+ \left. \left. 2 \left(\bar{w}_{(i^k)} - \bar{w}_{(k)} + \frac{\theta_i^{(i^k)} + \theta_i^{(k)}}{2} n_i^{(i^k)(k)} \right) \left(w_{(i^k)}^* - w_{(k)}^* + 3 \frac{\theta_i^{*(i^k)} + \theta_i^{*(k)}}{2} \xi_{(i^k)(k)} n_i^{(i^k)(k)} \right) \right] V_{(i^k)} \right] \\
+ \int_{-\frac{h}{2}}^{\frac{h}{2}} G z^3 dz \left\{ 4 \sum_i \frac{[(\bar{u}_i^{(i^k)} - \bar{u}_i^{(k)}) (\theta_j^{(i^k)} - \theta_j^{(k)}) + (\theta_i^{(i^k)} - \theta_i^{(k)}) (u_j^{*(i^k)} - u_j^{*(k)})] n_i^{(i^k)(k)} n_j^{(i^k)(k)}}{\xi_{(i^k)(k)}} V_{(i^k)} \right. \\
+ \left. \sum_i \left[w_{(i^k)}^* - w_{(k)}^* + \frac{3}{2} (\theta_i^{*(i^k)} + \theta_i^{*(k)}) \xi_{(i^k)(k)} n_i^{(i^k)(k)} \right] \left[\frac{\theta_z^{(i^k)} - \theta_z^{(k)}}{\xi_{(i^k)(k)}} + (u_j^{*(i^k)} + u_j^{*(k)}) n_j^{(i^k)(k)} \right] V_{(i^k)} \right\} \\
+ \int_{-\frac{h}{2}}^{\frac{h}{2}} \frac{G}{2} z^4 dz \left\{ 4 \sum_i \frac{[(u_i^{*(i^k)} - u_i^{*(k)}) n_i^{(i^k)(k)}]^2 + 2(\theta_i^{(i^k)} - \theta_i^{(k)}) (\theta_j^{(i^k)} - \theta_j^{(k)}) n_i^{(i^k)(k)} n_j^{(i^k)(k)} + (w_{(i^k)}^* - w_{(k)}^* + \frac{3}{2} (\theta_i^{*(i^k)} + \theta_i^{*(k)}) \xi_{(i^k)(k)} n_i^{(i^k)(k)})^2}{\xi_{(i^k)(k)}} V_{(i^k)} \right\} \\
+ 4 \int_{-\frac{h}{2}}^{\frac{h}{2}} G z^5 dz \sum_i \frac{(u_i^{*(i^k)} - u_i^{*(k)}) (\theta_j^{(i^k)} - \theta_j^{(k)}) n_i^{(i^k)(k)} n_j^{(i^k)(k)}}{\xi_{(i^k)(k)}} V_{(i^k)} + 4 \int_{-\frac{h}{2}}^{\frac{h}{2}} \frac{G}{2} z^6 dz \sum_i \frac{[(\theta_i^{*(i^k)} - \theta_i^{*(k)}) n_i^{(i^k)(k)}]^2}{\xi_{(i^k)(k)}} V_{(i^k)} \left. \right\}$$

$$\begin{aligned}
& + \frac{3}{\pi\delta^3 h^2} \left\{ \int_{-\frac{h}{2}}^{\frac{h}{2}} \frac{2Gv}{1-2\nu} dz \sum_i \left[\left(\frac{\theta_z^{(i^k)} + \theta_z^{(k)}}{2} \right) (\bar{u}_i^{(i^k)} - \bar{u}_i^{(k)}) n_i^{(i^k)(k)} + \left(\frac{\theta_z^{(i^k)} + \theta_z^{(k)}}{4} \right)^2 \xi_{(i^k)(k)} \right] V_{(i^k)} \right. \\
& + \int_{-\frac{h}{2}}^{\frac{h}{2}} \frac{2Gvz}{1-2\nu} dz \sum_i \left[(\dot{w}_{(i^k)}^* + \dot{w}_{(k)}^*) (\bar{u}_i^{(i^k)} - \bar{u}_i^{(k)}) n_i^{(i^k)(k)} + \frac{\theta_z^{(i^k)} + \theta_z^{(k)}}{2} \left((\theta_i^{(i^k)} - \theta_i^{(k)}) n_i^{(i^k)(k)} + \frac{\dot{w}_{(i^k)}^* + \dot{w}_{(k)}^*}{2} \xi_{(i^k)(k)} \right) \right] V_{(i^k)} \\
& + \int_{-\frac{h}{2}}^{\frac{h}{2}} \frac{2Gvz^2}{1-2\nu} dz \sum_i \left[(\dot{w}_{(i^k)}^* + \dot{w}_{(k)}^*) (\theta_i^{(i^k)} - \theta_i^{(k)}) n_i^{(i^k)(k)} + \frac{\theta_z^{(i^k)} + \theta_z^{(k)}}{2} (\dot{u}_i^{*(i^k)} - \dot{u}_i^{*(k)}) n_i^{(i^k)(k)} + \left(\frac{\dot{w}_{(i^k)}^* + \dot{w}_{(k)}^*}{2} \right)^2 \xi_{(i^k)(k)} \right] V_{(i^k)} \\
& + \int_{-\frac{h}{2}}^{\frac{h}{2}} \frac{2Gvz^3}{1-2\nu} dz \sum_i \left[(\dot{w}_{(i^k)}^* + \dot{w}_{(k)}^*) (\dot{u}_i^{*(i^k)} - \dot{u}_i^{*(k)}) n_i^{(i^k)(k)} + \frac{\theta_z^{(i^k)} + \theta_z^{(k)}}{2} (\theta_i^{*(i^k)} - \theta_i^{*(k)}) n_i^{(i^k)(k)} \right] V_{(i^k)} \\
& \left. + \int_{-\frac{h}{2}}^{\frac{h}{2}} \frac{2Gvz^4}{1-2\nu} dz \sum_i (\dot{w}_{(i^k)}^* + \dot{w}_{(k)}^*) (\theta_i^{*(i^k)} - \theta_i^{*(k)}) n_i^{(i^k)(k)} V_{(i^k)} \right\} \\
& + \frac{1}{h} \left(\frac{2}{\pi\delta^2 h} \right)^2 \left\{ \int_{-\frac{h}{2}}^{\frac{h}{2}} \frac{G}{2} \frac{4\nu-1}{1-2\nu} dz \left(\sum_i \frac{\bar{u}_i^{(i^k)} - \bar{u}_i^{(k)}}{\xi_{(i^k)(k)}} n_i^{(i^k)(k)} V_{(i^k)} \right)^2 + \int_{-\frac{h}{2}}^{\frac{h}{2}} \frac{G}{1-2\nu} z dz \sum_i \frac{\bar{u}_i^{(i^k)} - \bar{u}_i^{(k)}}{\xi_{(i^k)(k)}} n_i^{(i^k)(k)} V_{(i^k)} \sum_i \frac{\theta_j^{(i^k)} - \theta_j^{(k)}}{\xi_{(i^k)(k)}} n_j^{(i^k)(k)} V_{(i^k)} \right. \\
& + \int_{-\frac{h}{2}}^{\frac{h}{2}} \frac{G}{2} \frac{4\nu-1}{1-2\nu} z^2 dz \left[\left(\sum_i \frac{\theta_i^{(i^k)} - \theta_i^{(k)}}{\xi_{(i^k)(k)}} n_i^{(i^k)(k)} V_{(i^k)} \right)^2 + 2 \sum_i \frac{\bar{u}_i^{(i^k)} - \bar{u}_i^{(k)}}{\xi_{(i^k)(k)}} n_i^{(i^k)(k)} V_{(i^k)} \sum_i \frac{\dot{u}_j^{*(i^k)} - \dot{u}_j^{*(k)}}{\xi_{(i^k)(k)}} n_j^{(i^k)(k)} V_{(i^k)} \right] \\
& + \int_{-\frac{h}{2}}^{\frac{h}{2}} \frac{G}{1-2\nu} z^3 dz \left[\sum_i \frac{\bar{u}_i^{(i^k)} - \bar{u}_i^{(k)}}{\xi_{(i^k)(k)}} n_i^{(i^k)(k)} V_{(i^k)} \sum_i \frac{\theta_j^{*(i^k)} - \theta_j^{*(k)}}{\xi_{(i^k)(k)}} n_j^{(i^k)(k)} V_{(i^k)} + \sum_i \frac{\theta_i^{(i^k)} - \theta_i^{(k)}}{\xi_{(i^k)(k)}} n_i^{(i^k)(k)} V_{(i^k)} \sum_i \frac{\dot{u}_j^{*(i^k)} - \dot{u}_j^{*(k)}}{\xi_{(i^k)(k)}} n_j^{(i^k)(k)} V_{(i^k)} \right] \\
& + \int_{-\frac{h}{2}}^{\frac{h}{2}} \frac{G}{2} \frac{4\nu-1}{1-2\nu} z^4 dz \left[\left(\sum_i \frac{\dot{u}_i^{*(i^k)} - \dot{u}_i^{*(k)}}{\xi_{(i^k)(k)}} n_i^{(i^k)(k)} V_{(i^k)} \right)^2 + 2 \sum_i \frac{\theta_i^{(i^k)} - \theta_i^{(k)}}{\xi_{(i^k)(k)}} n_i^{(i^k)(k)} V_{(i^k)} \sum_i \frac{\theta_j^{*(i^k)} - \theta_j^{*(k)}}{\xi_{(i^k)(k)}} n_j^{(i^k)(k)} V_{(i^k)} \right] \\
& \left. + \int_{-\frac{h}{2}}^{\frac{h}{2}} \frac{G}{1-2\nu} z^5 dz \sum_i \frac{\dot{u}_i^{*(i^k)} - \dot{u}_i^{*(k)}}{\xi_{(i^k)(k)}} n_i^{(i^k)(k)} V_{(i^k)} \sum_i \frac{\theta_j^{*(i^k)} - \theta_j^{*(k)}}{\xi_{(i^k)(k)}} n_j^{(i^k)(k)} V_{(i^k)} + \int_{-\frac{h}{2}}^{\frac{h}{2}} \frac{G}{2} \frac{4\nu-1}{1-2\nu} z^6 dz \left(\sum_i \frac{\theta_i^{*(i^k)} - \theta_i^{*(k)}}{\xi_{(i^k)(k)}} n_i^{(i^k)(k)} V_{(i^k)} \right)^2 \right\}
\end{aligned}$$

(5.122a)

$$W_{FD}^{(i)} = \frac{3}{\pi \delta^3 h^2} \left\{ \int_{-\frac{h}{2}}^{\frac{h}{2}} \frac{G}{2} dz \left\{ 4 \sum_i \frac{[(\bar{u}_i^{(i)} - \bar{u}_i^{(j)}) n_i^{(i)(j)}]^2}{\xi_{(i^*)(k)}} V_{(i)} + \sum_i \left[\frac{1}{\xi_{(i^*)(j)}} \left(\bar{w}_{(i)} - \bar{w}_{(j)} + \frac{\theta_i^{(i)} + \theta_i^{(j)}}{2} \xi_{(i^*)(j)} n_i^{(i)(j)} \right)^2 + \left(\frac{\theta_z^{(i)} + \theta_z^{(j)}}{2} \right)^2 \xi_{(i^*)(j)} \right] V_{(i)} \right\} \right. \\
+ \int_{-\frac{h}{2}}^{\frac{h}{2}} G dz \left\{ 4 \sum_i \frac{(\bar{u}_i^{(i)} - \bar{u}_i^{(j)}) (\theta_j^{(i)} - \theta_j^{(j)}) n_i^{(i)(j)} n_j^{(i)(j)}}{\xi_{(i^*)(j)}} V_{(i)} \right. \\
+ \left. \sum_i \left[\left(\bar{w}_{(i)} - \bar{w}_{(j)} + \frac{\theta_i^{(i)} + \theta_i^{(j)}}{2} \xi_{(i^*)(j)} n_i^{(i)(j)} \right) \left(\frac{\theta_z^{(i)} - \theta_z^{(j)}}{\xi_{(i^*)(j)}} + (u_i^{*(i)} + u_i^{*(j)}) n_i^{(i)(j)} \right) + \frac{(\theta_z^{(i)} + \theta_z^{(j)}) (\dot{w}_{(i)} + \dot{w}_{(j)})}{2} \xi_{(i^*)(j)} \right] V_{(i)} \right\} \\
+ \int_{-\frac{h}{2}}^{\frac{h}{2}} \frac{G}{2} z^2 dz \left\{ 4 \sum_i \frac{[(\theta_i^{(i)} - \theta_i^{(j)}) n_i^{(i)(j)}]^2 + 2(\bar{u}_i^{(i)} - \bar{u}_i^{(j)}) (u_j^{*(i)} - u_j^{*(j)}) n_i^{(i)(j)} n_j^{(i)(j)}}{\xi_{(i^*)(j)}} V_{(i)} \right. \\
+ \left. \sum_i \left[\frac{1}{\xi_{(i^*)(k)}} (\theta_z^{(i)} - \theta_z^{(j)} + (u_i^{*(i)} + u_i^{*(j)}) \xi_{(i^*)(j)} n_i^{(i)(j)})^2 + (\dot{w}_{(i)} + \dot{w}_{(j)})^2 \xi_{(i^*)(j)} \right. \right. \\
+ \left. \left. 2 \left(\frac{\bar{w}_{(i)} - \bar{w}_{(j)}}{\xi_{(i^*)(j)}} + \frac{\theta_i^{(i)} + \theta_i^{(j)}}{2} n_i^{(i)(j)} \right) \left(\dot{w}_{(i)} - \dot{w}_{(j)} + 3 \frac{\theta_i^{*(i)} + \theta_i^{*(j)}}{2} \xi_{(i^*)(j)} n_i^{(i)(j)} \right) \right] V_{(i)} \right\} \\
+ \int_{-\frac{h}{2}}^{\frac{h}{2}} G^3 dz \left\{ 4 \sum_i \frac{[(\bar{u}_i^{(i)} - \bar{u}_i^{(j)}) (\theta_j^{*(i)} - \theta_j^{*(j)}) + (\theta_i^{(i)} - \theta_i^{(j)}) (u_j^{*(i)} - u_j^{*(j)})] n_i^{(i)(j)} n_j^{(i)(j)}}{\xi_{(i^*)(j)}} V_{(i)} \right. \\
+ \left. \sum_i \left[\dot{w}_{(i)} - \dot{w}_{(j)} + \frac{3}{2} (\theta_i^{*(i)} + \theta_i^{*(j)}) \xi_{(i^*)(j)} n_i^{(i)(j)} \right] \left[\frac{\theta_z^{(i)} - \theta_z^{(j)}}{\xi_{(i^*)(j)}} + (u_j^{*(i)} + u_j^{*(j)}) n_j^{(i)(j)} \right] V_{(i)} \right\} \\
+ \int_{-\frac{h}{2}}^{\frac{h}{2}} \frac{G}{2} z^4 dz \left\{ 4 \sum_i \frac{[(u_i^{*(i)} - u_i^{*(j)}) n_i^{(i)(j)}]^2 + 2(\theta_i^{(i)} - \theta_i^{(j)}) (\theta_j^{*(i)} - \theta_j^{*(j)}) n_i^{(i)(j)} n_j^{(i)(j)} + (\dot{w}_{(i)} - \dot{w}_{(j)} + \frac{3}{2} (\theta_i^{*(i)} + \theta_i^{*(j)}) \xi_{(i^*)(j)} n_i^{(i)(j)})^2}{\xi_{(i^*)(j)}} V_{(i)} \right\} \\
+ 4 \int_{-\frac{h}{2}}^{\frac{h}{2}} G^5 dz \sum_i \frac{(u_i^{*(i)} - u_i^{*(j)}) (\theta_j^{*(i)} - \theta_j^{*(j)}) n_i^{(i)(j)} n_j^{(i)(j)}}{\xi_{(i^*)(j)}} V_{(i)} + 4 \int_{-\frac{h}{2}}^{\frac{h}{2}} \frac{G}{2} z^6 dz \sum_i \frac{[(\theta_i^{*(i)} - \theta_i^{*(j)}) n_i^{(i)(j)}]^2}{\xi_{(i^*)(j)}} V_{(i)} \left. \right\}$$

$$\begin{aligned}
& + \frac{3}{\pi\delta^3 h^2} \left\{ \int_{-\frac{h}{2}}^{\frac{h}{2}} \frac{2G\nu}{1-2\nu} dz \sum_i \left[\left(\frac{\theta_z^{(i)} + \theta_z^{(j)}}{2} \right) (\bar{u}_i^{(i)} - \bar{u}_i^{(j)}) n_i^{(i)(j)} + \left(\frac{\theta_z^{(i)} + \theta_z^{(j)}}{4} \right)^2 \xi_{(i)(j)} \right] V_{(i)} \right. \\
& + \int_{-\frac{h}{2}}^{\frac{h}{2}} \frac{2G\nu z}{1-2\nu} dz \sum_i \left[(\dot{w}_{(i)} + \dot{w}_{(j)}) (\bar{u}_i^{(i)} - \bar{u}_i^{(j)}) n_i^{(i)(j)} + \frac{\theta_z^{(i)} + \theta_z^{(j)}}{2} \left((\theta_i^{(i)} - \theta_i^{(j)}) n_i^{(i)(j)} + \frac{\dot{w}_{(i)} + \dot{w}_{(j)}}{2} \xi_{(i)(j)} \right) \right] V_{(i)} \\
& + \int_{-\frac{h}{2}}^{\frac{h}{2}} \frac{2G\nu z^2}{1-2\nu} dz \sum_i \left[(\dot{w}_{(i)} + \dot{w}_{(j)}) (\theta_i^{(i)} - \theta_i^{(j)}) n_i^{(i)(j)} + \frac{\theta_z^{(i)} + \theta_z^{(j)}}{2} (u_i^{*(i)} - u_i^{*(j)}) n_i^{(i)(j)} + \left(\frac{\dot{w}_{(i)} + \dot{w}_{(j)}}{2} \right)^2 \xi_{(i)(j)} \right] V_{(i)} \\
& + \int_{-\frac{h}{2}}^{\frac{h}{2}} \frac{2G\nu z^3}{1-2\nu} dz \sum_i \left[(\dot{w}_{(i)} + \dot{w}_{(j)}) (u_i^{*(i)} - u_i^{*(j)}) n_i^{(i)(j)} + \frac{\theta_z^{(i)} + \theta_z^{(j)}}{2} (\theta_i^{*(i)} - \theta_i^{*(j)}) n_i^{(i)(j)} \right] V_{(i)} \\
& \left. + \int_{-\frac{h}{2}}^{\frac{h}{2}} \frac{2G\nu z^4}{1-2\nu} dz \sum_i (\dot{w}_{(i)} + \dot{w}_{(j)}) (\theta_i^{*(i)} - \theta_i^{*(j)}) n_i^{(i)(j)} V_{(i)} \right\} \\
& + \left(\frac{2}{\pi\delta^2 h} \right)^2 \left\{ \int_{-\frac{h}{2}}^{\frac{h}{2}} \frac{G}{2} \frac{4\nu - 1}{1-2\nu} dz \left(\sum_i \frac{\bar{u}_i^{(i)} - \bar{u}_i^{(j)}}{\xi_{(i)(j)}} n_i^{(i)(j)} V_{(i)} \right)^2 + \int_{-\frac{h}{2}}^{\frac{h}{2}} \frac{G}{1-2\nu} z dz \sum_i \frac{\bar{u}_i^{(i)} - \bar{u}_i^{(j)}}{\xi_{(i)(j)}} n_i^{(i)(j)} V_{(i)} \sum_i \frac{\theta_j^{(i)} - \theta_j^{(j)}}{\xi_{(i)(j)}} n_j^{(i)(j)} V_{(i)} \right. \\
& + \int_{-\frac{h}{2}}^{\frac{h}{2}} \frac{G}{2} \frac{4\nu - 1}{1-2\nu} z^2 dz \left[\left(\sum_i \frac{\theta_i^{(i)} - \theta_i^{(j)}}{\xi_{(i)(j)}} n_i^{(i)(j)} V_{(i)} \right)^2 + 2 \sum_i \frac{\bar{u}_i^{(i)} - \bar{u}_i^{(j)}}{\xi_{(i)(j)}} n_i^{(i)(j)} V_{(i)} \sum_i \frac{u_j^{*(i)} - u_j^{*(j)}}{\xi_{(i)(j)}} n_j^{(i)(j)} V_{(i)} \right] \\
& + \int_{-\frac{h}{2}}^{\frac{h}{2}} \frac{G}{1-2\nu} z^3 dz \left[\sum_i \frac{\bar{u}_i^{(i)} - \bar{u}_i^{(j)}}{\xi_{(i)(j)}} n_i^{(i)(j)} V_{(i)} \sum_i \frac{\theta_j^{*(i)} - \theta_j^{*(j)}}{\xi_{(i)(j)}} n_j^{(i)(j)} V_{(i)} + \sum_i \frac{\theta_i^{(i)} - \theta_i^{(j)}}{\xi_{(i)(j)}} n_i^{(i)(j)} V_{(i)} \sum_i \frac{u_j^{*(i)} - u_j^{*(j)}}{\xi_{(i)(j)}} n_j^{(i)(j)} V_{(i)} \right] \\
& + \int_{-\frac{h}{2}}^{\frac{h}{2}} \frac{G}{2} \frac{4\nu - 1}{1-2\nu} z^4 dz \left[\left(\sum_i \frac{u_i^{*(i)} - u_i^{*(j)}}{\xi_{(i)(j)}} n_i^{(i)(j)} V_{(i)} \right)^2 + 2 \sum_i \frac{\theta_i^{(i)} - \theta_i^{(j)}}{\xi_{(i)(j)}} n_i^{(i)(j)} V_{(i)} \sum_i \frac{\theta_j^{*(i)} - \theta_j^{*(j)}}{\xi_{(i)(j)}} n_j^{(i)(j)} V_{(i)} \right] \\
& \left. + \int_{-\frac{h}{2}}^{\frac{h}{2}} \frac{G}{1-2\nu} z^5 dz \sum_i \frac{u_i^{*(i)} - u_i^{*(j)}}{\xi_{(i)(j)}} n_i^{(i)(j)} V_{(i)} \sum_i \frac{\theta_j^{*(i)} - \theta_j^{*(j)}}{\xi_{(i)(j)}} n_j^{(i)(j)} V_{(i)} + \int_{-\frac{h}{2}}^{\frac{h}{2}} \frac{G}{2} \frac{4\nu - 1}{1-2\nu} z^6 dz \left(\sum_i \frac{\theta_i^{*(i)} - \theta_i^{*(j)}}{\xi_{(i)(j)}} n_i^{(i)(j)} V_{(i)} \right)^2 \right\}
\end{aligned}$$

(5.122b)

The complete PD EoM for functionally graded high order plate can be obtained by plugging (5.122a) and (5.122b) into (5.121) as

$$\begin{aligned}
& \rho_{(k)} \left(\ddot{u}_L^{(k)} + \frac{h^2}{12} \dot{u}_L^{*(k)} \right) \\
&= \frac{24}{\pi \delta^3 h^2} \left[\int_{-\frac{h}{2}}^{\frac{h}{2}} G dz \sum_j \frac{\bar{u}_l^{(j)} - \bar{u}_l^{(k)}}{\xi_{(j)(k)}} n_l^{(j)(k)} n_L^{(j)(k)} V_{(j)} + \int_{-\frac{h}{2}}^{\frac{h}{2}} \frac{G \nu}{1-2\nu} dz \sum_j \frac{\theta_z^{(j)} + \theta_z^{(k)}}{4} n_L^{(j)(k)} V_{(j)} \right. \\
&\quad + \int_{-\frac{h}{2}}^{\frac{h}{2}} G dz \sum_j \frac{\theta_l^{(j)} - \theta_l^{(k)}}{\xi_{(j)(k)}} n_l^{(j)(k)} n_L^{(j)(k)} V_{(j)} + \int_{-\frac{h}{2}}^{\frac{h}{2}} \frac{G \nu z}{1-2\nu} dz \sum_j \frac{w_{(j)}^* + w_{(k)}^*}{2} n_L^{(j)(k)} V_{(j)} \\
&\quad \left. + \int_{-\frac{h}{2}}^{\frac{h}{2}} G z^2 dz \sum_j \frac{u_l^{*(j)} - u_l^{*(k)}}{\xi_{(j)(k)}} n_l^{(j)(k)} n_L^{(j)(k)} V_{(j)} + \int_{-\frac{h}{2}}^{\frac{h}{2}} G z^3 dz \sum_j \frac{\theta_l^{*(j)} - \theta_l^{*(k)}}{\xi_{(j)(k)}} n_l^{(j)(k)} n_L^{(j)(k)} V_{(j)} \right] \\
&+ \frac{2}{\pi \delta^2 h^2} \left[\int_{-\frac{h}{2}}^{\frac{h}{2}} G \frac{4\nu-1}{1-2\nu} dz \sum_j \frac{\Theta_{(k)} + \Theta_{(j)}}{\xi_{(j)(k)}} n_L^{(j)(k)} V_{(j)} + \int_{-\frac{h}{2}}^{\frac{h}{2}} G \frac{4\nu-1}{1-2\nu} z dz \sum_j \frac{\Phi_{(k)} + \Phi_{(j)}}{\xi_{(j)(k)}} n_L^{(j)(k)} V_{(j)} \right. \\
&\quad \left. + \int_{-\frac{h}{2}}^{\frac{h}{2}} G \frac{4\nu-1}{1-2\nu} z^2 dz \sum_j \frac{\Theta_{(k)}^* + \Theta_{(j)}^*}{\xi_{(j)(k)}} n_L^{(j)(k)} V_{(j)} + \int_{-\frac{h}{2}}^{\frac{h}{2}} G \frac{4\nu-1}{1-2\nu} z^3 dz \sum_j \frac{\Phi_{(k)}^* + \Phi_{(j)}^*}{\xi_{(j)(k)}} n_L^{(j)(k)} V_{(j)} \right] + b_{u_L}^{(k)} \tag{5.123a}
\end{aligned}$$

$$\begin{aligned}
& \rho_{(k)} \left(\frac{h^2}{12} \ddot{\theta}_L^{(k)} + \frac{h^4}{80} \dot{\theta}_L^{*(k)} \right) \\
&= \frac{24}{\pi \delta^3 h^2} \left[\int_{-\frac{h}{2}}^{\frac{h}{2}} G dz \sum_j \frac{\bar{u}_l^{(j)} - \bar{u}_l^{(k)}}{\xi_{(j)(k)}} n_l^{(j)(k)} n_L^{(j)(k)} V_{(j)} + \int_{-\frac{h}{2}}^{\frac{h}{2}} \frac{G \nu z}{1-2\nu} dz \sum_j \frac{\theta_z^{(j)} + \theta_z^{(k)}}{4} n_L^{(j)(k)} V_{(j)} \right. \\
&\quad + \int_{-\frac{h}{2}}^{\frac{h}{2}} G z^2 dz \sum_j \frac{\theta_l^{(j)} - \theta_l^{(k)}}{\xi_{(j)(k)}} n_l^{(j)(k)} n_L^{(j)(k)} V_{(j)} + \int_{-\frac{h}{2}}^{\frac{h}{2}} \frac{G \nu z^2}{1-2\nu} dz \sum_j \frac{w_{(j)}^* + w_{(k)}^*}{2} n_L^{(j)(k)} V_{(j)} \\
&\quad \left. + \int_{-\frac{h}{2}}^{\frac{h}{2}} G z^3 dz \sum_j \frac{u_l^{*(j)} - u_l^{*(k)}}{\xi_{(j)(k)}} n_l^{(j)(k)} n_L^{(j)(k)} V_{(j)} + \int_{-\frac{h}{2}}^{\frac{h}{2}} G z^4 dz \sum_j \frac{\theta_l^{*(j)} - \theta_l^{*(k)}}{\xi_{(j)(k)}} n_l^{(j)(k)} n_L^{(j)(k)} V_{(j)} \right] \\
&- \frac{3}{\pi \delta^3 h^2} \left\{ \int_{-\frac{h}{2}}^{\frac{h}{2}} G dz \sum_j \left(\bar{w}_{(j)} - \bar{w}_{(k)} + \frac{\theta_l^{(j)} + \theta_l^{(k)}}{2} \frac{\xi_{(j)(k)}}{\xi_{(j)(k)}} n_l^{(j)(k)} \right) n_L^{(j)(k)} V_{(j)} \right. \\
&\quad \left. + \int_{-\frac{h}{2}}^{\frac{h}{2}} G dz \sum_j \left[\theta_z^{(j)} - \theta_z^{(k)} + (u_l^{*(j)} + u_l^{*(k)}) \frac{\xi_{(j)(k)}}{\xi_{(j)(k)}} n_l^{(j)(k)} \right] n_L^{(j)(k)} V_{(j)} \right\} \\
&\quad \left. + \int_{-\frac{h}{2}}^{\frac{h}{2}} G z^2 dz \sum_j \left(w_{(j)}^* - w_{(k)}^* + 3 \frac{\theta_l^{*(j)} + \theta_l^{*(k)}}{2} \frac{\xi_{(j)(k)}}{\xi_{(j)(k)}} n_l^{(j)(k)} \right) n_L^{(j)(k)} V_{(j)} \right\} \\
&+ \frac{2}{\pi \delta^2 h^2} \left(\int_{-\frac{h}{2}}^{\frac{h}{2}} G \frac{4\nu-1}{1-2\nu} z dz \sum_j \frac{\Theta_{(k)} + \Theta_{(j)}}{\xi_{(j)(k)}} V_{(j)} + \int_{-\frac{h}{2}}^{\frac{h}{2}} G \frac{4\nu-1}{1-2\nu} z^2 dz \sum_j \frac{\Phi_{(k)} + \Phi_{(j)}}{\xi_{(j)(k)}} V_{(j)} \right. \\
&\quad \left. + \int_{-\frac{h}{2}}^{\frac{h}{2}} G \frac{4\nu-1}{1-2\nu} z^3 dz \sum_j \frac{\Theta_{(k)}^* + \Theta_{(j)}^*}{\xi_{(j)(k)}} V_{(j)} + \int_{-\frac{h}{2}}^{\frac{h}{2}} G \frac{4\nu-1}{1-2\nu} z^4 dz \sum_j \frac{\Phi_{(k)}^* + \Phi_{(j)}^*}{\xi_{(j)(k)}} V_{(j)} \right) + b_{\theta_L}^{(k)} \tag{5.123b}
\end{aligned}$$

$$\begin{aligned}
& \rho_{(k)} \left(\frac{h^2}{12} \ddot{u}_L^{(k)} + \frac{h^4}{80} \dot{u}_L^{*(k)} \right) \\
&= \frac{24}{\pi \delta^3 h^2} \left[\int_{-\frac{h}{2}}^{\frac{h}{2}} \mathcal{G}^2 dz \sum_j \frac{\bar{u}_l^{(j)} - \bar{u}_l^{(k)}}{\xi_{(j)(k)}} n_l^{(j)(k)} n_L^{(j)(k)} V_{(j)} + \int_{-\frac{h}{2}}^{\frac{h}{2}} \frac{G \nu z^2}{1-2\nu} dz \sum_j \frac{\theta_z^{(j)} + \theta_z^{(k)}}{4} n_L^{(j)(k)} V_{(j)} \right. \\
&\quad \left. + \int_{-\frac{h}{2}}^{\frac{h}{2}} \mathcal{G}^3 dz \sum_j \frac{\theta_l^{(j)} - \theta_l^{(k)}}{\xi_{(j)(k)}} n_l^{(j)(k)} n_L^{(j)(k)} V_{(j)} + \int_{-\frac{h}{2}}^{\frac{h}{2}} \frac{G \nu z^3}{1-2\nu} dz \sum_j \frac{\dot{w}_{(j)} + \dot{w}_{(k)}}{2} n_L^{(j)(k)} V_{(j)} \right. \\
&\quad \left. + \int_{-\frac{h}{2}}^{\frac{h}{2}} \mathcal{G}^4 dz \sum_j \frac{u_l^{*(j)} - u_l^{*(k)}}{\xi_{(j)(k)}} n_l^{(j)(k)} n_L^{(j)(k)} V_{(j)} + \int_{-\frac{h}{2}}^{\frac{h}{2}} \mathcal{G}^5 dz \sum_j \frac{\theta_l^{*(j)} - \theta_l^{*(k)}}{\xi_{(j)(k)}} n_l^{(j)(k)} n_L^{(j)(k)} V_{(j)} \right] \\
&- \frac{6}{\pi \delta^3 h^2} \left\{ \int_{-\frac{h}{2}}^{\frac{h}{2}} \mathcal{G} dz \sum_j \left(\bar{w}_{(j)} - \bar{w}_{(k)} + \frac{\theta_l^{(j)} + \theta_l^{(k)}}{2} \xi_{(j)(k)} n_l^{(j)(k)} \right) n_L^{(j)(k)} V_{(j)} \right. \\
&\quad \left. + \int_{-\frac{h}{2}}^{\frac{h}{2}} \mathcal{G}^2 dz \sum_j \left[\theta_z^{(j)} - \theta_z^{(k)} + (u_l^{*(j)} + u_l^{*(k)}) \xi_{(j)(k)} n_l^{(j)(k)} \right] n_L^{(j)(k)} V_{(j)} \right\} \\
&\quad \left. + \int_{-\frac{h}{2}}^{\frac{h}{2}} \mathcal{G}^3 dz \sum_j \left(\dot{w}_{(j)} - \dot{w}_{(k)} + 3 \frac{\theta_l^{*(j)} + \theta_l^{*(k)}}{2} \xi_{(j)(k)} n_l^{(j)(k)} \right) n_L^{(j)(k)} V_{(j)} \right\} \\
&+ \frac{2}{\pi \delta^2 h^2} \left(\int_{-\frac{h}{2}}^{\frac{h}{2}} G \frac{4\nu-1}{1-2\nu} z^2 dz \sum_j \frac{\Theta_{(j)} + \Theta_{(k)}}{\xi_{(j)(k)}} n_L^{(j)(k)} V_{(j)} + \int_{-\frac{h}{2}}^{\frac{h}{2}} G \frac{4\nu-1}{1-2\nu} z^3 dz \sum_j \frac{\Phi_{(j)} + \Phi_{(k)}}{\xi_{(j)(k)}} n_L^{(j)(k)} V_{(j)} \right. \\
&\quad \left. + \int_{-\frac{h}{2}}^{\frac{h}{2}} G \frac{4\nu-1}{1-2\nu} z^4 dz \sum_j \frac{\Theta_{(j)}^* + \Theta_{(k)}^*}{\xi_{(j)(k)}} n_L^{(j)(k)} V_{(j)} + \int_{-\frac{h}{2}}^{\frac{h}{2}} G \frac{4\nu-1}{1-2\nu} z^5 dz \sum_j \frac{\Phi_{(j)}^* + \Phi_{(k)}^*}{\xi_{(j)(k)}} n_L^{(j)(k)} V_{(j)} \right)
\end{aligned} \tag{5.123c}$$

$$\begin{aligned}
& \rho_{(k)} \left(\frac{h^4}{80} \ddot{\theta}_L^{(k)} + \frac{h^6}{448} \ddot{\theta}_L^{*(k)} \right) \\
&= \frac{24}{\pi \delta^3 h^2} \left(\int_{-\frac{h}{2}}^{\frac{h}{2}} \mathcal{G}^3 dz \sum_j \frac{\bar{u}_l^{(j)} - \bar{u}_l^{(k)}}{\xi_{(j)(k)}} n_l^{(j)(k)} n_L^{(j)(k)} V_{(j)} + \int_{-\frac{h}{2}}^{\frac{h}{2}} \frac{G \nu z^3}{1-2\nu} dz \sum_j \frac{\theta_z^{(j)} + \theta_z^{(k)}}{4} n_L^{(j)(k)} V_{(j)} \right. \\
&\quad \left. + \int_{-\frac{h}{2}}^{\frac{h}{2}} \mathcal{G}^4 dz \sum_j \frac{\theta_l^{(j)} - \theta_l^{(k)}}{\xi_{(j)(k)}} n_l^{(j)(k)} n_L^{(j)(k)} V_{(j)} + \int_{-\frac{h}{2}}^{\frac{h}{2}} \frac{G \nu z^4}{1-2\nu} dz \sum_j \frac{\dot{w}_{(j)} + \dot{w}_{(k)}}{2} n_L^{(j)(k)} V_{(j)} \right. \\
&\quad \left. + \int_{-\frac{h}{2}}^{\frac{h}{2}} \mathcal{G}^5 dz \sum_j \frac{u_l^{*(j)} - u_l^{*(k)}}{\xi_{(j)(k)}} n_l^{(j)(k)} n_L^{(j)(k)} V_{(j)} + \int_{-\frac{h}{2}}^{\frac{h}{2}} \mathcal{G}^6 dz \sum_j \frac{\theta_l^{*(j)} - \theta_l^{*(k)}}{\xi_{(j)(k)}} n_l^{(j)(k)} n_L^{(j)(k)} V_{(j)} \right) \\
&- \frac{9}{\pi \delta^3 h^2} \left\{ \int_{-\frac{h}{2}}^{\frac{h}{2}} \mathcal{G}^2 dz \sum_j \left(\bar{w}_{(j)} - \bar{w}_{(k)} + \frac{\theta_l^{(j)} + \theta_l^{(k)}}{2} \xi_{(j)(k)} n_l^{(j)(k)} \right) n_L^{(j)(k)} V_{(j)} \right. \\
&\quad \left. + \int_{-\frac{h}{2}}^{\frac{h}{2}} \mathcal{G}^3 dz \sum_j \left[\theta_z^{(j)} - \theta_z^{(k)} + (u_l^{*(j)} + u_l^{*(k)}) \xi_{(j)(k)} n_l^{(j)(k)} \right] n_L^{(j)(k)} V_{(j)} \right\} \\
&\quad \left. + \int_{-\frac{h}{2}}^{\frac{h}{2}} \mathcal{G}^4 dz \sum_j \left(\dot{w}_{(j)} - \dot{w}_{(k)} + 3 \frac{\theta_l^{*(j)} + \theta_l^{*(k)}}{2} \xi_{(j)(k)} n_l^{(j)(k)} \right) n_L^{(j)(k)} V_{(j)} \right\} \\
&\frac{2}{\pi \delta^2 h^2} \left\{ \int_{-\frac{h}{2}}^{\frac{h}{2}} G \frac{4\nu-1}{1-2\nu} z^3 dz \sum_j \frac{\Theta_{(k)} + \Theta_{(j)}}{\xi_{(j)(k)}} n_L^{(j)(k)} V_{(j)} + \int_{-\frac{h}{2}}^{\frac{h}{2}} G \frac{4\nu-1}{1-2\nu} z^4 dz \sum_j \frac{\Phi_{(k)} + \Phi_{(j)}}{\xi_{(j)(k)}} n_L^{(j)(k)} V_{(j)} \right. \\
&\quad \left. + \int_{-\frac{h}{2}}^{\frac{h}{2}} G \frac{4\nu-1}{1-2\nu} z^5 dz \sum_j \frac{\Theta_{(k)}^* + \Theta_{(j)}^*}{\xi_{(j)(k)}} n_L^{(j)(k)} V_{(j)} + \int_{-\frac{h}{2}}^{\frac{h}{2}} G \frac{4\nu-1}{1-2\nu} z^6 dz \sum_j \frac{\Phi_{(k)}^* + \Phi_{(j)}^*}{\xi_{(j)(k)}} n_L^{(j)(k)} V_{(j)} \right\}
\end{aligned} \tag{5.123d}$$

$$\rho_{(k)} \left(\ddot{\bar{W}}_{(k)} + \frac{h^2}{12} \dot{W}_{(k)}^* \right) = \frac{6}{\pi \delta^3 h^2} \left[\int_{-\frac{h}{2}}^{\frac{h}{2}} \mathcal{G} z \sum_j \left(\frac{\bar{W}_{(j)} - \bar{W}_{(k)}}{\xi_{(j)(k)}} + \frac{\theta_l^{(j)} + \theta_l^{(k)}}{2} n_l^{(j)(k)} \right) V_{(j)} \right. \\ \left. + \int_{-\frac{h}{2}}^{\frac{h}{2}} \mathcal{G} z \sum_j \left[\frac{\theta_z^{(j)} - \theta_z^{(k)}}{\xi_{(j)(k)}} + (u_i^{*(j)} + u_i^{*(k)}) n_l^{(j)(k)} \right] V_{(j)} \right] + \mathcal{D}_z^{(k)} \quad (5.123e)$$

$$\rho_{(k)} \frac{h^2}{12} \ddot{\theta}_z^{(k)} = \frac{6}{\pi \delta^3 h^2} \left\{ \int_{-\frac{h}{2}}^{\frac{h}{2}} \mathcal{G} z \sum_j \left(\frac{\bar{W}_{(j)} - \bar{W}_{(k)}}{\xi_{(j)(k)}} + \frac{\theta_l^{(j)} + \theta_l^{(k)}}{2} n_l^{(j)(k)} \right) V_{(j)} \right. \\ \left. + \int_{-\frac{h}{2}}^{\frac{h}{2}} \mathcal{G}^2 z \sum_j \left[\frac{\theta_z^{(j)} - \theta_z^{(k)}}{\xi_{(j)(k)}} + (u_i^{*(j)} + u_i^{*(k)}) n_l^{(j)(k)} \right] V_{(j)} \right. \\ \left. + \int_{-\frac{h}{2}}^{\frac{h}{2}} \mathcal{G}^3 z \sum_j \left(\frac{W_{(j)}^* - W_{(k)}^*}{\xi_{(j)(k)}} + 3 \frac{\theta_l^{*(j)} + \theta_l^{*(k)}}{2} n_l^{(j)(k)} \right) V_{(j)} \right. \\ \left. - \int_{-\frac{h}{2}}^{\frac{h}{2}} \mathcal{G} \frac{1-\nu}{1-2\nu} dz \sum_j \frac{\theta_z^{(j)} + \theta_z^{(k)}}{4} \xi_{(j)(k)} V_{(j)} - \int_{-\frac{h}{2}}^{\frac{h}{2}} \frac{\mathcal{G} \nu}{1-2\nu} dz \sum_j (\bar{u}_l^{(j)} - \bar{u}_l^{(k)}) n_l^{(j)(k)} V_{(j)} \right. \\ \left. - \int_{-\frac{h}{2}}^{\frac{h}{2}} \mathcal{G} \frac{1-\nu}{1-2\nu} z dz \sum_j \frac{W_{(j)}^* + W_{(k)}^*}{2} \xi_{(j)(k)} V_{(j)} - \int_{-\frac{h}{2}}^{\frac{h}{2}} \frac{\mathcal{G} \nu z}{1-2\nu} dz \sum_j (\theta_l^{(j)} - \theta_l^{(k)}) n_l^{(j)(k)} V_{(j)} \right. \\ \left. - \int_{-\frac{h}{2}}^{\frac{h}{2}} \frac{\mathcal{G} \nu z^2}{1-2\nu} dz \sum_j (u_i^{*(j)} - u_i^{*(k)}) n_l^{(j)(k)} V_{(j)} - \int_{-\frac{h}{2}}^{\frac{h}{2}} \frac{\mathcal{G} \nu z^3}{1-2\nu} dz \sum_j (\theta_l^{*(j)} - \theta_l^{*(k)}) n_l^{(j)(k)} V_{(j)} \right\} \quad (5.123f)$$

$$\rho_{(k)} \left(\frac{h^2}{12} \ddot{W}_{(k)} + \frac{h^4}{80} \dot{W}_{(k)}^* \right) \\ = \frac{6}{\pi \delta^3 h^2} \left\{ \int_{-\frac{h}{2}}^{\frac{h}{2}} \mathcal{G}^2 z \sum_j \left(\frac{\bar{W}_{(j)} - \bar{W}_{(k)}}{\xi_{(j)(k)}} + \frac{\theta_l^{(j)} + \theta_l^{(k)}}{2} n_l^{(j)(k)} \right) V_{(j)} \right. \\ \left. + \int_{-\frac{h}{2}}^{\frac{h}{2}} \mathcal{G}^3 z \sum_j \left[\frac{\theta_z^{(j)} - \theta_z^{(k)}}{\xi_{(j)(k)}} + (u_i^{*(j)} + u_i^{*(k)}) n_l^{(j)(k)} \right] V_{(j)} \right. \\ \left. + \int_{-\frac{h}{2}}^{\frac{h}{2}} \mathcal{G}^4 z \sum_j \left(\frac{W_{(j)}^* - W_{(k)}^*}{\xi_{(j)(k)}} + 3 \frac{\theta_l^{*(j)} + \theta_l^{*(k)}}{2} n_l^{(j)(k)} \right) V_{(j)} - \int_{-\frac{h}{2}}^{\frac{h}{2}} \mathcal{G} z \sum_j \frac{\theta_z^{(j)} + \theta_z^{(k)}}{2} \xi_{(j)(k)} V_{(j)} \right. \\ \left. - 2 \int_{-\frac{h}{2}}^{\frac{h}{2}} \frac{\mathcal{G} \nu z^2}{1-2\nu} dz \sum_j (\theta_l^{(j)} + \theta_l^{(k)}) n_l^{(j)(k)} V_{(j)} - \int_{-\frac{h}{2}}^{\frac{h}{2}} \mathcal{G} \frac{1-\nu}{1-2\nu} z^2 dz \sum_j (W_{(j)}^* + W_{(k)}^*) \xi_{(j)(k)} V_{(j)} \right. \\ \left. - 2 \int_{-\frac{h}{2}}^{\frac{h}{2}} \frac{\mathcal{G} \nu z^3}{1-2\nu} dz \sum_j (u_i^{*(j)} - u_i^{*(k)}) n_l^{(j)(k)} V_{(j)} - 2 \int_{-\frac{h}{2}}^{\frac{h}{2}} \frac{\mathcal{G} \nu z^4}{1-2\nu} dz \sum_j (\theta_l^{*(j)} - \theta_l^{*(k)}) n_l^{(j)(k)} V_{(j)} \right\} \quad (5.123g)$$

where Θ and Φ can be defined as

$$\Theta_{(k)} = \frac{2}{\pi \delta^2 h} \sum_i \frac{\bar{u}_l^{(i^k)} - \bar{u}_l^{(k)}}{\xi_{i^k(k)}} n_l^{(i^k)(k)} V_{(i^k)} \quad \Theta_{(j)} = \frac{2}{\pi \delta^2 h} \sum_i \frac{\bar{u}_l^{(i^j)} - \bar{u}_l^{(j)}}{\xi_{i^j(j)}} n_l^{(i^j)(j)} V_{(i^j)}$$

$$\begin{aligned}
\Theta_{(k)}^* &= \frac{2}{\pi\delta^2 h} \sum_i \frac{u_i^{*(i^k)} - u_i^{*(k)}}{\xi_{(i^k)(k)}} n_i^{(i^k)(k)} V_{(i^k)} & \Theta_{(j)}^* &= \frac{2}{\pi\delta^2 h} \sum_i \frac{u_i^{*(i^j)} - u_i^{*(j)}}{\xi_{(i^j)(j)}} n_i^{(i^j)(j)} V_{(i^j)} \\
\Phi_{(k)} &= \frac{2}{\pi\delta^2 h} \sum_i \frac{\theta_i^{(i^k)} - \theta_i^{(k)}}{\xi_{(i^k)(k)}} n_i^{(i^k)(k)} V_{(i^k)} & \Phi_{(j)} &= \frac{2}{\pi\delta^2 h} \sum_i \frac{\theta_i^{(i^j)} - \theta_i^{(j)}}{\xi_{(i^j)(j)}} n_i^{(i^j)(j)} V_{(i^j)} \\
\Phi_{(k)}^* &= \frac{2}{\pi\delta^2 h} \sum_i \frac{\theta_i^{*(i^k)} - \theta_i^{*(k)}}{\xi_{(i^k)(k)}} n_i^{(i^k)(k)} V_{(i^k)} & \Phi_{(j)}^* &= \frac{2}{\pi\delta^2 h} \sum_i \frac{\theta_i^{*(i^j)} - \theta_i^{*(j)}}{\xi_{(i^j)(j)}} n_i^{(i^j)(j)} V_{(i^j)}
\end{aligned} \tag{5.124a – 24h}$$

In particular case, if Poisson's ratio $\nu(z) = \frac{1}{4}$, Eq.(24a, b, c, d) will reduce to bond based PD formulation as

$$\begin{aligned}
&\rho_{(k)} \left(\ddot{u}_L^{(k)} + \frac{h^2}{12} \ddot{u}_L^{*(k)} \right) \\
&= \frac{24}{\pi\delta^3 h^2} \left[\int_{-\frac{h}{2}}^{\frac{h}{2}} Gz \sum_j \frac{\bar{u}_i^{(j)} - \bar{u}_i^{(k)}}{\xi_{(j)(k)}} n_i^{(j)(k)} n_L^{(j)(k)} V_{(j)} + \int_{-\frac{h}{2}}^{\frac{h}{2}} \frac{Gv}{1-2\nu} dz \sum_j \frac{\theta_z^{(j)} + \theta_z^{(k)}}{4} n_L^{(j)(k)} V_{(j)} \right. \\
&\quad + \int_{-\frac{h}{2}}^{\frac{h}{2}} Gz dz \sum_j \frac{\theta_i^{(j)} - \theta_i^{(k)}}{\xi_{(j)(k)}} n_i^{(j)(k)} n_L^{(j)(k)} V_{(j)} + \int_{-\frac{h}{2}}^{\frac{h}{2}} \frac{Gvz}{1-2\nu} dz \sum_j \frac{\dot{w}_{(j)} + \dot{w}_{(k)}}{2} n_L^{(j)(k)} V_{(j)} \\
&\quad \left. + \int_{-\frac{h}{2}}^{\frac{h}{2}} Gz^2 dz \sum_j \frac{u_i^{*(j)} - u_i^{*(k)}}{\xi_{(j)(k)}} n_i^{(j)(k)} n_L^{(j)(k)} V_{(j)} + \int_{-\frac{h}{2}}^{\frac{h}{2}} Gz^3 dz \sum_j \frac{\theta_i^{*(j)} - \theta_i^{*(k)}}{\xi_{(j)(k)}} n_i^{(j)(k)} n_L^{(j)(k)} V_{(j)} \right] + b_{u_L}^{(k)} \tag{5.125a}
\end{aligned}$$

$$\begin{aligned}
&\rho_{(k)} \left(\frac{h^2}{12} \ddot{\theta}_L^{(k)} + \frac{h^4}{80} \ddot{\theta}_L^{*(k)} \right) \\
&= \frac{24}{\pi\delta^3 h^2} \left[\int_{-\frac{h}{2}}^{\frac{h}{2}} Gz dz \sum_j \frac{\bar{u}_i^{(j)} - \bar{u}_i^{(k)}}{\xi_{(j)(k)}} n_i^{(j)(k)} n_L^{(j)(k)} V_{(j)} + \int_{-\frac{h}{2}}^{\frac{h}{2}} \frac{Gvz}{1-2\nu} dz \sum_j \frac{\theta_z^{(j)} + \theta_z^{(k)}}{4} n_L^{(j)(k)} V_{(j)} \right. \\
&\quad + \int_{-\frac{h}{2}}^{\frac{h}{2}} Gz^2 dz \sum_j \frac{\theta_i^{(j)} - \theta_i^{(k)}}{\xi_{(j)(k)}} n_i^{(j)(k)} n_L^{(j)(k)} V_{(j)} + \int_{-\frac{h}{2}}^{\frac{h}{2}} \frac{Gvz^2}{1-2\nu} dz \sum_j \frac{\dot{w}_{(j)} + \dot{w}_{(k)}}{2} n_L^{(j)(k)} V_{(j)} \\
&\quad \left. + \int_{-\frac{h}{2}}^{\frac{h}{2}} Gz^3 dz \sum_j \frac{u_i^{*(j)} - u_i^{*(k)}}{\xi_{(j)(k)}} n_i^{(j)(k)} n_L^{(j)(k)} V_{(j)} + \int_{-\frac{h}{2}}^{\frac{h}{2}} Gz^4 dz \sum_j \frac{\theta_i^{*(j)} - \theta_i^{*(k)}}{\xi_{(j)(k)}} n_i^{(j)(k)} n_L^{(j)(k)} V_{(j)} \right] \\
&\quad - \frac{3}{\pi\delta^3 h^2} \left\{ \int_{-\frac{h}{2}}^{\frac{h}{2}} Gz \sum_j \left(\bar{w}_{(j)} - \bar{w}_{(k)} + \frac{\theta_z^{(j)} + \theta_z^{(k)}}{2} \frac{\xi_{(j)(k)}}{\xi_{(j)(k)}} n_i^{(j)(k)} \right) n_L^{(j)(k)} V_{(j)} \right. \\
&\quad \left. + \int_{-\frac{h}{2}}^{\frac{h}{2}} Gz dz \sum_j \left[\theta_z^{(j)} - \theta_z^{(k)} + (u_i^{*(j)} + u_i^{*(k)}) \frac{\xi_{(j)(k)}}{\xi_{(j)(k)}} n_i^{(j)(k)} \right] n_L^{(j)(k)} V_{(j)} \right. \\
&\quad \left. + \int_{-\frac{h}{2}}^{\frac{h}{2}} Gz^2 dz \sum_j \left(\dot{w}_{(j)} - \dot{w}_{(k)} + 3 \frac{\theta_z^{*(j)} + \theta_z^{*(k)}}{2} \frac{\xi_{(j)(k)}}{\xi_{(j)(k)}} n_i^{(j)(k)} \right) n_L^{(j)(k)} V_{(j)} \right\} + b_{\theta_L}^{(k)} \tag{5.125b}
\end{aligned}$$

$$\begin{aligned}
& \rho_{(k)} \left(\frac{h^2}{12} \ddot{u}_L^{(k)} + \frac{h^4}{80} \ddot{u}_L^{*(k)} \right) \\
& = \frac{24}{\pi \delta^3 h^2} \left[\int_{-\frac{h}{2}}^{\frac{h}{2}} \mathcal{G}^2 dz \sum_j \frac{\bar{u}_l^{(j)} - \bar{u}_l^{(k)}}{\xi_{(j)(k)}} n_l^{(j)(k)} n_L^{(j)(k)} V_{(j)} + \int_{-\frac{h}{2}}^{\frac{h}{2}} \frac{Gvz^2}{1-2\nu} dz \sum_j \frac{\theta_z^{(j)} + \theta_z^{(k)}}{4} n_L^{(j)(k)} V_{(j)} \right. \\
& \quad \left. + \int_{-\frac{h}{2}}^{\frac{h}{2}} \mathcal{G}^3 dz \sum_j \frac{\theta_l^{(j)} - \theta_l^{(k)}}{\xi_{(j)(k)}} n_l^{(j)(k)} n_L^{(j)(k)} V_{(j)} + \int_{-\frac{h}{2}}^{\frac{h}{2}} \frac{Gvz^3}{1-2\nu} dz \sum_j \frac{\dot{w}_{(j)} + \dot{w}_{(k)}}{2} n_L^{(j)(k)} V_{(j)} \right. \\
& \quad \left. + \int_{-\frac{h}{2}}^{\frac{h}{2}} \mathcal{G}^4 dz \sum_j \frac{u_l^{*(j)} - u_l^{*(k)}}{\xi_{(j)(k)}} n_l^{(j)(k)} n_L^{(j)(k)} V_{(j)} + \int_{-\frac{h}{2}}^{\frac{h}{2}} \mathcal{G}^5 dz \sum_j \frac{\theta_l^{*(j)} - \theta_l^{*(k)}}{\xi_{(j)(k)}} n_l^{(j)(k)} n_L^{(j)(k)} V_{(j)} \right] \\
& - \frac{6}{\pi \delta^3 h^2} \left\{ \int_{-\frac{h}{2}}^{\frac{h}{2}} \mathcal{G} dz \sum_j \left(\bar{w}_{(j)} - \bar{w}_{(k)} + \frac{\theta_l^{(j)} + \theta_l^{(k)}}{2} \xi_{(j)(k)} n_l^{(j)(k)} \right) n_L^{(j)(k)} V_{(j)} \right. \\
& \quad \left. + \int_{-\frac{h}{2}}^{\frac{h}{2}} \mathcal{G}^2 dz \sum_j \left[\theta_z^{(j)} - \theta_z^{(k)} + (u_l^{*(j)} + u_l^{*(k)}) \xi_{(j)(k)} n_l^{(j)(k)} \right] n_L^{(j)(k)} V_{(j)} \right\} \\
& \quad \left. + \int_{-\frac{h}{2}}^{\frac{h}{2}} \mathcal{G}^3 dz \sum_j \left(\dot{w}_{(j)} - \dot{w}_{(k)} + 3 \frac{\theta_l^{*(j)} + \theta_l^{*(k)}}{2} \xi_{(j)(k)} n_l^{(j)(k)} \right) n_L^{(j)(k)} V_{(j)} \right\}
\end{aligned} \tag{5.125c}$$

$$\begin{aligned}
& \rho_{(k)} \left(\frac{h^4}{80} \ddot{\theta}_L^{(k)} + \frac{h^6}{448} \ddot{\theta}_L^{*(k)} \right) \\
& = \frac{24}{\pi \delta^3 h^2} \left(\int_{-\frac{h}{2}}^{\frac{h}{2}} \mathcal{G}^3 dz \sum_j \frac{\bar{u}_l^{(j)} - \bar{u}_l^{(k)}}{\xi_{(j)(k)}} n_l^{(j)(k)} n_L^{(j)(k)} V_{(j)} + \int_{-\frac{h}{2}}^{\frac{h}{2}} \frac{Gvz^3}{1-2\nu} dz \sum_j \frac{\theta_z^{(j)} + \theta_z^{(k)}}{4} n_L^{(j)(k)} V_{(j)} \right. \\
& \quad \left. + \int_{-\frac{h}{2}}^{\frac{h}{2}} \mathcal{G}^4 dz \sum_j \frac{\theta_l^{(j)} - \theta_l^{(k)}}{\xi_{(j)(k)}} n_l^{(j)(k)} n_L^{(j)(k)} V_{(j)} + \int_{-\frac{h}{2}}^{\frac{h}{2}} \frac{Gvz^4}{1-2\nu} dz \sum_j \frac{\dot{w}_{(j)} + \dot{w}_{(k)}}{2} n_L^{(j)(k)} V_{(j)} \right. \\
& \quad \left. + \int_{-\frac{h}{2}}^{\frac{h}{2}} \mathcal{G}^5 dz \sum_j \frac{u_l^{*(j)} - u_l^{*(k)}}{\xi_{(j)(k)}} n_l^{(j)(k)} n_L^{(j)(k)} V_{(j)} + \int_{-\frac{h}{2}}^{\frac{h}{2}} \mathcal{G}^6 dz \sum_j \frac{\theta_l^{*(j)} - \theta_l^{*(k)}}{\xi_{(j)(k)}} n_l^{(j)(k)} n_L^{(j)(k)} V_{(j)} \right) \\
& - \frac{9}{\pi \delta^3 h^2} \left\{ \int_{-\frac{h}{2}}^{\frac{h}{2}} \mathcal{G}^2 dz \sum_j \left(\bar{w}_{(j)} - \bar{w}_{(k)} + \frac{\theta_l^{(j)} + \theta_l^{(k)}}{2} \xi_{(j)(k)} n_l^{(j)(k)} \right) n_L^{(j)(k)} V_{(j)} \right. \\
& \quad \left. + \int_{-\frac{h}{2}}^{\frac{h}{2}} \mathcal{G}^3 dz \sum_j \left[\theta_z^{(j)} - \theta_z^{(k)} + (u_l^{*(j)} + u_l^{*(k)}) \xi_{(j)(k)} n_l^{(j)(k)} \right] n_L^{(j)(k)} V_{(j)} \right\} \\
& \quad \left. + \int_{-\frac{h}{2}}^{\frac{h}{2}} \mathcal{G}^4 dz \sum_j \left(\dot{w}_{(j)} - \dot{w}_{(k)} + 3 \frac{\theta_l^{*(j)} + \theta_l^{*(k)}}{2} \xi_{(j)(k)} n_l^{(j)(k)} \right) n_L^{(j)(k)} V_{(j)} \right\}
\end{aligned} \tag{5.125d}$$

5.6.3 Numerical Results

To verify the validity of the PD formulation for functionally graded higher order plates, the PD solutions are compared with the corresponding finite element (FE) analysis results. In this study, the functionally graded material properties are chosen as Young's Modulus, E and shear modulus G and they are assumed to vary linearly through the thickness as

$$E(z) = (E_t - E_b) \frac{z}{h} + \frac{1}{2}(E_t + E_b) \quad (GPa) \tag{5.126a}$$

$$G(z) = \frac{E(z)}{2(1 + 0.3)} \quad (5.126b)$$

$$\nu(z) = 0.3 \quad (5.126c)$$

where E_t and E_b denote the Young's modulus of the top and bottom surfaces of the plate, and h denotes the total thickness of the plate.

In the following numerical cases, a functionally graded higher order plate with uniformity of thickness, which subjected to different boundary conditions is taken under consideration. The three dimensions length, width and thickness of the beam are chosen as $L \times W \times h = 1m \times 1m \times 0.15m$, respectively. The Young's modulus of the top and bottom surface are chosen as $E_t = 200 \text{ GPa}$ and $E_b = 100 \text{ GPa}$.

The PD models are discretized into one single row of material points through the thickness and 51×51 material points throughout the xy plane. Thus, the distance between two adjacent material points is $\Delta x = \frac{1}{51}m$. A fictitious region is introduced outside the edges as the external boundaries with a width of $6\Delta x$.

As references, the corresponding FE models are creating in ANSYS by using SHELL181 and SOLID185 elements, respectively. The FE SHELL model is meshed with 50×50 elements and divided into 30 layers. On the other hand, the SOLID model is meshed with 50×50 elements throughout the xy plane and 30 elements along the thickness. In order to obtain the functionally graded character, materials properties are assigned to the layers and elements through the thickness direction. The Young's modulus varies gradually over the thickness from the first layer $E_1 = 101.67 \text{ GPa}$ to the last layer $E_{30} = 198.33 \text{ GPa}$. The Poisson's ratio, $\nu = 0.3$, is applied for both models in ANSYS.

(Note that SHELL element and SOLID element are based on different elastic constitution. SHELL element is suitable for analysing moderately thick plate or shell structures, and it is referred to the first order shear deformation theory (partial Hooke's

Law). On the other hand, SOLID element is basically used for analysing 3D structure and governed by the complete 3D Hooke's Law, whose solution is more realistic. However, SHELL element specializes in modelling and analysing layered composite plates and shells better than SOLID element, thus both solutions are taken as references for our numerical verifications.)

5.6.3.1 Simply supported plate subjected to transverse loading

In the first example case, a simply supported functionally graded high order plate subjected to a distributed load of $p=100,00\text{N/m}$ through the central line is taken into consideration. For the PD model, the load is transformed into a body load of $b_z = \frac{p}{51 \times \Delta V} = 3.4 \times 10^6 \text{N/m}^3$ and it is imposed on a row of material points through the central line of the plate.

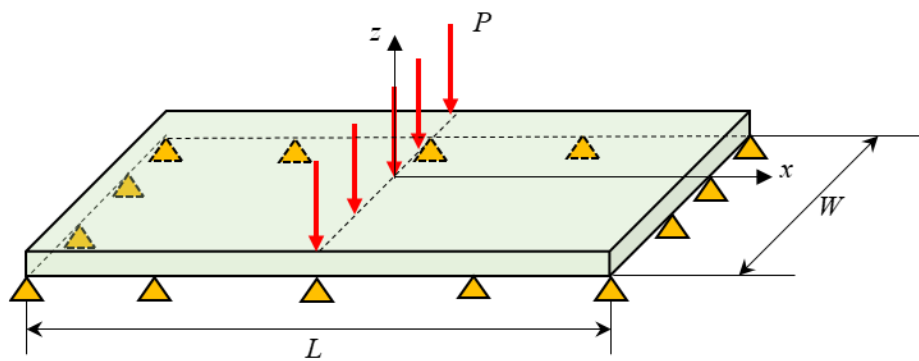


Figure 5.45. Simply supported plate subjected to transverse loading.

As shown in Fig. 5.46, PD solutions are compared against finite element (FE) analysis results obtained by using ANSYS Solid and Shell elements. Note that ANSYS Shell element is based on Mindlin plate theory. Compared to ANSYS Shell element, PD higher-order formulation performs better and represents a similar deformation variation with respect to ANSYS Solid element.

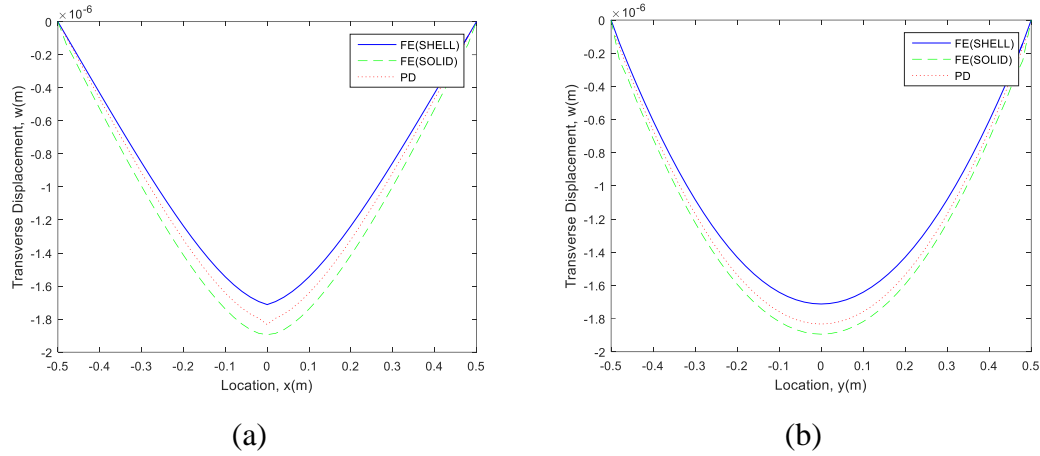


Figure 5.46 Variation of transverse displacements along (a) central x-axis and (b) central y-axis.

5.6.3.2 Fully clamped plate subjected to transverse loading

In the second example, a clamped functionally graded plate is considered as shown in Fig. 5.47. The plate is subjected to a distributed load of $P = 10000N/m$ along the central line.

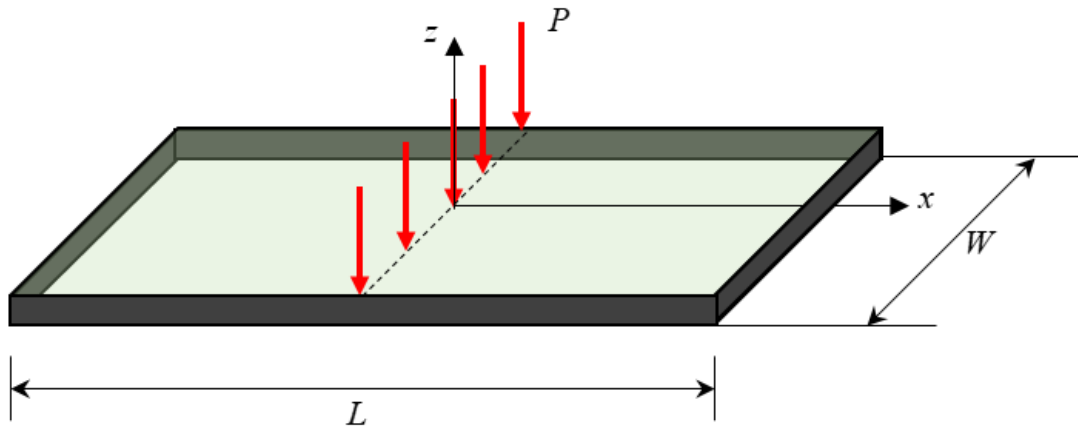


Figure 5.47. Clamped plate subjected to transverse loading.

As shown in Fig. 5.48, PD solutions are compared against finite element (FE) analysis results obtained by using ANSYS Solid and Shell elements. Compared to ANSYS Shell element, PD higher-order formulation performs better and represents a similar deformation variation with respect to ANSYS Solid element.

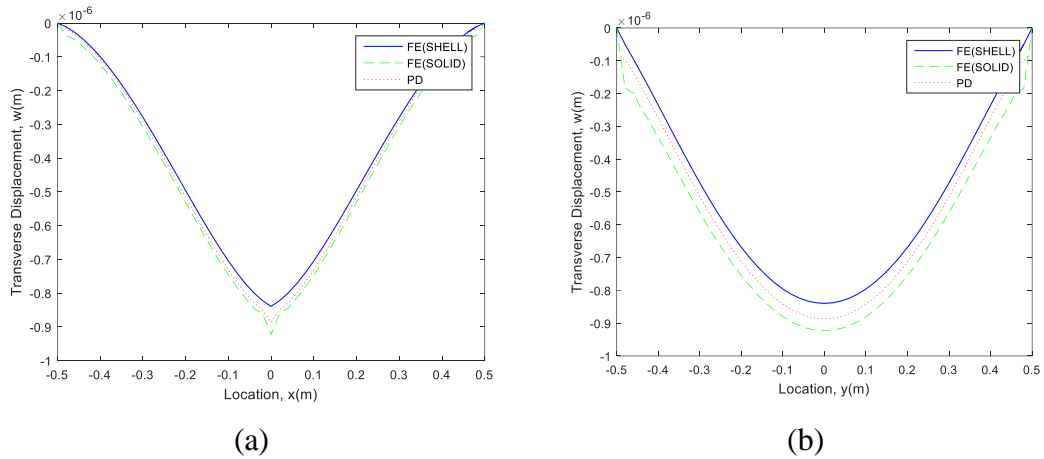


Figure 5.48 Variation of transverse displacements along (a) central x-axis and (b) central y-axis.

5.6.3.3 Mixed Boundary Conditions 1

In the third example, a functionally graded plate subjected to mixed boundary conditions (clamped-simply supported-clamped-simply supported) is considered as shown in Fig. 5.49. The plate is subjected to a distributed load of $P = 10000N/m$ along the central line.

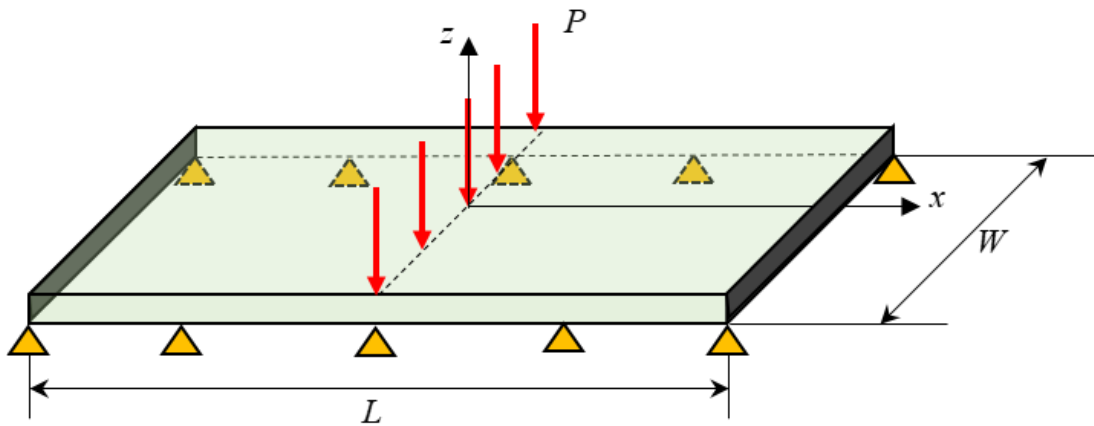


Figure 5.49 Functionally graded higher order plate subjected to mixed boundary conditions.

As shown in Fig. 5.50, PD solutions are compared against finite element (FE) analysis results obtained by using ANSYS Solid and Shell elements. Compared to ANSYS Shell element, PD higher-order formulation performs better and represents a similar deformation variation with respect to ANSYS Solid element.

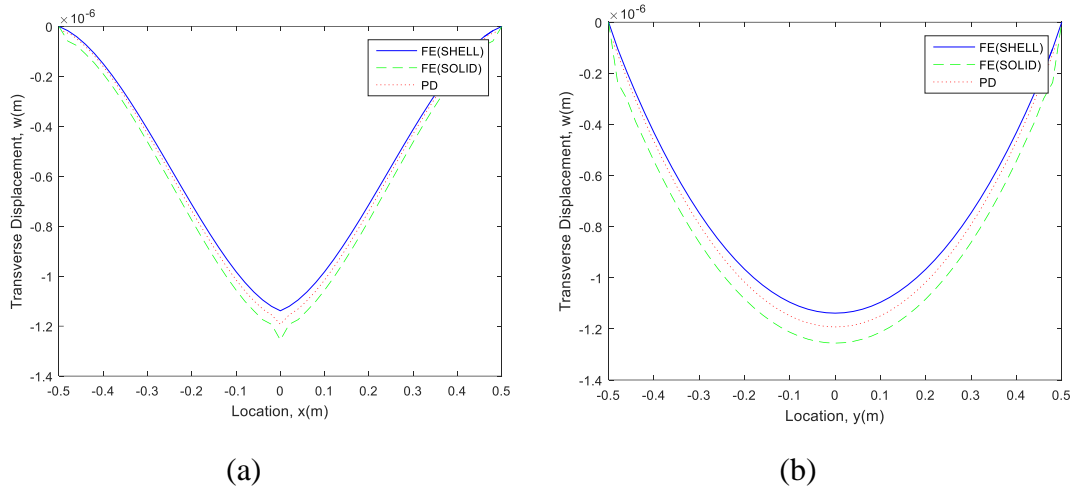


Figure 5.50 Variation of transverse displacements along (a) central x-axis and (b) central y-axis.

5.6.3.4 Mixed Boundary Conditions 2

In the third example, a functionally graded plate subjected to mixed boundary conditions (clamped-clamped-simply supported-simply supported) is considered as shown in Fig. 5.51. The plate is subjected to a distributed load of $P = 10000N/m$ along the central line.

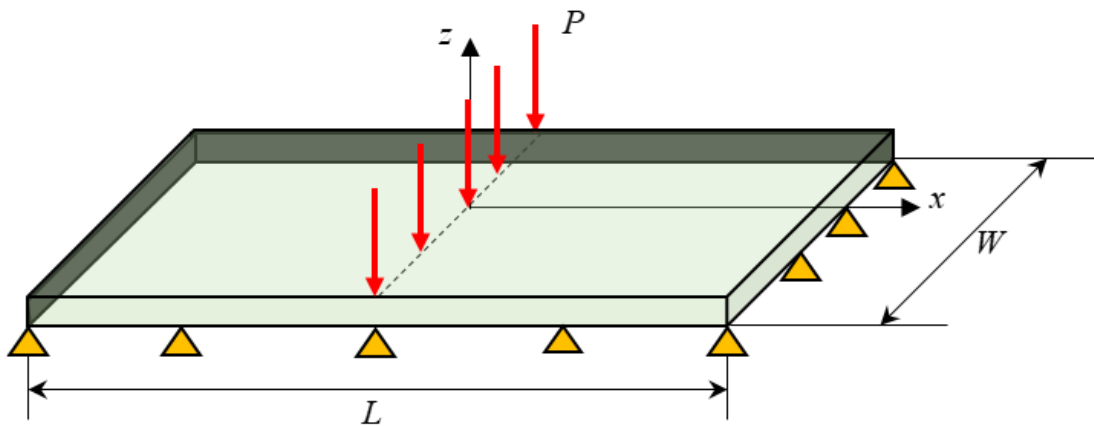


Figure 5.51 Functionally graded higher order plate subjected to mixed boundary conditions.

As shown in Fig. 5.52, PD solutions are compared against finite element (FE) analysis results obtained by using ANSYS Solid and Shell elements. Compared to ANSYS Shell

element, PD higher-order formulation performs better and represents a similar deformation variation with respect to ANSYS Solid element.

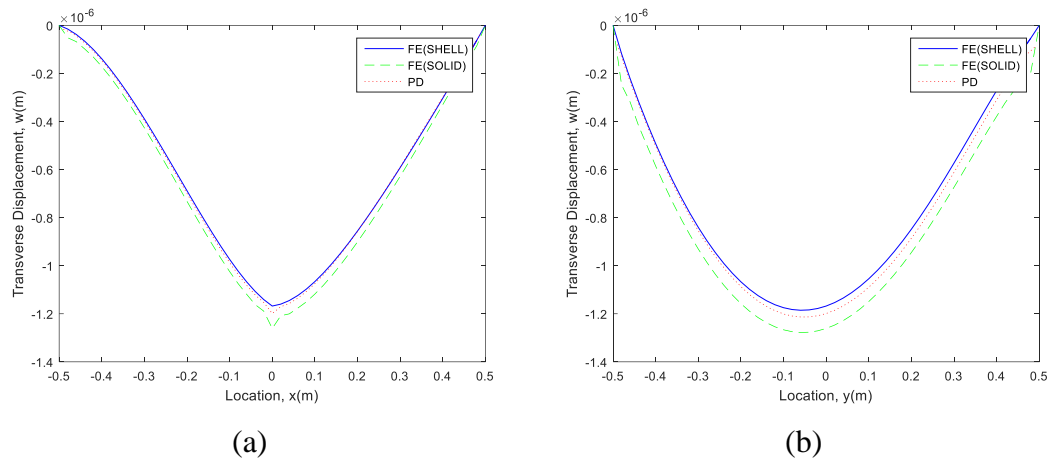


Figure 5.52 Variation of transverse displacements along (a) central x-axis and (b) central y-axis.

According to the results shown above, it can be seen clearly that SOLID element results in the maximum deflection among the three and SHELL the minimum, and the PD solution falls in between. This reflects that the PD high order plate formulations predict better in deformations than the classical plate theory (Mindlin plate theory).

5.7 Comparison Among PD Plate Theories

In the previous sections, different PD plate theories are introduced and verified by benchmark problems. In order to further investigate their feasibilities, three different PD FGM plate theories are compared by considering variation of thickness in this section. The length and width are chosen as $L = W = 1m$, three different thicknesses are considered as $h = 0.05m$, $0.10m$ and $0.15m$, which correspond to thin, moderate thick and thick plate, respectively. The material properties are assumed to vary linearly through the thickness as

$$E(z) = (E_t - E_b) \frac{z}{h} + \frac{1}{2}(E_t + E_b) \quad (GPa) \quad (5.127a)$$

$$G(z) = \frac{E(z)}{2(1 + 0.3)} \quad (5.127b)$$

$$v(z) = 0.3 \tag{5.127c}$$

in which $E_t = 200GPa$ and $E_b = 100GPa$ denote the Young's modulus of the top and bottom surface of the plate and h denotes the total thickness of the plate. The plate is subjected to simply supported boundary condition and a uniformly distributed load of $p = 10000N/m$ through the central line of the plate, as shown in Fig. 5.53.

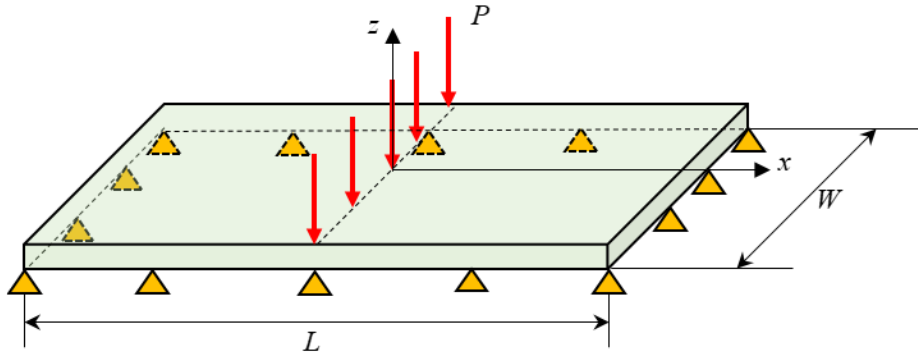


Figure 5.53 Simply supported plate subjected to transverse loading

The PD model is discretized into 101×101 material points throughout the xy plane. By contrast, the corresponding FE model is created in ANSYS by using SOLID185 element with meshing of 50×50 elements throughout the xy plane and 30 elements along the thickness direction. The comparison with respect to transverse deformation between three PD FGM theories and the corresponding FE solution are shown in the Fig. (5.54) to (5.56).

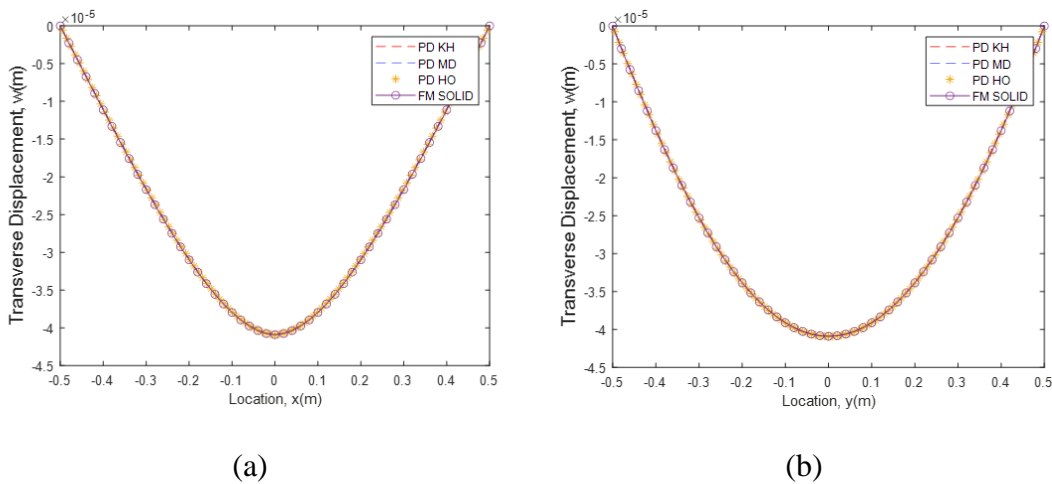


Figure 5.54 Variation of transverse displacements along (a) central x-axis and (b) central y-axis with thickness of $h = 0.05m$

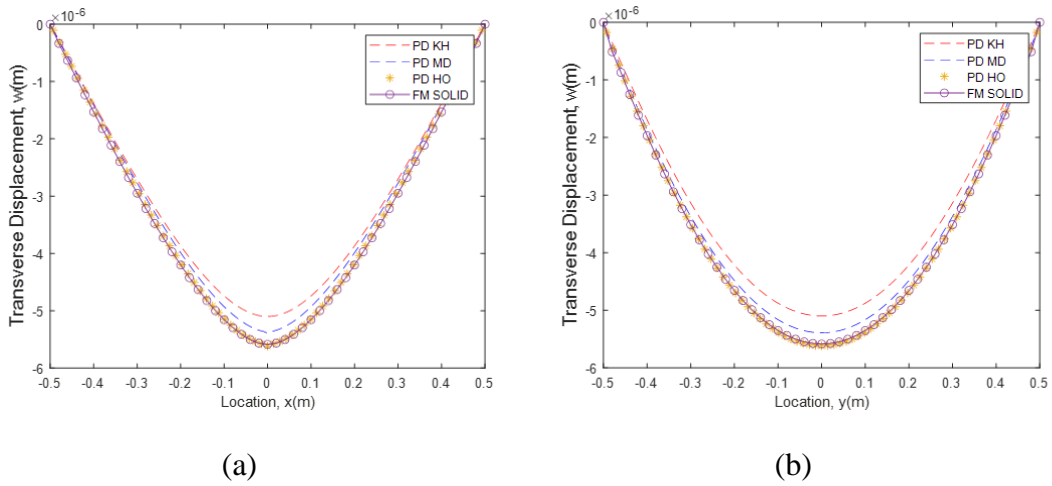


Figure 5.55 Variation of transverse displacements along (a) central x-axis and (b) central y-axis with thickness of $h = 0.10m$

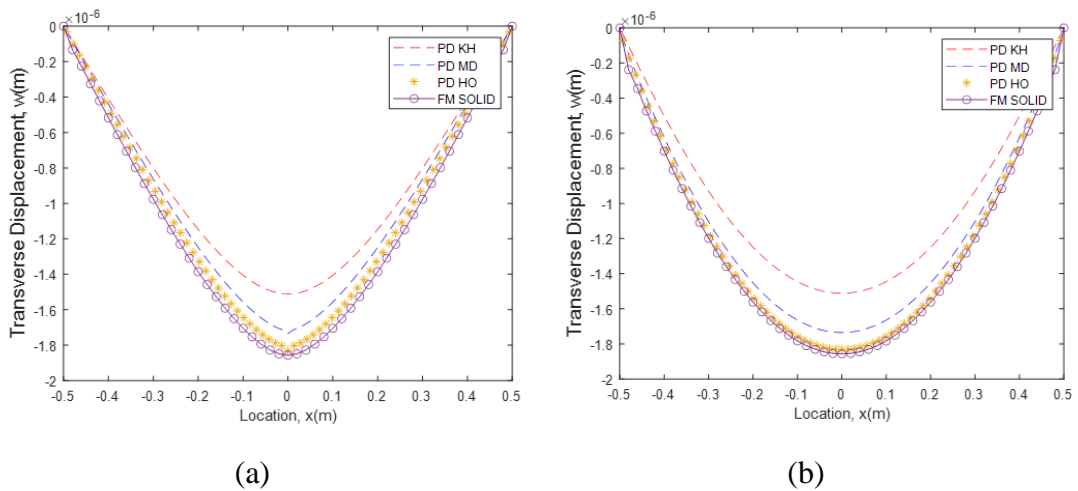


Figure 5.56 Variation of transverse displacements along (a) central x-axis and (b) central y-axis with thickness of $h = 0.15m$

As illustrated in Fig. 5.54, the results of all PD FGM plate theories consistent with each other when the plate is thin. However, as demonstrated in Fig. (5.55) and (5.56), as the thickness increases, the superiority of the FGM PD Mindlin and higher order plate theories becomes more noticeable, as the transverse shear deformations become more important, which is in line with our expectation. Particularly regarding thick plate, only higher order PD theory outputs accurate results. Moreover, since isotropic material can

be considered as a special case of FGM, a similar conclusion can be reasonably predicted with respect to the corresponding isotropic material models.

5.8 Conclusion

In this section, PD formulations for three representative plates that Kirchhoff Plate, Mindlin Plate and higher order deformable plate, as well as their FGM models, are presented. The equations of motion are obtained by utilizing Lagrange's equation. The derivation of PD SED functions and implementation of boundary conditions were described in Appendix A2 and B2, respectively. Several different benchmark problems were considered in each case, which were coding based on PD static solution method by using programming software Matlab. The PD results are compared against their corresponding finite element analysis results and a good agreement of displacement fields is observed between the two approaches. Therefore, it can be concluded that the developed approach can be used as an alternative approach for problems in which plate theories is applicable.

6. Implementation of Peridynamics Beam and Plate

Formulations in Finite Element Framework

Peridynamic (PD) theory is a new continuum mechanics formulation introduced to overcome the limitations of Classical Continuum Mechanics such as predicting crack initiation and propagation, and capturing nonlocal effects. PD theory is based on integro-differential equations and these equations are generally difficult to be solved by using analytical techniques. Therefore, numerical approximations, especially with meshless method, have been widely used. Numerical solution of three-dimensional models is usually computationally expensive and structural idealization can be utilized to reduce the computational time significantly. In this study, two of such structural idealization types are considered, namely Timoshenko beam and Mindlin plate, and their peridynamic formulations are briefly explained. Moreover, the implementation of these formulations in finite element framework is presented. To demonstrate the capability of the present approach, several case studies are considered including beam and plate bending due to transverse loading, buckling analysis and propagation of an initial crack in a plate under bending loading.

6.1. PD Timoshenko Beam and Mindlin Plate Formulation

6.1.1. PD Timoshenko Beam Formulation

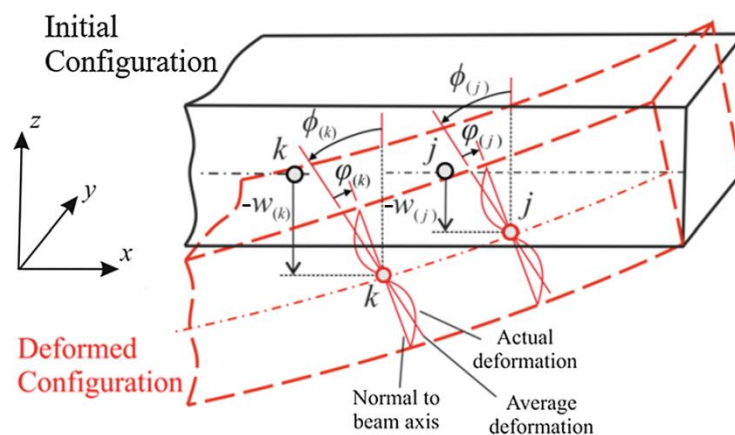


Figure 6.1 Initial and deformed configurations of a Timoshenko beam.

As explained in Chapter 4.1, according to the displacement notations and the positive stipulations shown in Fig. 6.1, the peridynamic equations of motion for a Timoshenko beam can be written as

$$\rho \ddot{w}_{(k)} = c_s \sum_{j=1}^{\infty} \left(\frac{w_{(j)} - w_{(k)}}{\xi_{(j)(k)}} - \frac{\phi_{(j)} + \phi_{(k)}}{2} \operatorname{sgn}(x_{(j)} - x_{(k)}) \right) V_{(j)} + \hat{b}_{(k)} \quad (6.1a)$$

and

$$\rho \frac{I}{A} \ddot{\phi}_{(k)} = c_b \sum_{j=1}^{\infty} \frac{\phi_{(j)} - \phi_{(k)}}{\xi_{(j)(k)}} V_{(j)} + \frac{1}{2} c_s \sum_{j=1}^{\infty} \left(\frac{w_{(j)} - w_{(k)}}{\xi_{(j)(k)}} \operatorname{sgn}(x_{(j)} - x_{(k)}) - \frac{\phi_{(j)} + \phi_{(k)}}{2} \right) \xi_{(j)(k)} V_{(j)} + \tilde{b}_{(k)} \quad (6.1b)$$

where $\hat{b}_{(k)}$ and $\tilde{b}_{(k)}$ represent body load and body moment terms, ρ , I , and A denote mass density, moment of inertia and cross-sectional area of the beam, respectively, and $V_{(j)}$ is the volume of material point j .

If peridynamic interactions are limited within the horizon of a material point, then these equations can be written in integral form as

$$\rho \ddot{w}(x, t) = c_s \int_H \left(\frac{w(x', t) - w(x, t)}{\xi} - \frac{\phi(x', t) + \phi(x, t)}{2} \operatorname{sgn}(x' - x) \right) dV' + \hat{b}(x, t) \quad (6.2a)$$

and

$$\begin{aligned} \frac{\rho I}{A} \ddot{\phi}(x, t) = & \int_H \left(c_b \frac{\phi(x', t) - \phi(x, t)}{\xi} \right) dV' \\ & + \int_H \left(\frac{1}{2} c_s \left(\frac{w(x', t) - w(x, t)}{\xi} \operatorname{sgn}(x' - x) - \frac{\phi(x', t) + \phi(x, t)}{2} \right) \xi \right) dV' + \tilde{b}(x, t) \end{aligned} \quad (6.2b)$$

The PD material constants c_s and c_b can be expressed in terms of shear and Young's moduli, G and, E as

$$c_s = \frac{2k_s G}{A\delta^2} \quad \text{and} \quad c_b = \frac{2EI}{\delta^2 A^2} \quad (6.3a, b)$$

where k_s is the shear correction factor.

For the material point k in a Timoshenko beam shown in Fig. 6.1, the peridynamic

interaction forces between material points j and k arising from transverse shear deformation, $\hat{f}_{(k)(j)}$ and bending, $\tilde{f}_{(k)(j)}$ can be defined for a linear material behavior as

$$\hat{f}_{(k)(j)} = c_s \varrho_{(k)(j)} \quad (6.4a)$$

and

$$\tilde{f}_{(k)(j)} = c_b \kappa_{(k)(j)} \quad (6.4b)$$

in which c_s and c_b are the peridynamics material constants associated with the transverse shear deformation and bending of the beam, respectively. Note that the unit of the force parameters given in Eqs. (6.4a) and (6.4b) are actually force per volume squared and couple of forces per volume squared, respectively, since in peridynamics the equations of motion are generally written in terms of general force density and the peridynamic forces are part of a volume integration. The transverse shear angle, $\varphi_{(k)(j)}$, arising from the interaction between material points j and k can be defined as the average of the transverse shear angles at these material points in the form

$$\varphi_{(k)(j)} = \left(\frac{w_{(j)} - w_{(k)}}{\xi_{(j)(k)}} - \frac{\phi_{(j)} + \phi_{(k)}}{2} \operatorname{sgn}(x_{(j)} - x_{(k)}) \right) \quad (6.5a)$$

Where w and ϕ represent the out-of-plane deflection and rotation of sections, respectively, $\operatorname{sgn}(\cdot)$ function provides the sign of the associated function, and $\xi_{(j)(k)}$ represents the initial distance between material points j and k .

The curvature, $\kappa_{(k)(j)}$, between the material points j and k can be expressed as

$$\kappa_{(k)(j)} = \left(\frac{\phi_{(j)} - \phi_{(k)}}{\xi_{(j)(k)}} \right) \quad (6.5b)$$

6.1.2. Peridynamic Mindlin Plate Formulation

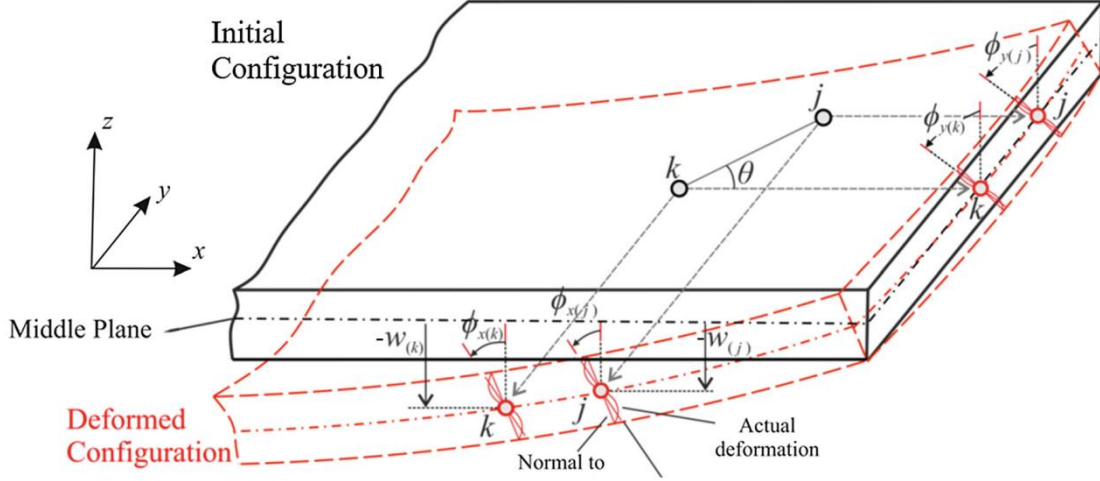


Figure 6.2 Initial and deformed configurations of a Mindlin plate.

As derived in Chapter 5.3, the PD bond-based ($\nu = 1/3$) formulations for Mindlin Plate can be written by utilizing the displacements notations and their positive stipulations given in Fig. 6.2 as

$$\begin{aligned} \rho_{(k)} \frac{h^2}{12} \ddot{\phi}_x^{(k)} = & c_s \sum_{j=1}^{\infty} \frac{1}{2} \frac{\xi}{\xi_{(j)(k)}} \left(\frac{w_{(j)} - w_{(k)}}{\xi_{(j)(k)}} - \frac{\phi_x^{(j)} + \phi_x^{(k)}}{2} \cos \theta - \frac{\phi_y^{(j)} + \phi_y^{(k)}}{2} \sin \theta \right) \cos \theta V_{(j)} \\ & + c_b \sum_{j=1}^{\infty} \left(\frac{\phi_x^{(j)} - \phi_x^{(k)}}{\xi_{(j)(k)}} \cos \theta + \frac{\phi_y^{(j)} - \phi_y^{(k)}}{\xi_{(j)(k)}} \sin \theta \right) \cos \theta V_{(j)} + \tilde{b}_{x(k)} \end{aligned} \quad (6.6a)$$

$$\begin{aligned} \rho_{(k)} \frac{h^2}{12} \ddot{\phi}_y^{(k)} = & c_s \sum_{j=1}^{\infty} \frac{1}{2} \frac{\xi}{\xi_{(j)(k)}} \left(\frac{w_{(j)} - w_{(k)}}{\xi_{(j)(k)}} - \frac{\phi_x^{(j)} + \phi_x^{(k)}}{2} \cos \theta - \frac{\phi_y^{(j)} + \phi_y^{(k)}}{2} \sin \theta \right) \sin \theta V_{(j)} + \\ & c_b \sum_{j=1}^{\infty} \left[\left(\frac{\phi_x^{(j)} - \phi_x^{(k)}}{\xi_{(j)(k)}} \right) \cos \theta + \left(\frac{\phi_y^{(j)} - \phi_y^{(k)}}{\xi_{(j)(k)}} \right) \sin \theta \right] \sin \theta V_{(j)} + \tilde{b}_{y(k)} \end{aligned} \quad (6.6b)$$

and

$$\rho \ddot{w}_{(k)} = c_s \sum_{j=1}^{\infty} \left(\frac{w_{(j)} - w_{(k)}}{\xi_{(j)(k)}} - \frac{\phi_{x(j)} + \phi_{x(k)}}{2} \cos \theta - \frac{\phi_{y(j)} + \phi_{y(k)}}{2} \sin \theta \right) V_{(j)} + \hat{b}_{(k)} \quad (6.6c)$$

with θ being the orientation of the bond with respect to x -axis, ϕ_x and ϕ_y are rotations around y - and x -axis, respectively. Here, the PD material constants c_s and c_b , which correspond to shear and bending effect, respectively, can be expressed in terms of Young's modulus, E , as

$$c_s = \frac{9\kappa_s^2 E}{4\pi\delta^3 h} \quad \text{and} \quad c_b = \frac{3Eh}{4\pi\delta^3} \quad (6.7a, b)$$

Eqs. (6.6) can be expressed in continuous form as

$$\begin{aligned}
\rho \frac{h^2}{12} \ddot{\phi}_x(\mathbf{x}, t) &= c_b \int_H \left[\left(\frac{\phi_x(\mathbf{x}', t) - \phi_x(\mathbf{x}, t)}{\xi} \right) \cos \theta + \left(\frac{\phi_y(\mathbf{x}', t) - \phi_y(\mathbf{x}, t)}{\xi} \right) \sin \theta \right] \cos \theta dV' \\
&+ \frac{1}{2} c_s \int_H \xi \left(\frac{w(\mathbf{x}', t) - w(\mathbf{x}, t)}{\xi} - \frac{\phi_x(\mathbf{x}', t) + \phi_x(\mathbf{x}, t)}{2} \cos \theta - \frac{\phi_y(\mathbf{x}', t) + \phi_y(\mathbf{x}, t)}{2} \sin \theta \right) \cos \theta dV' \\
&+ \tilde{b}_x(\mathbf{x}, t)
\end{aligned} \tag{6.8a}$$

$$\begin{aligned}
\rho \frac{h^2}{12} \ddot{\phi}_y(\mathbf{x}, t) &= c_b \int_H \left[\left(\frac{\phi_x(\mathbf{x}', t) - \phi_x(\mathbf{x}, t)}{\xi} \right) \cos \theta + \left(\frac{\phi_y(\mathbf{x}', t) - \phi_y(\mathbf{x}, t)}{\xi} \right) \sin \theta \right] \sin \theta dV' \\
&+ \frac{1}{2} c_s \int_H \xi \left(\frac{w(\mathbf{x}', t) - w(\mathbf{x}, t)}{\xi} - \frac{\phi_x(\mathbf{x}', t) + \phi_x(\mathbf{x}, t)}{2} \cos \theta - \frac{\phi_y(\mathbf{x}', t) + \phi_y(\mathbf{x}, t)}{2} \sin \theta \right) \sin \theta dV' \\
&+ \tilde{b}_y(\mathbf{x}, t)
\end{aligned} \tag{6.8b}$$

and

$$\rho \tilde{w}(\mathbf{x}, t) = c_s \int_H \left(\frac{w(\mathbf{x}', t) - w(\mathbf{x}, t)}{\xi} - \frac{\phi_x(\mathbf{x}', t) + \phi_x(\mathbf{x}, t)}{2} \cos \theta - \frac{\phi_y(\mathbf{x}', t) + \phi_y(\mathbf{x}, t)}{2} \sin \theta \right) dV' + \hat{b}(\mathbf{x}, t) \tag{6.8c}$$

Note that the peridynamic interactions can be restricted within the horizon of material points, H .

Considering the material point k as the point of interest as shown in Fig. 6.2, the transverse shear angle, $\varphi_{(k)(j)}$, between material points j and k can be defined as the average of the shear angles at these material points in the form

$$\varphi_{(k)(j)} = \frac{w_{(j)} - w_{(k)} - \phi_{(j)} + \phi_{(k)}}{\xi_{(j)(k)}} \tag{6.9}$$

where $\phi_{(j)}$ and $\phi_{(k)}$ represent the rotations with respect to the line of action between the material points j and k and can be defined as

$$\phi_{(j)} = \phi_x^{(j)} \cos \theta + \phi_y^{(j)} \sin \theta \tag{6.10a}$$

$$\phi_{(k)} = \phi_x^{(k)} \cos \theta + \phi_y^{(k)} \sin \theta \tag{6.10b}$$

As for the Timoshenko beam, the transverse shear angle and curvature, with respect to the line of action between the material points j and k can be defined as

$$\varphi_{(k)(j)} = \frac{w_{(j)} - w_{(k)}}{\xi_{(j)(k)}} - \left(\frac{\phi_{(k)} + \phi_{(j)}}{2} \right) \quad (6.11a)$$

$$\kappa_{(k)(j)} = \frac{\phi_{(j)} - \phi_{(k)}}{\xi_{(j)(k)}} \quad (6.11b)$$

When considering the material point j as the point of interest, the transverse shear angle and curvature for the interaction between the material points j and k become

$$\varphi_{(j)(k)} = \frac{w_{(k)} - w_{(j)}}{\xi_{(j)(k)}} - \left(-\frac{\phi_{(k)} + \phi_{(j)}}{2} \right) \quad (6.12a)$$

and

$$\kappa_{(j)(k)} = \frac{\phi_{(k)} - \phi_{(j)}}{\xi_{(j)(k)}} \quad (6.12b)$$

In order to include failure in the material response, the response functions in the equations of motion for the beam and plate can be modified through a history-dependent scalar value function, $H(x_{(j)} - x_{(k)}, t)$ as

$$\hat{f}_{(k)(j)} = H(x_{(j)} - x_{(k)}, t) c_s \varphi_{(k)(j)} \quad (6.13a)$$

and

$$\tilde{f}_{(k)(j)} = H(x_{(j)} - x_{(k)}, t) c_b \kappa_{(k)(j)} \quad (6.13b)$$

which is defined as

$$H(x_{(j)} - x_{(k)}, t) = \begin{cases} 1 & \text{if } \left| \kappa_{(k)(j)}(x_{(j)} - x_{(k)}, t) \right| < \kappa_c \text{ and } \left| \varphi_{(k)(j)}(x_{(j)} - x_{(k)}, t) \right| < \varphi_c \\ 0 & \text{otherwise} \end{cases} \quad (6.14)$$

where critical curvature and angle values can be expressed in terms of Mode-I and Mode-III critical energy release rates of the material, G_{Ic} and G_{IIIc} , as

$$\kappa_c = \sqrt{\frac{4G_{Ic}}{c_b h \delta^4}} \text{ and } \varphi_c = \sqrt{\frac{4G_{IIIc}}{c_s h \delta^4}}, \text{ respectively.} \quad (6.15a, b)$$

Please note that although it is possible to make connections to some of the existing approaches for fracture modelling (Marigo et al., 1989; Spagnuolo et al., 2017; Kezmane et al., 2017; Placidi, 2016), there are also certain differences between peridynamics and other existing techniques; especially the peridynamic bond concept and its breakage under certain conditions.

6.2 Implementation of Peridynamic Formulations in Finite Element Framework

As mentioned earlier, analytical solution of peridynamic equations of motion are usually not possible and numerical approaches are widely utilized. If meshless method is used for spatial discretization, the solution domain is divided into finite number of volumes and each volume is represented by a point located at its center as shown in Fig. 6.3. Each point is interacting with finite number of points located inside its horizon.

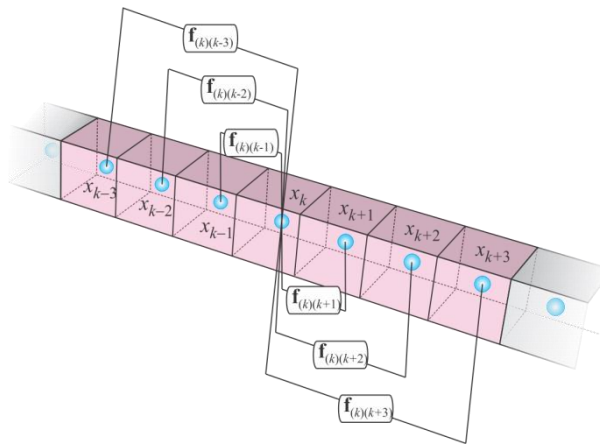


Figure 6.3 Meshless discretization of a domain and interaction between points inside the horizon of point k

Peridynamic formulations can be numerically implemented using different computer languages in either serial or parallel manner. Moreover, commercial finite element softwares such as ANSYS, Abaqus, etc. can also be utilized by following the approach presented in Macek and Silling (2007). In this study, the implementation procedure of peridynamic Timoshenko beam and Mindlin plate formulations in a commercial finite element software will be presented.

6.2.1 Calibration process to link PD and classical FE parameters

As mentioned earlier, the unit of the peridynamic interaction force parameters between material points j and k given in Eqs. (6.4a) and (6.4b) is generalized force per volume

squared. In order to convert these quantities to generalized force, these expressions should be multiplied by the volumes of the associated material points k and j as

$$\hat{F}_{(k)(j)} = c_b \kappa_{(k)(j)} V_{(k)} V_{(j)} \quad (6.16a)$$

and

$$\hat{F}_{(k)(j)} = c_s \varrho_{(k)(j)} V_{(k)} V_{(j)} \quad (6.16b)$$

In finite element framework, each peridynamic interaction can be represented using a Timoshenko beam element. Corresponding forces for a Timoshenko beam element can be expressed as

$$\hat{F}_{(k)(j)} = E_{(k)(j)} I \kappa_{(k)(j)} \quad (6.17a)$$

and

$$\hat{F}_{(k)(j)} = G_{(k)(j)} A \kappa_s \varrho_{(k)(j)} \quad (6.17b)$$

in which $E_{(k)(j)}$ and $G_{(k)(j)}$ represent the Young's modulus and shear modulus of the element, respectively, and I and A are the moment of inertia and cross-sectional area. Equating the corresponding forces given in Eqs. (6.16) and (6.17) yields

$$E_{(k)(j)} = \frac{c_b V_{(k)} V_{(j)}}{I} \quad (6.18a)$$

and

$$G_{(k)(j)} = \frac{c_s V_{(k)} V_{(j)}}{A \kappa_s} \quad (6.18b)$$

Note that Young's and shear moduli expressions given in Eqs. (18a,b) are not real material property values. Instead they are serving as the calibration parameters between peridynamics and finite element framework.

6.2.2 Implementation in ANSYS

As explained in the previous section, a peridynamic bond can be represented using a Timoshenko beam element after calibrating the material parameters given in Eqs. (6.18a,b) for both Timoshenko beam and Mindlin plate formulations. In this study, ANSYS, a commercial finite element software, is utilized. ANSYS has an extensive library of finite elements with a name defined as a combination of an element type and

a unique element number. A suitable element for the purpose of the current study is BEAM188. For the numerical implementation, first finite element nodes are created to represent material points. Then beam elements are created between material points to represent peridynamic interactions as shown in Fig. 6.4. Since in peridynamic theory a material point is interacting with other material points inside its horizon, a network of beam elements are generated to represent the numerical model as depicted in Fig. 6.5. As explained in section 6.2.1, the material properties of each beam element should be abided by Eqs. (6.18a, b). Regarding the transient analysis, MASS21 element will be introduced to attach on each node (PD material point) with ANSYS real constant of $r_{(k)} = \rho_{(k)}V_{(k)}$. Moreover, in order to simplify the preprocessor part, the PD model of Timoshenko beam/Mindlin plate is suggested to discretize into nodes (PD material points) uniformly, otherwise, unnecessary difficulties may occur when defining material properties of beam elements. If peridynamic failure criteria given in Eqs. (6.15a,b) are satisfied for a particular element, the element can be considered as broken utilizing EKILL command of ANSYS. Note that BEAM188 has 6 degrees-of-freedom. Therefore, it can both represent bending behavior and in-plane (membrane) behavior. Hence, it can capture the effect of in-plane loading on bending deformations as in the buckling analysis.

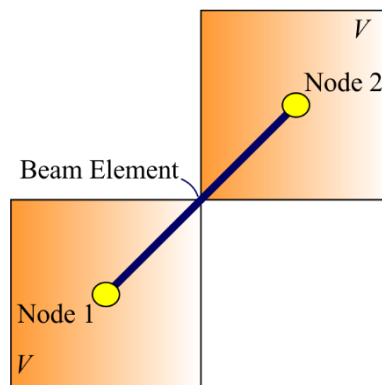


Figure 6.4 Beam element representing an interaction between PD points



Figure 6.5 Network of beam elements to represent interactions between PD points.

6.2.3 Application of boundary conditions and loading

Peridynamic equations given in Eqs. (6.1) and (6.6) are obtained using Lagrange's equations and without considering the boundaries. Although there are currently different techniques available in the literature, in this study, the displacement and rotation boundary conditions are applied by introducing a fictitious layer with a thickness equivalent to the size of horizon (Madenci and Oterkus, 2014). Moreover, the loading is applied to a single layer of material points as a body load or moment.

6.3 Numerical Results

In order to demonstrate the capability of the current approach, bending and buckling analyses are performed for both peridynamic Timoshenko beam and Mindlin plate formulations. The peridynamic solutions are compared against classical finite element method solutions. All PD and FE solutions were obtained by using ANSYS software. Moreover, a plate with an initial crack under bending loading is studied to demonstrate how cracks can propagate in the current approach. The horizon size was chosen as $\delta = 3.015\Delta x$ in all cases where Δx is the uniform grid spacing.

6.3.1 Timoshenko Beam

Beam Bending

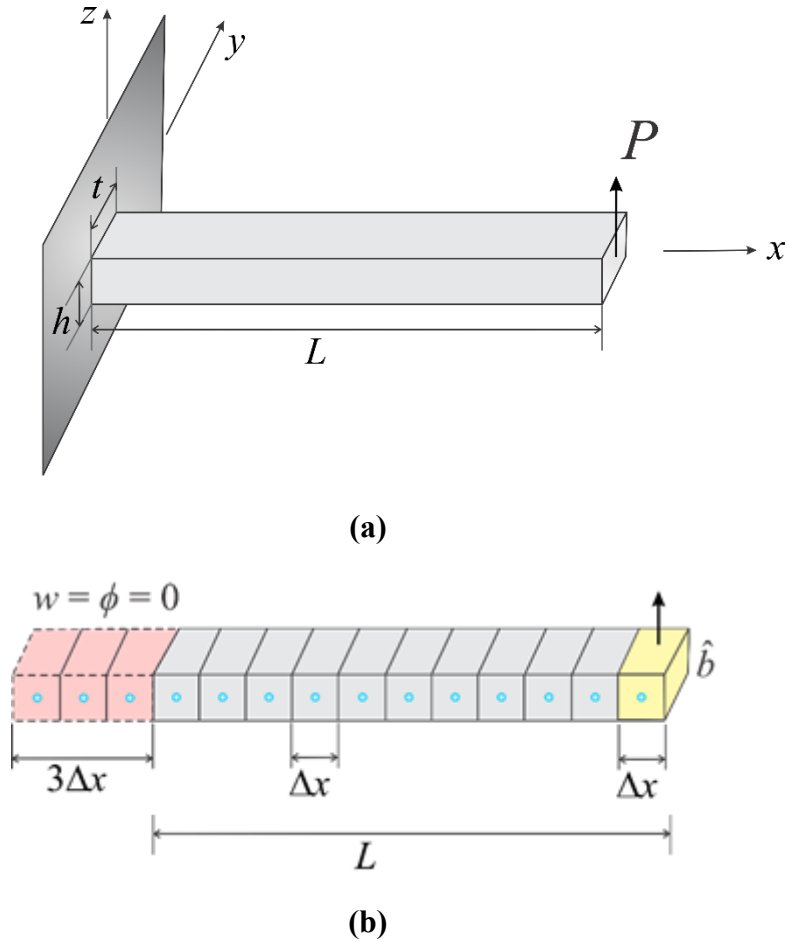
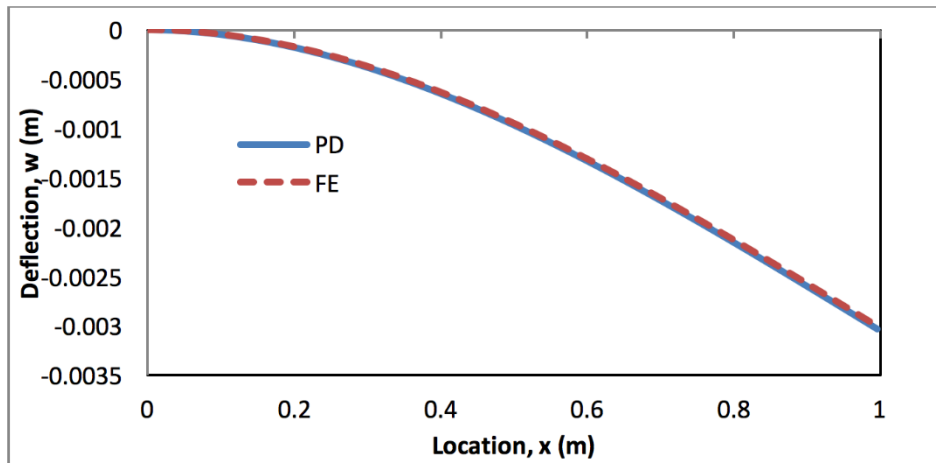


Figure 6.6 (a) A cantilever beam subjected to transverse loading and (b) its discretization.

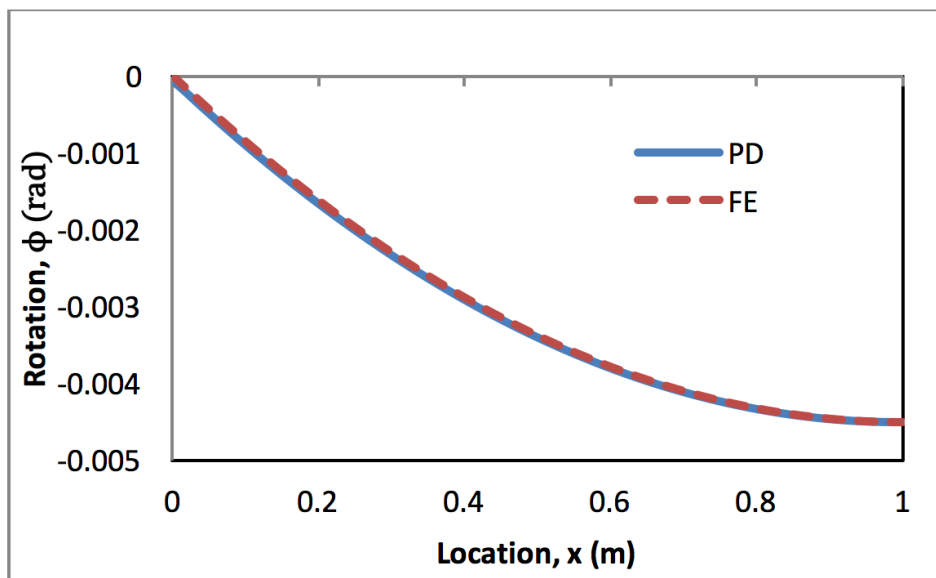
A cantilever beam shown in Fig. (6.6) with a length of $L = 1\text{ m}$ and a cross sectional area of $A = 0.1 \times 0.1\text{ m}^2$ is considered. The Young's modulus and Poisson's ratio are specified as $E = 200\text{ GPa}$ and $\nu = 1/3$, respectively. The beam is discretized into a single row of material points with a distance between each other of $\Delta x = 0.01\text{ m}$. As suggested by Madenci and Oterkus (2014), the left edge is constrained by introducing a fictitious region with a size of horizon, δ . Therefore, a total of 103 nodes are used in the model. A transverse concentrated force $P = -1000\text{ N}$ is applied to

the right end of the beam.

Fig. 6.7 shows the deflection and rotation results obtained from both PD and classical FE models. It can be clearly seen that the solutions from PD model are in very good agreement with classical FE solution. This verifies the capability of PD Timoshenko beam formulation to capture small bending deformations and rotations.



(a)



(b)

Figure 6.7 Variation of (a) deflection and (b) rotation along the cantilever beam.

Beam buckling

Same cantilever beam model considered in the previous case is tested for its buckling performance. When a structure is subjected to a compressive load, buckling may occur. The critical buckling load is the maximum load which a structure can resist buckling to occur.

ANSYS provides two techniques for buckling analysis which are eigenvalue analysis and geometrical non-linear analysis. Eigenvalue analysis provides the buckling load and mode shape for each buckling mode. Note that buckling mode only demonstrates the shape of the deformation. On the other hand, geometrical nonlinear analysis can provide both the buckling load and post-buckling behavior of the structure with real deformations.

Eigenvalue buckling analysis solution

According to Euler's formula, the theoretical critical buckling load for the cantilever beam subjected to fixed-free end conditions can be calculated as

$$F_{cr} = \frac{\pi^2 E I}{(2L)^2} = 4.11 \times 10^6 \text{ N} \quad (6.19)$$

The same problem is also solved by using classical finite element method and peridynamic model performing an eigenvalue analysis. Both PD and classical FE solutions of critical buckling load from eigenvalue buckling analysis yield the same value of $4.08 \times 10^6 \text{ N}$ which agree well with the theoretical value from Eq. (6.19). This clearly demonstrates that PD model of Timoshenko Beam has a good capability in eigenvalue analysis to predict critical buckling load.

Non-linear buckling analysis solution

The performance of geometrical non-linear buckling analysis of PD Timoshenko Beam is also studied. A total load of $F_x = -5 \times 10^6 \text{ N}$ is gradually applied to the beam at the right free end using 100 load steps. A sufficiently small transverse loading of $F_y =$

-20000 N (0.4% of F_x) is introduced to the free end to trigger the buckling behavior once the critical buckling load is reached.

In Fig. 6.8 the variation of deflections as the load increases is demonstrated. The solutions of PD and classical FE agree very well with each other and both predicts that the beam becomes unstable and buckles at a load of approximately $4 \times 10^6 \text{ N}$, which is slightly less than the eigenvalue solution of $4.08 \times 10^6 \text{ N}$ and theoretical value of $4.11 \times 10^6 \text{ N}$. Fig. 6.8 also shows the post-buckling behaviour of the column.

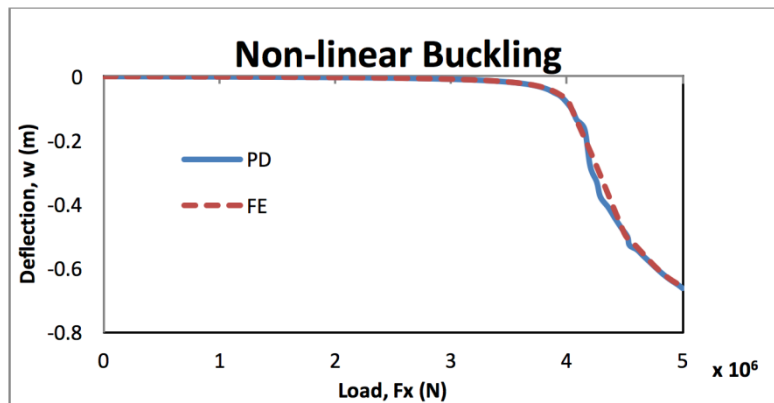


Figure 6.8 Variation of deflection as the applied load increases.

6.3.2 Mindlin Plate

In this section, the finite element implementation of PD Mindlin Plate formulation is investigated. As for the Timoshenko beam formulation, the PD Mindlin Plate formulation is tested for its bending and buckling analyses performance which include eigenvalue analysis and geometrical non-linear analysis. PD results are compared against regular FE models created using SHELL181 element of ANSYS. Moreover, a plate with an initial crack under bending loading is studied to demonstrate the failure prediction capability of the current formulation.

Bending

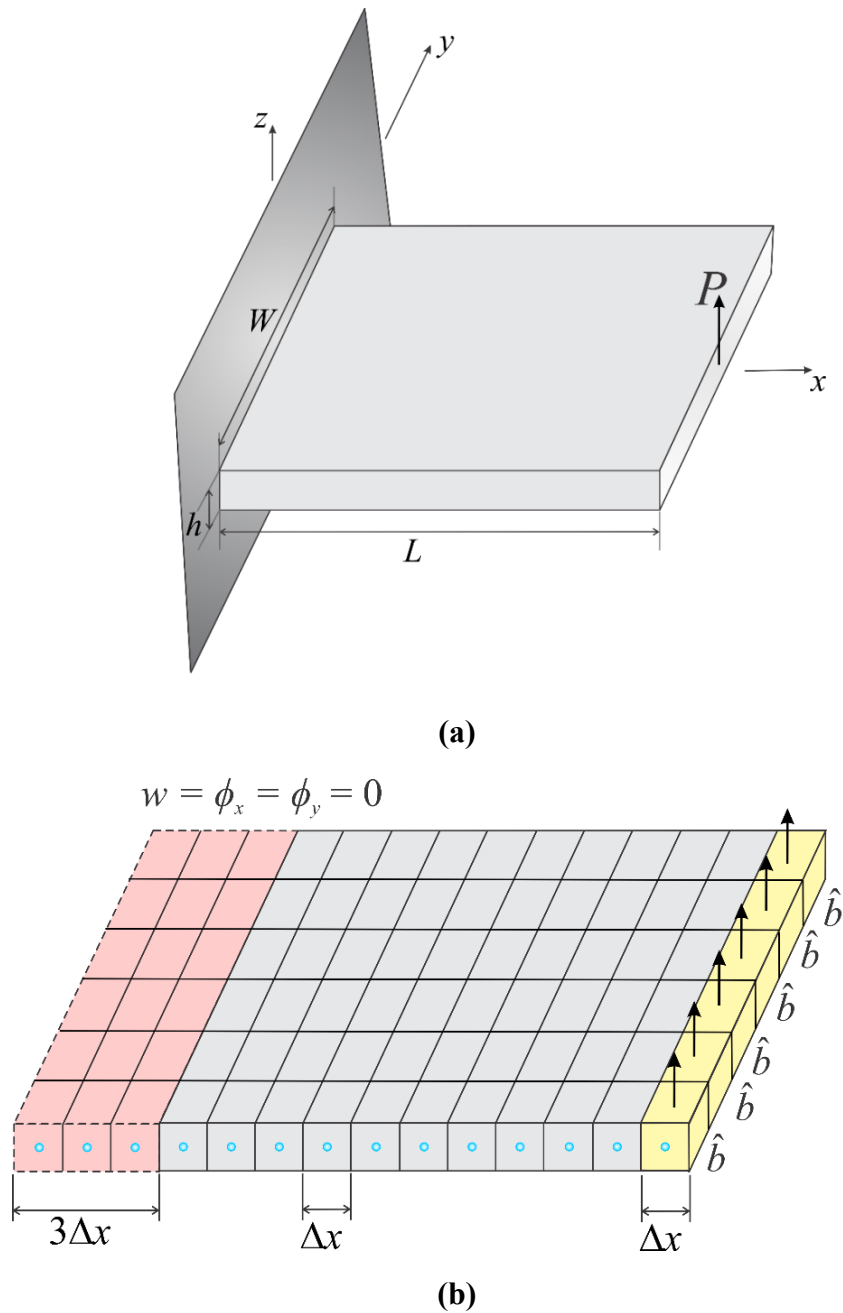
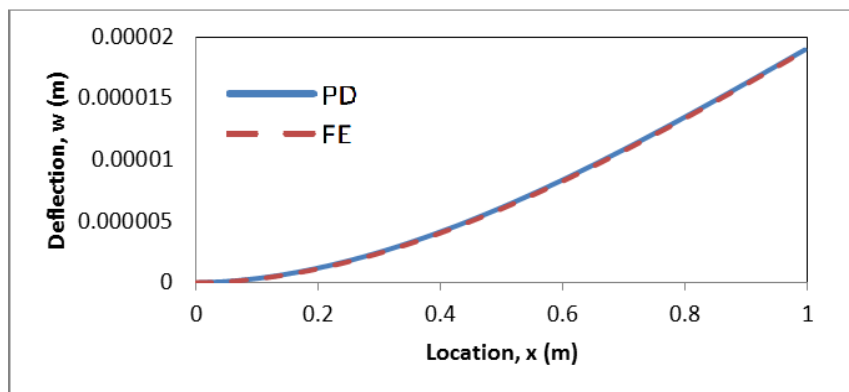


Figure 6.9 (a) A plate subjected to transverse force loading and (b) its discretization.

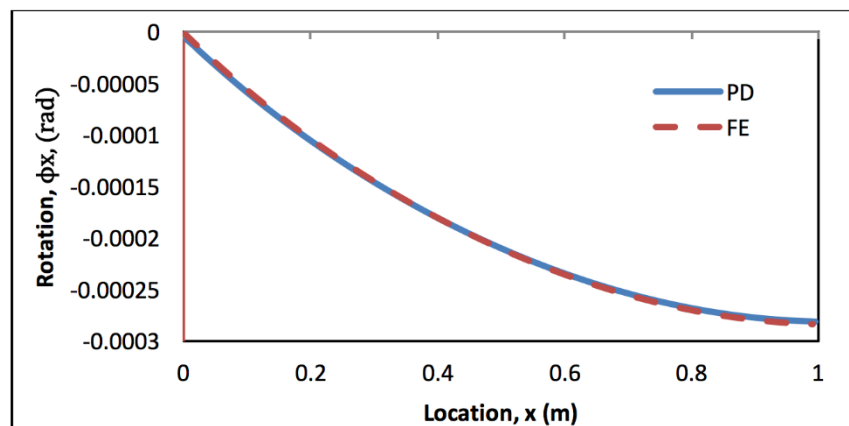
A cantilever plate with a length and width of $L = W = 1 \text{ m}$ and thickness of $h = 0.1 \text{ m}$ is considered as shown in Fig. 6.9. The Young's modulus and Poisson's ratio of the plate is $E = 200 \text{ GPa}$ and $\nu = 1/3$, respectively. The model is discretized into one single row of material points along the thickness and the distance between material points is $\Delta x = 0.01 \text{ m}$. The left edge is constrained by introducing a fictitious region

with a size of horizon, δ . A transverse load is applied to a single row of material points as a body load at the right edge of the plate with an amount of 10^7 N/m^3 .

As shown in Fig. 6.10, the PD and classical FE solutions yield similar variation in terms of deflection and rotation for the points located along the central x -axis. This shows that FE implementation of PD can accurately capture the bending behavior of the Mindlin plate.



(a)



(b)

Figure 6.10 Variation of (a) deflection and (b) rotation along the central x -axis of the plate.

Buckling

The cantilever plate considered in the previous case with same dimensions and material properties is also studied for its buckling behavior. As in the Timoshenko beam case,

both eigenvalue and non-linear buckling analysis are performed in this section.

Eigenvalue buckling analysis solution

The critical buckling load of the cantilever plate is first determined by performing an eigenvalue buckling analysis. Both PD and classical FE analyses yield same critical buckling load which is approximately equal to $4.35 \times 10^5 \text{ N}$.

Nonlinear buckling analysis solution

The performance of nonlinear buckling analysis of PD Mindlin plate is studied next. A total pressure of $P_x = -6 \times 10^8 \text{ N}$ is gradually applied to the free edge of the plate, which is equivalent to a concentrated force of $F_x = -6 \times 10^5 \text{ N}$, using 2000 load steps. To trigger the buckling behaviour, a sufficiently small transverse load of $F_y = 2400 \text{ N}$ (0.4% of F_x) is introduced to a single row of material points at the free edge.

In order to observe the buckling behaviour of the plate, the deflection of the central point at free edge ($x=L, y=0$) is recorded as the load increases. As depicted in Fig. 11, the PD and classical FE solutions are in very good agreement and both predicts that the plate buckles at a pressure loading of approximately $4.1 \times 10^8 \text{ Pa}$ which is slightly less than the eigenvalue solution of $4.35 \times 10^8 \text{ Pa}$. Fig. 6.11 also shows the post-buckling behaviour of the cantilever plate.

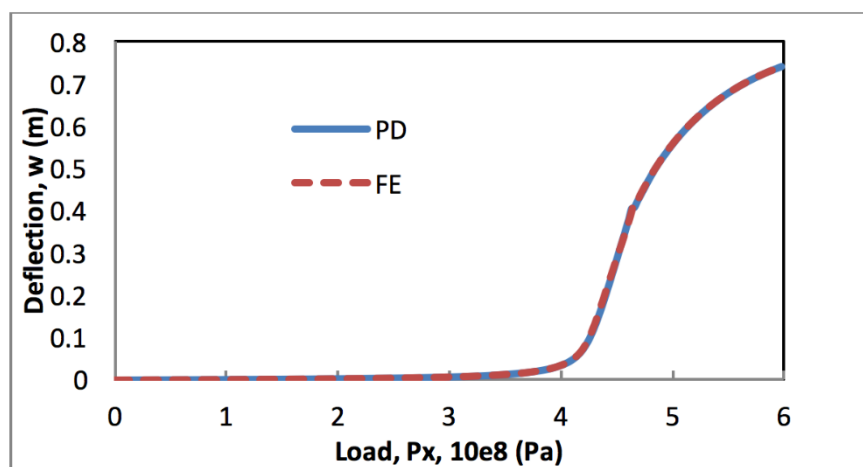


Figure 6.11 Variation of deflection as the applied load increases.

6.3.3 Plate with an initial crack subjected to pure bending loading

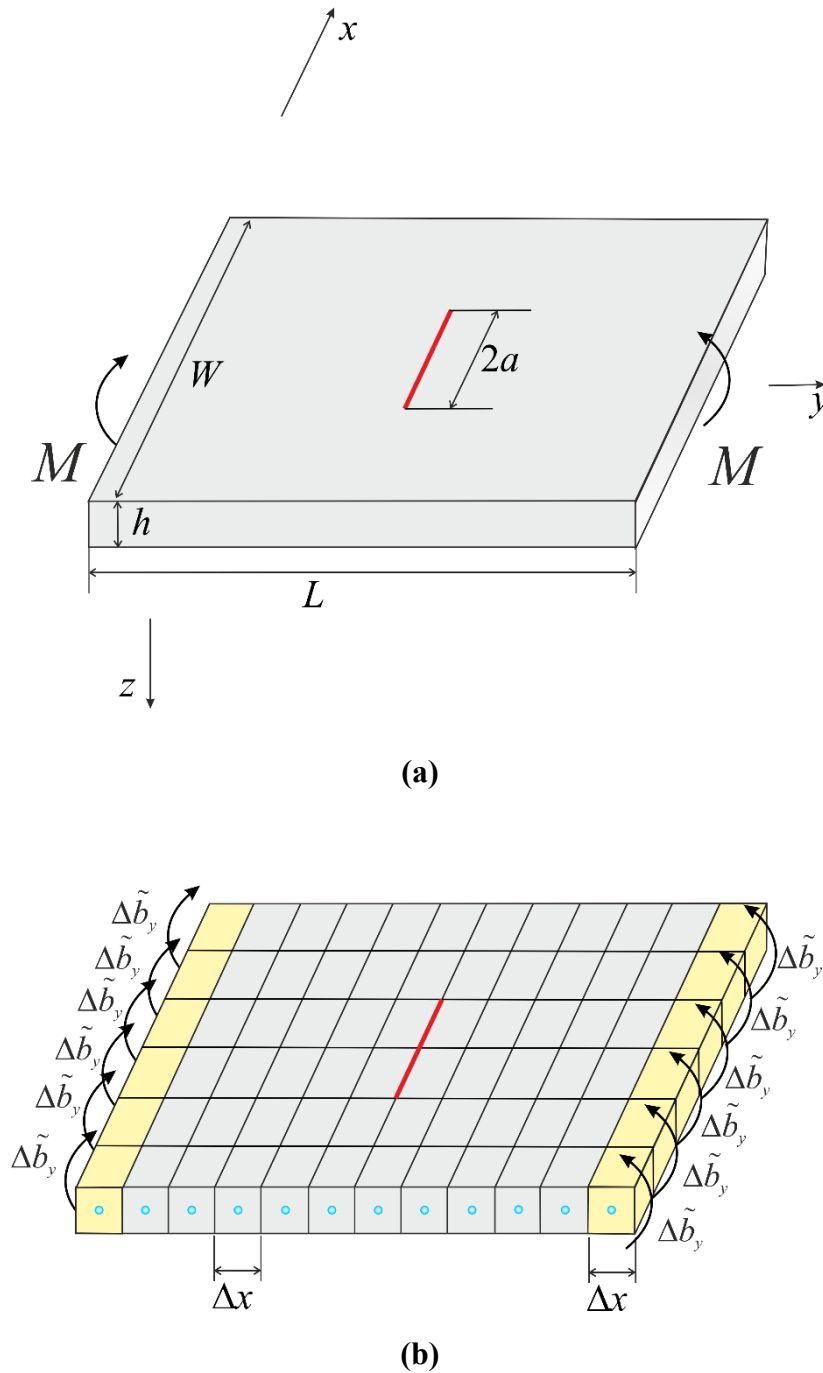
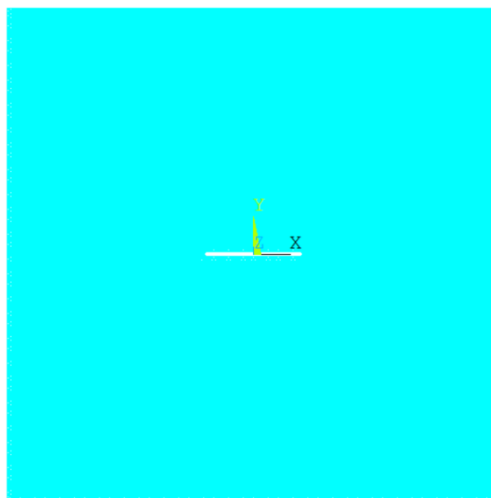


Figure 6.12 **(a)** A plate with a central crack subjected to pure bending loading and **(b)** its discretization.

As mentioned earlier, crack propagation prediction is one of the major strengths of PD theory. To demonstrate this capability, a square plate with an initial central crack aligned

horizontally is considered as shown in Fig. 6.12. The length and width of the square plate are $L = W = 1m$ with a thickness of $h = 0.1m$. The length of the initial crack is $2a = 0.2m$. The material is chosen as polymethyl-methacrylate (PMMA) which shows a brittle fracture behavior. The material properties of the plate are given as Young's modulus of $E = 3.227$ GPa, and Poisson's ratio of $\nu = 1/3$. The mode-I and mode-III fracture toughness are specified as $1.33 \text{ MPa}\sqrt{m}$ (Ayatollahi and Aliha, 2009) and $7.684 \text{ MPa}\sqrt{m}$ (Farshad and Flueler, 1998), respectively. The model is discretized into one single row of material points in the thickness direction. The distance between material points is $\Delta x = 0.01m$. The horizon size is chosen as $\delta = 3.015\Delta x$. A small increment of bending moment loading is applied through a single row of material points at the horizontal boundary regions of the plate. At each subsolution step, the deformation with respect to curvature and shear of each beam element (PD bond) will be evaluated based on Eqs. (6.11a, b), respectively, such that when the deformation of any certain beam element approaches the critical values according to Eqs. (6.15a, b), ANSYS EKILL command will be utilized to fail the element. Under the applied uniform bending, the crack starts to propagate when the resultant body load reaches $\tilde{b}_y = \pm 3.2 \times 10^6 \text{ N/m}$. This result is consistent with the result obtained by Diyaroglu et al. (2015), and as expected, the crack propagates towards the edges of the plate as the load increases as shown in Fig. 6.13.



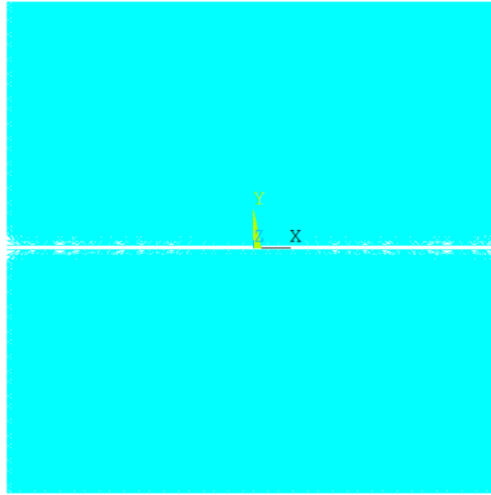


Figure 6.13 Propagation of a central crack in a plate subjected to uniform bending loading.

6.4 Conclusion

The main purpose of this study was to present finite element implementation of peridynamic Timoshenko and Mindlin plate formulations. The advantage of this approach is that only one single row of material point along the thickness is required, which not only decreases the memory consumption by reducing the number of the nodes and elements, but also brings efficiency on processing speed. The feasibility and accuracy of the current approach is verified by considering various benchmark problems and comparing peridynamic results against classical finite element solutions in bending and buckling cases. A good agreement is obtained between peridynamic and finite element analyses results. Moreover, crack growth in a plate subjected to bending loading case is studied to demonstrate the failure prediction capability of the current approach. As a future study, impact analysis will be considered to extend the usage of the current approach. Developed framework can also be used in other applications such as bone mechanics (Lekszycki and dell'Isola, 2012). Moreover, utilizing variational approach as presented in dell'Isola and Placidi (2012) and Placidi et al. (2008), the current formulation will be extended to represent the boundary conditions without utilizing fictitious regions.

7. Conclusion

The first two chapters of this thesis review the development of PD theory and classical beam and plate theories. As introduced above, the non-local character of PD theory makes it a very suitable tool for discontinuous simulation, such as prediction of crack initiation and propagation inside the structures. Moreover, it has a parameter named horizon, which allows representation of non-classical structural and material behaviour that is usually observed at small scale structures. Due to its inherent properties, PD is applicable for analysis of various physical problems including structural deformation, heat transfer, moisture diffusion, porous flow, etc. Moreover, PD is not limited to elasticity, but can represent plastic, viscoelastic and viscoplastic material behaviour. There has been a rapid progress on PD theory for solid mechanics in recent years, however, the investigations with respect to thin structures and functionally graded material are not much in the literature. The existing studies regarding beam and plate either only consider isotropic material, or contain limitation of Poisson's ratio. Therefore, this thesis emphasizes covering this gap and providing researchers with complete PD formulations for various types of isotropic and FGM beams and plates.

In Chapter 3, the most representative PD theories, which are bond-based, ordinary state-based and non-ordinary state-based peridynamic frameworks, are revisited. The novelty of this chapter was to provide an alternative derivation approach of peridynamics equations of motion from an analytical mechanics point of view. Under small deformation assumption, the peridynamics governing equations can be obtained by utilizing the Euler-Lagrange's equation and Taylor expansion. The emphasis of this idea is to convert strain energy density function from classical continuum mechanics form into peridynamics form, which is explained in detail. As it can be seen that all the peridynamics formulations derived in this chapter are in accordance with the previous researchers' results, e.g. Madenci and Oterkus (2014). In this sense, it can be believed

that this way of deriving peridynamics equations of motion can be a suitable alternative for deriving peridynamic formulations and reasonably applied in the following chapters. Moreover, PD numerical solution method with respect to dynamic and static analysis is explained, which indicates that PD solution procedure is more compact rather than FEM.

In Chapter 4, different types of beam theories including functionally graded material models are derived in peridynamics framework. The general idea of the derivation procedure inherits that given in Chapter 3, i.e. using the Euler-Lagrange's equation in conjunction with Taylor's expansion to determine the equations of motion. The peridynamic strain energy density and boundary conditions are discussed in Appendix A1 and B1 for this chapter, respectively. To verify the capability of these studies, peridynamic results are accordingly compared against finite element analysis results for each case under different types of boundary conditions and a very good agreement is obtained between the two approaches.

Chapter 5, which is an extension of Chapter 4, provides with three hierarchical classifications of plate theories comprising Kirchhoff Plate, Mindlin Plate and higher order deformable plate, and as well as their functionally graded material models in peridynamic framework. The derivation procedure is similar to the one given in Chapter 4 but extends the functions from one dimension to two dimensions. The discussion of strain energy density and boundary conditions are given in Appendix A2 and B2, respectively, as references for this chapter. The capability of this study is validated through comparing the displacement field obtained in peridynamic framework with finite element analysis results and a very good agreement is observed for each cases.

PD beams and plates formulations derived in Chapter 4 and 5 are not limited in static analysis, but can be applied to dynamics analysis as well. Regarding time dependent problems, the solution procedures can be referred to Section 3.3. The developed formulations can be utilised for failure analysis of beam and plate structures after incorporating a suitable failure criterion. Moreover, since PD is a non-local continuum

mechanics formulation and has a length scale parameter, i.e. horizon, the current formulations can be beneficial to represent non-classical deformation behaviour especially seen at small scales. Therefore, the developed formulation can be used for the analysis of nanobeams and nanoplates.

In Chapter 6, the implementation of peridynamic Timoshenko Beam and Mindlin Plate formulations in finite element framework is investigated, with Chapter 4.1, Chapter 5.3 and Diyaroglu et al. (2015) being the foundation . The feasibility and accuracy of the current approach is verified by considering various benchmark problems and comparing peridynamic results against classical finite element solutions in bending and buckling cases. A good agreement is obtained between peridynamics and finite element analyses results. Moreover, crack growth in a plate subjected to bending loading case is studied to demonstrate the failure prediction capability of the current approach.

7.1 Future Work

Although PD formulations for beams and plates with respect to thin, thick, isotropic and FGM are developed in this thesis, they are regarding small deformation assumption. PD formulations for large deformation of thin structures can be derived in a similar manner. In this respect, Green's strain tensor will be taken into account rather than small strain tensor and as a consequence, the final PD EoM will become non-linear form. Although solution of non-linear equation system is not as straightforward as that of linear, it may describe the structural failure due to deformation more accurately, especially for ductile material. With this in mind, PD large deformation theory may have broad application prospect in engineering which needs further studies.

In Chapter 5, the derivation of PD formulations for isotropic/FGM plates can be analogically extended to orthotropic material lamina and laminate. By doing this, a global stiffness matrix is need to be assembled by transforming each ply's local

coordinate system aligned with the principal material directions to the laminate coordinate system. Theories for calculating effective material constraints for laminates can be based on the work done by Chou and Carleone (1972) or Sun and Li (1988). Once the global stiffness matrix has been obtained, the rest of derivation can follow the similar procedures programmatically and this is left for a future study.

Implementation of PD beam and plate in finite element framework is explained in Chapter 6. This study is not limited to deformation analysis as given, but can be extended to contact analysis. In this regard, the current PD model can be coupled with ANSYS CONTA and TARGE elements such that structural failure simulation due to external impact loading can be solved. Moreover, with the help of the power of finite element software, additional types of analysis can be studied accordingly, such as modal analysis, harmonic response analysis, non-linear analysis, spectral analysis, etc., which will be left for future work.

Finally, material failure criterion based on PD theory can be further investigated. In classical fracture mechanics theory, various criteria of failure, such as criteria of maximum principal stress (MPSC), maximum shear stress (MSSC), maximum principal strain (MPSNC), maximum strain energy density (MSEDC) and maximum distortion energy density (MDEDC) are customized according to the material types. Regarding brittle materials e.g., cast iron, glass, Perspex, chalk, concrete, etc., MPSC, MPSNC and MSEDC are usually adopted, whereas ductile materials e.g., mild steel, alloy steel, etc., usually satisfy MSSC and MDEDC. These failure criteria are possible to be investigated accordingly based on PD framework. By doing this, each failure criteria can be expressed in terms of displacement only according to the material constitutive law, which can be further transformed into PD form by using Taylor's series expansion. As a consequence, the failure prediction applicability of PD theory with respect to material type can be therefore enhanced, and it will be left for future studies.

Appendix A. Peridynamics Strain Energy Density Functions

A1. PD SED for Beam Theories

The PD strain energy density function has a non-local form such that the strain energy of a certain material point k depends on both its displacement and all other material points in its family, which can be expressed as

$$W_D^{(k)} = W_D^{(k)}(\mathbf{u}_{(k)}, \mathbf{u}_{(1^k)}, \mathbf{u}_{(2^k)}, \mathbf{u}_{(3^k)}, \dots) \quad (\text{A1})$$

where $\mathbf{u}_{(k)}$ is the displacement vector of material point k and $\mathbf{u}_{(i^k)}$ ($i = 1, 2, 3, \dots$) is the displacement vector of the i th material point within the horizon of the material point k (see Figure A1 for Beam Model).

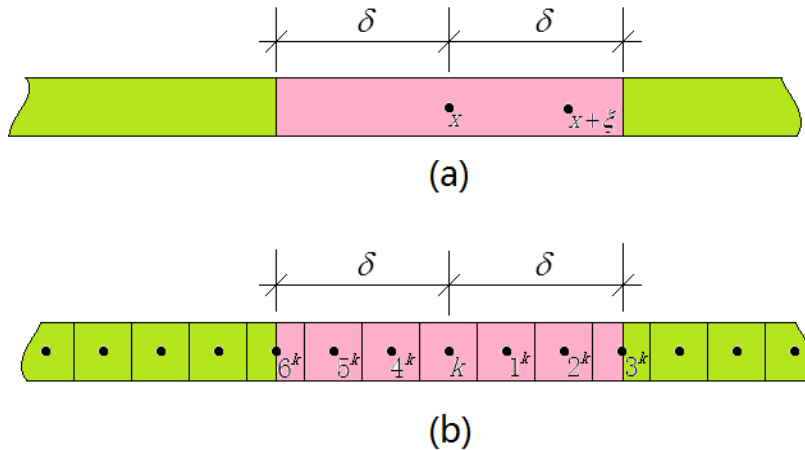


Figure A1 PD influence domain of beam model (a) and its discretization (b)

In this section, derivations of PD SED functions for beam theories are provided.

A1.1 Timoshenko Beam

As explained in Chapter 4.1, the strain energy density function for Timoshenko Beam based on classical continuum mechanics theory can be expressed as

$$W_{\text{CM}} = \frac{1}{2A} \left[E \left(\frac{\partial \theta}{\partial x} \right)^2 + \kappa GA \left(\theta + \frac{\partial w}{\partial x} \right)^2 \right] \quad (\text{A2})$$

In order to obtain the strain energy function in PD form, it is necessary to transform each local term in Eq. (A2) into their equivalent non-local form. This can be achieved by using Taylor expansion.

As shown in Figure A1(a), the rotational displacement function can be Taylor expanded up to 1st order term about point x as

$$\alpha(x + \xi) - \alpha(x) = \frac{\partial \alpha(x)}{\partial x} \xi \quad (\text{A3})$$

Squaring both sides of Eq. (A3) and dividing each terms by $|\xi|$ yields

$$\frac{[\alpha(x + \xi) - \alpha(x)]^2}{|\xi|} = \left(\frac{\partial \alpha(x)}{\partial x} \right)^2 |\xi| \quad (\text{A4})$$

Considering x as a constant point and integrating both side of Eq. (4) over a symmetric domain, $[-\delta, \delta]$, gives

$$\left(\frac{\partial \alpha(x)}{\partial x} \right)^2 = \frac{1}{\delta^2} \int_{-\delta}^{\delta} \frac{[\alpha(x + \xi) - \alpha(x)]^2}{|\xi|} d\xi \quad (\text{A5})$$

Taylor expand the transverse displacement rotational displacement functions and ignore the higher order terms:

$$w(x + \xi) - w(x) = \frac{\partial w(x)}{\partial x} \xi \quad (\text{A6a})$$

and

$$\frac{\alpha(x + \xi) + \alpha(x)}{2} \xi = \alpha(x) \xi \quad (\text{A6b})$$

Combining Eq.(A6a) and (A6b) gives

$$w(x + \xi) - w(x) + \frac{\alpha(x + \xi) + \alpha(x)}{2} \xi = \left(\alpha(x) + \frac{\partial w(x)}{\partial x} \right) \xi \quad (\text{A7})$$

Squaring both sides of Eq.(A7) and dividing each terms by $|\xi|$ results in

$$\frac{1}{|\xi|} \left(w(x + \xi) - w(x) + \frac{\alpha(x + \xi) + \alpha(x)}{2} \xi \right)^2 = \left(\alpha(x) + \frac{\partial w(x)}{\partial x} \right)^2 |\xi| \quad (\text{A8})$$

Considering x as a constant point and integrating both side of Eq.(A8) over a symmetric domain, $[-\delta, \delta]$, gives

$$\left(\alpha(x) + \frac{\partial w(x)}{\partial x} \right)^2 = \frac{1}{\delta^2} \int_{-\delta}^{\delta} \frac{1}{|\xi|} \left(w(x + \xi) - w(x) + \frac{\alpha(x + \xi) + \alpha(x)}{2} \xi \right)^2 d\xi \quad (\text{A9})$$

Eqs. (A5) and (A9) can be respectively discretized at material point k as

$$\left(\frac{\partial\theta_{(k)}}{\partial x}\right)^2 = \frac{1}{\delta^2 A} \sum_i \frac{(\theta_{(i^k)} - \theta_{(k)})^2}{|\xi_{(i^k)(k)}^\xi|} V_{(i^k)} \quad (\text{A10a})$$

$$\left(\theta_{(k)} + \frac{\partial w_{(k)}}{\partial x}\right)^2 = \frac{1}{\delta^2 A} \sum_i \frac{1}{|\xi_{(i^k)(k)}^\xi|} \left(w_{(i^k)} - w_{(k)} + \frac{\theta_{(i^k)} + \theta_{(k)}}{2} \xi_{(i^k)(k)}^\xi \right)^2 V_{(i^k)} \quad (\text{A10b})$$

Substituting Eqs. (A10a) and (A10b) into (A2) arises the SED function in PD form for material point k as

$$W_{\text{PD}}^{(k)} = \frac{1}{2\delta^2 A} \left[\frac{E}{A} \sum_i \frac{(\theta_{(i^k)} - \theta_{(k)})^2}{|\xi_{(i^k)(k)}^\xi|} V_{(i^k)} + \kappa G \sum_i \frac{\left(w_{(i^k)} - w_{(k)} + \frac{\theta_{(i^k)} + \theta_{(k)}}{2} \xi_{(i^k)(k)}^\xi \right)^2}{|\xi_{(i^k)(k)}^\xi|} V_{(i^k)} \right] \quad (\text{A11a})$$

Similarly, the PD strain energy density function for the material point j can be written by changing index as

$$W_{\text{PD}}^{(j)} = \frac{1}{2\delta^2 A} \left[\frac{E}{A} \sum_i \frac{[\theta_{(i^j)} - \theta_{(j)}]^2}{|\xi_{(i^j)(j)}^\xi|} V_{(i^j)} + \kappa G \sum_i \frac{\left(w_{(i^j)} - w_{(j)} + \frac{\theta_{(i^j)} + \theta_{(j)}}{2} \xi_{(i^j)(j)}^\xi \right)^2}{|\xi_{(i^j)(j)}^\xi|} V_{(i^j)} \right] \quad (\text{A11b})$$

A1.2 PD SED Function for Higher Order Deformable Beam

As explained in Chapter 4.2, the SED function for higher order deformable beam can be expressed based on classical continuum mechanics theory as

$$W_{\text{GM}} = \frac{1}{2A} \left\{ \frac{E}{1-\nu^2} \left[I \left(\left(\frac{\partial\theta}{\partial x} + 2w^* \right)^2 - 4(1-\nu) w^* \frac{\partial\theta}{\partial x} \right) + 2I^* \frac{\partial\theta^*}{\partial x} \left(\frac{\partial\theta}{\partial x} + 2w^* \right) + I^{**} \left(\frac{\partial\theta^*}{\partial x} \right)^2 \right] \right. \\ \left. + G \left[A \left(\theta + \frac{\partial w}{\partial x} \right)^2 + 2I \left(\theta + \frac{\partial w}{\partial x} \right) \left(3\theta^* + \frac{\partial w^*}{\partial x} \right) + I^* \left(3\theta^* + \frac{\partial w^*}{\partial x} \right)^2 \right] \right\} \quad (\text{A12})$$

Taylor expand the functions θ and w^* about point x and ignore the terms higher than 1st order:

$$\theta(x + \xi) - \theta(x) = \frac{\partial\theta(x)}{\partial x} \xi \quad (\text{A13a})$$

$$\left[w^*(x + \xi) + w^*(x) \right] \xi = 2w^*(x)\xi \quad (\text{A13b})$$

Combine Eq. (A13a) and (A13b) together gives

$$\alpha(x + \xi) - \alpha(x) + [\dot{w}(x + \xi) + \dot{w}(x)] \xi = \left(\frac{\partial \alpha(x)}{\partial x} + 2\dot{w}(x) \right) \xi \quad (\text{A14})$$

Square the both sides of Eq. (A14):

$$\frac{\{\alpha(x + \xi) - \alpha(x) + [\dot{w}(x + \xi) + \dot{w}(x)] \xi\}^2}{|\xi|} = \left(\frac{\partial \alpha(x)}{\partial x} + 2\dot{w}(x) \right)^2 |\xi| \quad (\text{A15})$$

Considering x as the fixed point, and integrating each terms of Eq. (A15) over a symmetric interval, $(\delta, -\delta)$, gives

$$\left(\frac{\partial \alpha(x)}{\partial x} + 2\dot{w}(x) \right)^2 = \frac{1}{\delta^2} \int_{-\delta}^{\delta} \frac{\{\alpha(x + \xi) - \alpha(x) + [\dot{w}(x + \xi) + \dot{w}(x)] \xi\}^2}{|\xi|} d\xi \quad (\text{A16a})$$

Following expressions can be obtain by using the analogical manner as

$$\frac{\partial \alpha(x)}{\partial x} \dot{w}(x) = \frac{1}{\delta^2} \int_{-\delta}^{\delta} [\alpha(x + \xi) - \alpha(x)] \frac{\dot{w}(x + \xi) + \dot{w}(x)}{2} \text{sgn}(\xi) d\xi \quad (\text{A16b})$$

$$\frac{\partial \theta'(x)}{\partial x} \left(\frac{\partial \alpha(x)}{\partial x} + 2\nu \dot{w}(x) \right) = \frac{1}{\delta^2} \int_{-\delta}^{\delta} \frac{\theta'(x + \xi) - \theta'(x)}{|\xi|} \left\{ \alpha(x + \xi) - \alpha(x) + \nu [\dot{w}(x + \xi) + \dot{w}(x)] \xi \right\} d\xi \quad (\text{A16c})$$

$$\left(\frac{\partial \theta'(x)}{\partial x} \right)^2 = \frac{1}{\delta^2} \int_{-\delta}^{\delta} \frac{[\theta'(x + \xi) - \theta'(x)]^2}{|\xi|} d\xi \quad (\text{A16d})$$

$$\left(\alpha(x) + \frac{\partial \nu(x)}{\partial x} \right)^2 = \frac{1}{\delta^2} \int_{-\delta}^{\delta} \frac{1}{|\xi|} \left(\nu(x + \xi) - \nu(x) + \frac{\alpha(x + \xi) + \alpha(x)}{2} \xi \right)^2 d\xi \quad (\text{A16e})$$

$$\left(\alpha(x) + \frac{\partial \nu(x)}{\partial x} \right) \left(3\theta'(x) + \frac{\partial \dot{w}(x)}{\partial x} \right) = \frac{1}{\delta^2} \int_{-\delta}^{\delta} \left\{ \frac{1}{|\xi|} \left(\nu(x + \xi) - \nu(x) + \frac{\alpha(x + \xi) + \alpha(x)}{2} \xi \right) \times \left(3 \frac{\theta'(x + \xi) + \theta'(x)}{2} \xi + \dot{w}(x + \xi) - \dot{w}(x) \right) \right\} d\xi \quad (\text{A16f})$$

$$\left(3\theta'(x) + \frac{\partial \dot{w}(x)}{\partial x} \right)^2 = \frac{1}{\delta^2} \int_{-\delta}^{\delta} \frac{1}{|\xi|} \left(3 \frac{\theta'(x + \xi) + \theta'(x)}{2} \xi + \dot{w}(x + \xi) - \dot{w}(x) \right)^2 d\xi \quad (\text{A16g})$$

Eqs. (A16) can be discretized as

$$\left(\frac{\partial \theta_{(k)}}{\partial x} + 2\dot{w}_{(k)} \right)^2 = \frac{1}{\delta^2 A} \sum_i \frac{[\theta_{(i^k)} - \theta_{(k)} + (\dot{w}_{(i^k)} + \dot{w}_{(k)}) \xi_{(i^k)(k)}]^2}{|\xi_{(i^k)(k)}|} V_{(i^k)} \quad (\text{A17a})$$

$$\frac{\partial \theta_{(k)}}{\partial x} \dot{w}_{(k)} = \frac{1}{\delta^2 A} \sum_i (\theta_{(i^k)} - \theta_{(k)}) \frac{\dot{w}_{(i^k)} + \dot{w}_{(k)}}{2} \text{sign}(\xi_{(i^k)(k)}) V_{(i^k)} \quad (\text{A17b})$$

$$\frac{\partial \theta'_{(k)}}{\partial x} \left(\frac{\partial \theta_{(k)}}{\partial x} + 2\nu \dot{w}_{(k)} \right) = \frac{1}{\delta^2 A} \sum_i \frac{\theta'_{(i^k)} - \theta'_{(k)}}{|\xi_{(i^k)(k)}|} [\theta_{(i^k)} - \theta_{(k)} + \nu (\dot{w}_{(i^k)} + \dot{w}_{(k)}) \xi_{(i^k)(k)}] V_{(i^k)} \quad (\text{A17c})$$

$$\left(\frac{\partial \theta_{(k)}^*}{\partial \mathbf{x}}\right)^2 = \frac{1}{\delta^2 A} \sum_i \frac{(\theta_{(i^k)}^* - \theta_{(k)}^*)^2}{|\xi_{(i^k)(k)}|} V_{(i^k)} \quad (\text{A17d})$$

$$\left(\theta_{(k)} + \frac{\partial W_{(k)}}{\partial \mathbf{x}}\right)^2 = \frac{1}{\delta^2 A} \sum_i \frac{1}{|\xi_{(i^k)(k)}|} \left(w_{(i^k)} - w_{(k)} + \frac{\theta_{(i^k)} + \theta_{(k)}}{2} \xi_{(i^k)(k)} \right)^2 V_{(i^k)} \quad (\text{A17e})$$

$$\left(\theta_{(k)} + \frac{\partial W_{(k)}}{\partial \mathbf{x}}\right) \left(3\theta_{(k)}^* + \frac{\partial W_{(k)}^*}{\partial \mathbf{x}} \right) = \frac{1}{\delta^2 A} \sum_i \left\{ \frac{1}{|\xi_{(i^k)(k)}|} \left(w_{(i^k)} - w_{(k)} + \frac{\theta_{(i^k)} + \theta_{(k)}}{2} \xi_{(i^k)(k)} \right) \right. \\ \left. \times \left(3 \frac{\theta_{(i^k)}^* + \theta_{(k)}^*}{2} \xi_{(i^k)(k)} + w_{(i^k)}^* - w_{(k)}^* \right) \right\} V_{(i^k)} \quad (\text{A17f})$$

$$\left(3\theta_{(k)}^* + \frac{\partial W_{(k)}^*}{\partial \mathbf{x}} \right)^2 = \frac{1}{\delta^2 A} \sum_i \frac{1}{|\xi_{(i^k)(k)}|} \left(3 \frac{\theta_{(i^k)}^* + \theta_{(k)}^*}{2} \xi_{(i^k)(k)} + w_{(i^k)}^* - w_{(k)}^* \right)^2 V_{(i^k)} \quad (\text{A17g})$$

Replacing the corresponding terms of Eq.(A2) with (A17) yields the SED function in PD form at material point k as

$$W_{\text{PD}}^{(k)} = \frac{1}{2\delta^2 A^2} \left\{ \frac{E}{1-\nu^2} \left[I \sum_{i^k} \frac{(\theta_{(i^k)} - \theta_{(k)})^2 + 2\nu (w_{(i^k)}^* + w_{(k)}^*) (\theta_{(i^k)} - \theta_{(k)}) \xi_{(i^k)(k)} + (w_{(i^k)}^* + w_{(k)}^*)^2 \xi_{(i^k)(k)}^2}{|\xi_{(i^k)(k)}|} V_{(i^k)} \right. \right. \\ \left. \left. + 2I^* \sum_{i^k} \frac{[\theta_{(i^k)} - \theta_{(k)} + \nu (w_{(i^k)}^* + w_{(k)}^*) \xi_{(i^k)(k)}] (\theta_{(i^k)}^* - \theta_{(k)}^*)}{|\xi_{(i^k)(k)}|} V_{(i^k)} \right. \right. \\ \left. \left. + I^{**} \sum_{i^k} \frac{(\theta_{(i^k)}^* - \theta_{(k)}^*)^2}{|\xi_{(i^k)(k)}|} V_{(i^k)} \right] \right. \\ \left. + G \left[A \sum_{i^k} \frac{1}{|\xi_{(i^k)(k)}|} \left(w_{(i^k)} - w_{(k)} + \frac{\theta_{(i^k)} + \theta_{(k)}}{2} \xi_{(i^k)(k)} \right)^2 V_{(i^k)} \right. \right. \\ \left. \left. + I^* \sum_{i^k} \frac{1}{|\xi_{(i^k)(k)}|} \left(w_{(i^k)}^* - w_{(k)}^* + 3 \frac{\theta_{(k)}^* + \theta_{(i^k)}^*}{2} \xi_{(i^k)(k)} \right)^2 V_{(i^k)} \right. \right. \\ \left. \left. + 2I \sum_{i^k} \frac{\left(w_{(i^k)} - w_{(k)} + \frac{\theta_{(i^k)} + \theta_{(k)}}{2} \xi_{(i^k)(k)} \right) \left(w_{(i^k)}^* - w_{(k)}^* + 3 \frac{\theta_{(k)}^* + \theta_{(i^k)}^*}{2} \xi_{(i^k)(k)} \right)}{|\xi_{(i^k)(k)}|} V_{(i^k)} \right] \right\} \quad (\text{A18a})$$

A similar form will hold for SED at material j if we replace the index k with j

$$\mathcal{W}_{\text{FD}}^{(j)} = \frac{1}{2\delta^2 A^2} \left\{ \begin{aligned} & \left[\begin{aligned} & I \sum_i \frac{(\theta_{(i^j)} - \theta_{(j)})^2 + 2\nu(\dot{w}_{(i^j)} + \dot{w}_{(j)})(\theta_{(i^j)} - \theta_{(j)})\xi_{(i^j)(j)} + (\dot{w}_{(i^j)} + \dot{w}_{(j)})^2 \xi_{(i^j)(j)}^2}{|\xi_{(i^j)(j)}|} V_{(i^j)} \\ & + 2I \sum_i \frac{(\theta_{(i^j)} - \theta_{(j)} + \nu(\dot{w}_{(i^j)} + \dot{w}_{(j)})\xi_{(i^j)(j)})(\theta_{(i^j)} - \theta_{(j)})}{|\xi_{(i^j)(j)}|} V_{(i^j)} \\ & + I \sum_i \frac{(\theta_{(i^j)} - \theta_{(j)})^2}{|\xi_{(i^j)(j)}|} V_{(i^j)} \end{aligned} \right] \\ & + G \left[\begin{aligned} & A \sum_i \frac{1}{|\xi_{(i^j)(j)}|} \left(w_{(i^j)} - w_{(j)} + \frac{\theta_{(i^j)} + \theta_{(j)}}{2} \xi_{(i^j)(j)} \right)^2 V_{(i^j)} \\ & + I \sum_i \frac{1}{|\xi_{(i^j)(j)}|} \left(\dot{w}_{(i^j)} - \dot{w}_{(j)} + 3 \frac{\theta_{(j)} + \theta_{(i^j)}}{2} \xi_{(i^j)(j)} \right)^2 V_{(i^j)} \\ & + 2I \sum_i \frac{\left(w_{(i^j)} - w_{(j)} + \frac{\theta_{(i^j)} + \theta_{(j)}}{2} \xi_{(i^j)(j)} \right) \left(\dot{w}_{(i^j)} - \dot{w}_{(j)} + 3 \frac{\theta_{(j)} + \theta_{(i^j)}}{2} \xi_{(i^j)(j)} \right)}{|\xi_{(i^j)(j)}|} V_{(i^j)} \end{aligned} \right] \end{aligned} \right\} \quad (\text{A18b})$$

A1.3 PD SED for FGM Euler Beam

As mentioned in Chapter 4.3, the SED of FGM Euler-Bernoulli beam can be expressed as

$$\mathcal{W}_{\text{con}} = \frac{1}{2A} \int_A \mathbf{E}(z) \left[\left(\frac{\partial u}{\partial x} \right)^2 - 2z \frac{\partial u}{\partial x} \frac{\partial^2 w}{\partial x^2} + z^2 \left(\frac{\partial^2 w}{\partial x^2} \right)^2 \right] dA \quad (\text{A19})$$

In order to obtain the corresponding SED function in PD form, each partial derivative term is needed to transform into the equivalent non-local term, and this can be achieved by using Taylor expansion.

If we Taylor expand the transverse displacement function w about point x and omit the higher order terms:

$$w(x + \xi) - w(x) = \frac{\partial w(x)}{\partial x} \xi + \frac{1}{2} \frac{\partial^2 w(x)}{\partial x^2} \xi^2 \quad (\text{A20})$$

Multiplying each term of Eq. (A20) by $\frac{1}{\xi^2}$ and integrating over a symmetric interval,

$(\delta, -\delta)$ yields

$$\frac{\partial^2 w(x)}{\partial x^2} = \frac{1}{\delta} \int_{-\delta}^{\delta} \frac{w(x + \xi) - w(x)}{\xi^2} d\xi \quad (\text{A21})$$

Note that the transverse displacement function $w(x)$ is related to the flexural deformation of the beam, thus, multiplying Eq. (A20) by $\frac{1}{\xi^2}$ is for the sake of ensuring the dimension of integrand of Eq. (A21) in accordance to the curvature, i.e., “1/length”.

Again, Taylor expand the axial displacement function u about point x and omit the higher order terms:

$$u(x + \xi) - u(x) = \frac{\partial u(x)}{\partial x} \xi \quad (\text{A22})$$

Multiplying each term of Eq.(A22) by $\frac{1}{\xi}$ and integrating over a symmetric interval,

$(\delta, -\delta)$ yields

$$\frac{\partial u(x)}{\partial x} = \frac{1}{2\delta} \int_{-\delta}^{\delta} \frac{u(x + \xi) - u(x)}{\xi} d\xi \quad (\text{A23})$$

Eqs. (A21) and (A23) can be discretized for material point k as

$$\frac{\partial u_{(k)}}{\partial x} = \frac{1}{2\delta A} \sum_i \frac{u_{(i^k)} - u_{(k)}}{\xi_{(i^k)(k)}} V_{(i^k)} \quad (\text{A24a})$$

$$\frac{\partial^2 w_{(k)}}{\partial x^2} = \frac{1}{\delta A} \sum_i \frac{w_{(i^k)} - w_{(k)}}{\xi_{(i^k)(k)}^2} V_{(i^k)} \quad (\text{A24b})$$

Utilizing the pre-obtained expression, Eq. (3.15b)

$$\left(\frac{\partial u_{(k)}}{\partial x} \right)^2 = \frac{1}{\delta^2 A} \sum_i \frac{(u_{(i^k)} - u_{(k)})^2}{|\xi_{(i^k)(k)}|} V_{(i^k)} \quad (\text{A24c})$$

and plugging Eqs. (A24) into (A19) arises the PD SED function for material point k as

$$W_{PD}^{(k)} = \frac{1}{2A} \frac{1}{\delta^2 A^2} \left[\begin{aligned} & A \int_A E(z) dA \sum_i \frac{(u_{(i^k)} - u_{(k)})^2}{|\xi_{(i^k)(k)}|} V_{(i^k)} + \int_A E(z) z^2 dA \left(\sum_i \frac{w_{(i^k)} - w_{(k)}}{\xi_{(i^k)(k)}^2} V_{(i^k)} \right)^2 \\ & - \int_A E(z) z dA \sum_i \frac{u_{(i^k)} - u_{(k)}}{\xi_{(i^k)(k)}} V_{(i^k)} \sum_i \frac{w_{(i^k)} - w_{(k)}}{\xi_{(i^k)(k)}^2} V_{(i^k)} \end{aligned} \right] \quad (\text{A25a})$$

Similarly, the PD strain energy density function for the material point j can be written by changing index as

$$W_{\text{pd}}^{(j)} = \frac{1}{2A} \frac{1}{\delta^2 A^2} \left[\int_A E(z) dA \sum_i \frac{(u_{(i^j)} - u_{(j)})^2}{|\xi_{(i^j)(j)}|} V_{(i^j)} + \int_A E(z) z^2 dA \left(\sum_i \frac{w_{(i^j)} - w_{(j)}}{\xi_{(i^j)(j)}^2} V_{(i^j)} \right)^2 \right. \\ \left. - \int_A E(z) z dA \sum_i \frac{u_{(i^j)} - u_{(j)}}{\xi_{(i^j)(j)}} V_{(i^j)} \sum_i \frac{w_{(i^j)} - w_{(j)}}{\xi_{(i^j)(j)}^2} V_{(i^j)} \right] \quad (\text{A25b})$$

A1.4 PD SED for FGM Timosheno Beam

As derived in Chapter 4.4, the SED function for FGM Timoshenko beam based on classical continuum mechanics theory can be expressed

$$W_{\text{cm}} = \frac{1}{2A} \left[\int_A E dA \left(\frac{\partial u}{\partial x} \right)^2 + \int_A E z^2 dA \left(\frac{\partial \theta}{\partial x} \right)^2 + 2 \int_A E z dA \frac{\partial u}{\partial x} \frac{\partial \theta}{\partial x} + \int_A \kappa G dA \left(\theta + \frac{\partial w}{\partial x} \right)^2 \right] \quad (\text{A26})$$

In order to obtain the strain energy density function in PD form, it is necessary to transform each term into an equivalent PD expression and this can be achieved by utilizing Taylor's expansion. If we expand the axial displacement u and rotational displacement θ about a point x and ignore the higher order terms:

$$u(x + \xi) - u(x) = \frac{\partial u(x)}{\partial x} \xi \quad (\text{A27a})$$

$$\theta(x + \xi) - \theta(x) = \frac{\partial \theta(x)}{\partial x} \xi \quad (\text{A27b})$$

Multiplying Eq. (A27a) with (A27b) and dividing each terms by $|\xi|$ yields

$$\frac{[u(x + \xi) - u(x)][\theta(x + \xi) - \theta(x)]}{|\xi|} = \frac{\partial \theta(x)}{\partial x} \frac{\partial u(x)}{\partial x} |\xi| \quad (\text{A28})$$

Considering x as a fix point and integrating each term over the interval $(-\delta, \delta)$ results in

$$\frac{\partial \theta(x)}{\partial x} \frac{\partial u(x)}{\partial x} = \frac{1}{\delta^2} \int_{-\delta}^{\delta} \frac{[u(x + \xi) - u(x)][\theta(x + \xi) - \theta(x)]}{|\xi|} d\xi \quad (\text{A29})$$

which can be discretized at material point k as

$$\frac{\partial \theta_{(k)}}{\partial x} \frac{\partial u_{(k)}}{\partial x} = \frac{1}{\delta^2 A} \sum_i \frac{(u_{(i^k)} - u_{(k)})(\theta_{(i^k)} - \theta_{(k)})}{|\xi_{(i^k)(k)}|} V_{(i^k)} \quad (\text{A30a})$$

Recalling the pre-proved results, Eqs. (3.15b), (A10a) and (A10b):

$$\left(\frac{\partial u_{(k)}}{\partial x} \right)^2 = \frac{1}{\delta^2 A} \sum_i \frac{(u_{(i^k)} - u_{(k)})^2}{|\xi_{(i^k)(k)}|} V_{(i^k)} \quad (\text{A30b})$$

$$\left(\frac{\partial\theta_{(k)}}{\partial\mathbf{x}}\right)^2 = \frac{1}{\delta^2\mathbf{A}} \sum_i \frac{(\theta_{(i^k)} - \theta_{(k)})^2}{|\xi_{(i^k)(k)}|} V_{(i^k)} \quad (\text{A30c})$$

$$\left(\theta_{(k)} + \frac{\partial W_{(k)}}{\partial\mathbf{x}}\right)^2 = \frac{1}{\delta^2\mathbf{A}} \sum_i \frac{1}{|\xi_{(i^k)(k)}|} \left(w_{(i^k)} - w_{(k)} + \frac{\theta_{(i^k)} + \theta_{(k)}}{2} \xi_{(i^k)(k)} \right)^2 V_{(i^k)} \quad (\text{A30d})$$

and substituting Eqs. (A30) into (A26) results in the PD SED function for material point k as

$$W_{\text{PD}}^{(k)} = \frac{1}{2\delta^2\mathbf{A}^2} \left[\int_A E d\mathbf{A} \sum_i \frac{(u_{(i^k)} - u_{(k)})^2}{|\xi_{(i^k)(k)}|} V_{(i^k)} + \int_A E z^2 d\mathbf{A} \sum_i \frac{(\theta_{(i^k)} - \theta_{(k)})^2}{|\xi_{(i^k)(k)}|} V_{(i^k)} \right. \\ \left. + 2 \int_A E z d\mathbf{A} \sum_i \frac{(u_{(i^k)} - u_{(k)})(\theta_{(i^k)} - \theta_{(k)})}{|\xi_{(i^k)(k)}|} V_{(i^k)} + \int_A \kappa G d\mathbf{A} \sum_i \frac{1}{|\xi_{(i^k)(k)}|} \left(w_{(i^k)} - w_{(k)} + \frac{\theta_{(i^k)} + \theta_{(k)}}{2} \xi_{(i^k)(k)} \right)^2 V_{(i^k)} \right] \quad (\text{A31a})$$

Similarly, the PD SED of a certain family member of k can be expressed as

$$W_{\text{PD}}^{(i)} = \frac{1}{2\delta^2\mathbf{A}^2} \left[\int_A E d\mathbf{A} \sum_i \frac{(u_{(i^i)} - u_{(j)})^2}{|\xi_{(i^i)(j)}|} V_{(i^i)} + \int_A E z^2 d\mathbf{A} \sum_i \frac{(\theta_{(i^i)} - \theta_{(j)})^2}{|\xi_{(i^i)(j)}|} V_{(i^i)} \right. \\ \left. + 2 \int_A E z d\mathbf{A} \sum_i \frac{(u_{(i^i)} - u_{(j)})(\theta_{(i^i)} - \theta_{(j)})}{|\xi_{(i^i)(j)}|} V_{(i^i)} + \int_A \kappa G d\mathbf{A} \sum_i \frac{1}{|\xi_{(i^i)(j)}|} \left(w_{(i^i)} - w_{(j)} + \frac{\theta_{(i^i)} + \theta_{(j)}}{2} \xi_{(i^i)(j)} \right)^2 V_{(i^i)} \right] \quad (\text{A31b})$$

A1.5 PD SED for FGM Higher Order Deformable Beam

As derived in Chapter 4.5, the strain energy density

$$\begin{aligned}
W_{\text{COM}} = & \frac{1}{2A} \left\{ \int_A \frac{E}{1-\nu^2} dA \left[\left(\frac{\partial u}{\partial x} \right)^2 + (\theta_z)^2 \right] + \int_A \frac{2Ez}{1-\nu^2} dA \left(\frac{\partial u}{\partial x} \frac{\partial \theta}{\partial x} + 2\theta_z \dot{w} \right) \right. \\
& + \int_A \frac{Ez^2}{1-\nu^2} dA \left[\left(\frac{\partial \theta}{\partial x} \right)^2 + 2 \frac{\partial u}{\partial x} \frac{\partial \dot{u}}{\partial x} + 4(\dot{w})^2 \right] + \\
& \left. \int_A \frac{2Ez^3}{1-\nu^2} dA \left(\frac{\partial u}{\partial x} \frac{\partial \theta^*}{\partial x} + \frac{\partial \theta}{\partial x} \frac{\partial \dot{u}}{\partial x} \right) + \int_A \frac{Ez^4}{1-\nu^2} dA \left[\left(\frac{\partial \dot{u}}{\partial x} \right)^2 + 2 \frac{\partial \theta}{\partial x} \frac{\partial \theta^*}{\partial x} \right] \right. \\
& \left. + \int_A \frac{2Ez^5}{1-\nu^2} dA \frac{\partial \dot{u}}{\partial x} \frac{\partial \theta^*}{\partial x} + \int_A \frac{Ez^6}{1-\nu^2} dA \left(\frac{\partial \theta^*}{\partial x} \right)^2 \right\} \\
& + \frac{1}{A} \left[\int_A \frac{E\nu z}{1-\nu^2} dA \frac{\partial u}{\partial x} \theta_z + \int_A \frac{E\nu z}{1-\nu^2} dA \left(2 \frac{\partial u}{\partial x} \dot{w} + \frac{\partial \theta}{\partial x} \theta_z \right) \right. \\
& + \int_A \frac{E\nu z^2}{1-\nu^2} dA \left(2 \frac{\partial \theta}{\partial x} \dot{w} + \frac{\partial \dot{u}}{\partial x} \theta_z \right) \\
& \left. + \int_A \frac{E\nu z^3}{1-\nu^2} dA \left(2 \frac{\partial \dot{u}}{\partial x} \dot{w} + \frac{\partial \theta^*}{\partial x} \theta_z \right) + \int_A \frac{2E\nu z^4}{1-\nu^2} dA \frac{\partial \theta^*}{\partial x} \dot{w} \right] \\
& + \frac{1}{2A} \left\{ \int_A \mathbf{G} dA \left(\theta + \frac{\partial w}{\partial x} \right)^2 + 2 \int_A \mathbf{G} dA \left(\theta + \frac{\partial w}{\partial x} \right) \left(2\dot{u} + \frac{\partial \theta_z}{\partial x} \right) \right. \\
& + \int_A \mathbf{G}^2 dA \left[\left(2\dot{u} + \frac{\partial \theta_z}{\partial x} \right)^2 + 2 \left(\theta + \frac{\partial w}{\partial x} \right) \left(3\theta^* + \frac{\partial \dot{w}}{\partial x} \right) \right] \\
& \left. + 2 \int_A \mathbf{G}^3 dA \left(2\dot{u} + \frac{\partial \theta_z}{\partial x} \right) \left(3\theta^* + \frac{\partial \dot{w}}{\partial x} \right) + \int_A \mathbf{G}^4 dA \left(3\theta^* + \frac{\partial \dot{w}}{\partial x} \right)^2 \right\}
\end{aligned} \tag{A32}$$

In order to obtain the strain energy density function in PD form, it is necessary to transform each term into an equivalent PD expression and this can be achieved by utilizing Taylor's expansion.

Eq. (A32) can be separated into three parts for simplification as

$$W_{\text{COM}} = W_{\text{COM}}^I + W_{\text{COM}}^{II} + W_{\text{COM}}^{III} \tag{A33}$$

where

$$\begin{aligned}
W_{\text{COM}}^I = & \frac{1}{2A} \left\{ \int_A \frac{E}{1-\nu^2} dA \left[\left(\frac{\partial u}{\partial x} \right)^2 + (\theta_z)^2 \right] + \int_A \frac{2Ez}{1-\nu^2} dA \left(\frac{\partial u}{\partial x} \frac{\partial \theta}{\partial x} + 2\theta_z \dot{w} \right) \right. \\
& + \int_A \frac{Ez^2}{1-\nu^2} dA \left[\left(\frac{\partial \theta}{\partial x} \right)^2 + 2 \frac{\partial u}{\partial x} \frac{\partial \dot{u}}{\partial x} + 4(\dot{w})^2 \right] \\
& \left. + \int_A \frac{2Ez^3}{1-\nu^2} dA \left(\frac{\partial u}{\partial x} \frac{\partial \theta^*}{\partial x} + \frac{\partial \theta}{\partial x} \frac{\partial \dot{u}}{\partial x} \right) + \int_A \frac{Ez^4}{1-\nu^2} dA \left[\left(\frac{\partial \dot{u}}{\partial x} \right)^2 + 2 \frac{\partial \theta}{\partial x} \frac{\partial \theta^*}{\partial x} \right] \right. \\
& \left. + \int_A \frac{2Ez^5}{1-\nu^2} dA \frac{\partial \dot{u}}{\partial x} \frac{\partial \theta^*}{\partial x} + \int_A \frac{Ez^6}{1-\nu^2} dA \left(\frac{\partial \theta^*}{\partial x} \right)^2 \right\}
\end{aligned} \tag{A34a}$$

$$W_{CCM}^I = \frac{1}{A} \left[\int_A \frac{Ev}{1-\nu^2} dA \frac{\partial u}{\partial x} \theta_z + \int_A \frac{Evz}{1-\nu^2} dA \left(2 \frac{\partial u}{\partial x} \dot{w} + \frac{\partial \theta}{\partial x} \theta_z \right) \right. \\ \left. + \int_A \frac{Evz^2}{1-\nu^2} dA \left(2 \frac{\partial \theta}{\partial x} \dot{w} + \frac{\partial u}{\partial x} \theta_z \right) \right. \\ \left. + \int_A \frac{Evz^3}{1-\nu^2} dA \left(2 \frac{\partial u}{\partial x} \dot{w} + \frac{\partial \theta}{\partial x} \theta_z \right) + \int_A \frac{2Evz^4}{1-\nu^2} dA \frac{\partial \theta}{\partial x} \dot{w} \right] \quad (A34b)$$

$$W_{CCM}^{III} = \frac{1}{2A} \left\{ \int_A \mathbf{G} dA \left(\theta + \frac{\partial W}{\partial x} \right)^2 + 2 \int_A \mathbf{G} z dA \left(\theta + \frac{\partial W}{\partial x} \right) \left(2u^* + \frac{\partial \theta_z}{\partial x} \right) \right. \\ \left. + \int_A \mathbf{G} z^2 dA \left[\left(2u^* + \frac{\partial \theta_z}{\partial x} \right)^2 + 2 \left(\theta + \frac{\partial W}{\partial x} \right) \left(3\theta^* + \frac{\partial \dot{w}}{\partial x} \right) \right] \right. \\ \left. + 2 \int_A \mathbf{G} z^3 dA \left(2u^* + \frac{\partial \theta_z}{\partial x} \right) \left(3\theta^* + \frac{\partial \dot{w}}{\partial x} \right) + \int_A \mathbf{G} z^4 dA \left(3\theta^* + \frac{\partial \dot{w}}{\partial x} \right)^2 \right\} \quad (A34c)$$

Next, Taylor's expansion will be utilised to determine the corresponding PD forms of Eqs. (A34a-c).

Transform W_{CCM}^I into PD form

Following relationship can be established by using Taylor's expansion as

$$\theta_z(x + \xi) = \theta_z(x) + \alpha(\xi) \quad (A35)$$

If we multiply both sides of Eq. (A4b) with ξ and perform some algebraic manipulations, the following relationship can be obtained as

$$\frac{\theta_z(x + \xi) + \theta_z(x)}{2} \xi = \theta_z(x) \xi + \alpha(\xi^2) \quad (A36)$$

Squaring Eq. (A36) and dividing each terms by $|\xi|$ and ignoring higher order terms yield

$$\left(\frac{\theta_z(x + \xi) + \theta_z(x)}{2} \right)^2 |\xi| = \theta_z^2(x) |\xi| \quad (A37)$$

Considering x as a fix point and integrating each term over the interval $(-\delta, \delta)$ results in

$$\theta_z^2(x) = \frac{1}{\delta^2} \int_{-\delta}^{\delta} \left(\frac{\theta_z(x + \xi) + \theta_z(x)}{2} \right)^2 |\xi| d\xi \quad (A38a)$$

Recalling the pre-obtained, Eq. (3.15a):

$$\left(\frac{\partial u(\mathbf{x})}{\partial \mathbf{x}}\right)^2 = \frac{1}{\delta^2} \int_{-\delta}^{\delta} \frac{[u(\mathbf{x} + \xi) - u(\mathbf{x})]^2}{|\xi|} d\xi \quad (\text{A38b})$$

and combining with Eq. (A38a) gives

$$\left(\frac{\partial u(\mathbf{x})}{\partial \mathbf{x}}\right)^2 + \theta_z^2(\mathbf{x}) = \frac{1}{\delta^2} \int_{-\delta}^{\delta} \left\{ \frac{[u(\mathbf{x} + \xi) - u(\mathbf{x})]^2}{|\xi|} + \left(\frac{\theta_z(\mathbf{x} + \xi) + \theta_z(\mathbf{x})}{2}\right)^2 |\xi| \right\} d\xi \quad (\text{A39a})$$

which can be discretized at material point k as

$$\left(\frac{\partial u_{(k)}}{\partial \mathbf{x}}\right)^2 + (\theta_z^{(k)})^2 = \frac{1}{\delta^2 A} \sum_i \left\{ \frac{[u_{(i^k)} - u_{(k)}]^2}{|\xi_{(i^k)(k)}^\xi|} + \left(\frac{\theta_z^{(i^k)} + \theta_z^{(k)}}{2}\right)^2 |\xi_{(i^k)(k)}^\xi| \right\} V_{(i^k)} \quad (\text{A39b})$$

Following a similar approach, the remaining local terms of W_{CCM}^I can be transformed

as

$$\begin{aligned} \frac{\partial u_{(k)}}{\partial \mathbf{x}} \frac{\partial \theta_{(k)}}{\partial \mathbf{x}} + 2\theta_z^{(k)} \dot{w}_{(k)} &= \frac{1}{\delta^2 A} \sum_i \left[\frac{(u_{(i^k)} - u_{(k)})(\theta_{(i^k)} - \theta_{(k)})}{|\xi_{(i^k)(k)}^\xi|} + \frac{w_{(i^k)}^\cdot + w_{(k)}^\cdot}{2} (\theta_z^{(i^k)} + \theta_z^{(k)}) |\xi_{(i^k)(k)}^\xi| \right] V_{(i^k)} \\ \left(\frac{\partial \theta_{(k)}}{\partial \mathbf{x}}\right)^2 + 2 \frac{\partial u_{(k)}}{\partial \mathbf{x}} \frac{\partial \dot{u}_{(k)}}{\partial \mathbf{x}} + 4(\dot{w}_{(k)})^2 &= \frac{1}{\delta^2 A} \sum_i \left[\frac{\theta_{(i^k)} - \theta_{(k)}}{|\xi_{(i^k)(k)}^\xi|} + 2 \frac{(u_{(i^k)} - u_{(k)})(\dot{u}_{(i^k)} - \dot{u}_{(k)})}{|\xi_{(i^k)(k)}^\xi|} + (w_{(i^k)}^\cdot + w_{(k)}^\cdot) |\xi_{(i^k)(k)}^\xi| \right] V_{(i^k)} \\ \frac{\partial u_{(k)}}{\partial \mathbf{x}} \frac{\partial \dot{\theta}_{(k)}}{\partial \mathbf{x}} + \frac{\partial \theta_{(k)}}{\partial \mathbf{x}} \frac{\partial \dot{u}_{(k)}}{\partial \mathbf{x}} &= \frac{1}{\delta^2 A} \sum_i \left[\frac{(u_{(i^k)} - u_{(k)})(\dot{\theta}_{(i^k)} - \dot{\theta}_{(k)})}{|\xi_{(i^k)(k)}^\xi|} + \frac{(\theta_{(i^k)} - \theta_{(k)})(\dot{u}_{(i^k)} - \dot{u}_{(k)})}{|\xi_{(i^k)(k)}^\xi|} \right] V_{(i^k)} \\ \left(\frac{\partial \dot{u}_{(k)}}{\partial \mathbf{x}}\right)^2 + 2 \frac{\partial \theta_{(k)}}{\partial \mathbf{x}} \frac{\partial \dot{\theta}_{(k)}}{\partial \mathbf{x}} &= \frac{1}{\delta^2 A} \sum_i \left[\frac{(\dot{u}_{(i^k)} - \dot{u}_{(k)})^2}{|\xi_{(i^k)(k)}^\xi|} + \frac{(\theta_{(i^k)} - \theta_{(k)})(\dot{\theta}_{(i^k)} - \dot{\theta}_{(k)})}{|\xi_{(i^k)(k)}^\xi|} \right] V_{(i^k)} \\ \frac{\partial \dot{u}_{(k)}}{\partial \mathbf{x}} \frac{\partial \dot{\theta}_{(k)}}{\partial \mathbf{x}} &= \frac{1}{\delta^2 A} \sum_i \frac{(\dot{u}_{(i^k)} - \dot{u}_{(k)})(\dot{\theta}_{(i^k)} - \dot{\theta}_{(k)})}{|\xi_{(i^k)(k)}^\xi|} V_{(i^k)} \\ \left(\frac{\partial \dot{\theta}_{(k)}}{\partial \mathbf{x}}\right)^2 &= \frac{1}{\delta^2 A} \sum_i \frac{(\dot{\theta}_{(i^k)} - \dot{\theta}_{(k)})^2}{|\xi_{(i^k)(k)}^\xi|} V_{(i^k)} \end{aligned} \quad (\text{A40a-f})$$

Substituting Eqs. (A39b), and (A40) into Eq. (A34a) results in the first part of the strain energy density function, W_{CCM}^I , for material point k in PD form as

$$W_{FD} = \frac{1}{2\delta^2 A^2} \left\{ \begin{aligned} & \int_A \frac{E}{1-\nu^2} dA \frac{1}{\delta^2 A} \sum_i \left\{ \frac{[u_{(i^k)} - u_{(k)}]^2}{|\xi_{(i^k)(k)}|} + \left(\frac{\theta_z^{(i^k)} + \theta_z^{(k)}}{2} \right)^2 |\xi_{(i^k)(k)}| \right\} V_{(i^k)} \\ & + \int_A \frac{2Ez}{1-\nu^2} dA \sum_i \left[\frac{(u_{(i^k)} - u_{(k)})(\theta_{(i^k)} - \theta_{(k)})}{|\xi_{(i^k)(k)}|} + \frac{w_{(i^k)}^* + w_{(k)}^*}{2} (\theta_z^{(i^k)} + \theta_z^{(k)}) |\xi_{(i^k)(k)}| \right] V_{(i^k)} \\ & + \int_A \frac{Ez^2}{1-\nu^2} dA \sum_i \left[\frac{\theta_{(i^k)} - \theta_{(k)}}{|\xi_{(i^k)(k)}|} + 2 \frac{(u_{(i^k)} - u_{(k)})(u_{(i^k)}^* - u_{(k)}^*)}{|\xi_{(i^k)(k)}|} + (w_{(i^k)}^* + w_{(k)}^*) |\xi_{(i^k)(k)}| \right] V_{(i^k)} \\ & + \int_A \frac{2Ez^3}{1-\nu^2} dA \sum_i \left[\frac{(u_{(i^k)} - u_{(k)})(\theta_{(i^k)}^* - \theta_{(k)}^*)}{|\xi_{(i^k)(k)}|} + \frac{(\theta_{(i^k)} - \theta_{(k)})(u_{(i^k)}^* - u_{(k)}^*)}{|\xi_{(i^k)(k)}|} \right] V_{(i^k)} \\ & + \int_A \frac{Ez^4}{1-\nu^2} dA \sum_i \left[\frac{(u_{(i^k)}^* - u_{(k)}^*)^2}{|\xi_{(i^k)(k)}|} + \frac{(\theta_{(i^k)} - \theta_{(k)})(\theta_{(i^k)}^* - \theta_{(k)}^*)}{|\xi_{(i^k)(k)}|} \right] V_{(i^k)} \\ & + \int_A \frac{2Ez^5}{1-\nu^2} dA \sum_i \frac{(u_{(i^k)}^* - u_{(k)}^*)(\theta_{(i^k)}^* - \theta_{(k)}^*)}{|\xi_{(i^k)(k)}|} V_{(i^k)} + \int_A \frac{Ez^6}{1-\nu^2} dA \sum_i \frac{(\theta_{(i^k)}^* - \theta_{(k)}^*)^2}{|\xi_{(i^k)(k)}|} V_{(i^k)} \end{aligned} \right\} \quad (A41)$$

Transform W_{CCM}^{II} into PD form

Following relationships can be established by using Taylor's expansion as

$$u(x + \xi) - u(x) = \frac{\partial u(x)}{\partial x} \xi + \alpha \xi^2 \quad (A42a)$$

$$\frac{\theta_z(x + \xi) + \theta_z(x)}{2} \xi = \theta_z(x) \xi + \alpha \xi^2 \quad (A42b)$$

Multiplying Eq. (A42a) with Eq. (A42b) and ignoring higher order terms yields

$$[u(x + \xi) - u(x)] \frac{\theta_z(x + \xi) + \theta_z(x)}{2} \text{sgn}(\xi) = \frac{\partial u(x)}{\partial x} \theta_z(x) |\xi| \quad (A43)$$

Integrating each terms of Eq. (A43) over the horizon yields

$$\frac{\partial u(x)}{\partial x} \theta_z(x) = \frac{1}{\delta^2} \int_{-\delta}^{\delta} [u(x + \xi) - u(x)] \frac{\theta_z(x + \xi) + \theta_z(x)}{2} \text{sgn}(\xi) d\xi \quad (A44a)$$

Eq. (A44a) can be written in discretized form for the material point k as

$$\frac{\partial u_{(k)}}{\partial x} \theta_z^{(k)} = \frac{1}{\delta^2 A} \sum_i (u_{(i^k)} - u_{(k)}) \frac{\theta_z^{(i^k)} + \theta_z^{(k)}}{2} \text{sgn}(\xi_{(i^k)(k)}) V_{(i^k)} \quad (A44b)$$

The remaining local terms of W_{CCM}^{II} can be written by following a similar approach as

$$2w_{(k)}^* \frac{\partial u_{(k)}}{\partial x} + \theta_z^{(k)} \frac{\partial \theta_{(k)}}{\partial x} = \frac{1}{\delta^2 A} \sum_i \left[(u_{(i^k)} - u_{(k)})(w_{(i^k)}^* + w_{(k)}^*) + (\theta_{(i^k)} - \theta_{(k)}) \frac{\theta_z^{(i^k)} + \theta_z^{(k)}}{2} \right] \text{sgn}(\xi_{(i^k)(k)}) V_{(i^k)}$$

$$2w_{(k)}^* \frac{\partial \theta_{(k)}}{\partial x} + \theta_z^{(k)} \frac{\partial u_{(k)}^*}{\partial x} = \frac{1}{\delta^2 A} \sum_i \left[(\theta_{(i^k)} - \theta_{(k)})(w_{(i^k)}^* + w_{(k)}^*) + (u_{(i^k)}^* - u_{(k)}^*) \frac{\theta_z^{(i^k)} + \theta_z^{(k)}}{2} \right] \text{sgn}(\xi_{(i^k)(k)}) V_{(i^k)}$$

$$2\dot{w}_{(k)} \frac{\partial \dot{u}_{(k)}}{\partial x} + \dot{\theta}_{(k)} \frac{\partial \dot{\theta}_{(k)}}{\partial x} = \frac{1}{\delta^2 A} \sum_i \left[(\dot{u}_{(i^k)} - \dot{u}_{(k)}) (\dot{w}_{(i^k)} + \dot{w}_{(k)}) + (\dot{\theta}_{(i^k)} - \dot{\theta}_{(k)}) \frac{\dot{\theta}_{(i^k)} + \dot{\theta}_{(k)}}{2} \right] \text{sgn}(\xi_{(i^k)(k)}) V_{(i^k)}$$

$$\dot{w}_{(k)} \frac{\partial \dot{\theta}_{(k)}}{\partial x} = \frac{1}{\delta^2 A} \sum_i (\dot{\theta}_{(i^k)} - \dot{\theta}_{(k)}) \frac{\dot{w}_{(i^k)} + \dot{w}_{(k)}}{2} \text{sgn}(\xi_{(i^k)(k)}) V_{(i^k)} \quad (\text{A45a-d})$$

Substituting Eqs. (A44b) and (A45) into Eq. (A34b) results in the second part of strain energy density function, W_{CCM}^{II} , in PD form as

$$w_{PD}^I = \frac{1}{\delta^2 A^2} \left[\begin{aligned} & \int_A \frac{Ev}{1-\nu^2} dA \sum_i (u_{(i^k)} - u_{(k)}) \frac{\theta_{(i^k)} + \theta_{(k)}}{2} \text{sgn}(\xi_{(i^k)(k)}) V_{(i^k)} \\ & + \int_A \frac{Evz}{1-\nu^2} dA \sum_i \left[(u_{(i^k)} - u_{(k)}) (\dot{w}_{(i^k)} + \dot{w}_{(k)}) + (\theta_{(i^k)} - \theta_{(k)}) \frac{\theta_{(i^k)} + \theta_{(k)}}{2} \right] \text{sgn}(\xi_{(i^k)(k)}) V_{(i^k)} \\ & + \int_A \frac{Evz^2}{1-\nu^2} dA \sum_i \left[(\theta_{(i^k)} - \theta_{(k)}) (\dot{w}_{(i^k)} + \dot{w}_{(k)}) + (u_{(i^k)} - u_{(k)}) \frac{\theta_{(i^k)} + \theta_{(k)}}{2} \right] \text{sgn}(\xi_{(i^k)(k)}) V_{(i^k)} \\ & + \int_A \frac{Evz^3}{1-\nu^2} dA \sum_i \left[(u_{(i^k)} - u_{(k)}) (\dot{w}_{(i^k)} + \dot{w}_{(k)}) + (\theta_{(i^k)} - \theta_{(k)}) \frac{\theta_{(i^k)} + \theta_{(k)}}{2} \right] \text{sgn}(\xi_{(i^k)(k)}) V_{(i^k)} \\ & + \int_A \frac{2Evz^4}{1-\nu^2} dA \sum_i (\theta_{(i^k)} - \theta_{(k)}) \frac{\dot{w}_{(i^k)} + \dot{w}_{(k)}}{2} \text{sgn}(\xi_{(i^k)(k)}) V_{(i^k)} \end{aligned} \right] \quad (\text{A46})$$

Transforming W_{CCM}^{III} into PD form

By following a similar approach as above, local terms in Eq. (A34c) can be transformed into PD form as

$$\left(\theta_{(k)} + \frac{\partial w_{(k)}}{\partial x} \right)^2 = \frac{1}{\delta^2 A} \sum_i \frac{\left(w_{(i^k)} - w_{(k)} + \frac{\theta_{(i^k)} + \theta_{(k)}}{2} \xi_{(i^k)(k)} \right)^2}{|\xi_{(i^k)(k)}|} V_{(i^k)}$$

$$\left(\theta_{(k)} + \frac{\partial w_{(k)}}{\partial x} \right) \left(2\dot{u}_{(k)} + \frac{\partial \dot{\theta}_{(k)}}{\partial x} \right)$$

$$= \frac{1}{\delta^2 A} \sum_i \left(w_{(i^k)} - w_{(k)} + \frac{\theta_{(i^k)} + \theta_{(k)}}{2} \xi_{(i^k)(k)} \right) \left[\frac{\theta_{(i^k)} - \theta_{(k)}}{|\xi_{(i^k)(k)}|} + (\dot{u}_{(i^k)} + \dot{u}_{(k)}) \text{sgn}(\xi_{(i^k)(k)}) \right] V_{(i^k)}$$

$$\left(\frac{\partial \dot{\theta}_{(k)}}{\partial x} + 2\dot{u}_{(k)} \right)^2 + 2 \left(\theta_{(k)} + \frac{\partial w_{(k)}}{\partial x} \right) \left(3\dot{\theta}_{(k)} + \frac{\partial \dot{w}_{(k)}}{\partial x} \right)$$

$$= \frac{1}{\delta^2 A} \sum_i \frac{\left[\frac{\theta_{(i^k)} - \theta_{(k)}}{|\xi_{(i^k)(k)}|} + (\dot{u}_{(i^k)} + \dot{u}_{(k)}) \text{sgn}(\xi_{(i^k)(k)}) \right]^2 + 2 \left(w_{(i^k)} - w_{(k)} + \frac{\theta_{(i^k)} + \theta_{(k)}}{2} \xi_{(i^k)(k)} \right) \left(\dot{w}_{(i^k)} - \dot{w}_{(k)} + 3 \frac{\theta_{(i^k)} + \theta_{(k)}}{2} \xi_{(i^k)(k)} \right)}{|\xi_{(i^k)(k)}|} V_{(i^k)}$$

$$\begin{aligned}
& \left(2\dot{u}_{(k)}^* + \frac{\partial \dot{\theta}_z^{(k)}}{\partial \mathbf{x}} \right) \left(3\dot{\theta}_{(k)}^* + \frac{\partial \dot{w}_{(k)}}{\partial \mathbf{x}} \right) \\
&= \frac{1}{\delta^2 A} \sum_i \frac{\left[\dot{\theta}_z^{(i^k)} - \dot{\theta}_z^{(k)} + (\dot{u}_{(i^k)}^* + \dot{u}_{(k)}^*) \xi_{\zeta_{(i^k)(k)}} \right] \left(\dot{w}_{(i^k)}^* - \dot{w}_{(k)}^* + 3 \frac{\dot{\theta}_{(i^k)}^* + \dot{\theta}_{(k)}^*}{2} \xi_{\zeta_{(i^k)(k)}} \right)}{|\xi_{\zeta_{(i^k)(k)}}|} V_{(i^k)} \\
& \left(3\dot{\theta}_{(k)}^* + \frac{\partial \dot{w}_{(k)}}{\partial \mathbf{x}} \right)^2 = \frac{1}{\delta^2 A} \sum_i \frac{\left(\dot{w}_{(i^k)}^* - \dot{w}_{(k)}^* + 3 \frac{\dot{\theta}_{(i^k)}^* + \dot{\theta}_{(k)}^*}{2} \xi_{\zeta_{(i^k)(k)}} \right)^2}{|\xi_{\zeta_{(i^k)(k)}}|} V_{(i^k)} \tag{A47a - e}
\end{aligned}$$

Substituting the equations given above into Eq. (A34c) allows W_{CCM}^{III} to be written in PD form as

$$W_{PD}^{III} = \frac{1}{2\delta^2 A^2} \left\{ \begin{aligned} & \int_A \alpha A \sum_i \frac{\left(w_{(i^k)} - w_{(k)} + \frac{\theta_{(i^k)} + \theta_{(k)}}{2} \xi_{\zeta_{(i^k)(k)}} \right)^2}{|\xi_{\zeta_{(i^k)(k)}}|} V_{(i^k)} + \int_A \mathbb{G}^2 dA \sum_i \frac{\left(\dot{w}_{(i^k)}^* - \dot{w}_{(k)}^* + 3 \frac{\dot{\theta}_{(i^k)}^* + \dot{\theta}_{(k)}^*}{2} \xi_{\zeta_{(i^k)(k)}} \right)^2}{|\xi_{\zeta_{(i^k)(k)}}|} V_{(i^k)} \\ & + 2 \int_A \mathbb{G} dA \sum_i \left(w_{(i^k)} - w_{(k)} + \frac{\theta_{(i^k)} + \theta_{(k)}}{2} \xi_{\zeta_{(i^k)(k)}} \right) \left[\frac{\dot{\theta}_z^{(i^k)} - \dot{\theta}_z^{(k)}}{|\xi_{\zeta_{(i^k)(k)}}|} + (\dot{u}_{(i^k)}^* + \dot{u}_{(k)}^*) \operatorname{sgn}(\xi_{\zeta_{(i^k)(k)}}) \right] V_{(i^k)} \\ & + \int_A \mathbb{G}^2 dA \sum_i \frac{\left[\dot{\theta}_z^{(i^k)} - \dot{\theta}_z^{(k)} + (\dot{u}_{(i^k)}^* + \dot{u}_{(k)}^*) \xi_{\zeta_{(i^k)(k)}} \right]^2 + 2 \left(w_{(i^k)} - w_{(k)} + \frac{\theta_{(i^k)} + \theta_{(k)}}{2} \xi_{\zeta_{(i^k)(k)}} \right) \left(\dot{w}_{(i^k)}^* - \dot{w}_{(k)}^* + 3 \frac{\dot{\theta}_{(i^k)}^* + \dot{\theta}_{(k)}^*}{2} \xi_{\zeta_{(i^k)(k)}} \right)}{|\xi_{\zeta_{(i^k)(k)}}|} V_{(i^k)} \\ & + 2 \int_A \mathbb{G}^3 dA \sum_i \frac{\left[\dot{\theta}_z^{(i^k)} - \dot{\theta}_z^{(k)} + (\dot{u}_{(i^k)}^* + \dot{u}_{(k)}^*) \xi_{\zeta_{(i^k)(k)}} \right] \left(\dot{w}_{(i^k)}^* - \dot{w}_{(k)}^* + 3 \frac{\dot{\theta}_{(i^k)}^* + \dot{\theta}_{(k)}^*}{2} \xi_{\zeta_{(i^k)(k)}} \right)}{|\xi_{\zeta_{(i^k)(k)}}|} V_{(i^k)} \end{aligned} \right\} \tag{A48}$$

Combining Eqs. (A41), (A46) and (A48) yields the PD SED function for material point k a

$$\begin{aligned}
W_{\text{D}}^{(k)} = \frac{1}{2\delta^2 A^2} & \left\{ \int_A \frac{E}{1-\nu^2} dA \frac{1}{\delta^2 A} \sum_I \left[\frac{(u_{(i^*)} - u_{(k)})^2}{|\xi_{(i^*)(k)}|} + \left(\frac{\theta_z^{(i^*)} + \theta_z^{(k)}}{2} \right)^2 \frac{1}{|\xi_{(i^*)(k)}|} \right] V_{(i^*)} + \int_A \frac{2Ez}{1-\nu^2} dA \sum_I \left[\frac{(u_{(i^*)} - u_{(k)})(\theta_{(i^*)} - \theta_{(k)})}{|\xi_{(i^*)(k)}|} + \frac{\dot{w}_{(i^*)} + \dot{w}_{(k)}}{2} (\theta_z^{(i^*)} + \theta_z^{(k)}) \frac{1}{|\xi_{(i^*)(k)}|} \right] V_{(i^*)} \right. \\
& + \int_A \frac{Ez^2}{1-\nu^2} dA \sum_I \left[\frac{\theta_{(i^*)} - \theta_{(k)}}{|\xi_{(i^*)(k)}|} + 2 \frac{(u_{(i^*)} - u_{(k)})(u_{(i^*)} - u_{(k)})}{|\xi_{(i^*)(k)}|} + (\dot{w}_{(i^*)} + \dot{w}_{(k)}) \frac{1}{|\xi_{(i^*)(k)}|} \right] V_{(i^*)} \\
& + \int_A \frac{2Ez^3}{1-\nu^2} dA \sum_I \left[\frac{(u_{(i^*)} - u_{(k)})(\theta_{(i^*)} - \theta_{(k)})}{|\xi_{(i^*)(k)}|} + \frac{(\theta_{(i^*)} - \theta_{(k)})(u_{(i^*)} - u_{(k)})}{|\xi_{(i^*)(k)}|} \right] V_{(i^*)} \\
& + \int_A \frac{Ez^4}{1-\nu^2} dA \sum_I \left[\frac{(u_{(i^*)} - u_{(k)})^2}{|\xi_{(i^*)(k)}|} + \frac{(\theta_{(i^*)} - \theta_{(k)})(\theta_{(i^*)} - \theta_{(k)})}{|\xi_{(i^*)(k)}|} \right] V_{(i^*)} + \int_A \frac{2Ez^5}{1-\nu^2} dA \sum_I \frac{(u_{(i^*)} - u_{(k)})(\theta_{(i^*)} - \theta_{(k)})}{|\xi_{(i^*)(k)}|} V_{(i^*)} + \int_A \frac{Ez^6}{1-\nu^2} dA \sum_I \frac{(\theta_{(i^*)} - \theta_{(k)})^2}{|\xi_{(i^*)(k)}|} V_{(i^*)} \\
& + \frac{1}{\delta^2 A^2} \left\{ \int_A \frac{Ev}{1-\nu^2} dA \sum_I (u_{(i^*)} - u_{(k)}) \frac{\theta_z^{(i^*)} + \theta_z^{(k)}}{2} \text{sgn}(\xi_{(i^*)(k)}) V_{(i^*)} + \int_A \frac{Evz}{1-\nu^2} dA \sum_I \left[(u_{(i^*)} - u_{(k)})(\dot{w}_{(i^*)} + \dot{w}_{(k)}) + (\theta_{(i^*)} - \theta_{(k)}) \frac{\theta_z^{(i^*)} + \theta_z^{(k)}}{2} \right] \text{sgn}(\xi_{(i^*)(k)}) V_{(i^*)} \right. \\
& + \int_A \frac{Evz^2}{1-\nu^2} dA \sum_I \left[(\theta_{(i^*)} - \theta_{(k)})(\dot{w}_{(i^*)} + \dot{w}_{(k)}) + (u_{(i^*)} - u_{(k)}) \frac{\theta_z^{(i^*)} + \theta_z^{(k)}}{2} \right] \text{sgn}(\xi_{(i^*)(k)}) V_{(i^*)} \\
& + \int_A \frac{Evz^3}{1-\nu^2} dA \sum_I \left[(u_{(i^*)} - u_{(k)})(\dot{w}_{(i^*)} + \dot{w}_{(k)}) + (\theta_{(i^*)} - \theta_{(k)}) \frac{\theta_z^{(i^*)} + \theta_z^{(k)}}{2} \right] \text{sgn}(\xi_{(i^*)(k)}) V_{(i^*)} + \int_A \frac{2Evz^4}{1-\nu^2} dA \sum_I (\theta_{(i^*)} - \theta_{(k)}) \frac{\dot{w}_{(i^*)} + \dot{w}_{(k)}}{2} \text{sgn}(\xi_{(i^*)(k)}) V_{(i^*)} \\
& + \frac{1}{2\delta^2 A^2} \left\{ \int_A \mathcal{G}^2 dA \sum_I \frac{\left(w_{(i^*)} - w_{(k)} + \frac{\theta_{(i^*)} + \theta_{(k)}}{2} \xi_{(i^*)(k)} \right)^2}{|\xi_{(i^*)(k)}|} V_{(i^*)} + 2 \int_A \mathcal{G}^2 dA \sum_I \left(w_{(i^*)} - w_{(k)} + \frac{\theta_{(i^*)} + \theta_{(k)}}{2} \xi_{(i^*)(k)} \right) \left[\frac{\theta_z^{(i^*)} - \theta_z^{(k)}}{|\xi_{(i^*)(k)}|} + (u_{(i^*)} + u_{(k)}) \text{sgn}(\xi_{(i^*)(k)}) \right] V_{(i^*)} \\
& + \int_A \mathcal{G}^2 dA \sum_I \frac{\left[\theta_z^{(i^*)} - \theta_z^{(k)} + (u_{(i^*)} + u_{(k)}) \xi_{(i^*)(k)} \right]^2 + 2 \left(w_{(i^*)} - w_{(k)} + \frac{\theta_{(i^*)} + \theta_{(k)}}{2} \xi_{(i^*)(k)} \right) \left(\dot{w}_{(i^*)} - \dot{w}_{(k)} + 3 \frac{\theta_{(i^*)} + \theta_{(k)}}{2} \xi_{(i^*)(k)} \right)}{|\xi_{(i^*)(k)}|} V_{(i^*)} \\
& + 2 \int_A \mathcal{G}^3 dA \sum_I \frac{\left[\theta_z^{(i^*)} - \theta_z^{(k)} + (u_{(i^*)} + u_{(k)}) \xi_{(i^*)(k)} \right] \left(\dot{w}_{(i^*)} - \dot{w}_{(k)} + 3 \frac{\theta_{(i^*)} + \theta_{(k)}}{2} \xi_{(i^*)(k)} \right)}{|\xi_{(i^*)(k)}|} V_{(i^*)} + \int_A \mathcal{G}^4 dA \sum_I \frac{\left(\dot{w}_{(i^*)} - \dot{w}_{(k)} + 3 \frac{\theta_{(i^*)} + \theta_{(k)}}{2} \xi_{(i^*)(k)} \right)^2}{|\xi_{(i^*)(k)}|} V_{(i^*)} \\
& \left. \right\}
\end{aligned} \tag{A49}$$

Regarding the PD SED for material point j , a similar form will hold if we replace the index k with j .

A2 PD SED for Plate Theories

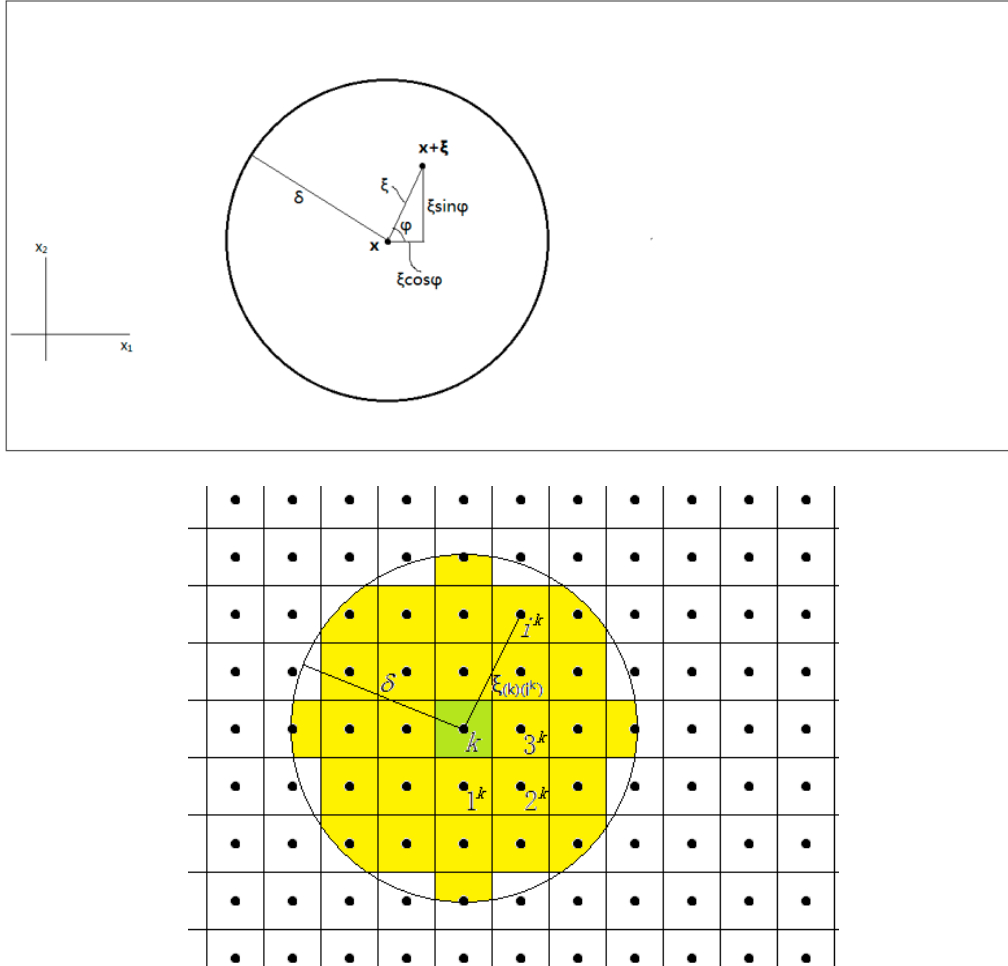


Figure A2. Peridynamic interaction between two material points

A2.1 Kirchhoff Plate

As explained in Chapter 5.1, the SED function for Kirchhoff Plate can be written as

$$W_{\text{KM}} = \frac{D}{2h} \left[\left(\frac{\partial^2 w}{\partial x_i \partial x_i} \right)^2 + (1 - \nu) \left(\frac{\partial^2 w}{\partial x_i \partial x_j} \frac{\partial^2 w}{\partial x_i \partial x_j} - \left(\frac{\partial^2 w}{\partial x_i \partial x_i} \right)^2 \right) \right] \quad (\text{A50})$$

The transverse displacement function, w , can be expanded in the form of Taylor series and can be written after ignoring higher order terms as

$$w(\mathbf{x} + \boldsymbol{\xi}) - w(\mathbf{x}) = \frac{\partial w(\mathbf{x})}{\partial x_i} \xi_i + \frac{1}{2} \frac{\partial^2 w(\mathbf{x})}{\partial x_i \partial x_j} \xi_i \xi_j \quad (\text{A51})$$

As shown in Fig. A2, $\xi = |\boldsymbol{\xi}|$ represents the distance between to material points and the unit orientation vector the unit orientation vector \mathbf{n} can be defined as

$$\mathbf{n} = \begin{Bmatrix} n_1 \\ n_2 \end{Bmatrix} = \begin{Bmatrix} \cos \varphi \\ \sin \varphi \end{Bmatrix} \quad (\text{A52})$$

Multiplying each term in Eq. (A52) by $\frac{n_L n_L}{\xi^2}$ and integrating over a circular horizon with central point of \mathbf{x} and radius of δ results in

$$\begin{aligned} \int_0^{2\pi} \int_0^\delta \frac{v(\mathbf{x} + \boldsymbol{\xi}) - v(\mathbf{x})}{\xi^2} n_\kappa n_L \xi d\xi d\varphi &= \frac{\partial v(\mathbf{x})}{\partial x_I} \int_0^{2\pi} \int_0^\delta n_I n_\kappa n_L d\xi d\varphi + \frac{1}{2} \frac{\partial^2 v(\mathbf{x})}{\partial x_I \partial x_J} \int_0^{2\pi} \int_0^\delta n_I n_J n_\kappa n_L \xi d\xi d\varphi \\ &= \frac{\pi \delta^2}{16} \frac{\partial^2 v(\mathbf{x})}{\partial x_I \partial x_J} (\delta_{IJ} \delta_{\kappa L} + \delta_{I\kappa} \delta_{JL} + \delta_{IL} \delta_{JK}) \\ &= \frac{\pi \delta^2}{16} \left(\frac{\partial^2 v(\mathbf{x})}{\partial x_I \partial x_I} \delta_{\kappa L} + 2 \frac{\partial^2 v(\mathbf{x})}{\partial x_\kappa \partial x_L} \right) \end{aligned} \quad (\text{A53a})$$

Similar expression can be obtained by using different free and dummy indices as

$$\int_0^{2\pi} \int_0^\delta \frac{v(\mathbf{x} + \boldsymbol{\xi}) - v(\mathbf{x})}{\xi^2} n_R n_S \xi d\xi d\varphi = \frac{\pi \delta^2}{16} \left(\frac{\partial^2 v(\mathbf{x})}{\partial x_J \partial x_J} \delta_{RS} + 2 \frac{\partial^2 v(\mathbf{x})}{\partial x_R \partial x_S} \right) \quad (\text{A53b})$$

Multiplying Eq. (A53a) by Eq. (A53b) gives

$$\begin{aligned} &\int_0^{2\pi} \int_0^\delta \frac{v(\mathbf{x} + \boldsymbol{\xi}) - v(\mathbf{x})}{\xi^2} n_R n_S \xi d\xi d\varphi \int_0^{2\pi} \int_0^\delta \frac{v(\mathbf{x} + \boldsymbol{\xi}) - v(\mathbf{x})}{\xi^2} n_\kappa n_L \xi d\xi d\varphi \\ &= \left(\frac{\pi \delta^2}{16} \right)^2 \left(\frac{\partial^2 v(\mathbf{x})}{\partial x_J \partial x_J} \delta_{RS} + 2 \frac{\partial^2 v(\mathbf{x})}{\partial x_R \partial x_S} \right) \left(\frac{\partial^2 v(\mathbf{x})}{\partial x_I \partial x_I} \delta_{\kappa L} + 2 \frac{\partial^2 v(\mathbf{x})}{\partial x_\kappa \partial x_L} \right) \end{aligned} \quad (\text{A54})$$

Multiplying both sides of Eq. (A54) with $\delta_{RS} \delta_{KL}$ and performing algebraic manipulations result in

$$\left(\frac{\partial^2 v(\mathbf{x})}{\partial x_I \partial x_I} \right)^2 = \left(\frac{4}{\pi \delta^2} \right)^2 \left(\int_0^{2\pi} \int_0^\delta \frac{v(\mathbf{x} + \boldsymbol{\xi}) - v(\mathbf{x})}{\xi^2} \xi d\xi d\varphi \right)^2 \quad (\text{A55})$$

Multiplying both sides of Eq. (A55) with $\delta_{RK} \delta_{SL}$ and performing algebraic manipulations result in

$$\begin{aligned} &\frac{\partial^2 v(\mathbf{x})}{\partial x_\kappa \partial x_L} \frac{\partial^2 v(\mathbf{x})}{\partial x_\kappa \partial x_L} - \left(\frac{\partial^2 v(\mathbf{x})}{\partial x_I \partial x_I} \right)^2 \\ &= \left(\frac{8}{\pi \delta^2} \right)^2 \int_0^{2\pi} \int_0^\delta \frac{v(\mathbf{x} + \boldsymbol{\xi}) - v(\mathbf{x})}{\xi^2} n_\kappa n_L \xi d\xi d\varphi \int_0^{2\pi} \int_0^\delta \frac{v(\mathbf{x} + \boldsymbol{\xi}) - v(\mathbf{x})}{\xi^2} n_\kappa n_L \xi d\xi d\varphi - \frac{5}{2} \left(\frac{\partial^2 v(\mathbf{x})}{\partial x_I \partial x_I} \right)^2 \end{aligned} \quad (\text{A56})$$

Substituting Eq. (A55) into the right hand side of Eq. (A56) and rearranging the free indices result in

$$\begin{aligned} & \frac{\partial^2 w(\mathbf{x})}{\partial x_K \partial x_L} \frac{\partial^2 w(\mathbf{x})}{\partial x_K \partial x_L} - \left(\frac{\partial^2 w(\mathbf{x})}{\partial x_I \partial x_I} \right)^2 \\ &= \left(\frac{4}{\pi \delta^2} \right)^2 \left[4 \int_0^{2\pi} \int_0^\delta \frac{w(\mathbf{x} + \boldsymbol{\xi}) - w(\mathbf{x})}{\xi^2} n_K n_L \xi d\xi d\varphi \int_0^{2\pi} \int_0^\delta \frac{w(\mathbf{x} + \boldsymbol{\xi}) - w(\mathbf{x})}{\xi^2} n_K n_L \xi d\xi d\varphi \right. \\ & \quad \left. - \frac{5}{2} \left(\int_0^{2\pi} \int_0^\delta \frac{w(\mathbf{x} + \boldsymbol{\xi}) - w(\mathbf{x})}{\xi^2} \xi d\xi d\varphi \right)^2 \right] \end{aligned} \quad (\text{A57})$$

Eqs. (A55) and (A57) can discretized as

$$\left(\frac{\partial^2 W_{(k)}}{\partial x_I \partial x_I} \right)^2 = \left(\frac{4}{\pi \delta^2 h} \right)^2 \left(\sum_i \frac{W_{(i^k)} - W_{(k)}}{\xi_{(i^k)(k)}^2} V_{(i^k)} \right)^2 \quad (\text{A58a})$$

and

$$\begin{aligned} & \frac{\partial^2 W_{(k)}}{\partial x_K \partial x_L} \frac{\partial^2 W_{(k)}}{\partial x_K \partial x_L} - \left(\frac{\partial^2 W_{(k)}}{\partial x_I \partial x_I} \right)^2 \\ &= \left(\frac{4}{\pi \delta^2 h} \right)^2 \left[4 \sum_i \frac{W_{(i^k)} - W_{(k)}}{\xi_{(i^k)(k)}^2} n_K^{(i^k)(k)} n_L^{(i^k)(k)} V_{(i^k)} \sum_i \frac{W_{(i^k)} - W_{(k)}}{\xi_{(i^k)(k)}^2} n_K^{(i^k)(k)} n_L^{(i^k)(k)} V_{(i^k)} \right. \\ & \quad \left. - \frac{5}{2} \left(\sum_i \frac{W_{(i^k)} - W_{(k)}}{\xi_{(i^k)(k)}^2} V_{(i^k)} \right)^2 \right] \end{aligned} \quad (\text{A58b})$$

Plugging Eqs. (A58) into (A50) results in the PD Kirchhoff Plate SED for material k as

$$W_{\text{PD}}^{(k)} = \frac{D}{h} \left(\frac{2}{\pi \delta^2 h} \right)^2 \left[(5\nu - 3) \left(\sum_i \frac{W_{(i^k)} - W_{(k)}}{\xi_{(i^k)(k)}^2} V_{(i^k)} \right)^2 + 8(1 - \nu) \sum_i \frac{W_{(i^k)} - W_{(k)}}{\xi_{(i^k)(k)}^2} n_K^{(i^k)(k)} n_L^{(i^k)(k)} V_{(i^k)} \sum_i \frac{W_{(i^k)} - W_{(k)}}{\xi_{(i^k)(k)}^2} n_K^{(i^k)(k)} n_L^{(i^k)(k)} V_{(i^k)} \right] \quad (\text{A59})$$

Regarding the PD SED for material point j , a similar form will hold if we replace the index k with j .

Moreover, particularly, for any shape of the Kirchhoff Plate subjected to fixed (simply-supported and clamped) boundary conditions only, the SED function, Eq. (A50), can be simplified as

$$W_{\text{GM}} = \frac{D}{2h} \left(\frac{\partial^2 w}{\partial x_I \partial x_I} \right)^2 \quad (\text{A60})$$

Proof:

The total strain energy, U , stored in the body can be obtained by integrating Eq. (A50) over the mid-plane as

$$\begin{aligned}
U &= \frac{D}{2h} \iint_{\Gamma} \left\{ \left(\frac{\partial^2 w}{\partial x_1 \partial x_1} \right)^2 + (1-\nu) \left[\frac{\partial^2 w}{\partial x_1 \partial x_2} \frac{\partial^2 w}{\partial x_1 \partial x_2} - \left(\frac{\partial^2 w}{\partial x_1 \partial x_2} \right)^2 \right] \right\} dx_1 dx_2 \\
&= \frac{D}{2h} \iint_{\Gamma} \left(\frac{\partial^2 w}{\partial x_1 \partial x_1} \right)^2 dx_1 dx_2 - \frac{D}{2h} \frac{1-\nu}{2} \iint_{\Gamma} \left[\frac{\partial^2 w}{\partial x_1 \partial x_1} \frac{\partial^2 w}{\partial x_2 \partial x_2} - \left(\frac{\partial^2 w}{\partial x_1 \partial x_2} \right)^2 \right] dx_1 dx_2
\end{aligned} \tag{A61}$$

where Γ represents the area of the mid-plane.

Following expressions will hold by calculus

$$\begin{aligned}
\frac{\partial^2 w}{\partial x_1 \partial x_1} \frac{\partial^2 w}{\partial x_2 \partial x_2} &= \frac{\partial}{\partial x_1} \left(\frac{\partial^2 w}{\partial x_2 \partial x_2} \frac{\partial w}{\partial x_1} \right) - \frac{\partial^3 w}{\partial x_1 \partial x_2 \partial x_2} \frac{\partial w}{\partial x_1} \\
&= \frac{\partial}{\partial x_1} \left(\frac{\partial^2 w}{\partial x_2 \partial x_2} \frac{\partial w}{\partial x_1} \right) - \frac{\partial}{\partial x_2} \left(\frac{\partial^2 w}{\partial x_1 \partial x_2} \frac{\partial w}{\partial x_1} \right) + \left(\frac{\partial^2 w}{\partial x_1 \partial x_2} \right)^2
\end{aligned} \tag{A62a}$$

$$\begin{aligned}
\frac{\partial^2 w}{\partial x_1 \partial x_1} \frac{\partial^2 w}{\partial x_2 \partial x_2} &= \frac{\partial}{\partial x_2} \left(\frac{\partial^2 w}{\partial x_1 \partial x_1} \frac{\partial w}{\partial x_2} \right) - \frac{\partial^3 w}{\partial x_2 \partial x_1 \partial x_1} \frac{\partial w}{\partial x_2} \\
&= \frac{\partial}{\partial x_2} \left(\frac{\partial^2 w}{\partial x_1 \partial x_1} \frac{\partial w}{\partial x_2} \right) - \frac{\partial}{\partial x_1} \left(\frac{\partial^2 w}{\partial x_1 \partial x_2} \frac{\partial w}{\partial x_2} \right) + \left(\frac{\partial^2 w}{\partial x_1 \partial x_2} \right)^2
\end{aligned} \tag{A62b}$$

Combining Eqs. (A52a) and (A52b) together gives

$$\frac{\partial^2 w}{\partial x_1 \partial x_1} \frac{\partial^2 w}{\partial x_2 \partial x_2} - \left(\frac{\partial^2 w}{\partial x_1 \partial x_2} \right)^2 = \frac{1}{2} \left[\begin{aligned} &\frac{\partial}{\partial x_1} \left(\frac{\partial^2 w}{\partial x_2 \partial x_2} \frac{\partial w}{\partial x_1} \right) - \frac{\partial}{\partial x_1} \left(\frac{\partial^2 w}{\partial x_1 \partial x_2} \frac{\partial w}{\partial x_2} \right) \\ &+ \frac{\partial}{\partial x_2} \left(\frac{\partial^2 w}{\partial x_1 \partial x_1} \frac{\partial w}{\partial x_2} \right) - \frac{\partial}{\partial x_2} \left(\frac{\partial^2 w}{\partial x_1 \partial x_2} \frac{\partial w}{\partial x_1} \right) \end{aligned} \right] \tag{A63}$$

Substituting Eq. (A63) into the second integration function of the RHS of (A61) and utilizing 2-Dimensional divergence theorem (Green's theorem) yields

$$\begin{aligned}
&\iint_{\Gamma} \left[\frac{\partial^2 w}{\partial x_1 \partial x_1} \frac{\partial^2 w}{\partial x_2 \partial x_2} - \left(\frac{\partial^2 w}{\partial x_1 \partial x_2} \right)^2 \right] dx_1 dx_2 \\
&= \frac{1}{2} \iint_{\Gamma} \left[\frac{\partial}{\partial x_1} \left(\frac{\partial^2 w}{\partial x_2 \partial x_2} \frac{\partial w}{\partial x_1} - \frac{\partial^2 w}{\partial x_1 \partial x_2} \frac{\partial w}{\partial x_2} \right) + \frac{\partial}{\partial x_2} \left(\frac{\partial^2 w}{\partial x_1 \partial x_1} \frac{\partial w}{\partial x_2} - \frac{\partial^2 w}{\partial x_1 \partial x_2} \frac{\partial w}{\partial x_1} \right) \right] dx_1 dx_2 \\
&= \frac{1}{2} \oint_{\partial \Gamma} \left[\left(\frac{\partial^2 w}{\partial x_2 \partial x_2} \frac{\partial w}{\partial x_1} - \frac{\partial^2 w}{\partial x_1 \partial x_2} \frac{\partial w}{\partial x_2} \right) \cos \theta + \left(\frac{\partial^2 w}{\partial x_1 \partial x_1} \frac{\partial w}{\partial x_2} - \frac{\partial^2 w}{\partial x_1 \partial x_2} \frac{\partial w}{\partial x_1} \right) \sin \theta \right] ds
\end{aligned} \tag{A64}$$

where $\partial \Gamma$ is the boundary of Γ and θ represents the angle between boundary normal and x_1 axis (see Fig. A3).

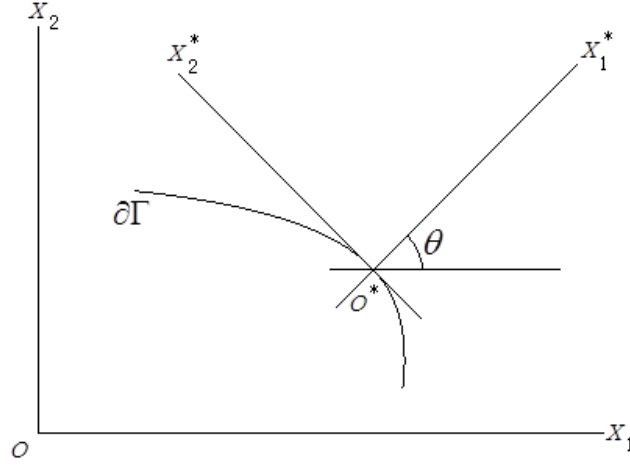


Figure A3 Global coordinate system and local coordinate system

When a simply connected plate is subjected to clamped boundary conditions, the boundaries are constrained to zero rotation, i.e. $\theta_1 = \frac{\partial w}{\partial x_1} = \theta_2 = \frac{\partial w}{\partial x_2} = 0$, thus integral function, (A53), equals to zero.

For some edges of a simply connected plated subjected to simply supported boundary conditions, if a local coordinate system $(x_1^* o^* x_2^*)$ is set at each edge, for instance as shown in Fig. A3, where x_1^* and x_2^* axis are set as the normal and tangent orientation to the boundary,

$$\theta_2^* = \frac{\partial w}{\partial x_2^*} = 0 \quad (\text{A65a})$$

$$\kappa_{11}^* = \frac{\partial^2 w}{\partial x_2^* \partial x_2^*} = 0 \quad (\text{A65b})$$

are satisfied on every edge. Moreover, the following expressions are satisfied according to the directional derivative relation:

$$\frac{\partial}{\partial x_1^*} = \cos \theta \frac{\partial}{\partial x_1} + \sin \theta \frac{\partial}{\partial x_2} \quad (\text{A66a})$$

$$\frac{\partial}{\partial x_2^*} = -\sin \theta \frac{\partial}{\partial x_1} + \cos \theta \frac{\partial}{\partial x_2} \quad (\text{A66b})$$

Thus one can obtained from Eqs. (A65a) and (A66b) that

$$\frac{\partial w}{\partial x_1} \sin \theta = \frac{\partial w}{\partial x_2} \cos \theta \quad (\text{A67})$$

Moreover, Eq. (A65b) can be transformed as

$$\begin{aligned}\frac{\partial^2 w}{\partial x_2^* \partial x_2^*} &= \frac{\partial}{\partial x_2^*} \left(\frac{\partial w}{\partial x_2^*} \right) = \left(-\sin \theta \frac{\partial}{\partial x_1} + \cos \theta \frac{\partial}{\partial x_2} \right) \left(-\sin \theta \frac{\partial w}{\partial x_1} + \cos \theta \frac{\partial w}{\partial x_2} \right) \\ &= \sin^2 \theta \frac{\partial^2 w}{\partial x_1^2} + \cos^2 \theta \frac{\partial^2 w}{\partial x_2^2} - 2 \sin \theta \cos \theta \frac{\partial^2 w}{\partial x_1 \partial x_2} = 0\end{aligned}\quad (\text{A68})$$

Substituting Eq. (A67) into (A64) meanwhile considering (A68) gives

$$\begin{aligned}&\iint_{\Gamma} \left[\frac{\partial^2 w}{\partial x_1 \partial x_1} \frac{\partial^2 w}{\partial x_2 \partial x_2} - \left(\frac{\partial^2 w}{\partial x_1 \partial x_2} \right)^2 \right] dx_1 dx_2 \\ &= \frac{1}{2} \oint_{\Sigma} \frac{\partial w}{\partial x_2} \frac{1}{\sin \theta} \left(\frac{\partial^2 w}{\partial x_2 \partial x_2} \cos^2 \theta + \frac{\partial^2 w}{\partial x_1 \partial x_1} \sin^2 \theta - 2 \frac{\partial^2 w}{\partial x_1 \partial x_2} \sin \theta \cos \theta \right) ds \\ &= 0\end{aligned}\quad (\text{A69})$$

Inserting Eq. (A68) into (A60) yields

$$\begin{aligned}U &= \frac{D}{2h} \iint_{\Gamma} \left(\frac{\partial^2 w}{\partial x_1 \partial x_1} \right)^2 dx_1 dx_2 - \frac{D}{2h} \frac{1-\nu}{2} \iint_{\Gamma} \left[\frac{\partial^2 w}{\partial x_1 \partial x_1} \frac{\partial^2 w}{\partial x_2 \partial x_2} - \left(\frac{\partial^2 w}{\partial x_1 \partial x_2} \right)^2 \right] dx_1 dx_2 \\ &= \frac{D}{2h} \iint_{\Gamma} \left(\frac{\partial^2 w}{\partial x_1 \partial x_1} \right)^2 dx_1 dx_2\end{aligned}\quad (\text{A70})$$

Thus the SED function becomes

$$W_{\text{COM}} = \frac{D}{2h} \left(\frac{\partial^2 w}{\partial x_1 \partial x_1} \right)^2 \quad \blacksquare$$

And its corresponding PD SED for material point k and its family member j become

$$W_{\text{PD}}^{(k)} = \frac{D}{2h} \left(\frac{4}{\pi \delta^2 h} \right)^2 \left(\sum_i \frac{w_{(i^k)} - w_{(k)}}{\xi_{(i^k)(k)}^2} V_{(i^k)} \right)^2 \quad (\text{A71a})$$

and

$$W_{\text{PD}}^{(j)} = \frac{D}{2h} \left(\frac{4}{\pi \delta^2 h} \right)^2 \left(\sum_i \frac{w_{(i^j)} - w_{(j)}}{\xi_{(i^j)(j)}^2} V_{(i^j)} \right)^2 \quad (\text{A71b})$$

A2.2 FGM Kirchhoff Plate

As explained in Chapter 5.2, the SED function of FGM Kirchhoff Plate can be expressed as

$$W_{\text{COM}} = W_{\text{COM}}^I + W_{\text{COM}}^{II} + W_{\text{COM}}^{III} \quad (\text{A72})$$

where

$$W_{\text{COM}}^I = \frac{1}{2h} \left[\int_{-\frac{h}{2}}^{\frac{h}{2}} \text{Gtz} (u_{,j} u_{,j} + u_{,j} u_{,j} + u_{,j} u_{,j}) + \int_{-\frac{h}{2}}^{\frac{h}{2}} \frac{E}{1-\nu^2} \frac{3\nu-1}{2} dz (u_{,j})^2 \right] \quad (\text{A73a})$$

$$W'_{\text{cm}} = \frac{1}{2h} \left[\int_{-\frac{h}{2}}^{\frac{h}{2}} \frac{Ez^2}{1-\nu^2} dz (w_{,11})^2 + 2 \int_{-\frac{h}{2}}^{\frac{h}{2}} Gz dz (w_{,1j}w_{,1j} - (w_{,11})^2) \right] \quad (\text{A73b})$$

$$W''_{\text{cm}} = -\frac{1}{h} \left\{ \int_{-\frac{h}{2}}^{\frac{h}{2}} \frac{Ez}{1-\nu^2} dz (u_{,1}w_{,1j}) + \int_{-\frac{h}{2}}^{\frac{h}{2}} Gz dz [(u_{,1j} + u_{,j1})w_{,1j} - 2u_{,1}w_{,1j}] \right\} \quad (\text{A73c})$$

Recall Eqs. (3.38a) and (3.38b):

$$\frac{\partial u_i^{(k)}}{\partial x_j} \frac{\partial u_j^{(k)}}{\partial x_i} + \frac{\partial u_i^{(k)}}{\partial x_i} \frac{\partial u_j^{(k)}}{\partial x_j} + \frac{\partial u_i^{(k)}}{\partial x_j} \frac{\partial u_j^{(k)}}{\partial x_i} = \frac{12}{\pi\delta^3 h} \sum_i \frac{(u_i^{(k)} - u_i^{(k)}) (u_j^{(k)} - u_j^{(k)})}{\xi_{(i^k)(k)}} n_i^{(i^k)(k)} n_j^{(j^k)(k)} V_{(i^k)} \quad (\text{A74a})$$

$$\frac{\partial u_i^{(k)}}{\partial x_i} = \frac{2}{\pi\delta^2 h} \sum_i \frac{u_i^{(i^k)} - u_i^{(k)}}{\xi_{(i^k)(k)}} n_i^{(i^k)(k)} V_{(i^k)} \quad (\text{A74b})$$

Inserting above into Eq. (A73a) results in

$$W'_{\text{D}} = \frac{6}{\pi\delta^3 h^2} \int_{-\frac{h}{2}}^{\frac{h}{2}} Gz dz \sum_i \frac{(u_i^{(i^k)} - u_i^{(k)}) (u_j^{(j^k)} - u_j^{(k)})}{\xi_{(i^k)(k)}} n_i^{(i^k)(k)} n_j^{(j^k)(k)} V_{(i^k)} + \frac{1}{2h} \int_{-\frac{h}{2}}^{\frac{h}{2}} \frac{E}{1-\nu^2} \frac{3\nu-1}{2} dz \left(\frac{2}{\pi\delta^2 h} \sum_i \frac{u_i^{(i^k)} - u_i^{(k)}}{\xi_{(i^k)(k)}} n_i^{(i^k)(k)} V_{(i^k)} \right)^2 \quad (\text{A75})$$

Recall Eqs. (A58a) and (A85b):

$$\left(\frac{\partial^2 W_{(k)}}{\partial x_i \partial x_i} \right)^2 = \left(\frac{4}{\pi\delta^2 h} \right)^2 \left(\sum_i \frac{W_{(i^k)} - W_{(k)}}{\xi_{(i^k)(k)}^2} V_{(i^k)} \right)^2 \quad (\text{A76a})$$

$$\frac{\partial^2 W_{(k)}}{\partial x_k \partial x_k} \frac{\partial^2 W_{(k)}}{\partial x_k \partial x_k} - \left(\frac{\partial^2 W_{(k)}}{\partial x_i \partial x_i} \right)^2 = \left(\frac{4}{\pi\delta^2 h} \right)^2 \left[4 \sum_i \frac{W_{(i^k)} - W_{(k)}}{\xi_{(i^k)(k)}^2} n_i^{(i^k)(k)} n_i^{(i^k)(k)} V_{(i^k)} \sum_i \frac{W_{(i^k)} - W_{(k)}}{\xi_{(i^k)(k)}^2} n_i^{(i^k)(k)} n_i^{(i^k)(k)} V_{(i^k)} - \frac{5}{2} \left(\sum_i \frac{W_{(i^k)} - W_{(k)}}{\xi_{(i^k)(k)}^2} V_{(i^k)} \right)^2 \right] \quad (\text{A76b})$$

Substituting above into Eq. (A73b) gives

$$W'_{\text{D}} = \frac{1}{2h} \left(\frac{4}{\pi\delta^2 h} \right)^2 \left\{ \int_{-\frac{h}{2}}^{\frac{h}{2}} \left(\frac{E}{1-\nu^2} - 5G \right) z^2 dz \left(\sum_i \frac{W_{(i^k)} - W_{(k)}}{\xi_{(i^k)(k)}^2} V_{(i^k)} \right)^2 + 8 \int_{-\frac{h}{2}}^{\frac{h}{2}} Gz dz \sum_i \frac{W_{(i^k)} - W_{(k)}}{\xi_{(i^k)(k)}^2} n_i^{(i^k)(k)} n_i^{(i^k)(k)} V_{(i^k)} \sum_i \frac{W_{(i^k)} - W_{(k)}}{\xi_{(i^k)(k)}^2} n_i^{(i^k)(k)} n_i^{(i^k)(k)} V_{(i^k)} \right\} \quad (\text{A77})$$

One can obtain with considering Eqs. (A53) and (A55) as

$$\frac{\partial^2 W(\mathbf{x})}{\partial x_i \partial x_j} = \frac{2}{\pi\delta^2} \left(4 \int_0^{2\pi} \int_0^\delta \frac{W(\mathbf{x} + \xi) - W(\mathbf{x})}{\xi^2} n_i n_j \xi d\xi d\varphi - \delta_{ij} \int_0^{2\pi} \int_0^\delta \frac{W(\mathbf{x} + \xi) - W(\mathbf{x})}{\xi^2} \xi d\xi d\varphi \right) \quad (\text{A78})$$

Recall Eq. (3.36)

$$\frac{\partial u_i(\mathbf{x})}{\partial x_j} = \frac{2}{\pi\delta^2} \int_0^{2\pi} \int_0^\delta \frac{u_i(\mathbf{x} + \boldsymbol{\xi}) - u_i(\mathbf{x})}{\xi} n_j \xi d\xi d\varphi \quad (\text{A79a})$$

$$\frac{\partial u_j(\mathbf{x})}{\partial x_j} = \frac{2}{\pi\delta^2} \int_0^{2\pi} \int_0^\delta \frac{u_j(\mathbf{x} + \boldsymbol{\xi}) - u_j(\mathbf{x})}{\xi} n_j \xi d\xi d\varphi \quad (\text{A79b})$$

Combining Eqs. (A79a) with (A79b) and multiplying with (A78) gives

$$\left(\frac{\partial u_i(\mathbf{x})}{\partial x_j} + \frac{\partial u_j(\mathbf{x})}{\partial x_j} \right) \frac{\partial^2 w(\mathbf{x})}{\partial x_i \partial x_j} = \left(\frac{4}{\pi\delta^2} \right)^2 \left[\begin{aligned} & \int_0^{2\pi} \int_0^\delta \left(\frac{u_i(\mathbf{x} + \boldsymbol{\xi}) - u_i(\mathbf{x})}{\xi} n_j + \frac{u_j(\mathbf{x} + \boldsymbol{\xi}) - u_j(\mathbf{x})}{\xi} n_i \right) \xi d\xi d\varphi \\ & \times \int_0^{2\pi} \int_0^\delta \frac{w(\mathbf{x} + \boldsymbol{\xi}) - w(\mathbf{x})}{\xi^2} n_i n_j \xi d\xi d\varphi \\ & - \frac{1}{2} \int_0^{2\pi} \int_0^\delta \frac{u_i(\mathbf{x} + \boldsymbol{\xi}) - u_i(\mathbf{x})}{\xi} n_j \xi d\xi d\varphi \int_0^{2\pi} \int_0^\delta \frac{w(\mathbf{x} + \boldsymbol{\xi}) - w(\mathbf{x})}{\xi^2} \xi d\xi d\varphi \end{aligned} \right] \quad (\text{A80})$$

One can obtain when considering Eqs. (3.37) and (A55) that

$$\frac{\partial u_i(\mathbf{x})}{\partial x_i} \frac{\partial^2 w(\mathbf{x})}{\partial x_j \partial x_j} = 2 \left(\frac{2}{\pi\delta^2} \right)^2 \int_0^{2\pi} \int_0^\delta \frac{u_i(\mathbf{x} + \boldsymbol{\xi}) - u_i(\mathbf{x})}{\xi} n_i \xi d\xi d\varphi \int_0^{2\pi} \int_0^\delta \frac{w(\mathbf{x} + \boldsymbol{\xi}) - w(\mathbf{x})}{\xi^2} \xi d\xi d\varphi \quad (\text{A81})$$

Eqs. (A80) and (A81) can be discretized as

$$\left(\frac{\partial u_i^{(k)}}{\partial x_j} + \frac{\partial u_j^{(k)}}{\partial x_j} \right) \frac{\partial^2 w_{(k)}}{\partial x_i \partial x_j} = \left(\frac{4}{\pi\delta^2 h} \right)^2 \left[\begin{aligned} & \sum_i \left(\frac{u_i^{(k)} - u_i^{(k)}}{\xi_{(i^k)(k)}} n_j^{(i^k)(k)} + \frac{u_j^{(k)} - u_j^{(k)}}{\xi_{(i^k)(k)}} n_i^{(i^k)(k)} \right) V_{(i^k)} \\ & \times \sum_i \frac{w_{(i^k)} - w_{(k)}}{\xi_{(i^k)(k)}^2} n_i^{(i^k)(k)} n_j^{(i^k)(k)} V_{(i^k)} \\ & - \frac{1}{2} \sum_i \frac{u_i^{(k)} - u_i^{(k)}}{\xi_{(i^k)(k)}} n_i^{(i^k)(k)} V_{(i^k)} \sum_i \frac{w_{(i^k)} - w_{(k)}}{\xi_{(i^k)(k)}^2} V_{(i^k)} \end{aligned} \right] \quad (\text{A82a})$$

$$\frac{\partial u_i^{(k)}}{\partial x_i} \frac{\partial^2 w_{(k)}}{\partial x_j \partial x_j} = 2 \left(\frac{2}{\pi\delta^2 h} \right)^2 \sum_i \frac{u_i^{(k)} - u_i^{(k)}}{\xi_{(i^k)(k)}} n_i^{(i^k)(k)} V_{(i^k)} \sum_i \frac{w_{(i^k)} - w_{(k)}}{\xi_{(i^k)(k)}^2} V_{(i^k)} \quad (\text{A82b})$$

Plugging Eqs. (A82a) and (A82b) into (A73c) arises

$$W_{\text{D}}^{II} = -\frac{2}{h} \left(\frac{2}{\pi\delta^2 h} \right)^2 \left[\begin{aligned} & \int_{-\frac{h}{2}}^{\frac{h}{2}} \left(\frac{E}{1-\nu^2} - 3G \right) \mathbf{z} d\mathbf{z} \sum_i \frac{u_i^{(k)} - u_i^{(k)}}{\xi_{(i^k)(k)}} n_i^{(i^k)(k)} V_{(i^k)} \sum_i \frac{w_{(i^k)} - w_{(k)}}{\xi_{(i^k)(k)}^2} V_{(i^k)} \\ & + 2 \int_{-\frac{h}{2}}^{\frac{h}{2}} \mathbf{G} \mathbf{z} d\mathbf{z} \left[\begin{aligned} & \sum_i \left(\frac{u_i^{(k)} - u_i^{(k)}}{\xi_{(i^k)(k)}} n_j^{(i^k)(k)} + \frac{u_j^{(k)} - u_j^{(k)}}{\xi_{(i^k)(k)}} n_i^{(i^k)(k)} \right) V_{(i^k)} \\ & \times \sum_i \frac{w_{(i^k)} - w_{(k)}}{\xi_{(i^k)(k)}^2} n_i^{(i^k)(k)} n_j^{(i^k)(k)} V_{(i^k)} \end{aligned} \right] \end{aligned} \right] \quad (\text{A83})$$

Inserting Eqs. (A75), (A77) and (A83) into (A72) results in the FGM Kirchhoff Plate SED in PD form as

$$\begin{aligned}
W_{FD}^{(k)} = & \frac{6}{\pi\delta^3 h^2} \int_{-\frac{h}{2}}^{\frac{h}{2}} Gz \sum_i \frac{(u_i^{(j^k)} - u_i^{(k)})(u_j^{(j^k)} - u_j^{(k)})}{\xi_{(i^k)(k)}} n_i^{(j^k)(k)} n_j^{(j^k)(k)} V_{(i^k)} \\
& + \frac{1}{2h} \left(\frac{2}{\pi\delta^2 h} \right)^2 \int_{-\frac{h}{2}}^{\frac{h}{2}} \frac{E}{1-\nu^2} \frac{3\nu-1}{2} dz \left(\sum_i \frac{u_i^{(j^k)} - u_i^{(k)}}{\xi_{(i^k)(k)}} n_i^{(j^k)(k)} V_{(i^k)} \right)^2 \\
& + \frac{2}{h} \left(\frac{2}{\pi\delta^2 h} \right)^2 \left\{ \int_{-\frac{h}{2}}^{\frac{h}{2}} \left(\frac{E}{1-\nu^2} - 5G \right) z^2 dz \left(\sum_i \frac{W_{(i^k)} - W_{(k)}}{\xi_{(i^k)(k)}^2} V_{(i^k)} \right)^2 \right. \\
& \left. + 8 \int_{-\frac{h}{2}}^{\frac{h}{2}} Gz^2 dz \sum_i \frac{W_{(i^k)} - W_{(k)}}{\xi_{(i^k)(k)}^2} n_i^{(j^k)(k)} n_j^{(j^k)(k)} V_{(i^k)} \sum_i \frac{W_{(i^k)} - W_{(k)}}{\xi_{(i^k)(k)}^2} n_i^{(j^k)(k)} n_j^{(j^k)(k)} V_{(i^k)} \right\} \quad (A84) \\
& - \frac{2}{h} \left(\frac{2}{\pi\delta^2 h} \right)^2 \left\{ \int_{-\frac{h}{2}}^{\frac{h}{2}} \left(\frac{E}{1-\nu^2} - 3G \right) z dz \sum_i \frac{u_i^{(j^k)} - u_i^{(k)}}{\xi_{(i^k)(k)}} n_i^{(j^k)(k)} V_{(i^k)} \sum_i \frac{W_{(i^k)} - W_{(k)}}{\xi_{(i^k)(k)}^2} V_{(i^k)} \right. \\
& \left. + 2 \int_{-\frac{h}{2}}^{\frac{h}{2}} Gz dz \left[\sum_i \left(\frac{u_i^{(j^k)} - u_i^{(k)}}{\xi_{(i^k)(k)}} n_j^{(j^k)(k)} + \frac{u_j^{(j^k)} - u_j^{(k)}}{\xi_{(i^k)(k)}} n_i^{(j^k)(k)} \right) V_{(i^k)} \right] \right. \\
& \left. \times \sum_i \frac{W_{(i^k)} - W_{(k)}}{\xi_{(i^k)(k)}^2} n_i^{(j^k)(k)} n_j^{(j^k)(k)} V_{(i^k)} \right\}
\end{aligned}$$

Moreover, in particular case, for any shape of the FGM Kirchhoff Plate subjected to fixed (simply-supported and clamped) boundary conditions only, the SED function can be simplified as

$$\begin{aligned}
W_{\text{com}} = & \frac{1}{2h} \left[\int_{-\frac{h}{2}}^{\frac{h}{2}} Gz (u_{i,j} u_{i,j} + u_{i,j} u_{j,i} + u_{i,i} u_{j,j}) + \int_{-\frac{h}{2}}^{\frac{h}{2}} \frac{E}{1-\nu^2} \frac{3\nu-1}{2} dz (u_{i,i})^2 \right] \\
& + \frac{1}{2h} \int_{-\frac{h}{2}}^{\frac{h}{2}} \frac{Ez^2}{1-\nu^2} dz (w_{,ii})^2 - \frac{1}{h} \int_{-\frac{h}{2}}^{\frac{h}{2}} \frac{Ez}{1-\nu^2} dz (u_{i,i} w_{,jj}) \quad (A85)
\end{aligned}$$

Proof

The total strain energy stored in the body can be casted as

$$U = \iint_{\Gamma} (W_{\text{com}} + W'_{\text{com}} + W''_{\text{com}}) dx_1 dx_2 = U_I + U_{II} + U_{III} \quad (A86)$$

where

$$U_I = \frac{1}{2h} \iint_{\Gamma} \left[\int_{-\frac{h}{2}}^{\frac{h}{2}} Gz (u_{i,j} u_{i,j} + u_{i,j} u_{j,i} + u_{i,i} u_{j,j}) + \int_{-\frac{h}{2}}^{\frac{h}{2}} \frac{E}{1-\nu^2} \frac{3\nu-1}{2} dz (u_{i,i})^2 \right] dx_1 dx_2 \quad (A87a)$$

$$U_{II} = \frac{1}{2h} \iint_{\Gamma} \int_{-\frac{h}{2}}^{\frac{h}{2}} \frac{Ez^2}{1-\nu^2} dz (w_{,ii})^2 dx_1 dx_2 + \frac{1}{h} \int_{-\frac{h}{2}}^{\frac{h}{2}} Gz^2 dz \iint_{\Gamma} (w_{,ij} w_{,ij} - (w_{,ii})^2) dx_1 dx_2 \quad (A87b)$$

$$U_{III} = -\frac{1}{h} \left\{ \int_{-\frac{h}{2}}^{\frac{h}{2}} \frac{Ez}{1-\nu^2} dz \iint_{\Gamma} (u_{i,i} w_{,jj}) dx_1 dx_2 \right. \\
\left. + \int_{-\frac{h}{2}}^{\frac{h}{2}} Gz dz \iint_{\Gamma} [(u_{i,j} + u_{j,i}) w_{,ij} - 2u_{i,i} w_{,jj}] dx_1 dx_2 \right\} \quad (A87c)$$

According to the differentiation definition for a compound function, it is clear that

$$\frac{\partial u_1}{\partial x_2} \frac{\partial^2 w}{\partial x_1 \partial x_2} = \frac{\partial}{\partial x_2} \left(u_1 \frac{\partial^2 w}{\partial x_1 \partial x_2} \right) - \frac{\partial}{\partial x_1} \left(u_1 \frac{\partial^2 w}{\partial x_2 \partial x_2} \right) + \frac{\partial u_1}{\partial x_1} \frac{\partial^2 w}{\partial x_2 \partial x_2} \quad (\text{A88a})$$

$$\frac{\partial u_2}{\partial x_1} \frac{\partial^2 w}{\partial x_1 \partial x_2} = \frac{\partial}{\partial x_1} \left(u_2 \frac{\partial^2 w}{\partial x_1 \partial x_2} \right) - \frac{\partial}{\partial x_2} \left(u_2 \frac{\partial^2 w}{\partial x_2 \partial x_2} \right) + \frac{\partial u_2}{\partial x_2} \frac{\partial^2 w}{\partial x_1 \partial x_1} \quad (\text{A88b})$$

Combining Eqs. (A88a) and (A88b) together gives

$$\begin{aligned} & \left(\frac{\partial u_1}{\partial x_2} + \frac{\partial u_2}{\partial x_1} \right) \frac{\partial^2 w}{\partial x_1 \partial x_2} - \left(\frac{\partial u_1}{\partial x_1} \frac{\partial^2 w}{\partial x_2^2} + \frac{\partial u_2}{\partial x_2} \frac{\partial^2 w}{\partial x_1^2} \right) \\ &= \frac{\partial}{\partial x_1} \left(u_2 \frac{\partial^2 w}{\partial x_1 \partial x_2} - u_1 \frac{\partial^2 w}{\partial x_2^2} \right) + \frac{\partial}{\partial x_2} \left(u_1 \frac{\partial^2 w}{\partial x_1 \partial x_2} - u_2 \frac{\partial^2 w}{\partial x_1^2} \right) \end{aligned} \quad (\text{A89})$$

According to the 2-Dimensional divergence theorem (Green's theorem), Eq. (A89) can be performed following manipulation

$$\begin{aligned} & \iint_{\Gamma} \left[\left(\frac{\partial u_1}{\partial x_2} + \frac{\partial u_2}{\partial x_1} \right) \frac{\partial^2 w}{\partial x_1 \partial x_2} - \left(\frac{\partial u_1}{\partial x_1} \frac{\partial^2 w}{\partial x_2^2} + \frac{\partial u_2}{\partial x_2} \frac{\partial^2 w}{\partial x_1^2} \right) \right] dx_1 dx_2 \\ &= \iint_{\Gamma} \frac{\partial}{\partial x_1} \left(u_2 \frac{\partial^2 w}{\partial x_1 \partial x_2} - u_1 \frac{\partial^2 w}{\partial x_2^2} \right) + \frac{\partial}{\partial x_2} \left(u_1 \frac{\partial^2 w}{\partial x_1 \partial x_2} - u_2 \frac{\partial^2 w}{\partial x_1^2} \right) dx_1 dx_2 \\ &= \oint_{\text{cr}} \left[\left(u_2 \frac{\partial^2 w}{\partial x_1 \partial x_2} - u_1 \frac{\partial^2 w}{\partial x_2^2} \right) \cos \theta - \left(u_1 \frac{\partial^2 w}{\partial x_1 \partial x_2} - u_2 \frac{\partial^2 w}{\partial x_1^2} \right) \sin \theta \right] ds \end{aligned} \quad (\text{A90})$$

For any shape of plate with boundaries are constrained as fixed, the in-plane displacements u_1 and u_2 are equal to zero. Therefore,

$$\iint_{\Gamma} \left[\left(\frac{\partial u_1}{\partial x_2} + \frac{\partial u_2}{\partial x_1} \right) \frac{\partial^2 w}{\partial x_1 \partial x_2} - \left(\frac{\partial u_1}{\partial x_1} \frac{\partial^2 w}{\partial x_2^2} + \frac{\partial u_2}{\partial x_2} \frac{\partial^2 w}{\partial x_1^2} \right) \right] dx_1 dx_2 = 0 \quad (\text{A91})$$

and

$$U_{III} = -\frac{1}{h} \int_{-\frac{h}{2}}^{\frac{h}{2}} \frac{Ez}{1-\nu^2} dz \iint_{\Gamma} (u_{i,j} w_{,j}) dx_1 dx_2 \quad (\text{A92a})$$

One can obtain by utilizing the pre-proved, Eq. (A69) that

$$U_{II} = \frac{1}{2h} \iint_{\Gamma} \int_{-\frac{h}{2}}^{\frac{h}{2}} \frac{Ez^2}{1-\nu^2} dz (w_{,ii})^2 dx_1 dx_2 \quad (\text{A92b})$$

Therefore, the total strain energy, Eq. (A86), stored in the body can be simplified as

$$\begin{aligned} U &= \frac{1}{2h} \iint_{\Gamma} \left[\int_{-\frac{h}{2}}^{\frac{h}{2}} G dz (u_{i,j} u_{i,j} + u_{i,j} u_{j,i} + u_{i,i} u_{j,j}) + \int_{-\frac{h}{2}}^{\frac{h}{2}} \frac{E}{1-\nu^2} \frac{3\nu-1}{2} dz (u_{i,i})^2 \right] dx_1 dx_2 \\ &+ \frac{1}{2h} \iint_{\Gamma} \int_{-\frac{h}{2}}^{\frac{h}{2}} \frac{Ez^2}{1-\nu^2} dz (w_{,ii})^2 dx_1 dx_2 - \frac{1}{h} \int_{-\frac{h}{2}}^{\frac{h}{2}} \frac{Ez}{1-\nu^2} dz \iint_{\Gamma} (u_{i,j} w_{,j}) dx_1 dx_2 \end{aligned} \quad (\text{A93})$$

And its corresponding strain energy density function becomes

$$W_{\text{com}} = \frac{1}{2h} \left[\int_{-\frac{h}{2}}^{\frac{h}{2}} Gz (u_{i,j} u_{i,j} + u_{i,j} u_{j,i} + u_{i,i} u_{j,j}) + \int_{-\frac{h}{2}}^{\frac{h}{2}} \frac{E}{1-\nu^2} \frac{3\nu-1}{2} dz (u_{i,i})^2 \right] \\ + \frac{1}{2h} \int_{-\frac{h}{2}}^{\frac{h}{2}} \frac{Ez^2}{1-\nu^2} dz (w_{i,i})^2 - \frac{1}{h} \int_{-\frac{h}{2}}^{\frac{h}{2}} \frac{Ez}{1-\nu^2} dz (u_{i,i} w_{j,j}) \quad \blacksquare$$

A2.3 Mindlin Plate

As explained in Chapter 5.3, the SED function for Mindlin Plate can be written as

$$W_{\text{com}} = \frac{G}{2} \frac{h^2}{12} \left[\left(\frac{\partial \theta_i}{\partial x_j} \frac{\partial \theta_i}{\partial x_j} + \frac{\partial \theta_i}{\partial x_j} \frac{\partial \theta_j}{\partial x_i} + \frac{\partial \theta_i}{\partial x_i} \frac{\partial \theta_j}{\partial x_j} \right) + \frac{3\nu-1}{1-\nu} \left(\frac{\partial \theta_i}{\partial x_i} \right)^2 \right] \\ + \kappa_s^2 \frac{G}{2} \left(\theta_i + \frac{\partial w}{\partial x_i} \right) \left(\theta_i + \frac{\partial w}{\partial x_i} \right) \quad (\text{A94})$$

If we recall Eqs. (3.38a, b) and replace the linear displacement, u , with the rotational displacement, θ , we have

$$\frac{\partial \theta_i^{(k)}}{\partial x_j} \frac{\partial \theta_i^{(k)}}{\partial x_j} + \frac{\partial \theta_i^{(k)}}{\partial x_i} \frac{\partial \theta_j^{(k)}}{\partial x_j} + \frac{\partial \theta_i^{(k)}}{\partial x_j} \frac{\partial \theta_j^{(k)}}{\partial x_i} = \frac{12}{\pi \delta^3 h} \sum_i \frac{(\theta_i^{(i^k)} - \theta_i^{(k)}) (\theta_j^{(i^k)} - \theta_j^{(k)})}{\xi_{(i^k)(k)}} n_i^{(i^k)(k)} n_j^{(i^k)(k)} V_{(i^k)} \quad (\text{A95a})$$

$$\frac{\partial \theta_i^{(k)}}{\partial x_i} = \frac{2}{\pi \delta^2 h} \sum_i \frac{\theta_i^{(i^k)} - \theta_i^{(k)}}{\xi_{(i^k)(k)}} n_i^{(i^k)(k)} V_{(i^k)} \quad (\text{A95b})$$

The following expressions can be obtained by utilizing Taylor expansion as

$$w(\mathbf{x} + \boldsymbol{\xi}) - w(\mathbf{x}) = \frac{\partial w(\mathbf{x})}{\partial x_i} \xi n_i + O(\xi^2) \quad (\text{A96a})$$

$$\frac{\theta_i(\mathbf{x} + \boldsymbol{\xi}) + \theta_i(\mathbf{x})}{2} \xi n_i = \theta_i(\mathbf{x}) \xi n_i + O(\xi^2) \quad (\text{A96b})$$

Combing Eqs. (A96a) with (A96b) and ignoring the big O notation gives

$$w(\mathbf{x} + \boldsymbol{\xi}) - w(\mathbf{x}) + \frac{\theta_i(\mathbf{x} + \boldsymbol{\xi}) + \theta_i(\mathbf{x})}{2} \xi n_i = \left(\frac{\partial w(\mathbf{x})}{\partial x_i} + \theta_i(\mathbf{x}) \right) \xi n_i \quad (\text{A97a})$$

or with another dummy index as

$$w(\mathbf{x} + \boldsymbol{\xi}) - w(\mathbf{x}) + \frac{\theta_j(\mathbf{x} + \boldsymbol{\xi}) + \theta_j(\mathbf{x})}{2} \xi n_j = \left(\frac{\partial w(\mathbf{x})}{\partial x_j} + \theta_j(\mathbf{x}) \right) \xi n_j \quad (\text{A97b})$$

Multiplying Eq. (A97a) with (A97b) and dividing each terms by the kernel function, ξ arises

$$\frac{1}{\xi} \left(w(\mathbf{x} + \boldsymbol{\xi}) - w(\mathbf{x}) + \frac{\theta_i(\mathbf{x} + \boldsymbol{\xi}) + \theta_i(\mathbf{x})}{2} \xi n_i \right)^2 = \left(\frac{\partial w(\mathbf{x})}{\partial x_i} + \theta_i(\mathbf{x}) \right) \left(\frac{\partial w(\mathbf{x})}{\partial x_j} + \theta_j(\mathbf{x}) \right) \xi n_i n_j \quad (\text{A98})$$

Considering \mathbf{x} as a fixed point, integrating both sides of Equation (A98) over a circular domain with centre of \mathbf{x} and radius of δ yields:

$$\begin{aligned}
& \int_0^{2\pi} \int_0^\delta \frac{1}{\xi} \left(w(\mathbf{x} + \boldsymbol{\xi}) - w(\mathbf{x}) + \frac{\theta_i(\mathbf{x} + \boldsymbol{\xi}) + \theta_i(\mathbf{x})}{2} \xi n_i \right)^2 \xi d\xi d\varphi \\
&= \left(\frac{\partial w(\mathbf{x})}{\partial x_i} + \theta_i(\mathbf{x}) \right) \left(\frac{\partial w(\mathbf{x})}{\partial x_j} + \theta_j(\mathbf{x}) \right) \int_0^{2\pi} \int_0^\delta \xi d\xi d\varphi \xi n_i n_j \\
&= \frac{\pi \delta^3}{3} \left(\frac{\partial w(\mathbf{x})}{\partial x_i} + \theta_i(\mathbf{x}) \right) \left(\frac{\partial w(\mathbf{x})}{\partial x_j} + \theta_j(\mathbf{x}) \right) \delta_{ij} \\
&= \frac{\pi \delta^3}{3} \left(\frac{\partial w(\mathbf{x})}{\partial x_i} + \theta_i(\mathbf{x}) \right) \left(\frac{\partial w(\mathbf{x})}{\partial x_i} + \theta_i(\mathbf{x}) \right)
\end{aligned} \tag{A99a}$$

which can be written in discretized form as

$$\left(\frac{\partial W_k}{\partial x_i} + \theta_i^{(k)} \right) \left(\frac{\partial W_k}{\partial x_i} + \theta_i^{(k)} \right) = \frac{3}{\pi \delta^3 h} \sum_i \frac{1}{\xi_{i^{(k)}(k)}} \left(w_{i^{(k)}} - w_k + \frac{\theta_i^{i^{(k)}} + \theta_i^{(k)}}{2} \xi_{i^{(k)}(k)} n_i^{i^{(k)}(k)} \right)^2 V_{i^{(k)}} \tag{A99b}$$

Substituting Eqs. (A95a, b) and (A99b) into (A94) results in the Mindlin Plate SED mat material point k , in PD form as

$$\begin{aligned}
W_{PD}^{(k)} &= \frac{G h^2}{2} \frac{12}{\pi \delta^3 h} \sum_i \left[\frac{\left(\theta_i^{i^{(k)}} - \theta_i^{(k)} \right) n_i^{i^{(k)}(k)}}{\xi_{i^{(k)}(k)}} \right]^2 V_{i^{(k)}} + \frac{3\nu - 1}{1 - \nu} \left(\frac{2}{\pi \delta^2 h} \sum_i \frac{\theta_i^{i^{(k)}} - \theta_i^{(k)}}{\xi_{i^{(k)}(k)}} n_i^{i^{(k)}(k)} V_{i^{(k)}} \right)^2 \\
&+ \kappa_s^2 \frac{G}{2} \frac{3}{\pi \delta^3 h} \sum_i \frac{1}{\xi_{i^{(k)}(k)}} \left(w_{i^{(k)}} - w_k + \frac{\theta_i^{i^{(k)}} + \theta_i^{(k)}}{2} \xi_{i^{(k)}(k)} n_i^{i^{(k)}(k)} \right)^2 V_{i^{(k)}}
\end{aligned} \tag{A100}$$

A2.4 FGM Mindlin Plate

As mentioned in Chapter 5.4, the SED function for FGM Mindlin Plate can be expressed as

$$\begin{aligned}
W_{\text{GM}} &= \frac{1}{2h} \left[\int_{-\frac{h}{2}}^{\frac{h}{2}} G z \left(\frac{\partial u_i}{\partial x_j} \frac{\partial u_i}{\partial x_j} + \frac{\partial u_i}{\partial x_j} \frac{\partial u_j}{\partial x_i} + \frac{\partial u_i}{\partial x_i} \frac{\partial u_j}{\partial x_j} \right) + \int_{-\frac{h}{2}}^{\frac{h}{2}} G^2 dz \left(\frac{\partial \theta_i}{\partial x_j} \frac{\partial \theta_i}{\partial x_j} + \frac{\partial \theta_i}{\partial x_j} \frac{\partial \theta_j}{\partial x_i} + \frac{\partial \theta_i}{\partial x_i} \frac{\partial \theta_j}{\partial x_j} \right) \right] \\
&+ 2 \int_{-\frac{h}{2}}^{\frac{h}{2}} G dz \left(\frac{\partial u_i}{\partial x_j} \frac{\partial \theta_i}{\partial x_j} + \frac{\partial u_i}{\partial x_j} \frac{\partial \theta_j}{\partial x_i} + \frac{\partial u_i}{\partial x_i} \frac{\partial \theta_j}{\partial x_j} \right) + \int_{-\frac{h}{2}}^{\frac{h}{2}} \kappa_s^2 G z \left(\theta_i + \frac{\partial w}{\partial x_i} \right) \left(\theta_i + \frac{\partial w}{\partial x_i} \right) \\
&+ \int_{-\frac{h}{2}}^{\frac{h}{2}} G \frac{3\nu - 1}{1 - \nu} dz \left(\frac{\partial u_i}{\partial x_i} \right)^2 + \int_{-\frac{h}{2}}^{\frac{h}{2}} G \frac{3\nu - 1}{1 - \nu} z^2 dz \left(\frac{\partial \theta_i}{\partial x_i} \right) + 2 \int_{-\frac{h}{2}}^{\frac{h}{2}} G \frac{3\nu - 1}{1 - \nu} z dz \frac{\partial u_i}{\partial x_i} \frac{\partial \theta_j}{\partial x_j}
\end{aligned} \tag{A101}$$

The following expressions can be established by referring to the derivation procedure of Eqs. (3.38a, b) and (A99b) as

$$\begin{aligned}
\frac{\partial u_i^{(k)}}{\partial x_j} \frac{\partial u_i^{(k)}}{\partial x_j} + \frac{\partial u_i^{(k)}}{\partial x_i} \frac{\partial u_j^{(k)}}{\partial x_j} + \frac{\partial u_i^{(k)}}{\partial x_j} \frac{\partial u_i^{(k)}}{\partial x_i} &= \frac{12}{\pi \delta^3 h} \sum_i \frac{\left[(u_i^{(k)} - u_i^{(k)}) n_i^{(i^k)(k)} \right]^2}{\xi_{(i^k)(k)}} V_{(i^k)} \\
\frac{\partial \theta_i^{(k)}}{\partial x_j} \frac{\partial \theta_i^{(k)}}{\partial x_j} + \frac{\partial \theta_i^{(k)}}{\partial x_i} \frac{\partial \theta_j^{(k)}}{\partial x_j} + \frac{\partial \theta_i^{(k)}}{\partial x_j} \frac{\partial \theta_j^{(k)}}{\partial x_i} &= \frac{12}{\pi \delta^3 h} \sum_i \frac{\left[(\theta_i^{(k)} - \theta_i^{(k)}) n_i^{(i^k)(k)} \right]^2}{\xi_{(i^k)(k)}} V_{(i^k)} \\
\frac{\partial u_i^{(k)}}{\partial x_j} \frac{\partial \theta_j^{(k)}}{\partial x_j} + \frac{\partial u_i^{(k)}}{\partial x_i} \frac{\partial \theta_j^{(k)}}{\partial x_j} + \frac{\partial u_i^{(k)}}{\partial x_j} \frac{\partial \theta_j^{(k)}}{\partial x_i} &= \frac{12}{\pi \delta^3 h} \sum_i \frac{(u_i^{(k)} - u_i^{(k)}) (\theta_j^{(k)} - \theta_j^{(k)})}{\xi_{(i^k)(k)}} n_i^{(i^k)(k)} n_j^{(i^k)(k)} V_{(i^k)} \\
\left(\frac{\partial w_{(k)}}{\partial x_i} + \theta_i^{(k)} \right) \left(\frac{\partial w_{(k)}}{\partial x_i} + \theta_i^{(k)} \right) &= \frac{3}{\pi \delta^3 h} \sum_i \frac{1}{\xi_{(i^k)(k)}} \left(w_{(i^k)} - w_{(k)} + \frac{\theta_i^{(i^k)} + \theta_i^{(k)}}{2} \xi_{(i^k)(k)} n_i^{(i^k)(k)} \right)^2 V_{(i^k)} \\
\frac{\partial u_i^{(k)}}{\partial x_i} &= \frac{2}{\pi \delta^2 h} \sum_i \frac{u_i^{(i^k)} - u_i^{(k)}}{\xi_{(i^k)(k)}} n_i^{(i^k)(k)} V_{(i^k)} \\
\frac{\partial \theta_i^{(k)}}{\partial x_i} &= \frac{2}{\pi \delta^2 h} \sum_i \frac{\theta_i^{(i^k)} - \theta_i^{(k)}}{\xi_{(i^k)(k)}} n_i^{(i^k)(k)} V_{(i^k)} \tag{A102a-f}
\end{aligned}$$

Plugging Eqs (A102a – f) into (A101) yields the SED at material point k in PD form

as

$$\begin{aligned}
W_{PD}^{(k)} &= \frac{6}{\pi \delta^3 h^2} \left\{ \int_{-\frac{h}{2}}^{\frac{h}{2}} G dz \sum_i \frac{\left[(u_i^{(i^k)} - u_i^{(k)}) n_i^{(i^k)(k)} \right]^2}{\xi_{(i^k)(k)}} V_{(i^k)} + \int_{-\frac{h}{2}}^{\frac{h}{2}} G z^2 dz \sum_i \frac{\left[(\theta_i^{(i^k)} - \theta_i^{(k)}) n_i^{(i^k)(k)} \right]^2}{\xi_{(i^k)(k)}} V_{(i^k)} \right. \\
&\quad \left. + \kappa_s^2 \int_{-\frac{h}{2}}^{\frac{h}{2}} \frac{G}{4} dz \sum_i \frac{1}{\xi_{(i^k)(k)}} \left(w_{(i^k)} - w_{(k)} + \frac{\theta_i^{(i^k)} + \theta_i^{(k)}}{2} n_i^{(i^k)(k)} \xi_{(i^k)(k)} \right)^2 V_{(i^k)} \right. \\
&\quad \left. 2 \int_{-\frac{h}{2}}^{\frac{h}{2}} G dz \sum_i \frac{(u_i^{(i^k)} - u_i^{(k)}) (\theta_j^{(i^k)} - \theta_j^{(k)})}{\xi_{(i^k)(k)}} n_i^{(i^k)(k)} n_j^{(i^k)(k)} V_{(i^k)} \right\} \tag{A103} \\
&\quad + \frac{1}{h} \left(\frac{2}{\pi \delta^2 h} \right)^2 \left[\int_{-\frac{h}{2}}^{\frac{h}{2}} \frac{G}{2} \frac{3\nu - 1}{1 - \nu} dz \left(\sum_i \frac{u_i^{(i^k)} - u_i^{(k)}}{\xi_{(i^k)(k)}} n_i^{(i^k)(k)} V_{(i^k)} \right)^2 \right. \\
&\quad \left. + \int_{-\frac{h}{2}}^{\frac{h}{2}} \frac{G}{2} \frac{3\nu - 1}{1 - \nu} z^2 dz \left(\sum_i \frac{\theta_i^{(i^k)} - \theta_i^{(k)}}{\xi_{(i^k)(k)}} n_i^{(i^k)(k)} V_{(i^k)} \right)^2 \right. \\
&\quad \left. + \int_{-\frac{h}{2}}^{\frac{h}{2}} G \frac{3\nu - 1}{1 - \nu} z dz \sum_i \frac{\theta_i^{(i^k)} - \theta_i^{(k)}}{\xi_{(i^k)(k)}} n_i^{(i^k)(k)} V_{(i^k)} \sum_i \frac{u_j^{(i^k)} - u_j^{(k)}}{\xi_{(i^k)(k)}} n_j^{(i^k)(k)} V_{(i^k)} \right]
\end{aligned}$$

A2.5 Higher Order Deformable Plate

As described in Chapter 4.5, the SED function can be given as

$$W_{\text{cm}} = \frac{G}{2} \left\{ \begin{aligned} & \frac{h^2}{12} \left[\frac{\partial \theta_i}{\partial x_j} \frac{\partial \theta_i}{\partial x_j} + \frac{\partial \theta_i}{\partial x_j} \frac{\partial \theta_j}{\partial x_i} + \frac{\partial \theta_i}{\partial x_i} \frac{\partial \theta_j}{\partial x_j} + 2 \left(\theta_i + \frac{\partial w}{\partial x_i} \right) \left(3\theta_i^* + \frac{\partial w^*}{\partial x_i} \right) \right] \\ & + \frac{8}{1-2\nu} \left[(1-\nu) (\dot{w})^2 + \nu \dot{w} \frac{\partial \theta_i}{\partial x_i} \right] \\ & + 2 \frac{h^4}{80} \left[\frac{\partial \theta_i}{\partial x_j} \frac{\partial \theta_i^*}{\partial x_j} + \frac{\partial \theta_i}{\partial x_j} \frac{\partial \theta_j^*}{\partial x_i} + \frac{\partial \theta_i}{\partial x_i} \frac{\partial \theta_i^*}{\partial x_i} \right. \\ & \left. + \frac{1}{2} \left(3\theta_i^* + \frac{\partial w^*}{\partial x_i} \right) \left(3\theta_i + \frac{\partial w}{\partial x_i} \right) + \frac{4\nu}{1-2\nu} \frac{\partial \theta_i^*}{\partial x_i} \dot{w} \right] \\ & + \left(\theta_i + \frac{\partial w}{\partial x_i} \right) \left(\theta_i + \frac{\partial w}{\partial x_i} \right) + \frac{h^6}{448} \left(\frac{\partial \theta_i^*}{\partial x_j} \frac{\partial \theta_i^*}{\partial x_j} + \frac{\partial \theta_i^*}{\partial x_j} \frac{\partial \theta_j^*}{\partial x_i} + \frac{\partial \theta_i^*}{\partial x_i} \frac{\partial \theta_j^*}{\partial x_j} \right) \\ & + \frac{4\nu-1}{1-2\nu} \left[\frac{h^2}{12} \left(\frac{\partial \theta_i}{\partial x_i} \right)^2 + \frac{h^6}{448} \left(\frac{\partial \theta_i^*}{\partial x_i} \right)^2 + 2 \frac{h^4}{80} \frac{\partial \theta_i}{\partial x_i} \frac{\partial \theta_j^*}{\partial x_j} \right] \end{aligned} \right\} \quad (\text{A104})$$

If we Taylor expand functions w^* and θ_i about point \mathbf{x}

$$\frac{\dot{w}(\mathbf{x} + \boldsymbol{\xi}) + \dot{w}(\mathbf{x})}{2} = \dot{w}(\mathbf{x}) \quad (\text{A105a})$$

$$\theta_i(\mathbf{x} + \boldsymbol{\xi}) - \theta_i(\mathbf{x}) = \frac{\partial \theta_i(\mathbf{x})}{\partial x_j} \xi n_j \quad (\text{A105b})$$

Multiplying Eq. (A105a) by (A105b) and multiplying each terms by the unit orientation vector gives

$$\frac{\dot{w}(\mathbf{x} + \boldsymbol{\xi}) + \dot{w}(\mathbf{x})}{2} [\theta_i(\mathbf{x} + \boldsymbol{\xi}) - \theta_i(\mathbf{x})] n_k = \dot{w}(\mathbf{x}) \frac{\partial \theta_i(\mathbf{x})}{\partial x_j} \xi n_j n_k \quad (\text{A106})$$

Considering \mathbf{x} as a fixed point, integrating both sides of Equation (A106) over a circular domain with centre of \mathbf{x} and radius of δ yields:

$$\dot{w}(\mathbf{x}) \frac{\partial \theta_i(\mathbf{x})}{\partial x_k} = \frac{3}{\pi \delta^3} \int_0^{2\pi} \int_0^\delta \frac{\dot{w}(\mathbf{x} + \boldsymbol{\xi}) + \dot{w}(\mathbf{x})}{2} [\theta_i(\mathbf{x} + \boldsymbol{\xi}) - \theta_i(\mathbf{x})] n_k \xi d\xi d\varphi \quad (\text{A107})$$

Multiplying both sides of Eq. (107) by δ_{IK} gives

$$\dot{w}(\mathbf{x}) \frac{\partial \theta_i(\mathbf{x})}{\partial x_i} = \frac{3}{\pi \delta^3} \int_0^{2\pi} \int_0^\delta \frac{\dot{w}(\mathbf{x} + \boldsymbol{\xi}) + \dot{w}(\mathbf{x})}{2} [\theta_i(\mathbf{x} + \boldsymbol{\xi}) - \theta_i(\mathbf{x})] n_i \xi d\xi d\varphi \quad (\text{A108a})$$

which can be discretized at material point k as

$$\dot{w}_{(k)}^* \frac{\partial \theta_i^{(k)}}{\partial x_i} = \frac{3}{\pi \delta^3 h} \sum_i \frac{\dot{w}_{(i^k)}^* + \dot{w}_{(k)}^*}{2} (\theta_i^{(i^k)} - \theta_i^{(k)}) n_i^{(i^k)(k)} V_{(i^k)} \quad (\text{A108b})$$

Following expressions can be obtained analogically

$$(\dot{w}_{(k)}^*)^2 = \frac{3}{2\pi \delta^3 h} \sum_i \left(\frac{\dot{w}_{(i^k)}^* + \dot{w}_{(k)}^*}{2} \right)^2 \xi_{(i^k)(k)} V_{(i^k)} \quad (\text{A109a})$$

$$\dot{w}_{(k)}^* \frac{\partial \theta_i^{(k)}}{\partial x_i} = \frac{3}{\pi \delta^3 h} \sum_i \frac{\dot{w}_{(i^k)}^* + \dot{w}_{(k)}^*}{2} (\theta_i^{(i^k)} - \theta_i^{(k)}) n_i^{(i^k)(k)} V_{(i^k)} \quad (\text{A109b})$$

The rest local terms of Eq. (A104) can be transformed into the equivalent non-local forms by referring to Eqs. (3.38a, b) and (A99b) as

$$\begin{aligned}
& \frac{\partial \theta_l^{(k)}}{\partial x_j} \frac{\partial \theta_l^{(k)}}{\partial x_j} + \frac{\partial \theta_l^{(k)}}{\partial x_l} \frac{\partial \theta_j^{(k)}}{\partial x_j} + \frac{\partial \theta_l^{(k)}}{\partial x_j} \frac{\partial \theta_j^{(k)}}{\partial x_l} = \frac{12}{\pi \delta^3 h} \sum_i \frac{\left[\left(\theta_l^{(i^k)} - \theta_l^{(k)} \right) n_l^{(i^k)(k)} \right]^2}{\xi_{(i^k)(k)}} V_{(i^k)} \\
& \left(\frac{\partial w_{(k)}}{\partial x_l} + \theta_l^{(k)} \right) \left(\frac{\partial w_{(k)}}{\partial x_l} + 3\theta_l^{*(k)} \right) \\
& = \frac{3}{\pi \delta^3 h} \sum_i \left(\frac{w_{(i^k)} - w_{(k)}}{\xi_{(i^k)(k)}} + \frac{\theta_l^{(i^k)} + \theta_l^{(k)}}{2} n_l^{(i^k)(k)} \right) \left(w_{(i^k)} - w_{(k)} + 3 \frac{\theta_l^{*(i^k)} + \theta_l^{*(k)}}{2} \xi_{(i^k)(k)} n_l^{(i^k)(k)} \right) V_{(i^k)} \\
& \frac{\partial \theta_l^{(k)}}{\partial x_j} \frac{\partial \theta_l^{*(k)}}{\partial x_j} + \frac{\partial \theta_l^{(k)}}{\partial x_l} \frac{\partial \theta_j^{*(k)}}{\partial x_j} + \frac{\partial \theta_l^{(k)}}{\partial x_j} \frac{\partial \theta_j^{*(k)}}{\partial x_l} = \frac{12}{\pi \delta^3 h} \sum_i \frac{\left(u_l^{(i^k)} - u_l^{(k)} \right) \left(\theta_j^{*(i^k)} - \theta_j^{*(k)} \right)}{\xi_{(i^k)(k)}} n_l^{(i^k)(k)} n_j^{(i^k)(k)} V_{(i^k)} \\
& \left(\frac{\partial w_{(k)}}{\partial x_l} + 3\theta_l^{*(k)} \right) \left(\frac{\partial w_{(k)}}{\partial x_l} + 3\theta_l^{*(k)} \right) = \frac{3}{\pi \delta^3 h} \sum_i \frac{1}{\xi_{(i^k)(k)}} \left(w_{(i^k)} - w_{(k)} + 3 \frac{\theta_l^{*(i^k)} + \theta_l^{*(k)}}{2} \xi_{(i^k)(k)} n_l^{(i^k)(k)} \right)^2 V_{(i^k)} \\
& \left(\frac{\partial w_{(k)}}{\partial x_l} + \theta_l^{(k)} \right) \left(\frac{\partial w_{(k)}}{\partial x_l} + \theta_l^{(k)} \right) = \frac{3}{\pi \delta^3 h} \sum_i \frac{1}{\xi_{(i^k)(k)}} \left(w_{(i^k)} - w_{(k)} + \frac{\theta_l^{(i^k)} + \theta_l^{(k)}}{2} \xi_{(i^k)(k)} n_l^{(i^k)(k)} \right)^2 V_{(i^k)} \\
& \frac{\partial \theta_l^{*(k)}}{\partial x_j} \frac{\partial \theta_l^{*(k)}}{\partial x_j} + \frac{\partial \theta_l^{*(k)}}{\partial x_l} \frac{\partial \theta_j^{*(k)}}{\partial x_j} + \frac{\partial \theta_l^{*(k)}}{\partial x_j} \frac{\partial \theta_j^{*(k)}}{\partial x_l} = \frac{12}{\pi \delta^3 h} \sum_i \frac{\left[\left(\theta_l^{*(i^k)} - \theta_l^{*(k)} \right) n_l^{(i^k)(k)} \right]^2}{\xi_{(i^k)(k)}} V_{(i^k)} \\
& \frac{\partial \theta_l^{(k)}}{\partial x_l} = \frac{2}{\pi \delta^2 h} \sum_i \frac{\theta_l^{(i^k)} - \theta_l^{(k)}}{\xi_{(i^k)(k)}} n_l^{(i^k)(k)} V_{(i^k)} \\
& \frac{\partial \theta_l^{*(k)}}{\partial x_l} = \frac{2}{\pi \delta^2 h} \sum_i \frac{\theta_l^{*(i^k)} - \theta_l^{*(k)}}{\xi_{(i^k)(k)}} n_l^{(i^k)(k)} V_{(i^k)} \tag{A110a – h}
\end{aligned}$$

Inserting above into (A104) results in the PD SED function as

$$\begin{aligned}
W_{FD}^{(k)} = \frac{G}{2} & \left\{ \begin{aligned} & \sum_i \left[\frac{(\theta_i^{i^k} - \theta_i^{(k)}) n_i^{i^k(k)}}{\xi_{(i^k)(k)}} \right]^2 V_{(i^k)} \\ & + \frac{h}{\pi \delta^3} \left[\sum_i \frac{1}{2} \left(\frac{w_{(i^k)} - w_{(k)}}{\xi_{(i^k)(k)}} + \frac{\theta_i^{i^k} + \theta_i^{(k)}}{2} n_i^{i^k(k)} \right) \left(w_{(i^k)} - w_{(k)} + 3 \frac{\theta_j^{*(i^k)} + \theta_j^{*(k)}}{2} \frac{\xi_{(i^k)(k)}}{\xi_{(i^k)(k)}} n_j^{i^k(k)} \right) V_{(i^k)} \right. \\ & \left. + \frac{1}{1-2\nu} \sum_i \left[(1-\nu) \left(\frac{w_{(i^k)}^* + w_{(k)}^*}{2} \right)^2 \xi_{(i^k)(k)} + \nu (w_{(i^k)}^* + w_{(k)}^*) (\theta_i^{i^k} - \theta_i^{(k)}) n_i^{i^k(k)} \right] V_{(i^k)} \right] \\ & + 2 \left[\frac{h^4}{80} + \frac{\nu}{1-2\nu} \frac{12}{\pi \delta^3 h} \sum_i \frac{w_{(i^k)}^* + w_{(k)}^*}{2} (\theta_i^{*(i^k)} - \theta_i^{*(k)}) n_i^{i^k(k)} V_{(i^k)} \right. \\ & \left. + \frac{1}{2} \frac{3}{\pi \delta^3 h} \sum_i \frac{1}{\xi_{(i^k)(k)}} \left(w_{(i^k)} - w_{(k)} + 3 \frac{\theta_i^{*(i^k)} + \theta_i^{*(k)}}{2} \frac{\xi_{(i^k)(k)}}{\xi_{(i^k)(k)}} n_i^{i^k(k)} \right)^2 V_{(i^k)} \right] \\ & + \frac{3}{\pi \delta^3 h} \sum_i \frac{1}{\xi_{(i^k)(k)}} \left(w_{(i^k)} - w_{(k)} + \frac{\theta_i^{i^k} + \theta_i^{(k)}}{2} \frac{\xi_{(i^k)(k)}}{\xi_{(i^k)(k)}} n_i^{i^k(k)} \right)^2 V_{(i^k)} \\ & + \frac{h^6}{448} \frac{12}{\pi \delta^3 h} \sum_i \left[\frac{(\theta_i^{*(i^k)} - \theta_i^{*(k)}) n_i^{i^k(k)}}{\xi_{(i^k)(k)}} \right]^2 V_{(i^k)} \\ & + \frac{4\nu - 1}{1 - 2\nu} \left[\frac{h^2}{12} \left(\frac{2}{\pi \delta^2 h} \sum_i \frac{\theta_i^{i^k} - \theta_i^{(k)}}{\xi_{(i^k)(k)}} n_i^{i^k(k)} V_{(i^k)} \right)^2 + \frac{h^6}{448} \left(\frac{2}{\pi \delta^2 h} \sum_i \frac{\theta_i^{*(i^k)} - \theta_i^{*(k)}}{\xi_{(i^k)(k)}} n_i^{i^k(k)} V_{(i^k)} \right)^2 \right] \\ & \left. + 2 \frac{h^4}{80} \left(\frac{2}{\pi \delta^2 h} \right)^2 \sum_i \frac{\theta_i^{i^k} - \theta_i^{(k)}}{\xi_{(i^k)(k)}} n_i^{i^k(k)} V_{(i^k)} \sum_i \frac{\theta_j^{*(i^k)} - \theta_j^{*(k)}}{\xi_{(i^k)(k)}} n_j^{i^k(k)} V_{(i^k)} \right] \end{aligned} \right\} \quad (A111)
\end{aligned}$$

The PD SED for material point j can be obtained by replacing the index k with j .

A2.6 FGM Higher Order Deformable Plate

As derived in Chapter 5.6, the SED function for FGM higher order plate can be written as

$$\begin{aligned}
W_{\text{cov}} = & \frac{1}{h} \left\{ \int_{-\frac{h}{2}}^{\frac{h}{2}} \frac{G}{2} dz \left[\frac{\partial \bar{u}_i}{\partial x_j} \frac{\partial \bar{u}_i}{\partial x_j} + \frac{\partial \bar{u}_i}{\partial x_j} \frac{\partial \bar{u}_j}{\partial x_i} + \frac{\partial \bar{u}_i}{\partial x_i} \frac{\partial \bar{u}_j}{\partial x_j} + \left(\theta_i + \frac{\partial \bar{w}}{\partial x_i} \right) \left(\theta_i + \frac{\partial \bar{w}}{\partial x_i} \right) + 2\theta_z^2 \right] \right. \\
& + \int_{-\frac{h}{2}}^{\frac{h}{2}} \frac{Gz}{2} dz \left[\frac{\partial \bar{u}_i}{\partial x_j} \frac{\partial \theta_i}{\partial x_j} + \frac{\partial \bar{u}_i}{\partial x_j} \frac{\partial \theta_j}{\partial x_i} + \frac{\partial \bar{u}_i}{\partial x_i} \frac{\partial \theta_j}{\partial x_j} + \left(\theta_i + \frac{\partial \bar{w}}{\partial x_i} \right) \left(2u_i^* + \frac{\partial \theta_z}{\partial x_i} \right) + 4\theta_z w^* \right] \\
& + \int_{-\frac{h}{2}}^{\frac{h}{2}} \frac{G}{2} z^2 dz \left[\frac{\partial \theta_i}{\partial x_j} \frac{\partial \theta_i}{\partial x_j} + \frac{\partial \theta_i}{\partial x_j} \frac{\partial \theta_j}{\partial x_i} + \frac{\partial \theta_i}{\partial x_i} \frac{\partial \theta_j}{\partial x_j} + 2 \left(\frac{\partial \bar{u}_i}{\partial x_j} \frac{\partial u_i^*}{\partial x_j} + \frac{\partial \bar{u}_i}{\partial x_j} \frac{\partial u_j^*}{\partial x_i} + \frac{\partial \bar{u}_i}{\partial x_i} \frac{\partial u_j^*}{\partial x_j} \right) \right. \\
& \left. + \left(2u_i^* + \frac{\partial \theta_z}{\partial x_i} \right) \left(2u_i^* + \frac{\partial \theta_z}{\partial x_i} \right) + 2 \left(\theta_i + \frac{\partial \bar{w}}{\partial x_i} \right) \left(3\theta_i^* + \frac{\partial w^*}{\partial x_i} \right) + 8(w^*)^2 \right] \\
& + \int_{-\frac{h}{2}}^{\frac{h}{2}} \frac{Gz^3}{2} dz \left[\left(\frac{\partial \bar{u}_i}{\partial x_j} \frac{\partial \theta_i^*}{\partial x_j} + \frac{\partial \bar{u}_i}{\partial x_j} \frac{\partial \theta_j^*}{\partial x_i} + \frac{\partial \bar{u}_i}{\partial x_i} \frac{\partial \theta_j^*}{\partial x_j} \right) + \left(\frac{\partial \theta_i}{\partial x_j} \frac{\partial u_i^*}{\partial x_j} + \frac{\partial \theta_i}{\partial x_j} \frac{\partial u_j^*}{\partial x_i} + \frac{\partial \theta_i}{\partial x_i} \frac{\partial u_j^*}{\partial x_j} \right) \right. \\
& \left. + \left(2u_i^* + \frac{\partial \theta_z}{\partial x_i} \right) \left(3\theta_i^* + \frac{\partial w^*}{\partial x_i} \right) \right] \\
& + \int_{-\frac{h}{2}}^{\frac{h}{2}} \frac{G}{2} z^4 dz \left[\left(\frac{\partial u_i^*}{\partial x_j} \frac{\partial u_i^*}{\partial x_j} + \frac{\partial u_i^*}{\partial x_j} \frac{\partial u_j^*}{\partial x_i} + \frac{\partial u_i^*}{\partial x_i} \frac{\partial u_j^*}{\partial x_j} \right) + 2 \left(\frac{\partial \theta_i}{\partial x_j} \frac{\partial \theta_i^*}{\partial x_j} + \frac{\partial \theta_i}{\partial x_j} \frac{\partial \theta_j^*}{\partial x_i} + \frac{\partial \theta_i}{\partial x_i} \frac{\partial \theta_j^*}{\partial x_j} \right) \right. \\
& \left. + \left(3\theta_i^* + \frac{\partial w^*}{\partial x_i} \right) \left(3\theta_i^* + \frac{\partial w^*}{\partial x_i} \right) \right] \\
& + \int_{-\frac{h}{2}}^{\frac{h}{2}} \frac{Gz^5}{2} dz \left(\frac{\partial u_i^*}{\partial x_j} \frac{\partial \theta_i^*}{\partial x_j} + \frac{\partial u_i^*}{\partial x_j} \frac{\partial \theta_j^*}{\partial x_i} + \frac{\partial u_i^*}{\partial x_i} \frac{\partial \theta_j^*}{\partial x_j} \right) \\
& + \int_{-\frac{h}{2}}^{\frac{h}{2}} \frac{G}{2} z^6 dz \left(\frac{\partial \theta_i^*}{\partial x_j} \frac{\partial \theta_i^*}{\partial x_j} + \frac{\partial \theta_i^*}{\partial x_j} \frac{\partial \theta_j^*}{\partial x_i} + \frac{\partial \theta_i^*}{\partial x_i} \frac{\partial \theta_j^*}{\partial x_j} \right) \\
& + \frac{1}{h} \left\{ \int_{-\frac{h}{2}}^{\frac{h}{2}} \frac{G\nu}{1-2\nu} dz \left(2 \frac{\partial \bar{u}_i}{\partial x_i} \theta_z + \theta_z^2 \right) + \int_{-\frac{h}{2}}^{\frac{h}{2}} \frac{2G\nu z}{1-2\nu} dz \left(2 \frac{\partial \bar{u}_i}{\partial x_i} w^* + \frac{\partial \theta_i}{\partial x_i} \theta_z + 2\theta_z w^* \right) \right. \\
& + \int_{-\frac{h}{2}}^{\frac{h}{2}} \frac{2G\nu z^2}{1-2\nu} dz \left[2 \frac{\partial \theta_i}{\partial x_i} w^* + \frac{\partial u_i^*}{\partial x_i} \theta_z + 2(w^*)^2 \right] \\
& + \int_{-\frac{h}{2}}^{\frac{h}{2}} \frac{2G\nu z^3}{1-2\nu} dz \left(2 \frac{\partial u_i^*}{\partial x_i} w^* + \frac{\partial u_i^*}{\partial x_i} \theta_z \right) + \int_{-\frac{h}{2}}^{\frac{h}{2}} \frac{4G\nu z^4}{1-2\nu} dz \frac{\partial \theta_i^*}{\partial x_i} w^* \\
& + \frac{1}{h} \left\{ \int_{-\frac{h}{2}}^{\frac{h}{2}} \frac{G(4\nu-1)}{2(1-2\nu)} dz \left(\frac{\partial \bar{u}_i}{\partial x_i} \right)^2 + \int_{-\frac{h}{2}}^{\frac{h}{2}} \frac{G(4\nu-1)}{1-2\nu} z dz \frac{\partial \bar{u}_i}{\partial x_i} \frac{\partial \theta_j}{\partial x_j} \right. \\
& + \int_{-\frac{h}{2}}^{\frac{h}{2}} \frac{G(4\nu-1)}{2(1-2\nu)} z^2 dz \left[\left(\frac{\partial \theta_i}{\partial x_i} \right)^2 + 2 \frac{\partial \bar{u}_i}{\partial x_i} \frac{\partial u_j^*}{\partial x_j} \right] + \int_{-\frac{h}{2}}^{\frac{h}{2}} \frac{G(4\nu-1)}{1-2\nu} z^3 dz \left(\frac{\partial \bar{u}_i}{\partial x_i} \frac{\partial \theta_j^*}{\partial x_j} + \frac{\partial \theta_i}{\partial x_i} \frac{\partial u_j^*}{\partial x_j} \right) \\
& + \int_{-\frac{h}{2}}^{\frac{h}{2}} \frac{G(4\nu-1)}{2(1-2\nu)} z^4 dz \left[\left(\frac{\partial u_i^*}{\partial x_i} \right)^2 + 2 \frac{\partial \theta_i}{\partial x_i} \frac{\partial \theta_j^*}{\partial x_j} \right] \\
& + \int_{-\frac{h}{2}}^{\frac{h}{2}} \frac{G(4\nu-1)}{1-2\nu} z^5 dz \frac{\partial u_i^*}{\partial x_i} \frac{\partial \theta_j^*}{\partial x_j} + \int_{-\frac{h}{2}}^{\frac{h}{2}} \frac{G(4\nu-1)}{2(1-2\nu)} z^6 dz \left(\frac{\partial \theta_i^*}{\partial x_i} \right)^2 \\
& \left. \right\} \\
\end{aligned} \tag{A112}$$

Referring to the previous derivative process, the local terms in Eq. (A112) can be transformed into non-local form as

$$\begin{aligned}
& \frac{\partial u_i^{(k)}}{\partial x_j} \frac{\partial u_i^{(k)}}{\partial x_j} + \frac{\partial u_i^{(k)}}{\partial x_i} \frac{\partial u_j^{(k)}}{\partial x_j} + \frac{\partial u_i^{(k)}}{\partial x_j} \frac{\partial u_j^{(k)}}{\partial x_i} + \left(\theta_i^{(k)} + \frac{\partial w_{(k)}}{\partial x_i} \right) \left(\theta_i^{(k)} + \frac{\partial w_{(k)}}{\partial x_i} \right) + 2(\theta_z^{(k)})^2 \\
&= \frac{12}{\pi \delta^3 h} \sum_i \frac{(u_i^{(k)} - u_i^{(k)}) (u_j^{(k)} - u_j^{(k)})}{\xi_{(i^k)(k)}} n_i^{(i^k)(k)} n_j^{(j^k)(k)} V_{(i^k)} \\
&+ \frac{3}{\pi \delta^3 h} \sum_i \left\{ \frac{1}{\xi_{(i^k)(k)}} \left[w_{(i^k)} - w_{(k)} + \frac{\theta_i^{(i^k)} + \theta_i^{(k)}}{2} \xi_{(i^k)(k)} n_i^{(i^k)(k)} \right]^2 + \xi_{(i^k)(k)} \left(\frac{\theta_z^{(i^k)} + \theta_z^{(k)}}{2} \right)^2 \right\} V_{(i^k)} \\
& \frac{\partial u_i^{(k)}}{\partial x_j} \frac{\partial \theta_j^{(k)}}{\partial x_j} + \frac{\partial u_i^{(k)}}{\partial x_j} \frac{\partial \theta_j^{(k)}}{\partial x_i} + \frac{\partial u_i^{(k)}}{\partial x_i} \frac{\partial \theta_j^{(k)}}{\partial x_j} + \left(\theta_i^{(k)} + \frac{\partial w_{(k)}}{\partial x_i} \right) \left(2u_i^{*(k)} + \frac{\partial \theta_z^{(k)}}{\partial x_i} \right) + 4\theta_z^{(k)} w_{(k)}^* \\
&= \frac{12}{\pi \delta^3 h} \sum_i \frac{(u_i^{(i^k)} - u_i^{(k)}) (\theta_j^{(i^k)} - \theta_j^{(k)})}{\xi_{(i^k)(k)}} n_i^{(i^k)(k)} n_j^{(j^k)(k)} V_{(i^k)} \\
&+ \frac{3}{\pi \delta^3 h} \sum_i \left[\left(w_{(i^k)} - w_{(k)} + \frac{\theta_i^{(i^k)} + \theta_i^{(k)}}{2} \xi_{(i^k)(k)} n_i^{(i^k)(k)} \right) \left(\frac{\theta_z^{(i^k)} - \theta_z^{(k)}}{\xi_{(i^k)(k)}} + (u_i^{*(i^k)} + u_i^{*(k)}) n_i^{(i^k)(k)} \right) \right. \\
&\quad \left. + \frac{(\theta_z^{(i^k)} + \theta_z^{(k)}) (w_{(i^k)}^* + w_{(k)}^*)}{2} \xi_{(i^k)(k)} \right] V_{(i^k)} \\
& \frac{\partial \theta_i^{(k)}}{\partial x_j} \frac{\partial \theta_i^{(k)}}{\partial x_j} + \frac{\partial \theta_i^{(k)}}{\partial x_j} \frac{\partial \theta_j^{(k)}}{\partial x_i} + \frac{\partial \theta_i^{(k)}}{\partial x_i} \frac{\partial \theta_j^{(k)}}{\partial x_j} + 2 \left(\frac{\partial u_i^{(k)}}{\partial x_j} \frac{\partial u_i^{*(k)}}{\partial x_j} + \frac{\partial u_i^{(k)}}{\partial x_j} \frac{\partial u_j^{*(k)}}{\partial x_i} + \frac{\partial u_i^{(k)}}{\partial x_i} \frac{\partial u_j^{*(k)}}{\partial x_j} \right) \\
&+ \left(2u_i^{*(k)} + \frac{\partial \theta_z^{(k)}}{\partial x_i} \right) \left(2u_i^{*(k)} + \frac{\partial \theta_z^{(k)}}{\partial x_i} \right) + 2 \left(\theta_i^{(k)} + \frac{\partial w_{(k)}}{\partial x_i} \right) \left(3\theta_i^{*(k)} + \frac{\partial w_{(k)}}{\partial x_i} \right) + 8(w_{(k)}^*)^2 \\
&= \frac{12}{\pi \delta^3 h} \sum_i \frac{\left[(\theta_i^{(i^k)} - \theta_i^{(k)}) n_i^{(i^k)(k)} \right]^2 + 2(u_i^{*(i^k)} - u_i^{*(k)}) (u_j^{*(i^k)} - u_j^{*(k)}) n_i^{(i^k)(k)} n_j^{(j^k)(k)}}{\xi_{(i^k)(k)}} V_{(i^k)} \\
&+ \frac{3}{\pi \delta^3 h} \sum_i \left\{ \frac{\left[\frac{\theta_z^{(i^k)} - \theta_z^{(k)}}{\xi_{(i^k)(k)}} + (u_i^{*(i^k)} + u_i^{*(k)}) \xi_{(i^k)(k)} n_i^{(i^k)(k)} \right]^2}{\xi_{(i^k)(k)}} + (w_{(i^k)}^* + w_{(k)}^*)^2 \xi_{(i^k)(k)} \right. \\
&\quad \left. + 2 \left(\frac{w_{(i^k)} - w_{(k)}}{\xi_{(i^k)(k)}} + \frac{\theta_i^{(i^k)} + \theta_i^{(k)}}{2} n_i^{(i^k)(k)} \right) \left(w_{(i^k)}^* - w_{(k)}^* + 3 \frac{\theta_i^{*(i^k)} + \theta_i^{*(k)}}{2} \xi_{(i^k)(k)} n_i^{(i^k)(k)} \right) \right\} V_{(i^k)} \\
& \frac{\partial u_i^{(k)}}{\partial x_j} \frac{\partial \theta_i^{*(k)}}{\partial x_j} + \frac{\partial u_i^{(k)}}{\partial x_i} \frac{\partial \theta_i^{*(k)}}{\partial x_j} + \frac{\partial u_i^{(k)}}{\partial x_i} \frac{\partial \theta_j^{*(k)}}{\partial x_j} + \frac{\partial \theta_i^{(k)}}{\partial x_j} \frac{\partial u_i^{*(k)}}{\partial x_j} + \frac{\partial \theta_j^{(k)}}{\partial x_i} \frac{\partial u_i^{*(k)}}{\partial x_j} + \frac{\partial \theta_i^{(k)}}{\partial x_i} \frac{\partial u_j^{*(k)}}{\partial x_j} \\
&+ \left(2u_i^* + \frac{\partial \theta_z}{\partial x_i} \right) \left(3\theta_i^* + \frac{\partial w^*}{\partial x_i} \right) \\
&= \frac{12}{\pi \delta^3 h} \sum_i \frac{\left[(u_i^{(i^k)} - u_i^{(k)}) (\theta_j^{*(i^k)} - \theta_j^{*(k)}) + (\theta_i^{(i^k)} - \theta_i^{(k)}) (u_j^{*(i^k)} - u_j^{*(k)}) \right] n_i^{(i^k)(k)} n_j^{(j^k)(k)}}{\xi_{(i^k)(k)}} V_{(i^k)} \\
&+ \frac{3}{\pi \delta^3 h} \sum_i \left[w_{(i^k)}^* - w_{(k)}^* + \frac{3}{2} (\theta_i^{*(i^k)} + \theta_i^{*(k)}) \xi_{(i^k)(k)} n_i^{(i^k)(k)} \right] \left[\frac{\theta_z^{(i^k)} - \theta_z^{(k)}}{\xi_{(i^k)(k)}} + (u_j^{*(i^k)} + u_j^{*(k)}) n_j^{(j^k)(k)} \right] V_{(i^k)}
\end{aligned}$$

$$\begin{aligned}
& \frac{\partial u_i^{*(k)}}{\partial x_j} \frac{\partial u_i^{*(k)}}{\partial x_j} + \frac{\partial u_i^{*(k)}}{\partial x_j} \frac{\partial u_j^{*(k)}}{\partial x_i} + \frac{\partial u_i^{*(k)}}{\partial x_i} \frac{\partial u_j^{*(k)}}{\partial x_j} + \\
& 2 \left(\frac{\partial \theta_i^{(k)}}{\partial x_j} \frac{\partial \theta_i^{*(k)}}{\partial x_j} + \frac{\partial \theta_j^{(k)}}{\partial x_i} \frac{\partial \theta_i^{*(k)}}{\partial x_j} + \frac{\partial \theta_i^{(k)}}{\partial x_i} \frac{\partial \theta_j^{*(k)}}{\partial x_j} \right) + \left(3\theta_i^{*(k)} + \frac{\partial \dot{w}_i^{(k)}}{\partial x_i} \right) \left(3\theta_i^{*(k)} + \frac{\partial \dot{w}_i^{(k)}}{\partial x_i} \right) \\
& = \frac{12}{\pi \delta^3 h} \sum_i \frac{\left[\left(u_i^{(i^k)} - u_i^{*(k)} \right) n_i^{(i^k)(k)} \right]^2 + 2 \left(\theta_i^{(i^k)} - \theta_i^{*(k)} \right) \left(\theta_j^{*(i^k)} - \theta_j^{*(k)} \right) n_i^{(i^k)(k)} n_j^{(i^k)(k)}}{\xi_{(i^k)(k)}} V_{(i^k)} \\
& + \frac{3}{\pi \delta^3 h} \sum_i \frac{\left(\dot{w}_i^{(i^k)} - \dot{w}_i^{(k)} + \frac{3}{2} \left(\theta_i^{*(i^k)} + \theta_i^{*(k)} \right) \xi_{(i^k)(k)} n_i^{(i^k)(k)} \right)^2}{\xi_{(i^k)(k)}} V_{(i^k)} \\
& \frac{\partial u_i^{*(k)}}{\partial x_j} \frac{\partial \theta_i^{*(k)}}{\partial x_j} + \frac{\partial u_j^{*(k)}}{\partial x_i} \frac{\partial \theta_i^{*(k)}}{\partial x_j} + \frac{\partial u_i^{*(k)}}{\partial x_i} \frac{\partial \theta_j^{*(k)}}{\partial x_j} \\
& = \frac{12}{\pi \delta^3 h} \sum_i \frac{\left(u_i^{*(i^k)} - u_i^{*(k)} \right) \left(\theta_j^{*(i^k)} - \theta_j^{*(k)} \right) n_i^{(i^k)(k)} n_j^{(i^k)(k)}}{\xi_{(i^k)(k)}} V_{(i^k)} \\
& \frac{\partial \theta_i^{*(k)}}{\partial x_j} \frac{\partial \theta_i^{*(k)}}{\partial x_j} + \frac{\partial \theta_i^{*(k)}}{\partial x_j} \frac{\partial \theta_j^{*(k)}}{\partial x_i} + \frac{\partial \theta_i^{*(k)}}{\partial x_i} \frac{\partial \theta_j^{*(k)}}{\partial x_j} = \frac{12}{\pi \delta^3 h} \sum_i \frac{\left[\left(\theta_i^{*(i^k)} - \theta_i^{*(k)} \right) n_i^{(i^k)(k)} \right]^2}{\xi_{(i^k)(k)}} V_{(i^k)} \\
& 2 \frac{\partial u_i^{(k)}}{\partial x_i} \theta_z^{(k)} + \left(\theta_z^{(k)} \right)^2 = \frac{3}{\pi \delta^3 h} \sum_i \left[\frac{\left(\theta_z^{(i^k)} + \theta_z^{(k)} \right) \left(u_i^{(i^k)} - u_i^{(k)} \right) n_i^{(i^k)(k)}}{+ \frac{1}{2} \left(\frac{\theta_z^{(i^k)} + \theta_z^{(k)}}{2} \right)^2 \xi_{(i^k)(k)}} \right] V_{(i^k)} \\
& 2 \frac{\partial u_i^{(k)}}{\partial x_i} \dot{w}_i^{(k)} + \frac{\partial \theta_i^{(k)}}{\partial x_i} \theta_z^{(k)} + 2 \theta_z^{(k)} \dot{w}_i^{(k)} \\
& = \frac{3}{\pi \delta^3 h} \sum_i \left[\frac{\left(\dot{w}_i^{(i^k)} + \dot{w}_i^{(k)} \right) \left(u_i^{(i^k)} - u_i^{(k)} \right) n_i^{(i^k)(k)} + \frac{\theta_z^{(i^k)} + \theta_z^{(k)}}{2} \left(\theta_i^{(i^k)} - \theta_i^{(k)} \right) n_i^{(i^k)(k)}}{+ \frac{\theta_z^{(i^k)} + \theta_z^{(k)}}{2} \frac{\dot{w}_i^{(i^k)} + \dot{w}_i^{(k)}}{2} \xi_{(i^k)(k)}} \right] V_{(i^k)} \\
& 2 \frac{\partial \theta_i^{(k)}}{\partial x_i} \dot{w}_i^{(k)} + \frac{\partial u_i^{*(k)}}{\partial x_i} \theta_z^{(k)} + 2 \left(\dot{w}_i^{(k)} \right)^2 \\
& = \frac{3}{\pi \delta^3 h} \sum_i \left[\frac{\left(\dot{w}_i^{(i^k)} + \dot{w}_i^{(k)} \right) \left(\theta_i^{(i^k)} - \theta_i^{(k)} \right) n_i^{(i^k)(k)} + \frac{\theta_z^{(i^k)} + \theta_z^{(k)}}{2} \left(u_i^{*(i^k)} - u_i^{*(k)} \right) n_i^{(i^k)(k)}}{\left(\frac{\dot{w}_i^{(i^k)} + \dot{w}_i^{(k)}}{2} \right)^2 \xi_{(i^k)(k)}} \right] V_{(i^k)} \\
& 2 \frac{\partial u_i^{*(k)}}{\partial x_i} \dot{w}_i^{(k)} + \frac{\partial \theta_i^{*(k)}}{\partial x_i} \theta_z^{(k)} = \frac{3}{\pi \delta^3 h} \sum_i \left[\frac{\left(\dot{w}_i^{(i^k)} + \dot{w}_i^{(k)} \right) \left(u_i^{*(i^k)} - u_i^{*(k)} \right) n_i^{(i^k)(k)} + \frac{\theta_z^{(i^k)} + \theta_z^{(k)}}{2} \left(\theta_i^{*(i^k)} - \theta_i^{*(k)} \right) n_i^{(i^k)(k)}}{\xi_{(i^k)(k)}} \right] V_{(i^k)} \\
& \frac{\partial \theta_i^{*(k)}}{\partial x_i} \dot{w}_i^{(k)} = \frac{3}{\pi \delta^3 h} \sum_i \frac{\dot{w}_i^{(i^k)} + \dot{w}_i^{(k)}}{2} \left(\theta_i^{*(i^k)} - \theta_i^{*(k)} \right) n_i^{(i^k)(k)} V_{(i^k)}
\end{aligned}$$

$$\frac{\partial \theta_i^{(k)}}{\partial x_i} = \frac{2}{\pi \delta^2 h} \sum_i \frac{\theta_i^{(i^k)} - \theta_i^{(k)}}{\xi_{(i^k)}^{(k)}} n_i^{(i^k)(k)} V_{(i^k)}$$

$$\frac{\partial u_i^{*(k)}}{\partial x_i} = \frac{2}{\pi \delta^2 h} \sum_i \frac{u_i^{*(i^k)} - u_i^{*(k)}}{\xi_{(i^k)}^{(k)}} n_i^{(i^k)(k)} V_{(i^k)}$$

$$\frac{\partial \theta_i^{*(k)}}{\partial x_i} = \frac{2}{\pi \delta^2 h} \sum_i \frac{\theta_i^{*(i^k)} - \theta_i^{*(k)}}{\xi_{(i^k)}^{(k)}} n_i^{(i^k)(k)} V_{(i^k)}$$

Plugging the above expressions into Eq. (A112) arises the PD SED for material point k as

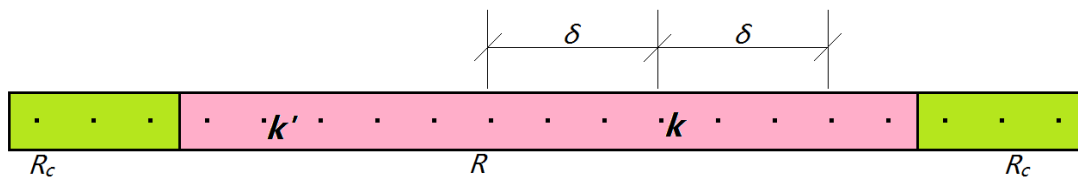
$$W_D^{(k)} = \frac{3}{\pi \delta^3 h^2} \left\{ \begin{aligned} & \int_{-\frac{h}{2}}^{\frac{h}{2}} \frac{G}{2} dz \left\{ 4 \sum_i \frac{[(u_i^{(i^k)} - u_i^{(k)}) n_i^{(i^k)(k)}]^2}{\xi_{(i^k)}^{(k)}} V_{(i^k)} + \sum_i \left[\frac{(w_{(i^k)} - w_k + \frac{\theta_i^{(i^k)} + \theta_i^{(k)}}{2} \xi_{(i^k)}^{(k)} n_i^{(i^k)(k)})^2}{\xi_{(i^k)}^{(k)}} + \left(\frac{\theta_z^{(i^k)} + \theta_z^{(k)}}{2} \right)^2 \xi_{(i^k)}^{(k)} \right] V_{(i^k)} \right\} \\ & + \int_{-\frac{h}{2}}^{\frac{h}{2}} G z dz \left\{ 4 \sum_i \frac{(u_i^{(i^k)} - u_i^{(k)}) (\theta_j^{(i^k)} - \theta_j^{(k)}) n_i^{(i^k)(k)} n_j^{(i^k)(k)}}{\xi_{(i^k)}^{(k)}} V_{(i^k)} \right. \\ & \left. + \sum_i \left[\frac{(w_{(i^k)} - w_k + \frac{\theta_i^{(i^k)} + \theta_i^{(k)}}{2} \xi_{(i^k)}^{(k)} n_i^{(i^k)(k)}) \left(\frac{\theta_z^{(i^k)} - \theta_z^{(k)}}{\xi_{(i^k)}^{(k)}} + (u_i^{(i^k)} + u_i^{*(k)}) n_i^{(i^k)(k)} \right)}{2} \right. \right. \\ & \left. \left. + \frac{(\theta_z^{(i^k)} + \theta_z^{(k)}) (w_{(i^k)} + \dot{w}_k)}{\xi_{(i^k)}^{(k)}} \right] V_{(i^k)} \right\} \\ & + \int_{-\frac{h}{2}}^{\frac{h}{2}} \frac{G}{2} z^2 dz \left\{ 4 \sum_i \frac{[(\theta_i^{(i^k)} - \theta_i^{(k)}) n_i^{(i^k)(k)}]^2 + 2(u_i^{(i^k)} - u_i^{(k)}) (u_j^{(i^k)} - u_j^{(k)}) n_i^{(i^k)(k)} n_j^{(i^k)(k)}}{\xi_{(i^k)}^{(k)}} V_{(i^k)} \right. \\ & \left. + \sum_i \left[\frac{1}{\xi_{(i^k)}^{(k)}} \left(\frac{\theta_z^{(i^k)} - \theta_z^{(k)}}{\xi_{(i^k)}^{(k)}} + (u_i^{(i^k)} + u_i^{*(k)}) \xi_{(i^k)}^{(k)} n_i^{(i^k)(k)} \right)^2 + (w_{(i^k)} + \dot{w}_k)^2 \xi_{(i^k)}^{(k)} \right. \right. \\ & \left. \left. + 2 \left(\frac{w_{(i^k)} - w_k + \frac{\theta_i^{(i^k)} + \theta_i^{(k)}}{2} \xi_{(i^k)}^{(k)} n_i^{(i^k)(k)} \right) \left(\dot{w}_{(i^k)} - \dot{w}_k + 3 \frac{\theta_i^{(i^k)} + \theta_i^{(k)}}{2} \xi_{(i^k)}^{(k)} n_i^{(i^k)(k)} \right) \right] V_{(i^k)} \right\} \\ & + \int_{-\frac{h}{2}}^{\frac{h}{2}} G z^3 dz \left\{ 4 \sum_i \frac{[(u_i^{(i^k)} - u_i^{(k)}) (\theta_j^{(i^k)} - \theta_j^{(k)}) + (\theta_i^{(i^k)} - \theta_i^{(k)}) (u_j^{(i^k)} - u_j^{(k)})] n_i^{(i^k)(k)} n_j^{(i^k)(k)}}{\xi_{(i^k)}^{(k)}} V_{(i^k)} \right. \\ & \left. + \sum_i \left[\dot{w}_{(i^k)} - \dot{w}_k + \frac{3}{2} (\theta_i^{(i^k)} + \theta_i^{(k)}) \xi_{(i^k)}^{(k)} n_i^{(i^k)(k)} \right] \left[\frac{\theta_z^{(i^k)} - \theta_z^{(k)}}{\xi_{(i^k)}^{(k)}} + (u_j^{(i^k)} + u_j^{*(k)}) n_j^{(i^k)(k)} \right] V_{(i^k)} \right\} \\ & + \int_{-\frac{h}{2}}^{\frac{h}{2}} \frac{G}{2} z^4 dz \left\{ 4 \sum_i \frac{[(u_i^{(i^k)} - u_i^{(k)}) n_i^{(i^k)(k)}]^2 + 2(\theta_i^{(i^k)} - \theta_i^{(k)}) (\theta_j^{(i^k)} - \theta_j^{(k)}) n_i^{(i^k)(k)} n_j^{(i^k)(k)}}{\xi_{(i^k)}^{(k)}} V_{(i^k)} \right. \\ & \left. + \sum_i \left[\frac{(w_{(i^k)} - \dot{w}_k + \frac{3}{2} (\theta_i^{(i^k)} + \theta_i^{(k)}) \xi_{(i^k)}^{(k)} n_i^{(i^k)(k)})^2}{\xi_{(i^k)}^{(k)}} \right] V_{(i^k)} \right\} \\ & + 4 \int_{-\frac{h}{2}}^{\frac{h}{2}} G z^5 dz \sum_i \frac{(u_i^{(i^k)} - u_i^{(k)}) (\theta_j^{(i^k)} - \theta_j^{(k)}) n_i^{(i^k)(k)} n_j^{(i^k)(k)}}{\xi_{(i^k)}^{(k)}} V_{(i^k)} + 4 \int_{-\frac{h}{2}}^{\frac{h}{2}} \frac{G}{2} z^5 dz \sum_i \frac{[(\theta_i^{(i^k)} - \theta_i^{(k)}) n_i^{(i^k)(k)}]^2}{\xi_{(i^k)}^{(k)}} V_{(i^k)} \end{aligned} \right\}$$

$$\begin{aligned}
& \left. \begin{aligned}
& \int_{-\frac{h}{2}}^{\frac{h}{2}} \frac{2G\nu}{1-2\nu} dz \sum_i \left[\left(\frac{\theta_z^{(i^*)} + \theta_z^{(k)}}{2} \right) (u_i^{(i^*)} - u_i^{(k)}) n_i^{(i^*)(k)} + \left(\frac{\theta_z^{(i^*)} + \theta_z^{(k)}}{4} \right)^2 \frac{\xi_{(i^*)(k)}}{\xi_{(i^*)(k)}} \right] V_{(i^*)} \\
& + \int_{-\frac{h}{2}}^{\frac{h}{2}} \frac{2G\nu z}{1-2\nu} dz \sum_i \left[(\dot{w}_{(i^*)} + \dot{w}_{(k)}) (u_i^{(i^*)} - u_i^{(k)}) n_i^{(i^*)(k)} + \frac{\theta_z^{(i^*)} + \theta_z^{(k)}}{2} \left((\theta_i^{(i^*)} - \theta_i^{(k)}) n_i^{(i^*)(k)} + \frac{\dot{w}_{(i^*)} + \dot{w}_{(k)}}{2} \frac{\xi_{(i^*)(k)}}{\xi_{(i^*)(k)}} \right) \right] V_{(i^*)} \\
& + \int_{-\frac{h}{2}}^{\frac{h}{2}} \frac{2G\nu z^2}{1-2\nu} dz \sum_i \left[(\dot{w}_{(i^*)} + \dot{w}_{(k)}) (\theta_i^{(i^*)} - \theta_i^{(k)}) n_i^{(i^*)(k)} + \frac{\theta_z^{(i^*)} + \theta_z^{(k)}}{2} (u_i^{(i^*)} - u_i^{(k)}) n_i^{(i^*)(k)} + \left(\frac{\dot{w}_{(i^*)} + \dot{w}_{(k)}}{2} \right)^2 \frac{\xi_{(i^*)(k)}}{\xi_{(i^*)(k)}} \right] V_{(i^*)} \\
& + \int_{-\frac{h}{2}}^{\frac{h}{2}} \frac{2G\nu z^3}{1-2\nu} dz \sum_i \left[(\dot{w}_{(i^*)} + \dot{w}_{(k)}) (u_i^{(i^*)} - u_i^{(k)}) n_i^{(i^*)(k)} + \frac{\theta_z^{(i^*)} + \theta_z^{(k)}}{2} (\theta_i^{(i^*)} - \theta_i^{(k)}) n_i^{(i^*)(k)} \right] V_{(i^*)} \\
& + \int_{-\frac{h}{2}}^{\frac{h}{2}} \frac{2G\nu z^4}{1-2\nu} dz \sum_i (\dot{w}_{(i^*)} + \dot{w}_{(k)}) (\theta_i^{(i^*)} - \theta_i^{(k)}) n_i^{(i^*)(k)} V_{(i^*)}
\end{aligned} \right\}
\end{aligned}$$

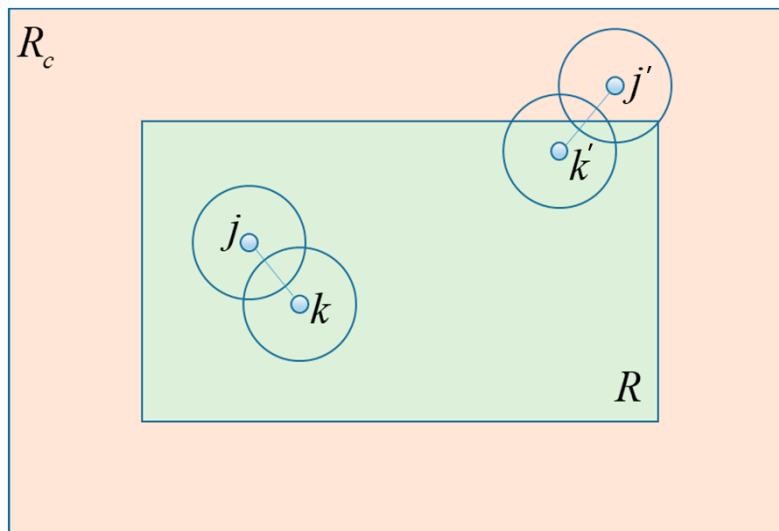
$$\begin{aligned}
& \left. \begin{aligned}
& \int_{-\frac{h}{2}}^{\frac{h}{2}} \frac{G}{2} \frac{4\nu - 1}{1 - 2\nu} dz \left(\sum_i \frac{u_i^{(i^*)} - u_i^{(k)}}{\xi_{(i^*)(k)}} n_i^{(i^*)(k)} V_{(i^*)} \right)^2 + \int_{-\frac{h}{2}}^{\frac{h}{2}} \frac{G}{2} \frac{4\nu - 1}{1 - 2\nu} z dz \sum_i \frac{u_i^{(i^*)} - u_i^{(k)}}{\xi_{(i^*)(k)}} n_i^{(i^*)(k)} V_{(i^*)} \sum_i \frac{\theta_j^{(i^*)} - \theta_j^{(k)}}{\xi_{(i^*)(k)}} n_j^{(i^*)(k)} V_{(i^*)} \\
& + \int_{-\frac{h}{2}}^{\frac{h}{2}} \frac{G}{2} \frac{4\nu - 1}{1 - 2\nu} z^2 dz \left[\left(\sum_i \frac{\theta_i^{(i^*)} - \theta_i^{(k)}}{\xi_{(i^*)(k)}} n_i^{(i^*)(k)} V_{(i^*)} \right)^2 + 2 \sum_i \frac{u_i^{(i^*)} - u_i^{(k)}}{\xi_{(i^*)(k)}} n_i^{(i^*)(k)} V_{(i^*)} \sum_i \frac{u_j^{(i^*)} - u_j^{(k)}}{\xi_{(i^*)(k)}} n_j^{(i^*)(k)} V_{(i^*)} \right] \\
& + \int_{-\frac{h}{2}}^{\frac{h}{2}} \frac{G}{2} \frac{4\nu - 1}{1 - 2\nu} z^3 dz \left[\sum_i \frac{u_i^{(i^*)} - u_i^{(k)}}{\xi_{(i^*)(k)}} n_i^{(i^*)(k)} V_{(i^*)} \sum_i \frac{\theta_j^{(i^*)} - \theta_j^{(k)}}{\xi_{(i^*)(k)}} n_j^{(i^*)(k)} V_{(i^*)} \right. \\
& \quad \left. + \sum_i \frac{\theta_i^{(i^*)} - \theta_i^{(k)}}{\xi_{(i^*)(k)}} n_i^{(i^*)(k)} V_{(i^*)} \sum_i \frac{u_j^{(i^*)} - u_j^{(k)}}{\xi_{(i^*)(k)}} n_j^{(i^*)(k)} V_{(i^*)} \right] \\
& + \int_{-\frac{h}{2}}^{\frac{h}{2}} \frac{G}{2} \frac{4\nu - 1}{1 - 2\nu} z^4 dz \left[\left(\sum_i \frac{u_i^{(i^*)} - u_i^{(k)}}{\xi_{(i^*)(k)}} n_i^{(i^*)(k)} V_{(i^*)} \right)^2 + 2 \sum_i \frac{\theta_i^{(i^*)} - \theta_i^{(k)}}{\xi_{(i^*)(k)}} n_i^{(i^*)(k)} V_{(i^*)} \sum_i \frac{\theta_j^{(i^*)} - \theta_j^{(k)}}{\xi_{(i^*)(k)}} n_j^{(i^*)(k)} V_{(i^*)} \right] \\
& + \int_{-\frac{h}{2}}^{\frac{h}{2}} \frac{G}{2} \frac{4\nu - 1}{1 - 2\nu} z^5 dz \sum_i \frac{u_i^{(i^*)} - u_i^{(k)}}{\xi_{(i^*)(k)}} n_i^{(i^*)(k)} V_{(i^*)} \sum_i \frac{\theta_j^{(i^*)} - \theta_j^{(k)}}{\xi_{(i^*)(k)}} n_j^{(i^*)(k)} V_{(i^*)} \\
& + \int_{-\frac{h}{2}}^{\frac{h}{2}} \frac{G}{2} \frac{4\nu - 1}{1 - 2\nu} z^6 dz \left(\sum_i \frac{\theta_i^{(i^*)} - \theta_i^{(k)}}{\xi_{(i^*)(k)}} n_i^{(i^*)(k)} V_{(i^*)} \right)^2
\end{aligned} \right\}$$

Appendix B Boundary Conditions for PD Beam and Plate Theories

The prerequisite of the derivation process of PD EoM is that the material point influence domain must be completely embedded in a material domain. For this reason, the PD EoM is valid only if the main material point, k , has intact horizon that is fully embedded in an actual material domain, R , as shown in Fig. B1. However, near the boundary points, k' , can have incomplete influence domains. Therefore, the supplemental equations valid for the fictitious boundary layer, R_c , outside the boundary of the actual material domain are necessary, as explained by Madenci and Oterkus. The length of this layer can be chosen as the size of the influence domain. The possible types of boundary conditions and their corrections are explained below for beams and plates from the PD point of view.



(a)



(b)

Figure B1 Introduction of fictitious boundary layers: (a) beam, (b) plate

B1 Boundary Conditions for PD Beams

B1.1 Timoshenko Beam

Clamped Boundary Condition

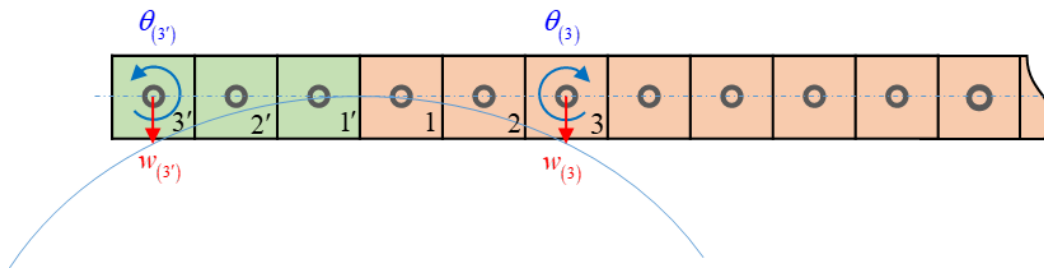


Figure B2 Application of clamped boundary conditions in PD theory

The clamped boundary condition for Timoshenko Beam may be achieved by enforcing mirror image of the transverse displacement field for the material points adjacent to the clamped end, and anti-symmetric image of rotational and axial displacements fields, as shown in Fig. (B2)

that

$$\begin{cases} w_{(i')} = w_{(i)} \\ w_{(1')} = w_{(1)} = 0 \quad \text{for } i = 1, 2, 3 \\ \theta_{(i')} = -\theta_{(i)} \end{cases} \quad (\text{B1})$$

Simply Supported Boundary Condition

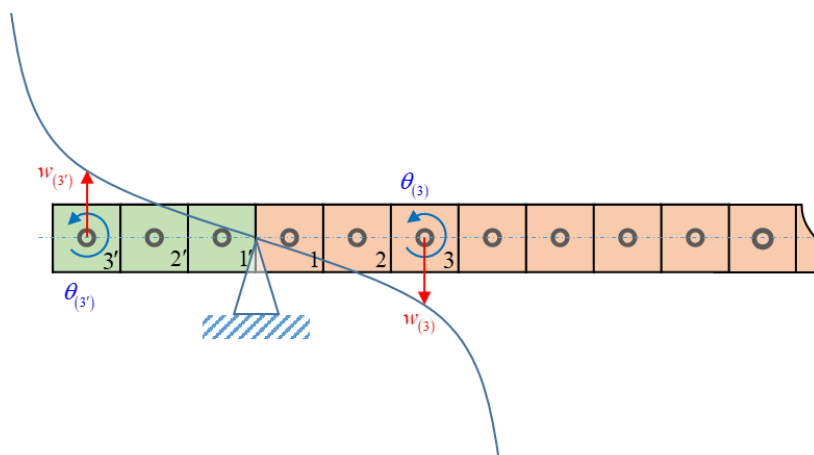


Figure B2 Application of simply supported boundary conditions in PD theory

The simply supported boundary condition may be satisfied by enforcing anti-symmetrical transverse displacement fields to the material points in the fictitious region as opposed to the actual displacement field, as shown in Fig. (B2). Thus, it is defined as

$$\begin{cases} w_{(i')} = -w_{(i)} \\ \theta_{(i')} = \theta_{(i)} \end{cases} \quad \text{for } i = 1, 2, 3 \quad (\text{B2})$$

B1.2 Higher Order Deformable Beam

Clamped boundary condition

To implement the clamped boundary condition, a fictitious boundary layer is created outside the actual material domain. The horizon size can be chosen as $\delta = 3\Delta x$ in which the discretization size is Δx . The clamped boundary condition constrains zero transverse displacement and zero rotation for the material point adjacent to the clamped end. In this study, this can be achieved by enforcing symmetrical displacement fields for w and w^* and anti-symmetrical displacement fields for θ and θ^* , respectively, to the material points in the fictitious region as opposed to the actual displacement field as

$$\begin{cases} w_{(i)} = w_{(i')} & w_{(i)}^* = w_{(i')}^* \\ w_{(1)} = w_{(1')} = w_{(1)}^* = w_{(1')}^* = 0 & i = 1, 2, 3 \\ \theta_{(i)} = -\theta_{(i')} & \theta_{(i)}^* = -\theta_{(i')}^* \end{cases} \quad (\text{B3})$$

Simply supported boundary condition

To implement the simply supported boundary condition, a fictitious layer is introduced outside the real material domain, whose size is again chosen to be equal to δ . From geometrical point of view, the simply supported boundary condition imposes zero transverse displacement and zero curvature for the material point adjacent to the constrained edge. In this study, this can be achieved by enforcing anti-symmetrical displacement fields for w and w^* and symmetrical displacement fields for θ and θ^* , respectively, to the material points in the fictitious region with respect to the actual displacement field as

$$\begin{cases} w_{(i)} = -w_{(i')} & w_{(i)}^* = -w_{(i')}^* \\ \theta_{(i)} = \theta_{(i')} & \theta_{(i)}^* = \theta_{(i')}^* \end{cases} \quad i=1,2,3 \quad (\text{B4})$$

B1.3 FGM Euler-Bernoulli Beam

Clamped Boundary Condition

According to Euler-Bernoulli Beam theory, the clamped boundary condition can be represented by constraining the transverse displacement and the rotation at the boundary. In PD framework, such boundary condition can be achieved by introducing a fictitious domain outside the boundary with a length equal to two times of the horizon size, δ so that all material points inside the actual solution domain have a complete horizon. In this study, the horizon size is chosen as $\delta = 3\Delta x$ where Δx is the distance between material points. Therefore, there are six additional material points inside the fictitious boundary region.

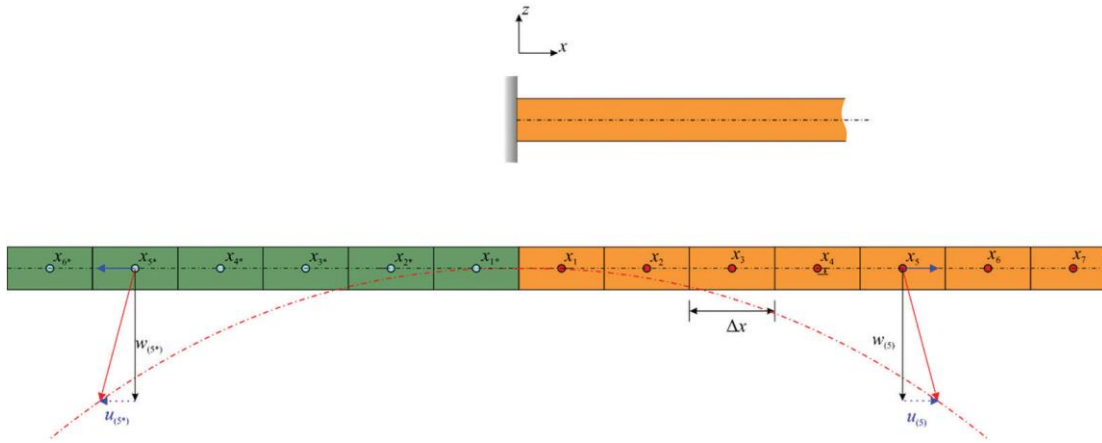


Figure B3: Application of clamped boundary condition

As shown in Fig. B3, clamped boundary conditions in PD framework can be achieved by imposing mirror images of the transverse displacements and anti-mirror axial displacements for the six material points in the actual and fictitious domains next to the boundary as

$$\begin{cases} w_{(i')} = w_{(i)} \\ w_{(i')} = w_{(1)} = 0 & i = 1, 2, \dots, 6 \\ u_{(i')} = -u_{(i)} \end{cases} \quad (\text{B5})$$

Simply Supported Boundary Condition

According to Euler-Bernoulli Beam theory, the simply supported boundary condition can be represented by constraining transverse displacement and curvature at the boundary.

In PD framework, this can be achieved by introducing a fictitious domain outside the boundary with a length equal to two times of the horizon size, δ . Moreover, as shown in Figs. B4, the transverse constraint condition can be satisfied by imposing anti-symmetrical transverse displacement fields to the six material points in the actual and fictitious domains next to the boundary which can be defined as

$$w_{(i^*)} = -w_{(i)} \quad i = 1, 2, \dots, 6 \quad (\text{B6})$$

However, for axial deformation, the application of simply supported boundary condition is different depending on the pinned support and roller support conditions.

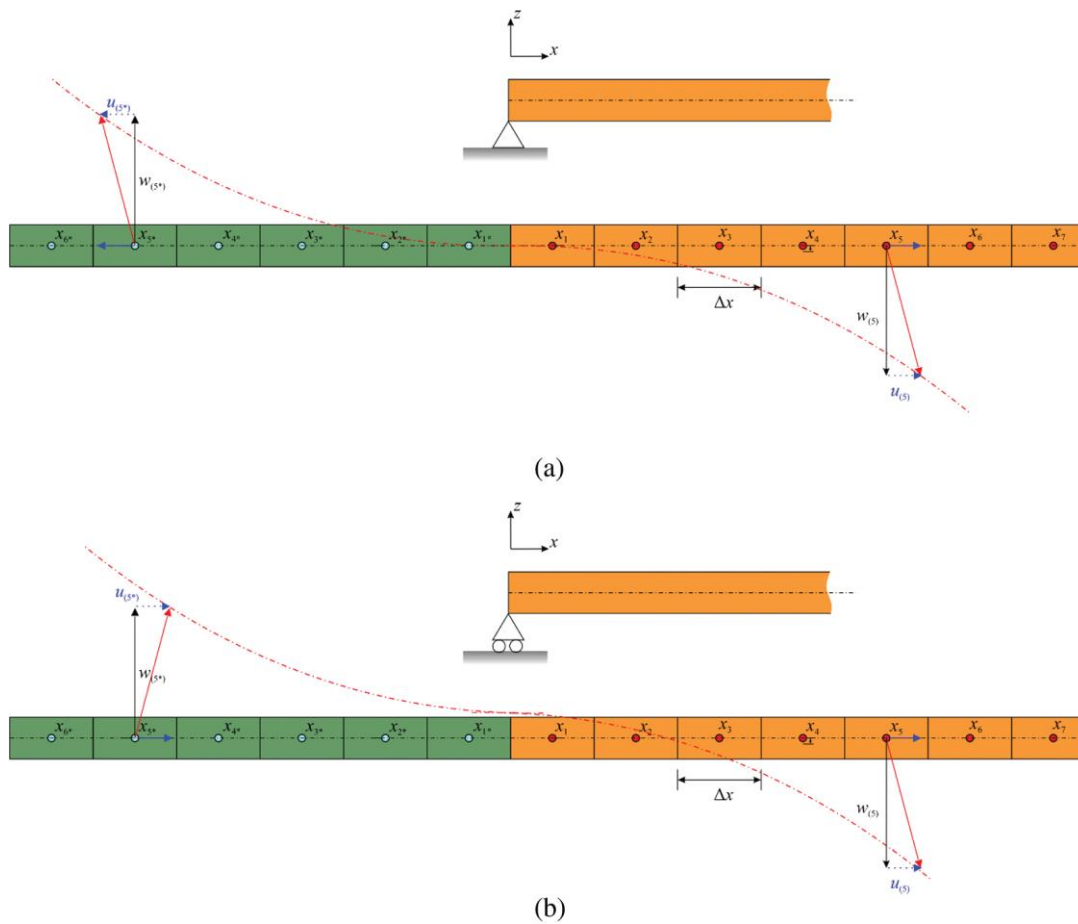


Figure B4 Application of simply supported boundary condition, (a) pinned support, (b) roller support

For pinned support condition, the axial deformations can be constrained by imposing anti-symmetrical displacement fields to the six material points in the actual and fictitious material domains next to the boundary, as shown in Fig. B4a, which can be defined as

$$u_{(i')} = -u_{(i)} \quad i = 1, 2, \dots, 6 \quad (\text{B7a})$$

On the other hand, the implementation of roller support boundary condition requires symmetrical displacement field adjacent to the boundary as (see Fig. B4b)

$$u_{(i')} = u_{(i)} \quad i = 1, 2, \dots, 6 \quad (\text{B7b})$$

B1.4 FGM Timoshenko Beam

Clamped boundary condition

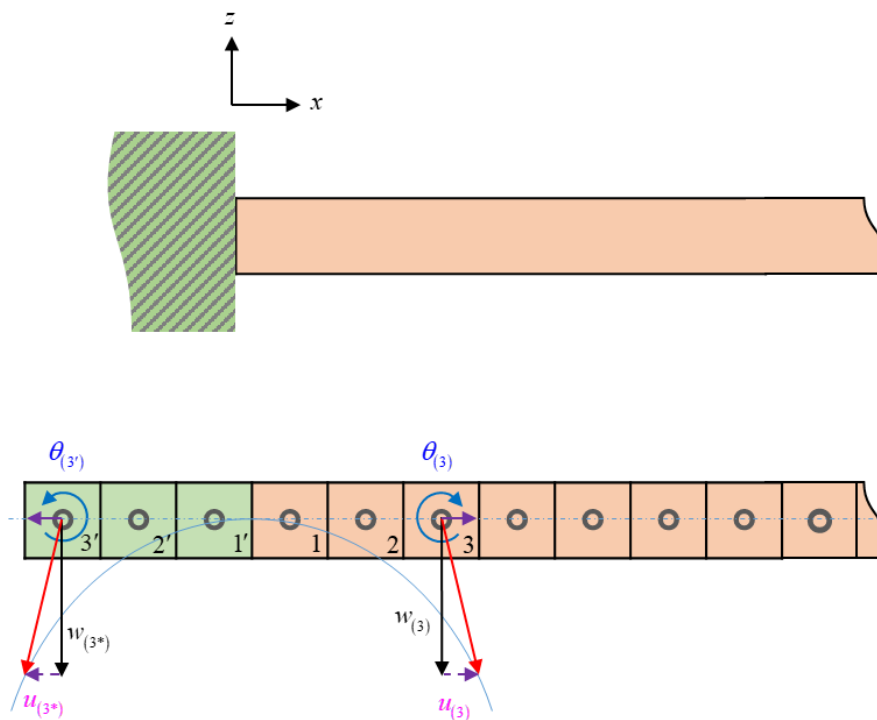


Figure B5 Application of clamped boundary conditions in peridynamic theory

Clamped boundary condition can be achieved by enforcing mirror image of the transverse displacement field for the material points adjacent to the clamped end and anti-symmetric image of rotational and axial displacements fields, as shown in Fig. B5, such that

$$\begin{cases} w_{(i')} = w_{(i)} & w_{(i')} = w_{(i)} = 0 \\ u_{(i')} = -u_{(i)} & \theta_{(i')} = -\theta_{(i)} \end{cases} \quad i = 1, 2, 3 \quad (\text{B8})$$

Simply supported boundary condition

To implement the simply supported boundary condition, the fictitious layer is introduced outside the real material domain, whose size is again chosen to be equal to δ . In Timoshenko Beam theory, the simply supported boundary condition imposes zero transverse displacement and zero curvature for the material point adjacent to the clamped end.

In our study, the above conditions can be satisfied by enforcing anti-symmetrical transverse displacement field and symmetrical rotational displacement field to the material points in the fictitious region with respect to the actual displacement field, as shown in Fig. B6, which is defined as

$$\begin{cases} w_{(i')} = -w_{(i)} \\ \theta_{(i')} = \theta_{(i)} \end{cases} \quad i = 1, 2, 3 \quad (\text{B9})$$

The discussion about simply supported boundary condition for axial deformation should be separated into two parts, which are pinned support and roller support, respectively. The implementation of axial deformation for pinned support is achieved by enforcing anti-symmetrical displacement field for fictitious material domain with respect to actual material domain, as shown in Fig. B6a, which can be defined as

$$u_{(i')} = -u_{(i)} \quad i = 1, 2, 3 \quad (\text{B10a})$$

On the other hand, the implementation for roller support boundary condition requires symmetrical displacement field adjacent to the boundary as (see Fig. B6b)

$$u_{(i')} = u_{(i)} \quad i = 1, 2, 3 \quad (\text{B10b})$$

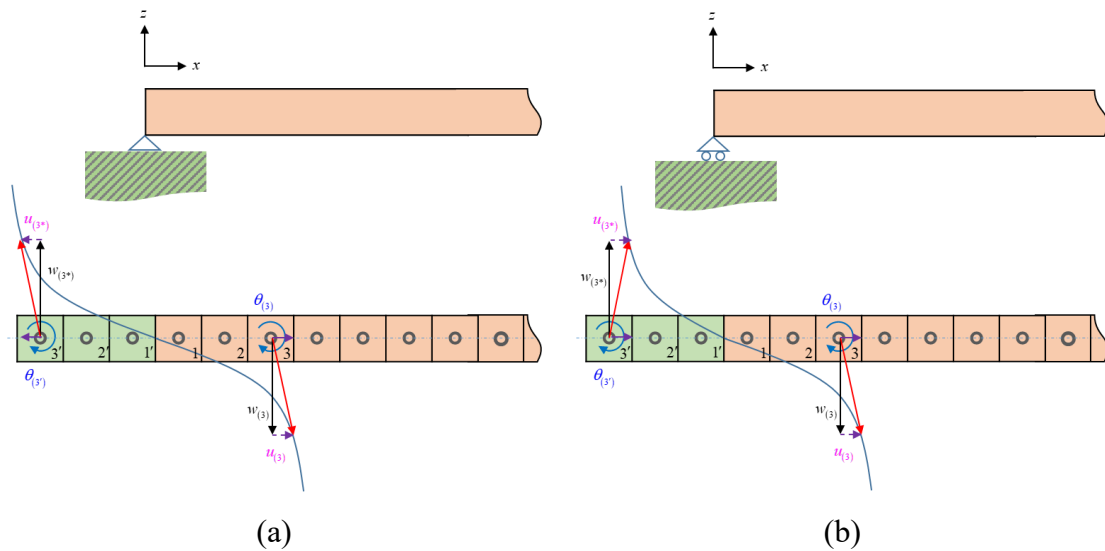


Figure B6: Application of simply supported boundary conditions, (a) pinned support and (b) roller support

B1.5 FGM Higher Order Deformable Beam

The clamped boundary condition

To implement the clamped boundary condition, a fictitious boundary layer is created outside the actual material domain. The horizon size can be chosen as $\delta = 3\Delta x$ in which the discretization size is Δx . This horizon size is sufficient enough to represent macro-scale displacement in our study. Hence, the size of the fictitious region is chosen as δ .

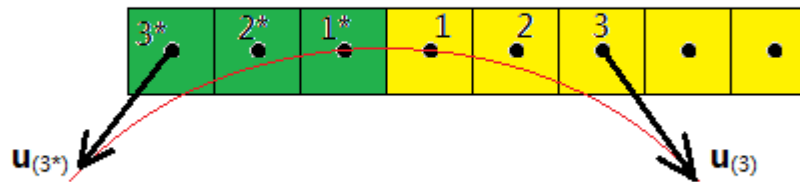


Figure B7 Application of clamped boundary conditions for FGM Higher Order Deformable Beam

The conditions that zero transverse displacement, zero axial displacement and zero rotation for

the material point adjacent to the clamped end can be achieved by enforcing the following displacements fields adjacent to the clamped boundary as (see Fig. B7)

$$\begin{cases} w_{(i^*)} = w_{(i)} & w_{(1^*)} = w_{(1)} = 0 \\ \dot{w}_{(i^*)} = \dot{w}_{(i)} & \dot{w}_{(1^*)} = \dot{w}_{(1)} = 0 \\ u_{(i^*)} = -u_{(i)} & u_{(i^*)}^* = -u_{(i)}^* \\ \theta_{(i^*)} = -\theta_{(i)} & \theta_{(i^*)}^* = -\theta_{(i)}^* \\ \theta_z^{(i^*)} = -\theta_z^{(i)} \end{cases} \quad i = 1, 2, 3 \quad (\text{B11})$$

Simply supported boundary condition

To implement the simply supported boundary condition, the fictitious layer is introduced outside the real material domain, whose size is again chosen to be equal to δ . In the classical beam theory, the discussion about simply supported boundary condition when considering axial displacement should be separated into two parts, which are pinned support and roller support, respectively (see Figure B8).

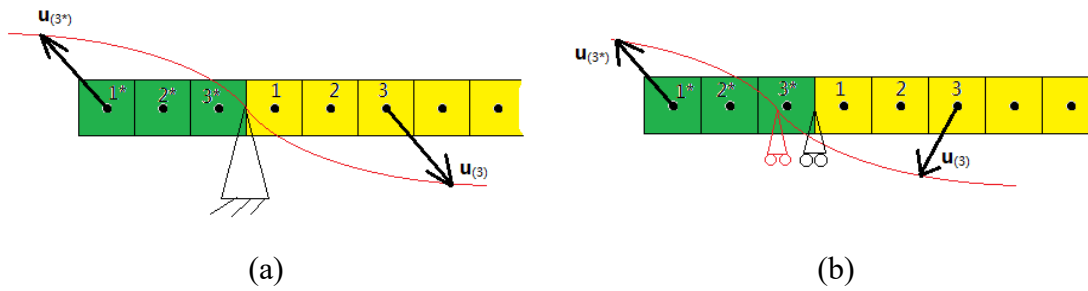


Figure B8 Application of simply supported boundary conditions, (a) pinned support and (b) roller support

For pinned support boundary condition, it imposed zero transverse displacement, zero axial displacement and zero curvature for the material point adjacent to the pinned supported end. In our study, these conditions can be achieved by enforcing the following displacements fields adjacent to the pinned end as

$$\begin{cases} w_{(i^*)} = -w_{(i)} & \dot{w}_{(i^*)} = -\dot{w}_{(i)} \\ u_{(i^*)} = -u_{(i)} & u_{(i^*)}^* = -u_{(i)}^* \\ \theta_{(i^*)} = \theta_{(i)} & \theta_{(i^*)}^* = \theta_{(i)}^* \\ \theta_z^{(i^*)} = -\theta_z^{(i)} \end{cases} \quad i = 1, 2, 3 \quad (\text{B12a})$$

On the other hand, for the roller supported boundary condition, it eliminates the constraint of axial displacements. This can be achieved in our study by enforcing the following

displacements fields

$$\begin{cases} w_{(i')} = -w_{(i)} & \dot{w}_{(i')} = -\dot{w}_{(i)} \\ u_{(i')} = u_{(i)} & \dot{u}_{(i')} = \dot{u}_{(i)} \\ \theta_{(i')} = \theta_{(i)} & \dot{\theta}_{(i')} = \dot{\theta}_{(i)} \\ \theta_z^{(i')} = -\theta_z^{(i)} \end{cases} \quad i = 1, 2, 3 \quad (\text{B12b})$$

B2 Boundary Conditions for PD Plates

B2.1 Kirchhoff Plate

Clamped Boundary Condition

To implement the clamped boundary condition (Figure B1b), a fictitious boundary layer is created outside the actual material domain. The horizon size can be chosen as $\delta = 3\Delta x$ in which the discretization size is Δx . This horizon size is sufficient enough to represent macro-scale displacements in plate problems. Hence, the width of the fictitious region is chosen as 2δ .

The clamped boundary condition for the vertical edges along the y -axis is obtained by imposing zero displacements and zero rotation for the material points adjacent to the clamped end and this can be achieved in PD framework by imposing symmetric displacement field near the boundary region as

$$\begin{cases} w_{(k)(-i)} = w_{(k)(i)} & \text{for } i = 1, 2, \dots, 6 \\ w_{(k)(-1)} = w_{(k)(1)} & k = 1, 2, \dots, n \end{cases} \quad (\text{B13})$$

where the first subscript represents the number of rows along the y -direction and the second subscript is for the number of columns along the x -direction (see Fig. B9).

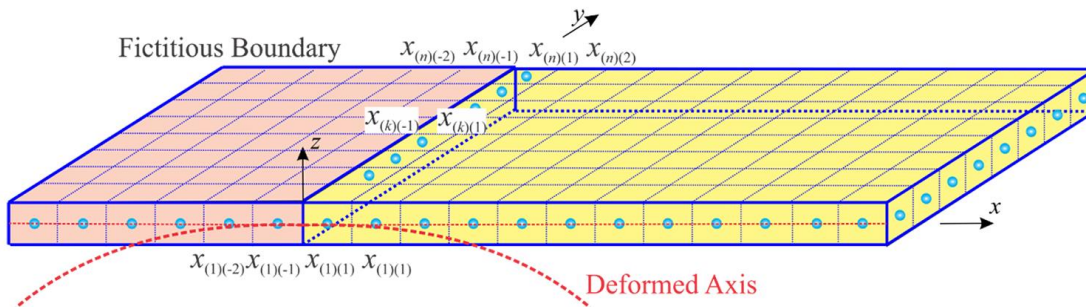


Figure B9 The clamped boundary condition

Similarly, for the horizontal direction edges parallel to the x-axis, the PD implementation can be analogically obtained as in Eq. (B13)

Simply Supported Boundary Condition

To implement the simply supported boundary condition, the fictitious boundary layer is again chosen to be equal to 2δ . The vertical direction boundaries (along the y-axis) are imposed to have zero displacements and curvatures, which can be implemented in PD frame work by enforcing anti-symmetrical displacement fields to the material points in the fictitious region as opposed to the actual displacement fields, as shown in Figure B10. Thus, it is defined as

$$w_{(k)(-i)} = -w_{(k)(i)} \quad \text{for} \quad \begin{matrix} i = 1, 2, \dots, 6 \\ k = 1, 2, \dots, n \end{matrix} \quad (\text{B14})$$

Similarly, the horizontal direction edges take a similar form as in Eq. (B14).

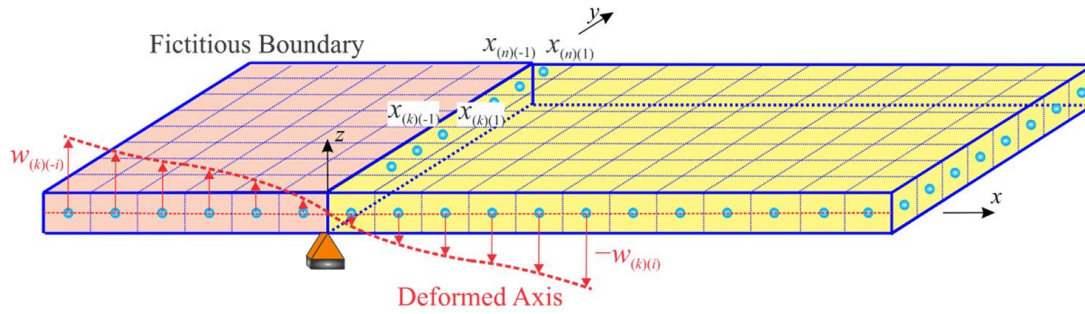


Figure B10 The simply supported boundary condition

B2.2 FGM Kirchhoff Plate

As shown in Fig. B11, unlike the boundaries implementation in isotropic Kirchhoff Plate, it has to take in-plane displacement into consideration for functionally graded material. Thus the corresponding displacements field near the boundaries can be defined as following

Clamped Boundary:

$$\begin{cases} w_{(k)(i')} = w_{(k)(i)} & w_{(k)(i')} = w_{(k)(1)} = 0 \\ u_{(k)(i')} = -u_{(k)(i)} & v_{(k)(i')} = -v_{(k)(i)} \end{cases} \quad \text{for} \quad \begin{matrix} i = 1, 2, \dots, 6 \\ k = 1, 2, \dots, n \end{matrix} \quad (\text{B15})$$

Simply Supported Boundary:

$$\begin{cases} w_{(k)(i')} = -w_{(k)(i)} \\ u_{(k)(i')} = -u_{(k)(i)} \\ v_{(k)(i')} = -v_{(k)(i)} \end{cases} \text{ for } \begin{matrix} i = 1, 2, \dots, 6 \\ k = 1, 2, \dots, n \end{matrix} \quad (\text{B16})$$

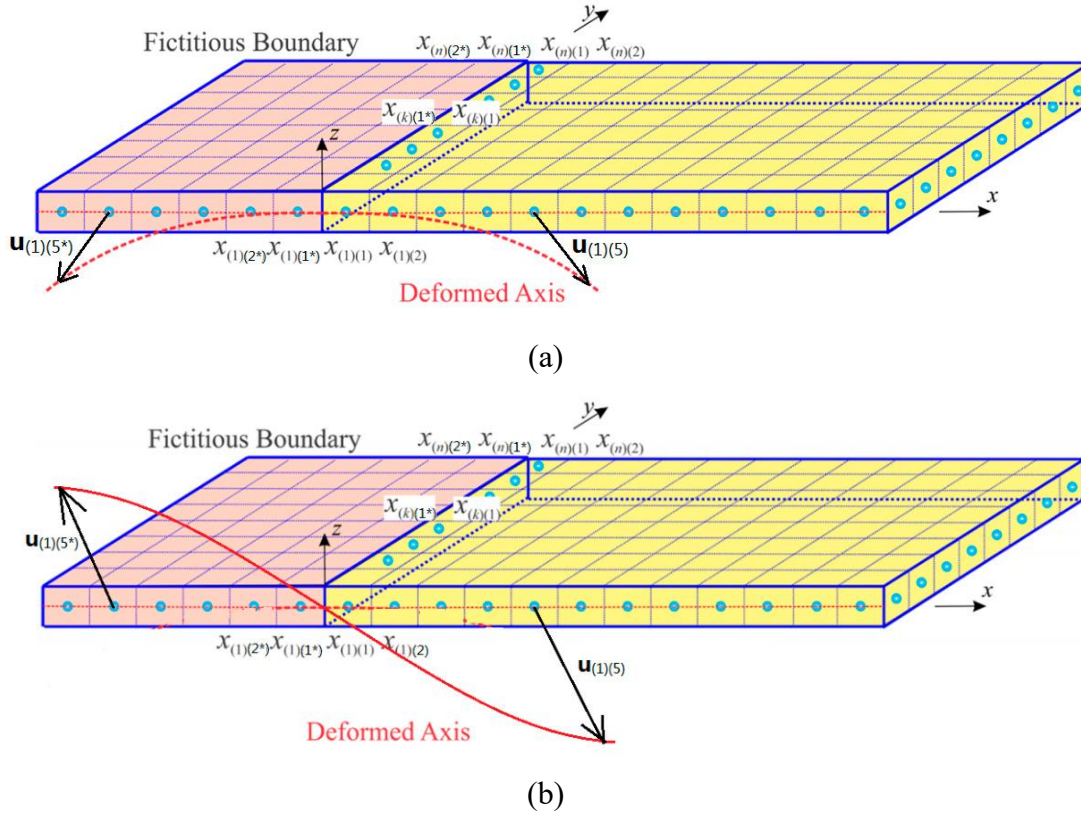


Figure B11 Applications of boundary conditions: (a) clamped, (b) simply supported

B2.3 Mindlin Plate

As shown in Fig. B1(b), the length of the fictitious domain, R_c , outside of the actual solution domain, R , can be chosen as the double size of the horizon if $\nu \neq 1/3$, or the size of the horizon if $\nu = 1/3$. The application procedure for two common types of boundary conditions, i.e. clamped and simply-supported, is given below.

Clamped Boundary

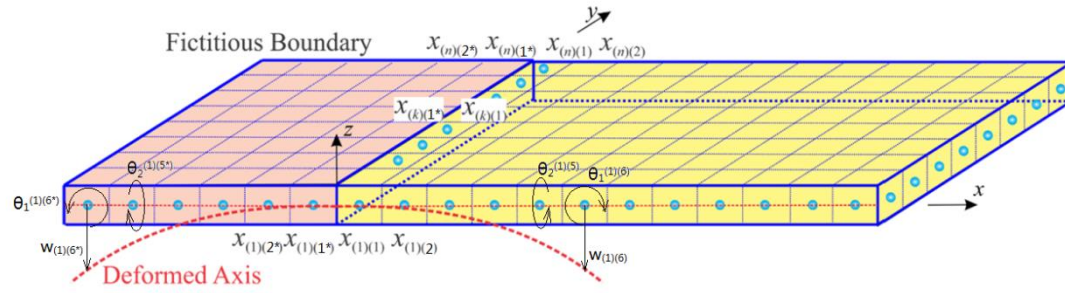


Figure B12. Application of clamped boundary condition in PD Mindlin Plate theory

As mentioned above, the clamped boundary condition imposes zero transverse displacement and zero rotation for the material point adjacent to the clamped end. In our study, these conditions can be achieved by enforcing mirror image of the transverse displacement field for the material points adjacent to the clamped end and anti-symmetric image of rotational displacements fields as shown in Fig. B12 as

$$\begin{aligned}
 w_{(n)(i^*)} &= w_{(n)(i)} \\
 w_{(n)(i^*)} &= w_{(n)(1)} = 0 \quad \text{for} \quad \begin{cases} i = 1, 2, \dots, 6 & \text{if } \nu \neq \frac{1}{3} \\ i = 1, 2, 3 & \text{if } \nu = \frac{1}{3} \end{cases} \\
 \theta_i^{(n)(i^*)} &= -\theta_i^{(n)(i)}
 \end{aligned} \tag{B17}$$

Simply Supported Boundary condition

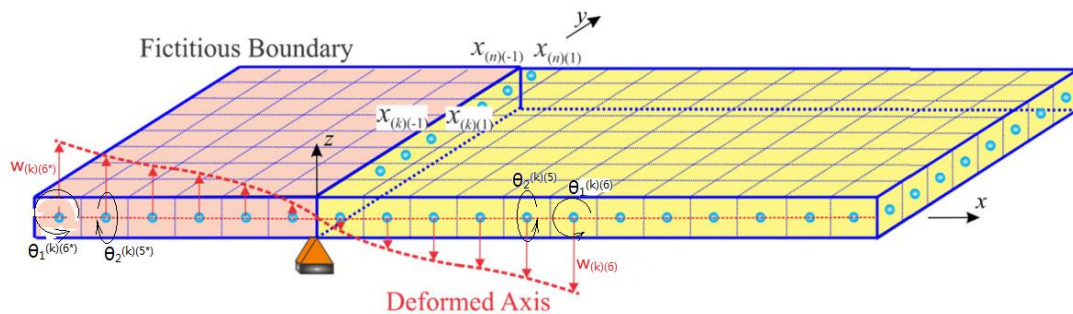


Figure B13. Application of simply supported boundary condition in PD Mindlin Plate theory

In Classical Mindlin plate theory, the simply supported boundary condition imposes zero transverse displacement and zero curvature for the material point adjacent to the boundary.

In our study, the transverse displacement boundary condition can be satisfied by enforcing anti-symmetrical transverse displacement fields to the material points in the fictitious region with respect to the actual displacement field, as shown in Fig. B13. Thus, it is defined as

$$w_{(n)(i')} = -w_{(n)(i)} \quad \text{for} \quad \begin{cases} i = 1, 2, \dots, 6 & \text{if } \nu \neq 1/3 \\ i = 1, 2, 3 & \text{if } \nu = 1/3 \end{cases} \quad (\text{B18})$$

The curvature condition can be satisfied by enforcing the following displacement fields adjacent to the edge $x_I = \text{constant}$ as

$$\begin{aligned} \theta_I^{n(i')} &= \theta_I^{n(i)} \\ \theta_J^{n(i')} &= -\theta_J^{n(i)} \quad (I \neq J) \quad \text{for} \quad \begin{cases} i = 1, 2, \dots, 6 & \text{if } \nu \neq 1/3 \\ i = 1, 2, 3 & \text{if } \nu = 1/3 \end{cases} \end{aligned} \quad (\text{B19})$$

B2.4 FGM Mindlin Plate

Regarding the functionally graded material, in-plane displacements effect has to be considered (see Fig. B11). Therefore, the displacements field near boundaries should be accordingly defined as

Clamped Boundary

$$\begin{aligned} u_I^{n(i')} &= -u_I^{n(i)} \\ w_{(n)(i')} &= w_{(n)(i)} \\ w_{(n)(i')} &= w_{(n)(i)} = 0 \\ \theta_I^{n(i')} &= -\theta_I^{n(i)} \end{aligned} \quad \text{for} \quad \begin{cases} i = 1, 2, \dots, 6 & \text{if } \nu \neq \frac{1}{3} \\ i = 1, 2, 3 & \text{if } \nu = \frac{1}{3} \end{cases} \quad (\text{B20})$$

Simply Supported Boundary

$$\begin{aligned} w_{(n)(i')} &= -w_{(n)(i)} \\ u_I^{n(i')} &= -u_I^{n(i)} \end{aligned} \quad \text{for} \quad \begin{cases} i = 1, 2, \dots, 6 & \text{if } \nu \neq 1/3 \\ i = 1, 2, 3 & \text{if } \nu = 1/3 \end{cases} \quad (\text{B21})$$

For the edge $x_I = \text{constant}$:

$$\begin{aligned} \theta_I^{n(i')} &= \theta_I^{n(i)} \\ \theta_J^{n(i')} &= -\theta_J^{n(i)} \quad (I \neq J) \quad \text{for} \quad \begin{cases} i = 1, 2, \dots, 6 & \text{if } \nu \neq 1/3 \\ i = 1, 2, 3 & \text{if } \nu = 1/3 \end{cases} \end{aligned} \quad (\text{B22})$$

B2.5 Higher Order Deformable Plate

The width of the fictitious boundary layer can be chosen as the size of the horizon for the Poisson's ratio value of $\nu=1/4$ or double size of the horizon for the Poisson's ratio of $\nu \neq 1/4$. Two common types of boundary conditions, i.e. clamped and simply supported, are explained below for PD higher-order plate formulation.

Clamped Boundary

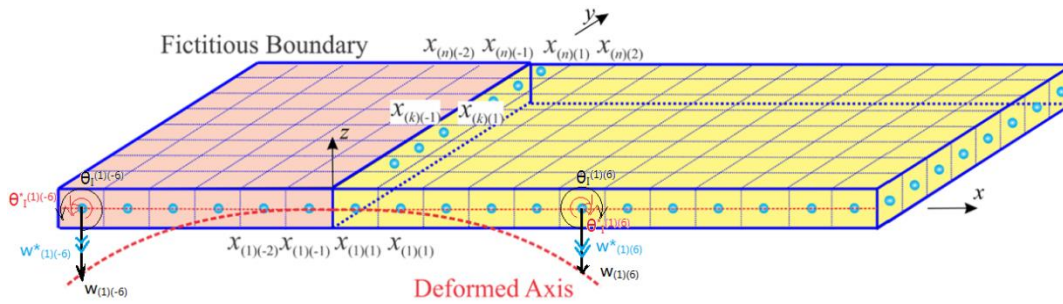


Figure B14 Application of clamped boundary condition of higher order plate

The clamped boundary constrains all degrees of freedom, and in PD framework, this can be achieved by enforcing the displacements field adjacent to the boundary as following

$$\begin{aligned} w_{(k)(-i)} &= w_{(k)(i)} & \dot{w}_{(k)(-i)} &= \dot{w}_{(k)(i)} \\ w_{(k)(-1)} &= w_{(k)(1)} = \dot{w}_{(k)(-1)} = \dot{w}_{(k)(1)} = 0 & \text{for } \begin{cases} i = 1, 2, \dots, 6 & \text{if } \nu \neq 1/4 \\ i = 1, 2, 3 & \text{if } \nu = 1/4 \end{cases} \\ \theta_1^{(k)(-i)} &= -\theta_1^{(k)(i)} & \theta_1^{(k)(-i)} &= -\theta_1^{(k)(i)} \end{aligned} \quad (B23)$$

Simply Supported Boundary

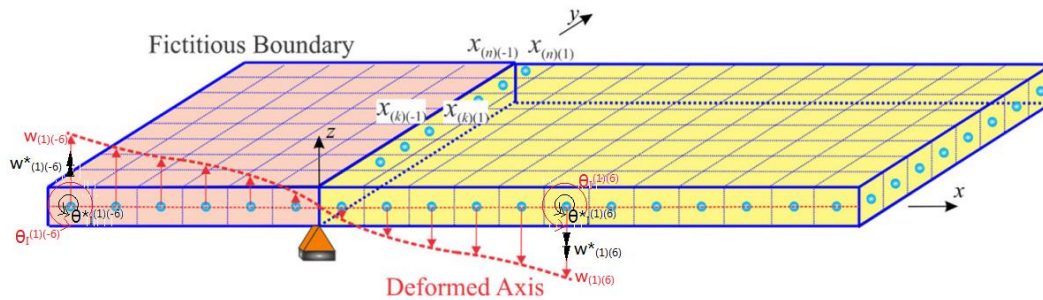


Figure B15 Application of simply supported boundary condition of higher order plate

Compare to clamped edge, simply supported boundary condition release the rotational constraint, and this can be achieved in PD framework by enforcing the following displacements field near the boundary as

$$\begin{aligned} w_{(k)(-i)} &= -w_{(k)(i)} & \text{for } & \begin{cases} i = 1, 2, \dots, 6 & \text{if } \nu \neq 1/4 \\ i = 1, 2, 3 & \text{if } \nu = 1/4 \end{cases} \\ \dot{w}_{(k)(-i)} &= -\dot{w}_{(k)(i)} \end{aligned} \quad (\text{B24})$$

and for the edge $x_I = \text{constant}$:

$$\begin{aligned} \theta_I^{(k)(-i)} &= \theta_I^{(k)(i)} \\ \theta_J^{(k)(-i)} &= -\theta_J^{(k)(i)} \\ \theta_I^{*(k)(-i)} &= \theta_I^{*(k)(i)} \\ \theta_J^{*(k)(-i)} &= -\theta_J^{*(k)(i)} \end{aligned} \quad (I \neq J) \text{ for } \begin{cases} i = 1, 2, \dots, 6 & \text{if } \nu \neq 1/4 \\ i = 1, 2, 3 & \text{if } \nu = 1/4 \end{cases} \quad (\text{B25})$$

B2.6 FGM Higher Order Deformable Plate

When take in-plane effect into consideration, the implementation of the displacements fields becomes following:

Clamped Boundary

$$\begin{aligned} u_I^{(n)(-i)} &= -u_I^{(n)(i)} & u_I^{*(n)(-i)} &= -u_I^{*(n)(i)} \\ w_{(k)(-i)} &= w_{(k)(i)} & \dot{w}_{(k)(-i)} &= \dot{w}_{(k)(i)} \\ w_{(k)(-1)} &= w_{(k)(1)} = \dot{w}_{(k)(-1)} = \dot{w}_{(k)(1)} = 0 & \text{for } & \begin{cases} i = 1, 2, \dots, 6 & \text{if } \nu \neq 1/4 \\ i = 1, 2, 3 & \text{if } \nu = 1/4 \end{cases} \\ \theta_I^{(k)(-i)} &= -\theta_I^{(k)(i)} & \theta_I^{*(k)(-i)} &= -\theta_I^{*(k)(i)} \\ \theta_z^{(k)(-i)} &= -\theta_z^{(k)(i)} \end{aligned} \quad (\text{B26})$$

Simply Supported Boundary

$$\begin{aligned} u_I^{(n)(-i)} &= -u_I^{(n)(i)} & u_I^{*(n)(-i)} &= -u_I^{*(n)(i)} \\ w_{(k)(-i)} &= -w_{(k)(i)} & \dot{w}_{(k)(-i)} &= -\dot{w}_{(k)(i)} \\ \theta_z^{(k)(-i)} &= -\theta_z^{(k)(i)} \end{aligned} \quad \text{for } \begin{cases} i = 1, 2, \dots, 6 & \text{if } \nu \neq 1/4 \\ i = 1, 2, 3 & \text{if } \nu = 1/4 \end{cases} \quad (\text{B27})$$

For the edge $x_I = \text{constant}$:

$$\begin{aligned} \theta_I^{(k)(-i)} &= \theta_I^{(k)(i)} \\ \theta_J^{(k)(-i)} &= -\theta_J^{(k)(i)} \\ \theta_I^{*(k)(-i)} &= \theta_I^{*(k)(i)} \\ \theta_J^{*(k)(-i)} &= -\theta_J^{*(k)(i)} \end{aligned} \quad (I \neq J) \text{ for } \begin{cases} i = 1, 2, \dots, 6 & \text{if } \nu \neq 1/4 \\ i = 1, 2, 3 & \text{if } \nu = 1/4 \end{cases} \quad (\text{B28})$$

Appendix C Nomenclature

A	Cross-section area	b	Body force
c	PD material constant	D	Bending rigidity
E	Young's modulus	G	Shear modulus
h	Thickness	I	2 nd moment of area
I^*, I^{**}	Higher order moment of area	I, J, K, \dots	Indices take up value of 1 and 2
i, j, k, \dots	Indices take up value of 1, 2 and 3	L	Lagrangian
\mathbf{n}	Unit orientation vector	T	Kinetic Energy
\mathbf{u}	Displacement vector	u	Displacement along x axis
\bar{u}	Displacement of central material point along x axis	u^*	Independent variable that contributes x direction deformation
U	Total potential energy	v	Displacement along y axis
\bar{v}	Displacement of central material point along y axis	v^*	Independent variable that contributes y direction deformation
V	Volume of material point	w	Displacement along z axis
\bar{w}	Displacement of central material point along z axis	w^*	Independent variable that contributes transverse deformation
W	Strain energy density		
α	Volume correction factor	β	Surface correction factor
γ	Shear strain	δ	PD horizon size
ε	Normal strain	θ	Rotational displacement
θ^*	Independent variable that contributes flexure deformation	κ	Shear correction factor
ν	Poisson's ratio	ξ	Distance between material points
ρ	Material density	σ	Normal stress
τ	Shear stress	φ	Orientation of bond w.r.t. x axis
CCM	Classical Continuum Mechanics	EoM	Equation of Motion
FE	Finite Element	FEM	Finite Element Method
PD	Perydynamics	SED	Strain Energy Density

Appendix D List of Figures & Tables

Figure 1.1	Beam cross sectional shapes
Figure 2.1	Deformation of Euler-Bernoulli Beam
Figure 2.2	Deformation of higher order beam
Figure 2.3	Deformation of Mindlin Plate
Figure 3.1	Interaction between material points
Figure 3.2	PD interaction between two material points inside the horizon
Figure 3.3	PD interaction between two material points
Figure 3.4	Material volumes in PD horizon
Figure 3.5	PD discretization method
Figure 3.6	Clamped – Free rod
Figure 3.7	PD discretization model of clamped – free rod
Figure 3.8	FEM and PD numerical solution procedure
Figure 4.1	Simply supported beam subjected to a central point force
Figure 4.2	Variation of (a) transverse displacement, (b) rotation along the beam
Figure 4.3	Clamped beam subjected to a central point force
Figure 4.4	Variation of (a) transverse displacement, (b) rotation along the beam
Figure 4.5	Beam subjected to a central point force and mixed boundary conditions
Figure 4.6	Variation of (a) transverse displacement, (b) rotation along the beam
Figure 4.7	Deformation of higher order deformable beam
Figure 4.8	Degrees-of-freedom per node used in higher-order beam theory
Figure 4.9	Simply supported beam subjected to distributed loading
Figure 4.10	Variation of transverse displacements along the beam
Figure 4.11	Simply supported beam subjected to concentrated load
Figure 4.12	Variation of transverse displacements along the beam
Figure 4.13	Clamped-clamped beam subjected to distributed loading
Figure 4.14	Variation of transverse displacements along the beam
Figure 4.15	Cantilever beam subjected to a point load at its free end
Figure 4.16	Variation of transverse displacements along the beam
Figure 4.17	Cantilever beam subjected to a moment at its free end
Figure 4.18	Variation of transverse displacements along the beam
Figure 4.19	Functionally graded Euler-Bernoulli beam
Figure 4.20	Functionally graded beam subjected to Pinned Support-Roller Support boundary condition
Figure 4.21	Variation of the Young's modulus in thickness direction for the FE model
Figure 4.22	Comparison of PD and FE results; (a) transverse displacement, (b) axial displacement
Figure 4.23	Functionally graded beam subjected to Pinned Support-Pinned Support boundary condition
Figure 4.24	Comparison of PD and FE results; (a) transverse displacement, (b) axial displacement

- Figure 4.25 Functionally graded beam subjected to Clamped-Clamped boundary condition
- Figure 4.26 Comparison of PD and FE results; (a) transverse displacement, (b) axial displacement
- Figure 4.27 Functionally graded beam subjected to Clamped-Free boundary condition
- Figure 4.28 Comparison of PD and FE results; (a) transverse displacement, (b) axial displacement
- Figure 4.29 Material variation along the thickness direction for the functionally graded material
- Figure 4.30 Timoshenko beam with pinned support – roller support boundary conditions
- Figure 4.31 Discretization, applied loading and fictitious region
- Figure 4.32 Material variation in the thickness direction for the finite element model
- Figure 4.33 Comparison of PD and FE results for (a) transverse displacements, (b) rotations, and (c) axial displacements
- Figure 4.34 Timoshenko beam with clamped – roller support boundary conditions
- Figure 4.35 Discretization, applied loading and fictitious region
- Figure 4.36 Comparison of PD and FE results for (a) transverse displacements, (b) rotations, and (c) axial displacements
- Figure 4.37 Timoshenko beam with clamped – free boundary conditions
- Figure 4.38 Discretization, applied loading and fictitious region
- Figure 4.39 Comparison of PD and FE results for (a) transverse displacements, (b) rotations, and (c) axial displacements
- Figure 4.40 PD model of functionally graded material beam
- Figure 4.41 Material variation in the thickness direction for the finite element model
- Figure 4.42 Beam with pinned support – roller support boundary conditions
- Figure 4.43 Discretization, applied loading and fictitious region
- Figure 4.44 Comparison of PD and FE results; (a) transverse displacement, (b) axial displacement
- Figure 4.45 Cantilever beam subjected to a point end load
- Figure 4.46 Variation of (a) transverse displacement, (b) axial displacement along the beam
- Figure 4.47 Clamped-simply supported beam subjected to transverse loading
- Figure 4.48 Variation of (a) transverse displacement, (b) axial displacement along the beam
- Figure 4.49 Simply supported FGM beam subjected to transverse load
- Figure 4.50 Deflections with thickness of $h = 0.05m$
- Figure 4.51 Deflections with thickness of $h = 0.10m$
- Figure 4.52 Deflections with thickness of $h = 0.15m$
- Figure 5.1 Peridynamic interactions in Kirchhoff plate theory
- Figure 5.2 The geometry of a clamped Kirchhoff plate
- Figure 5.3 The peridynamic discretization of Kirchhoff plate
- Figure 5.4 Comparison of the vertical displacement components of the (a) finite element and (b) peridynamic results (unit: m)

- Figure 5.5 Comparison of the vertical displacements along the (a) x- and (b) y-central axes. PD: peridynamic; FE: finite element
- Figure 5.6 The geometry of a simply supported Kirchhoff plate
- Figure 5.7 Comparison of the vertical displacement components of the (a) finite element and (b) peridynamic results (unit: m)
- Figure 5.8 Comparison of the vertical displacements along the (a) x- and (b) y-central axes. PD: peridynamic; FE: finite element
- Figure 5.9 Clamped plate subjected to transverse loading
- Figure 5.10 Variation of the Young's modulus in thickness direction for the FE model
- Figure 5.11 Variation of transverse displacements (a) PD, (b) FEM
- Figure 5.12 Variation of (a) transverse, w and (b) in-plane, u_1 , displacements along the central y -axis
- Figure 5.13 Simply supported plate subjected to transverse loading
- Figure 5.14 Variation of transverse displacements (a) PD, (b) FEM
- Figure 5.15 Variation of (a) transverse, w and (b) in-plane, u_1 , displacements along the central y -axis
- Figure 5.16 Simply supported plate subjected to inclined loading
- Figure 5.17 Variation of transverse displacements (a) PD, (b) FEM
- Figure 5.18 Variation of (a) transverse, w and (b) in-plane, u_1 , displacements along the central y -axis
- Figure 5.19 Degrees-of-freedom in peridynamic Mindlin formulation
- Figure 5.20 Simply supported plate subjected to transverse loading
- Figure 5.21 Discretisation and application of the body load
- Figure 5.22 Variation of transverse displacements along the central (a) x -axis, (b) y -axis
- Figure 5.23 Variation of rotations along the central (a) x -axis, (b) y -axis
- Figure 5.24 Clamped plate subjected to transverse loading
- Figure 5.25 Variation of transverse displacements along the central (a) x -axis, (b) y -axis.
- Figure 5.26 Variation of rotations along the central (a) x -axis, (b) y -axis
- Figure 5.27 Mindlin plate subjected to mixed boundary conditions
- Figure 5.28 Variation of transverse displacements along the central (a) x -axis, (b) y -axis
- Figure 5.29 Variation of rotations along the central (a) x -axis, (b) y -axis
- Figure 5.30 The positive set of the degrees - of - freedom for Mindlin plate formulation
- Figure 5.31 Variation of material properties through the thickness direction for the finite element model
- Figure 5.32 Numerical discretization, loading and fictitious region
- Figure 5.33 Comparison of PD and FEA results along the central x - and y - axes
- Figure 5.34 Fully clamped functionally graded Mindlin plate
- Figure 5.35 Comparison of PD and FEA results along the central x - and y - axes
- Figure 5.36 Functionally graded Mindlin plate subjected to mixed boundary conditions
- Figure 5.37 Comparison of PD and FEA results along the central x - and y - axes
- Figure 5.38 Simply supported plate subjected to transverse loading
- Figure 5.39 Application of transverse loading in PD model and fictitious region
- Figure 5.40 Variation of transverse displacements along (a) central x -axis and (b) central y -axis

- Figure 5.41 Clamped plate subjected to transverse loading
- Figure 5.42 Application of transverse loading in PD model and fictitious region
- Figure 5.43 Variation of transverse displacements along (a) central x-axis and (b) central y-axis
- Figure 5.44 Variation of transverse displacements along (a) central x-axis and (b) central y-axis
- Figure 5.45 Simply supported plate subjected to transverse loading
- Figure 5.46 Variation of transverse displacements along (a) central x-axis and (b) central y-axis
- Figure 5.47 Clamped plate subjected to transverse loading
- Figure 5.48 Variation of transverse displacements along (a) central x-axis and (b) central y-axis
- Figure 5.49 Functionally graded higher order plate subjected to mixed boundary conditions
- Figure 5.50 Variation of transverse displacements along (a) central x-axis and (b) central y-axis
- Figure 5.51 Functionally graded higher order plate subjected to mixed boundary conditions
- Figure 5.52 Variation of transverse displacements along (a) central x-axis and (b) central y-axis
- Figure 5.53 Simply supported plate subjected to transverse loading
- Figure 5.54 Variation of transverse displacements along (a) central x-axis and (b) central y-axis with thickness of $h = 0.05m$
- Figure 5.55 Variation of transverse displacements along (a) central x-axis and (b) central y-axis with thickness of $h = 0.10m$
- Figure 5.56 Variation of transverse displacements along (a) central x-axis and (b) central y-axis with thickness of $h = 0.15m$
- Figure 6.1 Initial and deformed configurations of a Timoshenko beam
- Figure 6.2 Initial and deformed configurations of a Mindlin plate
- Figure 6.3 Meshless discretization of a domain and interaction between points inside the horizon of point k
- Figure 6.4 Beam element representing an interaction between PD points
- Figure 6.5 Network of beam elements to represent interactions between PD points
- Figure 6.6 (a) A cantilever beam subjected to transverse loading and (b) its discretization
- Figure 6.7 Variation of (a) deflection and (b) rotation along the cantilever beam
- Figure 6.8 Variation of deflection as the applied load increases
- Figure 6.9 (a) A plate subjected to transverse force loading and (b) its discretization
- Figure 6.10 Variation of (a) deflection and (b) rotation along the central x-axis of the plate
- Figure 6.11 Variation of deflection as the applied load increases
- Figure 6.12 (a) A plate with a central crack subjected to pure bending loading and (b) its discretization

Figure 6.13	Propagation of a central crack in a plate subjected to uniform bending loading.
Figure A1	PD influence domain of beam model (a) and its discretization (b)
Figure A2	Peridynamic interaction between two material points
Figure B1	Introduction of fictitious boundary layers: (a) beam, (b) plate
Figure B2	Application of clamped boundary conditions in PD theory
Figure B3	Application of clamped boundary condition
Figure B4	Application of simply supported boundary condition, (a) pinned support, (b) roller support
Figure B5	Application of clamped boundary conditions in peridynamic theory
Figure B6	Application of simply supported boundary conditions, (a) pinned support and (b) roller support
Figure B7	Application of clamped boundary conditions for FGM Higher Order Deformable Beam
Figure B8	Application of simply supported boundary conditions, (a) pinned support and (b) roller support
Figure B9	The clamped boundary condition
Figure B10	The simply supported boundary condition
Figure B11	Applications of boundary conditions: (a) clamped, (b) simply supported
Figure B12	Application of clamped boundary condition in PD Mindlin Plate theory
Figure B13	Application of simply supported boundary condition in PD Mindlin Plate theory
Figure B14	Application of clamped boundary condition of higher order plate
Figure B15	Application of simply supported boundary condition of higher order plate
Table 2.1	Summary of beam theories
Table 2.2	Summary of plate theories

Reference

Silling, S.A., 2000. Reformulation of elasticity theory for discontinuities and long-range forces. *Journal of the Mechanics and Physics of Solids*, 48(1), pp.175-209.

F. I, A. D. Corte, R. Esposito, L. Russo, Some cases of unrecognized transmission of scientific knowledge : From Antiquity to Gabrio Piola's peridynamics and generalized continuum theories, *Advanced Structured Materials* 42 (2016) 77–128

Madenci, E. and Oterkus, E., *Peridynamic Theory and Its Applications*, Springer New York, New York, 2014.

Javili, A., Morasata, R., Oterkus, E. and Oterkus, S., 2019. Peridynamics review. *Mathematics and Mechanics of Solids*, 24(11), pp.3714-3739.

<https://theconstructor.org/structural-engg/types-beams-construction/24684/>

Komeili, A., Akbarzadeh, A. H., Doroushi, A., & Eslami, M. R. (2011). Static analysis of functionally graded piezoelectric beams under thermo-electro-mechanical loads. *Advances in Mechanical Engineering*, 3, 153731.

Heyliger P R, Reddy J N. A higher order beam finite element for bending and vibration problems[J]. *Journal of sound and vibration*, 1988, 126(2): 309-326.

Soldatos K P, Elishakoff I. A transverse shear and normal deformable orthotropic beam theory[J]. *JSV*, 1992, 155(3): 528-533.

Kant T, Marur S R, Rao G S. Analytical solution to the dynamic analysis of laminated beams using higher order refined theory[J]. *Composite Structures*, 1997, 40(1): 1-9.

Reissner E. The effect of transverse shear deformation on the bending of elastic plates[J]. *J. appl. Mech.*, 1945: A69-A77.

Mindlin R D. Thickness-shear and flexural vibrations of crystal plates[J]. *Journal of applied physics*, 1951, 22(3): 316-323.

Lo K H, Christensen R M, Wu E M. A high-order theory of plate deformation—Part 1: Homogeneous plates[J]. 1977.

Lo K H, Christensen R M, Wu E M. A high-order theory of plate deformation—part 2: laminated

plates[J]. 1977.

Reddy J N. A simple higher-order theory for laminated composite plates[J]. 1984.

Reddy J N. Energy and variational methods in applied mechanics: with an introduction to the finite element method[M]. New York: Wiley, 1984.

Reddy J N. A refined nonlinear theory of plates with transverse shear deformation[J]. *International Journal of solids and structures*, 1984, 20(9-10): 881-896.

Thai, H. T., Vo, T. P. (2012). Bending and free vibration of functionally graded beams using various higher-order shear deformation beam theories. *International Journal of Mechanical Sciences*, 62(1), 57-66.

Li, X. F. (2008). A unified approach for analyzing static and dynamic behaviors of functionally graded Timoshenko and Euler–Bernoulli beams. *Journal of Sound and vibration*, 318(4-5), 1210-1229.

Kadoli, R., Akhtar, K., Ganesan, N. (2008). Static analysis of functionally graded beams using higher order shear deformation theory. *Applied Mathematical Modelling*, 32(12), 2509-2525.

Kahrobaiyan, M. H., Rahaeifard, M., Tajalli, S. A., Ahmadian, M. T. (2012). A strain gradient functionally graded Euler–Bernoulli beam formulation. *International Journal of Engineering Science*, 52, 65-76.

Lu, C. F., Chen, W. Q., Xu, R. Q., Lim, C. W. (2008). Semi-analytical elasticity solutions for bi-directional functionally graded beams. *International Journal of Solids and Structures*, 45(1), 258-275.

Su, H., Banerjee, J. R., Cheung, C.W. (2013). Dynamic stiffness formulation and free vibration analysis of functionally graded beams. *Composite Structures*, 106, 854-862.

Şimşek, M., Kocatürk, T., Akbaş, Ş. D. (2012). Dynamic behavior of an axially functionally graded beam under action of a moving harmonic load. *Composite Structures*, 94(8), 2358-2364.

Li, S. R., Batra, R. C. (2013). Relations between buckling loads of functionally graded Timoshenko and homogeneous Euler–Bernoulli beams. *Composite Structures*, 95, 5-9.

Sankar, B. V. (2001). An elasticity solution for functionally graded beams. *Composites Science and Technology*, 61(5), 689-696.

Birsan, M., Altenbach, H., Sadowski, T., Eremeyev, V. A., Pietras, D. (2012). Deformation analysis of functionally graded beams by the direct approach. *Composites Part B: Engineering*, 43(3), 1315-1328.

Nguyen, T. K., Vo, T. P., Thai, H. T., 2013. Static and free vibration of axially loaded functionally graded beams based on the first-order shear deformation theory. *Composites Part B: Engineering*, 55, 147-157.

Filippi, M., Carrera, E., Zenkour, A. M. (2015). Static analyses of FGM beams by various theories and finite elements. *Composites Part B: Engineering*, 72, 1-9.

Vel, S.; Batra, R.C. Three-dimensional exact solution for the vibration of functionally graded rectangular plates. *J. Sound Vib.* **2004**, *272*, 703–730, doi:10.1016/s0022-460x(03)00412-7.

Shen, H.-S. Nonlinear bending response of functionally graded plates subjected to transverse loads and in thermal environments. *Int. J. Mech. Sci.* **2002**, *44*, 561–584, doi:10.1016/s0020-7403(01)00103-5.

Zenkour, A. Generalized shear deformation theory for bending analysis of functionally graded plates. *Appl. Math. Model.* **2006**, *30*, 67–84, doi:10.1016/j.apm.2005.03.009.

Bian, Z.; Chen, W.; Lim, C.W.; Zhang, N. Analytical solutions for single- and multi-span functionally graded plates in cylindrical bending. *Int. J. Solids Struct.* **2005**, *42*, 6433–6456, doi:10.1016/j.ijsolstr.2005.04.032.

Carrera, E.; Brischetto, S.; Cinefra, M.; Soave, M. Effects of thickness stretching in functionally graded plates and shells. *Compos. Part B Eng.* **2011**, *42*, 123–133, doi:10.1016/j.compositesb.2010.10.005.

Ferreira, A.; Batra, R.C.; Roque, C.; Qian, L.; Martins, P. Static analysis of functionally graded plates using third-order shear deformation theory and a meshless method. *Compos. Struct.* **2005**, *69*, 449–457, doi:10.1016/j.compstruct.2004.08.003.

Kashtalyan, M. Three-dimensional elasticity solution for bending of functionally graded rectangular plates. *Eur. J. Mech. A Solids* **2004**, *23*, 853–864.

Xiang, S.; Kang, G.-W. A n th-order shear deformation theory for the bending analysis on the functionally graded plates. *Eur. J. Mech. A Solids* **2013**, *37*, 336–343, doi:10.1016/j.euromechsol.2012.08.005.

<http://www.parash.xyz/2019/02/26/structural-engineering/>

Komeili A, Akbarzadeh AH, Doroushi A, Eslami MR. Static analysis of functionally graded piezoelectric beams under thermo-electro-mechanical loads. *Advances in Mechanical Engineering*.2011;3:153731.

Chen H, Kumar AV. Implicit Boundary Approach for Reissner-Mindlin Plates. In ASME 2013 International Design Engineering Technical Conferences and Computers and Information in Engineering Conference 2013 Aug 4. American Society of Mechanical Engineers Digital Collection.

Taylor, M., Steigmann, D.J.: A two-dimensional peridynamic model for thin plates. *Mathematics and Mechanics of Solids* **20**(8), 998-1010 (2015).

Diyaroglu, C., Oterkus, E., Oterkus, S.: An Euler–Bernoulli beam formulation in an ordinary state-based peridynamic framework. *Mathematics and Mechanics of Solids* **24**(2), 361-376 (2019).

Diyaroglu, C., Oterkus, E., Oterkus, S., Madenci, E.: Peridynamics for bending of beams and plates with transverse shear deformation. *International Journal of Solids and Structures* **69**, 152-168 (2015).

O'Grady, J., Foster, J.: Peridynamic beams: a non-ordinary, state-based model. *International Journal of Solids and Structures* **51**(18), 3177-3183 (2014).

O'Grady, J., Foster, J.: Peridynamic plates and flat shells: A non-ordinary, state-based model. *International Journal of Solids and Structures* **51**(25-26), 4572-4579 (2014).

Chowdhury, S.R., Roy, P., Roy, D., Reddy, J.N.: A peridynamic theory for linear elastic shells. *International Journal of Solids and Structures* **84**, 110-132 (2016).

Qian, L.F. and Batra, R.C., 2004. Transient thermoelastic deformations of a thick functionally graded plate. *Journal of Thermal Stresses*, **27**(8), pp.705-740.

Ferreira, A.J.M., Batra, R.C., Roque, C.M.C., Qian, L.F. and Martins, P.A.L.S., 2005. Static analysis of functionally graded plates using third-order shear deformation theory and a meshless method. *Composite structures*, **69**(4), pp.449-457.

Cheng, Z.Q. and Batra, R.C., 2000. Deflection relationships between the homogeneous Kirchhoff plate theory and different functionally graded plate theories. *Archives of Mechanics*, **52**(1), pp.143-158.

Batra, R.C., 2007. Higher-order shear and normal deformable theory for functionally graded incompressible linear elastic plates. *Thin-Walled Structures*, **45**(12), pp.974-982.

Belabed, Z., Houari, M.S.A., Tounsi, A., Mahmoud, S.R. and Bég, O.A., 2014. An efficient and simple higher order shear and normal deformation theory for functionally graded material (FGM) plates. *Composites Part B: Engineering*, **60**, pp.274-283.

Xiang, S. and Kang, G.W., 2013. A nth-order shear deformation theory for the bending analysis on the functionally graded plates. *European Journal of Mechanics-A/Solids*, **37**, pp.336-343.

Zhang, P., Qi, C., Fang, H. and He, W., 2020. Three dimensional mechanical behaviors of in-plane functionally graded plates. *Composite Structures*, p.112124.

F. Ebrahimi, M. Zia, Large amplitude nonlinear vibration analysis of functionally graded Timoshenko beams with porosities, *Acta Astronaut.* **116** (2015) 117–125.

F.F. Calim, Transient analysis of axially functionally graded Timoshenko beams with variable cross - section, *Compos. B Eng.* **98** (2016) 472–483.

M. Asghari, M. Rahaeifard, M.H. Kahrobaiyan, M.T. Ahmadian, The modified couple stress functionally graded Timoshenko beam formulation, *Mater. Des.* 32 (3) (2011) 1435–1443.

S.A. Tajalli, M. Rahaeifard, M.H. Kahrobaiyan, M.R. Movahhedy, J. Akbari, M. T. Ahmadian, Mechanical behavior analysis of size-dependent micro-scaled functionally graded Timoshenko beams by strain gradient elasticity theory, *Compos. Struct.* 102 (2013) 72–80. Z. Yang et al. *Thin-Walled Structures* 160 (2021) 10734316

F. Ebrahimi, M.R. Barati, A nonlocal higher-order shear deformation beam theory for vibration analysis of size-dependent functionally graded nanobeams, *Arabian J. Sci. Eng.* 41 (5) (2016) 1679–1690.

R. Kadoli, K. Akhtar, N. Ganesan, Static analysis of functionally graded beams using higher order shear deformation theory, *Appl. Math. Model.* 32 (12) (2008) 2509–2525.

M. Simsek, J.N. Reddy, Bending and vibration of functionally graded microbeams using a new higher order beam theory and the modified couple stress theory, *Int. J. Eng. Sci.* 64 (2013) 37–53.

S.R. Li, R.C. Batra, Relations between buckling loads of functionally graded Timoshenko and homogeneous Euler–Bernoulli beams, *Compos. Struct.* 95 (2013) 5–9.

Y. Sun, S.R. Li, R.C. Batra, Thermal buckling and post-buckling of FGM Timoshenko beams on nonlinear elastic foundation, *J. Therm. Stresses* 39 (1) (2016) 11–26.

A. Pydah, R.C. Batra, Shear deformation theory using logarithmic function for thick circular beams and analytical solution for bi-directional functionally graded circular beams, *Compos. Struct.* 172 (2017) 45–60.

J. Fariborz, R.C. Batra, Free vibration of bi-directional functionally graded material circular beams using shear deformation theory employing logarithmic function of radius, *Compos. Struct.* 210 (2019) 217–230.

A. Menasria, A. Kaci, A.A. Bousahla, F. Bourada, A. Tounsi, K.H. Benrahou, A. Tounsi, E.A. Adda Bedia, S.R. Mahmoud, A four-unknown refined plate theory for dynamic analysis of FG-sandwich plates under various boundary conditions, *Steel Compos. Struct.* 36 (3) (2020) 355–367.

A. Zine, A.A. Bousahla, F. Bourada, K.H. Benrahou, A. Tounsi, E.A. Adda Bedia, S. R. Mahmoud, A. Tounsi, Bending analysis of functionally graded porous plates via a refined shear deformation theory, *Comput. Concr.* 26 (1) (2020) 63–74.

M. Rabhi, K.H. Benrahou, A. Kaci, M.S.A. Houari, F. Bourada, A.A. Bousahla, A. Tounsi, E.A. Bedia, S.R. Mahmoud, A. Tounsi, A new innovative 3-unknowns HSDT for buckling and free vibration of exponentially graded sandwich plates resting on elastic foundations under various boundary conditions, *Geomech. Eng.* 22 (2) (2020) 119.

H. Matouk, A.A. Bousahla, H. Heireche, F. Bourada, E.A. Bedia, A. Tounsi, S. R. Mahmoud, A. Tounsi, K.H. Benrahou, Investigation on hygro-thermal vibration of P-FG and symmetric S-FG nanobeam using integral Timoshenko beam theory, *Adv. Nano Res.* 8 (4) (2020) 293–305.

S.C. Chikr, A. Kaci, A.A. Bousahla, F. Bourada, A. Tounsi, E.A. Bedia, S. R. Mahmoud, K.H. Benrahou, A. Tounsi, A novel four-unknown integral model for buckling response of FG sandwich plates resting on elastic foundations under various boundary conditions using Galerkin's approach, *Geomech. Eng.* 21 (5) (2020) 471–487.

S. Refrafi, A.A. Bousahla, A. Bouhadra, A. Menasria, F. Bourada, A. Tounsi, E. A. Bedia, S.R. Mahmoud, K.H. Benrahou, A. Tounsi, Effects of hygro-thermo- mechanical conditions on the buckling of FG sandwich plates resting on elastic foundations, *Comput. Concr.* 25 (4) (2020) 311–325.

M. Kaddari, A. Kaci, A.A. Bousahla, A. Tounsi, F. Bourada, A. Tounsi, E.A. Bedia, M. A. Al-Osta, A study on the structural behaviour of functionally graded porous plates on elastic foundation using a new quasi-3D model: bending and free vibration analysis, *Comput. Concr.* 25 (1) (2020) 37–57.

A. Tounsi, S.U. Al-Dulaijan, M.A. Al-Osta, A. Chikh, M.M. Al-Zahrani, A. Sharif, A. Tounsi, A four variable trigonometric integral plate theory for hygro-thermo- mechanical bending analysis of AFG ceramic-metal plates resting on a two- parameter elastic foundation, *Steel Compos. Struct.* 34 (4) (2020) 511.

A. Boussoula, B. Boucham, M. Bourada, F. Bourada, A. Tounsi, A.A. Bousahla, A. Tounsi, A simple n th-order shear deformation theory for thermomechanical bending analysis of different configurations of FG sandwich plates, *Smart Struct. Syst.* 25 (2) (2020) 197–218.

Madenci, E., Oterkus, E. (2014). *Peridynamic theory and its applications*. USA: Springer.

Seleson P., Littlewood D.J. (2018) Numerical Tools for Improved Convergence of Meshfree Peridynamic Discretizations. In: Voyiadjis G. (eds) *Handbook of Nonlocal Continuum Mechanics for Materials and Structures*. Springer, Cham. https://doi.org/10.1007/978-3-319-22977-5_39-1

Schoeftner J, Irschik H. Stress tracking in thin bars by eigenstrain actuation[J]. *Journal of Sound and Vibration*, 2016, 383: 35-45.

Bauchau OA, Craig JI. Euler-Bernoulli beam theory. In *Structural analysis 2009* (pp. 173-221). Springer, Dordrecht.

Timoshenko S. *History of strength of materials: with a brief account of the history of theory of elasticity and theory of structures*. Courier Corporation; 1983.

Soldatos KP, Elishakoff I. A transverse shear and normal deformable orthotropic beam theory. *Journal of Sound Vibration*. 1992 Jun;155(3):528-33.

Kant T, Gupta A. A finite element model for a higher-order shear-deformable beam theory. *Journal of sound and vibration*. 1988 Sep 8;125(2):193-202.

Love AE. XVI. The small free vibrations and deformation of a thin elastic shell. *Philosophical Transactions of the Royal Society of London.(A.)*. 1888 Dec 31(179):491-546.

Yang, Z., Oterkus, E., & Oterkus, S. (2020). Analysis of functionally graded Timoshenko beams by using peridynamics. *Journal of Peridynamics and Nonlocal Modeling*, 1-19.

Yang, Z., Oterkus, E., & Oterkus, S. (2020). A state-based peridynamic formulation for functionally graded Euler-Bernoulli beams. *CMES -Computer Modeling in Engineering and Sciences*, 124(2), 527-544.

Yang Z, Oterkus E, Oterkus S. A state-based peridynamic formulation for functionally graded Kirchhoff plates. *Mathematics and Mechanics of Solids*. 2020 Oct 13:1081286520963383.

Yang Z, Oterkus E, Oterkus S. Peridynamic formulation for higher order functionally graded beams. *Thin-Walled Structures*. 2020 Nov 28.

Yang Z, Oterkus E, Oterkus S. Peridynamic formulation for higher-order plate theory. *Journal of Peridynamics and Nonlocal Modeling*. 2020 Dec 9:1-26.

Yang, Z., Oterkus, S., & Oterkus, E. (2020). Peridynamic formulation for Timoshenko beam. *Procedia Structural Integrity*, 28, 464-471.

Yang, Z., Oterkus, E., & Oterkus, S. (2020). Peridynamic higher-order beam formulation. *Journal of Peridynamics and Nonlocal Modeling*, 1-17.

Yang, Z., Oterkus, E., & Oterkus, S. (2020). Peridynamic mindlin plate formulation for functionally graded materials. *Journal of Composites Science*,4(2), 76.

Yang, Z., Vazic, B., Diyaroglu, C., Oterkus, E., & Oterkus, S. (2020). A Kirchhoff plate formulation in a state-based peridynamic framework. *Mathematics and Mechanics of Solids*,25(3), 727-738.

Yang, Z., Oterkus, E., Nguyen, C. T., & Oterkus, S. (2019). Implementation of peridynamic beam and plate formulations in finite element framework. *Continuum Mechanics and Thermodynamics*,31(1), 301-315.